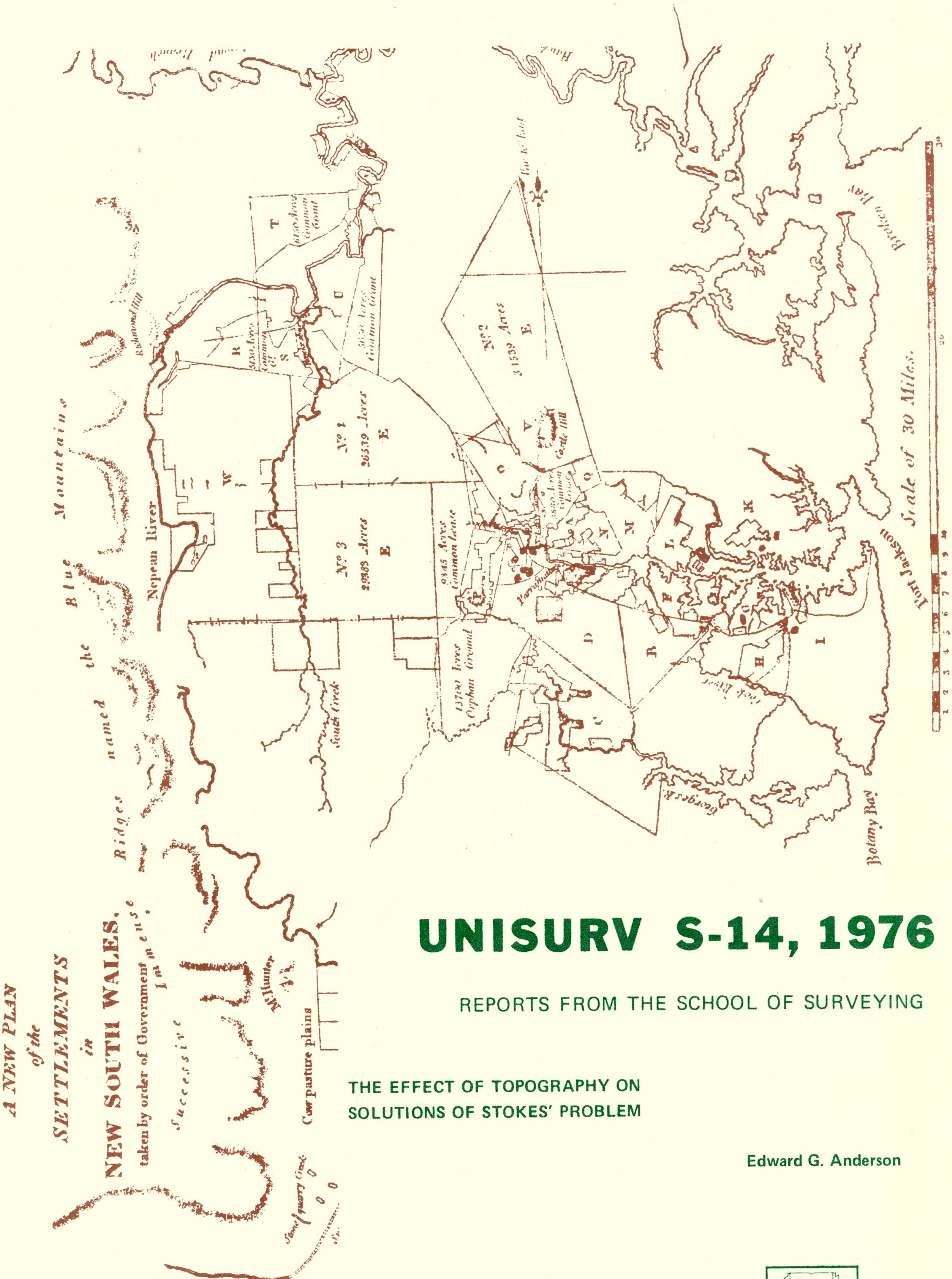

UNISURV S-14, 1976

REPORTS FROM THE SCHOOL OF SURVEYING

THE EFFECT OF TOPOGRAPHY ON SOLUTIONS OF STOKES' PROBLEM

Edward G. Anderson

UNIVERSITY OF NEW SOUTH WALES
KENSINGTON. N.S.W. AUSTRALIA

NATIONAL LIBRARY OF AUSTRALIA
CARD No. and ISBN
0 85839 021 3

KINGSFORD (OFFSET) PRINTING, SYDNEY, AUSTRALIA.

UNISURV REPORT NO. S14, 1976

THE EFFECT OF TOPOGRAPHY ON SOLUTIONS OF STOKES' PROBLEM

by

Edward G. Anderson

Received January, 1976

SCHOOL OF SURVEYING,
THE UNIVERSITY OF NEW SOUTH WALES,
P.O. BOX 1,
KENSINGTON, N.S.W., 2033, AUSTRALIA.

The attraction of the mountains is, at once, subtle and irresistible.

Abstract

This study is primarily directed towards a generalized evaluation of the gravitational effects of the earth's topography and isostatic compensation, determined globally at the geoid, the earth's surface, and at an altitude representative of satellite orbits. Equipotential undulations and components of the deflexion of the vertical are evaluated on a global $5^\circ \times 5^\circ$ grid. Emphasis is placed on applications pertaining to Stokes' problem and the associated treatment of the topography in the process of regularization of the earth, but this need not preclude wider applications of the quantitative results.

A mathematical model of the earth's topography and isostatic compensation, based on an ellipsoidal reference system and the Airy-Heiskanen isostatic compensation system, is established in isolation from all other natural energetic influences. Refinements of the model for the effects of sphericity and the polar ice caps are included. A global crustal density model, devised by de Graaff-Hunter is adopted. Geometric and physical properties of quadrature subdivisions of the topographic-isostatic model are investigated and an error analysis and a study of some practical consequences of adopting a rectangular parallelepiped approximation is undertaken.

Two different approaches to the mathematical formulation of the disturbing potential and attraction vector components of the quadrature model are developed. Firstly, rigorous closed form expressions are derived for use when the point of evaluation is close to, or in contact with, the gravitating material. The second approach involves open expansions of the potential and attraction components in terms of Legendre polynomials. Both sets of expressions apply to a rectangular parallelepiped and their scope is greatly enhanced by provision for vertical linear density variation.

Realization of the topographic model is in terms of available $5' \times 5'$ mean elevations covering North America, Europe, and Australia and $1^\circ \times 1^\circ$ mean ice thickness data for Antarctica and Greenland. The remaining coverage is completed by a simulation technique based on data transference depending on the correlation of topographic variance with elevation and using the global $1^\circ \times 1^\circ$ mean elevations to portray regional morphological trends. Projected applications of this technique to compress the storage of real digital topographic data are discussed.

Quantitative results of the computations are presented graphically and numerically, and analysed for spherical harmonic coefficients and degree variances up to degree and order (36,36). Specific examples of contributions to the topographic-isostatic effects, due to rock, ice, and marine topography in inner, mid, and outer zones, are given. The low degree harmonics of the distrubing potential are investigated to determine the mass imbalance of the topographic-isostatic model and its influence on the earth's centre of mass. An estimate of the mass of the terrestrial topography is computed. The significance of the results with respect to the general global qualities of the indirect effect for the free air geoid in the solution of Stokes' problem is examined and comparisons are made with extant determinations.

The mathematical formulations and computational techniques developed in this study are also utilized to evaluate the gravitational influence of a model of the atmosphere and assess its role in the geodetic boundary value problem. A stepwise linear density model of the atmosphere is defined and the consequent disturbing potential undulations and attraction vector components determined globally on a $30^\circ \times 30^\circ$ grid and harmonically analysed to the sixth degree. Estimates of the mass of the atmosphere are obtained directly by numerical integration and indirectly through the zero degree harmonic of the disturbing potential. The first degree harmonics are used to estimate the effect of the atmosphere on the earth's centre of mass.

Table of Contents

TABLE OF CONTENTS

TABLE OF CONTENTS

TABLE OF CONTENTS

TABLE OF CONTENTS

Index of Figures and Tables

FIGURES

INDEX OF FIGURES AND TABLES

INDEX OF FIGURES AND TABLES

INDEX OF FIGURES AND TABLES

TABLES

Index of Equations

Acknowledgements

Credit for the initial inspiration which is realized in this project must go to Associate Professor R. S. Mather, who also supervised the work. Acknowledgement for supervision during Dr. Mather's absence is also due to Professor P. V. Angus-Leppan and Dr. A. Stolz.

The writer wishes to record his gratitude for skillful and selfless assistance with the mathematical development provided by Mr. M. Maughan, whose enjoyment of a mathematical problem and appreciation of an elegant solution has lastingly stimulated the author. Other members of staff of the School of Surveying, University of New South Wales, who gave their time and experience generously in discussions include Associate Professor J. S. Allman, Dr. A. Stolz, and Mr. A. P. H. Werner. I am also grateful to all members of staff and post-graduate students of the School of Surveying for their professional guidance and enthusiastic fellowship over a much longer period than the duration of this study.

Topographic data for North America and Europe was made available to the School of Surveying by Mr. Thomas O. Seppelin, of the United States Defence Mapping Agency, Aerospace Center, and the use of the global data compiled by W. H. K. Lee of the University of California, Los Angeles is acknowledged. Australian data was originally compiled by Dr. Mather. Maps of Antarctic and Greenland ice thicknesses were generously supplied by Dr. W. F. Budd of the Antarctic Division, Australian Department of Supply. The author is also indepted to the New South Wales Surveyor General, Mr. L. N. Fletcher, for access to electronic digitizing equipment within the Department of Lands.

Substantial assistance with Assembler computer routines was given by Mr. B. Hirsch (School of Surveying), who also provided operational support during many long, wearisome hours of computing at night and on weekends and public holidays. For his unselfish attention to duties beyond the norm I extend my thanks.

The author's subsistence during the period of research was primarily provided by an Australian Government Postgraduate Research Award.

1

Introduction and Fundamental Definitions

1.1 PREAMBLE

STOKES' PROBLEM

HISTORICAL OVERVIEW. Orthodox solutions for a mathematical figure of the earth are, perforce, founded upon the theory of the potential—first expounded by Legendre and Laplace in 1785*. Treatises by George Green (in 1828) and C. F. Gauss (in 1841) dealt with the mathematical formulation of the potential function, thereby establishing the fundamental instruments for gravimetric resolution of the earth's shape. In particular, Gauss proposed adoption of an equipotential surface, coinciding with the oceans, as the basic figure. Consequently, a major preoccupation of physical geodesy has been the determination of that physically realizable surface—the geoid—which enjoys all the advantages and specialized properties of an equipotential surface, located strategically at man's intuitive datum: mean sea level.

Following Gauss, George Gabriel Stokes presented, in 1849, a formulated solution of the boundary value problem of physical geodesy, which provided the basis for a practical method of evaluating the geoidal undulations, using surface gravity measurements. Essentially, the technique relies on Stokes' theorem—that a function which is harmonic outside a bounding surface is uniquely determined by its values on that surface—and Dirichlet's principle, which asserts that such a function exists. Stokes' approach confronts specifically the *third boundary value problem*, wherein the boundary condition to be used in the solution of Laplace's differential equation, $\nabla^2 V = 0$, is a linear relation combining the potential and its normal derivative at the geoid: the *fundamental equation of physical geodesy*. Application of this equation to solve for the geoid using observed gravity values is, therefore, usually referred to as *Stokes' problem*, and this terminology is applied hereafter with that specific meaning. The solution of the basic differential equation by integration is embodied in *Stokes' formula* [HEISKANEN

* *LEGENDRE: Sur l'attraction des spheroids, Memoirs de Mathematique et de Physique, presentes a l'academie royale des sciences par divers savans, Tome X, 1785.*

P. S. LAPLACE: Theorie des attractions des spheroids et de la figure des planetes, Mec. Cel., *Tome III, ch. III, 1785.*

and MORITZ 1967, p.94]: essentially a global integration of observed gravity anomalies reduced to the bounding surface. Such an integral solution for the potential—or, by incorporating Bruns' theorem, the geoidal undulation—is possible through Stokes' formula only if the prevailing conditions satisfy Laplace's equation; that is, when there are no masses outside the geoid, so that the bounding potential function is harmonic.

GRAVITY REDUCTION—THE INDIRECT EFFECT. Compliance with this obligation has been achieved, customarily, by removing or redistributing the offending topographic masses, according to some mathematical procedure designed to *regularize* the earth. The *direct effect* of regularization on the surface gravity anomalies may be conjoined with their reduction from the point of measurement to the geoid; and the *indirect effect* on the potential function is usually relegated to a subsequent calculation to recover the geoid from the *cogeoid*, which results from the use of a regularized gravity anomaly field in the solution of Stokes' integral.

Many different methods of regularization have been proposed and used [*e.g.* HEISKANEN and MORITZ 1967, §§ 3.3, 3.5, 3.7], each with its associated reduction procedure and indirect effect formula. However, two techniques have proved to be particularly pertinent, at least from a practical viewpoint. Helmert's second method of condensation [*ibid*, p.145]—in which the external masses are condensed to a surface layer on the geoid—has acquired importance through its use as an intermediary in demonstrating the appropriateness of the other technique: the *free-air reduction*. It is justifiably reasoned that the Helmert reduction induces a very small indirect effect—of the order of one metre [*ibid*, p.145]—and that the direct effect is mostly negligible, so that the resulting cogeoid closely approximates the geoid. This is obvious enough, since the reduction procedure involves "lowering" both the topographic masses and the observation point to the geoid—the former by condensation and the latter by a free-air reduction. Hence the disposition of the gravitating masses with respect to the observation point is not greatly affected. If the direct effect is neglected, the Helmert reduction is identical to a free-air reduction, and it may be deduced that the free air geoid will have a similarly small indirect effect. MATHER [1968b]—drawing on the work of several authors [*e.g.* MOLODENSKY *et al* 1962; MORITZ 1965], wherein the relationship between regularized and non-regularized geoids has been established—has derived a complete definition of the non-regularized geoid and demonstrated that "*the Free Air Geoid is a good approximation to the non-regularized geoid*".

Of course, the free-air geoid, as with any other Stokesian boundary value solution, cannot escape the burden of dependence upon the distribution of masses between the geoid and the terrain surface. For a complete solution, knowledge of the density of the exterior masses is essential. Alternative solutions—which avoid this difficulty, but conceptually dispense with the geoid in the process—have originated in the proposals of Molodensky [HEISKANEN and MORITZ 1967, ch.8]. But, without being diverted by a needless discussion of the pro and contra arguments, it would be fair to suggest that these more modern techniques supplement, rather than supplant, the orthodox approach. There has indeed been a tendency for a proportion of the two theories to merge and, because of practical difficulties in implementing the Molodensky solution, the effects of topography come partly within the common ground [*e.g.* PELLINEN 1962]. Inasmuch as the particular topic of the present study has its origins in investigations of Stokes' problem, it will be confined to the basic tenets of that approach; but this need not preclude application of the more general conclusions to the alternative approach, in so far as they may be appropriate.

THE EFFECT OF TOPOGRAPHY. That the shape of the geoid should be influenced by the distribution of exterior masses may be discerned intuitively: since the upwards attraction of the topography reduces the vertical component of gravity at the geoid, the equipotential surfaces must be spaced more widely in that direction. This effect was appreciated more than a century ago, when experimenters such as J. H. Pratt observed deflexions of the vertical due to the Himalayan mountains, thereby incidentally discovering evidence of isostasy. But the unavoidable question: "By how much does the topography displace the earth's equipotential surfaces and thereby influence the solution of Stokes' problem?" remains difficult to answer precisely. Presumably the very smallness of the indirect effect for the free air geoid has been partly responsible for the dearth of attempts to ascertain its magnitude and global behaviour. As the need of greater accuracy in defining the geoid becomes more pressing and feasible, however, the significance of the indirect effect has expanded.

FRYER [1970] has recently obtained careful estimates of the global indirect effect for the free air geoid. Only the geoid-ellipsoid separation was considered, not the deflexions of the vertical. The formulae used were based on the development by MATHER [1968b, p.10 *et seq.*], in which a non-regularized geoid solution is derived in general form. Like the Stokes' solution for the free-air geoid itself, the indirect effect comprises a zero order term; a potential term with non-Stokesian characteristics, which is largely a function of the change in potential of the exterior masses when they are condensed; and a Stokesian term involving the *differential terrain correction*. Fryer was particularly concerned to examine the effect of the geoid on the Australian Geodetic Network, so the evaluations were made at a 5° grid interval in the Australian region and at 15° spacing for the remainder of the world. Global computation was mainly undertaken to evaluate the zero order term. The Stokesian and non-Stokesian terms were each evaluated twice; firstly by numerical integration and then, as verification, by a spherical harmonic analysis technique. Final global estimates—including sixth degree spherical harmonic coefficients of the differential terrain correction and contour plots of the non-Stokesian and Stokesian terms and the total indirect effect—are presented [FRYER 1970, pp.145, 153-5].

In drawing conclusions, Fryer expresses concern for the unexpectedly large magnitude of the indirect effect results. It has been further suggested that they exhibit unanticipated slow attenuation of magnitude with respect to distance from the major topographic masses—particularly the Himalayas. There is, however, no evidence of any flaw in the theoretical development and the ample checks seem to preclude computational errors, other than the admitted accuracy limitations imposed by the lack of detailed topographic data and computational expediencies.

POTENTIAL AND ATTRACTION OF THE TOPOGRAPHY

PROPOSED APPROACH. To further elucidate the contribution of the topography in solutions of Stokes' problem it is proposed, in the present study, to evaluate directly the gravitational potential and attraction of the earth's departure from the regularized Stokesian model. Conceptually the planned approach is to "create" a model of the topography and its isostatic compensation, in complete isolation from the rest of the earth and all other energetic influences such as the rotation, and to calculate its gravitational effect using fundamental Newtonian relationships. Consistency with the conditions of Stokes' problem is maintained by treating only isostatically compensated terrestrial topography and excluding the marine topography which is not part of the regularization process. The shaded portion of the earth in figure 1.1 illustrates the extent of the theoretical model. By so isolating the model, it was intended that any extraneous effects would be eliminated from the results and so not complicate the subsequent interpretation.

Generally the proposed approach may be visualized as a reversal of the process of evaluating the indirect effect. Instead of tracing the consequences of removing the exterior masses through the development of the Stokesian equations, the gravitational effects of creating the compensated topography are assessed and investigated directly. In this respect the underlying theoretical concepts of the study described here are simpler, a distinct advantage when interpreting the results. However, it should be noted that the quantities obtained are not identical with the indirect effect, but only part of it. Indeed, it must be emphasized that the present study is *not* an attempt to compute the indirect effect globally, but rather is designed to provide information fundamental to understanding the geodetic behaviour of the topographic effects.

WORKING HYPOTHESIS. A formal working hypothesis, which summarizes the motivation of the research described here, will provide a useful prescription to guide the experimental work. Taking into account

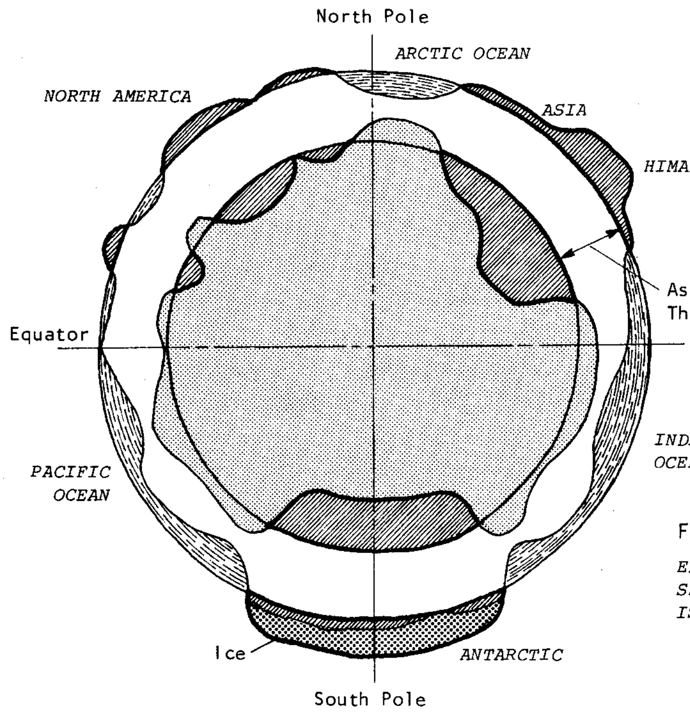

FIGURE 1.1

EXAGGERATED SECTION OF THE EARTH SHOWING EXTENT OF THE TOPOGRAPHIC-ISOSTATIC MODEL (Heavy outline)

the theoretical and experimental evidence accumulated to date in studies of the indirect effect for the free air geoid, it would be reasonable to suppose *that the effect of the topography and isostatic compensation on the non-regularized solution of Stokes' problem should be small—say, of the order of ten metres—and its magnitude should diminish rapidly with increasing distance from major topographic masses.* The latter contention is based on the presumption that the opposite effects of the topography and compensation should begin to cancel each other once the observation point is at a sufficient distance to impede discrimination of the effects of the two masses. In addition it may be anticipated that the somewhat random global distribution of topographic masses should cause considerable cancellation of the horizontal components of the gravity vector at an observation point, while, for a point at the geoid, the predominantly overlaying masses nearby should partially nullify the vertical gravitational effects of the more distant masses.

PREVIOUS EVALUATIONS OF TOPOGRAPHIC EFFECTS. Hitherto, evaluations of the gravitational effects of topography have been undertaken by a variety of methods and for a number of different purposes. Three such purposes are prominent:

(a) Reduction of gravity for geodetic purposes and preparation of isoanomaly maps.

(b) Extrapolation of gravity anomalies to unsurveyed areas.

(c) Geophysical studies and prospecting.

Examples of the first of these include the investigations in North America of HAYFORD and BOWIE [1912]; gravity reduction tables and maps in LAMBERT [1930], LAMBERT and DARLING [1936], CASSINIS *et al.* [1937], HEISKANEN and NISKANEN [1941], and BAESCHLIN [1948, pp.480 *et seq.*]; tables for topographic-isostatic deflexions of the vertical in [*ibid.*, pp.336 *et seq.*], LAMBERT and DARLING [1938], and DARLING [1949]; and isoanomaly maps [*e.g.* KÄRKI *et al.* 1961]. Since 1960 a sizeable quantity of work in this area has been published or referred to by the members of the Columbus Geodetic Group [HEISKANEN 1964]. In relation to the needs of the present investigation, all of these studies are either too limited in respect to the area covered or too coarse to provide the accurate detail sought. Usually such evaluations are based on a polar subdivision of the topography, which suits manual compilation procedures, rather than a "rectangular" geographical subdivision amenable to computer evaluations (see §2.3).

HEISKANEN [1953] and KUKKAMÄKI [1954] have discussed the application of electronic computers to the process of reducing gravity anomalies.

Evaluations for the second purpose have been performed by UOTILA [1964] and KIVIOJA [1964]. Uotila used a spherical harmonic analysis of 5°x5° mean topographic elevations to compute mean free air gravity anomalies due to topography and isostatic compensation in 5°x5° quadrature subdivisions with global coverage. Kivioja computed similar anomalies using a least squares technique to combine measured and geophysically extrapolated gravity. In both cases the results are in terms of area mean values, rather than a point-by-point evaluation, thus rendering them incompatible with the aims of the investigations proposed here. Furthermore, a considerable amount of smoothing is induced by the data and methods used, which could be expected to mask a good deal of the effects sought in the present study. This need not preclude their use as a check on general trends.

Calculations for geophysical purposes are well exemplified by the work of ST JOHN and GREEN [1967]. Generally such investigations differ from the geodetic variety only in ultimate intent and familiar techniques are employed. The author is not aware of any instances of this type of calculation with global scope.

A common trait of almost all of the previous attempts to compute the gravitational effects of topography has been the coarseness of the evaluation. This is understandable, in view of the magnitude of the computational task and the nature of the available data (*e.g.* see §2.3 *SIZE OF SUBDIVISIONS AND GRID INTERVALS*). Indeed the feasibility of the calculations undertaken for the present investigations was assured only by access to a quite large and reasonably fast digital computer, and then only by meticulous attention to the speed of the programmes and data accessing techniques. Although the extant information bears a superficial resemblance to the needs of the investigations proposed here, it is generally too deficient in detail to answer most of the questions which motivate this study.

EXTENSIONS OF THE INVESTIGATIONS

MARINE TOPOGRAPHIC EFFECTS. As the topographic irregularities in ocean areas occur *within* the bounding surface of the geoid, their influence is not properly a part of the Stokesian indirect effect. Even so, marine topographic corrections may be applied in gravity reduction procedures for the sake of conformity in geophysical interpretation. For this reason, extension of the calculations to include ocean areas can be justified. However, two major obstacles hinder the implementation of such a task: firstly, the inadequacy of bathymetric data, and secondly the constrictions of computational economy. A cursory examination of the marine topographic-isostatic influence was effected for a few special situations and the results are included in chapter 8.

ATMOSPHERIC EFFECTS. It is no longer needlessly pedantic—at least from a rigorous geodetic point of view—to suggest that the effects of the earth's atmosphere should be included in gravity reduction procedures and determinations of the figure of the earth [*e.g.* ECKER and MITTERMAYER 1969; MATHER 1973]. To assume that Laplace's equation holds at the surface of the earth—that is, within the atmosphere—is strictly no more tenable than to propound its validity at the geoid: the distinction made is merely a matter of degree.

Results of a global evaluation of the gravitational effects of a model of the earth's atmosphere are described in chapter 9. Specifications similar to those applied to the topographic calculations were sustained and the same standard of rigour was preserved. Identical topographic data was used to define the lower boundary of the atmosphere.

1.2 NOTATION

A guide to the symbols, mathematical conventions, and abbreviations utilized in this dissertation is provided in table 1.1. Generally, symbols are treated as a whole, including any prefixes, sub- or super-scripts, indices, and diacritical marks; and are listed in the table alphabetically in accordance with this rule. Only those qualifying symbols with a comprehensive connotation are listed separately. A distinction is drawn between subscripts which merely qualify the meaning of the main symbol and numerical subscripts (indices) which may take a range of values: the latter are usually denoted here by a script typeface. Some symbols which designate a physical concept or a commonly used geometrical location, rather than representing an algebraic quantity, are included.

Algebraic vector quantities are distinguished by the use of bold typeface and matrix quatities by large, upper-case type.

As an aid in identifying the meaning of a symbol, reference is made to the location of its first occurrence in the text. Also, to facilitate appreciation of the physical interpretation of the formulae, the fundamental dimensions and usual units for the quantity represented are stated where appropriate. Unlisted mathematical symbols are universally conventional.

1.3 UNITS

SI UNITS

In Australia, the Metric Conversion Act 1970 received Royal Assent on June 12 of that year [METRIC CONVERSION BOARD 1973]. Section 3 of the Act provides that the International System of Units (SI), as approved by the General Conference on Weights and Measures, shall be the sole system of measurement of physical quantities. The units and the correct manner of application are defined in Australian Standard—1000 [1970].

In accordance with these directives, SI units are used in this dissertation. As these units are not yet entirely familiar in the geodetic community, some care has been taken to state the unit used wherever necessary and in case of any possible confusion, the quantity is additionally expressed in terms of the old unit.

Two quantities in particular may cause some difficulty: gravitational force and gravitational potential. The author has published his ideas on appropriate SI units for these quantities elsewhere [ANDERSON 1973b; WERNER and ANDERSON 1973] and a lengthy reiteration here is unwarranted. However, a brief explanation of the use of the units *newton per kilogram* ($N\ kg^{-1}$) for gravitational attraction, instead of "metre per second squared" ($m\ s^{-2}$), and *joule per kilogram* ($J\ kg^{-1}$) for gravitational potential may be helpful.

The concept of "potential energy per unit mass" or "specific potential energy" is familiar in geodesy and is usually referred to simply as "gravitational potential". Thus the use of the unit $J\ kg^{-1}$ is a straightforward transition into SI terms. A possible alternative form, "metres squared per second squared" ($m^2\ s^{-2}$), is cumbersome and does not convey the physical meaning of the quantity represented. Consistency and clarity is achieved if the same treatment is applied to the unit of gravitational force, considering it as a measure of gravitational field strength rather than as an acceleration [KOEFOED 1967]. The idea of "specific force", expressed as $N\ kg^{-1}$, follows naturally [SWINDELLS 1971].

Use of $N\ kg^{-1}$ in the work described here was not, however, primarily based on these considerations. By choosing to use this form of the unit, the fact that the quantity measured is a *force*, due to a certain amount of topographic-isostatic mass, is emphasised, and this particular force is clearly distinguished from the common notion of the earth's total gravity. Because the topographic-isostatic masses are dealt with in isolation from the rest of the earth, the resulting forces may act in any direction (including upwards from the surface of the earth) and no sense of acceleration is involved. This abstract situation is conveyed comfortably by the concept of specific force.

Finally, it must be observed that the European Association of Exploration Geophysicists approved, in 1967, a resolution recommending the use of these SI units in gravimetry [KOEFOED 1973, pers. comm.].

SIZE OF UNITS AND CONVERSION FACTORS. Relationships between the units of gravitational force and potential are as follows:

1. INTRODUCTION AND FUNDAMENTAL DEFINITIONS

TABLE 1.1

NOTATION

SYMBOL	MEANING	§	PAGE	DIMENSIONS	UNIT
A	Area of a quadrature subdivision on a sphere.	3.4	49	L^2	
A_C	Area of a spherical cap.	3.4	49	L^2	
A_c	Area of horizontal cross-section of an isostatic compensation quad at mid height.	3.3	45	L^2	
A_r	Area of rectangular cross-section of parallelepiped in meridional plane.	3.4	54	L^2	
A_s	Area of a truncated sector of a circle.	3.4	54	L^2	
A_t	Area of horizontal cross-section of a topographic quad at mid height.	3.3	45	L^2	
A'	Area of a meridional sector of radius R_1.	3.4	50	L^2	
A''	Area of a meridional sector of radius R_2.	3.4	50	L^2	
$\mathbf{A}$	Matrix of parallelepiped dimension terms.	5.3	91		
a	(1) Semi-dimension of an arbitrary square prism.	2.3	24	L	
	(2) Semi-major axis of reference ellipsoid.	3.2	39	L	m
	(3) Semi-dimension of a parallelepiped in direction of x-axis.	3.4	48	L	
a	SUBSCRIPT: Qualified quantity refers to the atmosphere.	9.2	197		
B	(1) An arbitrary body.	1.4	16	--	--
	(2) Block shift applied to all 5' mean heights in a 1° quad.	6.4	109	L	
b	Semi-dimension of a parallelepiped in direction of y-axis.	3.4	48	L	
C_{nm}	Coefficient of the cosine term of a surface spherical harmonic.	8.4	183		
C_s	Arbitrary constant.	4.5	83	--	--
C_t	Arbitrary constant.	4.5	83	--	--
c	Semi-dimension of a parallelepiped in direction of z-axis.	3.4	48	L	
c	SUBSCRIPT: Qualified quantity refers to isostatic compensation.	3.2	40	--	--
c_b	Spatial distance to a bottom corner of a gravitating body from the evaluation point.	2.3	24	L	
c_t	Spatial distance to a top corner of a gravitating body from the evaluation point.	2.3	24	L	
D	Vertical gradient of volume density (= $d\sigma/dz$).	3.4	51	$M\,L^{-4}$	kg m^{-4}
D_a	Vertical density gradient of the atmosphere.	9.2	197	"	"
d	Spatial distance from evaluation point to an element or some specific part of a quad.	3.2	40	L	
d	PREFIX: Differential operator (total derivative).	1.4	16	--	--
$\mathbf{d}$	Position vector of evaluation point.	5.2	87	L	
d_b	Spatial distance from evaluation point to bottom edge of a gravitating body.	2.3	24	L	
d_t	Spatial distance from evaluation point to top edge of a gravitating body.	2.3	24	L	

TABLE 1.1 cont.

SYMBOL	MEANING	§	PAGE	DIMENSIONS	UNIT
d^*	Relative distance (with respect to radius of convergence) from evaluation point to a body.	2.3	26	0	--
$\vec{ds}$	Differential displacement vector.	1.4	16	L	
E					
e	(1) Eccentricity of the reference ellipsoid.	3.2	41	0	--
e	Exponential function of unit argument (base of natural logarithm) = 2.718 281 828 459 045	4.5	83	0	--
F	(1) Vertical scale factor applied to all 5' mean heights in a 1° quad.	6.4	109	0	--
	(2) Fractional part of an angular argument.	7.3	137	0	degree
$f_j(\ )$	Optional function of topographic ruggedness factors.	6.2	100		
$\mathfrak{f}$	Form factor of height distribution in a quad.	6.2	99	0	--
G	Rectangular component of gravitational attraction vector.	3.2	42	LT^{-2}	$N\ kg^{-1}$
G_{za}	Vertical component of gravity due to the lower atmosphere.	9.3	200	"	$\mu N\ kg^{-1}$
$\mathbf{G}$	Gravitational field strength vector. Specific force of attraction.	1.4	16	"	$N\ kg^{-1}$
g_0	Zero order, least squares linear regression coefficient of the vertical component of gravity due to the atmosphere.	9.3	200	"	$\mu N\ kg^{-1}$
g_1	First order, least squares linear regression coefficient of the vertical component of gravity due to the atmosphere.	9.3	200	"	"
$g(\phi,\lambda)$	An arbitrary function representing a computed topographic-isostatic gravitational effect.	8.4	183		
H	Mean height of a 1°x1°source quad.	6.4	109	L	m
H'	Known mean height of a 1°x1° quad containing simulated 5' mean heights.	6.4	109	L	m
h	(1) Height of a gravitating body.	2.3	24	L	
	(2) Cylindrical coordinate.	2.3	24	L	
	(3) Mean height of a 5'x5' quad.	3.2	40	L	m
h	SUBSCRIPT: Qualified quantity refers to the homogeneous part of the gravitating material.	4.3	67	--	--
h_c	Height of isostatic compensation (spherical model).	3.2	40	L	m
h_{cI}	Height of isostatic compensation ice correction.	3.3	46	L	m
h_I	Height (thickness) of ice sheet in topographic quad.	3.3	46	L	m
h_{jk}	Mean height of a 5' quad in a 1°x1° source quad.	6.4	109	L	m
h_p	Height of evaluation point P above reference level.	2.3	24	L	m
h_w	Height (depth) of ocean in a marine topographic quad.	8.3	181	L	m
$h(\phi,\lambda)$	General terrain surface function.	6.1	97	L	
$\bar{h}_c$	Height of isostatic compensation (plane model).	3.3	44	L	m
$\bar{h}_{cw}$	Height of isostatic compensation of marine topography (plane model).	8.3	181	L	m
h'_{jk}	Simulated mean height of a 5' quad in a 1°x1° quad.	6.4	109	L	m
$\tilde{h}$	Root mean square height of a quadrature subdivision.	6.2	99	L	m

TABLE 1.1 cont.

SYMBOL	MEANING	§	PAGE	DIMENSIONS	UNIT
I	Integer part of an angular argument.	7.3	137	0	degree
I	SUBSCRIPT: Qualified quantity refers to ice.	3.3	46	--	--
I_{kmn}	Inertial integrals of a body.	5.3	90	$L^{(k+m+n+3)}$	
$\mathbf{i}$	Unit vector parallel to geocentric X-axis.	3.4	52	0	--
i	SUBSCRIPT: Numerical index, conventionally ranging from 1 to 3 unless otherwise specified.	1.4	19	--	--
J					
$\mathbf{J}$	Jacobian determinant for transformation from cartesian to spherical coordinates.	3.4	52	L^2	
$\mathbf{j}$	Unit vector parallel to geocentric Y-axis.	3.4	52	0	--
j	SUBSCRIPT: Arbitrary numerical index.	2.3	25	--	--
K					
$\mathbf{K}$	Matrix of constant coefficients.	5.3	91	0	--
k	Universal gravitational constant ($= 6.67 \times 10^{-11}$).	1.4	16	$M^{-1}\,L^3\,T^{-2}$	$N\,m^2\,kg^{-2}$
$\mathbf{k}$	Unit vector parallel to geocentric Z-axis.	3.4	52	0	--
k	SUBSCRIPT: Arbitrary numerical index.	2.3	25	--	--
L_j	Abbreviation for a ℓog term in potential and attraction formulae. ($j = 1, 12$).	4.3	73	0	--
L	SUBSCRIPT: Qualified quantity refers to the lower half of a spherical tesseroid.	3.5	56	--	--
l	(1) Number of intervals of subdivision in Simpson numerical integration.	2.3	25	--	--
	(2) Length of topographic-isostatic dipole.	3.5	58	L	m
ℓ	SUBSCRIPT: Qualified quantity refers to the linear density part of a gravitating body.	4.3	67	--	--
M	(1) Mass.	1.4	16	M	kg
	(2) Location of a gravitating mass particle.	3.2	41	--	--
	(3) Mass of a spherical tesseroid.	3.4	51	M	kg
M_a	Mass of a specified part of the atmosphere.	9.4	213	"	"
M_c	Mass of an isostatic compensation quad.	3.3	44	"	"
M_E	Total mass of the earth ($= 5.976 \times 10^{24}$ kg).	8.4	185	"	"
M_T	Total mass of the terrestrial topography.	8.4	191	"	"
M_t	Mass of a topographic quad.	3.3	44	"	"
M_μ	Mass of a body of mean volume density σ_μ.	5.3	91	"	"
m	(1) Mass of a dimensionless particle.	1.4	16	"	"
	(2) Number of intervals of subdivision in Simpson numerical integration.	2.3	25	--	--
m	SUBSCRIPT: Qualified quantity refers to point M.	3.2	41	--	--
m	SUBSCRIPT: (1) Arbitrary numerical index.	4.3	74	--	--
	(2) Order of a surface spherical harmonic.	8.4	183	--	--
N	Height of geoidal undulations. Geoid-ellipsoid separation.	1.4	17	L	m
N_{10}	Computer precision: number of machine decimal digits.	4.5	84	0	--
n	(1) Number of intervals of subdivision in Simpson numerical integration.	2.3	25	--	--
	(2) Sample size from a bivariate population.	6.4	112	0	--
n	SUBSCRIPT: (1) Arbitrary numerical index.	4.3	74	--	--

TABLE 1.1 cont.

SYMBOL	MEANING	§	PAGE	DIMENSIONS	UNIT
n	SUBSCRIPT: (2) Degree of a surface spherical harmonic.	8.4	183	--	--
O	Location of geocentric origin of coordinates.	1.4	18	--	--
o	Location of local origin of coordinates.	4.3	66	--	--
o	SUBSCRIPT: Qualified quantity refers to "old" reference frame.	1.4	19	--	--
P	Location of evaluation point for mapping gravitational field.	1.4	18	--	--
P_n	Legendre polynomials of order n.	5.2	86	0	--
$\bar{P}_{nm}$	Fully normalized associated Legendre function of the first kind.	8.4	183	0	--
$\mathbf{P}_j$	Matrix of evaluation point coordinate terms.	5.3	91	L^j	
p	Perpendicular spatial distance from evaluation point to a face plane of a parallelepiped.	4.3	71	L	m
p	SUBSCRIPT: Qualified quantity refers to evaluation point.	2.3	24	--	--
Q	Location of evaluation sub-point at reference surface.	3.2	40	--	--
q	Arbitrary argument of the exponential function.	4.5	83	--	--
R	Geocentric radius.	1.4	18	L	m
R_C	Geocentric radius of the centroid of a meridian section of a spherical tesseroid.	3.4	50	"	"
R_c	Geocentric radius of the mid height of an isostatic compensation quad.	3.3	45	"	"
R_{cI}	Geocentric radius of the mid height of an isostatic compensation ice correction.	3.3	46	"	"
R_I	Geocentric radius of the mid height of ice in a topographic quad.	3.3	46	"	"
R_m	Local mean geocentric radius of the reference surface.	3.3	45	"	"
R_p	Geocentric radius of an evaluation point P.	8.4	184	"	"
R_t	Geocentric radius of mid height of a topographic quad.	3.3	45	"	"
R_μ	Geocentric radius of mid height of a quad.	3.4	53	"	"
R'	Geocentric radius of the centroid of a meridional sector of radius R_1.	3.4	50	"	"
R'_T	Approximate geocentric radius of the centre of mass of a small spherical tesseroid.	3.4	53	"	"
R''	Geocentric radius of the centroid of a meridional sector of radius R_2.	3.4	50	"	"
$\mathbf{R}$	Rotation matrix.	1.4	19	0	--
r	Radius of an arbitrary cylinder.	2.3	24	L	m
r_0	Spatial radius from evaluation sub-point Q to an arbitrary local sub-point at reference surface.	2.4	38	"	"
r^*	Radius of convergence of a gravitating body.	2.3	26	"	"
$\mathcal{r}$	Sample correlation coefficient of a bivariate distribution.	6.4	112	0	--
$\mathcal{r}_g$	Sample correlation coefficient of the vertical gravity due to the lower atmosphere with respect to the height of the evaluation point.	9.3	200	0	--

TABLE 1.1 cont.

SYMBOL	MEANING	§	PAGE	DIMENSIONS	UNIT
S	Relative ruggedness of 5' mean heights in a 1°x1° quad.	6.4	112	0	--
S_{nm}	Coefficient of the sine term of a surface spherical harmonic.	8.4	183		
s	(1) An arbitrary distance.	1.4	16	L	
	(2) Cylindrical coordinate.	2.3	24	L	
	(3) An arbitrary function of variables u and v.	4.5	83	--	--
$\mathcal{s}$	Standard deviation of known 5' mean heights in a 1°x1° source quad.	6.4	109	L	m
$\mathcal{s}^2$	Variance of height distribution in a quad.	6.2	99	L^2	m^2
$\mathcal{s}_0$	Sea level deviation of 5' mean heights in a 1°x1° quad.	6.4	112	L	m
$\mathcal{s}'$	Standard deviation of simulated 5' mean heights in a 1°x1° quad.	6.4	109	"	"
T	(1) Location of the centroid of a spherical tesseroid.	3.4	51	--	--
	(2) Crustal thickness from reference surface to isostatic compensation.	3.2	40	L	m
T_j	Abbreviation for a group of tan^{-1} terms in potential and attraction formulae. $(j = 1, 6)$.	4.3	74	0	angular
T	SUPERSCRIPT: Transpose of qualified matrix.	1.4	20	--	--
T	Geocentric position vector of the centre of mass of a spherical tesseroid.	3.4	51	L	m
t	(1) An arbitrary distance: magnitude of **t**.	5.2	85	L	m
	(2) An arbitrary function of variables u, v, and w.	4.2	64	--	--
t	Position vector of an elemental mass.	5.2	87	L	m
U	Gravitational potential of a spheropotential surface.	1.4	17	$L^2 T^{-2}$	$J\ kg^{-1}$
U	SUBSCRIPT: Qualified quantity refers to the upper half of a spherical tesseroid.	3.5	56	--	--
U_{ijk}	Value of the gravitational potential function due to a mass element with dimensions $\Delta a \times \Delta b \times \Delta c$.	2.3	25	$L^{-1} T^{-1}$	$J\ kg^{-1}\ m^{-3}$
u	(1) An arbitrary curvilinear coordinate.	1.4	20	0	
	(2) An arbitrary variable.	4.2	64	--	--
V	Gravitational disturbing potential. Specific potential energy.	1.4	16	$L^2 T^{-2}$	$J\ kg^{-1}$
V_ψ	Potential due to a topographic-isostatic dipole at an angular distance ψ.	3.5	60	"	"
V_0	Potential due to a rectangular parallelepiped at a point in the line of one edge.	4.3	66	"	"
v	(1) An arbitrary curvilinear coordinate.	1.4	20	0	
	(2) An arbitrary constant.	4.2	64	--	--
	(3) An arbitrary variable.	4.5	83	--	--
	(4) Volume of a spherical tesseroid.	3.4	49	L^3	m^3
W	Gravitational potential of a geopotential surface.	1.4	17	$L^2 T^{-2}$	$J\ kg^{-1}$
w	(1) An arbitrary curvilinear coordinate.	1.4	20	0	
	(2) An arbitrary constant.	4.2	64	--	--
	(3) An arbitrary variable.	4.5	83	--	--
w	SUBSCRIPT: Qualified quantity refers to the ocean.	8.3	181	--	--
X	Geocentric cartesian coordinate in direction of Greenwich meridian.	1.4	18	L	m

TABLE 1.1 cont.

SYMBOL	MEANING	§	PAGE	DIMENSIONS	UNIT
X	SUBSCRIPT: (1) Qualified quantity referred to X-axis.	1.4	20	--	--
	(2) Indicates component of qualified quantity parallel to X-axis.	3.2	43	--	--
X_E	X-component of displacement of centre of mass of the earth due to topographic-isostatic irregularities.	8.4	185	L	m
$\mathbf{X}$	Geocentric position vector of an element of mass.	3.4	52	"	"
x	Local cartesian coordinate in direction of prime vertical.	1.4	18	"	"
x	SUBSCRIPT: (1) Qualified quantity referred to x-axis.	3.2	42	--	--
	(2) Indicates component of qualified quantity parallel to x-axis.	3.2	42	--	--
Y	Geocentric cartesian coordinate in direction of normal to Greenwich meridian plane.	1.4	18	L	m
Y	SUBSCRIPT: (1) Qualified quantity referred to Y-axis.	1.4	20	--	--
	(2) Indicates component of qualified quantity parallel to Y-axis.	3.2	43	--	--
Y_E	Y-component of displacement of centre of mass of the earth due to topographic-isostatic irregularities.	8.4	185	L	m
y	Local cartesian coordinate in direction of meridian.	1.4	18	"	"
y	SUBSCRIPT: (1) Qualified quantity referred to y-axis.	3.2	42	--	--
	(2) Indicates component of qualified quantity parallel to y-axis.	3.2	42	--	--
Z	Geocentric cartesian coordinate in direction of earth's rotational axis.	1.4	18	L	m
Z	SUBSCRIPT: (1) Qualified quantity referred to Z-axis.	1.4	20	--	--
	(2) Indicates component of qualified quantity parallel to Z-axis.	3.2	43	--	--
Z_E	Z-component of displacement of centre of mass of the earth due to topographic-isostatic irregularities.	8.4	185	L	m
z	Local cartesian coordinate in direction of outwards spheroidal normal.	1.4	18	"	"
z	SUBSCRIPT: (1) Qualified quantity referred to z-axis.	3.2	42	--	--
	(2) Indicates component of qualified quantity parallel to z-axis.	3.2	42	--	--
z_0	Elevation in local system with respect to reference surface.	3.2	41	L	m
z	Transform of r assuming approximately standard normal distribution of variate.	6.4	112	0	--
	GREEK ALPHABET				
A					
α	(1) Local spherical coordinate: azimuth angle measured clockwise from North.	1.4	19	0	angular
	(2) Cylindrical coordinate.	2.3	24	0	angular
B					
β	Direction difference between position vectors to evaluation point and elemental mass.	5.2	85	0	angular

TABLE 1.1 cont.

SYMBOL	MEANING	§	PAGE	DIMENSIONS	UNIT
Γ					
γ_0	Normal gravity at the reference ellipsoid.	1.4	17	LT^{-2}	N kg^{-1}
Δ	PREFIX: Difference operator, indicating small difference in qualified quantity.	2.3	25	--	--
Δa	Interval of subdivision in Simpson numerical integration parallel to x-axis.	2.3	25	L	m
Δb	Interval of subdivision in Simpson numerical integration parallel to y-axis.	2.3	25	"	"
Δc	Interval of subdivision in Simpson numerical integration parallel to z-axis.	2.3	25	"	"
ΔM_B	Mass imbalance between topographic and isostatic compensation quads.	3.5	57	M	kg
ΔM_T	Residual topographic-isostatic mass imbalance indicated by zero degree harmonic of disturbing potential.	8.4	190	"	"
δ_{pq}	*Kronecker Delta* function.	2.3	25	0	--
Ε					
ε	Meridional semi-dimension of a spherical tesseroid ($= \frac{1}{2}\Delta\phi$).	3.4	50	0	angular
Ζ					
ζ	Deflexion of the vertical.	1.4	17	"	"
Η					
η	Prime vertical component of deflexion of the vertical.	1.4	17	"	"
Θ					
θ	Angle of rotation of a cartesian reference frame about one of its axes.	1.4	20	"	"
Ι					
ι					
Κ					
κ	An arbitrary positive integer.	5.3	91	--	--
Λ					
λ	Longitude measured eastwards from Greenwich meridian.	1.4	18	0	angular
Μ					
μ	An arbitrary positive integer.	5.3	91	--	--
μ	SUBSCRIPT: Mid value of the qualified quantity.	3.4	49	--	--
Ν					
ν	(1) An arbitrary positive integer. (2) Radius of curvature of the reference ellipsoid in the prime vertical.	5.3 3.2	91 41	-- L	-- m
Ξ					
ξ	Meridian component of the deflexion of the vertical.	1.4	17	0	angular
Ο					
ο					
Π					
π	Ratio of circumference of a circle to its diameter, (= 3.141 592 653 589 793).	2.3	24	0	--

TABLE 1.1 cont.

SYMBOL	MEANING	§	PAGE	DIMENSIONS	UNIT
Ρ					
ρ	Radius of curvature of the reference ellipsoid in the meridian.	3.3	45	L	m
Σ^2_n	Harmonic degree variance of degree n.	8.4	184	--	--
σ	Volume density.	2.3	24	ML^{-3}	kg m^{-3}
σ_a	Volume density of the atmosphere.	9.2	197	"	"
σ_{a0}	Homogeneous component of linear atmospheric density model: atmospheric density at the reference surface.	9.2	197	"	"
σ_c	Volume density of isostatic compensation.	3.3	45	"	"
σ_G	Apparent (extrapolated) volume density at geocentre.	3.4	51	"	"
σ_I	Volume density of polar ice in a topographic quad.	3.3	46	"	"
σ_p	Apparent (extrapolated) volume density at the level of the evaluation point.	4.3	67	"	"
σ_t	Volume density of a topographic quad, ("rock" density).	3.3	44	"	"
σ'_t	Pseudo topographic volume density comprising "rock" and air.	6.2	100	"	"
σ_w	Volume density of sea water in marine quad.	8.3	181	"	"
σ_μ	Mean volume density of a non-homogeneous body.	5.2	86	"	"
σ_0	Homogeneous component of linear volume density model: topographic density at the reference surface.	3.4	51	"	"
σ_1	Volume density of sub-crustal material.	3.3	44	"	"
Τ					
τ					
Υ					
υ	$sec\ \upsilon = f$ (form factor).	6.2	99	0	angular
Φ					
ϕ	Latitude measured north (positive) or south (negative) from equatorial plane.	1.4	18	"	"
Χ					
χ					
Ψ					
ψ	Local spherical coordinate: geocentric angular distance.	1.4	19	"	"
ψ_c	Angular radius of contact sub-zone.	2.3	26	"	"
ψ_0	Angular distance from evaluation point to topographic-isostatic dipole with null gravitational effect.	3.5	58	"	"
Ω					
ω	Prime vertical semi-dimension of a spherical tesseroid $(= \frac{1}{2}\Delta\lambda)$.	3.4	53	"	"
	MATHEMATICAL SYMBOLS				
$\boldsymbol{\nabla}$	Vector differential operator: $(= \sum \mathbf{i}[\partial / \partial x_i])$.	1.4	16	L^{-1}	
∇^2	Scalar Laplacian operator $(= \boldsymbol{\nabla}\cdot\boldsymbol{\nabla})$.	1.1	1	L^{-2}	
∂	Differential operator (Partial derivative).	1.4	20	--	--
^	DIACRITICAL: Estimated value of the qualified quantity.	3.3	45	--	--
~	DIACRITICAL: Root mean square value of the qualified quantity.	6.2	99	--	--

TABLE 1.1 cont.

SYMBOL	MEANING	§	PAGE	DIMENSIONS	UNIT
$\bar{\ }$	DIACRITICAL: (1) Mean value of qualified quantity.	6.4	112	--	--
	(2) Qualified quantity referred to plane reference system.	3.3	44	--	--
$\uparrow$	SUBSCRIPT: Maximum value of qualified quantity.	4.3	75	--	--
$\downarrow$	SUBSCRIPT: Minimum value of qualified quantity.	6.2	100	--	--
[ ]	Integer part of enclosed quantity.	4.3	75	--	--
$i\{\ \}$	SUBSCRIPT: i-th left to right permutation of the enclosed indices.	4.3	74	--	--
M{ }	Global mean value of the enclosed quantity.	8.4	190	--	--
o{ }	Order of magnitude of the enclosed quantity.	2.3	27	--	--
< >	SUBSCRIPT: Modular value of the enclosed index.	4.3	74	--	--
	ABBREVIATIONS				
ACIC	Aeronautical Chart and Information Center (U.S.A.) (now renamed DMA).	6.1	98	--	--
ANARE	Australian National Antarctic Research Expeditions.	6.3	103	--	--
DMA	Defence Mapping Agency (Aerospace Center), (U.S.A.)	6.3	103	--	--
GRS67	Geodetic Reference System 1967	9.1	196	--	--
IAG	International Association of Geodesy	3.2	39	--	--
ℓog	Natural logarithmic function ($\equiv \ell og_e$)	2.3	24	0	--
ℓog_{10}	Logarithm to base 10.	4.5	84	0	--
ppm	Part per million.	2.3	31	--	--
rms	Root mean square.	6.2	99	--	--
$sinh^{-1}$	Inverse hyperbolic sine function.	4.2	64	0	angular
tan^{-1}	Inverse tangent function.	4.2	64	"	"
UCLA	University of California, Los Angeles, U.S.A.	6.3	103	--	--
UNSW	University of New South Wales, Australia.	6.3	103	--	--

NOTES:

(a) The symbol 0 is used in the "dimensions" column to indicate a dimensionless quantity.

(b) Unused alphabetic symbols are listed with a blank entry to indicate that they are available for use.

(c) A blank entry in the "units" column indicates that the quantity may take a variety of units in different circumstances.

$1\ \mathrm{N\,kg^{-1}} = 1\ \mathrm{m\,s^{-2}} = 100\ \mathrm{cm\,s^{-2}} = 100\ \mathrm{gal} = 10^5\ \mathrm{mgal}$

$1\ \mathrm{\mu N\,kg^{-1}} = 1\ \mathrm{\mu m\,s^{-2}} = 0.1\ \mathrm{mgal} = 1$ (USA) gravity unit.

$1\ \mathrm{J\,kg^{-1}} = 1\ \mathrm{N\,m\,kg^{-1}} = 1\ \mathrm{m^2s^{-2}} = 100\ \mathrm{cm\,s^{-2}\cdot m} = 0.1\ \mathrm{kgal\,m}$

Thus the essential rule to be applied when converting either attraction or potential from SI to old units is: "*DIVIDE BY TEN*", since $10\ \mathrm{\mu N\,kg^{-1}} = 1$ mgal and $10\ \mathrm{J\,kg^{-1}} = 1$ kgal m.

1.4 DEFINITIONS

NEWTONIAN GRAVITATIONAL ATTRACTION AND POTENTIAL

According to Newton's gravitational theory, an *attracting force* **G** acts between two particles, with magnitude proportional to the product of their masses and inversely proportional to the square of the separating distance. If a particular particle is considered, the capacity of its attracting force to perform work—the potential energy—provides a convenient undirected measure of intensity at any point. This is usually assessed in terms of a scalar quantity: the *potential* V, which is the amount of work associated with the introduction of a test particle of unit mass, brought from an infinite distance to the required point. (Inherent in this definition is the notion that the potential is zero where the attracting force vanishes, that is, at an infinite distance).

Specifically, for a point at a distance s from a particle of mass m, the potential is:

$$V = \int_{\infty}^{s} \mathbf{G}\cdot \vec{ds} \tag{1.1}$$

$$= \int_{\infty}^{s} \frac{km}{s^2}\, ds$$

by Newton's law, since the mass of the test particle is unity. Hence,

$$V = \frac{-km}{s} \tag{1.2}$$

The potential, then, has the dimensions of enery per unit mass, $[L^2T^{-2}]$, (*i.e.* force × distance / mass) and is measured in joules/kg in SI units. Newton's gravitational constant of proportionality is:

$$k = 6.67 \times 10^{-11}\ \text{newton m}^2\text{kg}^{-2}$$

Inasmuch as the potential is a scalar quantity, the extension of equation 1.2 to a system of discrete particles requires merely the summation of the individual quantities, and thence, for a continuous mass distribution, the integration of a set of mass elements. Thus the potential at a point of a body B of mass M is:

$$V = k\iiint_B \frac{dM}{s}\ . \tag{1.3}$$

A corollary of 1.1 provides the means of determining the attraction vector in terms of the potential:

$$\mathbf{G} = \nabla V\ , \tag{1.4}$$

that is, the gravitational force is the gradient, or first derivative, of the potential.

It may be shown [*e.g.* MACMILLAN 1930, §§22-25] that the potential and its first derivatives—the attraction components—exist and are continuous everywhere: both within and without the gravitating mass distribution. This is not true of the second derivatives of the potential, which may be discontinuous at a point of discontinuity in the density of the surrounding material. Consequently, the gradient of the force field will change at the boundaries of a gravitating body. This latter property presents no particular theoretical difficulty in the evaluation of a gravitational field, but, as a matter of practical concern, may necessitate special procedures to prevent breakdown of computational formulae. It may also preclude analysis dependent on the *harmonic* nature of the potential function, which holds only outside the body [HEISKANEN and MORITZ 1967, p.5].

THE GEOID-ELLIPSOID SYSTEM

Throughout this study the development is related to the conventional geoid-ellipsoid system. Adherence to this system is largely a matter of historical congruity, in that the investigation is intrinsically concerned with the "classical" Stokes' problem and its solutions. In this context the geoid is accepted as the physically realizable determination of the earth's figure, and is defined to be that equipotential surface of the earth's gravitational field which coincides with a global "mean sea level". Such a surface, being partly within the solid boundary of the earth, is non-analytical. However, it departs only slightly from an oblate ellipsoid of revolution, which is analytical and is consequently adopted as the reference figure.

This reference surface—the ellipsoid—is defined to have the same potential as the geoid and its *normal* gravity field thereby provides a uniquely determined datum to which the non-analytical deviations of the actual field may be referred. The ellipsoid is, ideally, located with its centre coincident with the centre of mass of the earth and its minor axis collinear with the earth's rotational axis.

Just as the geoid does not coincide everywhere with the ellipsoid, the whole family of *geopotential surfaces* associated with the gravity field of the actual earth may depart from the numerically equivalent *spheropotential surfaces* of the reference system. These undulations may be entirely determined by their height N, measured along the ellipsoid normal (figure 1.2). Alternatively, the

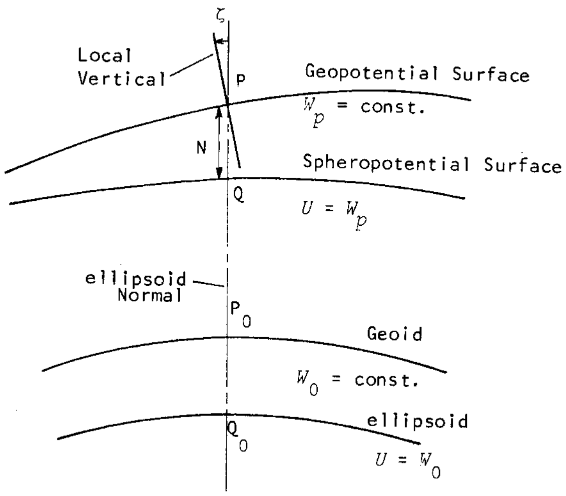

FIGURE 1.2

GEOPOTENTIAL UNDULATIONS AND DEFLEXIONS OF THE VERTICAL

departure may be measured in terms of the difference in direction of the actual gravity vector from the normal gravity vector; that is, the deflexion of the vertical ζ. The deflexion of the vertical may be resolved into its meridian and prime vertical components, ξ and η respectively.

If the departure, due to whatever cause, is treated as a residual *disturbing potential* V after subtracting the normal potential, the height of the undulations is given by Bruns' theorem as:

$$N = \frac{V}{\gamma_0} , \tag{1.5}$$

where γ_0 is the magnitude of normal gravity at the ellipsoid

And the components of the deflexion of the vertical are:

$$\xi = -\frac{1}{\gamma_0}\frac{\partial V}{\partial y}, \qquad \eta = -\frac{1}{\gamma_0}\frac{\partial V}{\partial x}, \tag{1.6}$$

where $\partial V/\partial y$ and $\partial V/\partial x$ are the meridian and prime vertical components of the disturbing gravity vector [HEISKANEN and MORITZ 1967, p.235].

COORDINATE SYSTEMS AND TRANSFORMATIONS

A number of different types of coordinate systems may be employed in the subsequent mathematical development, and the location and orientation of a reference frame may be varied to suit the prevailing circumstances. The basic systems and general forms for transformations are presented here, in mainly geometric terms, to provide a central definition. Specialized geodetic forms will be introduced as necessary, particularly in chapter 3.

Euclidean geometry is presumed adequate for what, in essence, amounts to a study of secondary effects, and a severely simplistic connexion of the physical realities to the chosen mathematical reference frames is adopted under the same pretext. The implications of these approximations may be appreciated by reference to the more rigorous and complete definitions of STOLZ [1972, ch.1].

CARTESIAN COORDINATE SYSTEMS. Conventional, right-handed, rectangular coordinate axes are employed quite generally, with the location and orientation dictated by the circumstances. Particular geodetic applications are (figure 1.3):

(a) *Geocentric Cartesian Axes* (X, Y, Z): wherein the origin O is chosen at the centre of mass of the earth (assumed to coincide with its centroid), the Z-axis is collinear with the rotational axis, and the X-axis is in the Greenwich meridian.

(b) *Local Cartesian Axes.* (x, y, z): centred on a particular spatial point P, the z-axis being directed along the outwards ellipsoidal normal at the point, the y-axis lying in the meridian plane, and the x-axis oriented in the direction of increasing longitude (*i.e.* eastwards).

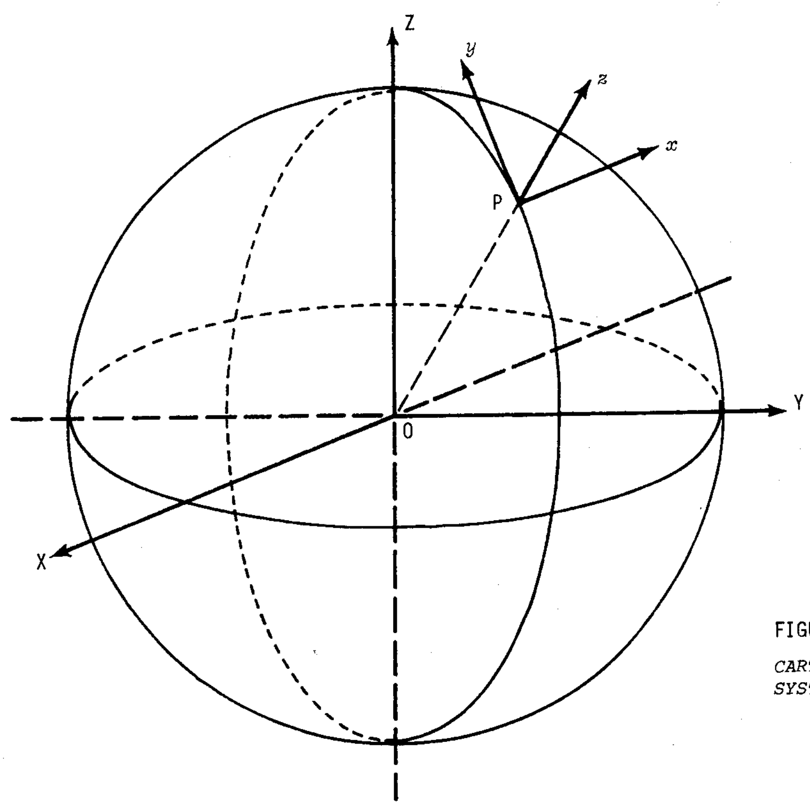

FIGURE 1.3

CARTESIAN COORDINATE SYSTEMS

1. INTRODUCTION AND FUNDAMENTAL DEFINITIONS

SPHERICAL COORDINATE SYSTEMS. Spherical coordinates are employed geocentrically, but with the orientation varied to provide (figure 1.4):

(a) *"Geographic" Coordinates* (ϕ, λ, R): defined conventionally, with latitude ϕ measured north or south (+ or -) with respect to the equatorial plane, longitude λ measured eastwards from the Greenwich meridian, and R being the geocentric radius.

(b) *Local Polar Coordinates* (ψ, α, R): where ψ is the angular distance with respect to the local spheroidal normal, α is the azimuth measured eastwards from the north branch of the local meridian, and R is the geocentric radius.

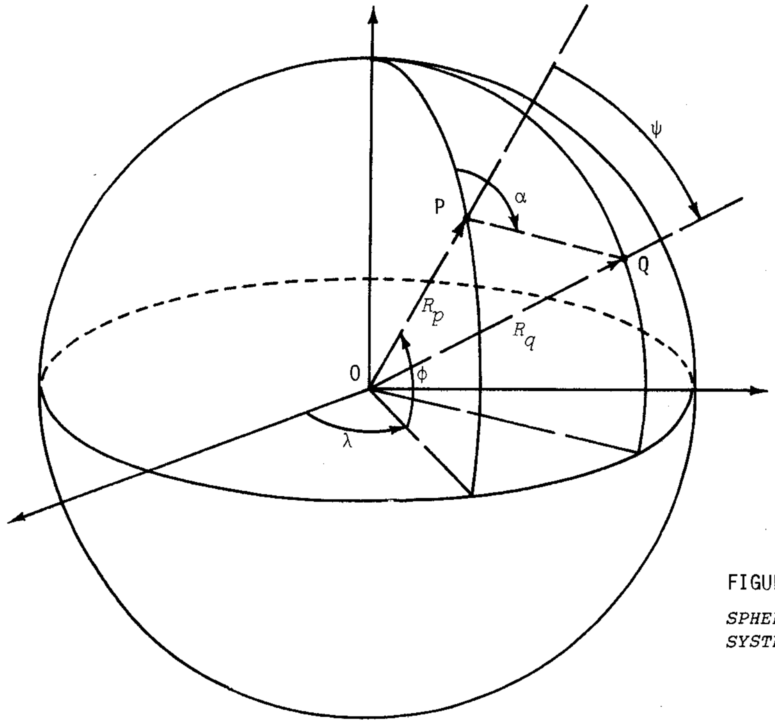

FIGURE 1.4
SPHERICAL COORDINATE SYSTEMS

TRANSFORMATIONS. The term transformation is applied variously to mean either the translation and rotation of a reference frame, or conversion between rectangular and orthogonal curvilinear coordinate systems.

Translation of the coordinate system is given by:

$$x_i = X_i - X_{io} \tag{1.7}$$

where x_i are the "new" coordinates,

X_i are the "old" coordinates, and

X_{io} are the old coordinates of the new origin.

When rotation is involved, the basic relation is [THOMPSON 1969, p.137]:

$$\begin{bmatrix} x \\ y \\ z \end{bmatrix} = \mathsf{R} \begin{bmatrix} X \\ Y \\ Z \end{bmatrix} \tag{1.8}$$

where R is the rotation matrix, being the product of the individual rotation matrices associated with each component rotation of the reference frame about a particular axis. Component rotations about each of the axes are given by:

$$\mathbf{R}_X = \begin{bmatrix} 1 & 0 & 0 \\ 0 & \cos\theta_X & \sin\theta_X \\ 0 & -\sin\theta_X & \cos\theta_X \end{bmatrix}, \quad \mathbf{R}_Y = \begin{bmatrix} \cos\theta_Y & 0 & -\sin\theta_Y \\ 0 & 1 & 0 \\ \sin\theta_Y & 0 & \cos\theta_Y \end{bmatrix}, \quad \mathbf{R}_Z = \begin{bmatrix} \cos\theta_Z & \sin\theta_Z & 0 \\ -\sin\theta_Z & \cos\theta_Z & 0 \\ 0 & 0 & 1 \end{bmatrix} \qquad (1.9)$$

where θ_X, θ_Y, θ_Z are the angles of rotation of the reference frame about the X, Y, Z axes respectively, considered to be positive in accordance with the "right-hand rule". The sequence of rotations is significant, pre-multiplication of the component matrices being requisite for each successive rotation. If negative rotations are involved the following relations are useful:

$$\mathbf{R}(-\theta) \equiv -\mathbf{R}(\theta) \equiv \mathbf{R}^{T}(\theta) \qquad (1.10)$$

When a transformation between rectangular and curvilinear coordinates is applied to variables under integration, the associated three dimensional Jacobian of the transformation is given by:

$$\left| \frac{\partial(x,y,z)}{\partial(u,v,w)} \right| = \begin{vmatrix} \partial x/\partial u & \partial x/\partial v & \partial x/\partial w \\ \partial y/\partial u & \partial y/\partial v & \partial y/\partial w \\ \partial z/\partial u & \partial z/\partial v & \partial z/\partial w \end{vmatrix}, \qquad (1.11)$$

and the elemental volume is

$$dx\ dy\ dz = \left| \frac{\partial(x,y,z)}{\partial(u,v,w)} \right| du\ dv\ dw \qquad (1.12)$$

ISOSTATIC COMPENSATION SYSTEMS

Experimental evidence demonstrates that the earth's topographic masses, above the geoid, are about 90% isostatically compensated by mass deficiencies within the crust. A number of mathematical models, approximating this natural phenomenon, have been proposed. Such models provide the basis for the methods of isostatic gravity reduction, associated with the regularization of the earth's crust to conform with the conditions of Stokes' solution. Their definition is, therefore, fundamental to this investigation.

Basically two systems have been proposed: the *Pratt-Hayford* and the *Airy-Heiskanen* systems. Both depend on the removal of the extra-geoidal masses and their relocation below the geoid, resulting in a homogeneous, regular crust. They differ only in the manner of distribution of the masses: the former postulates a sub-crustal "level of compensation", at which the masses of columns of the same cross-section are equal and the exterior mass may be re-distributed uniformly between this level and the geoid. The Airy-Heiskanen system supposes that there is a sub-crustal "root", of lesser density than the surrounding material, balancing the exterior mass. Regularization in this case may be achieved by relocating the topographic mass within the root.

A third system — the Vening Meinesz regional system — is a suggested modification of the Airy-Heiskanen model to admit regional, rather than localized, compensation. Although more realistic, it is not considered in this study, as it is needlessly complex.

A thorough definition of these systems needs to include provision for the ellipsoidal figure of the earth, so that the balanced columns of material converge appropriately towards the centre. The Airy-Heiskanen model, modified for sphericity, is applied throughout this study, and the reasons for this choice, a complete mathematical definition, and a discussion of the effects of different models are given in chapter 3.

When we mean to build,
We first survey the plot, then draw the model;
And when we see the figure of the house,
Then must we rate the cost of the erection;
Which if we find outweighs ability,
What do we then but draw anew the model
In fewer offices, or at last desist
To build at all? Much more, in this great work,
Which is almost to pluck a kingdom down
And set another up, should we survey
The plot of situation and the model,
Consent upon a sure foundataion,
Question surveyors, know our own estate,
How able such a work to undergo...

—*WILLIAM SHAKESPEARE*
in The Second Part of King Henry The Fourth.

2

Method of Evaluation

2.1 MAPPING THE GRAVITATIONAL FIELD

To determine the effect of the topography and compensation on the earth's total equipotential surfaces, it is necessary to "map" the gravitational field of the adopted topographic-isostatic model in three dimensions. Since the field is non-analytical, the process of mapping devolves to a point-by-point numerical evaluation of the representative function over whatever domain is required.

Global evaluation was judged essential, to provide a complete knowledge of the behaviour of the field and permit proper analysis of the results. However, complete mapping of the field in the vertical sense was not undertaken, rather evaluation was limited to three levels of prime interest: at the geoid, at the earth's surface, and at an altitude representative of satellite orbits. At each level, the field was mapped globally on a regular, geographical grid. Even though the field may be considered to be completely determined in terms of its intensity, as measured by the potential, a good deal more information is made available by simultaneously evaluating the attraction vector.

By treating the topographic-isostatic effect as a disturbing influence on the normal gravity field, Bruns' Theorem (equation 1.5) may be applied to convert the disturbing potential values to corresponding heights of undulations in the equipotential surfaces. Similarly, the horizontal components of the attraction vector may be expressed as topographic-isostatic deflexions of the vertical through the equations 1.6. The vertical component of the attraction vector may be thought of as the topographic-isostatic gravity disturbance.

2.2 REQUIREMENTS

Three prerequisite phases may be distinguished in the problem of mapping the gravitational field.

They are:

(a) theoretical definition of the mathematical models required to describe the geometry and composition of the topography and isostatic compensation;

(b) development of working formulae for the potential and attraction in terms of the adopted models; and,

(c) numerical elaboration of the models in a form suitable for use in the formulae.

Equations 1.3 and 1.4, which provide the starting point for formulation of the potential and attraction, are solely functions of the geometry and mass distribution of the topography and compensation. Because both these properties are non-analytical they must be modelled, either by approximate formulae or numerical data. The geometry of the topography and compensation enters the relations by way of the limits of integration and the distance of the mass element from the point of evaluation, while the mass element requires expression in terms of a density model. These aspects of the problem are treated in chapter 3.

Before computational routines can be designed the fundamental relations must be developed into working formulae, incorporating the adopted mathematical models. Proof of the formulae, by at least the application of elementary checks, should be undertaken and their theoretical validity and practical viability under the anticipated computational conditions should be ascertained. Chapters 4 and 5 comprise these topics.

Numerical realization of the topographic-isostatic model, in the form of digital topographic data, is described in chapter 6.

2.3 PRACTICAL CONSIDERATIONS AND PRELIMINARY INVESTIGATIONS

QUADRATURES TECHNIQUE

A "quadratures" technique is imposed on the evaluation of the gravity field integrals if digital data is to be employed in the topographic-isostatic model. (The term "quadrature"—strictly "cubature"—is used here in the classical sense, meaning the replacement of *integration* with respect to *curved* boundaries by *summation* over equivalent *rectangularized* domains.) It then remains to decide:

(a) the method of subdivision of the topographic-isostatic model,

(b) the size of the quadrature subdivisions (*"quads"*) and the evaluation grid interval, and

(c) the appropriate formulae, with regard to the degree of approximation which might be tolerated.

METHOD OF SUBDIVISION. A choice must be made between two fundamentally different methods of subdividing the earth's surface; based on either polar coordinates, local to the point of computation, or geographical coordinates, which are quite general. While the former method leads to advantageous simplicity in the associated formulae, it is burdened with the necessity to transform the digital data to different subdivision boundaries for use at each point. This is a serious encumbrance, since the transformation is complicated and must be repeated for every computation point. Consequently, it is better to expend some additional effort in the derivation of the rather more complex, geographical subdivision formulae, and thereby achieve considerable savings in the subsequent computation time.

Geographical subdivision may be either *equi-angular* or *equal area*, the former signifying equal intervals of both latitude and longitude, regardless of location, and the latter usually indicating that the intervals of longitude are varied at different latitudes to maintain approximately equal surface areas. Equi-angular subdivisions suffer from an important disadvantage, in that the number covering a specific area increases greatly at high latitudes. This is the prime reason for the introduction of the equal area method [PAUL 1973], which additionally provides a more equitable precision of representation at all latitudes. Though inherent bias of precision towards the poles is not a critical defect of the equi-angular method, the associated expansion of computation time may be a decisive factor. However, this must be balanced against the time consuming complications arising from the equal area approach, when adjacent zones comprising different areas of subdivision need to be introduced. This difficulty was deemed to outweigh the inefficiencies of the equi-angular subdivisions at high latitudes, which can be remedied somewhat by manipulating the interval of subdivision. Further, the availability of topographic data in equi-angular form obviates the need of conversion, which was a significant consideration in the preparation and maintenance of the data, (see chapter 6).

SIZE OF SUBDIVISIONS AND GRID INTERVALS. Selection of the size of quads and the evaluation grid interval must be a compromise between achieving requisite accuracy for the results and the feasibility of the computations. Despite the power and speed of electronic computation, it is possible to design an impractical computation scheme. For instance, to compute just the potential on a 1°x1° global grid, using 5'x5' quads of the terrestrial topography, would require about 2×10^{11} evaluations of whatever formula might be chosen — a task which, optimistically, could consume several hundred years of computer time. Clearly, if needless computation is to be avoided, some more rational scheme must be selected, based on a knowledge of the effect on overall accuracy of a sparser grid and coarser quadrature. Trial evaluations, designed to reveal the characteristic behaviour of the field, provide the most expeditious means of determining a suitable grid spacing. Even so, a compromise may be necessary here also.

Because the gravity field is a function of the reciprocal of the distance to the computation point, the contribution to the total effect of more distant topographic subdivisions is diminished and a greater degree of approximation in their evaluation can be tolerated. It is an accepted practice to take advantage of this property of the field by introducing a set of concentric "zones" surrounding the computation point. Within each zone a formula and size of quad can be selected, consistent with the desired accuracy but admitting the constraints of computation time. Evaluation in zones also permits a quantitative assessment of the separate contributions from each zone, thereby providing some perception of the characteristics of the overall effect. The choice of quad sizes within each zone is predominated by the selection of formulae.

FORMULAE. It is worth recalling at this point that the formulae sought are for a particular quadrature subdivision of the topographic model. Hence two levels of modelling must be discriminated: firstly the global topographic model and secondly, within that, the modelling of the individual quadrature subdivisions. Thus the total potential, for instance, may be conceptualized in the form

$$\textit{Total potential} = k \sum_{\substack{global\\model}}\sum \iiint_{\substack{quad.\\model}} \frac{dm}{s} \tag{2.1}$$

where the limits of integration are determined by the quadrature model, which may be — with increasing approximation — an ellipsoidal, spherical, or rectangular element of the global model, or a cylindrical approximation in certain circumstances. Solution of the integral may be achieved by rigorous analysis, numerical integration, or series expansion.

The geophysical literature is replete with formulae and methods for computing the "gravity anomaly" due to three dimensional bodies, particularly topographic masses and occasionally their compensation [*e.g.* see References in JOHNSON and LEE 1973, p.270]. In particular the formulae of NAGY [1966] and the methods proposed by ST JOHN and GREEN [1967] deserve consideration. Care must be exercised, however, in transferring these techniques into the context of a global evaluation, as their purposes and consequent specifications may differ substantially. It is also, perhaps, unfortunate that many of these works do not always fully recognize the great body of potential theory developed by European mathematicians during the middle and last decades of the nineteenth century and the thorough expositions of this material published in a subsequent revival of interest [*e.g.* KELLOGG 1929, MACMILLAN 1930].

A more recent and refined approach has been presented by JOHNSON and LITEHISER [1972], which rigorously accommodates sphericity of the body and includes a first order approximation of the effects of ellipticity. This work was published too late to be considered in the investigations described here. In any case, since the derivation has recourse to polar coordinates at the observation point, the resulting formulae are not compatible with the topographic model contemplated. The method appears to be further handicapped by being relatively slow in computation. An exhaustive analysis and evaluation of the effects of sphericity is also available in FRISCH [1960], again in terms of a local polar coordinate system.

For a variety of reasons, these formulations do not readily satisfy the specifications of a global evaluation, so a fresh approach was warranted.

PRELIMINARY INVESTIGATIONS

A preliminary investigation of possible computation schemes was undertaken, with the aim of determining:

(a) suitable sizes of quads and their interaction with formulae of different innate precisions, and

(b) an evaluation grid interval, consistent with the anticipated behaviour of the field to be mapped.

In studying the first of these questions two distinct situations were recognized, with different attendant requirements: firstly the case where the computation point comes into contact with the gravitating body, and secondly the situation where the body is sufficiently remote from the point to guarantee stability of any formulation. Each of these was investigated separately.

CONTACT SUB-ZONE. The area occupied by the four innermost quadrature subdivisions, immediately adjacent to the computation point, will be called the "contact sub-zone". (A complete definition of zones is deferred to §2.4). It is especially important because of its relatively large contribution to the total effect and because of the tendency to instability of any but rigorous formulae in this area. This last difficulty has commonly been circumvented by the simple expedient of the "cylindrical assumption" [MATHER 1968a p.92; FRYER 1970, p.99], whereby the contact sub-zone is approximated by a right cylinder of equivalent volume. Such a recourse is effective since it essentially reverts to a local polar coordinate system with the associated benefits of radial symmetry. However, the magnitude of the error introduced by this approximation has usually been ignored. For an exterior point P, the potential due to the cylinder of density σ in the configuration of figure 2.1 is [after HEISKANEN and MORITZ 1967, eq. 3-2]:

$$V_{cyl} = \pi k\sigma[(h_p - h)^2 - h_p^2 - (h_p - h)d_t + h_p d_b + r^2 \ell og\left(\frac{h_p + d_b}{h_p - h + d_t}\right)] \tag{2.2}$$

where: $d_t = [r^2 + (h_p - h)^2]^{\frac{1}{2}}$, and

$$d_b = [r^2 + h_p^2]^{\frac{1}{2}} .$$

Alternatively, if the four contact subdivisions are assumed to be the same height, the potential at P due to the total square prism with side $2a$ (figure 2.2) is:

$$V_{prism} = 8k\sigma \int_0^h \int_0^{\pi/4} \int_0^{a\,sec\,\alpha} \frac{s\ ds\ d\alpha\ dh}{[(h_p - h)^2 + s^2]^{\frac{1}{2}}}$$

where the symmetry of the prism is used by writing the integral in a cylindrical coordinate system (s,α,h). Straightforward integration techniques lead to the solution:

$$V_{prism} = 4k\sigma[\tfrac{\pi}{4}(h^2 - 2hh_p) + a^2\ell og\left(\frac{h_p + c_b}{h_p - h + c_t}\right) + 2ah_p\ \ell og\left(\frac{a + c_b}{d_b}\right) - 2a(h_p - h)\ell og\left(\frac{a + c_t}{d_t}\right)$$

$$+(h_p^2 - a^2)tan^{-1}\left(\frac{h_p}{c_b}\right) - ((h_p - h)^2 - a^2)tan^{-1}\left(\frac{h_p - h}{c_t}\right)], \tag{2.3}$$

where: $d_t = [a^2 + (h_p - h)^2]^{\frac{1}{2}}$,

$d_b = [a^2 + h_p^2]^{\frac{1}{2}}$,

$c_t = [2a^2 + (h_p - h)^2]^{\frac{1}{2}}$,

$c_b = [2a^2 + h_p^2]^{\frac{1}{2}}$.

Equations 2.2 and 2.3 both provide rigorous solutions in terms of geometrically approximate quadrature models.

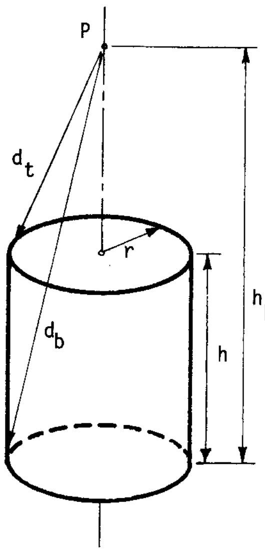

FIGURE 2.1
POTENTIAL OF A RIGHT CYLINDER

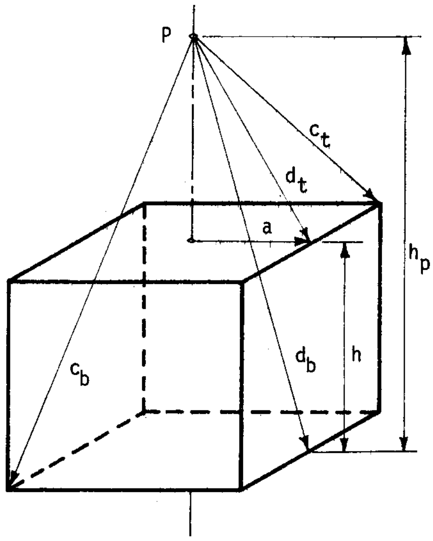

FIGURE 2.2
POTENTIAL OF A RIGHT SQUARE PRISM

Multiple numerical integration ("cubature") may also be called upon to evaluate the integral in equation 2.1. Simpson's rule [WILLERS 1948, p.125 *et seq.*] may be extended to replace the triple integral, giving the potential of a quad as

$$V_{quad} = \frac{\Delta a\ \Delta b\ \Delta c}{27} \sum_{i=0}^{l} \sum_{j=0}^{m} \sum_{k=0}^{n} [(3 - \delta_{i0} - \delta_{il} - (-1)^i) \times (3 - \delta_{j0} - \delta_{jm} - (-1)^j)$$

$$\times (3 - \delta_{k0} - \delta_{kn} - (-1)^k)\ U_{ijk}], \tag{2.4}$$

where: Δa, Δb, Δc, are the chosen intervals of subdivision of the function arguments;

l, m, n are the number of such intervals respectively, and must be even numbers;

U_{ijk} is the value of the potential function due to the mass element designated by the indices;

and δ_{pq} is the *Kronecker Delta* defined by:

$$\begin{cases} \delta_{pq} = 0 & \text{if } p \neq q, \\ \delta_{pq} = 1 & \text{if } p = q. \end{cases} \tag{2.5}$$

This form of solution has advantageous flexibility, in that it may be applied in terms of an ellipsoidal, spherical, or rectangular quadrature model with equal ease. However, the stability of the solution in the contact sub-zone must be investigated.

Prototype computer routines were developed for the Hewlett-Packard 9810 and 9830 programmable calculators (see §7.3) to enable a comparison of these formulae under a variety of realistic circumstances. Some of the results are summarized in table 2.1.

TABLE 2.1

COMPARISON OF FORMULAE FOR THE POTENTIAL OF THE CONTACT SUB-ZONE

Height of topography, h = 5000 m
Height of computation point = h_p
Density = 2670 kg/m^3

Radius of Sub-zone, ψ_c = 0.1°
Relative distance $d^* = (h_p - h/2) / r^*$
Radius of convergence = r^*

FORMULA	No. of intervals	h_p = 20 000 m			h_p = 5000 m		
		d^*	Potential†	% error	d^*	Potential†	% error
Square Prism (eq. 2.3) a = 11 120 m, r^* = 15 923 m		1.10	22.5767	--	0.16	57.6694	--
Cylinder (equivalent volume) (eq. 2.2) r = 12 547 m, r^* = 12 794 m		1.37	22.6572	0.357	0.20	58.0273	0.621
Numerical integration (eq. 2.4) Simpson's rule							
Spherical quadrature model, arguments ϕ, λ, R; $\Delta\phi = \Delta\lambda = \pm 0.1°$, 6371 km $\leq R \leq$ 6376 km	$l=m=n=2$	1.10	22.8226	1.089	0.16	78.8846	36.8
	=4		22.5913	0.065		55.2440	-4.21
	=6		22.5883	0.051		60.8312	5.48
	=8		22.5876	0.048		57.0232	-1.12
	=10		22.5874	0.047		58.8329	2.02
	=12		--	--		57.3914	-0.48
Rectangular quadrature model, arguments x, y, z; $\Delta x = \Delta y = \pm$11 120 m, z = 5000 m	$l=m=n=2$	1.10	22.8106	1.0360	0.16	78.8387	36.7
	=4		22.5807	0.0177		55.2258	-4.24
	=6		22.5777	0.0044		60.8056	5.44
	=8		22.5770	0.0013		57.0044	-1.15
	=10		22.5768	0.0004		58.8110	1.98
	=12		--	--		57.3728	-0.51

†*Units for potential are J/kg*

**The asterisk is used here as a mathematical symbol (see text below)*

The height (h = 5000 m) and density (σ = 2670 kg/m^3) of the topography are assumed to be constant over the whole contact sub-zone, which has an angular radius of approximately $\psi_c = 0.1°$. Four formulations are compared for two different configurations: first with the computation point at some distance from the topography (h_p = 20 000 m), and then in contact with the topographic surface (h_p = 5000 m). Rigorous computation for a square prism is presumed nearest to reality, so the percentage errors are calculated with respect to this result—a negative error indicating under-estimation of the reference value.

As expected, the more compact shape of the cylinder causes over-estimation of the potential. In the most important case—the contact situation—the accuracy of the cylindrical assumption is poor, and hardly tolerable. Although it improves for a more remote point, as the shape of the quadrature model becomes less influential, accuracy to the order of the flattening is not achieved at the "radius of convergence".

Radius of convergence r^* is here defined to be the radius of the smallest sphere which can contain the whole of the gravitating body. The *relative distance* d^* of the computation point is then defined as the ratio of the distance between the computation point and the centre of mass of the body, to the radius of convergence. This concept, which allows comparison of results regardless of the actual size of the body and its true distance from the computation point, is a corollary of the "perspectivity" theorem [MACMILLAN 1930, p.9].

Numerical integration, using Simpson's rule, is compared for both spherical and rectangular quadrature models. Agreement between these models approaches one tenth of the order of the flattening *i.e.* $o\{0.1 f\}$. This is considered analytically in §3.4. Convergence of the numerical integration at a relative distance greater than unity ($h_p = 20\,000$ m) is rapid as the number of intervals is increased, a satisfactory result being achieved with four intervals. In contrast, the contact situation is unstable, and oscillating convergence as the number of intervals is increased invalidates the normal rules for extrapolation of the result. A satisfactory accuracy is not achieved with twelve intervals. Computation time is also a significant factor in this context, since it increases as the cube of the number of intervals. Also, even though the spherical quadrature model should be more realistic than the rectangular model, it consumes approximately three times as much computation time, because of the necessity to evaluate trigonometric functions.

The accuracy of the cylindrical assumption and numerical integration, as a function of the relative distance, was further investigated. In figure 2.3 the plotted results show that the error of the cylindrical model is stable within the radius of convergence and falls below the order of the flattening at a relative distance of about 1.5. Numerical integration evinces marked instability immediately within the radius of convergence, but performs well and consistently outside this limit. Neither the cylindrical assumption nor the numerical integration method provides acceptable accuracy in the contact sub-zone.

To further elucidate the quantitative properties of the gravity field at or near contact conditions, the computer routines were used to separately investigate the effects of changing height of topography and changing height of computation point. Figure 2.4 illustrates the first of these effects as determined by evaluation of the rigorous formula for a square prism. The computation point is held at the surface by setting its height equal to that of the topography throughout. An almost linear relationship between both potential and vertical gravity and the height of topography in the contact sub-zone is apparent. In figure 2.5 the stability of the rigorous formula is demonstrated, the height of the computation point being varied from 0 to 30 km, while the height of topography is held constant at 5000 m. Continuity of the potential and gravity functions is illustrated, even when the computation point is within the boundaries of the gravitating material, and the finite discontinuity of the second derivative of the potential is exemplified by the change of gradient of the vertical gravity at the topographic surface. This behaviour accords with the theory referred to in §1.4.

Having thus demonstrated the viability of the rigorous formulation, an investigation of the contact sub-zone effect under real conditions was undertaken. A profile (figure 2.6) was computed at 5' intervals on the 19° north parallel of latitude, between longitudes 260° and 264° east. This region was chosen because 5'x5' mean topographic elevation data was available (see §6.3) and the effects of steep topographic gradients, high elevations, and the sea coast are all present. Only the four 5'x5' contact quadrature subdivisions and their isostatic compensation (as defined in §3.3) were considered and the computation point was assumed to be at the mean height of these four blocks. As might be anticipated by the relationship portrayed in figure 2.4, the potential is highly correlated with the

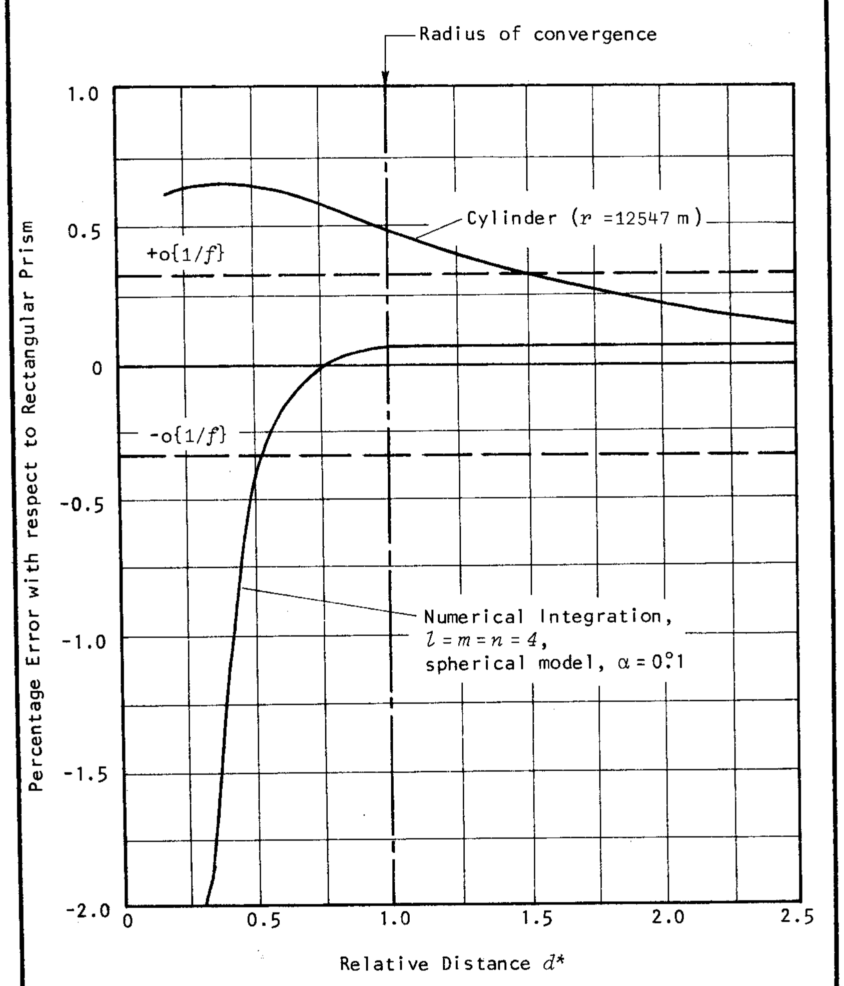

FIGURE 2.3

ACCURACY OF THE CYLINDRICAL APPROXIMATION AND NUMERICAL INTEGRATION AS A FUNCTION OF RELATIVE DISTANCE

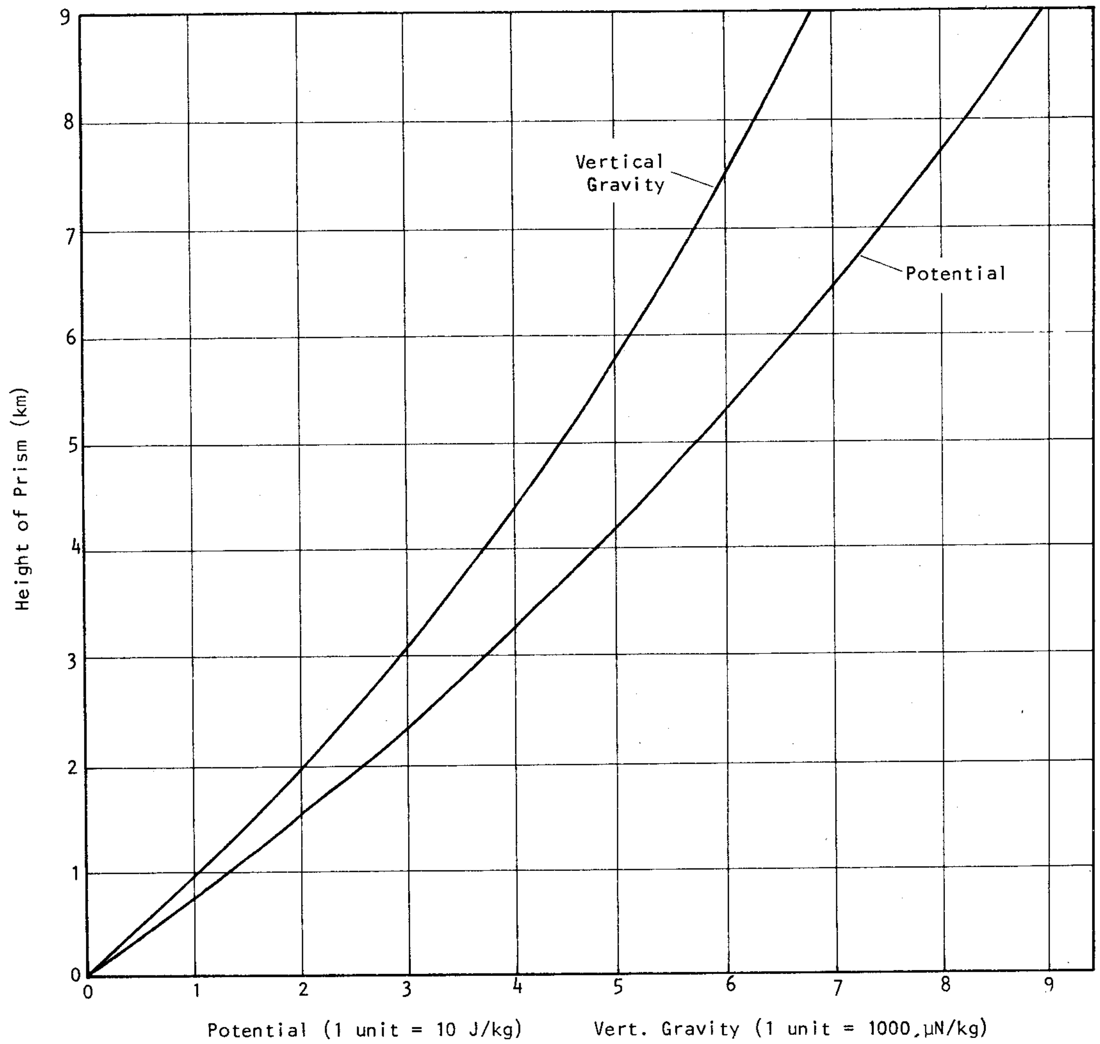

FIGURE 2.4

POTENTIAL AND VERTICAL GRAVITY AT SURFACE DUE TO A SQUARE PRISM (a = 11 119.5 m) AS A FUNCTION OF ITS HEIGHT

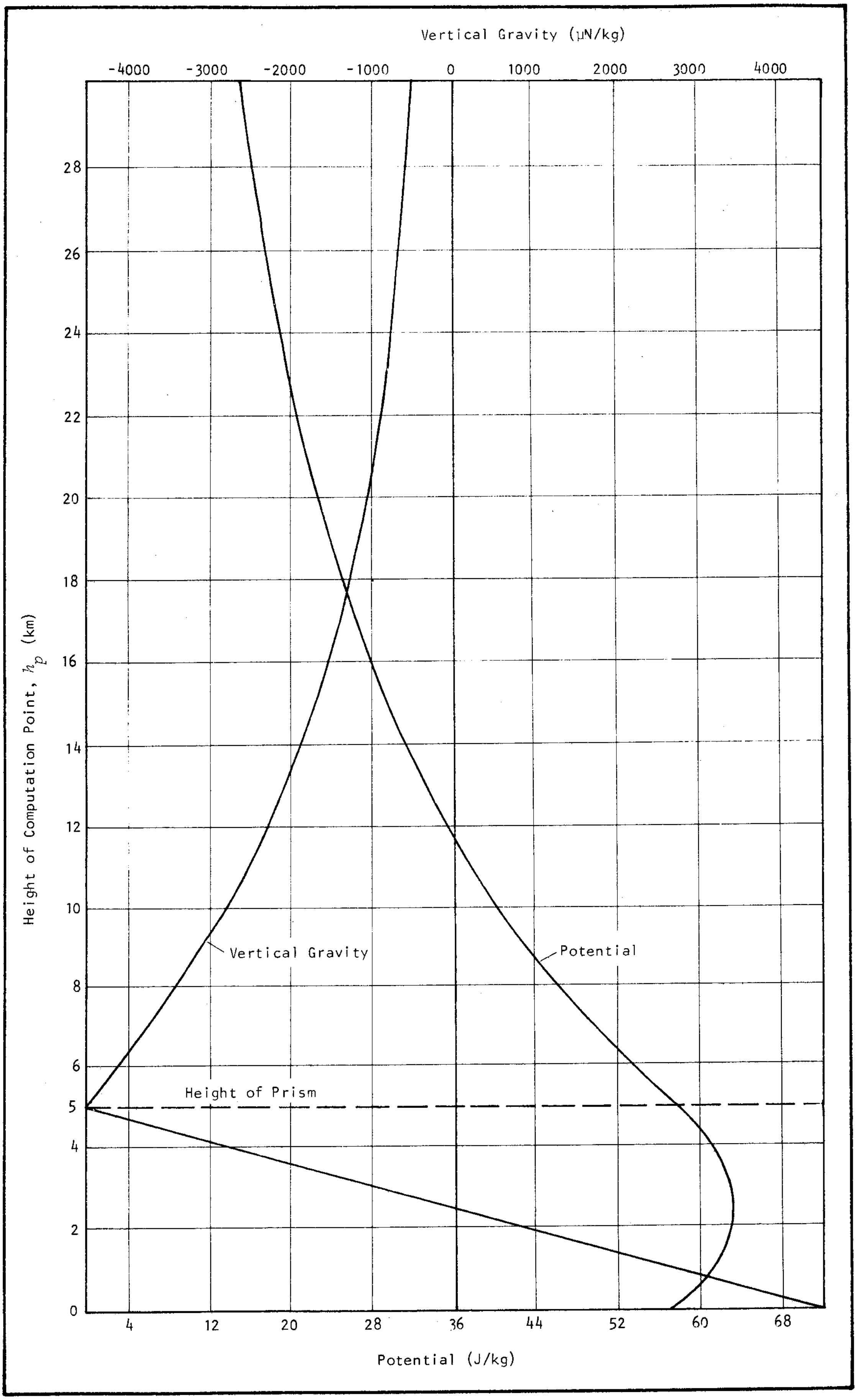

FIGURE 2.5

POTENTIAL AND VERTICAL GRAVITY DUE TO A SQUARE PRISM (a = 11 119.5 m, h = 5000 m) AS A FUNCTION OF HEIGHT OF THE COMPUTATION POINT

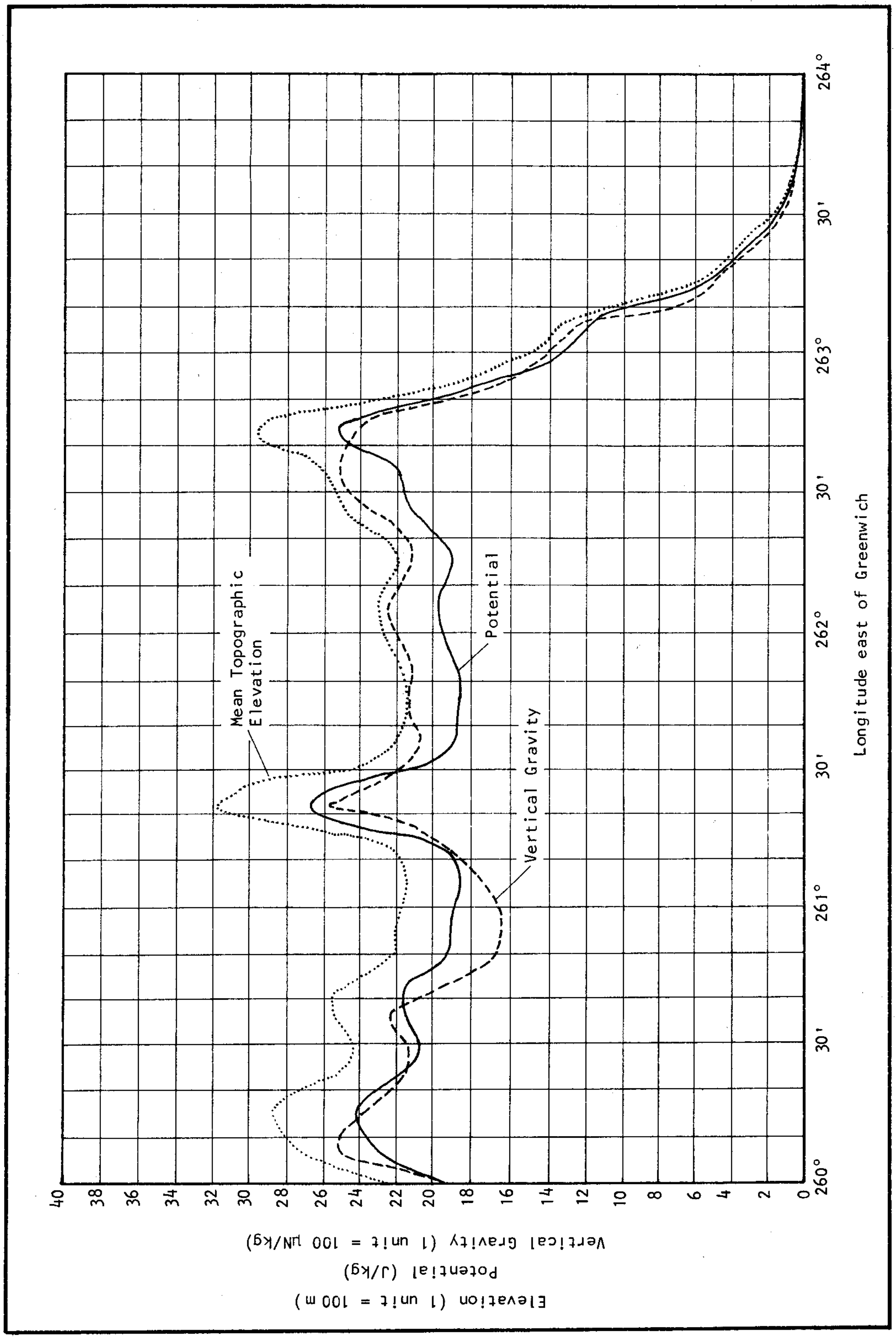

FIGURE 2.6

PROFILE ON LATITUDE 19°N (part of Eastern Sierra Madre, Mexico) SHOWING POTENTIAL AND VERTICAL GRAVITY DUE TO CONTACT SUB-ZONE mean topographic elevation. However, in the case of the vertical gravity component, this effect is noticeably modified; apparently by the uneven heights of the four contact blocks in areas of "rugged" topography. This reconfiguration of the topographic masses does not greatly alter the value of the potential from what it would be if the four blocks were of equal elevation, since the total mass is unchanged and the spatial distribution is affected only slightly. In contrast the value of vertical gravity may be changed substantially, because uneven terrain effectively imposes a deficiency of mass below the computation point, combined with a surplus above. Vertical gravity may thus be systematically diminished.

NON-CONTACT ZONES. Beyond the contact zone, where instability of the formulation is no longer significant, the simplicity of numerical integration would appear to have the advantage over a rigorous formula. But the tests described above indicated that even this technique was relatively expensive in terms of computation time. A faster, but no less accurate, method would be desirable.

Logically, the gravitational effect of any quadrature subdivision may be thought of as comprising a primary part, which is a function only of the mass, and a number of lesser secondary parts, determined by the shape, orientation, and density distribution. Further, the influence of these secondary parts should decrease as the relative distance from the computation point is increased. An empirical formulation of this concept may be derived, but it can be shown (see chapter 5) that a rigorous mathematical development involving series expansion of the potential function in terms of Legendre polynomials leads to a comparable result. Thus the first (zero order) term of the series in equation 5.21 depends on the mass of the body, while the higher order terms may be interpreted as expressing its geometric configuration. And the influence of the higher order terms is significantly moderated by the reciprocal distance coefficients. Equations 5.21, 5.32, 5.33, and 5.46 then provide a relatively rapid solution for potential and attraction components, so long as the series are convergent.

In passing, it may be noted that these expansions are sometimes called "multipole" formulae, which highlights the geometric interpretation whereby the gravitating body is represented as a three-dimensional array of "poles" or point masses. Indeed, this construction is discernible in all of the formulae considered here; appearing in the rigorous forms as functions of the distances from the computation point to the prism corners and explicitly in the numerical integration technique by virtue of the subdivision into mass elements. Also it is this property which admits the various empirical "point mass", "line mass", and "surface mass" approximations which are often employed.

Computer routines for the HP 9830 and IBM 360/50 (§7.3) were used to study the convergence of the series formulae. Figure 2.7 illustrates the error (in parts per million) of the series formula for potential, compared to the rigorous formula (equation 4.34), as a function of relative distance of the computation point. The potential is due to a homogeneous square prism with dimensions 5'x5'x9000 m, which is almost a cube, since $5' \simeq 9268$ m at the equator. Therefore the error is quite small. Curve 1 is the error in using only the first (zero order) term, and is thus equivalent to the point mass assumption. Successively including the second and third terms reduces the error to the level depicted by curves 2 and 3, respectively. However, the improvement achieved by inclusion of these extra terms is disproportionately small in comparison with the large amount of additional computation needed.

If the proportions of the prism are changed so that the height is approximately 1% of the base dimension, the error arising from use of the first term alone is much greater, and behaves as shown in figure 2.8. Three curves are plotted to show the effect of different sizes of prism: (1) 5'x5'x100 m, (2) 1°x1°x1000 m, and (3) 5°x5°x5000 m. In each case the improvement gained by including the second term stabilizes to a particular value for relative distances greater than about 6, (see table 2.2). Also, beyond this distance the improvement afforded by inclusion of the third term becomes neglibible.

Generally it is apparent that the potential may be computed by means of the point mass assumption if the quadratures subdivision is at a relative distance from the computation point greater than 10. Hence, in the non-contact zones, the point mass formula provides a most expeditious solution.

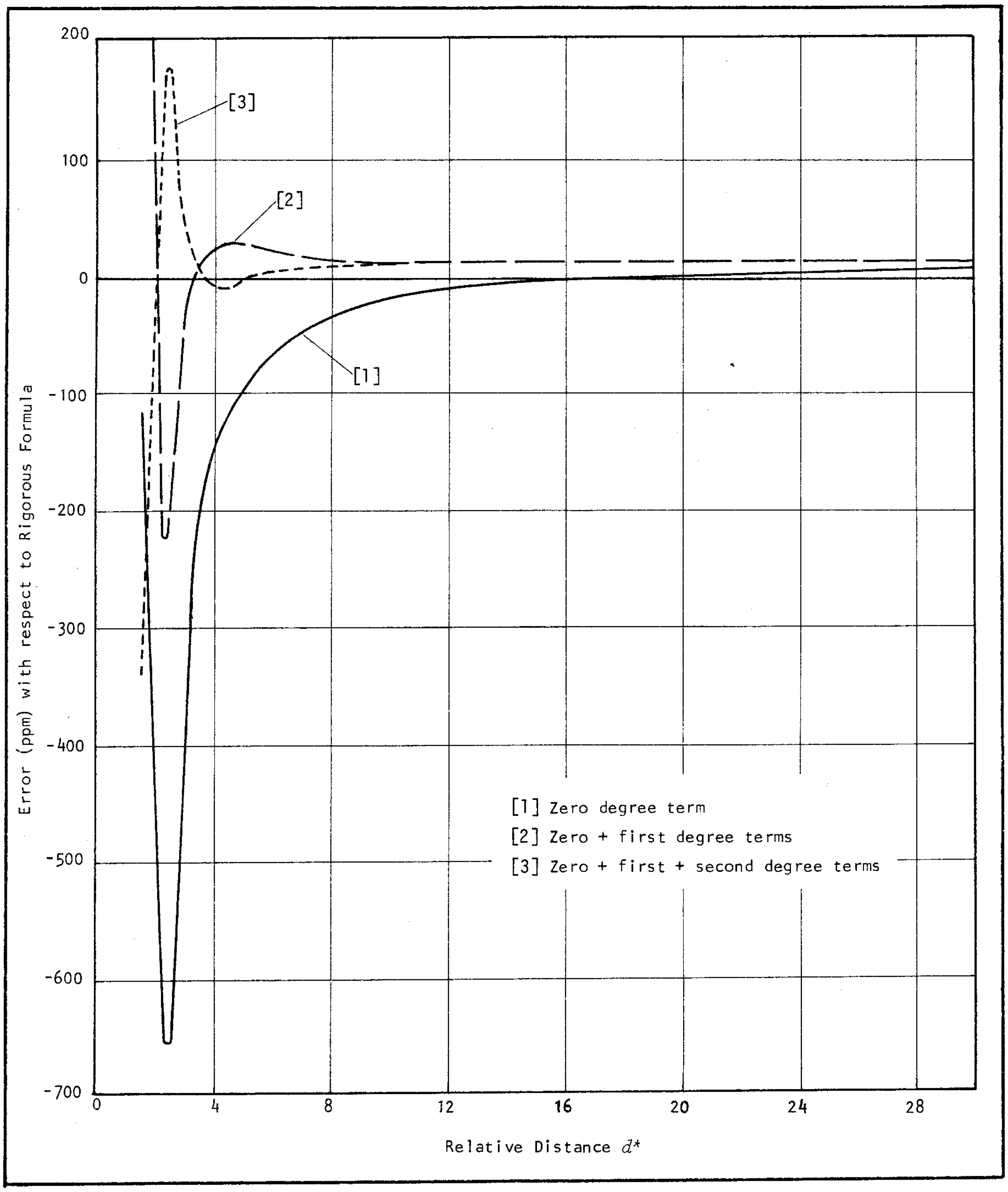

FIGURE 2.7

ERROR IN SERIES EXPANSION OF POTENTIAL OF HOMOGENEOUS SQUARE PRISM (5' x 5' x 9000 m) AS A FUNCTION OF RELATIVE DISTANCE

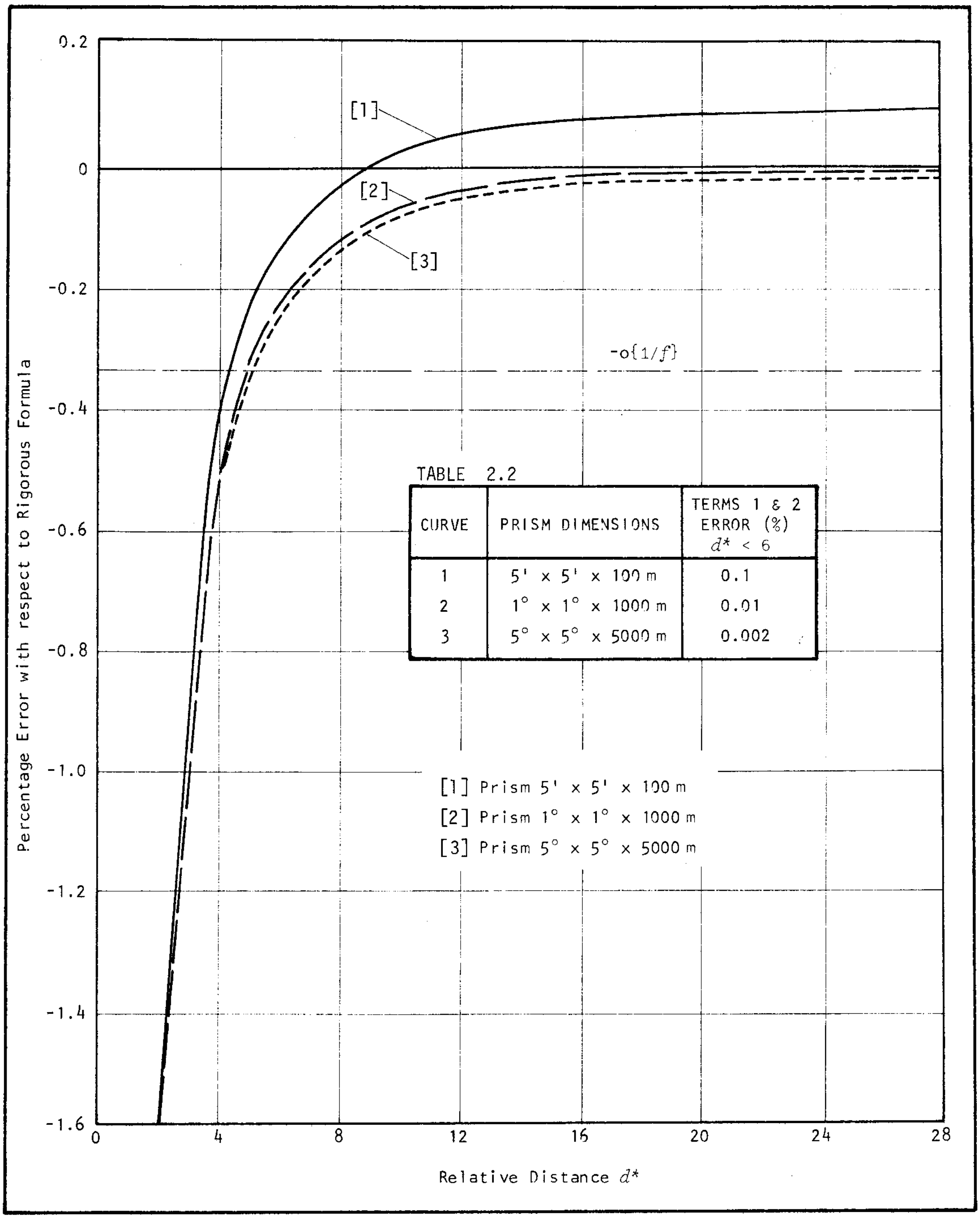

TABLE 2.2

CURVE	PRISM DIMENSIONS	TERMS 1 & 2 ERROR (%) $d^* < 6$
1	5' x 5' x 100 m	0.1
2	1° x 1° x 1000 m	0.01
3	5° x 5° x 5000 m	0.002

FIGURE 2.8

ERROR IN ZERO DEGREE TERM OF SERIES EXPANSION OF POTENTIAL DUE TO A SQUARE PRISM AS A FUNCTION OF RELATIVE DISTANCE

A further source of error, with special significance in the more distant zones where quadrature subdivisions may be large, is that occasioned by the suppression of the regional topographic surface gradient within a subdivision. This will occur for instance in a $1°\times1°$ subdivision when the mean height is presumed to prevail over the whole area, whereas the surface gradient could be more realistically represented by four $\frac{1}{2}°\times\frac{1}{2}°$ subdivisions of different heights. The configuration is represented in figure 2.9: the computation point P is located on a spherical reference surface at an angular distance ψ from a $1°\times1°$ subdivision in which the mean topographic height is h. An extreme instance of the effect of topographic gradient is introduced by assuming that both of the $\frac{1}{2}°\times\frac{1}{2}°$ subdivisions nearest to P are lower than the remainder by an amount Δh. If the potential and vertical ("radial") component of gravity at P due to the 1° block of height h are computed, it may be supposed that they will be in error by an amount equal to the change induced by transferring the mass 'A' to fill the space 'B', (figure 2.9). This change was computed using the point mass formula and expressed as a percentage of the "more correct" value due to the total mass, indicated by shading in figure 2.9. Results for both potential and vertical gravity, and five different combinations of h and Δh, are graphed as functions of ψ in figures 2.10 and 2.11. Two trends are evident: for a given mean height (h) the error increases for a greater gradient (Δh), and for a given gradient it is increased at lower mean heights. The former effect is self evident; the latter is partly a consequence of the mass redistribution being brought closer to the computation point, but primarily arises from the intrinsic reduction of the total mass.

Since topographic gradients tend to correlate positively with mean elevation (see §6.4), the seriousness of the second trend is diminished somewhat. However, it may be expected to become significant near extensive mountain masses and elevated continental coasts. Generally, other than in these special circumstances, the error shoud not accumulate systematically. Inspection of the graphs suggests that a workable compromise, between excessive computation and an acceptable error level under average conditions, can be achieved by maintaining a relative distance of at least 10, from the computation point to the subdivision. (A more complicated procedure, designed to cope with this effect, was incorporated and successfully tested in prototype computer routines. This remedy— which relied on dynamic variation of zone boundary definitions and quadrature subdivision sizes, depending on the configuration of mean elevations [ANDERSON 1973a p.113] — was found to slow the routines intolerably, and also made the subsequent interpretation of zone contributions awkward.)

EVALUATION GRID INTERVAL. Obviously it is desirable to choose the spacing between successive computation points—the evaluation grid interval—small enough to detect significant variations in the fields. The question thus devolves to: What are significant variations, and over what distance might they be expected to occur? In figure 2.6 the profile obtained indicates that fluctuations of the order of one metre may occur in the equipotential surfaces over distances less than $\frac{1}{2}°$, arising from the contact sub-zone alone. But such localized effects are not the primary concern of this study: the long-wave trends —with wavelengths near or exceeding continental scale—are of the greatest import. To ascertain these qualities requires the low degree terms in the ultimate analysis of the results to be strongly determined, which may be achieved by a reasonable degree of over-determination of the analysis solution. This again implies the need for a fine grid, albeit not perhaps as fine as the representation of localized fluctuations would dictate.

While it would be agreeable to base the choice on these considerations alone, unfortunately the limits of computation time will impose an overwhelming constraint. It must be remembered that the amount of computation increases as an inverse square of the grid interval and is further compounded twelve times for evaluation of the potential and three components of the attraction vector at three different elevations.

An assessment of these factors indicated that it would be prudent—at least initially—to evaluate on a global $5°\times5°$ grid. This would permit an effective appraisal of the behaviour of the fields and leave open at least two options for more detailed investigation: interpolation at a finer interval,

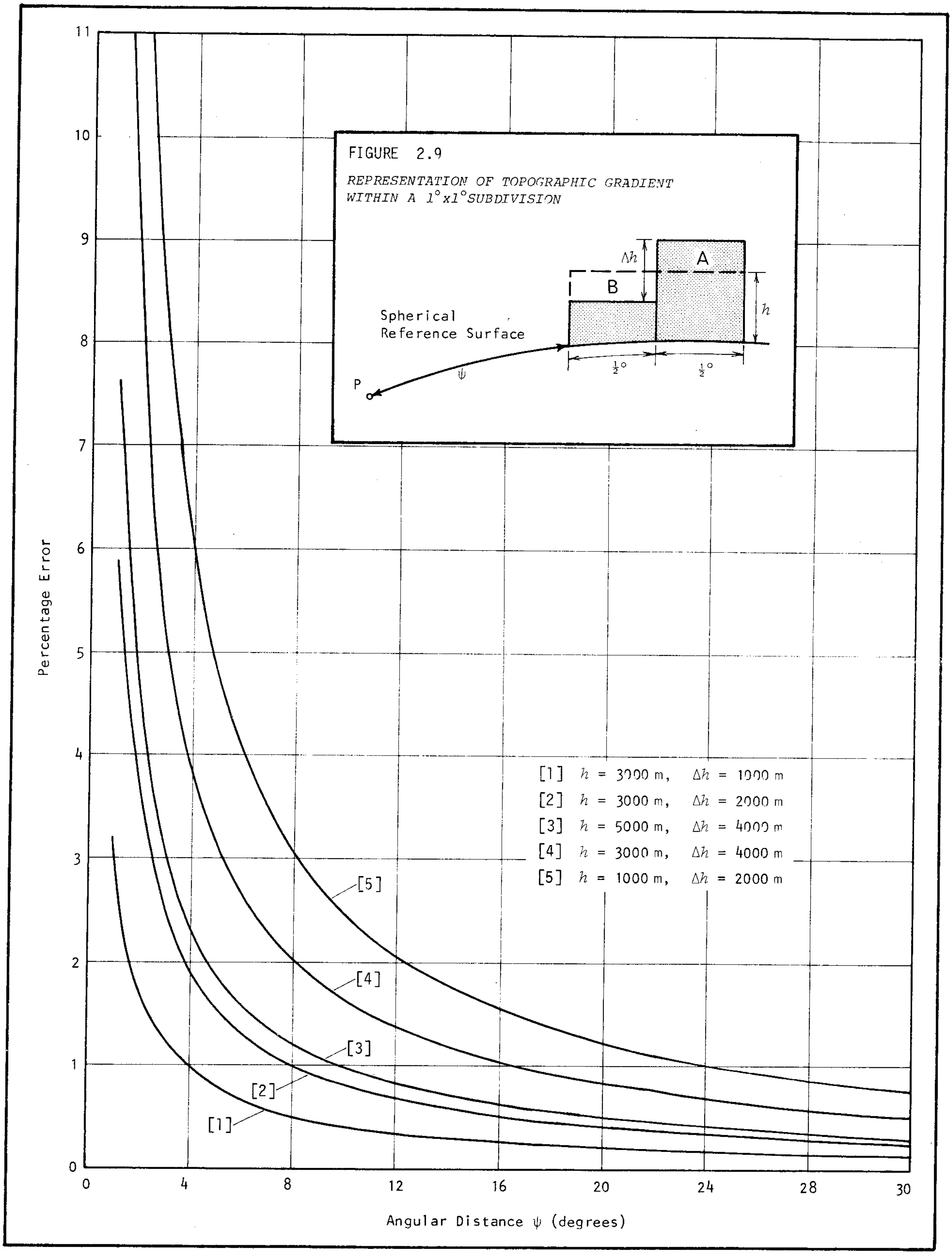

FIGURE 2.9

REPRESENTATION OF TOPOGRAPHIC GRADIENT WITHIN A 1°x1° SUBDIVISION

FIGURE 2.10

ERROR IN POTENTIAL DUE TO SUPPRESSION OF TOPOGRAPHIC GRADIENT IN A 1°x1° SUBDIVISION AS A FUNCTION OF ANGULAR DISTANCE TO THE COMPUTATION POINT

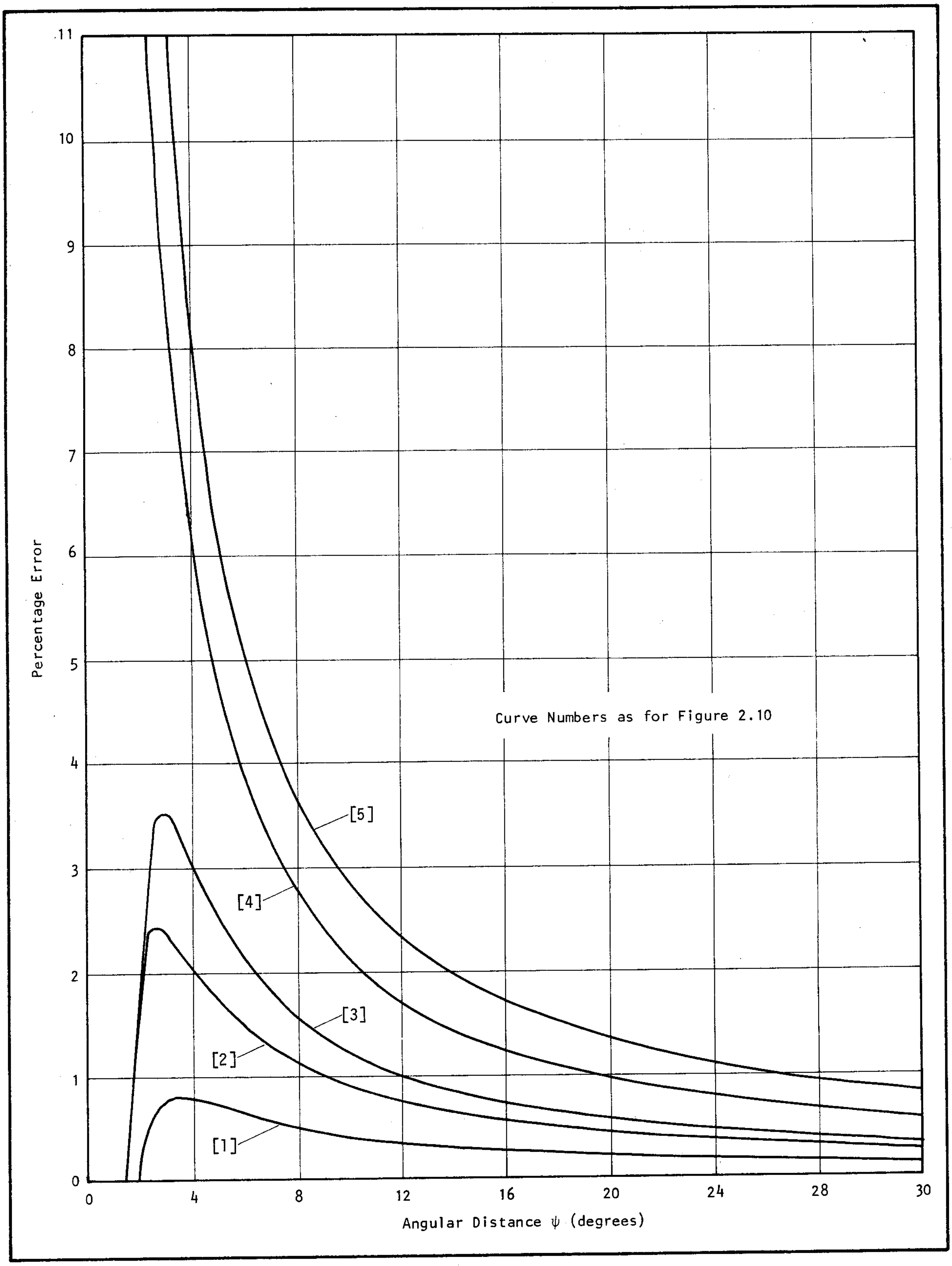

FIGURE 2.11

ERROR IN VERTICAL GRAVITY DUE TO SUPPRESSION OF TOPOGRAPHIC GRADIENT IN A $1^{\circ} x 1^{\circ}$ SUBDIVISION AS A FUNCTION OF ANGULAR DISTANCE TO THE COMPUTATION POINT if the smoothness of the field should prove suitable, or selective additional evaluation in areas where this might be warranted by the results. Accordingly, the computation routines should be designed to operate on a 5° grid, but with provision to accommodate a 1° interval, which can be invoked selectively.

If the evaluation grid is extended to provide complete global coverage, the "orthogonality relations" (see §8.2) may be applied in the harmonic analysis of the results, with concomitant simplification of that process. Conventionally the origin for a global grid is the intersection of the equator and the prime meridian, and if this is adopted the difficulties of evaluation at the poles arises. The poles are burdened by the confluence of a number of limiting conditions, which can be expected to tax the viability of most computational algorithms and, indeed, some of the basic definitions. In particular, a definitive meaning of geographical longitude and the horizontal components of the attraction vector, resolved into a local cartesian system, must be stated in these circumstances, to permit orderly use of these quantities in the computations and subsequent analysis. Theoretically, the value of longitude is usually of no consequence at the poles, but in practice—at least in computer routines—it is safer to consistently assign it a value of zero. It then follows that the x-axis of a local reference frame will be directed along the 90° east meridian from either pole, and the y-axis will be directed along the 180° east meridian at the north pole and along the prime meridian at the south pole (see figure 2.12).

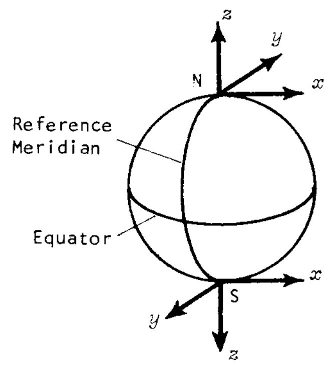

FIGURE 2.12

LOCAL CARTESIAN AXES AT THE POLES

This definition will serve in the interpretation of the components of the deflexion of the vertical (equations 1.6) at the poles.

2.4 SPECIFICATION OF METHOD

Upon taking into account the results of §2.3, and considering the constraints of computation time and computer storage space, the following broad conclusions, concerning the design of a computation scheme, may be drawn.

(a) A quadratures technique, using various sizes of equi-angular geographical subdivisions, grouped in zones determined by distance from the computation point, appears to provide the best overall method.

(b) Two distinct situations concerning the disposition of the subdivisions with respect to the computation point—broadly classifiable as "contact" and "non-contact"—dominate the selection of formulae.

(c) Adequate precision in evaluating the effect of the contact sub-zone necessitates a rigorous formula, for at least a rectangular approximation of the subdivisions.

(d) Because the total number of evaluations for the contact sub-zone will be small, any increase in computation time occasioned by the additional complexity of a rigorous formula will be negligible.

(e) Quadrature subdivisions in the contact sub-zone should be as small as available digital data will permit, so as to bestow maximum validity upon the rectangular approximation and minimise the effects of mass redistribution.

(f) No appreciable error is introduced by applying the point mass assumption to non-contact zone subdivisions if their relative distance from the computation point is greater than 10.

(g) Maintaining this relative distance of 10 also seems to provide an optimum solution to the problem of falsification of topographic gradients caused by the use of a digital mean height model within subdivisions.

(h) On *prima facie* grounds, a 5°x5° evaluation grid interval appears suitable, but the ability to selectively compute on a 1°x1° grid should be reserved. Global evaluation is highly desirable.

In view of these conclusions the following detailed specifications were adopted for the method of computation.

(a) The gravitational potential and the three components of the attraction vector should be evaluated at all points.

(b) Evaluations should be made at three elevations, namely: the geoid, the terrestrial surface, and at 1000 km above the reference surface, to indicate the effects at a representative satellite altitude.

(c) An ability to compute at an evaluation grid interval down to 1°, at all three elevations, should be retained.

(d) The definition of zones and sub-zones, and the associated equi-angular quad sizes and formulae should be as set out in table 2.3.

TABLE 2.3
DEFINITION OF ZONES AND ASSOCIATED QUADRATURE SUBDIVISIONS AND FORMULAE

ZONE	SUB-ZONE	DEFINITIVE RADIUS LIMITS† (km)	ANGULAR LIMITS (Approximate)	QUADRATURE SUBDIVISION	FORMULA
Inner	Contact	Four adjacent blocks	--	5' x 5'	Parallelepiped
	Inner	$r_0 < 111.2$	$\psi < 1°$	5' x 5'	Parallelepiped
Mid	Near	$111.2 \leq r_0 < 556$	$1° \leq \psi \leq 5°$	5' x 5'	Point mass
	Mid	$556 < r_0 < 1112$	$5° < \psi < 10°$	30' x 30'	Point mass
Outer	Outer	$1112 \leq r_0 \leq 5560$	$10° \leq \psi \leq 50°$	1° x 1°	Point mass
	Remote	$5560 < r_0$	$50° < \psi$	5° x 5°	Point mass

†*Definition of "rectangular" sub-zones, bounded by a single meridian or parallel on each side (e.g. as used by* FRYER [1970, p.114]*), is unmanageable when global summations are involved, because of convergence of the meridians towards the poles. Such a definition becomes meaningless when one of the poles lies within a sub-zone. Moreover — since it is time consuming and not necessary to evaluate* ψ *for each quad if computations are in terms of geocentric cartesian coordinates (see §3.2) — the definition of sub-zones using angular distance from the computation point would also be inconvenient. For these reasons the spatial radius* r_0 *(see figure 3.1), which is easily computed by a formula similar to equation 3.4, was used to delimit the sub-zones. The values given in kilometres, though approximate equivalents of the angular quantities, are definitive.*

3

Topographic-Isostatic Model

3.1 INTRODUCTION

In the last chapter it was stated that the geometry and composition of the topographic-isostatic model enter the problem directly through the integral equations. A rigorous, mathematical difinition of these aspects of the model will now be presented. Some practical consequences of the adopted model will also be investigated.

COMPONENTS OF THE MODEL. The major components of the model are illustrated in figure 3.1. All dimensions are referred to a *reference surface* which thereby determines the global geometry of the model. This is further affected by the choice of an *isostatic compensation system* and the presumed *density model*. At a finer level, the geometry of an individual *quadrature subdivision* must be investigated and its contribution to the total model defined.

3.2 REFERENCE SURFACE AND ASSOCIATED GEOMETRY

DEFINITION

Strictly, as a direct consequence of the Stokes' approach, the reference surface should be the geoid. This dependence is further amplified by the usual inherent relation between measured topographic data and the geoid. However, use of the geoid as a reference surface in the context of a basic topographic-isostatic model is intolerable, largely because of its non-analytical nature. In any case, the effect of the geoidal undulations on the solution of the problem in hand can be expected to be negligible. A spheroidal surface provides a suitable alternative and the *Reference Ellipsoid 1967* [I.A.G. 1967] ($a = 6\,378\,160$ m, $f = 1/298.25$) was adopted. Normal gravity on this surface, which is necessary in the application of equations 1.5 and 1.6, is given by [I.A.G. 1971]:

$$\gamma_0 \text{ (N/kg)} = 9.780\,318\,(1 + 5.3024 \times 10^{-3} \sin^2\phi - 5.9 \times 10^{-6} \sin^2 2\phi). \tag{3.0}$$

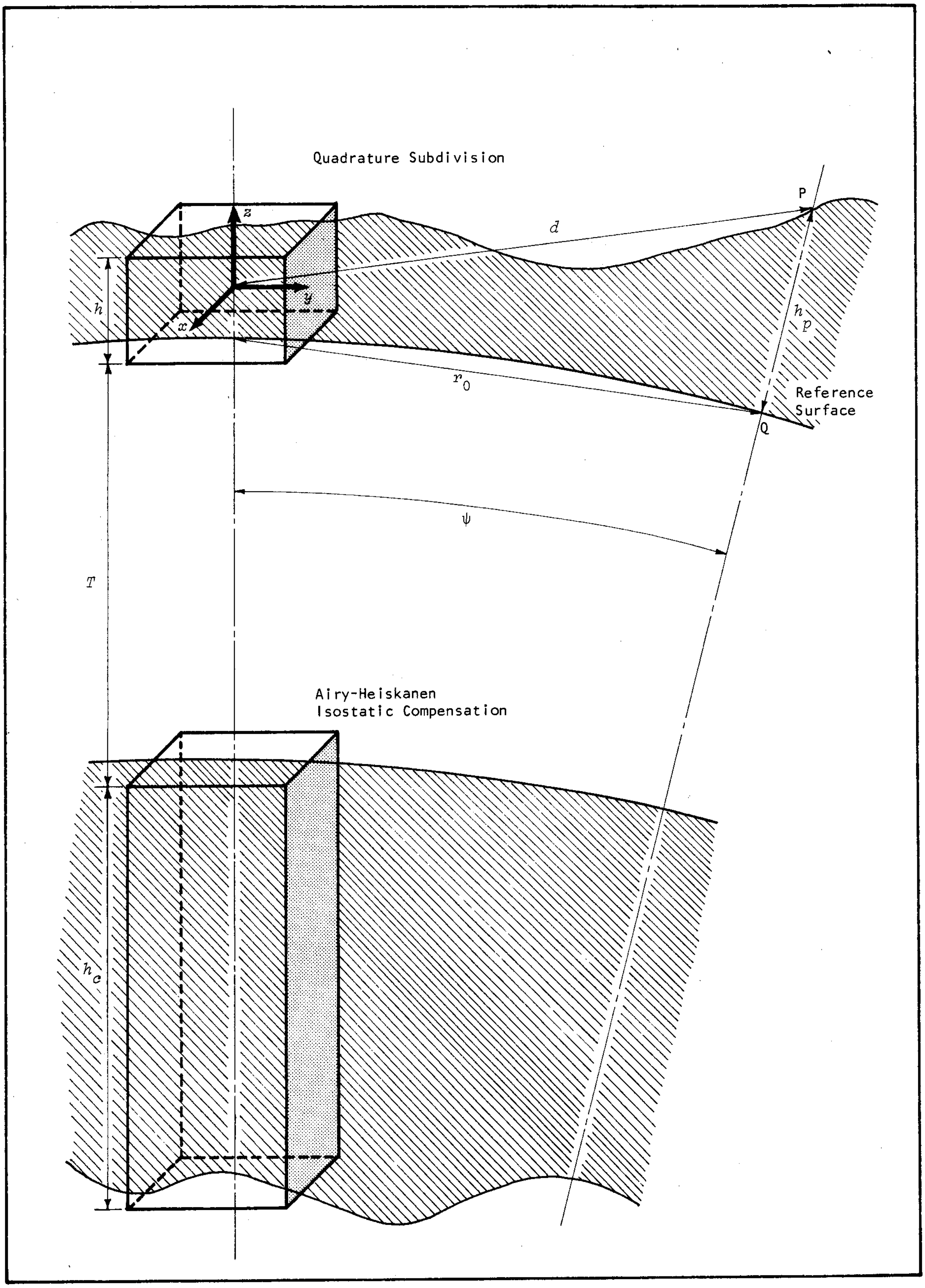

FIGURE 3.1

GEOMETRY OF THE TOPOGRAPHIC-ISOSTATIC MODEL

It might be argued that a spherical reference surface would be adequate—with accuracy to the order of the flattening—but, in terms of cartesian geometry, there is little advantage in this simplification. This is evident in the coordinate transformation equations developed below. The influence of the degree of curvature of the reference surface is investigated in §3.5.

SPATIAL GEOMETRY

TRANSFORMATIONS IN A CARTESIAN SYSTEM. With the reference surface defined, it becomes possible to write the various coordinate transformation equations—which will be required later—in specific form. Since gravity evaluation invariably requires a knowledge of the *spatial* ("straight line") *distance* d between the evaluation point P and a gravitating mass particle at M (figure 3.2), it is logical, and simpler, to work in a consistent cartesian coordinate system. The geocentric cartesian system (X,Y,Z) defined in §1.4 is suitable.

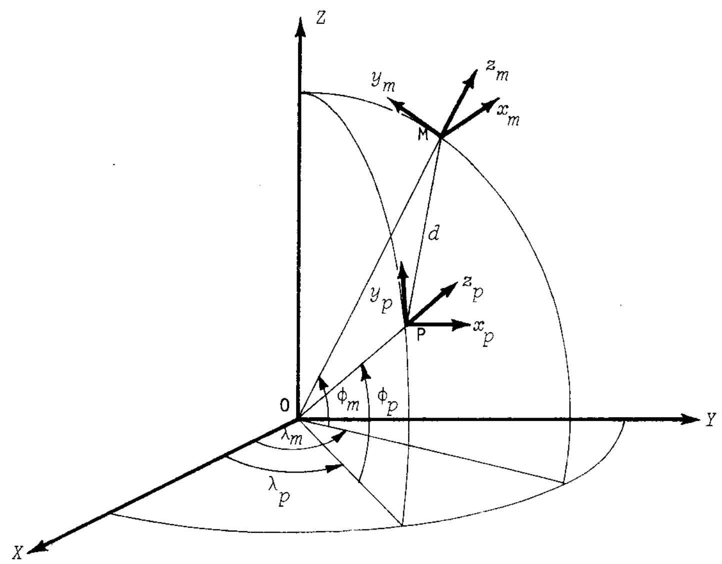

FIGURE 3.2
COORDINATE TRANSFORMATIONS

Applying the plane geometry of a meridional ellipse, the transformation from "geodetic" coordinates (ϕ,λ,z_0) of any point to the geocentric cartesian system may be written as [HEISKANEN and MORITZ 1967, p.182]:

$$X = (\nu + z_0)\ \cos\phi\ \cos\lambda$$
$$Y = (\nu + z_0)\ \cos\phi\ \sin\lambda$$
$$Z = [\nu(1 - e^2) + z_0]\ \sin\phi\ , \qquad (3.1)$$

where ν is the prime vertical radius of curvature of the ellipsoid, given by:

$$\nu = \frac{a}{(1 - e^2\ \sin^2\phi)^{\frac{1}{2}}}\ , \qquad (3.2)$$

and e is the ellipsoidal eccentricity, which is related to the flattening by the equation

$$e^2 = 2f - f^2. \qquad (3.3)$$

Then the spatial distance d between P and M is given by

$$d = [(X_p - X_m)^2 + (Y_p - Y_m)^2 + (Z_p - Z_m)^2]^{\frac{1}{2}} \qquad (3.4)$$

where (X_p, Y_p, Z_p) are the geocentric coordinates of P,

and (X_m, Y_m, Z_m) are the coordinates of M in the same system.

On occasion it will also be necessary to transform a gravity vector, expressed in a local cartesian system at M, to a similar local system at P. This may be achieved by a series of axes rotations; whence, by equation 1.8:

$$\begin{bmatrix} G_{xp} \\ G_{yp} \\ G_{zp} \end{bmatrix} = \mathsf{R} \begin{bmatrix} G_{xm} \\ G_{ym} \\ G_{zm} \end{bmatrix} , \tag{3.5}$$

where: G_{xm}, G_{ym}, G_{zm} are the components of a gravity vector $\mathbf{G}$ at M in the local system (x_m, y_m, z_m),

G_{xp}, G_{yp}, G_{zp} are the components of $\mathbf{G}$ in the local system (x_p, y_p, z_p) at P,

and R is the combined rotation matrix given by

$$\mathsf{R} = \mathsf{R}_4 \, \mathsf{R}_3 \, \mathsf{R}_2 \, \mathsf{R}_1 \tag{3.6}$$

where the individual rotation matrices are defined in table 3.1 (with reference to figure 3.2).

TABLE 3.1
SPECIFICATION OF ROTATION MATRICES

MATRIX	ANGLE OF ROTATION	AXIS OF ROTATION	RESULT
R_1	$-(90° - \phi_m)$	x_m	$z_m \parallel Z$
R_2	$-(90° + \lambda_m)$	Z	$x_m \parallel X$
R_3	$(90° + \lambda_m)$	Z	$X \parallel x_p$
R_4	$(90° - \phi_m)$	x_p	$Z \parallel z_p$

Use of equations 1.9 provides the values of the individual matrices:

$$\mathsf{R}_1 = \begin{bmatrix} 1 & 0 & 0 \\ 0 & \sin\phi_m & -\cos\phi_m \\ 0 & \cos\phi_m & \sin\phi_m \end{bmatrix} , \quad \mathsf{R}_2 = \begin{bmatrix} -\sin\lambda_m & -\cos\lambda_m & 0 \\ \cos\lambda_m & -\sin\lambda_m & 0 \\ 0 & 0 & 1 \end{bmatrix}$$

$$\mathsf{R}_3 = \begin{bmatrix} -\sin\lambda_p & \cos\lambda_p & 0 \\ -\cos\lambda_p & -\sin\lambda_p & 0 \\ 0 & 0 & 1 \end{bmatrix} \quad \mathsf{R}_4 = \begin{bmatrix} 1 & 0 & 0 \\ 0 & \sin\phi_p & \cos\phi_p \\ 0 & -\cos\phi_p & \sin\phi_p \end{bmatrix} . \tag{3.7}$$

Although it is possible to evaluate R, subsequent applications of this theory will be better served by separating the transformation process into two stages: first a transformation to the geocentric system and then a separate transformation from the geocentric to the local system at P. The first stage is represented by

$$\begin{bmatrix} G_X \\ G_Y \\ G_Z \end{bmatrix} = \mathbf{R}_2 \mathbf{R}_1 \begin{bmatrix} G_{xm} \\ G_{ym} \\ G_{zm} \end{bmatrix}, \tag{3.8}$$

which leads to the working equations

$$\begin{aligned} G_X &= G_{zm} \cos \lambda_m \cos \phi_m - G_{ym} \cos \lambda_m \sin \phi_m - G_{xm} \sin \lambda_m, \\ G_Y &= G_{zm} \sin \lambda_m \cos \phi_m - G_{ym} \sin \lambda_m \sin \phi_m - G_{xm} \cos \lambda_m, \\ G_Z &= G_{zm} \sin \phi_m + G_{ym} \cos \phi_m. \end{aligned} \tag{3.9}$$

Similarly the second stage is

$$\begin{bmatrix} G_{xp} \\ G_{yp} \\ G_{zp} \end{bmatrix} = \mathbf{R}_4 \mathbf{R}_3 \begin{bmatrix} G_X \\ G_Y \\ G_Z \end{bmatrix}, \tag{3.10}$$

which becomes

$$\begin{aligned} G_{xp} &= G_{yp} \cos \lambda_p - G_{xp} \sin \lambda_p, \\ G_{yp} &= G_{zp} \cos \phi_p - G_{yp} \sin \phi_p \sin \lambda_p - G_{xp} \sin \phi_p \cos \lambda_p, \\ G_{zp} &= G_{zp} \sin \phi_p + G_{yp} \cos \phi_p \sin \lambda_p + G_{xp} \cos \phi_p \cos \lambda_p. \end{aligned} \tag{3.11}$$

A further prerequisite of the later development is the ability to express the coordinates of P (x_{pm}, y_{pm}, z_{pm}) in terms of the local cartesian system at M. This coordinate change may be envisaged as an application of the second stage of the transformation just outlined, where the vector concerned is now the position vector of P with respect to M. Alternatively, systematic utilization of the translation equations 1.7 and rotation equation 3.10 provides the same result, namely

$$\begin{aligned} x_{pm} &= (Y_p - Y_m) \cos \lambda_m - (X_p - X_m) \sin \lambda_m, \\ y_{pm} &= (Z_p - Z_m) \cos \phi_m - (Y_p - Y_m) \sin \phi_m \sin \lambda_m - (X_p - X_m) \sin \phi_m \cos \lambda_m, \\ z_{pm} &= (Z_p - Z_m) \sin \phi_m + (Y_p - Y_m) \cos \phi_m \sin \lambda_m + (X_p - X_m) \cos \phi_m \cos \lambda_m. \end{aligned} \tag{3.12}$$

TRANSFORMATIONS IN A SPHERICAL SYSTEM. In some circumstances a spherical approximation of the reference surface may be preferable, and a transformation to local polar coordinates at P may be useful. Solution of the spherical triangle NPM (figure 3.3) then gives:

$$\cos \psi = \sin \phi_p \sin \phi_m + \cos \phi_p \cos \phi_m \cos (\lambda_m - \lambda_p) \tag{3.13}$$

and

$$\tan \alpha = \frac{\sin (\lambda_m - \lambda_p)}{\tan \phi_m \cos \phi_p - \sin \phi_p \cos (\lambda_m - \lambda_p)} \tag{3.14}$$

Application of the cosine rule in the plane triangle of the normal section (OPM) (figure 3.4) provides the distance d:

$$d^2 = 2(R + h_p)(R + h_m)(1 - \cos \psi) + (h_p - h_m)^2. \tag{3.15}$$

The relative simplicity of the cartesian approach is immediately evident. And it is significant

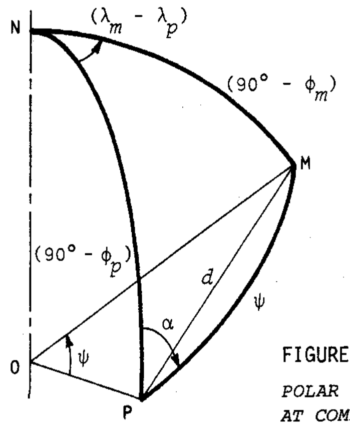

FIGURE 3.3
POLAR COORDINATES AT COMPUTATION POINT

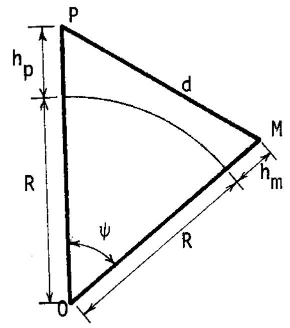

FIGURE 3.4
NORMAL SECTION THROUGH PM.

that the geometry of the reference surface enters the development only in the transformation to a geocentric system (equation 3.1). Thereafter, plane cartesian geometry prevails.

3.3 ISOSTATIC COMPENSATION SYSTEM

DEFINITION

Of the systems outlined in §1.4, the Airy-Heiskanen isostatic compensation model was adopted as one which reasonably fits the available evidence, without introducing the unmanageable complexity of a regional model (such as Vening Meinesz') into the process of storing and accessing the digital data. It has the further advantage of conforming with other studies, thus facilitating comparison of results. HEISKANEN and MORITZ [1967, p.135] give a fundamental definition of the system and this is assumed here as a basis for further refinement.

Figure 3.5 depicts the basic hypothesis of floating equilibrium, the condition for this status being

$$\bar{h}_c(\sigma_1 - \sigma_t) = h\sigma_t, \tag{3.16}$$

where all symbols are as defined in the figure. This condition presumes *mass equilibrium* between the topography and its compensation. Crustal thickness (at "mean sea level") is assumed to be constant at

$$T = 30\,000 \text{ metres.} \tag{3.17}$$

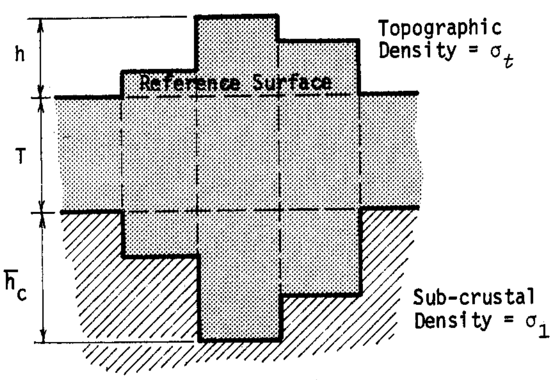

FIGURE 3.5 *AIRY-HEISKANEN ISOSTATIC COMPENSATION SYSTEM*

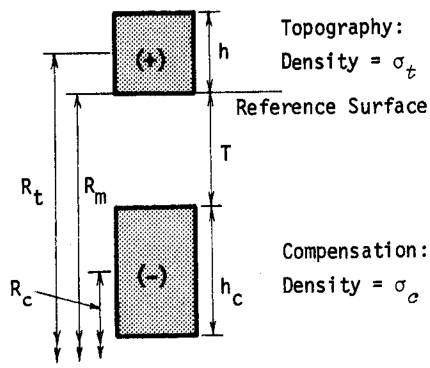

FIGURE 3.6 *TOPOGRAPHIC-ISOSTATIC MODEL*

If, as in the present study, the topography and compensation are artificially isolated from the remainder of the earth's structure, the model shown in figure 3.6 results. Here the topographic mass M_t, of density σ_t, is "balanced" by the mass *deficiency* M_c of the compensation, where its density is given by

$$\sigma_c = \sigma_t - \sigma_1. \tag{3.18}$$

Given the densities and the height of topography, it is possible to deduce the height of the compensation by rewriting equation 3.16, thus

$$\bar{h}_c = \frac{\sigma_t h}{\sigma_c}. \tag{3.19}$$

CORRECTION FOR SPHERICITY. Equation 3.19 tacitly includes a plane reference surface in the model. This is not sufficiently accurate and a correction for the effect of sphericity must be introduced. Its magnitude may be such as to alter $\bar{h}_c$ by up to 1.7%.

As the correction sought is small, the compound curvature of the spheroidal reference surface may be replaced locally by a spherical surface. The radius of this assumed sphere R_m is usually made equal to the local mean radius of the spheroid, that is

$$R_m = (\rho\nu)^{\frac{1}{2}}, \tag{3.20}$$

where ρ and ν are the radii of curvature of the spheroid in the meridian and prime vertical normal sections, respectively. Under these conditions the topographic-isostatic masses are

$$\begin{aligned} M_t &\simeq \sigma_t h A_t, \\ M_c &\simeq \sigma_c h_c A_c, \end{aligned} \tag{3.21}$$

where A_t and A_c are the areas of "mean" sections of the topographic and compensatory blocks respectively, and h_c is the *corrected* height of compensation. (These equations are approximate, but adequate for the purpose: exact expressions are given in §3.4). Substituting equation 3.32 for the areas and equating the two masses leads to

$$\begin{aligned} h_c &= \frac{\sigma_t R_t^2 h}{\sigma_c R_c^2} \\ &= \frac{\bar{h}_c R_t^2}{R_c^2}, \end{aligned} \tag{3.22}$$

where R_t and R_c are the spherical radii of the mid heights of the topography and compensation respectively, (figure 3.6). Thus

$$R_t = R_m + h_t/2 . \tag{3.23}$$

In equation 3.22 R_c is a function of h_c and is therefore unknown; however, an iterative procedure—beginning with an estimate of h_c $(\hat{h}_c)$ from equation 3.19—provides an acceptable solution. Then an estimate of R_c given by

$$\hat{R}_c = R_m - T + \hat{h}_c/2 , \tag{3.24}$$

may be used to solve equation 3.22. Further iteration is possible, but unnecessary. Initially, each iteration improves the value of h_c by about 0.01%. It should be noted that h_c is a negative quantity, according to the definition of σ_c in equation 3.18.

ICE CORRECTION. Substantial areas of ice occur in Antarctica and Greenland. These ice sheets reach thicknesses up to 4800 and 3300 metres respectively and comprise the major bulk of the topographic volume. They cannot be ignored in the definition of a topographic-isostatic model.

FRYER [1970, p.116], in his formulation of the indirect effect, took account of only the Antarctic ice by condensing it to an equivalent rock thickness, according to the ice/rock density contrast. He was then able to proceed with a *global* rock density function. For a number of reasons adoption of this procedure in the present investigation was considered unsatisfactory:

(a) The mass redistribution involved in condensation would induce sizeable errors in the potential and gravity due to the inner zones.

(b) Inclusion of the "equivalent" rock thickness in a global density function, derived empirically from geological sampling (see below) is a questionable procedure.

(c) Recent radar profiling and other techniques have provided a remarkable improvement in the knowledge of the physical characteristics, including thickness, of the ice caps [BUDD *et al.* 1971], so that a more realistic model, which can incorporate this data, is justifiable.

In order to study their effects, a decision was made to separately compute the contributions to the total potential and gravity due to the ice, using specially developed routines (see §7.3). However, difficulties in computer scheduling and data management made it necessary to complete the main computations using a global density model in which the volumes known to be occupied by ice were assumed to be composed of rock. It was then possible to rectify the excess contributions of this false model by separately evaluating a set of "ice corrections", based on a model of the ice/rock contrast. This "less direct" procedure does not greatly detract from the initial objective of studying the global effects of the ice caps on the gravity field.

Figure 3.7 illustrates the derivation of the topographic-isostatic model for the ice correction.

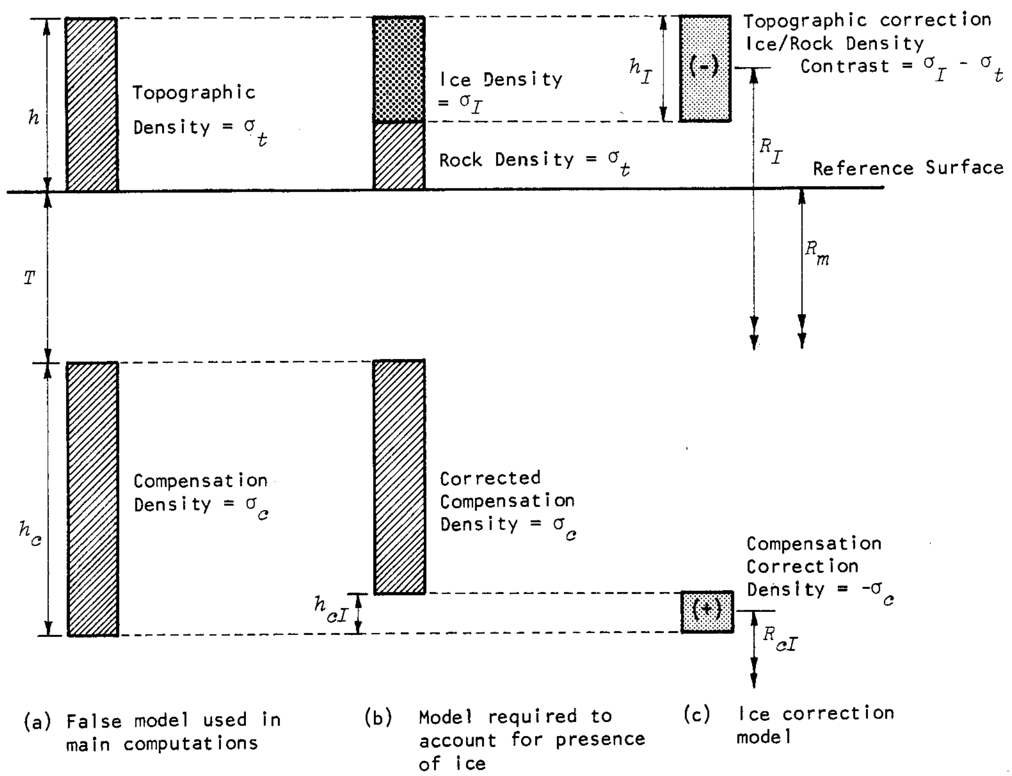

FIGURE 3.7 *TOPOGRAPHIC-ISOSTATIC MODEL FOR ICE CORRECTIONS*

(a) shows the false model adopted in the main computations, where the topography is assumed to be entirely rock of density σ_t. In (b) the model required to correctly account for the presence of ice, of density σ_I and height h_I, is shown. Here the height of compensation has to be reduced by an amount h_{cI} to allow for the reduction in topographic mass. The difference between these models gives the necessary ice correction model (c); comprising a topographic component of density equal to the ice/rock contrast and height equal to the ice thickness, and a compensation component of height h_{cI} and density equal to the normal compensation density with opposite sign. A correction for sphericity may be applied in the same manner as outlined above, so that to maintain equilibrium the height of the compensation correction must be

$$h_{cI} = \frac{(\sigma_I - \sigma_t)h_I R_I^2}{-\sigma_c R_{cI}^2} \tag{3.25}$$

where: σ_I is the density of ice,

h_I is the ice thickness,

and R_I is the spherical radius of the mid height of the ice, given by

$$R_I = R_m + h + h_I/2. \tag{3.26}$$

In equation 3.25 R_{cI}, which is the spherical radius of the mid height of the compensation correction, is unknown, but it can be determined from an estimate of the value of h_{cI} given by

$$\hat{h}_{cI} = \frac{(\sigma_I - \sigma_t)h_I}{\sigma_c}, \tag{3.27}$$

whence

$$R_{cI} = R_m - T + h_c + \hat{h}_{cI}/2 . \tag{3.28}$$

As before, a single iteration is sufficient. It should be observed that h_I is a negative quantity and h_{cI} is positive, while the density of the topographic component is negative and that of the compensation component is positive.

Computation of the ice corrections was made to conform to the specifications stated in §2.4.

DENSITY MODEL

The composition of the topography and isostatic compensation needs to be defined in terms of some global density model. Once again the non-analytical nature of such a physical characteristic must be overcome by introduction of some analytical function or a global, digital model. The latter alternative cannot easily be realized at this time, even though it might be feasible. Global topographic density functions are, however, available and have been employed in recent studies of Stokes' problem [*e.g.* MATHER 1968a, p.9; FRYER 1970, p.114]. For the sake of congruity, the function used in these studies, and originally proposed by de GRAAFF-HUNTER [1966], has been maintained here. This formula, which was based on global sampling, relates the density of a topographic column to the height of the terrain surface thus:

$$\sigma_t \text{ (kg m}^{-3}) = \begin{cases} 2770 - h/21 & \text{for } h \le 2100 \text{ metres} \\ 2670 & \text{for } h > 2100 \text{ metres} \end{cases} \tag{3.29}$$

Constant values were adopted for the sub-crustal density [after HEISKANEN and MORITZ 1967, p.135] and the density of ice [BALMINO *et al* 1973] as follows:

$$\text{Sub-crustal density } \sigma_1 = 3270 \text{ kg m}^{-3}, \tag{3.30}$$

$$\text{Density of ice } \sigma_I = 917 \text{ kg m}^{-3}. \tag{3.31}$$

3.4 QUADRATURE MODELS — THE TESSEROID AND ITS GEOMETRIC APPROXIMATION

DEFINITION

Depending on need, a quadrature subdivision may be defined geometrically in terms of ellipsoidal, spherical, or rectangular coordinate systems. Should the ellipsoidal form be chosen, a rigorous definition of the quadrature model would embody parts of three pairs of surfaces: (a) a pair of confocal spheroids, determined by the definitive parameters of the reference surface and the height of the subdivision; (b) a pair of similarly confocal hyperboloids, related to the latitude bounds of the subdivision; and (c) a pair of meridional planes, defining the longitude boundaries. In most cases the simpler geometry of a spherical approximation to the ellipsoidal model ensures adequate accuracy. The spherical model, which results as a limiting case of the ellipsoidal definition, is similarly constructed of portions of three pairs of surfaces: (a) two concentric spheres, defined by the local mean radius (R_m) (equation 3.20) and the height (h) of the subdivision; (b) two coaxial cones, defined by the latitude bounds of the subdivision (ϕ_1, ϕ_2); and (c) a pair of meridional planes, defined by the longitude boundaries (λ_1, λ_2), (see figure 3.8).

Succinct terminology for such shapes seems to be unresolved. As a matter of convenience, they will be referred to hereafter by the generic term "tesseroid", qualified by "ellipsoidal" or "spherical" as may be appropriate.

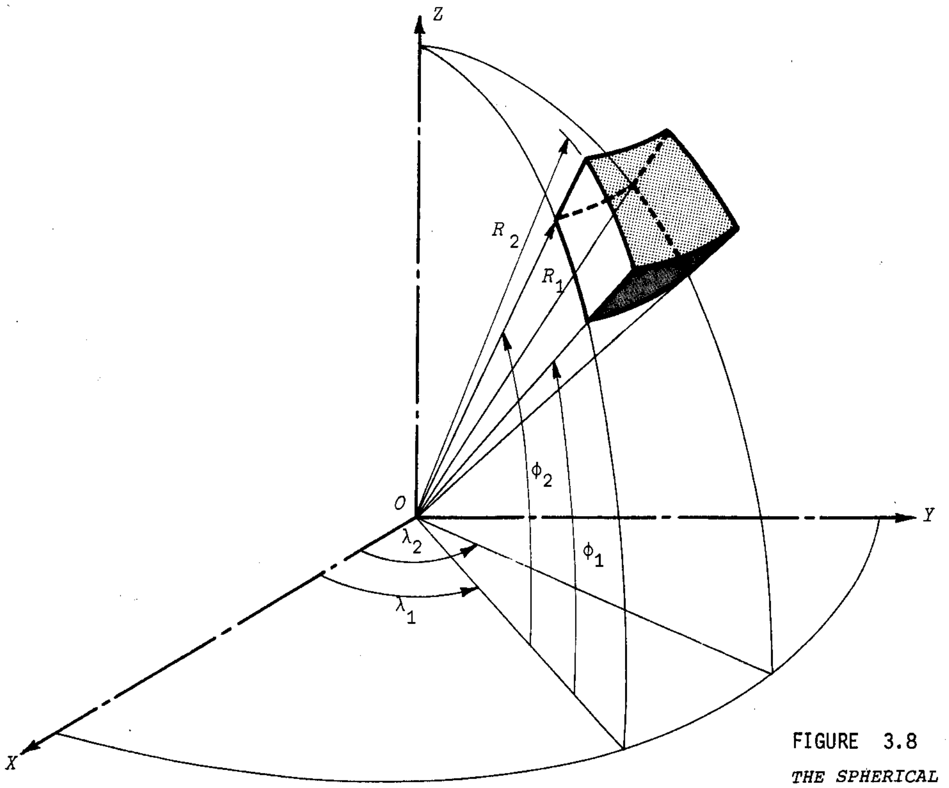

FIGURE 3.8
THE SPHERICAL TESSEROID

Formulation of the inner zone effects necessitates approximation of the tesseroid by a rectangular quadrature model. For this purpose a rectangular parallelepiped of equivalent volume, with dimensions $2a$, $2b$, $2c$, may be "fitted" to the tesseroid.

GEOMETRIC AND PHYSICAL PROPERTIES

AREA OF A QUADRATURE SUBDIVISION ON A SPHERE. Usually the surface area of a quadrature subdivision with latitude and longitude dimensions $\Delta\phi$ and $\Delta\lambda$, at mid-latitude ϕ_μ on a sphere of radius R, is taken to be

$$A \simeq R^2 \cos \phi_\mu \, \Delta\phi \, \Delta\lambda, \tag{3.32}$$

which is substantially correct, in so far as the elements of latitude and longitude are small. When the subdivision is not small (such as occurs in the outer zone), or an exact expression is required, the area may be derived by differencing two spherical caps, bounded by the parallels of latitude ϕ_1 and ϕ_2 (figure 3.9).

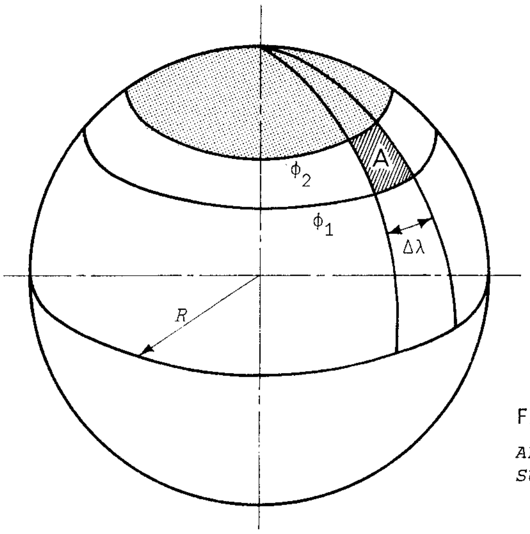

FIGURE 3.9
AREA OF A QUADRATURE SUBDIVISION ON A SPHERE

Since the area of a spherical cap is

$$A_C = 2\pi R^2(1 - \sin \phi),$$

the area of the subdivision must be

$$A = R^2(\sin \phi_2 - \sin \phi_1) \, \Delta\lambda, \tag{3.33}$$

where $\Delta\lambda$ is the longitude difference in radians.

This formula reduces to equation 3.32 if $\Delta\phi$ is small, since

$$\sin \phi_2 - \sin \phi_1 = 2 \cos \left(\frac{\phi_2 + \phi_1}{2}\right) \sin \left(\frac{\phi_2 - \phi_1}{2}\right)$$

$$\simeq \cos \phi_\mu \, \Delta\phi.$$

VOLUME OF A SPHERICAL TESSEROID. Although the volume of a spherical tesseroid may be derived using conventional solid geometry—by a combination of cones and segments of spheres—a more elegant solution is available through the application of the second theorem of Pappus. This theorem states that: *"If a plane area revolve about an axis in its plane, not intersecting it, the volume generated is equal to the area multiplied by the length of the path of its mean centre"* [LAMB 1956, p.266]. "Mean centre" is understood to be synonymous with "centroid".

In figure 3.10 the required volume v will be obtained by revolving the area A_s of the truncated sector *IJKL* (*i.e.* meridian section of the tesseroid) through an angle $\Delta\lambda$ about axis *OZ*. Hence the volume is

$$v = \textit{area IJKL} \times \textit{arc length of centroid path}$$

$$= A_s \times R_C \cos\left(\frac{\phi_2 + \phi_1}{2}\right) \Delta\lambda \tag{3.34}$$

where R_C is the spherical radius of the centroid C of the area $IJKL$, which must lie on its axis of symmetry OE. Equating moments about O gives

$$A_s R_C = A''R'' - A'R' , \tag{3.35}$$

where: R', R'' are the geocentric spherical radii of the centroids of the sectors OIJ and OKL, and A', A'' are the areas of those sectors respectively.

The radii are given by [BULLEN 1951, p.169]

$$R' = \frac{2R_1 \sin\varepsilon}{3\varepsilon}, \qquad R'' = \frac{2R_2 \sin\varepsilon}{3\varepsilon}, \tag{3.36}$$

and the areas by

$$A' = \varepsilon R_1^2, \qquad A'' = \varepsilon R_2^2, \tag{3.37}$$

where

$$\varepsilon = \tfrac{1}{2}(\phi_2 - \phi_1). \tag{3.38}$$

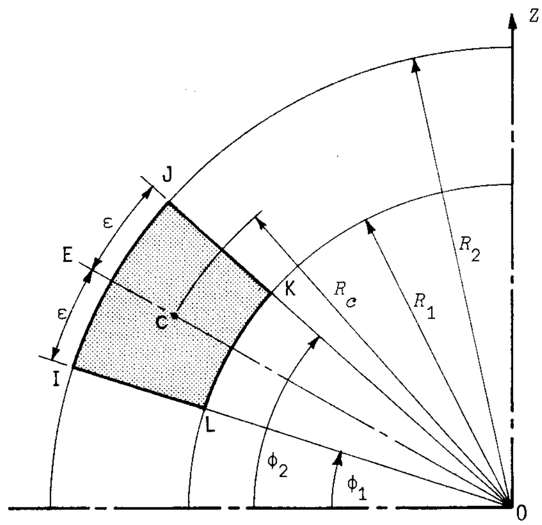

FIGURE 3.10
VOLUME OF A SPHERICAL TESSEROID

Substituting equations 3.36 and 3.37 into 3.35 gives

$$A_s R_C = \frac{2}{3}(R_2^3 - R_1^3) \sin\varepsilon, \tag{3.35a}$$

which may be substituted into equation 3.34 to give the volume

$$v = \frac{\Delta\lambda}{3}(R_2^3 - R_1^3) \times 2 \sin\left(\frac{\phi_2 - \phi_1}{2}\right) \cos\left(\frac{\phi_2 + \phi_1}{2}\right)$$

$$= \frac{\Delta\lambda}{3}(R_2^3 - R_1^3)(\sin\phi_2 - \sin\phi_1). \tag{3.39}$$

This result may be checked by integrating equation 3.33 with respect to R.

MASS OF A NON-HOMOGENEOUS SPHERICAL TESSEROID. The density model defined in §3.3 assumes homogeneity within each quadrature subdivision. How much this model departs from reality is generally uncertain, but it may be supposed that some degree of vertical density stratification occurs in the topography. Almost any such distribution could be modelled by varying the parameters of a vertical *linear* density function of the form

$$\sigma = \sigma_0 + Dz, \tag{3.40}$$

where: z is altitude in a local coordinate system;

σ_0 is a homogeneous component of the density, being the density at zero altitude;

D is the vertical density gradient.

Introduction of this function allows the theoretical development to be applied in an investigation of the effects of density distribution. Also, the linear function is indispensable in the study of atmospheric effects (chapter 9). In the following development the somewhat artificial concept of density as a function of geocentric spherical radius — rather than altitude — will be required. For this purpose equation 3.40 may be transformed as follows:

$$\begin{aligned} \sigma &= \sigma_0 + D(R - R_m) \\ &= \sigma_G + DR, \end{aligned} \tag{3.41}$$

where σ_G is the "apparent" density at the geocentre, given by

$$\sigma_G = \sigma_0 - DR_m. \tag{3.42}$$

Then to obtain the mass of a spherical tesseroid M it is necessary to perform integration with respect to the spherical radius only. Thus, using the aforenamed symbols,

$$M = \int_{R_1}^{R_2} \sigma \, dv$$

and, substituting equations 3.41 and 3.33,

$$M = A \int_{R_1}^{R_2} (\sigma_G + DR) R^2 \, dR, \tag{3.43}$$

where A is the surface area of the quadrature subdivision on a unit sphere. Expanding equation 3.43 and integrating the separate components leads to

$$M = A\left[\frac{\sigma_G}{3} (R_2^3 - R_1^3) + \frac{D}{4} (R_2^4 - R_1^4) \right]. \tag{3.44}$$

CENTRE OF MASS OF A NON-HOMOGENEOUS SPHERICAL TESSEROID. Implementation of the point mass assumption outlined for the non-contact zones in §2.3 requires that the mass of the quadrature subdivision be concentrated at its centre of mass. When the density is non-homogeneous the centroid and centre of mass of the tesseroid do not coincide. Further, since the tesseroid has only one symmetry plane — the meridian plane of mid longitude — neither of these points lies in the surfaces of mid latitude or mid radius. Consequently the centre of mass T is best located by a geocentric position vector $\mathbf{T}$, defined by [BULLEN 1951, p.166]:

$$M\mathbf{T} = \iiint_v \sigma \, \mathbf{X} \, dv, \tag{3.45}$$

where

$$\mathbf{X} = X\mathbf{i} + Y\mathbf{j} + Z\mathbf{k} \tag{3.46}$$

is the position vector of an element of mass σdv, which has geocentric coordinates (X,Y,Z), and $\mathbf{i}$, $\mathbf{j}$, $\mathbf{k}$ are unit vectors parallel to the geocentric cartesian axes. Resolution into components gives the coordinates of the centre of mass (X_T, Y_T, Z_T)

$$MX_T = \iiint_v \sigma X dv, \qquad MY_T = \iiint_v \sigma Y dv, \qquad MZ_T = \iiint_v \sigma Z dv. \tag{3.47}$$

Solution of these integrals is best achieved after transformation to a spherical reference frame, in which

$$\begin{aligned} X &= R \cos\phi \cos\lambda, \\ Y &= R \cos\phi \sin\lambda, \\ Z &= R \sin\phi, \end{aligned} \tag{3.48}$$

and

$$\begin{aligned} dv &= dX\, dY\, dZ \\ &= \mathrm{J}\, d\phi\, d\lambda\, dR, \end{aligned} \tag{3.49}$$

where the transformation Jacobian (equation 1.11) is

$$\mathrm{J} = R^2 \cos\phi. \tag{3.50}$$

If the same radial density function (equation 3.41) is assumed, equations 3.47 become

$$MX_T = \int_{R_1}^{R_2}\int_{\lambda_1}^{\lambda_2}\int_{\phi_1}^{\phi_2} (\sigma_G + DR)\, R^3 \cos^2\phi \cos\lambda \, d\phi\, d\lambda\, dR,$$

$$MY_T = \int_{R_1}^{R_2}\int_{\lambda_1}^{\lambda_2}\int_{\phi_1}^{\phi_2} (\sigma_G + DR)\, R^3 \cos^2\phi \sin\lambda \, d\phi\, d\lambda\, dR,$$

$$MZ_T = \int_{R_1}^{R_2}\int_{\lambda_1}^{\lambda_2}\int_{\phi_1}^{\phi_2} (\sigma_G + DR)\, R^3 \sin\phi \cos\lambda \, d\phi\, d\lambda\, dR. \tag{3.51}$$

Successive application of standard integral forms and some slight rearrangement of the trigonometric terms leads to the solutions, wherein M is given by equation 3.44:

$$X_T = \frac{(\Delta\phi + \cos 2\phi_\mu \sin\Delta\phi)(\sin\lambda_2 - \sin\lambda_1)\left\{\frac{\sigma_G}{4}(R_2^4 - R_1^4) + \frac{D}{5}(R_2^5 - R_1^5)\right\}}{2\Delta\lambda(\sin\phi_2 - \sin\phi_1)\left\{\frac{\sigma_G}{3}(R_2^3 - R_1^3) + \frac{D}{4}(R_2^4 - R_1^4)\right\}},$$

$$Y_T = \frac{(\Delta\phi + \cos 2\phi_\mu \sin\Delta\phi)(\cos\lambda_1 - \cos\lambda_2)\left\{\frac{\sigma_G}{4}(R_2^4 - R_1^4) + \frac{D}{5}(R_2^5 - R_1^5)\right\}}{2\Delta\lambda(\sin\phi_2 - \sin\phi_1)\left\{\frac{\sigma_G}{3}(R_2^3 - R_1^3) + \frac{D}{4}(R_2^4 - R_1^4)\right\}},$$

$$Z_T = \frac{\sin 2\phi_\mu \sin \Delta\phi \left\{ \frac{\sigma_G}{4} (R_2^4 - R_1^4) + \frac{D}{5} (R_2^5 - R_1^5) \right\}}{2(\sin \phi_2 - \sin \phi_1) \left\{ \frac{\sigma_G}{3} (R_2^3 - R_1^3) + \frac{D}{4} (R_2^4 - R_1^4) \right\}} . \tag{3.52}$$

These expressions may be usefully abbreviated to:

$$X_T = \frac{(2\varepsilon + \cos 2\phi_\mu \sin 2\varepsilon) \cos \lambda_\mu \sin \omega}{4\omega \cos \phi_\mu \sin \varepsilon} R_T'$$

$$Y_T = X_T \tan \lambda_\mu ,$$

$$Z_T = \frac{\sin 2\phi_\mu \sin 2\varepsilon}{4 \cos \phi_\mu \sin \varepsilon} R_T' ; \tag{3.53}$$

in which the following new notation has been introduced:

$$\lambda_\mu = \tfrac{1}{2}(\lambda_2 + \lambda_1), \tag{3.54}$$

$$\omega = \tfrac{1}{2}(\lambda_2 - \lambda_1) = \tfrac{1}{2}\Delta\lambda, \tag{3.55}$$

and

$$R_T' = \frac{\frac{\sigma_G}{4}(R_2^4 - R_1^4) + \frac{D}{5}(R_2^5 - R_1^5)}{\frac{\sigma_G}{3}(R_2^3 - R_1^3) + \frac{D}{4}(R_2^4 - R_1^4)} . \tag{3.56}$$

Simple dependence between X_T and Y_T arises because of longitudinal symmetry.

For small quadrature subdivisions — that is, when $\Delta\phi$ and $\Delta\lambda$ are both small — the equations 3.53 may be reduced to:

$$X_T \simeq R_T' \cos \phi_\mu \cos \lambda_\mu,$$

$$Y_T \simeq R_T' \cos \phi_\mu \sin \lambda_\mu,$$

$$Z_T \simeq R_T' \sin \phi_\mu; \tag{3.57}$$

and comparison with equations 3.48 shows that under these circumstances the centre of mass T has the approximate spherical coordinates $(\phi_\mu, \lambda_\mu, R_T')$. These relations hold to better than 0.1% for a 5°x5° quad. Since the height of a quad is small in comparison with the earth's radius, in equation 3.56:

$$R_2 - R_1 << R_\mu,$$

where

$$R_\mu = \tfrac{1}{2}(R_2 + R_1), \tag{3.58}$$

whence

$$R_T' \simeq R_\mu$$

for a *homogeneous* tesseroid, and the centre of mass may be considered to approximately coincide with its "mid point" $(\phi_\mu, \lambda_\mu, R_\mu)$.

EQUIVALENT RECTANGULAR PARALLELEPIPED. When replacing the spherical tesseroid by a rectangular parallelepiped the following criteria are exerted presumptively in the fitting process:

(a) equivalent volume,

(b) coincidence of centroids (but not necessarily centres of mass),

(c) alignment of equivalent axes.

Fulfilment of (a) necessitates definition of the dimensions of the parallelepiped in terms of those of the tesseroid. Equivalence of axes is taken to mean that respective dimensions are:

$$2a \equiv \Delta\lambda, \qquad 2b \equiv \Delta\phi, \qquad 2c \equiv \Delta R;$$

so that (a,b,c) are measured on the (x,y,z) axes respectively, of a local cartesian coordinate system. In achieving equivalent volume, recourse may be had once more to the theorems of Pappus and a corollary which generalizes the allowable motion of the generating area [LAMB 1956, p.268]. Thus equation 3.34 may be extended to

$$A_r \times 2a = A_s \times R_C \cos \tfrac{1}{2}(\phi_2 + \phi_1)\ \Delta\lambda. \tag{3.59}$$

where A_r is the rectangular area of the parallelepiped in the yz-plane. And, if a is defined by

$$2a = R_C \cos \tfrac{1}{2}(\phi_2 + \phi_1)\ \Delta\lambda, \tag{3.60}$$

then

$$A_r = A_s. \tag{3.61}$$

Applying Pappus' first theorem, which is merely a two-dimensional analogue of the second theorem, gives the area A_s swept out by the line of length $R_2 - R_1$, and equation 3.61 becomes (see figure 3.11):

$$2b \times 2c = \Delta\phi\ R_\mu \times (R_2 - R_1). \tag{3.62}$$

Then b and c may be defined by

$$2b = \Delta\phi\ R_\mu \tag{3.63}$$

and

$$\begin{aligned} 2c &= R_2 - R_1, \\ &= \Delta R. \end{aligned} \tag{3.64}$$

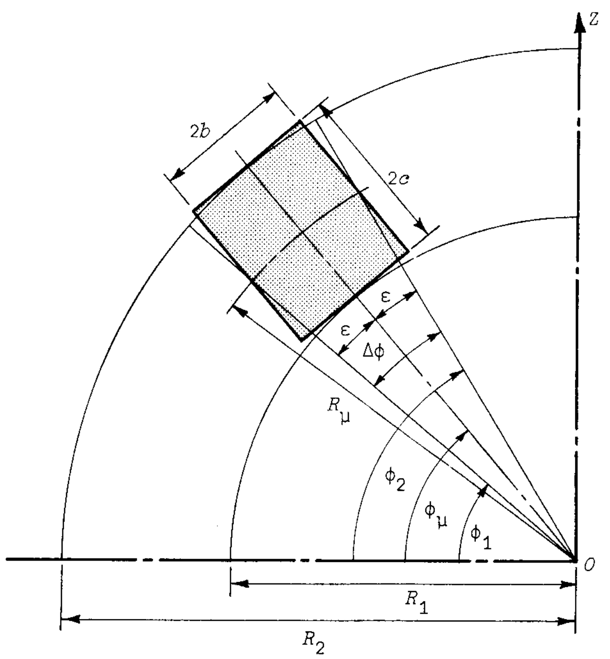

FIGURE 3.11
EQUIVALENT RECTANGULAR PARALLELEPIPED

To complete the definition of a an evaluation of R_C is required, which may be obtained by rewriting equation 3.35a thus:

$$R_C = \frac{2\, sin\, \varepsilon\, (R_2^3 - R_1^3)}{3A_s} \tag{3.65}$$

$$= \frac{2\, sin\, \varepsilon\, (R_2^3 - R_1^3)}{3\varepsilon(R_2^2 - R_1^2)}\,, \tag{3.66}$$

since A_s — the area of a truncated sector — is (see equations 3.37)

$$A_s = \varepsilon(R_2^2 - R_1^2). \tag{3.67}$$

Combining equations 3.60, 3.63 and 3.64 gives the volume of the equivalent parallelepiped as

$$v = R_C\, R_\mu\, cos\, \phi_\mu\, \Delta\phi\, \Delta\lambda\, \Delta R \tag{3.68}$$

$$\simeq R_\mu^2\, cos\, \phi_\mu\, \Delta\phi\, \Delta\lambda\, \Delta R. \tag{3.69}$$

Equation 3.69 demonstrates that the parallelepiped with the same height and mid altitude cross-sectional area as the tesseroid has approximately the same volume. In other words, the parallelepiped which possesses the "mean" dimensions of the tesseroid is almost volumetrically equivalent: a property which stems directly from the principle underlying the theorems of Pappus.

3.5 ERROR ANALYSIS AND PRACTICAL CONSEQUENCES OF MODEL

ERRORS IN RECTANGULAR PARALLELEPIPED MODEL

If a rectangular parallelepiped is to be adopted as the quadrature model two aspects of the resulting accuracy of representation are of sufficient consequence to warrant quantitative investigation. Both may engender systematic errors. First it must be ascertained that the mass of a subdivision is determined with adequate accuracy, and then the effect of mass displacement, arising from the changed shape of the subdivision, must be gauged.

VOLUMETRIC ACCURACY. Assuming homogeneity and no error in the density model defined by equations 3.29, the remaining source of error in mass representation lies in the adopted formula for volume. Equation 3.68 is rigorous, but the much simpler approximation offered by equation 3.69 is an attractive alternative. The errors introduced by this approximation, expressed with respect to the rigorous formula, are set out in table 3.2 for some typical situations.

TABLE 3.2
Volumetric Accuracy of Rectangular Parallelepiped Model

APPLICATION	LOCATION (metres)	DIMENSIONS	REL. ACCURACY $= \frac{R_C - R_\mu}{R_C}$
1. Inner Zone Topography	R_μ = 6 375 500	$\Delta\phi = \Delta\lambda = 0^\circ\!.1$ ΔR = 9000m	1 / 25 000 000 (0.04 ppm)
2. Inner Zone Compensation	R_μ = 6 321 000	$\Delta\phi = \Delta\lambda = 0^\circ\!.1$ ΔR = 40 000m	1 / 300 000 (33 ppm)
3. Remote Sub-zone Topography	R_μ = 6 373 500	$\Delta\phi = \Delta\lambda = 5^\circ$ ΔR = 5000m	1 / 3150 (317 ppm)
4. Remote Sub-zone Compensation	R_μ = 6 330 000	$\Delta\phi = \Delta\lambda = 5^\circ$ ΔR = 22 250m	1 / 3160 (316 ppm)

ERROR DUE TO MASS DISPLACEMENT. Transfiguration of a quadrature subdivision from a spherical tesseroid to a rectangular parallelepiped involves the displacement of a certain amount of mass, generally towards the geocentre. Although it is difficult to determine exactly the effect of this mass redistribution on the potential and attraction fields, a reasonable estimate may be made by adopting a point mass representation of the quantities involved. To some extent the inaccuracies of this approximation are internally cancelled by studying the *relative* disturbance of the fields.

Again assuming homogeneity, the amount of mass ΔM to be moved from above to below the mid altitude of the subdivision is (figure 3.12)

$$\begin{aligned} \Delta M &= \sigma(v_U - v_L) \\ &= \frac{\sigma\,\Delta\lambda}{6}(\sin\phi_2 - \sin\phi_1)(R_2^3 - 2R_\mu^3 + R_1^3), \end{aligned} \qquad (3.70)$$

where: v_U is the volume of the tesseroid above the mid altitude, and

v_L is the volume of the tesseroid below the mid altitude.

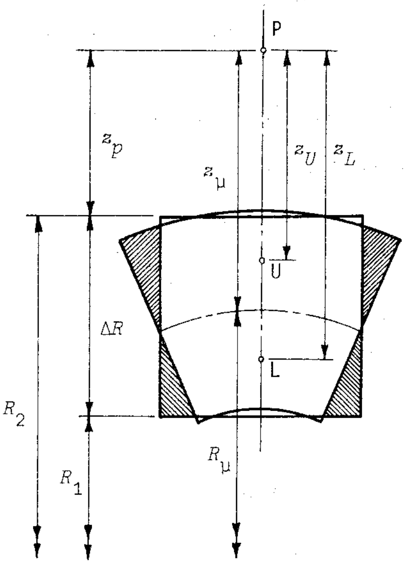

FIGURE 3.12

EFFECT OF MASS DISPLACEMENT IN ASSUMED QUADRATURE MODEL

Relative to the total mass this is

$$\frac{\Delta M}{M} = \frac{R_2^3 + R_1^3 - 2R_\mu^3}{R_2^3 - R_1^3}, \qquad (3.71)$$

which is a function of the height of the subdivision and its geocentric radius only. To anticipate the worst case it might be supposed that the computation point P is immediately above the subdivision, which is of maximum height ΔR, whence the disturbance of the potential and vertical component of gravity is greatest. Under these conditions the change in potential ΔV and gravity ΔG is due to the displacement of the point mass ΔM from U to L: the centres of mass of the upper and lower portions of the subdivision respectively. Expressed relative to the total field, these changes are

$$\frac{\Delta V}{V} = \frac{\Delta M\,(z_L - z_U)\,z_\mu}{M\,z_U\,z_L}, \qquad (3.72)$$

and

$$\frac{\Delta G}{G} = \frac{\Delta M \; (z_L^2 - z_U^2) \; z_\mu^2}{M \; z_U^2 \; z_L^2} \, , \tag{3.73}$$

where the origin of a local cartesian reference frame is chosen at P, so that z_U, z_L, and z_μ are the distances from P to U, L, and the mid point of the subdivision respectively, and are given by:

$$\begin{aligned} z_U &= z_p + \Delta R/4, \\ z_L &= z_p + 3\Delta R/4, \\ z_\mu &= z_p + \Delta R/4. \end{aligned} \tag{3.74}$$

Table 3.3 contains evaluations of equations 3.71, 3.72, and 3.73 for the same situations dealt with in table 3.2. While the accuracy of the parallelepiped model evinced by these results appears to approach the lower limit of acceptability, the extreme adversity of the situations depicted must be emphasized.

TABLE 3.3
GRAVITY ERRORS DUE TO MASS DISPLACEMENT IN RECTANGULAR PARALLELEPIPED MODEL

APPLICATION (see table 3.2)	LOCATION and HEIGHT (metres)	z_p (metres)	$\Delta M/M$	$\Delta V/V$	$\Delta G/G$
1.	R_μ = 6 375 500 ΔR_1 = 9000	0	1 / 1417	1 / 1063	1 / 398
2.	R_μ = 6 321 000 ΔR_2 = 40 000	$T + \Delta R_1$ = 39 000	1 / 316	1 / 906	1 / 440
3.	R_μ = 6 373 500 ΔR_3 = 5000	0	1 / 2549	1 / 1912	1 / 717
4.	R_μ = 6 330 000 ΔR_4 = 22 250	$T + \Delta R_3$ = 35 000	1 / 569	1 / 2325	1 / 1145

MASS BALANCE OF TOPOGRAPHY AND ISOSTATIC COMPENSATION

In checking the accuracy of the balance achieved between the masses of the topography and isostatic compensation it will be shown that there is no significant dependence on whether the rigour of equation 3.44 is employed or an approximation based on equation 3.69 is made. Homogeneity is again assumed. Following the latter course, the masses of the topography and compensation are:

$$M_t \simeq \sigma_t \; h \; R_t^2 \; \cos \phi_\mu \; \Delta\phi \; \Delta\lambda,$$

and

$$M_c \simeq \sigma_c \; h_c \; R_c^2 \; \cos \phi_\mu \; \Delta\phi \; \Delta\lambda. \tag{3.75}$$

Hence the *relative* mass balance error is

$$\begin{aligned} \frac{\Delta M_B}{M_t} &= \frac{M_t - M_c}{M_t} \\ &= \frac{\sigma_t \; R_t^2 \; h - \sigma_c \; R_c^2 \; h_c}{\sigma_t \; R_t^2 \; h} \, . \end{aligned} \tag{3.76}$$

Equation 3.76 is free of latitude and longitude dependent terms and is not a function of the area of the subdivision. Consequently, the approximations introduced through equations 3.75 are exceedingly good ones, as exemplified by the quantitative results in table 3.2 for small subdivisions. Therefore equation 3.76 provides an accurate estimate of the error in mass balance which might originate in the adoption of equations 3.22 and 3.24 to define the height of compensation h_c. Using these relations in a quantitative analysis of the error shows that it is greatest when the height of the topography h is maximum. For the maximum anticipated topographic height of 9000 m the error is 1/9100, and it rapidly reduces to 1/20 500 when $h = 5000$ m .

LOCATION OF NULL TOPOGRAPHIC-ISOSTATIC GRAVITATIONAL EFFECT

Since the masses of the topography and compensation are made equal and opposite, each quadrature subdivision may be treated as a gravitational dipole [HEISKANEN and MORITZ 1967, p.149]. Because of the curvature of the reference surface the orientation of this dipole may be such as to nullify its gravitational effect at the computation point P. If, in figure 3.13, M_1 and M_2 are the centres of mass of the topography and compensation, then P will be a null point when $d_1 = d_2$. The locus of all such points is a plane which is normal to, and bisects, the dipole: thus, if C is the mid point of the dipole PCO is a right angle triangle. Then

$$\cos\,\psi_0 = \frac{R_t - l/2}{R_p} \tag{3.77}$$

where l, the dipole length, is given by (see figure 3.6)

$$l = T + \frac{h + h_c}{2} \,. \tag{3.78}$$

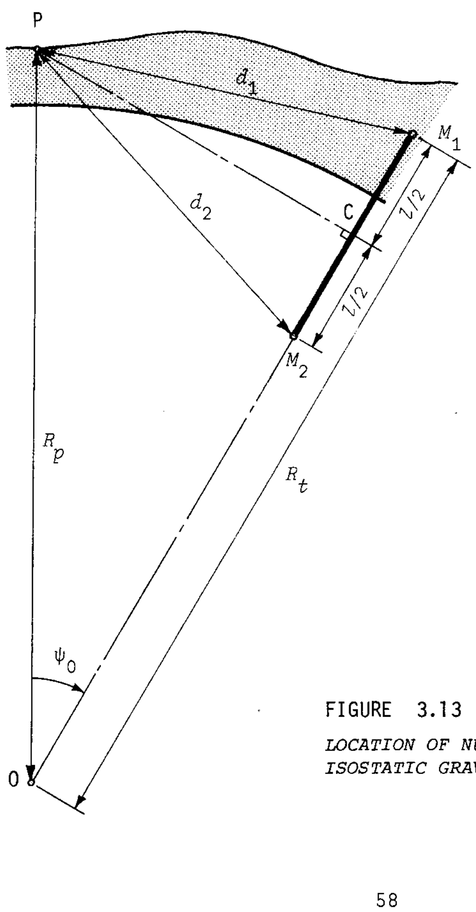

FIGURE 3.13

LOCATION OF NULL TOPOGRAPHIC-ISOSTATIC GRAVITATIONAL EFFECT

Skewness of the normals at P and M_1 precludes a rigorous interpretation of this result in relation to a spheroidal reference surface. However, if a spherical approximation ($R = 6371$ km) is substituted, and O is recognized as the geocentre, then R_p and R_t are geocentric radii and ψ_0 measures the angular distance of the quadrature subdivision from P. Subdivisions closer to P than this will contribute positively to the total potential and the attraction will be directed towards the dipole, whereas a negative contribution and reversal of the attraction will be generated by more distant subdivisions. Values of ψ_0, computed from equation 3.77, are plotted against topographic height for three typical computation point heights in figure 3.14. A sphericity correction has been applied to

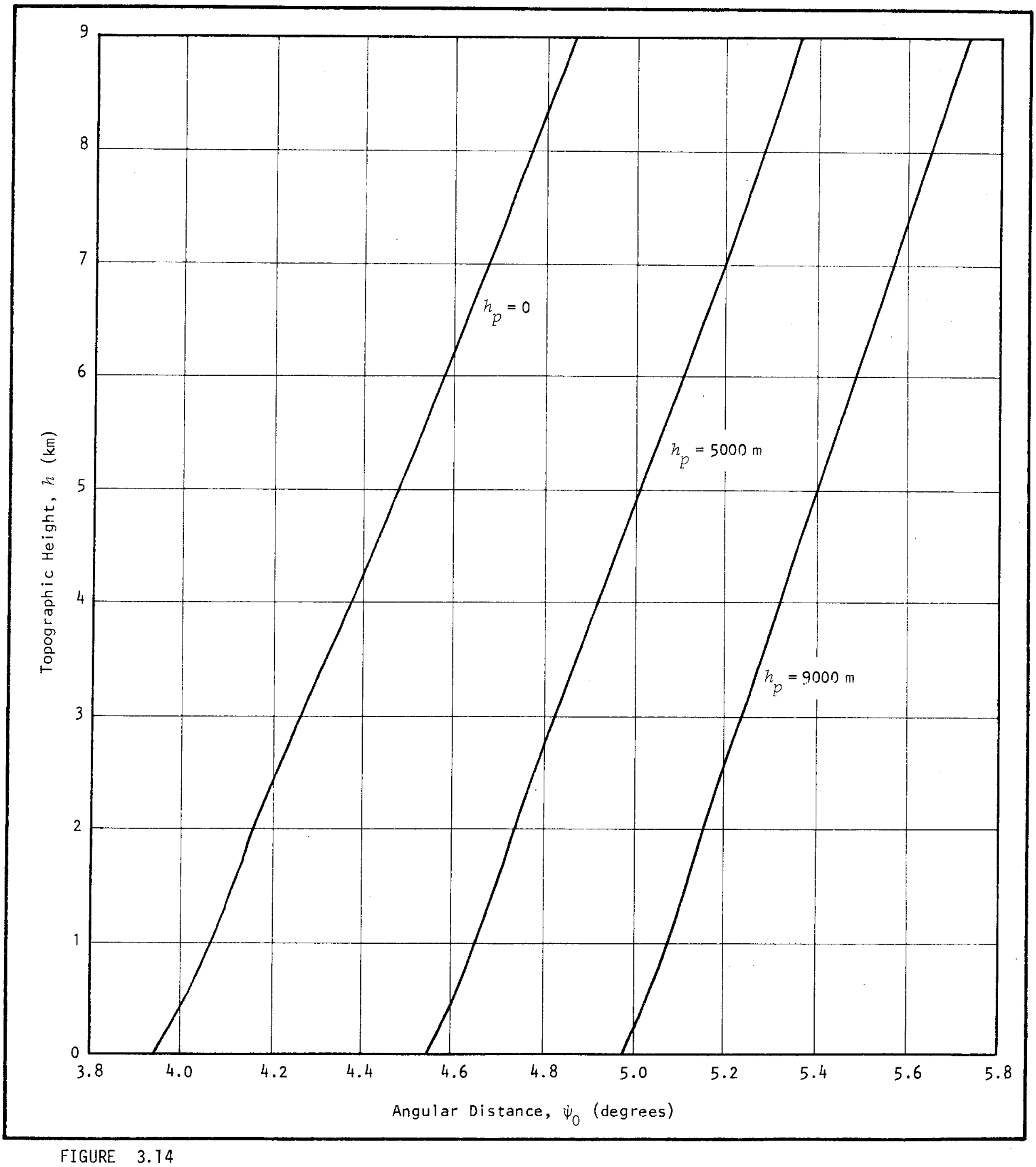

FIGURE 3.14

ANGULAR DISTANCE OF NULL TOPOGRAPHIC-ISOSTATIC EFFECT AS A FUNCTION OF TOPOGRAPHIC HEIGHT AND HEIGHT OF COMPUTATION POINT the compensation and the density model defined by equations 3.29 has been included. These results indicate that the null or "cross-over" distance is generally a little less than 5°, with about 1° variation each way. For a computation point 1000 km above the reference surface—that is, at satellite altitude—ψ_0 is about 30.5° and varies less than 0.1°.

CONSEQUENCES OF GRAVITATIONAL DIPOLE CROSS-OVER. The phenomenon just described may be supposed to occur in reality; it is not merely a mathematical attribute of the adopted models. One consequence of this property of a dipole field is considerable instability in its gravitational effect with respect to its orientation near cross-over. This behaviour is well illustrated by the discontinuity exhibited in the graph in figure 3.15, where changes in the potential of a dipole ΔV_ψ, caused by a change in orientation $\Delta\psi$, expressed as a percentage of the potential V of the dipole at mean orientation are plotted against angular distance ψ. Thus the ordinates plotted are

$$\frac{\Delta V_\psi}{V}\,(\%) = \frac{2(V_{\psi+\Delta\psi} - V_\psi)}{V_{\psi+\Delta\psi} + V_\psi} \times 100, \tag{3.79}$$

where the potential of the dipole is (see figure 3.13)

$$V_\psi = kM\left(\frac{1}{d_1} - \frac{1}{d_2}\right), \tag{3.80}$$

in which d_1 and d_2 are given by equation 3.15 with $R = 6371$ km. The common factor kM is eliminated when equation 3.80 is substituted into equation 3.79. Allowing for sphericity, a dipole length of $l = 54\,872$ m has been used, corresponding to topographic height $h = 9000$ m and density $\sigma_t = 2670$ kg/m³. The computation point has been taken at the reference surface and the change in orientation $\Delta\psi$ equals 0.1°. Quite large relative changes in the potential are seen to occur as a result of slight changes in the orientation of a quadrature subdivision in the inner and mid zones, particularly near the cross-over distance where there is a discontinuity. Of course the large percentage changes illustrated here must not be construed necessarily to indicate the total effect at the computation point: while the *change* in potential is large, its *absolute value* is small, approaching zero at cross-over. Consequently the influence of those subdivisions which happen to lie near the cross-over distance must be considered within the context of the remaining *global* topographic-isostatic effect, wherein their contribution whould be relatively small. Nevertheless, knowledge of this behaviour foreshadows difficulties in any attempt to analyse the total gravitational effect at a point in terms of the contributions from separate zones, or to imbue such contributions with a particular physical meaning. In some special circumstances, where there is a preponderance of topography at the cross-over distance and a lack nearer the computation point, only slight changes in the orientation of the topographic-isostatic model—such as may be occasioned by the difference in curvature between a spherical or ellipsoidal reference surface—may influence the overall results considerably. In effect, such a configuration may be regarded as causing a sizeable portion of the topography to "vanish into the discontinuity" only to "reappear" suddenly if there is a change in any factor which determines the cross-over distance.

Orientation of a particular quad, or group of quads in a region, with respect to a computation point is determined by many factors, including: reference surface curvature, latitude and longitude, heights of computation point and topography, definition of topographic-isostatic model, sphericity and ice corrections, and density model. When conjoined with the unsystematic distribution of the topography, these factors make prediction of the gravitational effects at any point, according to any simplistic or "intuitive" scheme, a futile task. Not only the magnitude of the effect but the sign of the potential and particularly the direction of the attraction vector are obscured by the multiple interactions of these elements.

Despite the complexity, some generalizations concerning the contribution of particular zones may

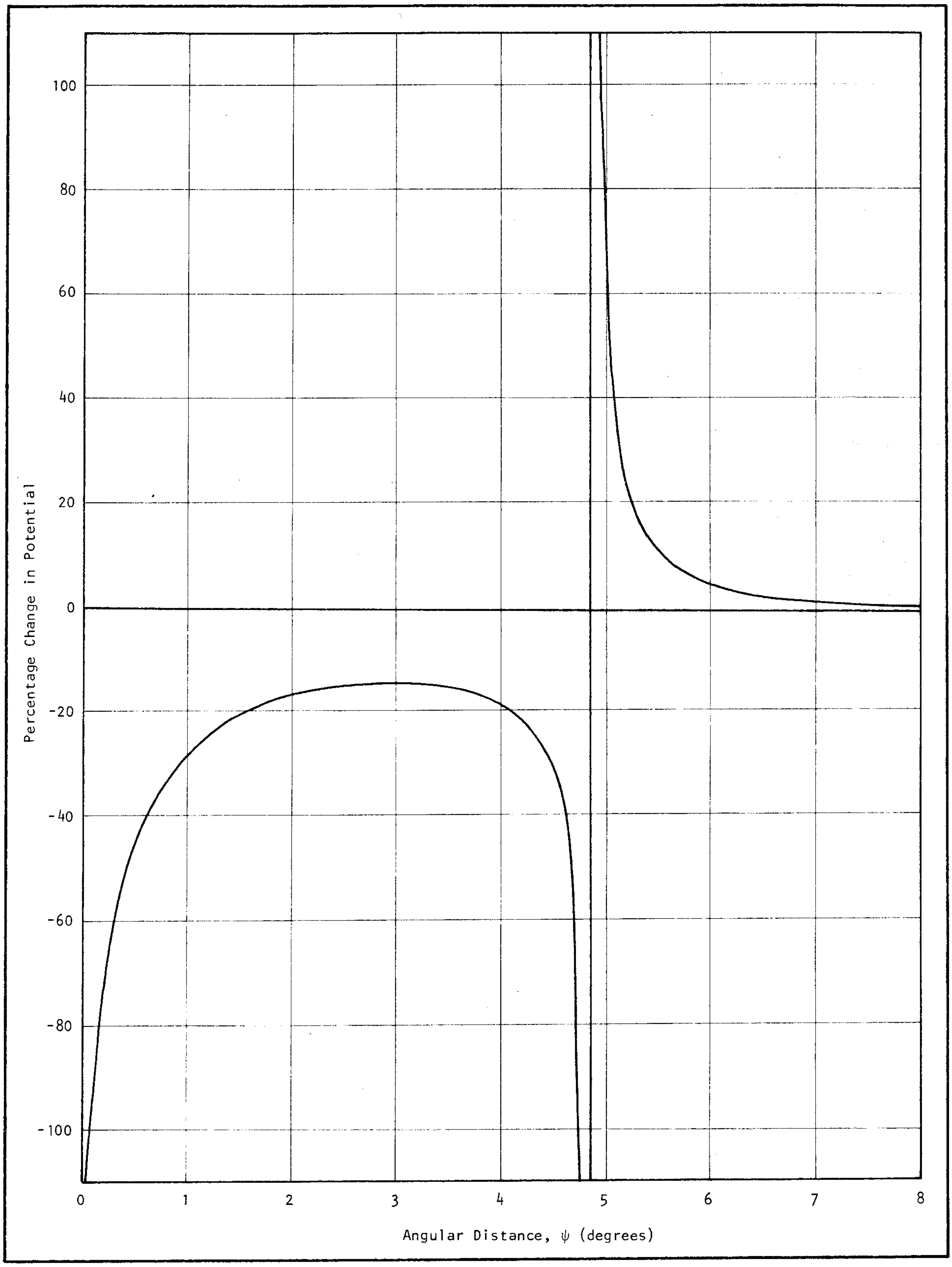

FIGURE 3.15

RELATIVE CHANGE IN POTENTIAL DUE TO A MASS DIPOLE OF LENGTH l = 54 872 m AS A FUNCTION OF ANGULAR DISTANCE TO THE COMPUTATION POINT be made for geoidal or surface points.

(a) The outer zone will always contribute negatively to the potential and attraction vector components.

(b) In the inner zone, contributions to the potential will be positive, but no general rule applies to the attraction components.

(c) Contributions from the mid zone may be either positive or negative depending on whether the topography in the near sub-zone or mid sub-zone is predominant.

(d) All of the aforementioned effects will be reversed when considering the contributions of the ice corrections.

3.6 SUMMARY OF MODEL

The various components of the topographic-isostatic model are specified in table 3.4, along with a list of text and external references.

TABLE 3.4

SPECIFICATION OF TOPOGRAPHIC-ISOSTATIC MODEL

ITEM		SPECIFICATION	REFERENCES
Global Model	Reference Surface	Reference Ellipsoid 1967 Semi-major axis = 6 378 160 m Flattening = 1 / 298.25	[I.A.G. 1967]
	Normal Gravity	γ_0 (N/kg) = 9.780 318 (1 + 5.3024 × 10^{-3} $sin^2\phi$ - 5.9 × 10^{-6} $sin^2 2\phi$)	[I.A.G. 1971]
	Isostatic Compensation System	Airy-Heiskanen System, modified for sphericity and ice correction where necessary. Crustal Thickness T = 30 000 m Sub-crustal Density σ_1 = 3270 kg/m³ Ice Density σ_I = 917 kg/m³	Basic Model: [HEISKANEN and MORITZ 1967, p.135] and equation 3.16 Sphericity: eq. 3.22 Ice Correction: eq. 3.25.
	Topographic Density	de Graaff-Hunter Formula	[de GRAAFF-HUNTER 1966] and equation 3.29
Quadrature Model		INNER ZONE: Rectangular parallelepiped of equivalent volume, "coincident" with the spherical tesseroid. Equivalent volume dimensions: $2a = R_\mu \cos\phi_\mu \Delta\lambda$, $2b = R_\mu \Delta\phi$, $2c = \Delta R$. MID and OUTER ZONES: Point mass at "mid point" of spherical tesseroid.	Equivalent volume: equation 3.69. Mass: equation 3.75

4

Gravity Field of a Non-homogeneous, Rectangular Parallelepiped

4.1 INTRODUCTION

As a result of the preliminary investigations and theoretical development described in the preceeding chapters, it was found that the most satisfactory quadrature model in the inner zone is a rectangular parallelepiped. This represents a compromise between the undue complexity of a spherical tesseroid and the inadequate precision of geometrically reduced models. However, the prototype formula (equation 2.3) derived to investigate the potential is a special case. A more general form, which admits variety of prism dimensions and does not restrict the spatial interrelation between the computation point and the prism, must be developed to satisfy the computation specifications in §2.4. Also, a formulation for the attraction components remains to be derived.

Solutions for the potential and attraction vector due to a *homogeneous* rectangular parallelepiped have appeared in the literature [e.g. MACMILLAN 1930, p.72 *et seq.*†]: the originality of the development given here rests upon the incorporation of a *vertical linear density function*. This greatly increases the flexibility of the result, indeed to an extent whereby virtually any vertically heterogeneous and/or discontinuous mass distribution could be handled, (*e.g.* see chapter 9).

Except for an occasional appeal to symmetry, thus avoiding repetitious working, a rigorous analytical procedure has been followed throughout, without resort to geometrical argument to sustain the development. This contrasts with Macmillan's approach, but, even though some discernment of the physical meaning of the expressions may be sacrificed, consistency of procedure is maintained between the constant and variable density parts of the development. Many of Macmillan's assumptions concerning geometry and symmetry cannot necessarily be extrapolated to the linear density case and, perhaps surprisingly, differentiation of the potential expressions to obtain the attraction components does not provide a method less complicated than integration of the fundamental forms.

The procedure adopted for both the potential and attraction components is to first expand the integrals which describe a special case, where the computation point is confined to lie in the line of one edge of the parallelepiped. This abbreviates the working expressions. Then the result is generalized by a combination of four parallelepipeds, each of which conforms to the limitations of the special case, juxtaposed so as to characterize the required general form. Recurring basic integrals are listed at the

† *Macmillan's spelling of* parallelepiped *(i.e. parallelopiped) does not conform with current English usage.*

beginning.

In the treatment of the attraction the question of correct sign is resolved by defining the vector as though it originates *at the computation point* P, not at the attracting body. Constants of integration, where applicable, are implied, but their presence is superfluous when definite integrals are evaluated.

4.2 BASIC INTEGRALS

Some integrals which occur commonly in the following development may, with convenience, be stated in general form here. The symbol u is used for the principal variable, v and w are constants, and t is a variable function of u, v, and w. Standard forms may be found in GRÖBNER and HOFREITER [1961] or SPEIEGEL [1968, p.57 *et seq.*].

Four standard forms which recur are:

(a)
$$\int \frac{du}{(u^2 + v^2)^{\frac{1}{2}}} = sinh^{-1}\left(\frac{u}{v}\right) \tag{4.1a}$$

$$= \ell og\left(\frac{u + (u^2 + v^2)^{\frac{1}{2}}}{v}\right)^{\dagger}, \tag{4.1b}$$

(b)
$$\int \frac{du}{u^2 + v^2} = \frac{1}{v}\, tan^{-1}\left(\frac{u}{v}\right), \tag{4.2}$$

(c)
$$\int \frac{u\, du}{(u^2 + v^2)^{3/2}} = -(u^2 + v^2)^{-\frac{1}{2}}, \tag{4.3}$$

(d)
$$\int \frac{u^2\, du}{(u^2 + v^2)^{3/2}} = -u(u^2 + v^2)^{-\frac{1}{2}} + sinh^{-1}\left(\frac{u}{v}\right). \tag{4.4}$$

For simplicity the $sinh^{-1}$ form is retained in derivations, but the logarithmic form is more suitable in computer evaluations. A useful, general relationship between the two forms is:

$$\ell og\left(\frac{(u^2 + v^2)^{\frac{1}{2}} - u}{(u^2 + v^2)^{\frac{1}{2}} + u}\right) = \ell og\left(\frac{u^2 + v^2 - u^2}{[(u^2 + v^2)^{\frac{1}{2}} + u^2]^2}\right)$$

$$= -2\ \ell og\left(\frac{u + (u^2 + v^2)^{\frac{1}{2}}}{v}\right)$$

$$= -2\ sinh^{-1}\left(\frac{u}{v}\right). \tag{4.5}$$

Further integration often involves the following four general forms, for which "integration by parts" usually provides a successful start.

(e)
$$\int sinh^{-1}\left(\frac{w}{(u^2 + v^2)^{\frac{1}{2}}}\right) du = u\ sinh^{-1}\left(\frac{w}{(u^2 + v^2)^{\frac{1}{2}}}\right) + \int \frac{wu^2 du}{(u^2 + v^2)(u^2 + v^2 + w^2)^{\frac{1}{2}}}. \tag{4.6}$$

The integral of the last term can be separated into two integrals:

$$\int \frac{w\, du}{(u^2 + v^2 + w^2)^{\frac{1}{2}}} - \int \frac{wv^2 du}{(u^2 + v^2)(u^2 + v^2 + w^2)^{\frac{1}{2}}},$$

in which the first is standard, giving

† *This form is more general than the reduced versions often given.*

$$w \sinh^{-1}\left(\frac{u}{(v^2 + w^2)^{\frac{1}{2}}}\right), \tag{4.7}$$

and the second may be standardized by substituting

$$u = t\left(\frac{v^2 + w^2}{w^2 - t^2}\right)^{\frac{1}{2}} \quad \text{and} \quad du = \frac{w^2(v^2 + w^2)^{\frac{1}{2}}}{(w^2 - t^2)^{3/2}}\, dt.$$

This leads to:

$$-v^2 \int \frac{dt}{t^2 + v^2} = -v \tan^{-1}\left(\frac{t}{v}\right) = -v \tan^{-1}\left(\frac{wu}{v(u^2 + v^2 + w^2)^{\frac{1}{2}}}\right). \tag{4.8}$$

Combining 4.6, 4.7, and 4.8 provides the solution:

$$\int \sinh^{-1}\left(\frac{w}{(u^2 + v^2)^{\frac{1}{2}}}\right) du = u \sinh^{-1}\left(\frac{w}{(u^2 + v^2)^{\frac{1}{2}}}\right) + w \sinh^{-1}\left(\frac{u}{(v^2 + w^2)^{\frac{1}{2}}}\right)$$

$$-v \tan^{-1}\left(\frac{wu}{v(u^2 + v^2 + w^2)^{\frac{1}{2}}}\right). \tag{4.9}$$

(f)

$$\int u \tan^{-1}\left(\frac{vw}{u(u^2 + v^2 + w^2)^{\frac{1}{2}}}\right) du = \frac{u^2}{2} \tan^{-1}\left(\frac{vw}{u(u^2 + v^2 + w^2)^{\frac{1}{2}}}\right)$$

$$- \int \frac{u^2}{2}\left(1 + \frac{v^2w^2}{u^2(u^2 + v^2 + w^2)}\right)^{-1}\left(\frac{-vw[(u^2 + v^2 + w^2) + u^2]}{u^2(u^2 + v^2 + w^2)^{3/2}}\right) du. \tag{4.10}$$

The integral of the last term expands to:

$$\frac{vw}{2}\left(\int \frac{u^2\,du}{(u^2 + v^2)(u^2 + v^2 + w^2)^{\frac{1}{2}}} + \int \frac{u^2\,du}{(u^2 + w^2)(u^2 + v^2 + w^2)^{\frac{1}{2}}}\right),$$

and the solution of these standard forms, when substituted into 4.10, gives the final result:

$$\int u \tan^{-1}\left(\frac{vw}{u(u^2 + v^2 + w^2)^{\frac{1}{2}}}\right) du = \frac{u^2}{2} \tan^{-1}\left(\frac{vw}{u(u^2 + v^2 + w^2)^{\frac{1}{2}}}\right) - \frac{v^2}{2} \tan^{-1}\left(\frac{uw}{v(u^2 + v^2 + w^2)^{\frac{1}{2}}}\right)$$

$$- \frac{w^2}{2} \tan^{-1}\left(\frac{uv}{w(u^2 + v^2 + w^2)^{\frac{1}{2}}}\right) + vw \sinh^{-1}\left(\frac{u}{(v^2 + w^2)^{\frac{1}{2}}}\right). \tag{4.11}$$

(g)

$$\int u \sinh^{-1}\left(\frac{w}{(u^2 + v^2)^{\frac{1}{2}}}\right) du = \frac{u^2}{2} \sinh^{-1}\left(\frac{w}{(u^2 + v^2)^{\frac{1}{2}}}\right)$$

$$- \int \frac{u^2}{2}\left(1 + \frac{w^2}{(u^2 + v^2)}\right)^{-\frac{1}{2}}\left(\frac{-uw}{(u^2 + v^2)^{3/2}}\right) du. \tag{4.12}$$

Rearrangement of the last term gives:

$$\frac{w}{2}\int \frac{u^3\,du}{(u^2 + v^2)(u^2 + v^2 + w^2)^{\frac{1}{2}}} = \frac{w}{2}\int \frac{u\,du}{(u^2 + v^2 + w^2)^{\frac{1}{2}}} - \frac{v^2w}{2}\int \frac{u\,du}{(u^2 + v^2)(u^2 + v^2 + w^2)^{\frac{1}{2}}}$$

$$= \frac{w}{2}(u^2 + v^2 + w^2)^{\frac{1}{2}} - \frac{v^2w}{2}\int \frac{t\,dt}{(t^2 + w^2)t}, \tag{4.13}$$

where $u^2 + v^2 + w^2 = t^2$ and $u\,du = t\,dt.$

The last term of 4.13 becomes:

$$-\frac{v^2}{4}\left(\int\frac{dt}{t-w}-\int\frac{dt}{t+w}\right)=\frac{-v^2}{4}\,\ell og\left(\frac{t-w}{t+w}\right). \tag{4.14}$$

Replacing t in 4.14 and collecting terms provides the solution:

$$\int u\,\sinh^{-1}\left(\frac{w}{(u^2+v^2)^{\frac{1}{2}}}\right)du=\frac{u^2}{2}\sinh^{-1}\left(\frac{w}{(u^2+v^2)^{\frac{1}{2}}}\right)$$

$$+\frac{w}{2}(u^2+v^2+w^2)^{\frac{1}{2}}-\frac{v^2}{4}\,\ell og\left(\frac{(u^2+v^2+w^2)^{\frac{1}{2}}-w}{(u^2+v^2+w^2)^{\frac{1}{2}}+w}\right). \tag{4.15}$$

(h) $$\int u^2\tan^{-1}\left(\frac{vw}{u(u^2+v^2+w^2)^{\frac{1}{2}}}\right)du=\frac{u^3}{3}\tan^{-1}\left(\frac{vw}{u(u^2+v^2+w^2)^{\frac{1}{2}}}\right)$$

$$-\int\frac{u^3}{3}\left(1+\frac{v^2w^2}{u^2(u^2+v^2+w^2)}\right)^{-1}\left(\frac{vw(2u^2+v^2+w^2)}{u^2(u^2+v^2+w^2)^{3/2}}\right)du \tag{4.16}$$

The remaining integral expands to:

$$\frac{vw}{3}\left(\int\frac{u^3du}{(u^2+v^2)(u^2+v^2+w^2)^{\frac{1}{2}}}+\int\frac{u^3du}{(u^2+w^2)(u^2+v^2+w^2)^{\frac{1}{2}}}\right)=\frac{vw}{3}\left(2\int\frac{u\,du}{(u^2+v^2+w^2)^{\frac{1}{2}}}\right.$$

$$\left.-v^2\int\frac{u\,du}{(u^2+v^2)(u^2+v^2+w^2)^{\frac{1}{2}}}-w^2\int\frac{u\,du}{(u^2+w^2)(u^2+v^2+w^2)^{\frac{1}{2}}}\right). \tag{4.17}$$

Solutions of the three standard forms in 4.17 may be substituted into 4.16 for the final result:

$$\int u^2\tan^{-1}\left(\frac{vw}{u(u^2+v^2+w^2)^{\frac{1}{2}}}\right)du=\frac{u^3}{3}\tan^{-1}\left(\frac{vw}{u(u^2+v^2+w^2)^{\frac{1}{2}}}\right)+\frac{2vw}{3}(u^2+v^2+w^2)^{\frac{1}{2}}$$

$$-\frac{v^3}{3}\,\ell og\left(\frac{(u^2+v^2+w^2)^{\frac{1}{2}}-w}{(u^2+v^2+w^2)^{\frac{1}{2}}+w}\right)-\frac{w^3}{6}\,\ell og\left(\frac{(u^2+v^2+w^2)^{\frac{1}{2}}-v}{(u^2+v^2+w^2)^{\frac{1}{2}}+v}\right). \tag{4.18}$$

4.3 POTENTIAL

SPECIAL CASE

Consider the potential V_0 of a rectangular paralellepiped with sides x_1, y_1, and z_1 at a point P_0 in the line of one edge—extended if necessary (see figure 4.1). Let the origin O_0 of a rectangular coordinate system (x_0, y_0, z_0) be at one corner of the parallelepiped, and the axes coincide with the edges. Let the coordinates of P_0 be (0, 0, z_2).

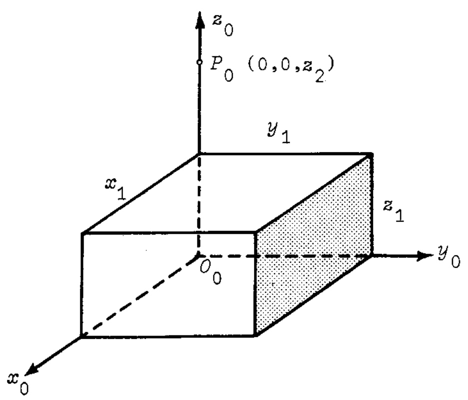

FIGURE 4.1

RECTANGULAR PARALLELEPIPED —SPECIAL CASE

Assume that the density of the parallelepiped is a linear function of z_0, namely:

$$\sigma = \sigma_p + D(z_0 - z_2), \tag{4.19}$$

where σ_p is the apparent density at the height of the point P_0, and

D is the vertical density gradient.

Applying equation 1.3, the potential at P_0 will be,

$$V_0 = k\int_0^{z_1}\int_0^{y_1}\int_0^{x_1}\frac{\sigma\, dx_0\, dy_0\, dz_0}{[x_0^2 + y_0^2 + (z_0 - z_2)^2]^{\frac{1}{2}}} \tag{4.20}$$

$$= k\sigma_p\int_0^{z_1}\int_0^{y_1}\int_0^{x_1}\frac{dx_0\, dy_0\, dz_0}{[x_0^2 + y_0^2 + (z_0 - z_2)^2]^{\frac{1}{2}}}$$

$$+ Dk\int_0^{z_1}\int_0^{y_1}\int_0^{x_1}\frac{(z_0 - z_2)\, dx_0\, dy_0\, dz_0}{[x_0^2 + y_0^2 + (z_0 - z_2)^2]^{\frac{1}{2}}} \tag{4.21}$$

$$= V_{0h} + V_{0\ell},$$

where V_{0h} is the potential due to a homogeneous prism of density σ_p, and

$V_{0\ell}$ is the potential due to a superposed prism of linear density $D(z_0 - z_2)$.

The definite integral in the term for V_{0h} may be expanded as follows:

$$\frac{V_{0h}}{k\sigma_p} = \int_0^{z_1}\int_0^{y_1}\left|\sinh^{-1}\left(\frac{x_0}{[y^2 + (z_0 - z_2)^2]^{\frac{1}{2}}}\right)\right|_0^{x_1} dy_0\, dz_0$$

$$= \int_0^{z_1}\int_0^{y_1}\sinh^{-1}\left(\frac{x_1}{[y_0^2 + (z_0 - z_2)^2]^{\frac{1}{2}}}\right) dy_0\, dz_0$$

$$= \int_0^{z_1}\left| y_0\sinh^{-1}\left(\frac{x_1}{[y_0^2 + (z_0 - z_2)^2]^{\frac{1}{2}}}\right) + x_1\sinh^{-1}\left(\frac{y_0}{[x_1^2 + (z_0 - z_2)^2]^{\frac{1}{2}}}\right)\right.$$

$$\left. - (z_2 - z_0)\tan^{-1}\left(\frac{x_1 y_0}{(z_0 - z_2)[x_1^2 + y_0^2 + (z_0 - z_2)^2]^{\frac{1}{2}}}\right)\right|_0^{y_1} dz_0$$

$$= \int_0^{z_1}\left\{ y_1\sinh^{-1}\left(\frac{x_1}{[y_1^2 + (z_0 - z_2)^2]^{\frac{1}{2}}}\right) + x_1\sinh^{-1}\left(\frac{y_1}{[x_1^2 + (z_0 - z_2)^2]^{\frac{1}{2}}}\right)\right.$$

$$\left. - (z_0 - z_2)\tan^{-1}\left(\frac{x_1 y_1}{(z_0 - z_2)[x_1^2 + y_1^2 + (z_0 - z_2)^2]^{\frac{1}{2}}}\right)\right\} dz_0 \tag{4.22}$$

$$= \left\{ y_1\left((z_0 - z_2)\sinh^{-1}\left(\frac{x_1}{[y_1^2 + (z_0 - z_2)^2]^{\frac{1}{2}}}\right) + x_1\sinh^{-1}\left(\frac{z_0 - z_2}{(x_1^2 + y_1^2)^{\frac{1}{2}}}\right)\right.\right.$$

$$\left.\left. - y_1\tan^{-1}\left(\frac{x_1(z_0 - z_2)}{y_1[x_1^2 + y_1^2 + (z_0 - z_2)^2]^{\frac{1}{2}}}\right)\right)\right.$$

$$+ x_1\left\{(z_0 - z_2)\sinh^{-1}\left[\frac{y_1}{[x_1^2 + (z_0 - z_2)^2]^{\frac{1}{2}}}\right] + y_1\sinh^{-1}\left[\frac{z_0 - z_2}{(x_1^2 + y_1^2)^{\frac{1}{2}}}\right]\right.$$

$$\left. - x_1 \tan^{-1}\left[\frac{y_1(z_0 - z_2)}{x\,[x_1^2 + y_1^2 + (z_0 - z_2)^2]^{\frac{1}{2}}}\right]\right\}$$

$$- \frac{1}{2}\left\{(z_0 - z_2)^2 \tan^{-1}\left[\frac{x_1 y_1}{(z_0 - z_2)[x_1^2 + y_1^2 + (z_0 - z_2)^2]^{\frac{1}{2}}}\right] - y_1^2 \tan^{-1}\left[\frac{x_1(z_0 - z_2)}{y_1[x_1^2 + y_1^2 + (z_0 - z_2)^2]^{\frac{1}{2}}}\right]\right.$$

$$\left.\left. - x_1^2 \tan^{-1}\left[\frac{y_1(z_0 - z_2)}{x_1[x_1^2 + y_1^2 + (z_0 - z_2)^2]^{\frac{1}{2}}}\right] + 2x_1y_1 \sinh^{-1}\left[\frac{z_0 - z_2}{(x_1^2 + y_1^2)^{\frac{1}{2}}}\right]\right\}\right|_0^{z_1}.$$

Then evaluating at the limits:

$$\frac{V_{0h}}{k\sigma_p} = x_1y_1 \sinh^{-1}\left[\frac{z_1 - z_2}{(x_1^2 + y_1^2)^{\frac{1}{2}}}\right] - x_1y_1 \sinh^{-1}\left[\frac{-z_2}{(x_1^2 + y_1^2)^{\frac{1}{2}}}\right]$$

$$+ y_1(z_1 - z_2) \sinh^{-1}\left[\frac{x_1}{[y_1^2 + (z_1 - z_2)^2]^{\frac{1}{2}}}\right] + y_1z_2 \sinh^{-1}\left[\frac{x_1}{(y_1^2 + z_2^2)^{\frac{1}{2}}}\right]$$

$$+ x_1(z_1 - z_2) \sinh^{-1}\left[\frac{y_1}{[x_1^2 + (z_1 - z_2)^2]^{\frac{1}{2}}}\right] + x_1z_2 \sinh^{-1}\left[\frac{y_1}{(x_1^2 + z_2^2)^{\frac{1}{2}}}\right]$$

$$- \frac{x_1^2}{2} \tan^{-1}\left[\frac{y_1(z_1 - z_2)}{x_1[x_1^2 + y_1^2 + (z_1 - z_2)^2]^{\frac{1}{2}}}\right] + \frac{x_1^2}{2} \tan^{-1}\left[\frac{-y_1z_2}{x_1(x_1^2 + y_1^2 + z_2^2)^{\frac{1}{2}}}\right]$$

$$- \frac{y_1^2}{2} \tan^{-1}\left[\frac{x_1(z_1 - z_2)}{y_1[x_1^2 + y_1^2 + (z_1 - z_2)^2]^{\frac{1}{2}}}\right] + \frac{y_1^2}{2} \tan^{-1}\left[\frac{-x_1z_2}{y_1(x_1^2 + y_1^2 + z_2^2)^{\frac{1}{2}}}\right]$$

$$- \frac{(z_1 - z_2)^2}{2} \tan^{-1}\left[\frac{x_1y_1}{(z_1 - z_2)[x_1^2 + y_1^2 + (z_1 - z_2)^2]^{\frac{1}{2}}}\right] + \frac{z_2^2}{2} \tan^{-1}\left[\frac{x_1y_1}{-z_2(x_1^2 + y_1^2 + z_2^2)^{\frac{1}{2}}}\right]. \tag{4.23}$$

Now, returning to equation 4.21, the definite integral in the term for $V_{0\ell}$ may be written as

$$\frac{V_{0\ell}}{kD} = \int_0^{z_1}(z_0 - z_2)\int_0^{y_1}\int_0^{x_1}\frac{dx_0\, dy_0}{[x_0^2 + y_0^2 + (z_0 - z_2)^2]^{\frac{1}{2}}}\, dz_0. \tag{4.24}$$

And the double integral in x_0 and y_0 may be expanded using the result given in equation 4.22, so that 4.24 becomes

$$\frac{V_{0\ell}}{kD} = \int_0^{z_1}(z_0 - z_2)\left\{y_1 \sinh^{-1}\left[\frac{x_1}{[y_1^2 + (z_0 - z_2)^2]^{\frac{1}{2}}}\right] + x_1 \sinh^{-1}\left[\frac{y_1}{[x_1^2 + (z_0 - z_2)^2]^{\frac{1}{2}}}\right]\right.$$

$$\left. - (z_0 - z_2) \tan^{-1}\left[\frac{x_1y_1}{(z_0 - z_2)[x_1^2 + y_1^2 + (z_0 - z_2)^2]^{\frac{1}{2}}}\right]\right\} dz_0$$

$$= \Bigg| \frac{y_1}{2}(z_0 - z_2)^2 \sinh^{-1}\left(\frac{x_1}{[y_1^2 + (z_0 - z_2)^2]^{\frac{1}{2}}}\right) + \frac{x_1 y_1}{2}[x_1^2 + y_1^2 + (z_0 - z_2)^2]^{\frac{1}{2}}$$

$$- \frac{y_1^3}{4} \log\left(\frac{[x_1^2 + y_1^2 + (z_0 - z_2)^2]^{\frac{1}{2}} - x_1}{[x_1^2 + y_1^2 + (z_0 - z_2)^2]^{\frac{1}{2}} + x_1}\right)$$

$$+ \frac{x_1}{2}(z_0 - z_2)^2 \sinh^{-1}\left(\frac{y_1}{[x_1^2 + (z_0 - z_2)^2]^{\frac{1}{2}}}\right) + \frac{x_1 y_1}{2}[x_1^2 + y_1^2 + (z_0 - z_2)^2]^{\frac{1}{2}}$$

$$- \frac{x_1^3}{4} \log\left(\frac{[x_1^2 + y_1^2 + (z_0 - z_2)^2]^{\frac{1}{2}} - y_1}{[x_1^2 + y_1^2 + (z_0 - z_2)^2]^{\frac{1}{2}} + y_1}\right)$$

$$- \frac{(z_0 - z_2)^3}{3} \tan^{-1}\left(\frac{x_1 y_1}{(z_0 - z_2)[x_1^2 + y_1^2 + (z_0 - z_2)^2]^{\frac{1}{2}}}\right) - \frac{2x_1 y_1}{3}[x_1^2 + y_1^2 + (z_0 - z_2)^2]^{\frac{1}{2}}$$

$$+ \frac{x_1^3}{6} \log\left(\frac{[x_1^2 + y_1^2 + (z_0 - z_2)^2]^{\frac{1}{2}} - y_1}{[x_1^2 + y_1^2 + (z_0 - z_2)^2]^{\frac{1}{2}} + y_1}\right) + \frac{y_1^3}{6} \log\left(\frac{[x_1^2 + y_1^2 + (z_0 - z_2)^2]^{\frac{1}{2}} - x_1}{[x_1^2 + y_1^2 + (z_0 - z_2)^2]^{\frac{1}{2}} + x_1}\right) \Bigg|_0^{z_1}.$$

Hence,

$$\frac{V_{0\ell}}{kD} = \frac{y_1(z_1 - z_2)^2}{2} \sinh^{-1}\left(\frac{x_1}{[y_1^2 + (z_1 - z_2)^2]^{\frac{1}{2}}}\right) - \frac{y_1 z_2^2}{2} \sinh^{-1}\left(\frac{x_1}{[y_1^2 + z_2^2]^{\frac{1}{2}}}\right)$$

$$+ \frac{x_1(z_1 - z_2)^2}{2} \sinh^{-1}\left(\frac{y_1}{[x_1^2 + (z_1 - z_2)^2]^{\frac{1}{2}}}\right) - \frac{x_1 z_2^2}{2} \sinh^{-1}\left(\frac{y_1}{[x_1^2 + z_2^2]^{\frac{1}{2}}}\right)$$

$$- \frac{y_1^3}{12} \log\left(\frac{[x_1^2 + y_1^2 + (z_1 - z_2)^2]^{\frac{1}{2}} - x_1}{[x_1^2 + y_1^2 + (z_1 - z_2)^2]^{\frac{1}{2}} + x_1}\right) + \frac{y_1^3}{12} \log\left(\frac{[x_1^2 + y_1^2 + z_2^2]^{\frac{1}{2}} - x_1}{[x_1^2 + y_1^2 + z_2^2]^{\frac{1}{2}} + x_1}\right)$$

$$- \frac{x_1^3}{12} \log\left(\frac{[x_1^2 + y_1^2 + (z_1 - z_2)^2]^{\frac{1}{2}} - y_1}{[x_1^2 + y_1^2 + (z_1 - z_2)^2]^{\frac{1}{2}} + y_1}\right) + \frac{x_1^3}{12} \log\left(\frac{[x_1^2 + y_1^2 + z_2^2]^{\frac{1}{2}} - y_1}{[x_1^2 + y_1^2 + z_2^2]^{\frac{1}{2}} + y_1}\right)$$

$$+ \frac{x_1 y_1}{3}[x_1^2 + y_1^2 + (z_1 - z_2)^2]^{\frac{1}{2}} - \frac{x_1 y_1}{3}[x_1^2 + y_1^2 + z_2^2]^{\frac{1}{2}}$$

$$- \frac{(z_1 - z_2)^3}{3} \tan^{-1}\left(\frac{x_1 y_1}{(z_1 - z_2)[x_1^2 + y_1^2 + (z_1 - z_2)^2]^{\frac{1}{2}}}\right) - \frac{z_2^3}{3} \tan^{-1}\left(\frac{x_1 y_1}{-z_2[x_1^2 + y_1^2 + z_2^2]^{\frac{1}{2}}}\right). \quad (4.25)$$

POTENTIAL AT A GENERAL POINT

To generalize the preceeding development for a point P, not specially related to the position and orientation of the parallelepiped, it will be convenient to choose the origin O_μ of a new rectangular reference frame (x,y,z) at the centroid of the parallelepiped with axes parallel to the edges, and let the coordinates of P in this system be (x_p, y_p, z_p). Let the sides of the parallelepiped be $2a$, $2b$, and $2c$, and its density σ be given by:

$$\sigma = \sigma_p + D(z - z_p). \quad (4.26)$$

Then, with reference to figure 4.2, the potential V of the parallelepiped $ABCDEFGH$ is given by:

$$V = V_1 - V_2 - V_3 + V_4 \tag{4.27}$$

where V_1 is the potential at P due to prism $IKMDNRTH$,
V_2 is the potential at P due to prism $IKLANRSE$,
V_3 is the potential at P due to prism $JKMCQRTG$, and
V_4 is the potential at P due to prism $JKLBQRSF$.

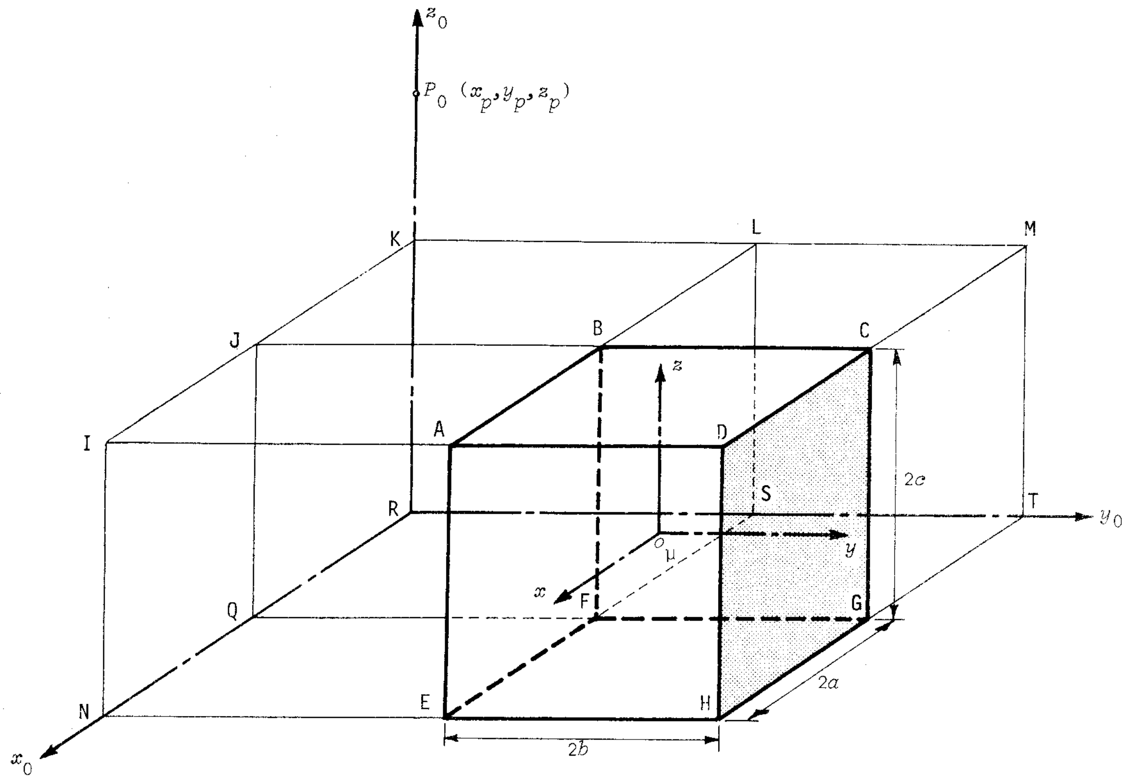

FIGURE 4.2

RECTANGULAR PARALLELEPIPED—GENERAL CASE

Each of these four potentials may be expressed in a form similar to 4.21 with appropriate integration limits, hence

$$V = (V_{1h} - V_{2h} - V_{3h} + V_{4h}) + (V_{1\ell} - V_{2\ell} - V_{3\ell} + V_{4\ell}) \tag{4.28}$$

$$= V_h + V_\ell, \tag{4.29}$$

where the subscripts h and ℓ relate to the homogeneous and linear parts of the density function, respectively. Each term in equation 4.28 may be expanded by using either equation 4.23 or 4.25, and observing the necessary relationships between the various parallelepiped sides and the coordinates of P for each configuration. There are sixteen such relationships and they are as set out in table 4.1.

TABLE 4.1
RELATIONS FOR TRANSLATION OF PARALLELEPIPED FORMULAE FROM SPECIAL TO GENERAL CASE

PARALLELEPIPED:	1	2	3	4
$x_1 =$	$-(x_p - a)$	$-(x_p - a)$	$-(x_p + a)$	$-(x_p + a)$
$y_1 =$	$-(y_p - b)$	$-(y_p + b)$	$-(y_p - b)$	$-(y_p + b)$
$z_1 - z_2 =$	$-(z_p - c)$	$-(z_p - c)$	$-(z_p - c)$	$-(z_p - c)$
$z_2 =$	$z_p + c$	$z_p + c$	$z_p + c$	$z_p + c$

At the same time, the $sinh^{-1}$ terms may be converted to logarithmic form and consistency of signs achieved by noting that both $sinh^{-1}$ and tan^{-1} are odd functions, so that:

$$sinh^{-1}(-u) = -sinh^{-1}u$$

and

$$tan^{-1}(-u) = -tan^{-1}\,u.$$

Considerable abbreviation is attained by introducing the following notation:

$$d_{111} = [(x_p + a)^2 + (y_p + b)^2 + (z_p + c)^2]^{\frac{1}{2}}$$

$$d_{112} = [(x_p + a)^2 + (y_p + b)^2 + (z_p - c)^2]^{\frac{1}{2}}$$

etc. ...

$$d_{222} = [(x_p - a)^2 + (y_p - b)^2 + (z_p - c)^2]^{\frac{1}{2}}\ , \tag{4.30}$$

where the subscipts 1 and 2 are associated with the positive and negative signs respectively. There are eight possible values for d, which are interpreted geometrically as the distances from P to each of the eight corners of the parallelepiped. Similarly, the six quantities: $(x_p + a)$, $(y_p + b)$, $\ldots(z_p - c)$ represent the perpendicular distances from P to each of the face planes of the parallelepiped, and may be abbreviated thus:

$$p_{x1} = (x_p + a)$$

$$p_{y1} = (y_p + b)$$

etc. ...

$$p_{z2} = (z_p - c). \tag{4.31}$$

Then, for example, the potential due to the first parallelepiped may be written as:

$$\frac{V_{1h}}{k\sigma_p} = p_{x2}\,p_{y2}\,\ell og\left(\frac{d_{221} + p_{z1}}{d_{220}}\right) - p_{x2}\,p_{y2}\,\ell og\left(\frac{d_{222} + p_{z2}}{d_{220}}\right)$$

$$+ p_{y2}\,p_{z1}\,\ell og\left(\frac{d_{221} + p_{x2}}{d_{021}}\right) - p_{y2}\,p_{z2}\,\ell og\left(\frac{d_{222} + p_{x2}}{d_{022}}\right)$$

$$+ p_{x2}\,p_{z1}\,\ell og\left(\frac{d_{221} + p_{y2}}{d_{201}}\right) - p_{x2}\,p_{z2}\,\ell og\left(\frac{d_{222} + p_{y2}}{d_{202}}\right)$$

$$+\frac{p_{x2}^2}{2}\tan^{-1}\left(\frac{p_{y2}\,p_{z2}}{p_{x2}\,d_{222}}\right)-\frac{p_{x2}^2}{2}\tan^{-1}\left(\frac{p_{y2}\,p_{z1}}{p_{x2}\,d_{221}}\right)$$

$$+\frac{p_{y2}^2}{2}\tan^{-1}\left(\frac{p_{x2}\,p_{z2}}{p_{y2}\,d_{222}}\right)-\frac{p_{y2}^2}{2}\tan^{-1}\left(\frac{p_{x2}\,p_{z1}}{p_{y2}\,d_{221}}\right)$$

$$+\frac{p_{z2}^2}{2}\tan^{-1}\left(\frac{p_{x2}\,p_{y2}}{p_{z2}\,d_{222}}\right)-\frac{p_{z1}^2}{2}\tan^{-1}\left(\frac{p_{x2}\,p_{y2}}{p_{z1}\,d_{221}}\right), \qquad (4.32)$$

in which a useful extension of the aforementioned notation has been introduced, whereby the subscript 0 is used to indicate a missing term in the expression for d, thus:

$$d_{012} = [(y_p + b)^2 + (z_p - c)^2]^{\frac{1}{2}} \qquad (4.30a)$$

etc. ...

The linear density part is:

$$\frac{V_{1\ell}}{kD} = \frac{p_{y2}\,p_{z2}^2}{2}\,\ell og\left(\frac{d_{222}+p_{x2}}{d_{022}}\right)-\frac{p_{y2}\,p_{z1}^2}{2}\,\ell og\left(\frac{d_{221}+p_{x2}}{d_{021}}\right)$$

$$+\frac{p_{x2}\,p_{z2}^2}{2}\,\ell og\left(\frac{d_{222}+p_{y2}}{d_{202}}\right)-\frac{p_{x2}\,p_{z1}^2}{2}\,\ell og\left(\frac{d_{221}+p_{y2}}{d_{201}}\right)$$

$$+\frac{p_{y2}^3}{12}\,\ell og\left(\frac{d_{222}+p_{x2}}{d_{222}-p_{x2}}\right)-\frac{p_{y2}^3}{12}\,\ell og\left(\frac{d_{221}+p_{x2}}{d_{221}-p_{x2}}\right)$$

$$+\frac{p_{x2}^3}{12}\,\ell og\left(\frac{d_{222}+p_{y2}}{d_{222}-p_{y2}}\right)-\frac{p_{x2}^3}{12}\,\ell og\left(\frac{d_{221}+p_{y2}}{d_{221}-p_{y2}}\right)$$

$$+\frac{1}{3}p_{x2}\,p_{y2}\,d_{222}-\frac{1}{3}p_{x2}\,p_{y2}\,d_{221}$$

$$-\frac{p_{z2}^3}{3}\tan^{-1}\left(\frac{p_{x2}\,p_{y2}}{p_{z2}\,d_{222}}\right)+\frac{p_{z1}^3}{3}\tan^{-1}\left(\frac{p_{x2}\,p_{y2}}{p_{z1}\,d_{221}}\right). \qquad (4.33)$$

In combining the homogeneous parts of the four parallelepipeds, it is possible to merge pairs of ℓog terms with the same coefficients, so that the complete expression for V_h will contain twelve ℓog terms and twenty-four $\tan^{-1}$ terms. There is no need to elaborate the expressions for the remaining six terms of equation 4.28—due to the other three parallelepipeds—since they are similar to, and may be obtained from, equations 4.32 and 4.33. Simple interchanging of appropriate subscripts, to reflect the changes of sign apparent in table 4.1, is necessary. Thus, all numeric subscripts associated with y are changed to obtain the V_2 terms; those assocated with x for the V_3 terms; and subscripts relating to both x and y for the V_4 terms. The final expression for the potential due to the homogeneous part is:

$$
\begin{aligned}
\frac{V_h}{k\sigma_p} = {} & p_{x1}\, p_{y1}\, \ell og\left(\frac{d_{111} + p_{z1}}{d_{112} + p_{z2}}\right) - p_{x1}\, p_{y2}\, \ell og\left(\frac{d_{121} + p_{z1}}{d_{122} + p_{z2}}\right) \\
& + p_{x2}\, p_{y2}\, \ell og\left(\frac{d_{221} + p_{z1}}{d_{222} + p_{z2}}\right) - p_{x2}\, p_{y1}\, \ell og\left(\frac{d_{211} + p_{z1}}{d_{212} + p_{z2}}\right) \\
& + p_{x1}\, p_{z1}\, \ell og\left(\frac{d_{111} + p_{y1}}{d_{121} + p_{y2}}\right) - p_{x1}\, p_{z2}\, \ell og\left(\frac{d_{112} + p_{y1}}{d_{122} + p_{y2}}\right) \\
& + p_{x2}\, p_{z2}\, \ell og\left(\frac{d_{212} + p_{y1}}{d_{222} + p_{y2}}\right) - p_{x2}\, p_{z1}\, \ell og\left(\frac{d_{211} + p_{y1}}{d_{221} + p_{y2}}\right) \\
& + p_{y1}\, p_{z1}\, \ell og\left(\frac{d_{111} + p_{x1}}{d_{211} + p_{x2}}\right) - p_{y1}\, p_{z2}\, \ell og\left(\frac{d_{112} + p_{x1}}{d_{212} + p_{x2}}\right) \\
& + p_{y2}\, p_{z2}\, \ell og\left(\frac{d_{122} + p_{x1}}{d_{222} + p_{x2}}\right) - p_{y2}\, p_{z1}\, \ell og\left(\frac{d_{121} + p_{x1}}{d_{221} + p_{x2}}\right) \\
& + \frac{p_{x1}^2}{2}\left\{ tan^{-1}\left(\frac{p_{y1}\, p_{z2}}{p_{x1}\, d_{112}}\right) - tan^{-1}\left(\frac{p_{y1}\, p_{z1}}{p_{x1}\, d_{111}}\right) + tan^{-1}\left(\frac{p_{y2}\, p_{z1}}{p_{x1}\, d_{121}}\right) - tan^{-1}\left(\frac{p_{y2}\, p_{z2}}{p_{x1}\, d_{122}}\right)\right\} \\
& + \frac{p_{x2}^2}{2}\left\{ tan^{-1}\left(\frac{p_{y1}\, p_{z1}}{p_{x2}\, d_{211}}\right) - tan^{-1}\left(\frac{p_{y1}\, p_{z2}}{p_{x2}\, d_{212}}\right) + tan^{-1}\left(\frac{p_{y2}\, p_{z2}}{p_{x2}\, d_{222}}\right) - tan^{-1}\left(\frac{p_{y2}\, p_{z1}}{p_{x2}\, d_{221}}\right)\right\} \\
& + \frac{p_{y1}^2}{2}\left\{ tan^{-1}\left(\frac{p_{x2}\, p_{z1}}{p_{y1}\, d_{211}}\right) - tan^{-1}\left(\frac{p_{x2}\, p_{z2}}{p_{y1}\, d_{212}}\right) + tan^{-1}\left(\frac{p_{x1}\, p_{z2}}{p_{y1}\, d_{112}}\right) - tan^{-1}\left(\frac{p_{x1}\, p_{z1}}{p_{y1}\, d_{111}}\right)\right\} \\
& + \frac{p_{y2}^2}{2}\left\{ tan^{-1}\left(\frac{p_{x1}\, p_{z1}}{p_{y2}\, d_{121}}\right) - tan^{-1}\left(\frac{p_{x2}\, p_{z1}}{p_{y2}\, d_{221}}\right) + tan^{-1}\left(\frac{p_{x2}\, p_{z2}}{p_{y2}\, d_{222}}\right) - tan^{-1}\left(\frac{p_{x1}\, p_{z2}}{p_{y2}\, d_{122}}\right)\right\} \\
& + \frac{p_{z1}^2}{2}\left\{ tan^{-1}\left(\frac{p_{x1}\, p_{y2}}{p_{z1}\, d_{121}}\right) - tan^{-1}\left(\frac{p_{x1}\, p_{y1}}{p_{z1}\, d_{111}}\right) + tan^{-1}\left(\frac{p_{x2}\, p_{y1}}{p_{z1}\, d_{211}}\right) - tan^{-1}\left(\frac{p_{x2}\, p_{y2}}{p_{z1}\, d_{221}}\right)\right\} \\
& + \frac{p_{z2}^2}{2}\left\{ tan^{-1}\left(\frac{p_{x1}\, p_{y1}}{p_{z2}\, d_{112}}\right) - tan^{-1}\left(\frac{p_{x1}\, p_{y2}}{p_{z2}\, d_{122}}\right) + tan^{-1}\left(\frac{p_{x2}\, p_{y2}}{p_{z2}\, d_{222}}\right) - tan^{-1}\left(\frac{p_{x2}\, p_{y1}}{p_{z2}\, d_{212}}\right)\right\} . \qquad (4.34)
\end{aligned}
$$

Since the ℓog and tan^{-1} terms in this expression recur frequently in the remaining development, it will be advantageous to adopt the following abbreviated notation, in which the sequential order of the terms in 4.34 is definitive with respect to the numeric subscripts:

$$L_1 = \ell og\left(\frac{d_{111} + p_{z1}}{d_{112} + p_{z2}}\right),$$

$$L_2 = \ell og\left(\frac{d_{121} + p_{z1}}{d_{122} + p_{z2}}\right),$$

etcetera, through to L_{12};

$$T_1 = \left\{ \tan^{-1}\left(\frac{p_{y1}\, p_{z2}}{p_{x1}\, d_{112}}\right) - \tan^{-1}\left(\frac{p_{y1}\, p_{z1}}{p_{x1}\, d_{111}}\right) + \tan^{-1}\left(\frac{p_{y2}\, p_{z1}}{p_{x1}\, d_{121}}\right) - \tan^{-1}\left(\frac{p_{y2}\, p_{z2}}{p_{x1}\, d_{122}}\right)\right\},$$

and so on, up to T_6.

When the four expressions representing the potential due to the linear density parallelepipeds are combined, similar merging of pairs of ℓog terms occurs and further reduction of the ℓog terms connected with the coefficient p^3 may be effected; for instance:

$$\frac{p_{x1}^3}{12}\left\{\ell og\left(\frac{d_{122} - p_{y2}}{d_{122} + p_{y2}}\right) - \ell og\left(\frac{d_{112} - p_{y1}}{d_{112} + p_{y1}}\right)\right\} = \frac{p_{x1}^3}{12}\,\ell og\left(\frac{d_{122} - p_{y2}}{d_{122} + p_{y2}} \cdot \frac{d_{112} + p_{y1}}{d_{112} - p_{y1}}\right)$$

$$= \frac{p_{x1}^3}{12}\,\ell og\left(\frac{d_{122}^2 - p_{y2}^2}{(d_{122} + p_{y2})^2} \cdot \frac{(d_{112} + p_{y1})^2}{d_{112}^2 - p_{y1}^2}\right)$$

$$= \frac{p_{x1}^3}{6}\,\ell og\left(\frac{d_{112} + p_{y1}}{d_{122} + p_{y2}}\right),$$

in which the last step is achieved by expanding the d^2 terms using equations 4.30.

A final grouping of like terms leads to the expression for the potential due to the linear density part:

$$\frac{V_\ell}{kD} = \frac{p_{x1}}{6}\left(3p_{z2}^2 + p_{x1}^2\right) L_6 - \frac{p_{x1}}{6}\left(3p_{z1}^2 + p_{x1}^2\right) L_5 + \frac{p_{x2}}{6}\left(3p_{z1}^2 + p_{x2}^2\right) L_8 - \frac{p_{x2}}{6}\left(3p_{z2}^2 + p_{x2}^2\right) L_7$$
$$+ \frac{p_{y1}}{6}\left(3p_{z2}^2 + p_{y1}^2\right) L_{10} - \frac{p_{y1}}{6}\left(3p_{z1}^2 + p_{y1}^2\right) L_9 + \frac{p_{y2}}{6}\left(3p_{z1}^2 + p_{y2}^2\right) L_{12} - \frac{p_{y2}}{6}\left(3p_{z2}^2 + p_{y2}^2\right) L_{11}$$
$$+ \frac{p_{x1}\, p_{y2}}{3}\left(d_{121} - d_{122}\right) - \frac{p_{x1}\, p_{y1}}{3}\left(d_{111} - d_{112}\right) + \frac{p_{x2}\, p_{y1}}{3}\left(d_{211} - d_{212}\right) - \frac{p_{x2}\, p_{y2}}{3}\left(d_{221} - d_{222}\right)$$
$$- \frac{p_{z1}^3}{3} T_5 - \frac{p_{z2}^3}{3} T_6 \qquad (4.35)$$

Substitution of equations 4.34 and 4.35 into 4.29 gives the total potential V due to a parallelepiped with a vertical linear density model.

A more concise form of the expressions for the homogeneous and linear parts of the potential is achieved by introducing an indexed notation, which is more amenable to transcription to a computer algorithm. Thus:

$$V_h = k\sigma_p \sum_{i=1}^{3} \sum_{m=1}^{2} \sum_{n=0}^{1} (-1)^n \left\{ p_{im}\, p_{<i+1><m+n>}\, \ell og\left(\frac{d_{i\{m<m+n>1\}} + p_{<i+2>1}}{d_{i\{m<m+n>2\}} + p_{<i+2>2}}\right) + \sum_{j=1}^{2} (-1)^j \frac{p_{im}^2}{2} \tan^{-1}\left(\frac{p_{<i+1><m+n>}\, p_{<i+2>j}}{p_{im}\, d_{i\{m<m+n>j\}}}\right)\right\}, \qquad (4.34a)$$

and

$$V_\ell = \frac{kD}{3} \sum_{m=1}^{2} \sum_{n=0}^{1} (-1)^{n+1} \left[\sum_{i=1}^{2} \left(\frac{p_{<i+1>m}}{2} \left(3p^2_{3<m+n>} + p^2_{<i+1>m}\right) \log \left(\frac{d_{i\{1m\}<m+n>} + p_{i1}}{d_{i\{2m\}<m+n>} + p_{i2}} \right) \right) \right.$$
$$\left. + \sum_{j=1}^{2} (-1)^{j+1} \left(p_{1m}\, p_{2<m+n>}\, d_{m<m+n>j} + p^3_{3j} \tan^{-1} \left(\frac{p_{1m}\, p_{2<m+n>}}{p_{3j}\, d_{m<m+n>j}} \right) \right) \right], \tag{4.35a}$$

where equations 4.30 and 4.31 are rewritten in the indexed forms:

$$d_{mnj} = [p^2_{1m} + p^2_{2n} + p^2_{3j}]^{\frac{1}{2}} \tag{4.30b}$$

and

$$p_{im} = x_{ip} + (-1)^{m+1}\, a_i. \tag{4.31a}$$

Equivalence of notation between 4.31 and 4.31a may be represented as follows:

$$\left. \begin{array}{ll} (x_p, y_p, z_p) & \equiv x_{ip} \\ a, b, c & \equiv a_i \end{array} \right\} \quad (i = 1,3).$$

Additional special notation used includes:

(a) $<m+n>$ which indicates the modular value of the enclosed index†. This is effectively the remainder after dividing $m+n$ by the maximum value taken by the first of the enclosed indices; in this case m. It is given by:

$$<m+n> = (m+n) - \left[\frac{m+n}{m_\dagger} \right] m_\dagger$$

where [ ] indicates the integer part of the enclosed quantity and $m_\dagger$ is the maximum value of m.

(b) $i\{mnj\}$ indicating the ith left to right permutation of the enclosed indices; whence,

$$i\{mnj\} = \begin{cases} mnj & \text{when } i = 1 \\ jmn & \text{when } i = 2 \\ njm & \text{when } i = 3. \end{cases}$$

Application of these formulae for the potential requires a knowledge of only six quantities: the parallelepiped dimensions given by a, b, and c, and the coordinates of P in the local system (x_p, y_p, z_p). Parallelepiped dimensions are defined for the quadrature model in table 3.4. The requisite coordinates of P are given by equations 3.12, where the local reference frame is positioned at the mid point O_μ of the quadrature subdivision, given by $(\phi_\mu, \lambda_\mu, R_\mu)$.

4.4 COMPONENTS OF ATTRACTION

SPECIAL CASE

Returning to the configuration described at the beginning of §4.3 and figure 4.1, the gravitational attraction vector acting on unit mass at point P_0, due to the parallelepiped, may be determined by its rectangular components parallel to the stated reference frame. By considering the magnitudes of the force vector components, treatment of the attraction may proceed in a similar manner to that of the

†*Given by the Fortran IV function subprogramme MOD(Arg 1, Arg 2).*

potential, in terms of scalar equations throughout. Further, the summation technique applied to combine superposed parts remains valid—since $\nabla(V_h + V_\ell) = \nabla V_h + \nabla V_\ell$—enabling both the introduction of a linear density function and later extension from the special to the more general case.

According to equation 1.4 the attraction vector is

$$\mathbf{G}_0 = \nabla V_0 = G_{x0}\mathbf{i} + G_{y0}\mathbf{j} + G_{z0}\mathbf{k} \tag{4.36}$$

where $\mathbf{i}$, $\mathbf{j}$, $\mathbf{k}$ are unit vectors parallel to x_0, y_0, z_0 respectively, and

$$G_{x0} = \partial V_0/\partial x, \quad G_{y0} = \partial V_0/\partial y, \quad G_{z0} = \partial V_0/\partial z.$$

Retaining the linear density function stated in 4.19, the attraction components are obtained by differentiating equation 4.21. With some limitations on the applicability of the result [MACMILLAN 1930, p.25], it is permissible to interchange the order of differentiation and integration, so that:

$$G_{x0} = G_{x0h} + G_{x0\ell}$$

$$= k\sigma_p \int_0^{z_1}\int_0^{y_1}\int_0^{x_1} \frac{x_0\,dx_0\,dy_0\,dz_0}{[x_0^2 + y_0^2 + (z_0 - z_2)^2]^{3/2}} + kD\int_0^{z_1}\int_0^{y_1}\int_0^{x_1} \frac{x_0(z_0 - z_2)\,dx_0\,dy_0\,dz_0}{[x_0^2 + y_0^2 + (z_0 - z_2)^2]^{3/2}} \tag{4.37a}$$

$$G_{y0} = G_{y0h} + G_{y0\ell}$$

$$= k\sigma_p \int_0^{z_1}\int_0^{y_1}\int_0^{x_1} \frac{y_0\,dx_0\,dy_0\,dz_0}{[x_0^2 + y_0^2 + (z_0 - z_2)^2]^{3/2}} + kD\int_0^{z_1}\int_0^{y_1}\int_0^{x_1} \frac{y_0(z_0 - z_2)\,dx_0\,dy_0\,dz_0}{[x_0^2 + y_0^2 + (z_0 - z_2)^2]^{3/2}} \tag{4.37b}$$

$$G_{z0} = G_{z0h} + G_{z0\ell}$$

$$= k\sigma_p \int_0^{z_1}\int_0^{y_1}\int_0^{x_1} \frac{(z_0 - z_2)\,dx_0\,dy_0\,dz_0}{[x_0^2 + y_0^2 + (z_0 - z_2)^2]^{3/2}} + kD\int_0^{z_1}\int_0^{y_1}\int_0^{x_1} \frac{(z_0 - z_2)^2\,dx_0\,dy_0\,dz_0}{[x_0^2 + y_0^2 + (z_0 - z_2)^2]^{3/2}} \tag{4.37c}$$

where h and ℓ indicate homogeneous and linear parts as before.

Because of symmetry, it is not necessary to further develop the expressions for the y components, since the result will be the same as that for x, with x and y interchanged throughout. Dealing with the x component first, the homogeneous part is a standard integral in x_0, (equation 4.3):

$$\frac{G_{x0h}}{k\sigma_p} = \int_0^{z_1}\int_0^{y_1}\int_0^{x_1} \frac{x_0\,dx_0\,dy_0\,dz_0}{[x_0^2 + y_0^2 + (z_0 - z_2)^2]^{3/2}}$$

$$= \int_0^{z_1}\int_0^{y_1} \left(\frac{1}{[y_0^2 + (z_0 - z_2)^2]^{\frac{1}{2}}} - \frac{1}{[x_1^2 + y_0^2 + (z_0 - z_2)^2]^{\frac{1}{2}}}\right) dy_0\,dz_0$$

which, by equation 4.1a

$$= \int_0^{z_1} \left\{ \sinh^{-1}\left(\frac{y_1}{z_0 - z_2}\right) - \sinh^{-1}\left(\frac{y_1}{[x_1^2 + (z_0 - z_2)^2]^{\frac{1}{2}}}\right)\right\} dz_0 \tag{4.38}$$

$$= \left| (z_0 - z_2)\sinh^{-1}\left(\frac{y_1}{z_0 - z_2}\right) + y_1\sinh^{-1}\left(\frac{z_0 - z_2}{y_1}\right)\right.$$

$$- (z_0 - z_2)\, sinh^{-1}\left(\frac{y_1}{[x_1^2 + (z_0 - z_2)^2]^{\frac{1}{2}}}\right) - y_1\, sinh^{-1}\left(\frac{z_0 - z_2}{[x_1^2 + y_1^2]^{\frac{1}{2}}}\right)$$

$$+ x_1\, tan^{-1}\left(\frac{y_1(z_0 - z_2)}{x_1[x_1^2 + y_1^2 + (z_0 - z_2)^2]^{\frac{1}{2}}}\right)\Bigg|_0^{z_1},$$

the last step being achieved by treating both terms of 4.38 as the general form given in equation 4.9. Evaluation at the limits gives:

$$\frac{G_{x0h}}{k\sigma_p} = (z_1 - z_2) sinh^{-1}\left(\frac{y_1}{z_1 - z_2}\right) - z_2\, sinh^{-1}\left(\frac{y_1}{z_2}\right) + y_1\, sinh^{-1}\left(\frac{z_1 - z_2}{y_1}\right) + y_1\, sinh^{-1}\left(\frac{z_2}{y_1}\right)$$

$$- (z_1 - z_2)\, sinh^{-1}\left(\frac{y_1}{[x_1^2 + (z_1 - z_2)^2]^{\frac{1}{2}}}\right) - z_2\, sinh^{-1}\left(\frac{y_1}{[x_1^2 + z_2^2]^{\frac{1}{2}}}\right)$$

$$- y_1\, sinh^{-1}\left(\frac{z_1 - z_2}{[x_1^2 + y_2^2]^{\frac{1}{2}}}\right) - y_1\, sinh^{-1}\left(\frac{z_2}{[x_1^2 + y_2^2]^{\frac{1}{2}}}\right)$$

$$+ x_1\, tan^{-1}\left(\frac{y_1(z_1 - z_2)}{x_1[x_1^2 + y_1^2 + (z_1 - z_2)^2]^{\frac{1}{2}}}\right) + x_1\, tan^{-1}\left(\frac{y_1\, z_2}{x_1[x_1^2 + y_2^2 + z_2^2]^{\frac{1}{2}}}\right) \tag{4.39}$$

The linear density term in the expression for G_{x0} may be written:

$$\frac{G_{x0\ell}}{kD} = \int_0^{z_1} (z_0 - z_2) \int_0^{y_1} \int_0^{x_1} \frac{x_0\, dx_0\, dy_0\, dz_0}{[x_0^2 + y_0^2 + (z_0 - z_2)^2]^{3/2}}$$

which, on substituting the result for the double integral given in equation 4.38,

$$= \int_0^{z_1} (z_0 - z_2)\left\{sinh^{-1}\left(\frac{y_1}{z_0 - z_2}\right) - sinh^{-1}\left(\frac{y_1}{[x_1^2 + (z_0 - z_2)^2]^{\frac{1}{2}}}\right)\right\} dz_0$$

$$= \Bigg| \frac{(z_0 - z_2)^2}{2}\, sinh^{-1}\left(\frac{y_1}{z_0 - z_2}\right) + \frac{y_1}{2}\, [y_1^2 + (z_0 - z_2)^2]^{\frac{1}{2}}$$

$$- \frac{(z_0 - z_2)^2}{2}\, sinh^{-1}\left(\frac{y_1}{[x_1^2 + (z_0 - z_2)^2]^{\frac{1}{2}}}\right) - \frac{y_1}{2}\, [x_1^2 + y_1^2 + (z_0 - z_2)^2]^{\frac{1}{2}}$$

$$+ \frac{x_1}{4}\, \ell og\left(\frac{[x_1^2 + y_1^2 + (z_0 - z_2)^2]^{\frac{1}{2}} - y_1}{[x_1^2 + y_1^2 + (z_0 - z_2)^2]^{\frac{1}{2}} + y_1}\right)\Bigg|_0^{z_1};$$

using the general form given in 4.15. Evaluating at the limits gives the expression for the x component in the special case:

$$\frac{G_{x0\ell}}{kD} = \frac{(z_1 - z_2)^2}{2} \sinh^{-1}\left(\frac{y_1}{z_1 - z_2}\right) + \frac{z_2^2}{2} \sinh^{-1}\left(\frac{y_1}{z_2}\right)$$

$$- \frac{(z_1 - z_2)^2}{2} \sinh^{-1}\left(\frac{y_1}{[x_1^2 + (z_1 - z_2)^2]^{\frac{1}{2}}}\right) + \frac{z_2^2}{2} \sinh^{-1}\left(\frac{y_1}{[x_1^2 + z_2^2]^{\frac{1}{2}}}\right)$$

$$+ \frac{x_1^2}{4} \log\left(\frac{[x_1^2 + y_1^2 + (z_1 - z_2)^2]^{\frac{1}{2}} - y_1}{[x_1^2 + y_1^2 + (z_1 - z_2)^2]^{\frac{1}{2}} + y_1}\right) - \frac{x_1^2}{4} \log\left(\frac{[x_1^2 + y_1^2 + z_2^2]^{\frac{1}{2}} - y_1}{[x_1^2 + y_1^2 + z_2^2]^{\frac{1}{2}} + y_1}\right)$$

$$+ \frac{y_1}{2} [y_1^2 + (z_1 - z_2)^2]^{\frac{1}{2}} - \frac{y_1}{2} [y_1^2 + z_2^2]^{\frac{1}{2}}$$

$$- \frac{y_1}{2} [x_1^2 + y_1^2 + (z_1 - z_2)^2]^{\frac{1}{2}} + \frac{y_1}{2} [x_1^2 + y_1^2 + z_2^2]^{\frac{1}{2}}. \tag{4.40}$$

In treating the z component, symmetry is of further advantage in establishing the homogeneous part, which is obtained directly by interchanging x and $(z_0 - z_2)$ in the expression for G_{x0h}, before evaluating at the limits of z_0. Hence,

$$\frac{G_{z0h}}{k\sigma_p} = \left| x_1 \sinh^{-1}\left(\frac{y_1}{x_1}\right) + y_1 \sinh^{-1}\left(\frac{x_1}{y_1}\right) - x_1 \sinh^{-1}\left(\frac{y_1}{[x_1^2 + (z_0 - z_2)^2]^{\frac{1}{2}}}\right) - y_1 \sinh^{-1}\left(\frac{x_1}{[y_1^2 + (z_0 - z_2)^2]^{\frac{1}{2}}}\right)\right.$$

$$\left. + (z_0 - z_2) \tan^{-1}\left(\frac{x_1 y_1}{(z_0 - z_2)[x_1^2 + y_1^2 + (z_0 - z_2)^2]^{\frac{1}{2}}}\right)\right|_0^{z_0}$$

$$= x_1 \sinh^{-1}\left(\frac{y_1}{[x_1^2 + z_2^2]^{\frac{1}{2}}}\right) - x_1 \sinh^{-1}\left(\frac{y_1}{[x_1^2 + (z_1 - z_2)^2]^{\frac{1}{2}}}\right)$$

$$+ y_1 \sinh^{-1}\left(\frac{x_1}{[y_1^2 + z_2^2]^{\frac{1}{2}}}\right) - y_1 \sinh^{-1}\left(\frac{x_1}{[y_1^2 + (z_1 - z_2)^2]^{\frac{1}{2}}}\right)$$

$$+ (z_1 - z_2) \tan^{-1}\left(\frac{x_1 y_1}{(z_1 - z_2)[x_1^2 + y_2^2 + (z_1 - z_2)^2]^{\frac{1}{2}}}\right) - z_2 \tan^{-1}\left(\frac{x_1 y_1}{z_2[x_1^2 + y_1^2 + z_2^2]^{\frac{1}{2}}}\right). \tag{4.41}$$

In equation 4.37c the linear part of the z component is a standard integral in z_0 given by equation 4.4:

$$\frac{G_{z0\ell}}{kD} = \int_0^{x_1} \int_0^{y_1} \int_0^{z_1} \frac{(z_0 - z_2)^2 \, dz_0 \, dy_0 \, dx_0}{[x_0^2 + y_0^2 + (z_0 - z_2)^2]^{3/2}}$$

$$= \int_0^{x_1} \int_0^{y_1} \left(\sinh^{-1}\left(\frac{z_1 - z_2}{[x_0^2 + y_0^2]^{\frac{1}{2}}}\right) + \sinh^{-1}\left(\frac{z_2}{[x_0^2 + y_0^2]^{\frac{1}{2}}}\right) \right.$$

$$\left. - \frac{z_1 - z_2}{[x_0^2 + y_0^2 + (z_1 - z_2)^2]^{\frac{1}{2}}} - \frac{z_2}{[x_0^2 + y_0^2 + z_2^2]^{\frac{1}{2}}} \right) dy_0 \, dx_0$$

Integration with respect to y_0 involves the results 4.1a and 4.9, and after cancellation of some terms:

$$\frac{G_{z0\ell}}{kD} = \int_0^{x_1} \left\{ y_1 \,sinh^{-1}\left(\frac{z_1 - z_2}{[x_0^2 + y_1^2]^{\frac{1}{2}}}\right) + y_1 \,sinh^{-1}\left(\frac{z_2}{[x_0^2 + y_1^2]^{\frac{1}{2}}}\right) - x_0 tan^{-1}\left(\frac{y_1(z_1 - z_2)}{x_0[x_0^2 + y_1^2 + (z_1 - z_2)^2]^{\frac{1}{2}}}\right) - x_0 tan^{-1}\left(\frac{y_1 \, z_2}{x_0[x_0^2 + y_1^2 + z_2^2]^{\frac{1}{2}}}\right)\right\} dx_0 .$$

Substitution of the general forms given in 4.9 and 4.11 and collection of terms leads to:

$$\begin{aligned}\frac{G_{z0\ell}}{kD} = \Bigg| & x_0 y_1 \,sinh^{-1}\left(\frac{z_1 - z_2}{[x_0^2 + y_1^2]^{\frac{1}{2}}}\right) + x_0 y_1 \,sinh^{-1}\left(\frac{z_2}{[x_0^2 + y_1^2]^{\frac{1}{2}}}\right) \\ & - \frac{y_1^2}{2} tan^{-1}\left(\frac{x_0(z_1 - z_2)}{y_1[x_0^2 + y_1^2 + (z_1 - z_2)^2]^{\frac{1}{2}}}\right) - \frac{y_1^2}{2} tan^{-1}\left(\frac{x_0 \, z_2}{y_1[x_0^2 + y_1^2 + z_2^2]^{\frac{1}{2}}}\right) \\ & - \frac{x_0^2}{2} tan^{-1}\left(\frac{y_1(z_1 - z_2)}{x_0[x_0^2 + y_1^2 + (z_1 - z_2)^2]^{\frac{1}{2}}}\right) - \frac{x_0^2}{2} tan^{-1}\left(\frac{y_1 \, z_2}{x_0[x_0^2 + y_1^2 + z_2^2]^{\frac{1}{2}}}\right) \\ & + \frac{(z_1 - z_2)^2}{2} tan^{-1}\left(\frac{x_0 \, y_1}{(z_1 - z_2)[x_0^2 + y_1^2 + (z_1 - z_2)^2]^{\frac{1}{2}}}\right) + \frac{z_2^2}{2} tan^{-1}\left(\frac{x_0 \, y_1}{z_2[x_0^2 + y_1^2 + z_2^2]^{\frac{1}{2}}}\right)\Bigg|_0^{x_1} .\end{aligned}$$

In evaluating at the limits all terms vanish when $x_0 = 0$, so that:

$$\begin{aligned}\frac{G_{z0\ell}}{kD} = \; & x_1 y_1 \,sinh^{-1}\left(\frac{z_1 - z_2}{[x_1^2 + y_1^2]^{\frac{1}{2}}}\right) + x_1 y_1 \,sinh^{-1}\left(\frac{z_2}{[x_1^2 + y_1^2]^{\frac{1}{2}}}\right) \\ & - \frac{y_1^2}{2} tan^{-1}\left(\frac{x_1(z_1 - z_2)}{y_1[x_1^2 + y_1^2 + (z_1 - z_2)^2]^{\frac{1}{2}}}\right) - \frac{y_1^2}{2} tan^{-1}\left(\frac{x_1 \, z_2}{y_1[x_1^2 + y_1^2 + z_2^2]^{\frac{1}{2}}}\right) \\ & - \frac{x_1^2}{2} tan^{-1}\left(\frac{y_1(z_1 - z_2)}{x_1[x_1^2 + y_1^2 + (z_1 - z_2)^2]^{\frac{1}{2}}}\right) - \frac{x_1^2}{2} tan^{-1}\left(\frac{y_1 \, z_2}{x_1[x_1^2 + y_1^2 + z_2^2]^{\frac{1}{2}}}\right) \\ & + \frac{(z_1 - z_2)^2}{2} tan^{-1}\left(\frac{x_1 \, y_1}{(z_1 - z_2)[x_1^2 + y_1^2 + (z_1 - z_2)^2]^{\frac{1}{2}}}\right) + \frac{z_2^2}{2} tan^{-1}\left(\frac{x_1 \, y_1}{z_2[x_1^2 + y_1^2 + z_2^2]^{\frac{1}{2}}}\right) .\end{aligned} \tag{4.42}$$

ATTRACTION AT A GENERAL POINT

Generalization of the attraction may proceed along the same lines as used in §4.3, since the components are unchanged by a parallel translation of the reference frame to the centroid of the general parallelepiped and the combination of superposed parts requires only summation of scalar components. Then, adopting the same configuration of four parallelepipeds as before, the attraction of the general parallelepiped *ABCDEFGH* (figure 4.2) is given by (*cf.* 4.28 and 4.29):

$$G_x = (G_{x1h} - G_{x2h} - G_{x3h} + G_{x4h}) + (G_{x1\ell} - G_{x2\ell} - G_{x3\ell} + G_{x4\ell}) \tag{4.43}$$

$$= G_{xh} + G_{x\ell}; \tag{4.44}$$

with similar relations for G_y and G_z. Expansion of these equations is effected by substitution of expressions in the form of 4.39 and 4.40 for G_x (and G_y by symmetry), and 4.41 and 4.42 for G_z. The replacements of table 4.1 remain applicable and again the notation of 4.30 and 4.31 may be used. Then, taking the first parallelepiped as an example, the homogeneous and linear parts are:

$$\frac{G_{x1h}}{k\sigma_p} = -p_{z2}\ \ell og\left(\frac{p_{y2}+d_{022}}{p_{z2}}\right) + p_{z1}\ \ell og\left(\frac{p_{y2}+d_{021}}{p_{z1}}\right) + p_{y1}\ \ell og\left(\frac{d_{022}+p_{z2}}{-p_{y2}}\right) - p_{y1}\ \ell og\left(\frac{d_{021}+p_{z1}}{-p_{y2}}\right)$$

$$- p_{z2}\ \ell og\left(\frac{p_{y2}+d_{222}}{d_{202}}\right) + p_{z1}\ \ell og\left(\frac{p_{y2}+d_{221}}{d_{201}}\right) - p_{y2}\ \ell og\left(\frac{d_{222}+p_{z2}}{d_{220}}\right) + p_{y2}\ \ell og\left(\frac{d_{221}+p_{z1}}{d_{220}}\right)$$

$$+ p_{x2}\ tan^{-1}\left[\frac{p_{y2}\ p_{z2}}{p_{x2}\ d_{222}}\right] - p_{x2}\ tan^{-1}\left[\frac{p_{y2}\ p_{z1}}{p_{x2}\ d_{221}}\right], \qquad (4.45)$$

$$\frac{G_{x1\ell}}{kD} = \frac{p_{z2}^2}{2}\ \ell og\left(\frac{d_{022}+p_{y2}}{p_{z2}}\right) - \frac{p_{z1}^2}{2}\ \ell og\left(\frac{d_{021}+p_{y2}}{p_{z1}}\right) + \frac{p_{z2}^2}{2}\ \ell og\left(\frac{d_{222}+p_{y2}}{d_{202}}\right) - \frac{p_{z1}^2}{2}\ \ell og\left(\frac{d_{221}+p_{y2}}{d_{202}}\right)$$

$$- \frac{p_{x2}^2}{4}\ \ell og\left[\frac{d_{222}+p_{y2}}{d_{222}-p_{y2}}\right] + \frac{p_{x1}^2}{4}\ \ell og\left[\frac{d_{221}+p_{y2}}{d_{221}-p_{y2}}\right] - \frac{p_{y2}}{2}\ (d_{022} - d_{021} - d_{222} + d_{221}); \qquad (4.46)$$

and, as in §4.3, the remaining terms of 4.43 are obtained by appropriate manipulation of subscripts. When the terms for the homogeneous part are combined the first four ℓog terms may be cancelled and pairs with the same coefficients merged, so that, in the notation of §4.3:

$$\frac{G_{xh}}{k\sigma_p} = p_{y1}\ L_1 - p_{y2}\ L_2 + p_{y2}\ L_3 - p_{y1}\ L_4 + p_{z1}\ L_5 - p_{z2}\ L_6 + p_{z2}\ L_7 - p_{z1}\ L_8 + p_{x1}\ T_1 + p_{x2}\ T_2 \qquad (4.47)$$

Similarly, cancellation and merging of terms occurs in the linear part, leading to:

$$\frac{G_{x\ell}}{kD} = \frac{1}{2}(p_{z2}^2 + p_{x1}^2)L_6 - \frac{1}{2}(p_{z1}^2 + p_{x1}^2)L_5 + \frac{1}{2}(p_{z1}^2 + p_{x2}^2)L_8 - \frac{1}{2}(p_{z2}^2 + p_{x2}^2)L_7$$

$$+ \frac{p_{y1}}{2}\ (d_{211} - d_{212} - d_{111} + d_{112}) + \frac{p_{y2}}{2}\ (d_{121} - d_{122} - d_{221} + d_{222}). \qquad (4.48)$$

Combining 4.47 and 4.48 in accordance with 4.44 provides the total x component of the attraction, and the total y component by symmetry. Expansion of the z component proceeds in a like manner, using 4.41 and 4.42:

$$\frac{G_{z1h}}{k\sigma_p} = p_{x2}\ \ell og\left(\frac{d_{221}+p_{y2}}{d_{201}}\right) - p_{x2}\ \ell og\left(\frac{d_{222}+p_{y2}}{d_{202}}\right) + p_{y2}\ \ell og\left(\frac{d_{221}+p_{x2}}{d_{021}}\right) - p_{y1}\ \ell og\left(\frac{d_{222}+p_{x2}}{d_{022}}\right)$$

$$- p_{z1}\ tan^{-1}\left[\frac{p_{x2}\ p_{y2}}{p_{z1}\ d_{221}}\right] + p_{z2}\ tan^{-1}\left[\frac{p_{x2}\ p_{y2}}{p_{z2}\ d_{222}}\right], \qquad (4.49)$$

$$\frac{G_{z1\ell}}{kD} = p_{x2}\ p_{y2}\ \ell og\left(\frac{d_{221}+p_{z1}}{d_{220}}\right) - p_{x2}\ p_{y2}\ \ell og\left(\frac{d_{222}+p_{z2}}{d_{220}}\right)$$

$$+ \frac{p_{x2}^2}{2}\left[tan^{-1}\left[\frac{p_{y2}\ p_{z2}}{p_{x2}\ d_{222}}\right] - tan^{-1}\left[\frac{p_{y2}\ p_{z1}}{p_{x2}\ d_{221}}\right]\right] + \frac{p_{y2}^2}{2}\left[tan^{-1}\left[\frac{p_{x2}\ p_{z2}}{p_{y2}\ d_{222}}\right] - tan^{-1}\left[\frac{p_{x2}\ p_{z1}}{p_{y2}\ d_{221}}\right]\right]$$

$$+\frac{p_{z1}^2}{2}\tan^{-1}\left\{\frac{p_{x2}\,p_{y2}}{p_{z1}\,d_{221}}\right\} - \frac{p_{z2}^2}{2}\tan^{-1}\left\{\frac{p_{x2}\,p_{y2}}{p_{z2}\,d_{222}}\right\}. \tag{4.50}$$

Once again, manipulation of numeric subscripts provides the remaining terms of G_{zh} and $G_{z\ell}$. When combined, no cancellation of these terms occurs, but combination of terms with like coefficients leads to:

$$\frac{G_{zh}}{k\sigma_p} = p_{x1}L_5 - p_{x1}L_6 + p_{x2}L_7 - p_{x2}L_8 + p_{y1}L_9 - p_{y1}L_{10} + p_{y2}L_{11} - p_{y2}L_{12} + p_{z1}T_5 + p_{z2}T_6 \tag{4.51}$$

and

$$\frac{G_{z\ell}}{kD} = p_{x1}p_{y1}L_1 - p_{x1}p_{y2}L_2 + p_{x2}p_{y2}L_3 - p_{x2}p_{y1}L_4$$

$$+\frac{p_{x1}^2}{2}T_1 + \frac{p_{x2}^2}{2}T_2 + \frac{p_{y1}^2}{2}T_3 + \frac{p_{y2}^2}{2}T_4 - \frac{p_{z1}^2}{2}T_5 - \frac{p_{z2}^2}{2}T_6 \tag{4.52}$$

The total z component of the attraction is then available by combining 4.51 and 4.52.

All of the terms which make up the expressions for the attraction components have previously occurred in the potential equations. Consequently, separate computer algorithms are not necessary, as the attraction components can be computed concurrently within the potential algorithm.

Parallelepiped dimensions and coordinates of P are determined in the same way as for the potential. The attraction components resulting from the above formulae, while evaluated as though originating at P, are oriented parallel to the axes of the local reference frame at the centroid of the parallelepiped. Consequently, before a global accumulation can be effected at P, the components arising from individual quads must be transformed into the same reference system, preferably a local system at P. Computation time is saved if the accumulation is made in a geocentrically oriented system, followed by a final transformation of the total components to the local system at P. Thus, before summation, the transformation stated in equations 3.9 is applied to the results for each quad, and the final transformation of the accumulated components is in accordance with equations 3.11.

4.5 CHECKS AND PRACTICAL CONSIDERATIONS IN EVALUATION OF THE FORMULAE

CHECKS

Verification of the formulae derived in sections 4.3 and 4.4 may be implemented in different ways. None of these assures absolute and independent validity. Nevertheless they at least test internal consistency and conformity with the physical realities of the model which the formulae purport to represent. Possible checks include:

(a) Reduction to a simpler model for which correct formulae are independently known.
(b) Consistency with the symmetry of the model.
(c) Dimensional conformity.
(d) Theoretical and numerical agreement between the potential and attraction formulae in accordance with equation 1.4.

REDUCTION CHECKS. If the linear component of the density is removed, all of the formulae involving the remaining homogeneous density component are directly comparable with the results given by MACMILLAN [1930, p.78 *et seq.*]. Additionally, if the dimensions of the parallelepiped are set so that $b = a$ and the coordinates of P are chosen with $x_p = y_p = 0$, then the configuration of figure 2.2 is obtained. Under these conditions the following checks are substantiated:

(a) equation 4.34 agrees with equation 2.3,

(b) equation 4.47 reduces to zero, and

(c) equation 4.51 agrees with the partial derivative of equation 2.3 with respect to h_p.

Further reduction of the parallelepiped to planes and lines, oriented in a variety of ways with respect to P, provides formulae for both potential and attraction which may be compared with results given by MACMILLAN [1930] in §§7,8,18, and 31.

SYMMETRY CHECKS. Triple symmetry of the parallelepiped is reflected in the formulae as follows:

(a) x, y, and z all appear uniformly in equation 4.34, as do x and y in equations 4.35, 4.51, and 4.52; and y and z in equation 4.47.

(b) x and z are interchangeable between equations 4.47 and 4.51.

DIMENSIONAL CHECKS. Dimensions of all quantities are listed in §1.2. A comparison of the dimensions to be expected on the left and right hand sides of the potential and attraction equations is made in table 4.2. Every term on the right hand side of a formula should conform with the tablulated dimensions.

TABLE 4.2

DIMENSIONAL CONFORMITY OF EQUATIONS FOR POTENTIAL AND ATTRACTION

QUANTITY	NOTATION	L.H.S. DIMENSIONS	R.H.S. DIMENSION
Potential — homogeneous part	$\frac{V_h}{k\sigma_p}$	$\frac{[L^2 T^{-2}]}{[M^{-1} L^3 T^{-2}][M L^{-3}]}$	$[L^2]$
Potential — Linear part	$\frac{V_\ell}{kD}$	$\frac{[L^2 T^{-2}]}{[M^{-1} L^3 T^{-2}][M L^{-4}]}$	$[L^3]$
Attraction — Homogeneous part	$\frac{G_h}{k\sigma_p}$	$\frac{[L T^{-2}]}{[M^{-1} L^3 T^{-2}][M L^{-3}]}$	$[L]$
Attraction — Linear part	$\frac{G_\ell}{kD}$	$\frac{[L T^{-2}]}{[M^{-1} L^3 T^{-2}][M L^{-4}]}$	$[L^2]$

ATTRACTION COMPONENTS BY PARTIAL DIFFERENTIATION OF POTENTIAL. MACMILLAN [1930, p.80] demonstrates that the partial differentiation of potential formulae for *homogeneous* bodies may proceed with certain terms containing the independent variable treated as constants. In particular, the potential formula given by equation 4.34 may be differentiated with respect to x_p, y_p, or z_p with the ℓog and tan^{-1} terms held constant, thus easily yielding the homogeneous parts of the three attraction components. This process does not necessarily hold for the linear density parts and the differentiation procedure is thereby rendered intractable.

However, numerical differentiation offers a simple method of not only checking the formulae, but also the correctness of their transcription into computer routines. The technique involves evaluation of the potential and attraction components for a particular position of the computation point P, followed by successive re-evaluations of the potential for points displaced from P by small amounts in the directions of the reference frame axes. If the displacements are sufficiently small, the change in potential should equal the attraction component in the direction of the displacement. In practice a displacement of one metre was found to give results which were consistent within the precision of the computer routines. Because the linear density model incorporated in the formulae (equation 4.26) uses

P, rather than the coordinate origin, as a datum, it is essential to take account of the change in σ_p consequent upon the small displacement of P.

VIABILITY OF THE FORMULAE

All of the formulae must be shown to be viable—that is, retain meaning—in all of the possible circumstances in which they might be applied. There are two aspects to this problem: firstly, the formulae must remain theoretically sound, and secondly arrangements must be made to ensure that they do not fail for practical reasons—such as underflow or overflow conditions, or the lack of precision—during computer evaluation.

LIMITING CONVERGENCE OF FORMULAE. As all of the possible forms which terms may assume are represented in equation 4.34, it will be necessary to consider only this formula. Two situations may occur in which some terms could become indeterminate: the denominator in the argument of a $\log$ term could become zero, or the same may happen to a $\tan^{-1}$ term. In the former case, consideration of the geometry shows that the numerator cannot simultaneously become zero, however this need not be so in the case of the $\tan^{-1}$ terms. Geometrically, all such situations can be brought about only by the computation point coming into the plane of at least one face of the parallelepiped—the extreme case being coincidence with a corner. Inspection of the quantities involved indicates that the coefficient of the particular term in question must also become zero.

Treating the $\tan^{-1}$ terms first: they are seen to occur in groups of four, and each term can assume values only in the range $-\pi$ to $+\pi$. Whatever limit may be taken by these terms, it will be possible to combine them in pairs with equal value but opposite sign, so that the difference is zero.

The $\log$ terms may be generalized as:

$$uv \log\left(\frac{[u^2 + v^2 + w_1^2]^{\frac{1}{2}} + w_1}{[u^2 + v^2 + w_2^2]^{\frac{1}{2}} + w_2}\right), \tag{4.53}$$

in which u and v may be zero simultaneously and the denominator will be zero if w_2 is negative. In this case, the limiting value of the term is given by:

$$\begin{aligned} &\lim_{s,t\to 0} \left\{s \log[(u^2 + v^2 + w_1^2)^{\frac{1}{2}} + w_1] - s \log t\right\} \\ &\qquad = 0 + \lim_{s,t\to 0} (s \log t), \end{aligned} \tag{4.54}$$

where $s = uv$ and $t = (u^2 + v^2 + w_2^2) + w_2$; since the argument of the first $\log$ term is non-zero. Putting:

$$s = C_s\, e^{-q}, \quad t = C_t\, e^{-q},$$

where e is the exponential function for unit argument, and C_s and C_t are constants such that:

$$1 < \left\{ \begin{matrix} C_s \\ C_t \end{matrix} \right\} < e,$$

converts equation 4.54 to:

$$\lim_{q\to\infty} C_s\, e^{-q} \log(C_t\, e^{-q}) = -C_s \lim_{q\to\infty}\left(\frac{q}{e^q}\right) + C_s \lim_{q\to\infty}\left(\frac{\log C_t}{e^q}\right) = 0 + 0; \tag{4.55}$$

following HARDY [1958, ex. XXVII, (3)].

COMPUTATIONAL VIABILITY. Since both of the limiting conditions investigated above converge to zero, it is a simple matter to test for a denominator which may approach zero and omit computation of that term if necessary.

Theoretically, no difficulty should arise from the arguments of the ℓog terms becoming negative, because the magnitude of the "diagonal" distance d always exceeds that of the perpendicular distance p. Unfortunately, inadequate computational precision may generate this condition in special circumstances. For instance, in equation 4.53, if

$$u^2 + v^2 << w_1^2 \tag{4.56}$$

so that

$$\ell og_{10}\, w_1^2 - \ell og_{10}(u^2 + v^2) > N_{10},$$

where N_{10} is the number of machine decimal digits, then the machine sum $(u^2 + v^2 + w_1^2)$ will equal w_1^2 and further loss of precision in the square root function may produce a zero or negative value for the numerator when w_1 is negative. The same process may affect the denominator. By this means division of numerator by denominator may generate machine overflow or an attempt to find the logarithm of a negative argument may result. A procedure which circumvents this difficulty may be devised as follows. In equation 4.53 let

$$\begin{aligned} d &= (u^2 + v^2 + w_1^2)^{\frac{1}{2}} \\ &= (s^2 + w_1^2)^{\frac{1}{2}} \\ &= |w_1| \left(1 + \frac{s^2}{w_1^2}\right)^{\frac{1}{2}} \end{aligned}$$

Then, since $s^2/w_1^2 < 1$ by equation 4.56, expansion by the binomial theorem gives

$$d = |w_1| + \frac{s^2}{2|w_1|} - \frac{s^4}{8|w_1|^3} + \ldots \tag{4.57}$$

and the numerator is given by

$$\frac{s^2}{2|w_1|} - \frac{s^4}{8|w_1|^3} + \ldots \tag{4.58}$$

when w_1 is negative.

5

Gravity Field of a Non-homogeneous Body at a Distant Point

5.1 INTRODUCTION

The following development is based on that given by MACMILLAN [1930, p.81 *et seq*.], extended to incorporate a linear density model. In addition, the components of attraction are formulated by differentiation of the potential.

Essentially, the method relies on the fundamental dependence of the gravitational potential on the "reciprocal distance" and the possibility of expanding this harmonic function in terms of Legendre's polynomials. Integration of the resulting series may proceed conventionally, under conditions for which it is convergent. Differentiation of the result, with respect to a chosen reference frame, will then provide the components of the attraction vector.

The advantageous consequences of symmetry, utilized in chapter 4, remain prominent in the following derivation and subsequent verification of formulae.

5.2 EXPANSION OF THE RECIPROCAL DISTANCE IN LEGENDRE POLYNOMIALS

In figure 5.1, B is a finite, irregular body and P any distant point. Let o_0 be the origin of an arbitrarily chosen cartesian reference frame (x,y,z), in which the coordinates of P are (x_p,y_p,z_p) and of dM—an element of mass of B—are (x,y,z). Let dM be at a distance t from the origin and s from P, and the distance $o_0P = d$.

The potential of B at P is (eq. 1.3):

$$V = k\iiint_B \frac{dM}{s}$$

and by plane trigonometry,

$$s^2 = d^2 + t^2 - 2td \cos \beta \tag{5.1}$$

where β is the angle between the directions of dM and P from the origin. From equation 5.1 the reciprocal distance is:

5. NON-HOMOGENEOUS BODY AT A DISTANT POINT

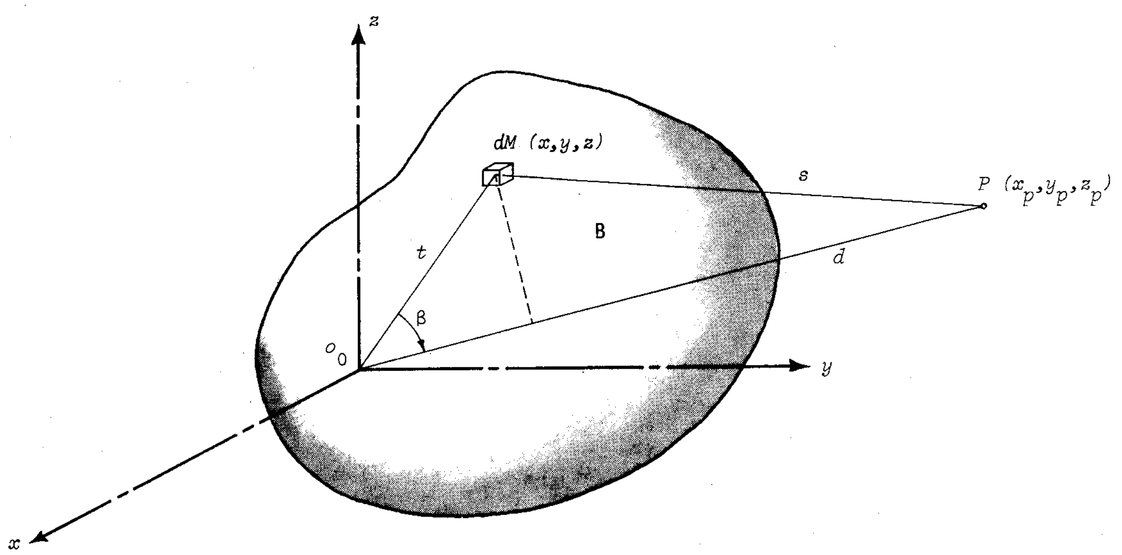

FIGURE 5.1

NON-HOMOGENEOUS IRREGULAR BODY AND A DISTANT POINT

$$\frac{1}{s} = \frac{1}{d}\left(1 - \frac{2t}{d}\cos\beta + \frac{t^2}{d^2}\right)^{-\frac{1}{2}}$$

which, for $t/d < 1$, may be expanded as a power series by application of the binomial theorem. Hence,

$$\frac{1}{s} = \frac{1}{d}\left\{1 + \cos\beta\,\frac{t}{d} + \frac{1}{2}(3\cos^2\beta - 1)\frac{t^2}{d^2} + \frac{1}{2}(5\cos^3\beta - 3\cos\beta)\frac{t^3}{d^3}\right.$$
$$\left. + \frac{1}{8}(35\cos^4\beta - 30\cos^2\beta + 3)\frac{t^4}{d^4} + \ldots\right\} \tag{5.2}$$

and the coefficients are Legendre's polynomials, usually designated by $P_n(\cos\beta)$. Allowing limitations on the closeness of P to the body, it can be shown [MACMILLAN 1930, p.83] that this series is absolutely and uniformly convergent, and, therefore, may be integrated term by term to yield the potential:

$$V = \frac{k}{d}\iiint_B dM + \frac{k}{d^2}\iiint_B t\cos\beta\,dM + \frac{k}{2d^3}\iiint_B (3t^2\cos^2\beta - t^2)dM$$
$$+ \frac{k}{2d^4}\iiint_B (5t^3\cos^3\beta - 3t^3\cos\beta)dM + \frac{k}{8d^5}\iiint_B (35t^4\cos^4\beta - 30t^4\cos^2\beta + 3t^4)dM + \ldots \tag{5.3}$$

$$= V_0 + V_1 + V_2 + V_3 + V_4 + \ldots \tag{5.4}$$

Assuming a linear density model of the form:

$$\sigma = \sigma_\mu + Dz, \tag{5.5}$$

where σ_μ is the mean density of the body, the elemental mass becomes:

$$dM = \sigma\,dv = \sigma\,dx\,dy\,dz \tag{5.6}$$

dv being the equivalent elemental volume.

Substituting equation 5.6 into 5.3, and treating each integral in turn gives:

$$V_0 = \frac{k}{d}\iiint\limits_B \sigma\, dx\, dy\, dz$$

$$= \frac{k\sigma_\mu}{d}\iiint\limits_B dx\, dy\, dz + \frac{kD}{d}\iiint\limits_B z\, dx\, dy\, dz \tag{5.7}$$

$$V_1 = \frac{k\sigma_\mu}{d^2}\iiint\limits_B t\cos\beta\, dx\, dy\, dz + \frac{kD}{d^2}\iiint\limits_B zt\cos\beta\, dx\, dy\, dz$$

Projection of the position vector of dM onto that of P will provide an expression for $t\cos\beta$, and may be achieved in terms of their scalar product; hence:

$$\mathbf{t}\cdot\mathbf{d} = td\cos\beta = xx_p + yy_p + zz_p,$$

since

$$t^2 = x^2 + y^2 + z^2 \tag{5.8}$$

and

$$d^2 = x_p^2 + y_p^2 + z_p^2, \tag{5.9}$$

and therefore

$$t\cos\beta = \frac{xx_p}{d} + \frac{yy_p}{d} + \frac{zz_p}{d}. \tag{5.10}$$

Then,

$$V_1 = \frac{k\sigma_\mu}{d^3}\left(x_p\iiint\limits_B x\, dx\, dy\, dz + y_p\iiint\limits_B y\, dx\, dy\, dz + z_p\iiint\limits_B z\, dx\, dy\, dz\right)$$

$$+ \frac{kD}{d^3}\left(x_p\iiint\limits_B xz\, dx\, dy\, dz + y_p\iiint\limits_B yz\, dx\, dy\, dz + z_p\iiint\limits_B z^2\, dx\, dy\, dz\right), \tag{5.11}$$

$$V_2 = \frac{k\sigma_\mu}{2d^3}\iiint\limits_B (3t^2\cos^2\beta - t^2)\, dx\, dy\, dz + \frac{kD}{2d^3}\iiint\limits_B z(3t^2\cos^2\beta - t^2)\, dx\, dy\, dz.$$

Substituting equation 5.10 and employing 5.8 and 5.9 gives:

$$V_2 = \frac{k\sigma_\mu}{2d^5}\left((2x_p^2 - y_p^2 - z_p^2)\iiint\limits_B x^2\, dx\, dy\, dz + (2y_p^2 - x_p^2 - z_p^2)\iiint\limits_B y^2\, dx\, dy\, dz\right.$$

$$+ (2z_p^2 - x_p^2 - y_p^2)\iiint\limits_B z^2\, dx\, dy\, dz + 6x_py_p\iiint\limits_B xy\, dx\, dy\, dz$$

$$\left. + 6x_pz_p\iiint\limits_B xz\, dx\, dy\, dz + 6y_pz_p\iiint\limits_B yz\, dx\, dy\, dz\right)$$

$$+ \frac{kD}{2d^5}\left(C_{21}\iiint\limits_B x^2 z \, dx\, dy\, dz + C_{22}\iiint\limits_B y^2 z \, dx\, dy\, dz + C_{23}\iiint\limits_B z^3 \, dx\, dy\, dz\right.$$

$$\left. + C_{24}\iiint\limits_B xyz \, dx\, dy\, dz + C_{25}\iiint\limits_B xz^2 \, dx\, dy\, dz + C_{26}\iiint\limits_B yz^2 \, dx\, dy\, dz\right), \qquad (5.12)$$

in which

$$C_{21} = (2x_p^2 - y_p^2 - z_p^2),$$

$$C_{22} = (2y_p^2 - x_p^2 - z_p^2),$$

etc. ...

$$C_{26} = 6y_p z_p.$$

Since the coefficients of the integrals in the homogeneous part of each potential term are always repeated sequentially in the linear density part, this abbreviated notation will be employed in the expressions for the remaining potential terms. Hence, C_{31} to C_{310} represent, sequentially, the coefficients of the ten integrals in the homogeneous part of V_3 and similarly C_{41} to C_{415} in V_4. Then, continuing with the potential terms:

$$V_3 = \frac{k\sigma_\mu}{2d^4}\iiint\limits_B (5t^3 \cos^3\beta - 3t^3 \cos\beta)\, dx\, dy\, dz + \frac{kD}{2d^4}\iiint\limits_B z(5t^3 \cos^3\beta - 3t^3 \cos\beta)\, dx\, dy\, dz$$

$$= \frac{k\sigma_\mu}{2d^7}\left((2x_p^3 - 3x_p y_p^2 - 3x_p z_p^2)\iiint\limits_B x^3 \, dx\, dy\, dz + (2y_p^3 - 3x_p^2 y_p - 3y_p z_p^2)\iiint\limits_B y^3 \, dx\, dy\, dz\right.$$

$$+ (2z_p^3 - 3x_p^2 z_p - 3y_p^2 z_p)\iiint\limits_B z^3 \, dx\, dy\, dz + (12x_p^2 y_p - 3y_p^3 - 3y_p z_p^2)\iiint\limits_B x^2 y \, dx\, dy\, dz$$

$$+ (12y_p^2 z_p - 3x_p^2 z_p - 3z_p^3)\iiint\limits_B y^2 z \, dx\, dy\, dz + (12x_p z_p^2 - 3x_p y_p^2 - 3x_p^3)\iiint\limits_B xz^2 \, dx\, dy\, dz$$

$$+ (12x_p^2 z_p - 3y_p^2 z_p - 3z_p^3)\iiint\limits_B x^2 z \, dx\, dy\, dz + (12x_p y_p^2 - 3x_p z_p^2 - 3x_p^3)\iiint\limits_B xy^2 \, dx\, dy\, dz$$

$$\left. + (12y_p z_p^2 - 3x_p^2 y_p - 3y_p^3)\iiint\limits_B yz^2 \, dx\, dy\, dz + 30x_p y_p z_p\iiint\limits_B xyz \, dx\, dy\, dz\right)$$

$$+ \frac{kD}{2d^7}\left(C_{31}\iiint\limits_B x^3 z \, dx\, dy\, dz + C_{32}\iiint\limits_B y^3 z \, dx\, dy\, dz + C_{33}\iiint\limits_B z^4 \, dx\, dy\, dz\right.$$

$$+ C_{34}\iiint\limits_B x^2 yz \, dx\, dy\, dz + C_{35}\iiint\limits_B y^2 z^2 \, dx\, dy\, dz + C_{36}\iiint\limits_B xz^3 \, dx\, dy\, dz$$

$$+ C_{37}\iiint\limits_B x^2z^2\ dx\ dy\ dz + C_{38}\iiint\limits_B xy^2z\ dx\ dy\ dz + C_{39}\iiint\limits_B yz^3\ dx\ dy\ dz$$

$$\left. + C_{310}\iiint\limits_B xyz^2\ dx\ dy\ dz\right\};\tag{5.13}$$

$$V_4 = \frac{k\sigma_\mu}{8d^5}\iiint\limits_B (35t^4\ \cos^4\beta - 30t^4\ \cos^2\beta + 3t^4)\ dx\ dy\ dz$$

$$+ \frac{kD}{8d^5}\iiint\limits_B z(35t^4\ \cos^4\beta - 30t^4\ \cos^2\beta + 3t^4)\ dx\ dy\ dz,$$

$$= \frac{k\sigma_\mu}{8d^9}\left\{(8x_p^4 + 3y_p^4 + 3z_p^4 - 24x_p^2y_p^2 - 24x_p^2z_p^2 + 6y_p^2z_p^2)\iiint\limits_B x^4\ dx\ dy\ dz\right.$$

$$+ (3x_p^4 + 8y_p^4 + 3z_p^4 - 24x_p^2y_p^2 + 6x_p^2z_p^2 - 24y_p^2z_p^2)\iiint\limits_B y^4\ dx\ dy\ dz$$

$$+ (3x_p^4 + 3y_p^4 + 8z_p^4 + 6x_p^2y_p^2 - 24x_p^2z_p^2 - 24y_p^2z_p^2)\iiint\limits_B z^4\ dx\ dy\ dz$$

$$+ (80x_p^3y_p - 60x_py_p^3 - 60x_py_pz_p^2)\iiint\limits_B x^3y\ dx\ dy\ dz + (80x_p^3z_p - 60x_pz_p^3 - 60x_py_p^2z_p)\iiint\limits_B x^3z\ dx\ dy\ dz$$

$$+ (80x_py_p^3 - 60x_p^3y_p - 60x_py_pz_p^2)\iiint\limits_B xy^3\ dx\ dy\ dz + (80y_p^3z_p - 60y_pz_p^3 - 60x_p^2y_pz_p)\iiint\limits_B y^3z\ dx\ dy\ dz$$

$$+ (80x_pz_p^3 - 60x_p^3z_p - 60x_py_p^2z_p)\iiint\limits_B xz^3\ dx\ dy\ dz + (80y_pz_p^3 - 60y_p^3z_p - 60x_p^2y_pz_p)\iiint\limits_B yz^3\ dx\ dy\ dz$$

$$+ (-24x_p^4 - 24y_p^4 + 6z_p^4 + 162x_p^2y_p^2 - 18x_p^2z_p^2 - 18y_p^2z_p^2)\iiint\limits_B x^2y^2\ dx\ dy\ dz$$

$$+ (-24x_p^4 + 6y_p^4 - 24z_p^4 - 18x_p^2y_p^2 + 162x_p^2z_p^2 - 18y_p^2z_p^2)\iiint\limits_B x^2z^2\ dx\ dy\ dz$$

$$+ (6x_p^4 - 24y_p^4 - 24z_p^4 - 18x_p^2y_p^2 - 18x_p^2z_p^2 + 162y_p^2z_p^2)\iiint\limits_B y^2z^2\ dx\ dy\ dz$$

$$+ (360x_p^2 y_p z_p - 60y_p^3 z_p - 60y_p z_p^3)\iiint\limits_B x^2 yz \, dx \, dy \, dz$$

$$+ (360x_p y_p^2 z_p - 60x_p^3 z_p - 60x_p z_p^3)\iiint\limits_B xy^2 z \, dx \, dy \, dz$$

$$\left. + (360x_p y_p z_p^2 - 60x_p^3 y_p - 60x_p y_p^3)\iiint\limits_B xyz^2 \, dx \, dy \, dz \right\}$$

$$+ \frac{kD}{8d^9}\left\{C_{41}\iiint\limits_B x^4 z \, dx \, dy \, dz + C_{42}\iiint\limits_B y^4 z \, dx \, dy \, dz + C_{43}\iiint\limits_B z^5 \, dx \, dy \, dz\right.$$

$$+ C_{44}\iiint\limits_B x^3 yz \, dx \, dy \, dz + C_{45}\iiint\limits_B x^3 z^2 \, dx \, dy \, dz + C_{46}\iiint\limits_B xy^3 z \, dx \, dy \, dz$$

$$+ C_{47}\iiint\limits_B y^3 z^2 \, dx \, dy \, dz + C_{48}\iiint\limits_B xz^4 \, dx \, dy \, dz + C_{49}\iiint\limits_B yz^4 \, dx \, dy \, dz$$

$$+ C_{410}\iiint\limits_B x^2 y^2 z \, dx \, dy \, dz + C_{411}\iiint\limits_B x^2 z^3 \, dx \, dy \, dz + C_{412}\iiint\limits_B y^2 z^3 \, dx \, dy \, dz$$

$$\left. + C_{413}\iiint\limits_B x^2 yz^2 \, dx \, dy \, dz + C_{414}\iiint\limits_B xy^2 z^2 \, dx \, dy \, dz + C_{415}\iiint\limits_B xyz^3 \, dx \, dy \, dz\right\}. \quad (5.14)$$

Combining expressions 5.7, 5.11, 5.12, 5.13, and 5.14 in accordance with equation 5.4 provides an open form expression for the potential at P due to a general body with the linear density model indicated by equation 5.5. The whole expression is apparently a function of the *inertial integrals* of the body, the coefficients of which depend only on the position of the point P.

5.3 THE RECTANGULAR PARALLELEPIPED

If the general body of the preceeding section is defined specifically to be a rectangular parallelepiped with sides $2a$, $2b$, and $2c$—positioned with its centroid at the origin c_0 and oriented so that its edges are parallel to the coordinate axes—it is a simple matter to evaluate the inertial integrals in the expression for the potential. They may be treated in general form as:

$$I_{kmn} = \iiint\limits_B x^k \, y^m \, z^n \, dx \, dy \, dz,$$

which, for the parallelepiped being considered, becomes:

$$I_{kmn} = \int_{-a}^{a}\int_{-b}^{b}\int_{-c}^{c} x^k \, y^m \, z^n \, dx \, dy \, dz$$

$$= \int_{-a}^{a}\int_{-b}^{b} x^k \, y^m \left|\frac{z^{n+1}}{n+1}\right|_{-c}^{c} dx \, dy$$

$$= \int_{-a}^{a} \int_{-b}^{b} x^k\, y^m \left[\frac{c^{n+1}}{n+1} - \frac{(-c)^{n+1}}{n+1}\right] dx\, dy,$$

wherein, if n is odd, the bracketted term causes the whole expression to vanish. But, for n even,

$$I_{kmn} = \frac{2c^{2\nu+1}}{2\nu + 1} \int_{-a}^{a} \int_{-b}^{b} x^k\, y^m\, dx\, dy$$

where $2\nu = n$ and ν is any positive integer.

The remaining integrals behave identically, so that, finally:

$$I_{kmn} = \frac{2a^{2\kappa+1}\; 2b^{2\mu+1}\; 2c^{2\nu+1}}{(2\kappa + 1)(2\mu + 1)(2\nu + 1)}$$

where $2\kappa = k$, $2\mu = m$, $2\nu = n$; κ and μ being any positive integers. But $I_{kmn} = 0$ if any of k, m, or n are odd, reflecting the triply symmetric geometry of the parallelepiped.

Hence, generally:

$$I_{2\kappa,2\mu,2\nu} = \frac{v\; a^{2\kappa}\; b^{2\mu}\; c^{2\nu}}{(2\kappa + 1)(2\mu + 1)(2\nu + 1)} \tag{5.15}$$

where v is the volume of the parallelepiped, and

κ, μ, ν are any positive integers.

Use of 5.15 now enables evaluation of the potential terms V_0, V_1, V_2, V_3, and V_4 of §5.2, which become in matrix notation:

$$V_0 = \frac{k\sigma_\mu v}{d} = \frac{kM_\mu}{d}, \tag{5.16}$$

where M_μ is the mass of the parallelepiped assuming homogeneity with mean density σ_μ.

$$V_1 = \frac{kDv}{3d^3}\, \mathbf{A}_1\, \mathbf{K}_1\, \mathbf{P}_1, \tag{5.17}$$

where $\mathbf{A}_1 = c^2$, $\mathbf{K}_1 = 1$, $\mathbf{P}_1 = z_p$.

$$V_2 = \frac{kM_\mu}{6d^5}\, \mathbf{A}_2 \mathbf{K}_2 \mathbf{P}_2, \tag{5.18}$$

where $\mathbf{A}_2 = [a \quad b \quad c\,]$,

$$\mathbf{K}_2 = \begin{bmatrix} 2 & -1 & -1 \\ -1 & 2 & -1 \\ -1 & -1 & 2 \end{bmatrix}, \mathbf{P}_2 = \begin{bmatrix} x_p \\ y_p \\ z_p \end{bmatrix}.$$

$$V_3 = \frac{kDv}{30d^7}\, \mathbf{A}_3 \mathbf{K}_3 \mathbf{P}_3 \tag{5.19}$$

where $\mathbf{A}_3 = [a^2c^2 \quad b^2c^2 \quad c^4]$,

$$\mathbf{K}_3 = \begin{bmatrix} 20 & -5 & -5 \\ -5 & 20 & -5 \\ -9 & -9 & 6 \end{bmatrix}, \quad \mathbf{P}_3 = \begin{bmatrix} x_p^2\, z_p \\ y_p^2\, z_p \\ z_p^{\,3} \end{bmatrix}.$$

$$V_4 = \frac{kM_\mu}{72d^9}\, \mathbf{A}_4 \mathbf{K}_4 \mathbf{P}_4 \tag{5.20}$$

where

$$\mathbf{A}_4 = [a^4 \quad b^4 \quad c^4 \quad a^2b^2 \quad a^2c^2 \quad b^2c^2],$$

$$\mathbf{K}_4 = \begin{bmatrix} 8 & 3 & 3 & -24 & -24 & 6 \\ 3 & 8 & 3 & -24 & 6 & -24 \\ 3 & 3 & 8 & 6 & -24 & -24 \\ -24 & -24 & 6 & 162 & -18 & -18 \\ -24 & 6 & -24 & -18 & 162 & -18 \\ 6 & -24 & -24 & -18 & -18 & 162 \end{bmatrix}, \quad \mathbf{P}_4 = \begin{bmatrix} x_p^4 \\ y_p^4 \\ z_p^4 \\ x_p^2y_p^2 \\ x_p^2z_p^2 \\ y_p^2z_p^2 \end{bmatrix}.$$

Substituting the potential terms V_0 to V_4 into equation 5.4 gives the total potential of the parallelepiped:

$$V = kM_\mu \left(\frac{1}{d} + \frac{1}{6d^5}\mathbf{A}_2\mathbf{K}_2\mathbf{P}_2 + \frac{1}{72d^9}\mathbf{A}_4\mathbf{K}_4\mathbf{P}_4 + \ldots\right)$$

$$+ \; kDv\left(\frac{1}{3d^3}\mathbf{A}_1\mathbf{K}_1\mathbf{P}_1 + \frac{1}{30d^7}\mathbf{A}_3\mathbf{K}_3\mathbf{P}_3 + \ldots\right) \qquad (5.21)$$

where $\mathbf{A}$, $\mathbf{K}$, and $\mathbf{P}$ are the matrices of parallelepiped dimension terms, constant coefficients, and point coordinate terms, respectively.

5.4 ATTRACTION COMPONENTS BY DIFFERENTIATION OF POTENTIAL

Partial differentiation of the potential series 5.21 with respect to each coordinate of P will provide the rectangular components of the attraction vector at that point. In so doing, the $\mathbf{A}$ and $\mathbf{K}$ matrices may be treated as constants, while the $\mathbf{P}$ matrices and d are the variables. Differentiation of the various powers of d is best expressed in general form, thus:

since $d^{-\kappa} = \left(x_p^2 + y_p^2 + z_p^2\right)^{-\kappa/2}$,

then

$$\frac{\partial d^{-\kappa}}{\partial x_{pi}} = -\kappa x_{pi}\, d^{-(\kappa+2)}, \qquad (5.22)$$

where $x_{pi} = x_p$, y_p, or z_p.

Beginning with the x-component:

$$G_x = \frac{\partial V}{\partial x_p} = \frac{\partial V_0}{\partial x_p} + \frac{\partial V_1}{\partial x_p} + \frac{\partial V_2}{\partial x_p} + \frac{\partial V_3}{\partial x_p} + \frac{\partial V_4}{\partial x_p} + \ldots$$

$$= G_{x0} + G_{x1} + G_{x2} + G_{x3} + G_{x4} + \ldots \qquad (5.23)$$

Treating each term in turn gives:

$$G_{x0} = \frac{\partial}{\partial x_p}\left(\frac{kM_\mu}{d}\right)$$

$$= \frac{-kM_\mu x_p}{d^3} \qquad (5.24)$$

$$G_{x1} = \frac{kDvc^2 z_p}{3} \frac{\partial}{\partial x_p} (d^{-3})$$

$$= \frac{-kDvx_p}{d^5} c^2 z_p$$

$$= \frac{-kDvx_p}{d^5} \mathbf{A}_1 \mathbf{K}_1 \mathbf{P}_1. \tag{5.25}$$

$$G_{x2} = \frac{kM_\mu}{6} \mathbf{A}_2 \mathbf{K}_2 \frac{\partial}{\partial x_p} \left(\frac{\mathbf{P}_2}{d^5}\right)$$

$$= \frac{kM_\mu}{6} \mathbf{A}_2 \mathbf{K}_2 \begin{bmatrix} 2x_p d^{-5} - 5x_p^3 d^{-7} \\ -5x_p y_p^2 d^{-7} \\ -5x_p z_p^2 d^{-7} \end{bmatrix}$$

$$= \frac{kM_\mu x_p}{6d^5} \mathbf{A}_2 \mathbf{K}_{x2} - \frac{5kM_\mu x_p}{6d^7} \mathbf{A}_2 \mathbf{K}_2 \mathbf{P}_2, \tag{5.26}$$

where

$$\mathbf{K}_{x2} = \begin{bmatrix} 4 \\ -2 \\ -2 \end{bmatrix}. \tag{5.27}$$

$$G_{x3} = \frac{kDv}{30} \mathbf{A}_3 \mathbf{K}_3 \frac{\partial}{\partial x_p} \left(\frac{\mathbf{P}_3}{d^7}\right)$$

$$= \frac{kDv}{30} \mathbf{A}_3 \mathbf{K}_3 \begin{bmatrix} 2x_p z_p d^{-7} - 7x_p^3 z_p d^{-9} \\ - 7x_p y_p^2 z_p d^{-9} \\ - 7x_p z_p^3 d^{-9} \end{bmatrix}$$

$$= \frac{kDvx_p}{30d^7} \mathbf{A}_3 \mathbf{K}_{x3} \mathbf{P}_1 - \frac{7kDvx_p}{30d^9} \mathbf{A}_3 \mathbf{K}_3 \mathbf{P}_3, \tag{5.28}$$

where

$$\mathbf{K}_{x3} = \begin{bmatrix} 40 \\ -10 \\ -18 \end{bmatrix}. \tag{5.29}$$

$$G_{x4} = \frac{kM_\mu}{72} \mathbf{A}_4 \mathbf{K}_4 \frac{\partial}{\partial x_p} \left(\frac{\mathbf{P}_4}{d^9}\right)$$

$$= \frac{kM_\mu}{72} \mathsf{A}_4 \mathsf{K}_4 \begin{bmatrix} 4x_p^3 d^{-9} - 9x_p^5 d^{-11} \\ -9x_p y_p^4 d^{-11} \\ -9x_p z_p^4 d^{-11} \\ 2x_p y_p^2 d^{-9} - 9x_p^3 y_p^2 d^{-11} \\ 2x_p z_p^2 d^{-9} - 9x_p^3 z_p^2 d^{-11} \\ -9x_p y_p^2 z_p^2 d^{-11} \end{bmatrix}$$

$$= \frac{kM_\mu x_p}{72d^9} \mathsf{A}_4 \mathsf{K}_{x4} \mathsf{P}_2 - \frac{9kM_\mu x_p}{72d^{11}} \mathsf{A}_4 \mathsf{K}_4 \mathsf{P}_4, \tag{5.30}$$

where

$$\mathsf{K}_{x4} = \begin{bmatrix} 32 & -48 & -48 \\ 12 & -48 & 12 \\ 12 & 12 & -48 \\ -96 & 324 & -36 \\ -96 & -36 & 324 \\ 24 & -36 & -36 \end{bmatrix}. \tag{5.31}$$

The combination of terms provides the series for the x-component of the attraction at P:

$$G_x = -kM_\mu x_p \left\{\frac{1}{d^3} - \frac{1}{6d^5}\mathsf{A}_2 \mathsf{K}_{x2} + \frac{5}{6d^7}\mathsf{A}_2 \mathsf{K}_2 \mathsf{P}_2 - \frac{1}{72d^9}\mathsf{A}_4 \mathsf{K}_{x4} \mathsf{P}_2 + \frac{9}{72d^{11}}\mathsf{A}_4 \mathsf{K}_4 \mathsf{P}_4 - \dots\right\}$$
$$- kDvx_p \left\{\frac{1}{d^5}\mathsf{A}_1 \mathsf{K}_1 \mathsf{P}_1 - \frac{1}{30d^7}\mathsf{A}_3 \mathsf{K}_{x3} \mathsf{P}_1 + \frac{7}{30d^9}\mathsf{A}_3 \mathsf{K}_3 \mathsf{P}_3 - \dots\right\}. \tag{5.32}$$

Due to symmetry, the expression for G_y is available by interchanging x with y and a with b in equation 5.32. In practice, this is more easily achieved by an appropriate permutation of the K matrices. Therefore:

$$G_y = -kM_\mu y_p \left\{\frac{1}{d^3} - \frac{1}{6d^5}\mathsf{A}_2 \mathsf{K}_{y2} + \frac{5}{6d^7}\mathsf{A}_2 \mathsf{K}_2 \mathsf{P}_2 - \frac{1}{72d^9}\mathsf{A}_4 \mathsf{K}_{y4} \mathsf{P}_2 + \frac{9}{72d^{11}}\mathsf{A}_4 \mathsf{K}_4 \mathsf{P}_4 - \dots\right\}$$
$$- kDvy_p \left\{\frac{1}{d^5}\mathsf{A}_1 \mathsf{K}_1 \mathsf{P}_1 - \frac{1}{30d^7}\mathsf{A}_3 \mathsf{K}_{y3} \mathsf{P}_1 + \frac{7}{30d^9}\mathsf{A}_3 \mathsf{K}_3 \mathsf{P}_3 - \dots\right\}, \tag{5.33}$$

where

$$\mathsf{K}_{y2} = \begin{bmatrix} -2 \\ 4 \\ -2 \end{bmatrix}, \quad \mathsf{K}_{y3} = \begin{bmatrix} -10 \\ 40 \\ 18 \end{bmatrix}, \qquad (5.34),\ (5.35)$$

and

$$\mathsf{K}_{y4} = \begin{bmatrix} -48 & 12 & 12 \\ -48 & 32 & -48 \\ 12 & 12 & -48 \\ 324 & -96 & -36 \\ -36 & 24 & -36 \\ -36 & -96 & 324 \end{bmatrix}. \tag{5.36}$$

To find the z-component, differentiation with respect to z_p proceeds in a like manner so that:

$$G_z = G_{z0} + G_{z1} + G_{z2} + G_{z3} + G_{z4} + \ldots \tag{5.37}$$

Treating each term in turn gives:

$$G_{z0} = kM_\mu \frac{\partial}{\partial z_p}\left(\frac{1}{d}\right) = \frac{-kM_\mu z_p}{d^3} \tag{5.38}$$

$$G_{z1} = \frac{kDvc^2}{3}\frac{\partial}{\partial z_p}\left(\frac{z_p}{d^3}\right) = \frac{kDvc^2}{3d^3} - \frac{kDvc^2 z_p^2}{d^5} = \frac{kDv}{3d^3}\mathsf{A}_1\mathsf{K}_1 - \frac{kDvz_p}{d^5}\mathsf{A}_1\mathsf{K}_1\mathsf{P}_1. \tag{5.39}$$

$$G_{z2} = \frac{kM_\mu}{6}\mathsf{A}_2\mathsf{K}_2\frac{\partial}{\partial z_p}\left(\frac{\mathsf{P}_2}{d^5}\right)$$

$$= \frac{kM_\mu}{6}\mathsf{A}_2\mathsf{K}_2\begin{bmatrix} -5x_p^2 z_p d^{-7} \\ -5y_p^2 z_p d^{-7} \\ 2z_p d^{-5} - 5z_p^3 d^{-7}\end{bmatrix} = \frac{kM_\mu z_p}{6d^5}\mathsf{A}_2\mathsf{K}_{z2} - \frac{5kM_\mu z_p}{6d^7}\mathsf{A}_2\mathsf{K}_2\mathsf{P}_2, \tag{5.40}$$

where

$$\mathsf{K}_{z2} = \begin{bmatrix} -2 \\ -2 \\ 4\end{bmatrix}. \tag{5.41}$$

$$G_{z3} = \frac{kDv}{30}\mathsf{A}_3\mathsf{K}_3\frac{\partial}{\partial z_p}\left(\frac{\mathsf{P}_3}{d^7}\right)$$

$$= \frac{kDv}{30}\mathsf{A}_3\mathsf{K}_3\begin{bmatrix} x_p^2 d^{-7} - 7x_p^2 z_p^2 d^{-9} \\ y_p^2 d^{-7} - 7y_p^2 z_p^2 d^{-9} \\ 3z_p^2 d^{-7} - 7z_p^4 d^{-9}\end{bmatrix} = \frac{kDv}{30d^7}\mathsf{A}_3\mathsf{K}_{z3}\mathsf{P}_2 - \frac{7kDvz_p}{30d^9}\mathsf{A}_3\mathsf{K}_3\mathsf{P}_3, \tag{5.42}$$

where

$$\mathsf{K}_{z3} = \begin{bmatrix} 20 & -5 & -15 \\ -5 & 20 & -15 \\ -9 & -9 & 18\end{bmatrix}. \tag{5.43}$$

$$G_{z4} = \frac{kM_\mu}{72}\mathsf{A}_4\mathsf{K}_4\frac{\partial}{\partial z_p}\left(\frac{\mathsf{P}_4}{d^9}\right)$$

$$= \frac{kM_\mu}{72}\mathsf{A}_4\mathsf{K}_4\begin{bmatrix} -9x_p^4 z_p d^{-11} \\ -9y_p^4 z_p d^{-11} \\ 4z_p^3 d^{-9} - 9z_p^5 d^{-11} \\ -9x_p^2 y_p^2 z_p d^{-11} \\ 2x_p^2 z_p d^{-9} - 9x_p^2 z_p^3 d^{-11} \\ 2y_p^2 z_p d^{-9} - 9y_p^2 z_p^3 d^{-11}\end{bmatrix}$$

$$= \frac{kM_\mu z_p}{72d^9} \mathbf{A}_4 \mathbf{K}_{z4} \mathbf{P}_2 - \frac{9kM_\mu z_p}{72d^{11}} \mathbf{A}_4 \mathbf{K}_4 \mathbf{P}_4, \tag{5.44}$$

where

$$\mathbf{K}_{z4} = \begin{bmatrix} -48 & 12 & 12 \\ 12 & -48 & 12 \\ -48 & -48 & 32 \\ -36 & -36 & 24 \\ 324 & -36 & -96 \\ -36 & 324 & -96 \end{bmatrix}. \tag{5.45}$$

Whence

$$G_z = -kM_\mu z_p \left\{ \frac{1}{d^3} - \frac{1}{6d^5} \mathbf{A}_2 \mathbf{K}_{z2} + \frac{5}{6d^7} \mathbf{A}_2 \mathbf{K}_2 \mathbf{P}_2 - \frac{1}{72d^9} \mathbf{A}_4 \mathbf{K}_{z4} \mathbf{P}_2 + \frac{9}{72d^{11}} \mathbf{A}_4 \mathbf{K}_4 \mathbf{P}_4 - \dots \right\}$$

$$- kDvz_p \left\{ - \frac{1}{3z_p d^3} \mathbf{A}_1 \mathbf{K}_1 + \frac{1}{d^5} \mathbf{A}_1 \mathbf{K}_1 \mathbf{P}_1 - \frac{1}{30z_p d^7} \mathbf{A}_3 \mathbf{K}_{z3} \mathbf{P}_2 + \frac{7}{30d^9} \mathbf{A}_3 \mathbf{K}_3 \mathbf{P}_3 - \dots \right\}. \tag{5.46}$$

5.5 CHECKS AND PRACTICAL CONSIDERATIONS

All of the checks listed in §4.5 are equally applicable to the series formulae just derived. In addition, the formulae may be compared numerically with the closed forms developed in §§4.3 and 4.4. Symmetry is easily checked by inspection of all the $\mathbf{A}$ and $\mathbf{P}$ matrices, while the dimensional consistency is readily perceived by determining the dimensions of these same arrays. All of the formulae and their computer algorithms were also checked by the numerical differentiation techniques referred to earlier.

Convergence of the series was discussed and verified numerically under a variety of circumstances in §2.3 under the sub-heading "Non-contact Zones". It must be emphasised that these forms are based on the premise of reasonable separation between the computation point and the gravitating body. When the computation point is brought too near the body it becomes dangerous to infer from a simple numerical comparison of a pair of successive terms that absolute convergence of the series persists. Under some conditions the potential and gravity series may become *conditionally convergent* [HARDY 1958, §§193-6] or oscillatory.

Any such difficulties are obviated in the present study by applying these formulae only well beyond the radius of convergence.

6

Digital Topographic Data

6.1 INTRODUCTION AND DEFINITION

All of the definitive components which contribute to the topographic-isostatic model developed in chapter 3 are functions of the height of the topography, measured from the reference surface. Realization of this theoretical model in a practical form, suitable for digital computation, requires a global set of numerical height values. Many methods of numerical representation of the topography are possible—and some of these will be considered in §6.2—but most of the options are pre-emptively removed by the preceeding choice of method of evaluation and theoretical definition of a quadrature model. Indeed, the notion of "quadrature" includes "rectangularization" of the topographic surface, which thereby circumscribes the range of suitable topographic models. This is exemplified by the introduction in §3.4 of an upper bounding surface—curvilinear or plane—which is representative of a constant value of topographic height h (or geocentric radius R_2) over the finite area of a quadrature subdivision.

Consequently, the most suitable, and simplest, form of numerical data is a set of *mean topographic heights*; a single value representing the height of each quadrature subdivision. Here the term "mean topographic height" is understood to be defined as the expected value of the continuous height distribution for the area of quadrature subdivision, given by:

$$h = \frac{\iint_{quad} h(\phi,\lambda)\ d\phi\ d\lambda}{\iint_{quad} d\phi\ d\lambda} \tag{6.1}$$

$$= \frac{v_{quad}}{A_{quad}} , \tag{6.2}$$

where $h(\phi,\lambda)$ is a function defining the terrain surface at all points of the quadrature subdivision,

v_{quad} is the volume of the quadrature subdivision, and

A_{quad} is its area.

Thus the representation of the topographic surface by its mean value does not, theoretically, change the volume of a quadrature subdivision, only the spatial distribution of its composition: in effect material above the mean level is displaced to occupy the spaces below that level. Some effects of this mass displacement were considered at the end of §2.3 under the heading "Non-contact Zones". Of course, the most obvious, and significant, are the smoothing of topographic gradients and the creation of surface discontinuities at subdivision boundaries.

Invariably, the terrain surface is non-analytical, so the integral in the numerator of equation 6.1 cannot be evaluated by other than numerical or sampling techniques. Methods of compiling digital data, implemented by the United States Aeronautical Chart and Information Center (ACIC) (now renamed the Defence Mapping Agency, Aerospace Center), have been detailed by CZARNECKI [1970].

Whatever method of compilation is used, a definitive statement of what, exactly, is to be regarded as the topographic surface is prerequisite. Such a definition could refer to the *solid earth* boundary, except for the ambiguity posed by the presence of large bodies of water and ice. Water may occur as oceans or significant "inland" lakes and the policy to be adopted in disinguishing between these and their treatment must be settled. Likewise, the treatment of substantial areas of ice and land below sea level must be decided. ACIC commonly classify their data in seven ways [ACIC 1965] as follows:

(a) all positive land,
(b) all ocean,
(c) some negative land,
(d) both land and ocean,
(e) surface of ice,
(f) land or ocean below ice,
(g) a significant lake.

CZARNECKI [1970] describes ACIC's treatment of these categories with particular reference to the use of density factors to "compress" or "expand" the material as necessary. Before using the data it is important to determine whether or not it has undergone such treatment.

Despite the importance of the definitions underlying the compilation of data, usually the user has no control of these decisions as they are appropriated by the compiler.

6.2 ALTERNATIVE TOPOGRAPHIC MODELS

Mean heights are by no means the only method of representing the topography. Alternative models may be categorized as *actual* or *artificial*, according to whether the numeric data purports to represent the true topographic surface or some mathematical conception devoid of physical reality. Also, the model may be either *continuous* or *discrete*. Mean height data belongs to the latter category in each case.

Althought a detailed examination of alternative models is not within the ambit of this thesis, superficial consideration of some of the possibilities will provide a background to highlight the implications of the adopted mean height model. Factors which might be embodied—separately or combined—in a topographic model are:

(a) the root mean square height,
(b) the variance,
(c) higher order statistical moments,
(d) other stochastic parameters,
(e) point mass parameters and inertial integrals,
(f) plane polynomial coefficients,
(g) trigonometric (and other transcendental function) coefficients (*e.g.* Fourier coefficients),
(h) harmonic coefficients (*e.g.* Legendre coefficients), and
(i) morphometric parameters.

Some of these are generic, in that a number of distinct alternatives within a group may be related through a unifying principle.

ROOT MEAN SQUARE HEIGHTS AND VARIANCE. Essentially the root mean square (rms) height $\tilde{h}$ of a quadrature subdivision, given by

$$\tilde{h}^2 = \frac{\iint_{quad} h^2(\phi,\lambda)\, d\phi\, d\lambda}{A_{quad}}, \tag{6.3}$$

appears as the statistical second moment of the height distribution function *about the "origin"*. It is, therefore, distinguishable from the variance s^2, given by

$$s^2 = \frac{\iint_{quad} [h(\phi,\lambda) - h]^2\, d\phi\, d\lambda}{A_{quad}}, \tag{6.4}$$

which is the same order moment taken *about the mean height* h. Hence the variance is purely a measure of the variability or "ruggedness" of the topography, whereas the rms height combines this concept with an indication of the mean height as well. Analytically this may be demonstrated by expanding the integrand of equation 6.4; whence,

$$s^2 = \tilde{h}^2 - h^2. \tag{6.5}$$

In figure 6.1 this relationship is portrayed geometrically, showing the simple dependence of the rms height on both the mean height and the variance. Instead of using the variance to describe the ruggedness of the topography, the concept of *form factor* f, given by (see figure 6.1)

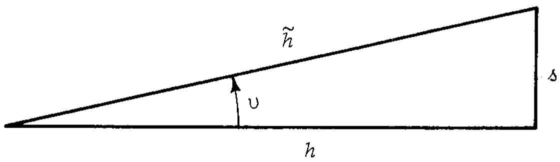

FIGURE 6.1

ROOT MEAN SQUARE HEIGHT, MEAN HEIGHT, AND VARIANCE

$$f = \sec \upsilon = \frac{\tilde{h}}{h}, \tag{6.6}$$

may be borrowed from electrical wave measurement theory [SKILLING 1957, p.111]. The main advantage of this parameter is its dimensionless nature.

While the rms height conveys more information than the mean height, it cannot be employed alone as a simple replacement for the latter in a topographic model because it would falsify the volume of the topography. However—with suitable modifications to the density functions, designed to preserve correct topographic mass—it could be used in conjunction with the mean height to alleviate the artificial disturbance of the gravity field associated with the mass displacements inherent in the simple mean height model. Many variations of the basic principle are possible, depending on the way the density fuction is modified. For instance, two of the simplest models are illustrated by figure 6.2.

In each case a density discontinuity is proposed which divides the topography into upper and lower portions. The usual density function is retained for the lower portion, while the density of the upper portion is diminished to characterize the combination of rock and air densities which occur there. Logically, the bounding discontinuity could be set at the level of the minimum height $h_{\downarrow}$, so that the lower portion is uncontaminated by air, and the upper portion extended upwards to the maximum topographic

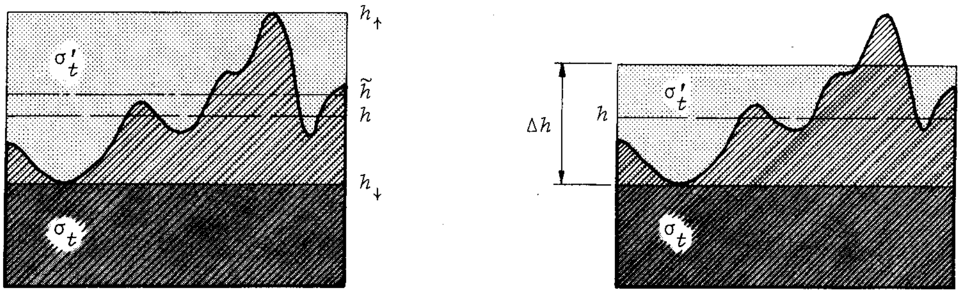

(a) (b)

FIGURE 6.2

ALTERNATIVE TOPOGRAPHIC MODELS INCORPORATING RUGGEDNESS

height $h_\uparrow$ (see figure 6.2a). To preserve topographic mass the density of the upper portion σ'_t would need to be

$$\sigma'_t = \frac{\sigma_t\ (h - h_\downarrow)}{(h_\uparrow - h_\downarrow)} . \tag{6.7}$$

Some of the attributes of this model, without density modification, have been essayed by FRYER [1970, p.110 *et seq.*] in calculations of the indirect effect on gravity. Compared to the ordinary mean height model the first alternative would change the resulting potential only slightly (about 1% for the contact sub-zone), but the effect on the vertical component of gravity would be dramatic (up to 35%) because a sizeable portion of the mass is moved from below the computation point and redistributed above it.

A refinement of this model, capable of better "realism", can be devised by relating the height of the upper portion Δh and its density σ'_t to the ruggedness of the topography, expressed by the rms height or variance (figure 6.2b). Thus,

$$\left.\begin{matrix} \Delta h \\ \sigma'_t \end{matrix}\right\} = \left\{\begin{matrix} f_1(\tilde{h}) \\ f_2(s^2) . \end{matrix}\right. \tag{6.8}$$

The particular functional relationship chosen for equation 6.8 may be determined by an empirical investigation of real topographic situations, with the aim of achieving the most accurate portrayal of the gravity field in the required circumstances of application of the model. Incorporation of linear density functions, instead of homogeneity, could improve the verity of the model without unduly burdening the computations.

HIGHER ORDER STATISTICAL MOMENTS; OTHER STOCHASTIC PARAMETERS. Higher statistical moments may be used to refine a topographic model since they usually convey additional information about the "shape" of the topographic surface. For instance the third and fourth moments about the mean are sometimes taken to indicate the "skewness" and "kurtosity", respectively, of the distribution function. One way of incorporating these parameters into the model is via the functional relationships expressed in equation 6.8, or—more effectively—through the definitive parameters of linear density functions.

A number of parameters, associated with the prediction of values which are presumed to behave according to a stochastic process, may also be utilized to impart additional reality into a basic model. Care must be excercised in applying such techniques because the fundamental hypothesis of "randomness" in the topography may not be valid: indeed, systematic geomorphology (see *MORPHOMETRIC PARAMETERS* below) manifests non-stochastic processes in topographic formation.

POINT MASSES AND INERTIAL INTEGRALS. Any mass distribution may be simulated by a set of positive and/or negative point masses, for purposes of studying its gravitational field [*e.g.* FISCHER 1973, §4]. A recent review of pertinent techniques has been given by HOPKINS [1973], wherein surface mass layers are examined also. With little difficulty these methods could be used to model the topographic irregularities above the minimum height level $h_{\downarrow}$. Quite simple models could be expected to yield substantial improvements in the modelling accuracy.

Alternatively, empirically derived inertial integrals (see §5.3) are capable of concisely symbolizing the topographic morphology. However the additional complexity of this approach, in comparison with point masses, would need to be justified.

FITTED, QUASI-ACTUAL MODELS. Items (f), (g), and (h) listed above furnish, by one means or another, a continuous, analytical surface which can be "fitted" as closely as desired to the actual topographic surface. Generally, they may be expected to produce rather more complex formulations of the gravitational effect than the models dealt with heretofore, but their appeal may lie in their potential for greater realism. For applications over small quadrature subdivisions this realism may be costly in terms of the amount of digital data required. Fitting procedures for polynomial, trigonometric, and harmonic functions are given by MILNE [1949].

Representation by polynomial functions may be thought of as a generalization of the mean height model outlined in §6.1. With increasing accuracy, and intricacy, the surface can be endowed with slope and curvature. A cursory study of a model comprising a truncated parallelepiped with a sloping plane top surface (*i.e.* a first order polynomial in x and y) established the feasibility of this refinement, but especially good reasons would be necessary to warrant embarking upon the computational complexities of evaluating the resulting formulae. Modifications of the density function, to allow for departures from the basic model, are applicable here as in the mean height model.

Methods which rely on combinations of multi-frequency periodic functions have been a popular expedient for topographic modelling, [*e.g.* UOTILA 1964; LEE and KAULA 1967; BALMINO *et al.* 1973]. But when accurate delineation of the more detailed characteristics of the topography is sought the efficiency of this approach is imperilled by the multiplicity of requisite coefficients.

This is more a consequence of the intrinsic "angularity" of many topographic forms than of any tendency to manifestly short wavelengths. Because of the natural "smoothness" of trigonometric functions, the presence of only one sharp change in an otherwise broadly undulating topographic surface insinuates the higher harmonics into the model. It is well known—at least by landscape artists and some geologists and geomorphologists—that topographic shapes fundamentally comprise plane, rather than curved, surfaces and it appears probable that more concise modelling might be achieved in terms of first order, or at most second order, polynomial functions of height. Thus, instead of the truncated parallelepipeds conforming with quadrature boundaries as referred to above, topographic data could comprise a set of *empirically located* plane surfaces, delimited by their intersections with adjacent planes. Such a representation is essentially an "actual topographic gradient" model, and thereby contrasts with procedures involving "artificial" location of surfaces. One benefit of this approach would be the economy of representation attained in extensive areas of plane but sloping terrain, such as occurs commonly in shield regions.

MORPHOMETRIC PARAMETERS. Morphometry—the quantification and mathematical analysis of landforms and their genetic processes—is gaining respectability among geomorphologists, as a means of systematically quantifying their studies [*e.g.* JENNINGS 1971]. In the search for topographically descriptive parameters, many purely geometric indices and statistical measures have been devised, but the repetoire has also been enriched by a number of more abstract concepts concerned with the motive energy of the causative processes: for example, "relief energy" and "dynamic equilibrium" of slopes and other erosional situations. At present these parameters are inadequate to convey, unaided, a total description of the topographic surface. Nevertheless, they may be engaged as a powerful adjunct to the other modelling methods outlined here. Essentially, they provide the link whereby the real characteristics of the topography can be quantified and adapted to the systematic, but elementary and artificial, notation of a chosen mathematical model. For instance, parameters which distinguish between a mountainous area and an equally rugged, high, disected plateau, devoid of "peaks", could be incorporated in the functional relations expressed by equation 6.8 or used to resolve a distribution of point masses.

6.3 AVAILABLE DATA

SOURCES, COVERAGE, AND ACCURACY

Six digital datasets, listed in table 6.1, provided the topographic source material in the form of area mean height values. These datasets were modified in a variety of ways and a number of different working datasets, designed to meet the demands of the computations, were compiled from them. Modifications of the source data were necessary for three reasons:

(a) to correct errors and omissions,

(b) to attain compatibility between common areas of datasets with different quad sizes, and

(c) to compile terrestrial versions of the data.

Additionally, datasets with 30'x30' and 5°x5° quad sizes were generated.

Error screening is dealt with in the following sub-section. Compatibility of datasets was achieved by recomputing values for larger quads wherever source data was available for corresponding smaller subdivisions. A *terrestrial* dataset is one which has been generated from source data wherein all negative values have been replaced by zeros. Thus no negative values can occur and, in conformity with the conditions of Stokes' model, only topographic material above the geoid is taken into account. This contrasts with *marine* data, which is composed of the negative values in ocean areas only. In table 6.1, the term *solid surface* is used to refer to data which includes both hypsometric and bathymetric values. The "mechanics" of computer data preparation and management are described in §7.4.

UCLA 1° DATA. Global coverage of 1°x1° solid surface, mean elevations was provided by this dataset. The quad boundaries are integer values of latitude and longitude. Using values generated from the available 5' data, this dataset was "updated" to achieve compatibility. During this process it was possible to compare the UCLA values with the, presumably, more accurate generated values, thus obtaining a realistic estimate of the accuracy of the UCLA data. Out of 4175 common, positive values, 363 (8.7%) were discrepant by more than 200 metres. The overall rms discrepancy for terrestrial values was 162 metres. A number of gross errors, evidently involving a factor of ten, were detected. World, outline base maps, used in chapter 8 to present results data, were prepared from computer plots of the zero elevation contour of the UCLA data.

DMA 5' DATA. Coverage is illustrated by the reproduced computer maps in figures 6.3 and 6.4. The accuracy of this data varies and an assessment is coded along with each 5' value [ACIC 1965]. Apart from an initial inspection, this information was not referred to again and was not stored in working datasets.

UNSW 5' DATA. This data covers an area bounded by parallels 10° and 44° south and meridians 111° and 154° east. A computer map of the data is reproduced in figure 6.5, illustrating the locations of positive and negative quads. Originally the data was compiled as 6'x6' mean values in feet by R. S. Mather, using the "estimation method" [CZARNECKI 1970]. These values were converted to metric 5' means by the author, using two-dimensional, linear interpolation. Although the accuracy of the data is

TABLE 6.1

SOURCE TOPOGRAPHIC DATA

DATASET	REGION	TYPE	QUAD SIZE	NUMBER OF QUADS	ORIGINAL SOURCE*	COMPILER
1	Global	Solid surface	1°x1°	64 800	UCLA	W.H.K. Lee†
2	North America	Solid surface	5'x5'	337 248	DMA	--
3	Europe	Solid surface	5'x5'	229 248	DMA	--
4	Australia	Solid surface	5'x5'	215 568	UNSW	R.S. Mather†
5	Antarctica	Ice thickness	1°x1°	9 000	ANARE	E.G. Anderson
6	Greenland	Ice thickness	1°x1°	1 650	ANARE	E.G. Anderson

**Abbreviations:* *UCLA = University of California, Los Angeles*
DMA = Defence Mapping Agency, (Aerospace Center), U.S.A.
UNSW = University of New South Wales, Australia
ANARE = Australian National Antarctic Research Expeditions

†*Source data substantially modified by the author.*

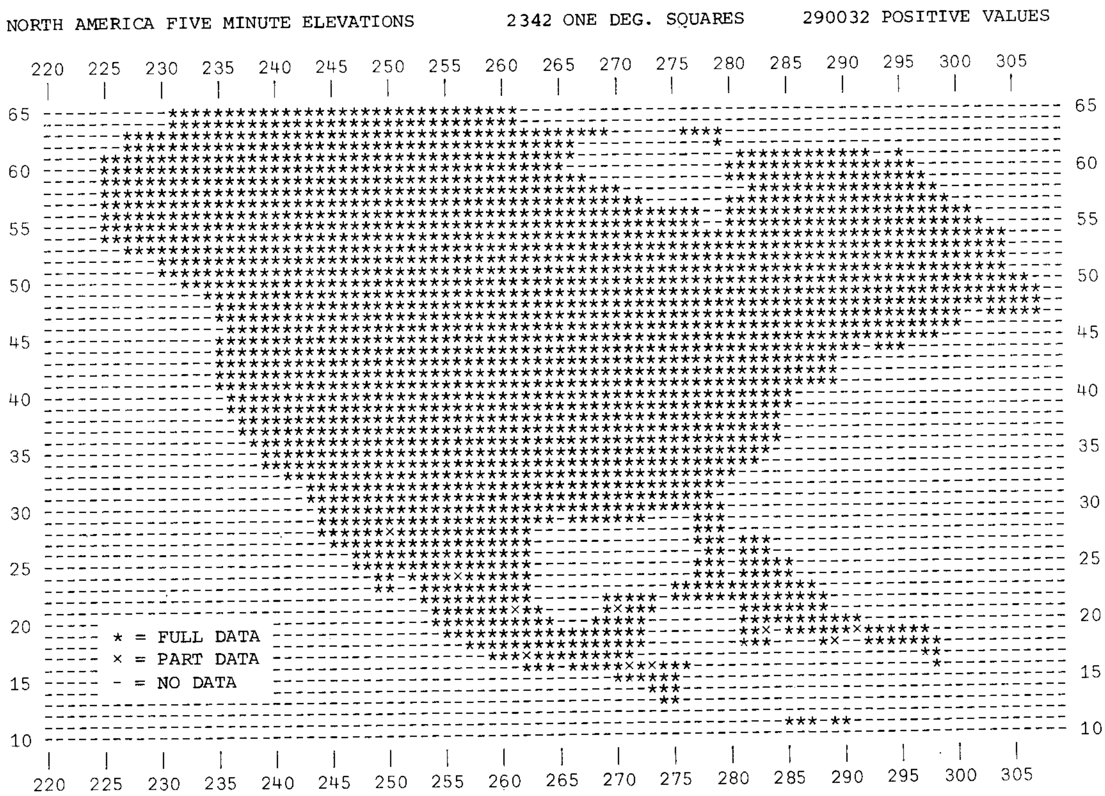

FIGURE 6.3

COMPUTER GENERATED MAP SHOWING EXTENT OF NORTH AMERICAN 5'x5' MEAN ELEVATION COVERAGE

EUROPEAN FIVE MINUTE ELEVATIONS 1592 ONE DEG. SQUARES 175691 POSITIVE VALUES

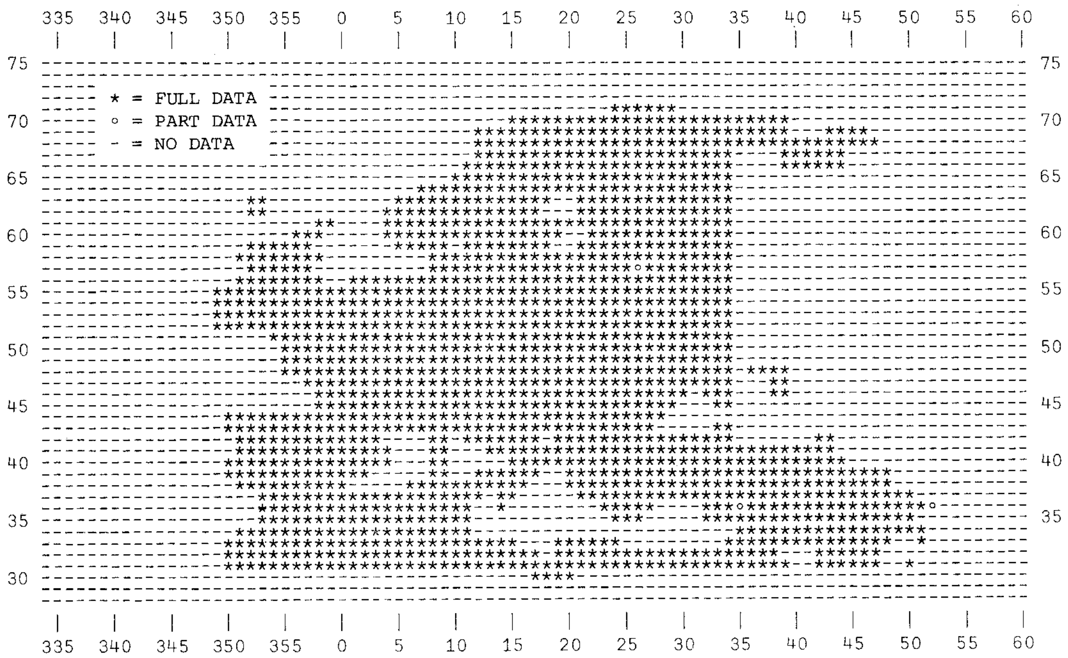

FIGURE 6.4

COMPUTER GENERATED MAP SHOWING EXTENT OF EUROPEAN 5'x5' MEAN ELEVATION COVERAGE

AUSTRALIAN FIVE MINUTE ELEVATIONS

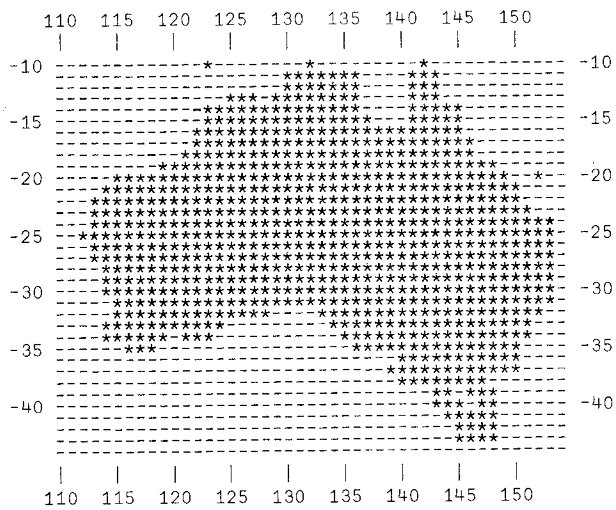

817 POSITIVE ONE DEG. SQUARES
101884 POSITIVE VALUES
1497 TOTAL ONE DEG. SQUARES
35928 CARDS

* = POSITITVE DATA VALUES
- = NEGATIVE DATA VALUES

TAPE FILE: DSN=AUSTFIVE,VOL=SER=UCC319,DCB=(RECFM=FB,LRECL=80,BLKSIZE=1920),LABEL=1

FIGURE 6.5

COMPUTER GENERATED MAP SHOWING EXTENT OF POSITIVE 5'x5' MEAN ELEVATIONS IN AUSTRALIA uncertain, random checks suggest that the terrestrial values are acceptable; however, much of the bathymetry—which was not used in this study—must be regarded as estimates only.

ICE THICKNESS DATA. Mean ice thicknesses for 1° quads were compiled by the author using an area estimation method and maps supplied by W. F. Budd of ANARE [BUDD *et al.* 1971; BUDD 1972, pers. comm.]. Dataset number 5, Antartica, covers the whole area south of latitude -65° and the Greenland data (dataset number 6) extends north of latitude 60° between meridians 285° and 340° east. Though no certain estimate of the accuracy is available, the data is compiled from the best extant information. Substantial differences have been noted between this information and that available from earlier maps, compiled before the advent or extensive use of aerial radar profiling. On an area basis the 1° quads used for this data are comparable with quad sizes ranging between approximately 30' and 5' at the equator.

ERROR SCREENING

With more than 0.85 million data values it is not feasible to detect errors by manual inspection of numerical listings. For this reason a variety of statistical error screening techniques were implemented on the computer, backed up by a visual screening procedure based on computer gererated, graphical illustrations of the data. Computer routines designed for these purposes and methods of maintaining the fidelity of the screened data are described in §§7.3 and 7.4.

STATISTICAL SCREENING TECHNIQUES. During initial transfer of the source data from magnetic tape, all of the card images were checked to ensure the sensibility of all numerical values and location maps were generated. Height values were tested for range ($-11\,000\,\mathrm{m} < h < 9\,000\,\mathrm{m}$) and location parameters (latitude and longitude, degrees and minutes) were checked for omissions, duplications, and range consistent with the boundaries of the particular dataset. By this means a number of gross errors—mispunchings, physical tape errors, and original card-to-tape transfer errors—were detected and eliminated.

Less obvious errors were sought by numerically comparing every value with the eight (or, at margins, less) surrounding values. An error was signalled if the value differed from the mean of the surrounding values by more than a tolerable amount. This tolerance could be set at any integral number of standard deviations of the surrounding values. A listing of signalled values and computer map then facilitated the final decision to retain or reject a value. Missing data was also signalled by the computer routines and the gaps were subsequently filled, either by reference to topographic maps or by linear interpolation.

GRAPHICAL SCREENING TECHNIQUES. Certain error conditions could not be detected by the statistical screening: for instance, when large errors occur in adjacent values. Initially an attempt to overcome this difficulty was implemented by quantitatively "mapping" the data using the computer line printer. An example of the print-out appears in figure 6.6. Alphabetic, numeric, and special characters were used to demarcate successive levels, so that an abrupt change in the pattern could indicate an error. While these maps could be generated rapidly by the computer, the subsequent visual scanning was found to be time consuming and laborious, though reasonably effective.

An alternative method, involving computer generated graph plots of longitudinal profiles of the data, proved to be most effective in detecting errors, and additionally provided a concise, visual impression of the data. Profiles were plotted at 5' intervals of latitude wherever data was available so that every 5'x5' mean elevation was represented. Figure 6.7 illustrates a portion of the computer plot for North America in the vicinity of the Gulf of California and the Mexican Sierra Madre. Three gross errors—two of them adjacent—are apparent near longitude 254° east and a value is omitted at latitude 23° 30' north, longitude 256° 45' east. A number of missing card images are evident between longitudes 261° and 262° east. About 300 defective or missing card images (0.32% of total) were detected in the DMA 5' data.

POSITIVE ELEVATIONS:

LAT = 20 LON = 270

Error at 18° 55'/270° 30'

Erroneous card at 15° 15'/271° 30'

Missing value at 15° 15'/271° 55'

```
     |            |            |            |            |
     BBCCCCCCCCCCBBBBBBAAAAAAAAAAAAA------..........................
     BBBCCCCCCCCCBBABBBAAAAAAAAAAAAA------..........................
     BBBCCCCCCCCCBBABBBAAAAAAAAAAAAA------..........................
     BBCCCCCCCCCCBBBBBBBAAAAAAAAAAA-------..........................
     BBCCCCCCCCCCCCCBBBAAAAAAAAAAA--------..........................
     BBCCCCDDDCCCCCCCCBBBBAAAAAAAAAAA-----..........................
     BBCCCCDDDCCCCCCCCBBBBBAAAAAAAAA------..........................
     BCCCCDDDCCCCCCCBBBBBBBAAAAAAA-------...........................
     BCCCDDDCCCCCCCCBBBABBBAAAAAA-A------...........................
     CCCCDDDDCCCCCCCBBBBBBBBAAAAAAA-------..........................
     CCCDEEDDDDCCCCCBBBBBBAAAAAAAA-------...........................
  -  CCDDEEEDCCCCCCCBBBBBAAAAAAAAAA-------.......................... -
  →→ CCDDDDKDDDCCCCCBBBBAAAAAAAAAA--------..........................
     CDDDDEEDDDCCCCCBBBAAAAAAAAAAA--------..........................
     CDDDEEDDDDCCCCCBBAAAAAAA-AAAA--------..........................
     DDDDEEEDDDDCCCBBBAAAAAA--AAA---------..........................
     DDDEEEEEEDDCCCBBBAAAAAA--AAA---------..........................
     DDEEEEEEEEEDDCCCBBAAAA--AAAA---------..........................
     DDDEEEEEEEDDDCCBBAAAAA---AAA---------..........................
     DDDDDEEEEEDDCCCBBAAA----AA----------...........................
     CCCDDDEEEEDDCCBBBAAAAAAA--A----------..........................
     CCDDEEEEEEEDDCCBBAAAAAAAA------------..........................
     CDDEEEEEEEEDDDCCBBBAAAAAA------------..........................
  -  DDEEEEEEEEEDDDDCBBBAAAAAA-A----------.......................... -
     DDDDDDDDDDBBDDCBAAAAAAA--------------..........................
     EDDDDEDDDDBBCCAAAAAAAAA--------------..........................
     EFFFFFEDCCCCCBBBAAAAAAA--------------..........................
     EFFFGFECCCCCBBBBAAAAAA---------------..........................
     FFGGFFCCCECCBBBAAAAAAA---------------..........................
     FGGGFCDDEECCCBAAAAAAAA---------------..........................
     FGHGDDEEEECCBBBBBAAAA----------------..........................
     FGHGDEEEEDCCBBBBBABBA----------------..........................
     EFHGEFEEDDCCBBBBBABBA----------------..........................
     DFFFFEEEDECCCCCDCBBBB----------------..........................
     DFFFGGFEFFEEEFFEDDED-----------------..........................
  -  DDFGHGFFEEEGILNJKHGEA----------------.......................... -
     CBBDEFGFEGGIKNOKPRHEB---.......................................
     EFFGGGFEFHIIMMKNNHEEA---.......................................
     DEEGHGFEGIIJKOKROCEBA---.......................................
     DDDEHHGFHIJJKNOJIEHBA---.......................................
     DDEFGGIGJKJKNPOJECBB----.......................................
     DDEEFHJIKNMMPMHCBBBA----.......................................
     DEEEFHHJOSPOJHDBBBA-----.......................................
     DDEGHIILOPOMHFCBBA------.......................................
     DDFIIJKMNNJGCCBAAA------.......................................
     DDDFIIJLJIGEBEB---------.......................................
     DDEFGGGGIFECCBB---------.......................................
  -  DDDEEFGGFECBAA----------....................................... -
     DDDDFGFGCAAAA------------------------------------AAA-------AA
     DDDFGGEGEBBBDBA-----------AAA---------------AGGGKDAAAAAABSKB
     FGEEEEEEEFDBBBABA-AAA----DFAAAAAAA-----BFGBACGMGDCBBGGGMMERCD
     JHKIIJJINKKBACMKBBAAA-BIHAACCFJJDBAACGM2PEEHJFCBCEGMPJEJJDDG
     NSMINNOQKGFAAINMFBAADHROCAAAHMMEGCDMGDSSVSGECCCDGFGGEEMMGEGH
     MMMPMOJKH---BEFGABDMTXUICBAAILEFJSPY22YSMPDDCEGMRJGEMPPJEGGG
     SXROKFBA---BGCBDJLNNUTPHAABINOYYG2YYMMMGJGEGPSPMTMJMPPMEMMJJ
     BXOGAAAAAFGIBBGOPLLIIGFHCBFMNKY2YVSPKMGMSGY2YY2YPJNSSPFJSSMM
  →→ PGKJJJRMRPIBEIKQOK....AØBCOGFJYYVPVVSS.YSSMP22YYMJMSVMMPVSPM
     1CA2Z3ZZOGGILXQQLJMTQQMJCHQISZVAYPSYAVYYAYSPYYYXMMMSAMMMMKJH
     KNJLKWTIGJOMY3ROQRRWSINLDDGGFMY2SMVYPM2AJVVS2YXYPSYYVJJFGGFE
  -  EE3VSKMLKUSOVYNRRSPOKJRMDHMKRZS2RAYPSSYSY2A2ZYVAJVJGEEFGEDED -
     |            |            |            |            |
```

HYPSOMETRIC INTERVAL = 100 METRES - = NEGATIVE VALUE . = DATA NOT AVAILABLE

FIGURE 6.6

EXAMPLE OF LINE PRINTER MAP OF 5' MEAN ELEVATION DATA

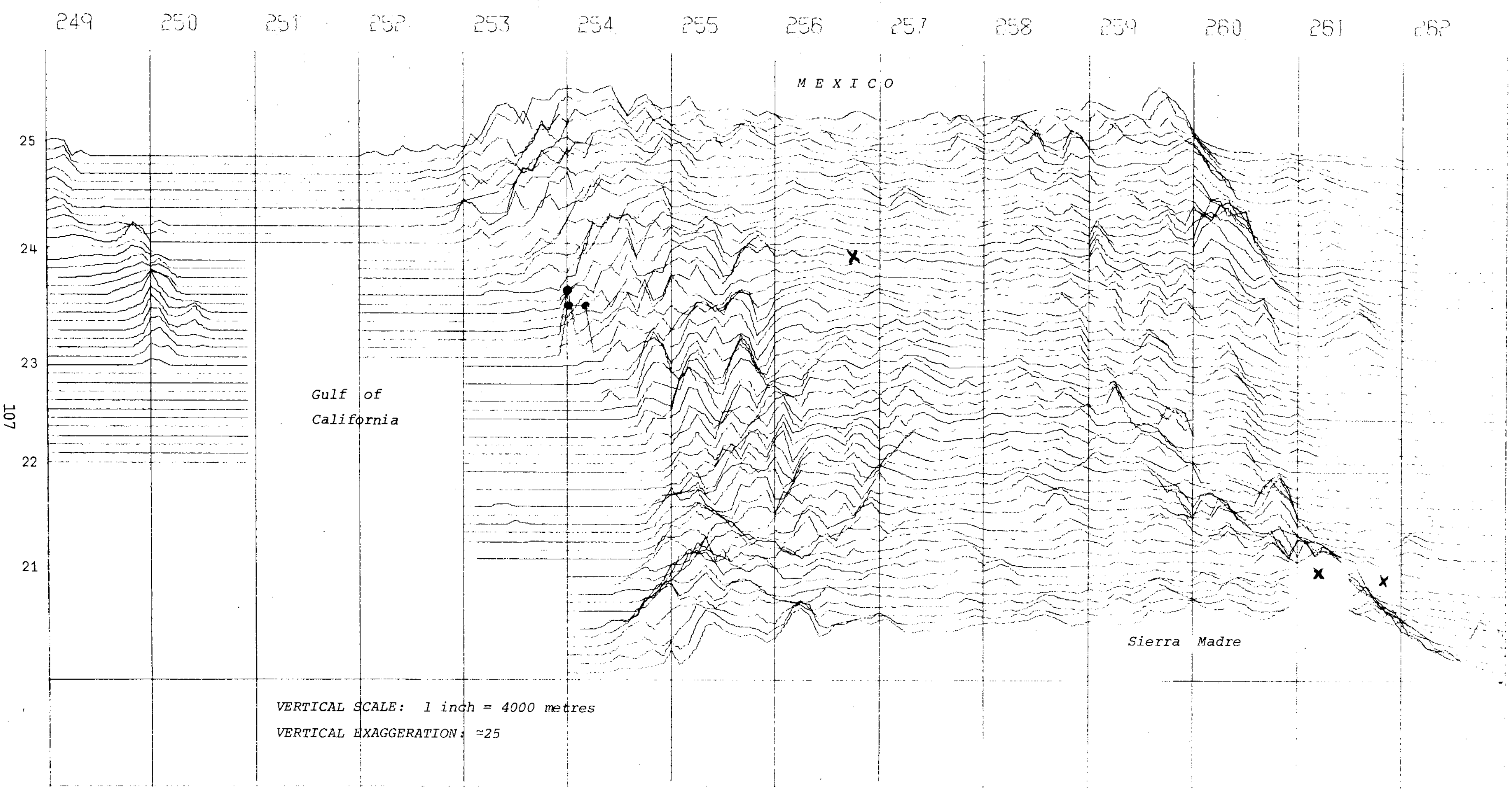

FIGURE 6.7

EXAMPLE OF COMPUTER GENERATED GRAPH PLOT OF 5'x5' MEAN ELEVATIONS USED IN ERROR SCREENING

6.4 SIMULATED DATA

FEASIBILITY OF COMPLETING DATA COVERAGE

Global data for quad sizes less than $1°x1°$ was not available, so a study was made of the feasibility of compiling terrestrial 5' mean elevations for the unrepresented areas. Enquires regarding holdings of maps at suitable scales within Australia revealed a paucity and investigations into the possibility of acquiring these—where available—indicated that cost alone would be prohibitive. Consequently, the study was diverted to the problem of compiling data from very small scale maps and atlases.

Initially, timed trials of an inter-contour, area estimation method, as well as the "point method" [CZARNECKI 1970], were performed, using transparent grid overlays and manual recording procedures. Estimation of areas was found to be somewhat more accurate and faster, but both methods proved to be too slow. A considerable improvement was achieved by entering estimates directly into an electronic desk calculator, where they were processed and the resulting mean heights automatically printed; however, the estimation procedure could not be hastened sufficiently. Several methods of automating the "map reading" process were investigated, including the possibility of scanning photographic reproductions of the maps in a "Topocart-Orthophot-Orograph" photogrammetric instrument [*e.g.* HOLDEN 1974, p.37 *et seq.*] to digitally derive inter-contour areas, and the use of a computer controlled "digitizer" for the same purpose. Although these techniques were capable of rapidly digitizing the maps, the cost—in terms of subsequent computer time necessary to transform the raw data into mean heights—was too high when the whole job was taken into account.

Eventually, it was concluded that compilation of the required data was not feasible with the available resources.

METHOD OF SIMULATING DATA

As it was deemed essential to accomplish the evaluation of the gravitational effects on a world-wide grid according to a consistent specification, the possibility of completing the data coverage by simulation was examined. The philosophy underlying this decision included the idea that the advantages accruing from the ability to globally analyse the results, particularly in terms of harmonic coefficients, outweighed the fact that such results were partly a function of an artificial model. At least it would be possible to demonstrate the effects of a *particular* topographic model and any lack of realism need not detract from the broad conclusions drawn from the observed behaviour of that model. Also, it must be stressed that the simulated data enters the calculation pertaining to the inner and mid zones only, and does not, therefore, influence the results for the outer zone.

SIMULATION BY DATA TRANSFERENCE. All of the usual methods of interpolating or predicting data values were judged to yield over-smoothened results, and a method of generating data with characteristics harmonious with the existing "real" data was sought. A simple scheme, based on the concept of transferring blocks of real data to areas lacking coverage, was chosen. In addition to its simplicity this method enjoys the advantage of being founded upon a principle which is not merely mathematical, but which has some measure of geomorphological justification. Furthermore, the capacity to save computer storage by rapidly generating simulated values as they are needed, and to do this through the same computer routines used to access the real data, are important practical attributes.

The fundamental contention, upon which the method relies, is that it should be possible to find a block of data within the available 5' datasets which has similar morphological features to a block for which simulated values are sought. This similarity need be only qualitative, since variations of orientation and scale can be built into the generating procedure. Thus, choosing a 1° quad as the basic unit of the scheme, all of the simulated 5' mean elevations h'_{jk} in a quad can be related to known 5' data values h_{jk} in a *source quad* through the equation

$$h'_{jk} = B + Fh_{jk} \quad (j = 1,12;\ k = 1,12), \tag{6.9}$$

where B is a constant *block shift*, and

F is a constant vertical *scale factor*.

Then, since B and F are both constants within a 1° quad, it follows that the mean height H' of the simulated 1° quad must be related to the mean height H of the source quad by the similar equation:

$$H' = B + FH. \tag{6.10}$$

Because H' and H can both be assigned values for all 1° quads, using the UCLA global dataset, then, if F is chosen according to some morphological criterion, the value of B is constrained to satisfy the equation

$$B = H' - FH. \tag{6.11}$$

F is perceptibly connected with the desired ruggedness of the simulated topography, defined by its standard deviation:

$$s' = \left\{\frac{\sum_{j=1}^{12}\sum_{k=1}^{12}(h'_{jk} - H')^2}{144}\right\}^{\frac{1}{2}}. \tag{6.12}$$

Substituting equations 6.9 and 6.10 into 6.12 leads to:

$$s' = F\left\{\frac{\sum_{j=1}^{12}\sum_{k=1}^{12}(h_{jk} - H)^2}{144}\right\}$$

$$= Fs,$$

whence

$$F = \frac{s'}{s}, \tag{6.13}$$

where s is the standard deviation of the source quad, which can be determined from its known 5' values. Care must be exercised to ensure that this quantity does not approach zero. Thus F acts as a scale factor which changes the ruggedness of the source quad to provide a suitable variance in the simulated quad. But what is the appropriate ruggedness for a simulated quad?

The available terrestrial 5' data was analysed to see if any correlation could be observed between the standard deviation of a 1° quad and its mean height. Results are presented graphically in figures 6.8 (a) to (c), and 6.9, and numerically in table 6.2. In the figures—which are computer generated "scatter diagrams"—the plotted numbers represent frequencies from the bivariate population (H,s), classified into discrete intervals. A class interval of 100 metres was used for H and 20 metres for s in all cases. Frequencies exceeding 9 are denoted by an asterisk. Figures 6.8 (a), (b), and (c) illustrate analysis of datasets 2, 3, and 4 respectively (see table 6.1), while figure 6.9 depicts the result for all three datasets combined. A marked trend towards smaller standard deviations occuring at higher elevations is apparent in the North American and Australian data, which contrasts with the reverse tendency in Europe. This could be a reflection of the extensive "shield" regions in the former continents. Europe is also more rugged overall. Not surprisingly, the extraordinary occurrence of a standard deviation of almost 1000 metres in the European data is due to the quad containing Mt. Blanc.

CORRELATION OF TOPOGRAPHIC STANDARD DEVIATION WITH MEAN ELEVATION
FOR ONE DEGREE QUADS
DATA SET 2 -- NORTH AMERICA

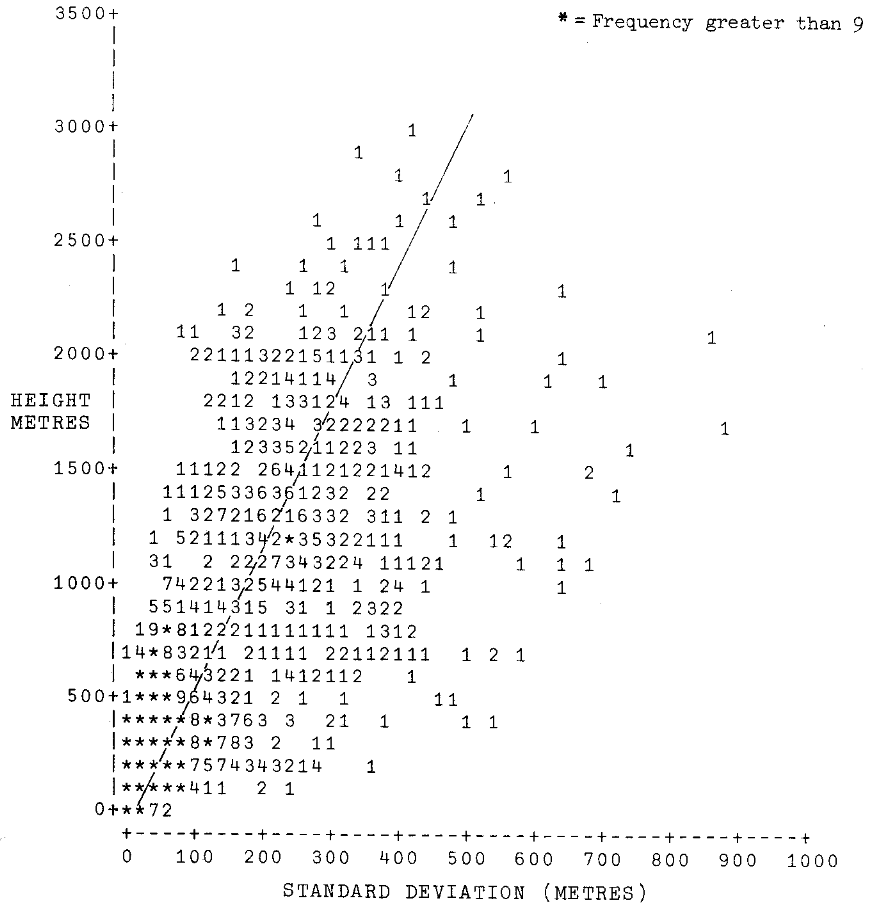

(a) North America

CORRELATION OF TOPOGRAPHIC STANDARD DEVIATION WITH MEAN ELEVATION
FOR ONE DEGREE QUADS
DATA SET 3 -- EUROPE

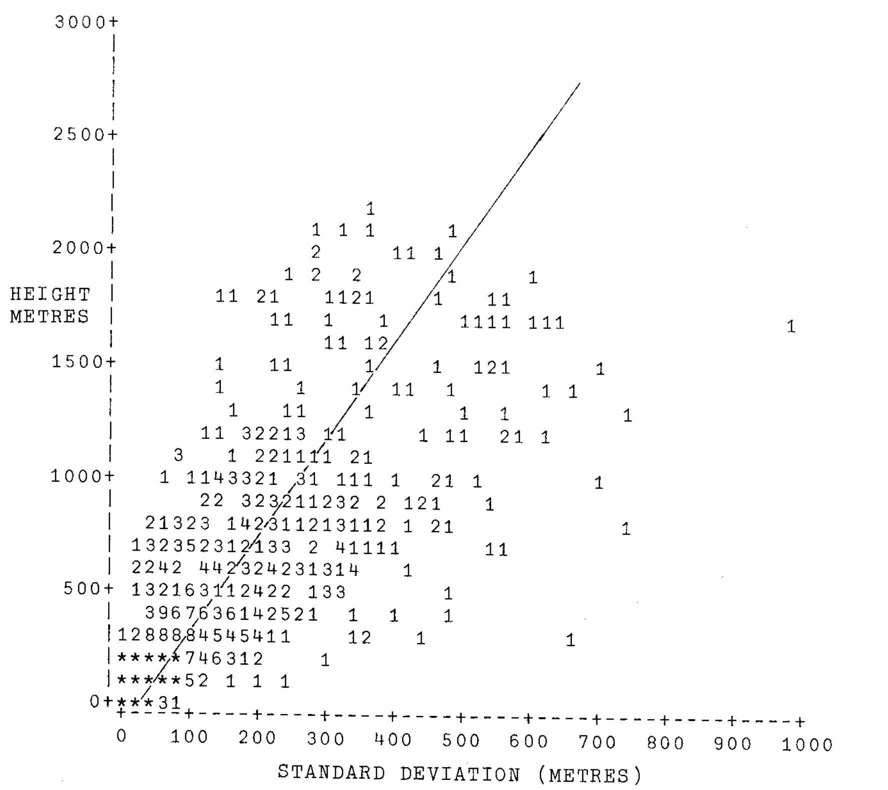

(b) Europe

FIGURE 6.8

COMPUTER GENERATED SCATTER DIAGRAMS OF MEAN HEIGHT VERSUS STANDARD DEVIATION OF TOPOGRAPHIC DATA

CORRELATION OF TOPOGRAPHIC STANDARD DEVIATION WITH MEAN ELEVATION
FOR ONE DEGREE QUADS
DATA SET 4 -- AUSTRALIA

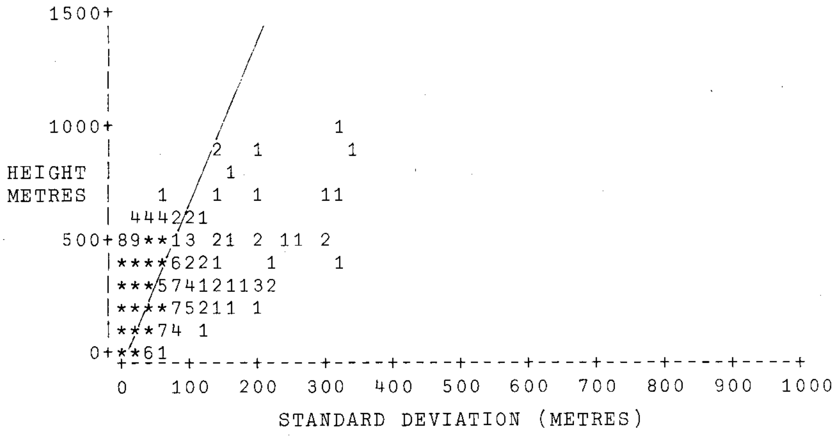

(c) Australia

FIGURE 6.8 Continued

COMPUTER GENERATED SCATTER DIAGRAM

CORRELATION OF TOPOGRAPHIC STANDARD DEVIATION WITH MEAN ELEVATION
FOR ONE DEGREE QUADS
DATA SET 2+3+4 -- ALL DATA

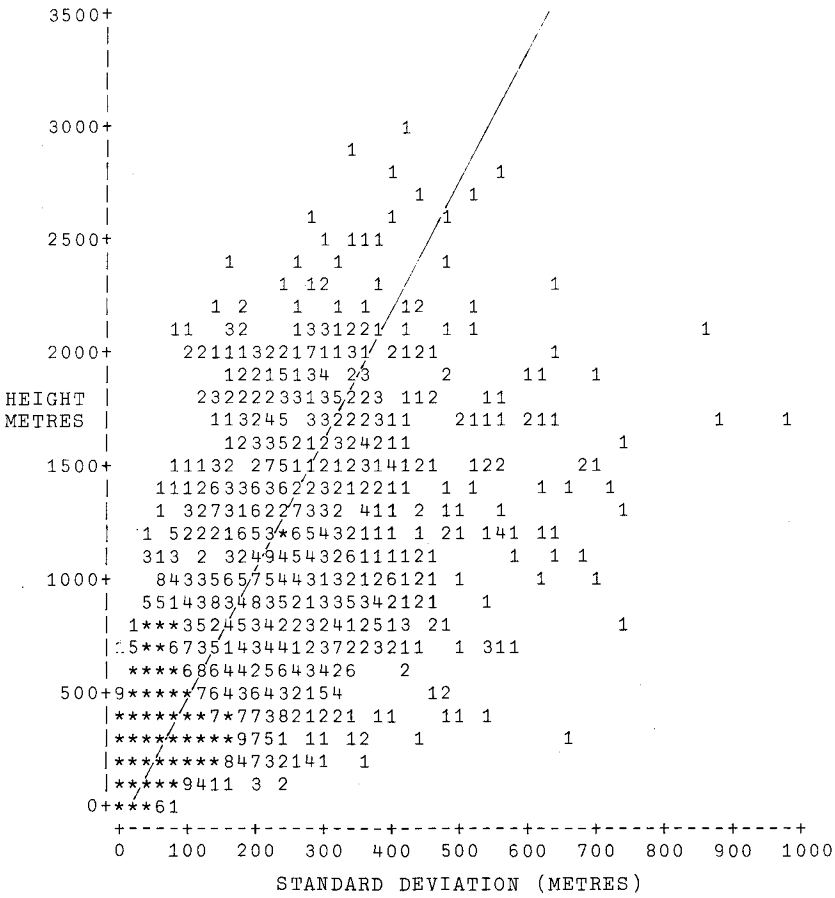

FIGURE 6.9

COMPUTER GENERATED SCATTER DIAGRAM FOR ALL AVAILABLE DATA

TABLE 6.2

CORRELATION AND REGRESSION OF TOPOGRAPHIC MEAN ELEVATIONS AND STANDARD DEVIATIONS

ITEM			DATASET 2 Nth. America	DATASET 3 Europe	DATASET 4 Australia	2 + 3 + 4 All data
(1)	n		1 785	888	609	3 282
(2)	$\sum H$	(m)	1 253 956	453 390	181 768	1 889 313
(3)	$\sum s$	(m)	231 707	127 732	30 220	389 658
(4)	$\sum H^2$	(m^2)	1 506 608 000	440 506 100	72 545 730	2 019 660 000
(5)	$\sum s^2$	(m^2)	62 291 780	38 234 880	3 022 837	103 549 500
(6)	$\sum Hs$	(m^2)	264 012 800	113 776 500	11 601 750	389 390 800
(7)	$\bar{H}$	(m)	702.50	510.80	298.47	575.65
(8)	$\bar{s}$	(m)	129.81	143.84	49.62	118.73
(9)	r		0.713	0.754	0.489	0.714
(10)	z		37.7	29.2	13.2	51.3
(11)	s_0	(m)	16.1	25.1	7.49	16.8
(12)	S		0.162	0.232	0.141	0.177

In table 6.2 item 1 is the number of positive quads in the dataset, that is, the sample size. Items 2 to 6 are the sample sums, sums of squares, and sum of products of the variates and items 7 and 8 are the overall mean values of the mean heights and standard deviations. The sample correlation coefficient r is item 9. Australian elevations evince a much lower correlation than the other datasets. This peculiarity is thought to be associated with the continent's geological antiquity and distinctive, stable tectonic history, which has resulted in the vast plateau regions between 200 and 450 metres elevation over more than three-quarters of the total area [MATHER *et al.* 1971, §1.2].

To test whether the observed degree of correlation is significant it is usual to first convert r to a value z which has an approximately standard normal distribution. Then, to test the null hypothesis that the correlation coefficient of the population is zero, z is given by [FREUND 1962, p.311]:

$$z = \frac{(n - 3)^{\frac{1}{2}}}{2} \, \ell og \, \frac{(1 + r)}{(1 - r)} \, . \tag{6.14}$$

Tabulated values of z (item 10) all greatly exceed the two-tail, 1% level of significance ($z_{0.005} = 2.58$) for a normal distribution, thereby forcing rejection of the null hypothesis and demonstrating an indubitable correlation in all datasets. Strictly, this test is only valid if the sampled population is normally distributed and the accompanying scatter diagrams patently suggest that this is not so. However, the very high statistical significance of the results well justifies the conclusion of correltation between 1° mean heights and standard deviations.

This established correlation provides a means of gauging a suitable degree of ruggedness for the simulated quads. All that is required to predict a standard deviation, given the mean height, are the least squares linear regression coefficients s_0 and S [*ibid.*, §13.5] in the equation:

$$s' = s_0 + SH', \tag{6.15}$$

where s_0 is the *sea level deviation*, and

S is the deviation rate or *relative ruggedness*.

Values of these coefficients are given by items 11 and 12, and the resulting regression lines have been added to the accompanying figures. Because the combination of all data is more likely to include a typical range of morphological traits than an individual dataset, it was chosen to provide the definitive values of the regression coefficients. Hence,

$$s_0 = 16.8 \text{ metres}, \quad S = 0.177 \tag{6.16}$$

were adopted.

Despite an apparent lack of normality in the distribution, it is not unreasonable to study the reliability of these coefficients under the assumptions of *normal regression analysis* [*ibid.*, §13.4.2], since the resulting statistics provide at least some measure, however rough, of the efficacy of the adopted prediction technique. To this end, confidence intervals were constructed for the regression coefficients and *limits of prediciton* for s' were established within the range of H'. In table 6.3 the standard deviations and 0.95 and 0.99 confidence intervals are given for s_0 and S, along with the associated marginal and conditional standard deviations. Figure 6.10 shows the 0.99 limits of prediction of the standard deviation of a 1° quad, and demonstrates that the maximum reliability is achieved at the mean point of the distribution.

TABLE 6.3

REGRESSION COEFFICIENT CONFIDENCE INTERVALS FOR COMBINED DATA

Marginal standard deviation of H: s_H = 532.91 m
Marginal standard deviation of s: s_s = 132.12 m
Conditional standard deviation of s given H: $s_{s|H}$ = 92.45 m

COEFFICIENT	STANDARD DEVIATION	CONFIDENCE INTERVAL 0.95	CONFIDENCE INTERVAL 0.99
s_0	2.375 m	$s_0 \pm 4.66$ m	$s_0 \pm 6.13$ m
S	0.00303	$S \pm 0.00594$	$S \pm 0.00782$

CHOICE OF SOURCE QUAD. Using equations 6.11, 6.13, 6.15, and 6.16 it is now possible to solve the *transfer equation*—equation 6.9—to obtain simulated 5' mean elevations from those contained in a source quad. But it remains to decide how to choose the source quad.

Two related criteria were considered mandatory in selecting the source data:

(a) Actual regional topographic trends within the simulated 1° quad should be realized by the simulated values.

(b) Simulated 5' values at the boundaries of contiguous 1° quads should "match up" so as to avoid large discontinuities.

In most cases it is reasonable to suppose that any major trends in the topography may extend beyond the boundaries of a 1° quad; at least this could be expected to be true of the most important trend—the regional average gradient. It follows that the mean heights of 1° quads adjacent to that which is to be simulated may be employed to assess such trends, and thus predicate both of the above criteria in the choice of a source quad. A suitable source quad is, therefore, distinguished by having a pattern of surrounding quads which is similar to that of the simulated quad, and may be found by a process of least squares fitting. The governing condition of this process is:

$$\sum_{n=1}^{8} (H_n - H'_n + H' - H)^2 = \text{minimum}, \tag{6.17}$$

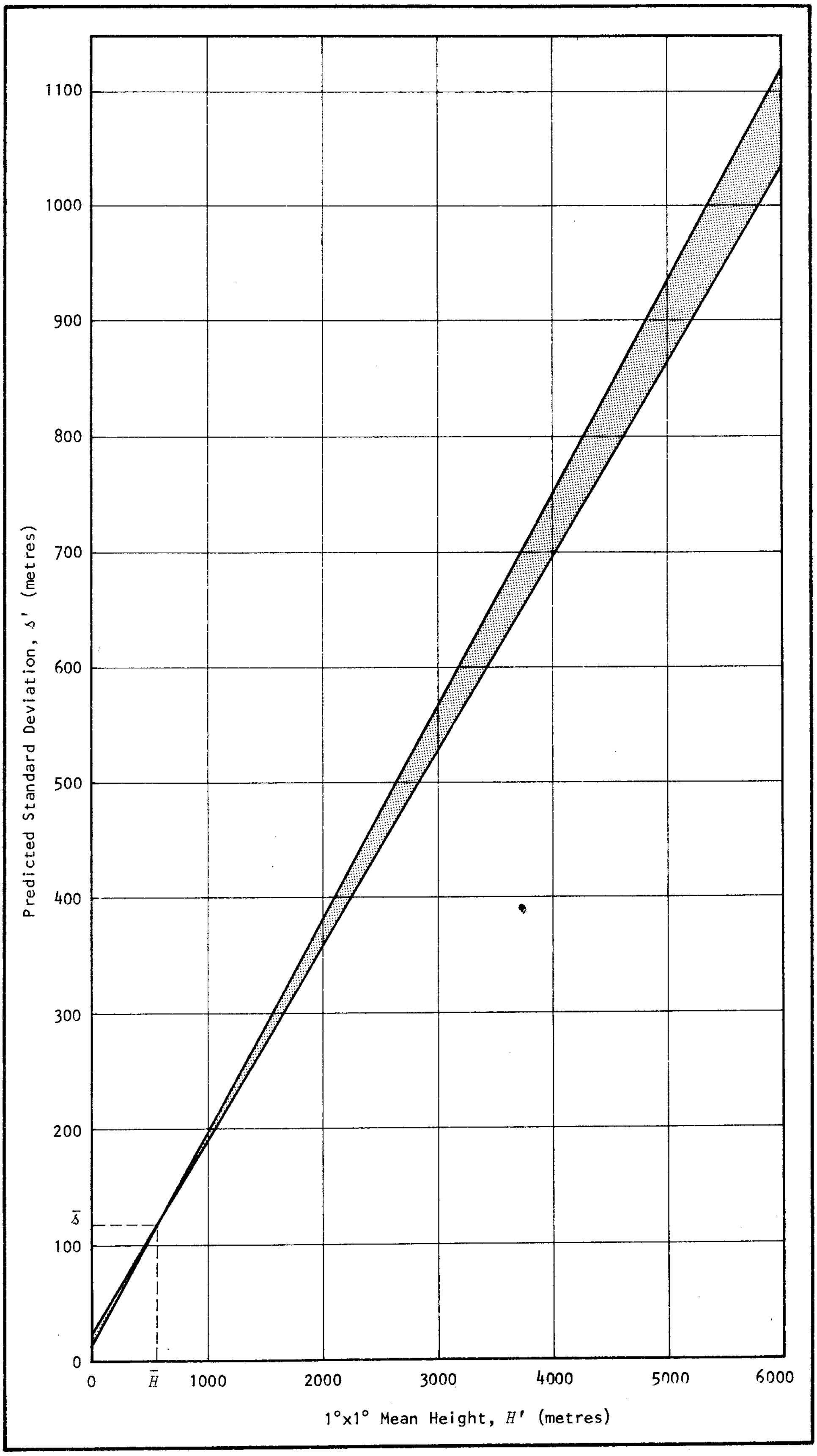

FIGURE 6.10

0.99 LIMITS OF PREDICTION OF THE STANDARD DEVIATION OF ELEVATIONS IN A 1°x1° QUAD AS A FUNCTION OF ITS MEAN HEIGHT, BASED ON ALL AVAILABLE DATA where H_n and H_n' are the mean heights of the eight 1° quads surrounding the source and simulated quads respectively. In effect, the quads surrounding the source are block shifted by the difference between the simulated and source quads before attempting the fit.

During the search for a best-fitting group of quads there is no reason to presume that the orientation of the source group has any importance, as long as any change of orientation before fitting is duplicated in the subsequent transfer of 5' values. Orientation of the source group, and hence the 5' source data, greatly improves the probability of finding a good fit. By extending the orientation procedure to allow mirror-images of the source data—which are equivalent to the topographic surface turned upside-down—the number of orientations is doubled to give eight possibilities. For example, figure 6.11 illustrates the relationship between the simulated and source groups when the latter is oriented eastwards and mirror-imaged. Practically, the orientation of the data is achieved by manipulating the indices in equation 6.17 and, accordingly, in the transfer equation, 6.9.

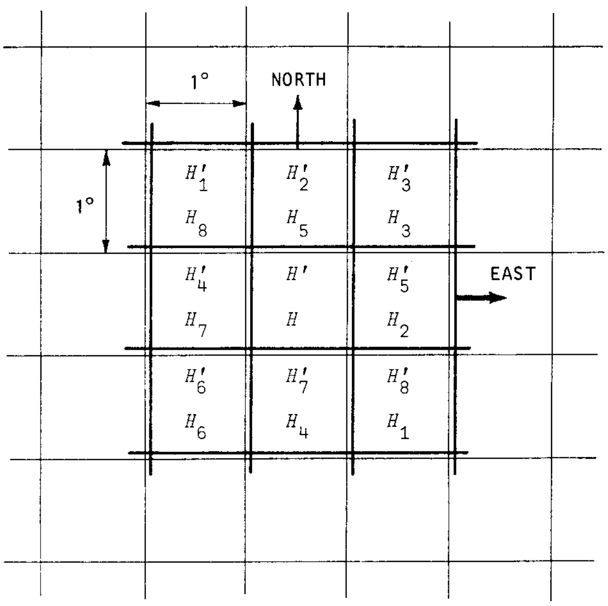

FIGURE 6.11

ORIENTATION OF SOURCE GROUP TO THE EAST AND MIRROR-IMAGED

STORAGE OF THE SIMULATED DATA. It is unnecessary and wasteful of storage space to permanently store the simulated 5' data. Implementation of the transfer equation involves trivial computations, so that the simulated values are easily generated from the source data whenever necessary. Only four simulation parameters for each 1° quad need to be permanently stored: the block shift B, the scale factor F, an orientation parameter, and an identification number to point to the chosen source quad. These parameters may be stored conveniently in an index dataset, along with the identification numbers used to index 1° quads of real 5' data. Data access routines are described in §7.4.

EXAMPLES OF SIMULATED DATA

Perhaps the best test of the simulated data is its appearance. Visualization and comparison of simulated values with real data was possible by using the computer plotting routines developed for graphical error screening. In figure 6.12 (a) and (b) a single 1° wide strip of simulated 5' data is shown with real data on either side for comparison. The simulated strip is bordered by the parallels 41° and 40° North and extends from longitude 236°, at the west coast of the U.S.A., across the highest part of the

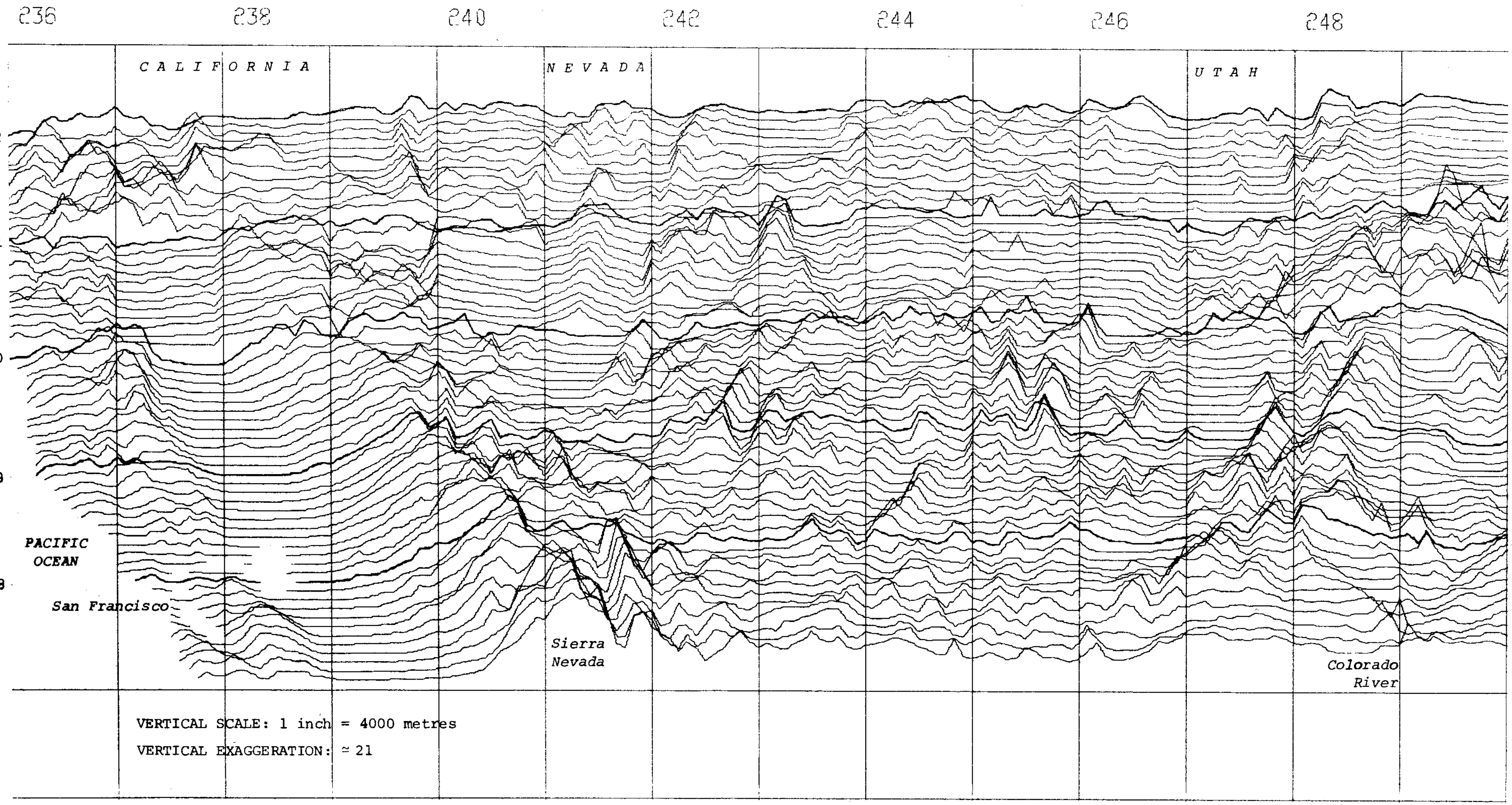

FIGURE 6.12(a)

COMPARISON OF SIMULATED 5' DATA (BETWEEN LATITUDES 41° AND 40°N) WITH REAL DATA

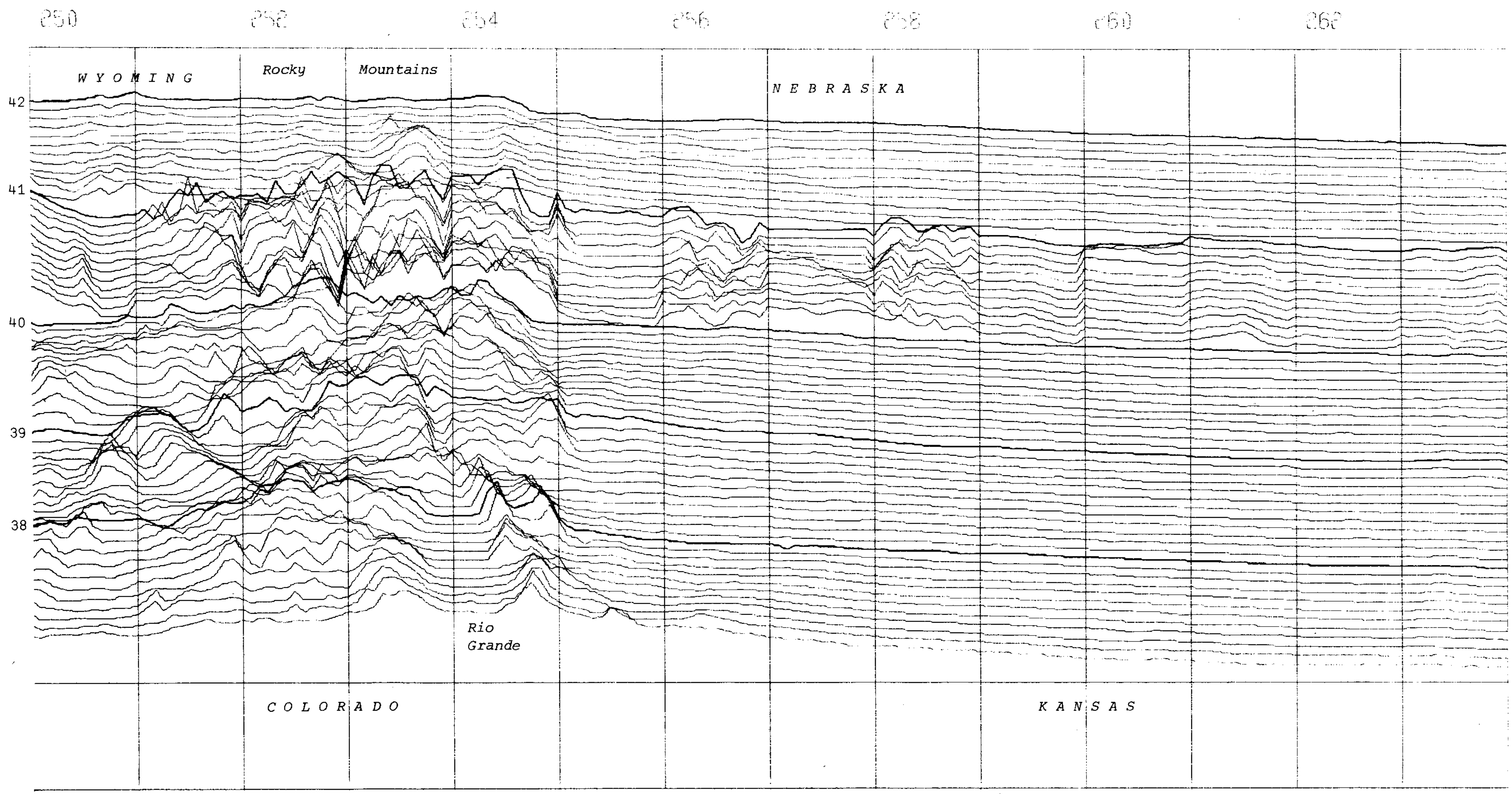

FIGURE 6.12(b)

COMPARISON OF SIMULATED 5' DATA (BETWEEN LATITUDES 41° AND 40°N) WITH REAL DATA

TABLE 6.4

EXAMPLES OF TOPOGRAPHIC DATA SIMULATION PARAMETERS

SIMULATED QUAD LAT.	LON.	H'	SOURCE QUAD LAT.	LON.	H	F	B	Orien-tation
			See figure 6.12(a)					
41	236	800	51	237	1508	0.39	211	W
41	237	600	58	226	248	0.28	530	N
41	238	1400	52	244	1916	0.84	-209	S
41	239	1500	59	227	1216	0.91	393	N
41	240	1550	64	239	328	7.27	-834	S
41	241	1550	60	237	496	3.34	-106	E
41	242	1650	64	236	384	1.79	962	E
41	243	1700	62	237	323	3.24	653	E
41	244	1900	60	288	228	10.00	-380	S
41	245	1800	58	292	151	10.00	290	W
41	246	1600	61	243	259	6.24	-16	W
41	247	1385	60	232	823	1.72	-30	E
41	248	2300	59	235	1398	0.94	985	E
41	249	2800	47	238	1244	1.46	983	S
			See figure 6.12(b)					
41	250	1950	59	240	476	3.04	502	W
41	251	2250	57	237	1006	2.06	177	S
41	252	2700	62	232	1550	2.16	-647	W
41	253	3000	63	233	1704	2.80	-1771	E
41	254	2800	45	250	2417	1.02	334	N
41	255	1500	39	255	1717	0.98	-182	N
41	256	1500	61	234	970	1.64	-90	E
41	257	1500	60	245	586	1.26	761	N
41	258	1300	62	232	1550	1.07	-358	E
41	259	760	61	244	230	3.43	-28	W
41	260	750	64	239	328	3.73	-473	S
41	261	750	61	239	550	1.51	-80	W
41	262	400	63	245	190	2.30	-36	E
41	263	350	64	255	265	1.57	-66	W
			See figure 6.14					
36	65	2700	26	259	1621	0.66	1630	E
36	66	2900	47	12	1420	0.85	1693	S
36	67	2900	38	43	1988	0.87	1170	S
36	68	2200	39	254	2595	1.03	-472	E
36	69	2600	21	260	2056	1.66	-812	E
36	70	4000	47	10	2109	1.46	920	N
36	71	3100	19	262	1920	1.-5	124	W
36	72	3100	29	251	1786	1.40	599	E'
36	73	3000	23	260	776	1.30	1991	W
36	74	3200	33	353	783	1.56	1978	S'
36	75	4000	39	41	1410	1.81	1447	E'
36	76	4800	53	233	1222	2.16	2160	N
36	77	5000	45	245	2234	3.32	-2416	S'
36	78	5000	59	227	1216	2.90	1473	W'

Rocky Mountains to longitude 264°. A list of the source quads used and the appropriate simulation parameters is given in table 6.4. This example illustrates simulation of a wide range of topographic forms with considerable variation in both elevation and ruggedness. Generally, topographic trends and continuity at 1° quad boundaries have been accomplished remarkably well. A few minor exceptions—for example, the boundary discontinuities associated with the quads at longitudes 249°, 253°, and 254°—appear to have been caused, in part, by termination of the scan for a source quad before the *best* least squares fit was reached. This measure, which was introduced to economize computation time, was implemented by accepting the first source group with a sum of squares below a specified tolerance, rather than finding the absolute minimum solution of equation 6.17. In addition, for this particular example only, the fit of mirror-images of the source group was not included in the scan; a device which, despite its time saving qualities, was found to severely handicap the fitting procedure. Consequently, the quality of some of the resulting simulated data is less than the best that could be achieved by the transfer method. Another minor imperfection arises from the inability of the regression coefficients (equation 6.16) to cope with all possible topographic forms. Thus, in figure 6.12(b), the ruggedness of the quads at longitudes 256° to 258° is an over-estimate of the prevailing conditions in that particular region. Furthermore, to facilitate computer storage and constrain excessive values, an upper limit of 10.00 was applied to the scale factor F.

Figures 6.13 and 6.14 enable comparison of real and simulated data in the most mountainous regions. The first figure illustrates real 5' data covering the area between latitudes 50° and 45° north and longitudes 5° to 19° east, which includes the European Alps. Comparable simulated data is depicted in the second figure, covering the western extremity of the Himalayas between latitudes 40° and 35° north and from longitude 65° to 79°. The Hindu Kush, Pamirs, and Karakoram Range are encompassed, and elevations ranging from 450 to 8000 metres occur. Source quads and simulation parameters for the 1° strip at latitude 36° North are listed in the last part of table 6.4. Again some 1° boundary discontinuities are evident, but their magnitude is not unreasonable in the context of such rugged topography.

IMPROVEMENT OF THE METHOD AND ALTERNATIVE APPLICATIONS

Many refinements of the transfer method of simulating topographic data could be implemented to improve the results. Some of these are discussed in the following list.

(a) A higher order or different type of transfer equation could be employed. By this means, factors other than linear magnification of ruggedness, based on specific morphometric properties, could be incorporated. Local topographic trends, within the limits of a 1° quad, could be taken into account.

(b) Processes supplementary to the simple transfer equation—such as "tilting" or "bending" of the simulated surface within a 1° quad—could be applied to minimize boundary discontinuities. This procedure has the advantage that it could be implemented in a second phase, independent of whatever initial transfer process was used.

(c) Curvilinear, instead of linear, regression could be applied to determine the required standard deviation of the simulated quad.

(d) Instead of a single set of "global" regression coefficients, a number of sets of regional coefficients could be utilized. It was demonstrated earlier that the correlation of elevations with their standard deviation is a function of regional geomorphology (see table 6.2) and it follows that the accuracy of the regression coefficients could be improved by first categorizing the data according to regional traits. A fairly simple set of categories —including provision for high and low plateaux, rugged mountains, gentle undulations, and smooth plains—would effect a considerable improvement.

(e) The technique of item (d) could be extended so as to circumscribe the choice of a source quad within the limits of a particular morphological region. Thus data would be transferred only between regions of the same category.

While all such refinements could be expected to consume extra computer time in the process of generating the simulated data, this difficulty need not extend to the process of accessing the data. In this respect, the time consumed in the initial simulation process must be treated as a "once off", capital outlay.

ALTERNATIVE APPLICATIONS. A beneficial byproduct of the transfer method is the great saving in computer

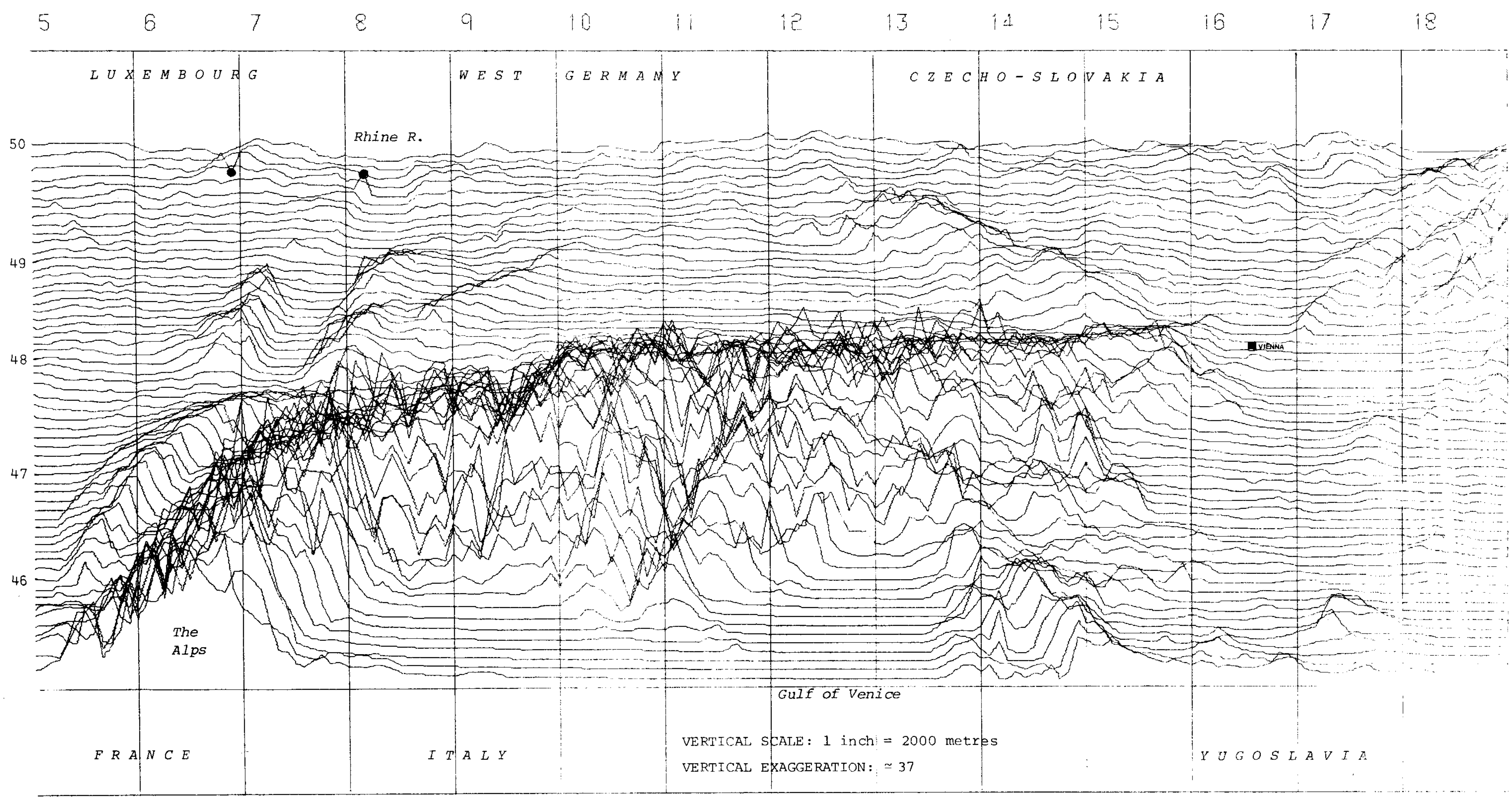

FIGURE 6.13

PROFILES OF REAL 5'x5' MEAN ELEVATION DATA FOR EUROPE INCLUDING THE ALPS

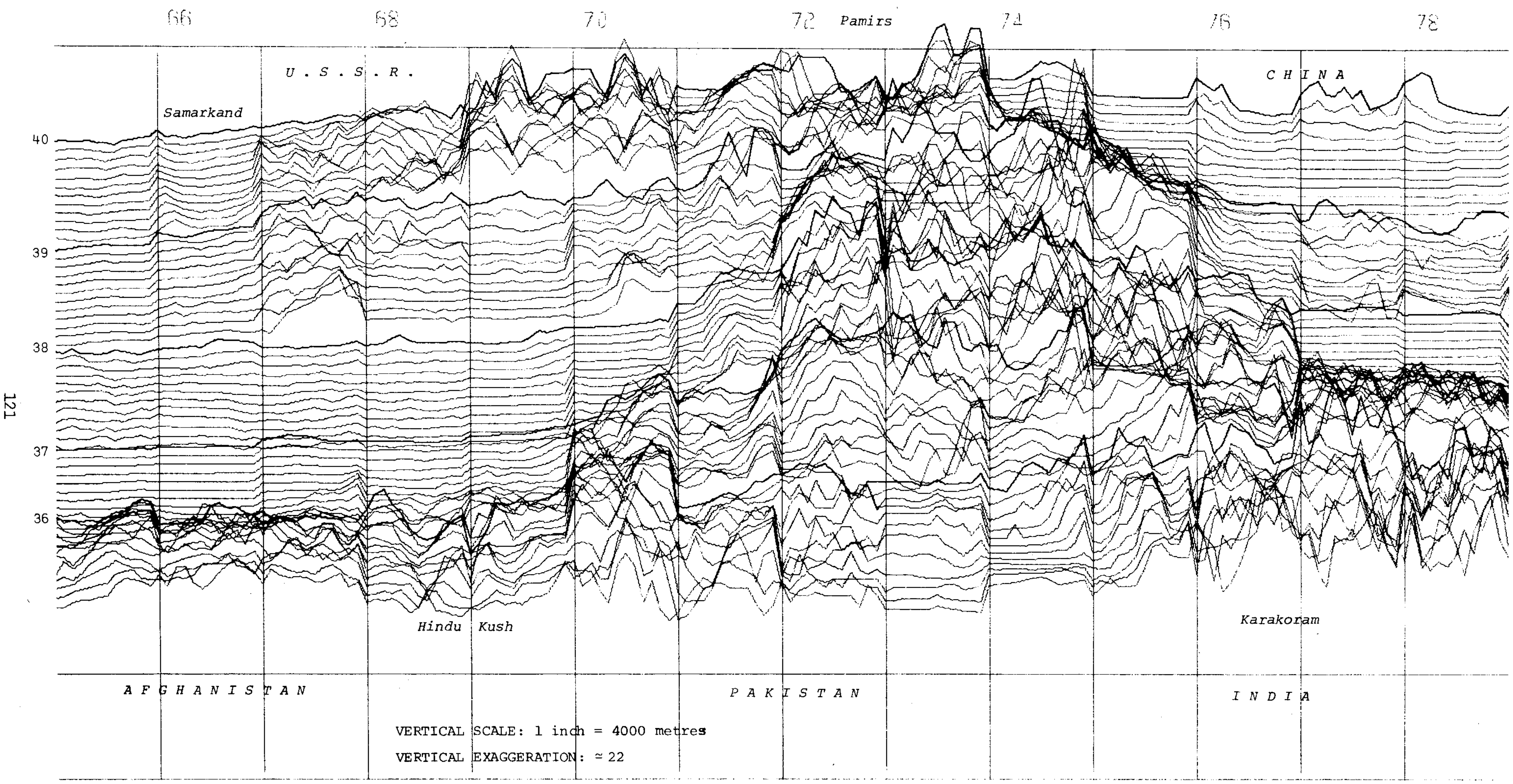

FIGURE 6.14

PROFILES OF SIMULATED 5'x5' MEAN ELEVATION DATA FOR PART OF THE HIMALAYAS storage: in effect, the large number of data values for each quad are compressed into just a few simulation parameters. If it were available, storage of global 5' data, comprising more than nine million values when ocean areas are included, could become a serious difficulty for many types of computer. However, the transfer method offers a systematic means of compressing the data, in such a manner that it can be re-generated easily whenever necessary. The technique would involve first establishing a basic set of source data containing quads chosen for their capacity to represent the necessary range of topographic forms. Then, by a process of fitting the remaining real data to the basic set, particular source quads and regeneration parameters to be used in the transfer equation could be resolved. Because real 5' values would be available in the quad to be generated as well as the source quad, the fitting process could be pursued to a suitable degree of accuracy by manipulating the size of a source quad, the scope of the basic source set, and the transfer parameters.

7

Computation Procedures and Data Management

7.1 INTRODUCTION

DESIGN OF THE COMPUTATIONAL SYSTEM

In a research project such as that reported in this thesis, where experimental testing and investigation are primarily accomplished by numerical computation, the validity of the conclusions is wholly dependent on the viability of the total *computational system*, under all of the conditions to which it may be subjected. The total computational system is here defined to comprise the computation and control routines, and the model and results datasets. It is thus distinguished from the *computer system*—that is, the "hardware"—and the *operating system*, which includes the routines supplied by the manufacturer to control the computer and peripheral devices. A substantial description of the computational system is included here in recognition of its crucial role in fulfilling the aims of this study.

Because of the large amount of computation involved (several hundred hours of computer time) and the extensive model and results datasets required, the problems posed in designing a computational system assume major significance. Limitations on access to the large, central computing facility at the University of New South Wales dictated a multi-job method of processing, in which the same computational procedure may require submission of many separate jobs. A protracted period (approaching two years) was, therefore, necessary to complete the computations and analysis. Some of the requirements for a successful computational system, taking into account this overriding constraint, may be listed as follows:

(a) Fidelity of the datasets, particularly the model data, must be maintained over a long period and it should be possible to check their status in this respect.

(b) Provision must be made for *automatic* continuity of computation from one job to the next.

(c) Results data must be maintained in such a manner that any single job cannot destroy or inadvertantly alter previously accumulated results.

(d) When a job is required to run for a lengthy period (say more than half an hour), provision should be made to periodically secure its accumulated results against programme or machine failure.

(e) In case of errors or machine failure, it must be possible to restore the prior situation and restart computation at the appropriate point.

(f) As far as possible the routines should be self-managing and their status and continuity should not depend on external record-keeping or manual intervention.

At least, in some respects, the environment in which these requirements must be achieved can be described as "hostile". For instance, some of the disturbing influences that the computational system must withstand are:

(a) computer or operating system failure;

(b) failure of part of the computational system itself;

(c) occasional errors, either physical or logical, in peripheral data storage;

(d) operating system or operator cancellation and restoring of a job, or multiple runs of the same job;

(e) out-of-sequence running of jobs;

(f) erroneous jobs, due to incorrect, missing, or disarranged control cards or instructions;

(g) changes in the computer system hardware; and

(h) new releases of the operating system.

The possibility of any of these influences becoming significant increases greatly with the number of separate jobs, the amount of computation time, and the total period during which the computations are implemented. In case it should be thought that preparation for all of these contingencies involves undue caution, it may be noted that all of the enumerated disturbances eventuated on a number of occasions during the computations. They were successfully handled by the computation system with a minimum of manual intervention.

In order to satisfy all of the requirements and cope with the additional demands of the environment, the following features were incorporated in the design of the computation system:

(a) In addition to the main computation routines, a library of compatible subroutines was established for data management and access and easy display of current status.

(b) All routines and datasets were permanently loaded onto personal disk storage packs. Routines were stored in load module form (that is, in machine code ready for immediate transfer to the computer core) [IBM 1969, Part 1] and most datasets were established in direct access rather than sequential form [IBM 1970a, p.93; IBM 1968, p.62 *et seq.*]. Job procedures, including all of the necessary job control card images, were also stored on disk.

(c) Check parameters, incorporating geographical coordinates and time and date of storage, were included in each model data record.

(d) Computation progressed in blocks with storage of results on completion of each block and at the end of each job.

(e) Automatic continuity of computation was assured by storage in the results datasets of a set of *link parameters* containing sufficient information to recommence computation after an interruption. These parameters were updated by the computation routines only after storage of each block of results was completed. Because of automatic continuity, the job control cards were identical from one job to the next—unless manual intervention was required—so that multiple or out-of-sequence runs were harmless.

(f) An automatic log of times and dates of all computation jobs was maintained in the results datasets.

(g) Each computation job contained interval timing routines to enable orderly closure of the job before operating system time limits were imposed [IBM 1971, pp229-230].

(h) Default values of all *computation* and *control parameters* were established automatically within the routines at the commencement of each job.

(i) Values of the control and computation parameters, as well as the link parameters, could be established manually at the commencement of each job through a parameter list on the job control cards [IBM 1966a, p.15]. By this means, the need for "data" cards to be included with each job was obviated, thus reducing the possibility of errors, but the option of overriding the default values of any of the parameters was retained. Restarting after unscheduled interruptions was thus simplified.

(j) The number of job control cards was minimized to eight cards in the worst case.

(k) A library of utility routines was established to simplify regular saving of datasets by copying to magnetic tapes. A routine to provide a concise map of the volume table of contents of the disk packs was also developed (see programme VTOCMAP, appendix A).

As the author was permitted to operate the University's central computer at certain times, advantage was taken of this opportunity to undertake particularly long job runs. For this purpose a number of special features were added to the computation routines, making it possible to communicate with and control them through the operator's console. Additionally, the console could be used to start any of the routines in the computational system by calling up and modifying or adding to the card images of the job procedures stored on disk, or by entering a new job in the form of card images. This feature eliminated the need to manually input cards through the card reader, thus reducing the possibility of operator errors.

7.2 COMPUTER SYSTEMS

IBM SYSTEM 360/50

All of the main computations and analysis of results were implemented on the University of New South Wales' IBM System 360, Model 50 computer. The available configuration, including modifications made during the period of computation, is depicted schematically in figure 7.1. New releases of the operating system (OS/360) were implemented twice, so that the computation system was run successively under releases 17.6, 20.6, and 21. "Multiprogramming with a variable number of tasks" (MVT) became possible with the last release and teleprocessing with a number of remote, time-share terminals was added. HASP (Houston Automatic Spooling) was available on the last release.

NUMERIC AND CHARACTER REPRESENTATION. Several different types of data representation were employed in the computations. Figure 7.2 illustrates the binary form and the allowable numeric range of each type [IBM 1966b]. Single precision representation (approximatley 7 significant decimal digits) was adequate for all of the computations except the spherical harmonic analysis (see §8.4), wherein double precision was used to represent values of the associated Legendre function. Evaluation of this function for high degrees is also hampered by the limited range of the floating point representation, since the register capacity is exceeded by factorials greater than 56!. This difficulty was avoided by using two separate numbers to represent factorials: a floating point number for the fractional part and an integer for the decimal exponent.

As almost all of the model data comprised values within a suitably narrow range, it was possible to effect a considerable saving of storage space by using half word integers for this purpose. A further saving was obtained by storing some of the logical information pertaining to certain results data in the form of single binary bits or, in some instances, by combining two decimal quantities in a single half-word integer (see §7.4).

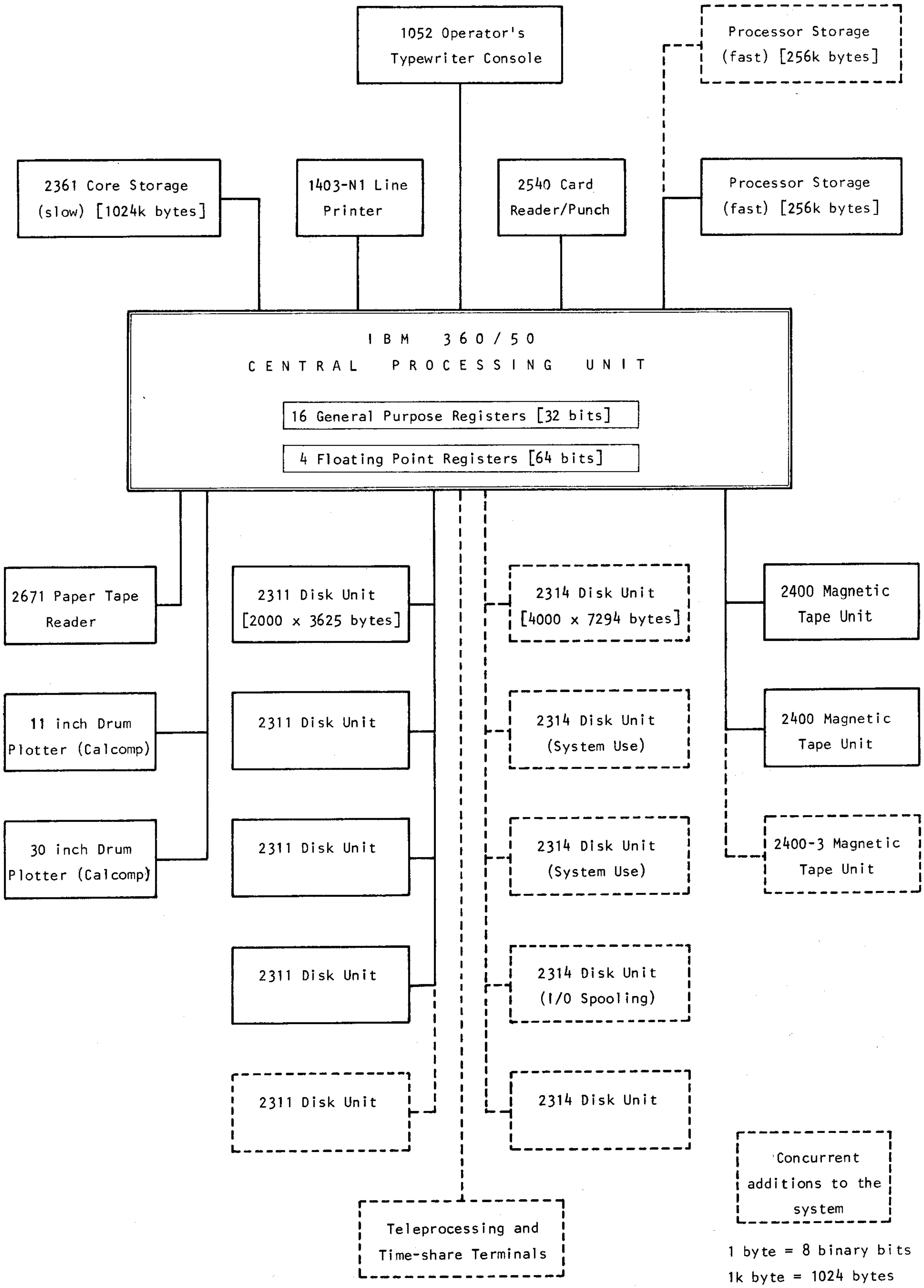

FIGURE 7.1

UNIVERSITY OF NEW SOUTH WALES IBM 360/50 COMPUTER SYSTEM

(a) One Byte (= 8 bits):

```
0      7
|11000110|
```

Representing: 1 character, 2 hexadecimal digits, or 8 binary bits.

(b) One Half-word (= 16 bits):

```
0 1              15
|11000110|11100100|
|S|<------N------>|
```

Representing: 1 half-word integer, comprising 1 sign bit (S), and 15 numeric bits (N).

Decimal range: -32 768 to +32 767

(c) One Full-word (= 32 bits):

```
0 1                                31
|11000110|11100100|11000011|11010010|
|S|<--------------N---------------->|
```

(i) Representing: 1 full-word integer, comprising 1 sign bit and 31 numeric bits.

Decimal range: -2 147 483 648 to +2 147 483 647

```
0 1     7 8                        31
|11100010|11001000|11001001|11100011|
|S|<-C-->|<-------------F---------->|
```

(ii) Representing: 1 short (single precision) floating point number; comprising 1 sign bit; 7 characteristic bits (C), representing the exponent of 16 biassed to a positive value; and 24 fraction bits (F), equivalent to 6 hexadecimal digits or approximately 7 significant decimal digits.

Decimal range: approximately 5.4×10^{-79} to 7.2×10^{75} (positive or negative)

(d) One Double word (= 64 bits):

```
0 1     7 8                                                        63
|11000110|11100100|11000011|11010010|11100100|11010101|11100010|11100110|
|S|<-C-->|<-----------------------------F------------------------------>|
```

Representing: 1 long (double precision) floating point number, constructed in the same manner as (c)(ii), but with 56 fraction bits, equivalent to 14 hexadecimal digits or approximately 16 significant decimal digits.

Decimal range: as for (c)(ii).

FIGURE 7.2

BINARY DATA REPRESENTATION

HEWLETT-PACKARD 9810 AND 9830 PROGRAMMABLE CALCULATORS

A number of prototype and investigatory routines were developed for the HP-9810 and HP-9830 calculators. Both are electronic programmable desk calculators rather than computers in the strict sense of that term, but the 9830 in particular has comprehensive programming and peripheral storage ability.

The 9810 is programmed by a sequence of coded keyboard steps and data may be stored in a bank of floating point registers. Twelve significant decimal digits are retained in all arithmetic operations and the numeric range is from 10^{-99} to 10^{99} for positive or negative values. A small built-in printer is provided and plug-in, read-only-memory (ROM) units extend the range of mathematical functions and enable alphanumeric printing. Programmes and data may be loaded from or stored onto magnetic cards. The particular configuration available accomodates 2036 programme steps and 111 data values. An output typewriter, a small plotter, and a cassette tape storage unit became available during the course of this project.

An "interpreter" using the *BASIC* language and conventional typewriter keyboard entry provide a very flexible programming medium in the HP-9830. Precision and numeric range are similar to the 9810, while the configuration used had a storage capacity of 5856 sixteen-bit words to accommodate both programme instructions and data. A cassette tape storage unit for programmes or data is built-in and plug-in ROM units provide extended mathematical functions, including matrix algebra. During the period of use an output typewriter, a free-motion "digitizer" and an additional cassette storage unit were annexed.

7.3 COMPUTATION AND ANALYSIS ROUTINES

Logically, the computational system may be divided into two parts: (a) the computation sub-system, including the routines designed to perform the main body of the calculations in evaluating the gravitational effects and those involved in the subsequent analysis and presentation of the results, and (b) the data management sub-system, which comprises the routines used to prepare, maintain, and display the model and results data. The data management sub-system is described in §7.4.

Space will not permit a detailed description of all of the computer routines, however, a compendium containing their main attributes, arranged alphabetically according to the routine names, is available in appendix A. Investigatory routines, developed for the Hewlett-Packard computers are included in the compendium.

COMPUTATION SUB-SYSTEM

Figure 7.4 illustrates schematically the interrelation of computer routines and datasets forming the computation sub-system. A key to the symbols used in this and subsequent figures is available in figure 7.3. There are seven main computation programmes: INNZONE (7.4,C6)*, MIDZONE (7.4,J6), and OUTZONE (7.4,O6), which compute the effects of the terrestrial topography and compensation in the inner, mid, and outer zones; INNICEC (7.4,A6), MIDICEC (7.4, H6), and OUTICEC (7.4,M6), which compute the corrections due to the polar ice sheets; and INNCONT (7.4,F6), which computes the effect of a discrepancy in the mean heights of the topographic quads in the contact sub-zone. Discussion of the reasons for including the last named programme is deferred to §8.2.

PROCESSES COMMON TO ALL MAIN COMPUTATION PROGRAMMES. Many of the processes involved in the seven main computation programmes are common to them all and so may be dealt with collectively. Figure 7.5 is an annotated flow chart of the common parts of these programmes. As mentioned in §7.1, a number of special features were incorporated in all of the programmes to permit manual intervention and generally enhance the flexibility of the computation sub-system. These include:

(a) The ability to impose any required time limit on a particular job.

(b) Control over the storage of results data in the results dataset.

(c) The possibility of nominating a particular job as either a *normal* or a *special* run. A normal run is one in which the job automatically continues the computations in accordance with the

**Notation in parentheses refers to a figure number and a coordinate reference within that figure.*

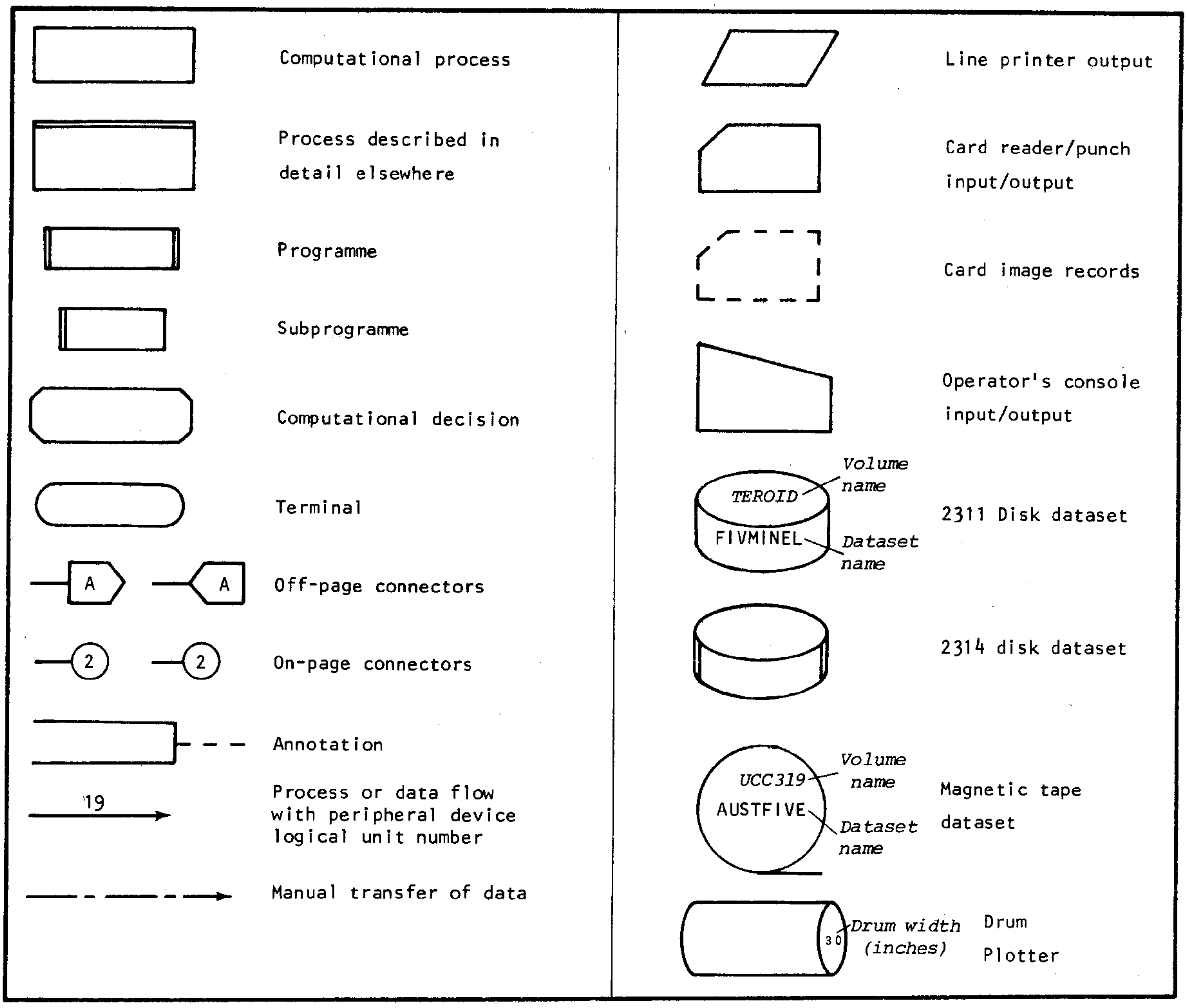

FIGURE 7.3
KEY TO SYMBOLS

link parameters stored by the preceeding job. A special run is defined by the manual entry, via the parameter list, of special values of any of the link parameters so that the job runs out of the normal sequence without upsetting it.

(d) The ability to display on the opertor's console the current status of a programme during execution, at predetermined regular intervals or at any time by command.

(e) Control of an executing programme by a set of commands entered through the operator's console, thus making it possible to:(i) hold the programme in an idle state until released, (ii) display the current values of the parameter list, (iii) change the programme from "fast" to "slow" areas of main storage or vice-versa, (iv) reset the values of the link parameters or revert to anicedent values, (v) close the programme after storage of accumulated results and optionally invoke recommencement of a new job, or (vi) abort execution immediately.

An abstract of the printed output of a typical run of programme OUTZONE (see figure 7.6) will serve to illustrate the options available in all of the main computation programmes and the form of the

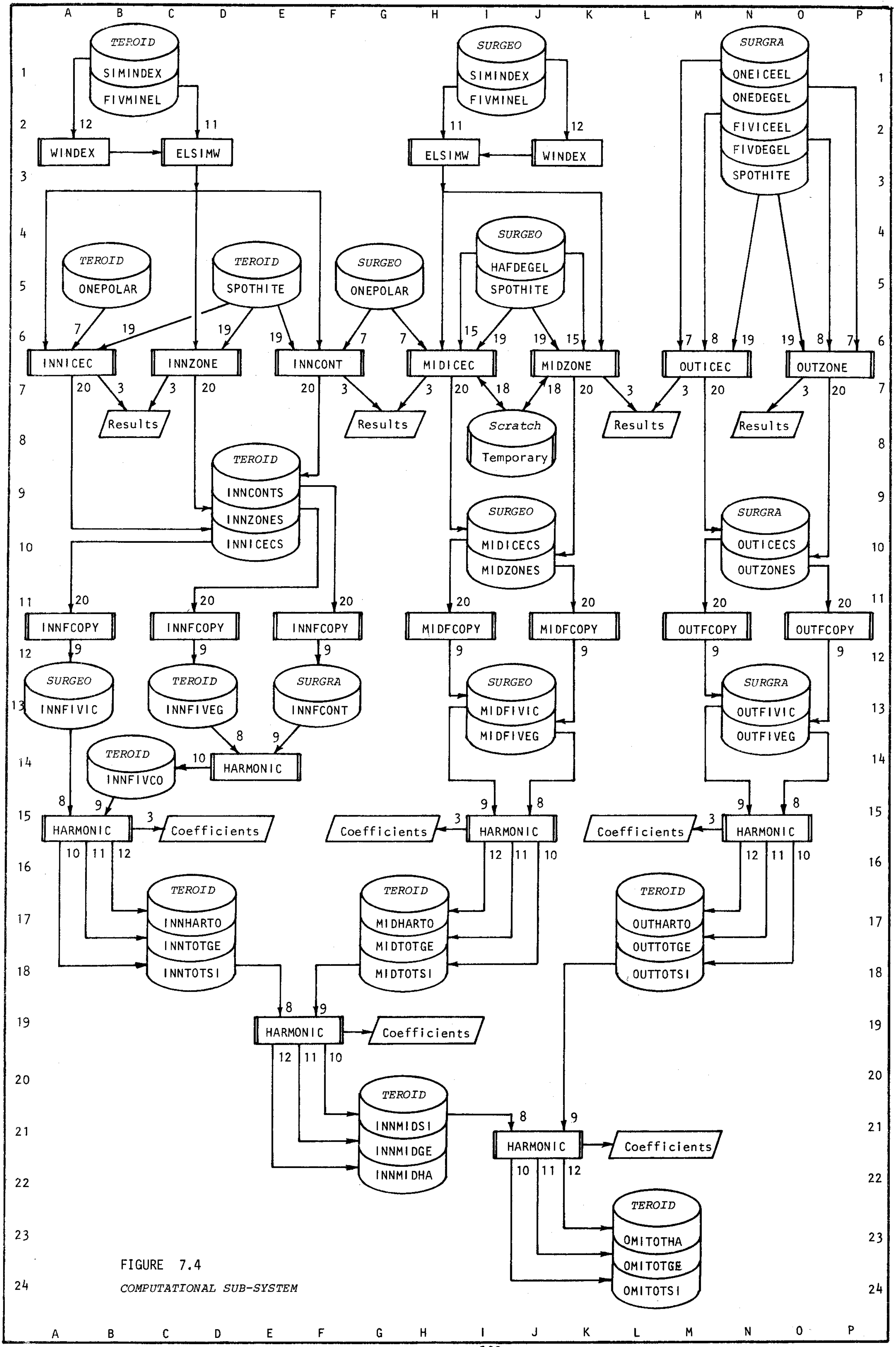

FIGURE 7.4

COMPUTATIONAL SUB-SYSTEM

FIGURE 7.5a

FLOW CHART OF PROCESSES COMMON TO ALL MAIN COMPUTATION ROUTINES

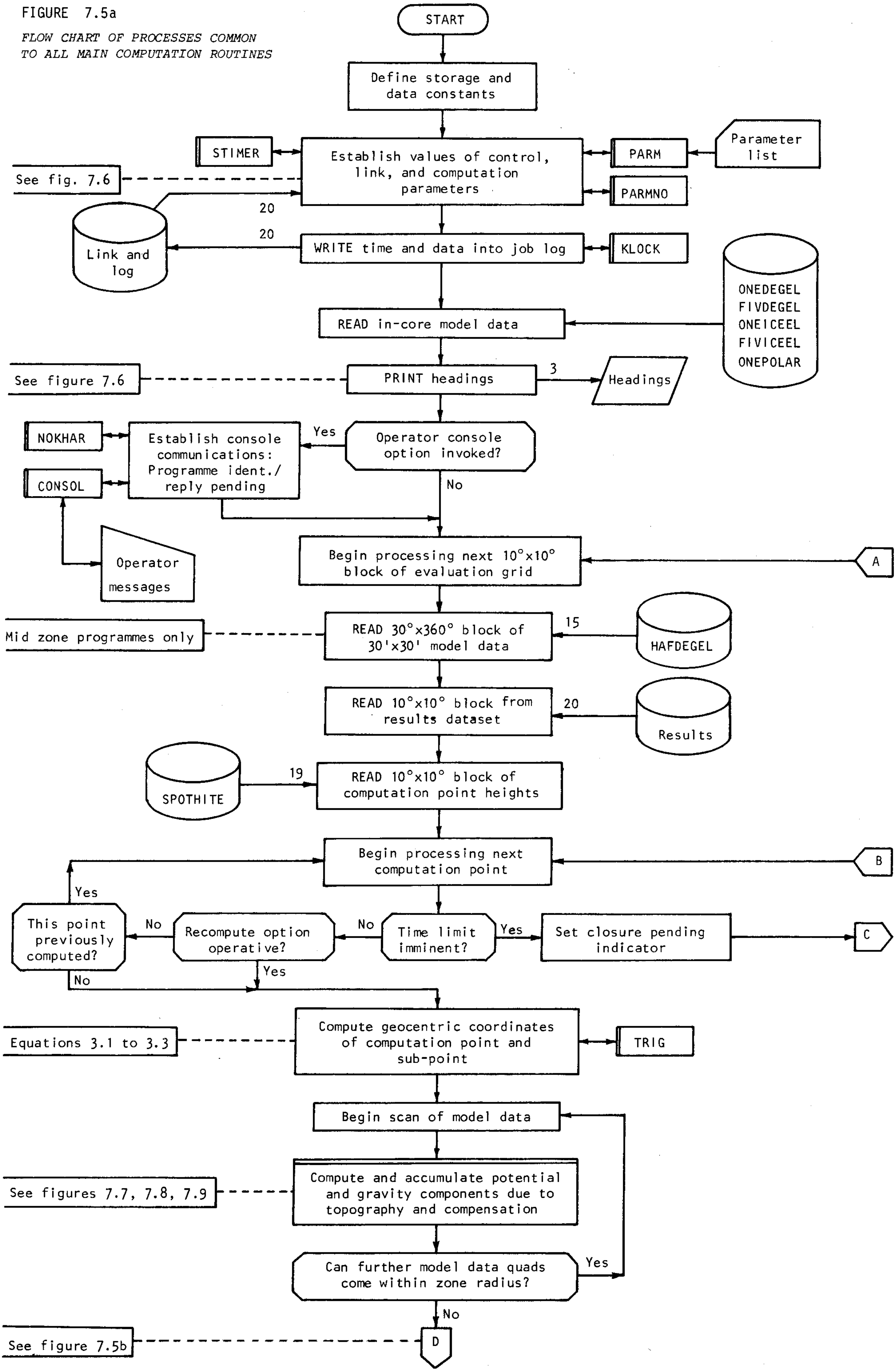

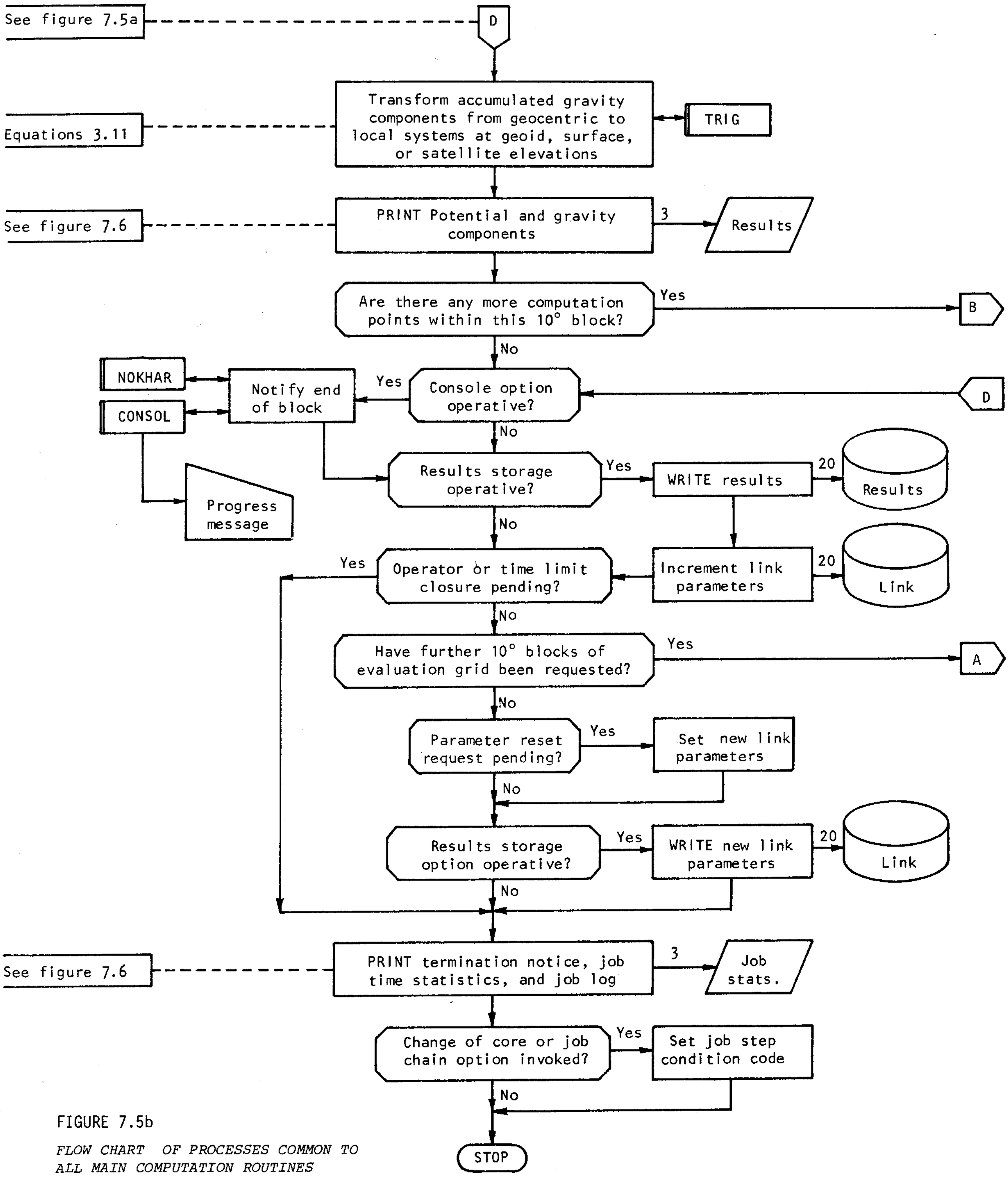

FIGURE 7.5b

FLOW CHART OF PROCESSES COMMON TO ALL MAIN COMPUTATION ROUTINES

```
==========================
OUTZONE NORMAL  RUN NO.  5                DATE  74.148/ 1.59
==========================
```

HOLD = NO	TIME = 19	CONSOLE LEVEL = 2	CONSOLE RATE = 5	SOLUTION WRITE LEVEL=1
BLOCK NW CORNER = 90/ 0	EXTENT = 180/360	BLOCK RESTART = 30/220	GRID RESTART = 6/ 1	GRID INTERVAL = 5
ORBITAL HEIGHT = 1000000	ISOSTATIC DEPTH = 30000	OUTER ZONE AT 5560000	MID ZONE AT 1112000	DENSITY = 2700-H/21

```
UNITS    POTENTIAL:    JOULES/KG
=====    GRAVITY:      MICRONEWTONS/KG
         (<<<< INDICATES SCALED VALUES)
```

FIGURE 7.6a

TYPICAL PRINTED OUTPUT FROM PROGRAMME OUTZONE (FIRST PAGE)

```
TEN DEGREE BLOCK: LOC = 94   LAT = 70   LON = 210   INDEX = 30/220

 LAT  LON  ELEV       5X5   1X1                  POTENTIAL   VERT GRAV    NTH. GRAV     EAST GRAV
---------------------------------------------------------------------------------------------------

  65  210   247       810  5757     ORBITAL  :     1.297      -3.261       -0.641         3.722
                                    GEOIDAL  :    -8.143       6.630       -0.283        -0.227
                                    SURFACE  :    -8.142       6.630       -0.283        -0.226

  65  215   626       813  5631     ORBITAL  :     2.265      -4.511       -1.520         3.307
                                    GEOIDAL  :    -8.117       6.634       -0.228        -0.276
                                    SURFACE  :    -8.112       6.633       -0.228        -0.273
===================================================================================================
TEN DEGREE BLOCK: LOC = 95   LAT = 70   LON = 220   INDEX = 30/230

 LAT  LON  ELEV       5X5   1X1                  POTENTIAL   VERT GRAV    NTH. GRAV     EAST GRAV
---------------------------------------------------------------------------------------------------

  70  220    94       794  6073     ORBITAL  :     0.583      -0.685       -4.289         0.959
                                    GEOIDAL  :    -8.366       7.469       -0.162        -0.220
                                    SURFACE  :    -8.366       7.468       -0.162        -0.220

  70  225    -3       797  5984     ORBITAL  :     0.719      -0.406       -4.477         0.276
                                    GEOIDAL  :    -8.399       7.913       -0.109        -0.231

  65  220  1190       817  5492     ORBITAL  :     3.060      -5.349       -2.537         2.447
                                    GEOIDAL  :    -8.115       6.871       -0.167        -0.313
                                    SURFACE  :    -8.107       6.869       -0.170        -0.307

  65  225   918       820  5383     ORBITAL  :     3.563      -5.552       -3.505         1.187
                                    GEOIDAL  :    -8.150       7.438       -0.103        -0.325
                                    SURFACE  :    -8.143       7.436       -0.105        -0.321
===================================================================================================

...................................................................................................

STIMERED-- TOTAL TIME = 4.11 HRS.   THIS RUN = 19.00 MINS.
RESTART POINT = ( 30/240)  (  1/  1)


LOG OF RUNS
-----------

  1    4141/ 630       4148/  58
  2    4141/ 709       4148/ 119
  3    4145/  23
```

FIGURE 7.6b

TYPICAL PRINTED OUTPUT FROM PROGRAMME OUTZONE (SECOND AND LAST PAGES) printed results. On the first page the programme name, type of run, and date and time are stated and a table of the operational values of the control parameters (first line), link parameters (second line), and computation parameters (third line) are listed. The meaning of each of these parameters and the possible options, taken in sequence, are as follows:

(a)	HOLD	= YES	Stop execution and await additional operator instructions before commencing computations;
		= NO	Proceed normally.
(b)	TIME	= t	Close execution normally after t minutes of CPU time.
(c)	CONSOLE LEVEL	= 0	No messages of any kind are to be transmitted to the operator's console;
		= 1	Progress reports only, to be transmitted to the console—no operator control is possible;
		= 2	Full operator control through console commands is required.
(d)	CONSOLE RATE	= n	($n \leq 5$) Progress reports to be displayed on the console after every n 10°x10° blocks of the evaluation grid have been completed.
(e)	SOLUTION WRITE LEVEL	= 0	No results data to be written into the results dataset—does not affect printed results;
		= 1	Only results for points not previously computed are to be written into the results dataset;
		= 2	All results to be written into the results dataset, regardless of previous computation.
(f)	BLOCK NW CORNER	= ℓ_1/ℓ_2	ℓ_1 and ℓ_2 are the latitude and longitude in degrees of the north-west corner of the area of evaluation grid to be processed by this and subsequent jobs.
(g)	EXTENT	= ℓ_3/ℓ_4	ℓ_3 and ℓ_4 are the dimensions in degrees of the area of evaluation grid to be processed.
(h)	BLOCK RESTART	= ℓ_5/ℓ_6	ℓ_5 and ℓ_6 specify the position of the first 10°x10° block of evaluation grid to be processed by this job.
(i)	GRID RESTART	= ℓ_7/ℓ_8	ℓ_7 and ℓ_8 specify the position within the 10°x10° block of the first computation point to be processed by this job.
(j)	GRID INTERVAL	= ℓ_9	ℓ_9 is the grid interval in degrees between successive computation points.
(k)	ORBITAL HEIGHT	= c_1	c_1 specifies the height in metres of the computation point to be used for evaluation at satellite orbit altitude (outer zone only).
(l)	ISOSTATIC DEPTH	= c_2	c_2 is the crustal thickness T to be used (see equation 3.17).
(m)	SUB-ZONE LIMITS		The remaining computation parameters specify the radii r_0 in metres of the outer-most limits of the sub-zone boundaries (see table 2.3).

Values of any of these parameters could be passed to the programme via the parameter list (PARM option) on the job control cards.

Results for computation points within each 10°x10° block are printed on following pages. Each point is identified by its geographical coordinates and a count of the number of quads of each size, which contribute to the total effect at that point, is listed. The potential and attraction components for each elevation of the computation point are then tabulated. When the computation point lies in an ocean area or its terrestrial elevation is that of mean sea level, computation and results for the earth's surface are suppressed and only the evaluation at geoid and satellite orbit elevation is performed and printed.

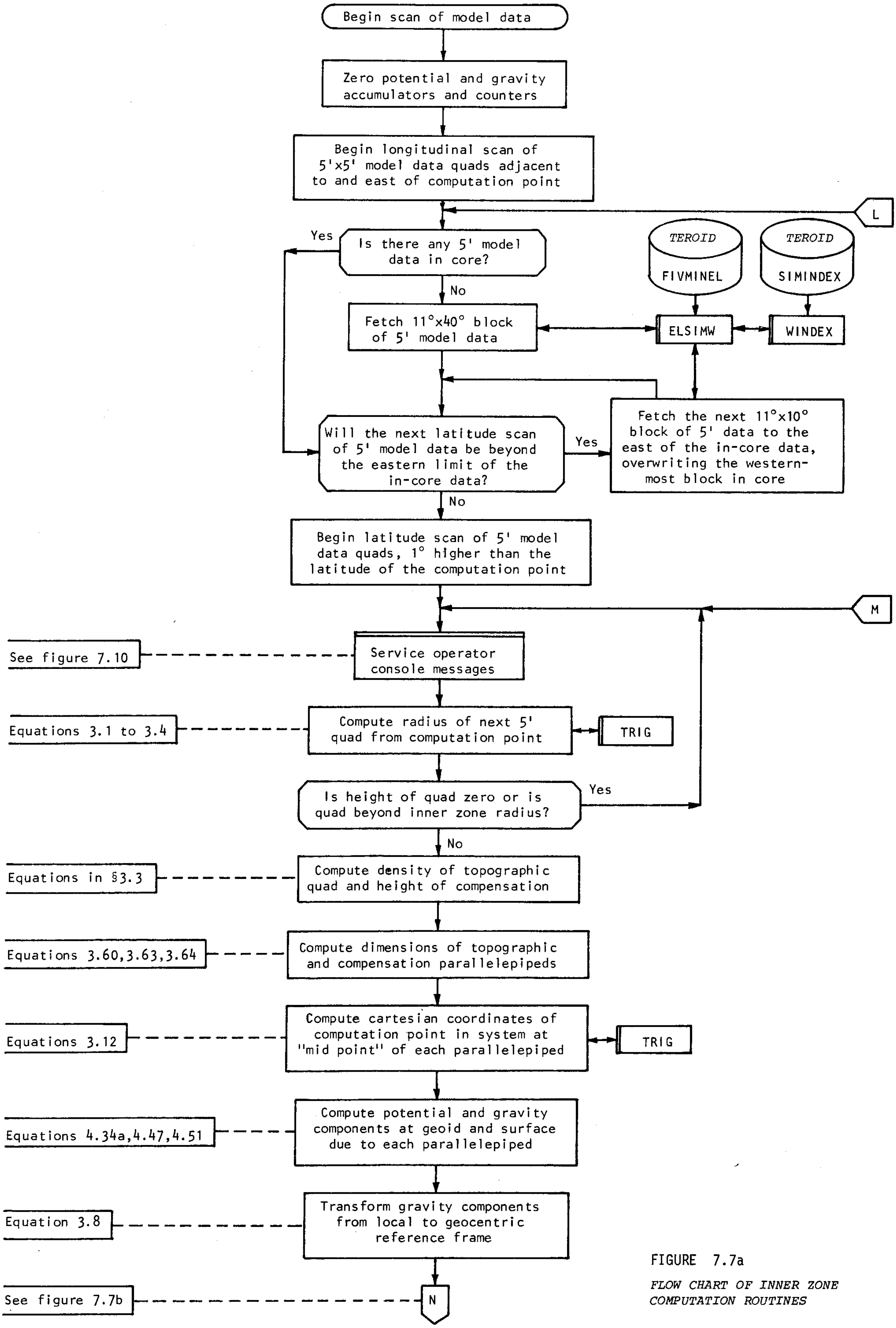

FIGURE 7.7a

FLOW CHART OF INNER ZONE COMPUTATION ROUTINES

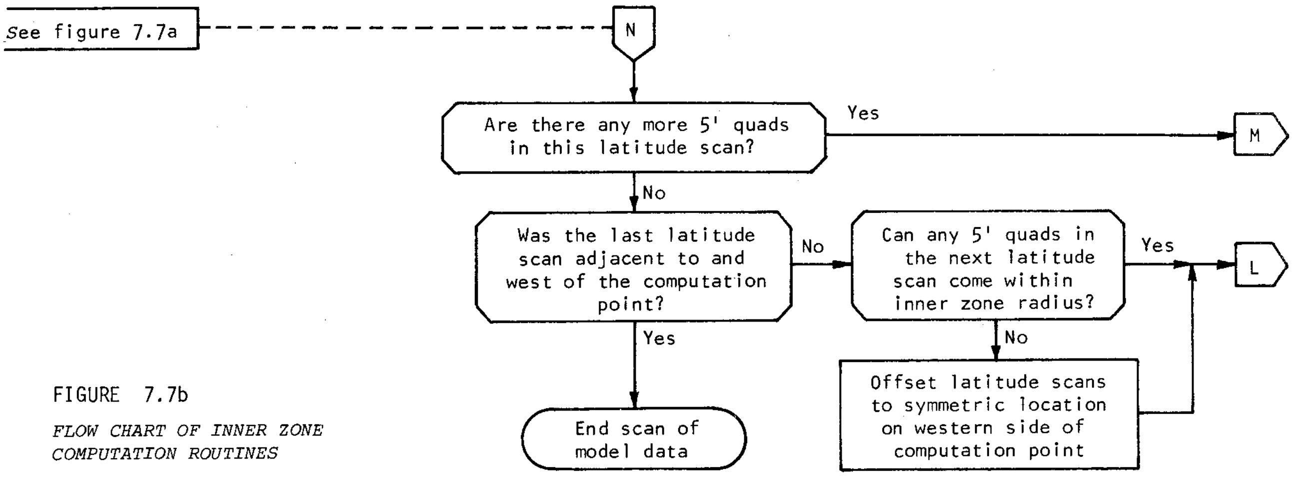

FIGURE 7.7b

FLOW CHART OF INNER ZONE COMPUTATION ROUTINES

On the last page the manner in which the job ended, the run times, and the restart parameter values are printed, and a full listing of the current job log is tabulated.

PROCESSES COMMON TO PROGRAMMES FOR EACH ZONE. All of the main computation programmes work by scanning the model data and computing the contribution of each quad within a particular zone to the total effect at the computation point. However, the method of computing the contribution differs from zone to zone. This part of the processing is described for each zone in turn by the flow charts in figure 7.7, 7.8, and 7.9. Annotation of these charts provides cross-references to the equations involved in the computations.

Separation of the main computations into subroutines, though it might have been convenient, was assiduously avoided since the accrued time consumed in transferring too and from such routines can severely slow the programmes. Moreover, repeated computation of sine and cosine functions is a common retarding factor in programme execution. This effect was minimized by relacing the IBM built-in functions SIN and COS by a single subroutine TRIG, which was capable of returning values of both functions in approximately half the time of the IBM routines with equivalent accuracy (see programme TRIGTIME in appendix A). Subroutine TRIG uses a table of the sine function at 1° intervals from 0° to 90° and a series expansion of the remaining fractional part of the argument to return single precision values of the sine and cosine of any angle in degrees. Thus:

$$\sin\,(I + F) = \sin I \cos F + \cos I \sin F$$
$$\cos\,(I + F) = \cos I \cos F - \sin I \sin F, \qquad (7.1)$$

where I is the integer part of the argument in degrees,

F is the fractional part, and

$$\sin F \simeq F \times \frac{\pi}{180}$$
$$\cos F \simeq 1 - \tfrac{1}{2}\sin^2 F, \quad \text{for } |F| < 0.5°. \qquad (7.2)$$

Within each programme there is a section which services the operator console requests. A flow chart for this section, illustrating the effect of each of the available operator commands, is given in figure 7.10.

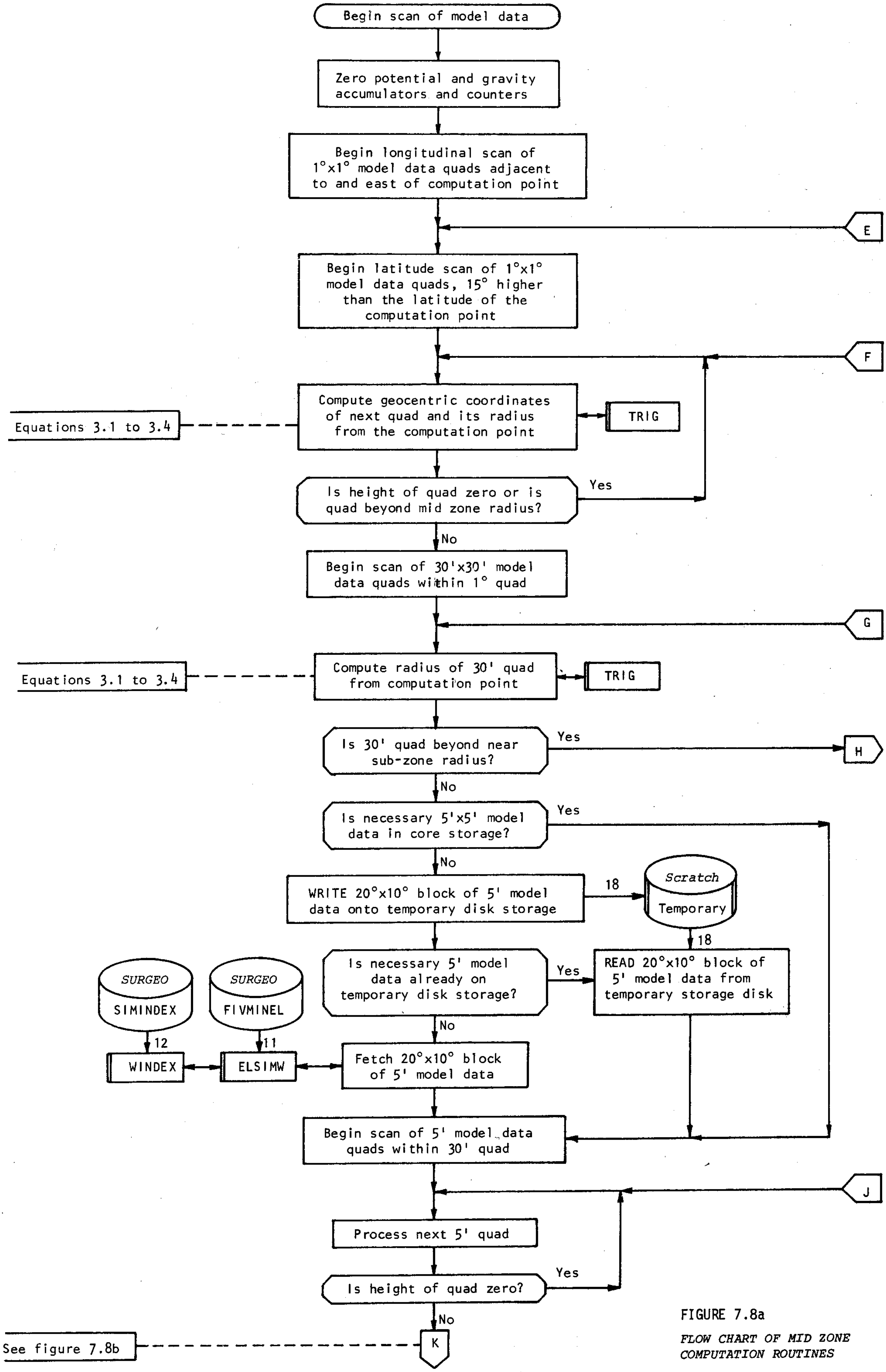

FIGURE 7.8a

FLOW CHART OF MID ZONE COMPUTATION ROUTINES

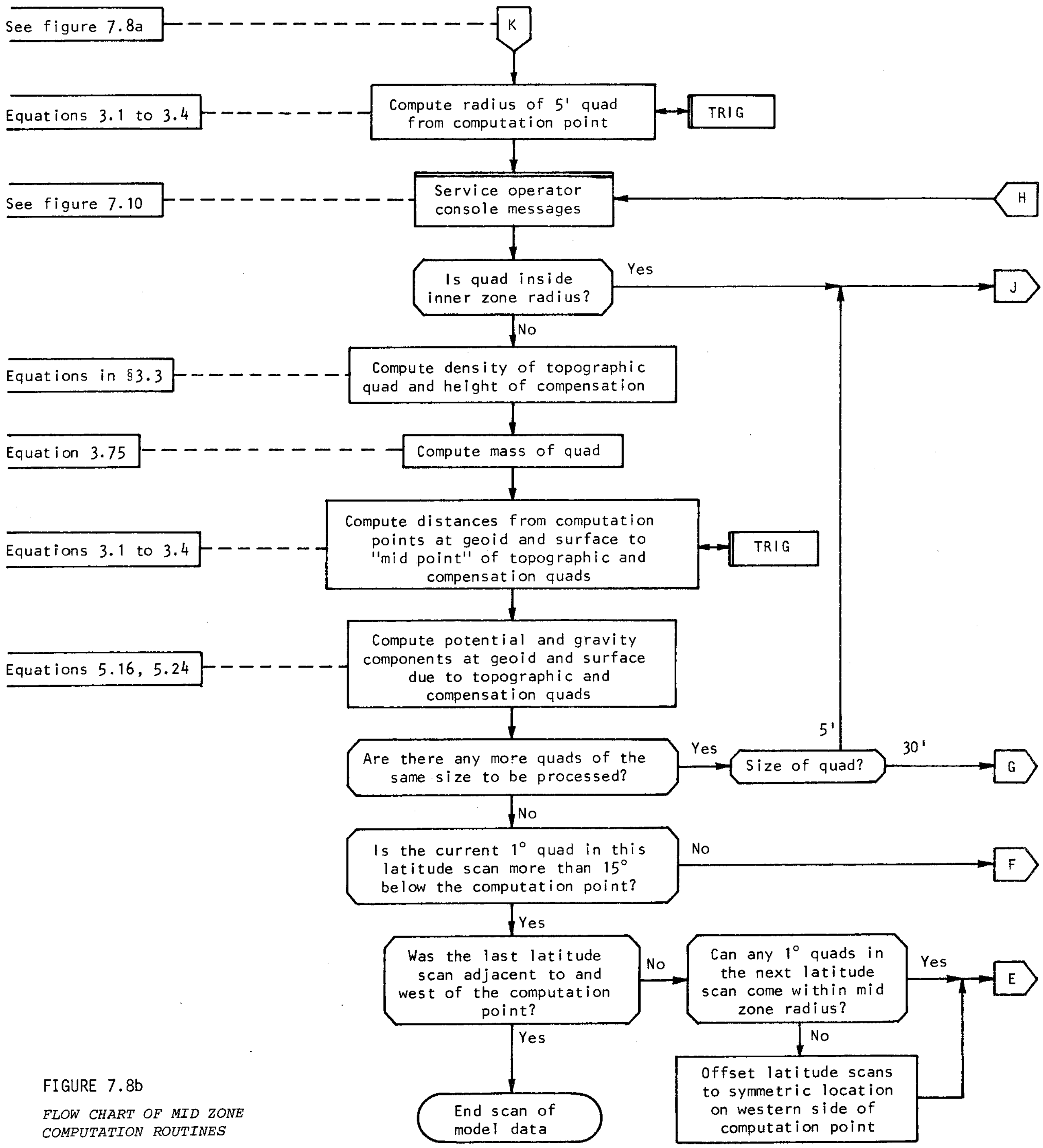

FIGURE 7.8b

FLOW CHART OF MID ZONE COMPUTATION ROUTINES

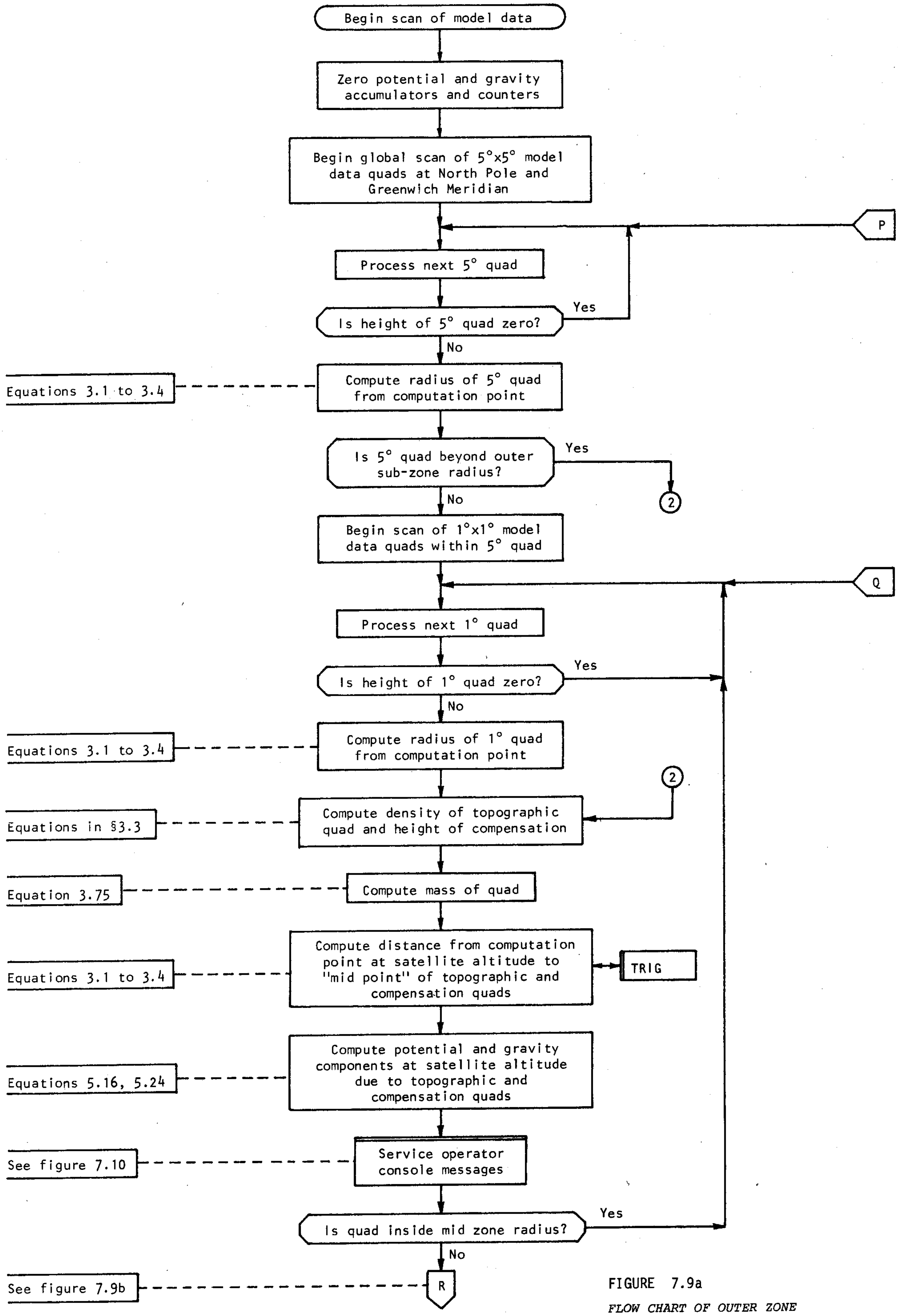

FIGURE 7.9a

FLOW CHART OF OUTER ZONE COMPUTATION ROUTINES

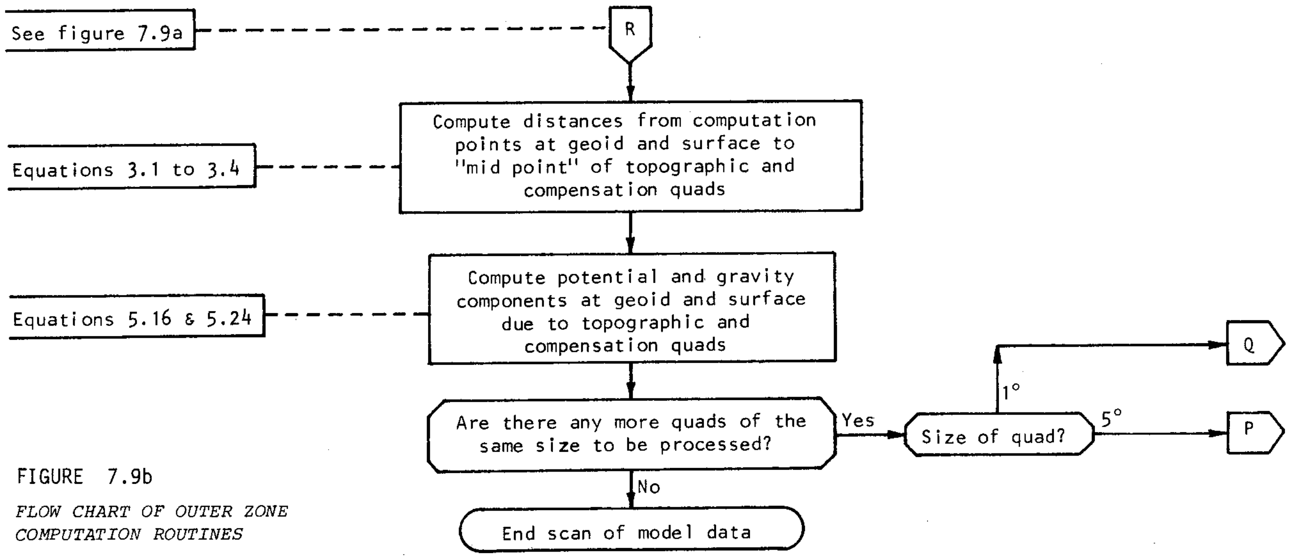

FIGURE 7.9b
FLOW CHART OF OUTER ZONE COMPUTATION ROUTINES

JOB STATISTICS. Table 7.1 contains an analysis of the number of job runs and CPU times for each of the seven main computation programmes. In addition, a significant amount of time was consumed in simulation of 5' topographic data, programme TOPOSIM taking 60.5 hours of CPU time for 86 jobs. Approximately 20 hours was estimated to have been used in harmonic analysis and synthesis.

TABLE 7.1
JOB STATISTICS

EFFECT	INNER ZONE		MID ZONE		OUTER ZONE		TOTAL	
	Jobs	Time (h)	Jobs	Time (h)	Jobs	Time (h)	Jobs	Time (h)
Topographic effect	41	30	45	28	46	21	132	79
Ice correction	10	6	16	6.6	19	6.2	45	18.8
Contact effect	3	1.5	--	--	--	--	3	1.5
Total	54	37.5	61	34.6	65	27.2	180	99.3

AUTOMATIC JOB STARTING PROGRAMMES. Adjunctive programmes and datasets used to provide the automatic job starting feature of the computational system, referred to in §7.1, are illustrated in figure 7.11.

ANALYSIS PROGRAMMES. Because of the requirement for a 1° evaluation grid interval, the results datasets accessed by the computation programmes—that is, INNZONES, INNICECS, and INNCONTS (7.4,D9) for the inner zone; MIDZONES and MIDICECS (7.4, I10) for the mid zone; and OUTZONES and OUTICECS (7.4,N10) for the outer zone—were large enough to accommodate this amount of data. However, when computation on a 5° evaluation grid was completed, these results were extracted and stored in smaller datasets to save space. This was effected by the programmes INNFCOPY, MIDFCOPY, and OUTFCOPY (7.4,A-P11) and the 5° grid

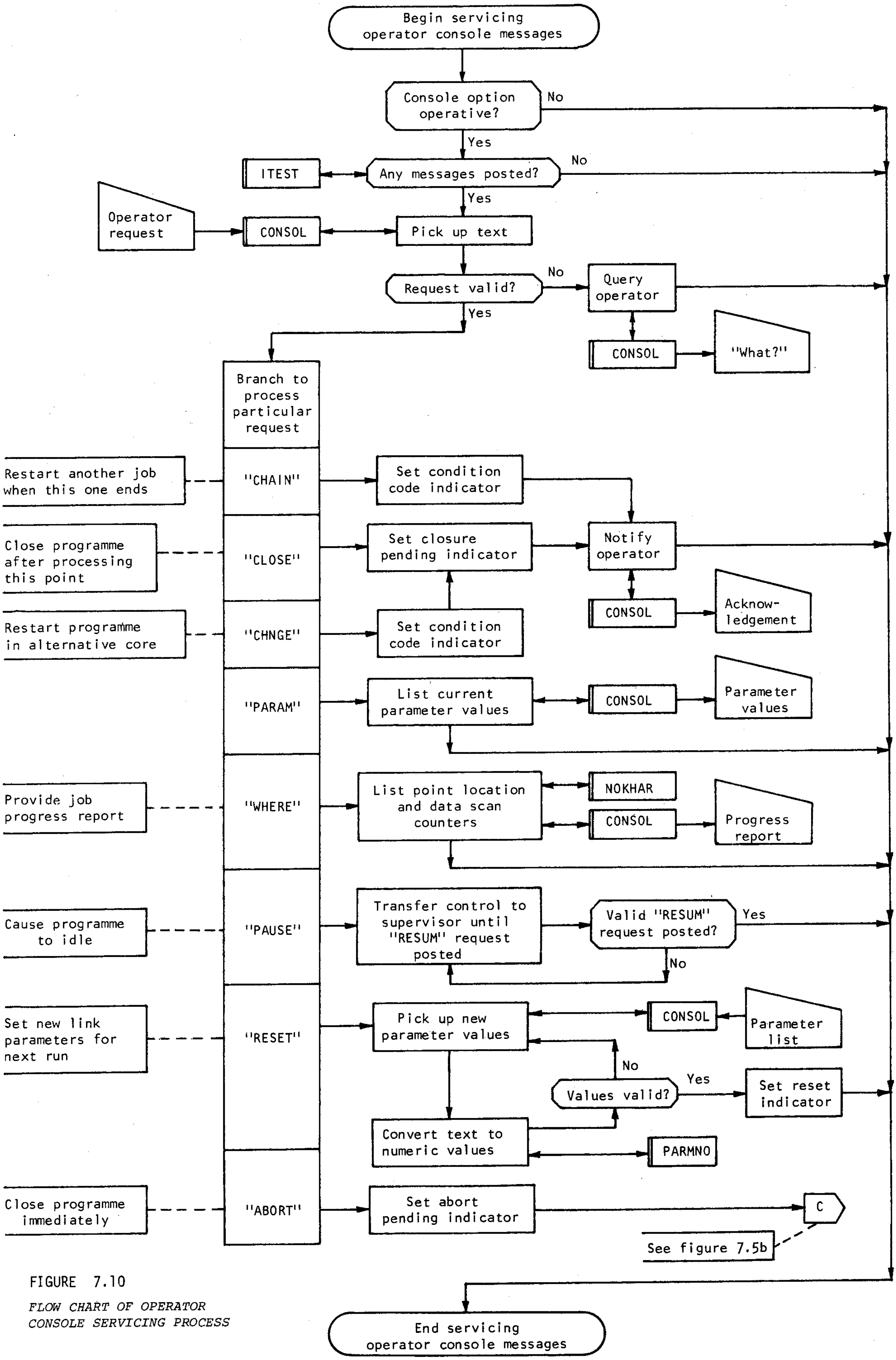

FIGURE 7.10

FLOW CHART OF OPERATOR CONSOLE SERVICING PROCESS

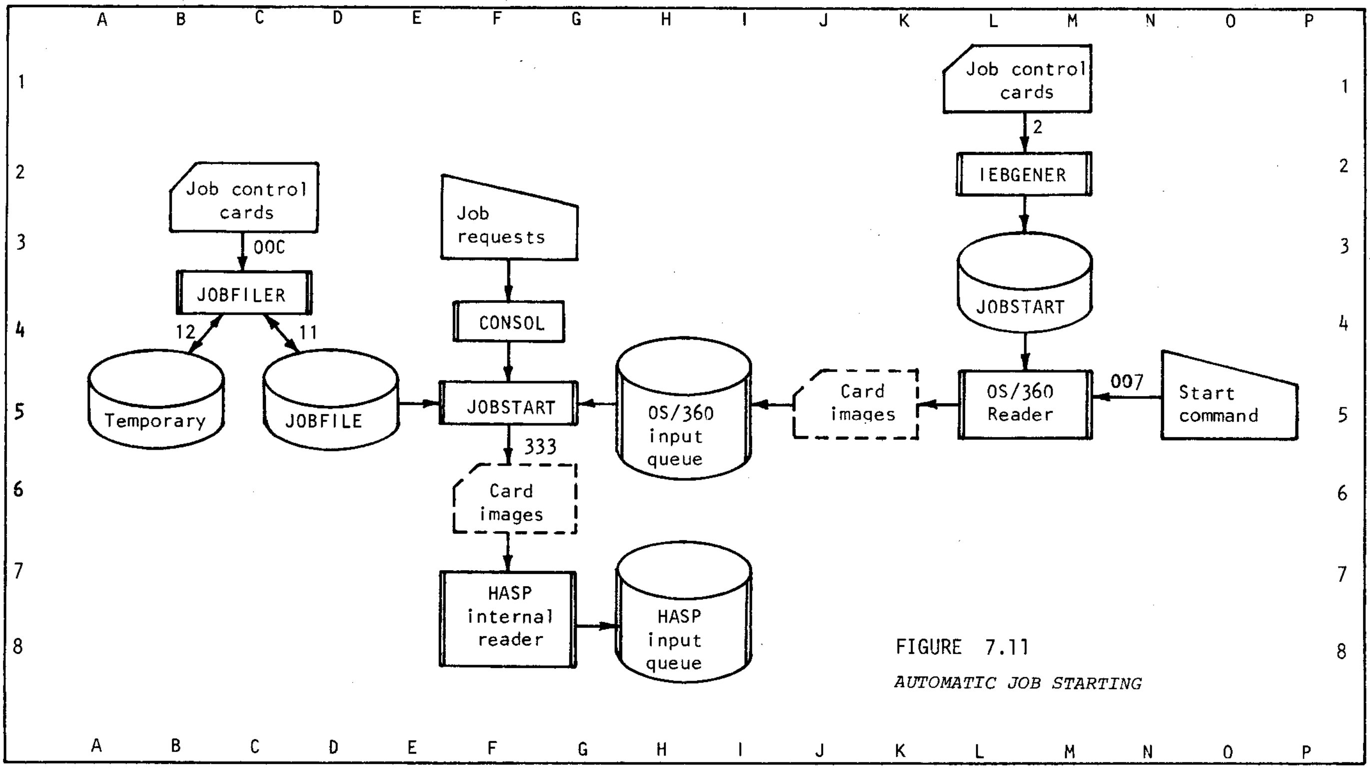

FIGURE 7.11

AUTOMATIC JOB STARTING

FIGURE 7.12

GENERALIZED PROCESS OF ANALYSIS, SYNTHESIS, AND PRESENTATION OF RESULTS

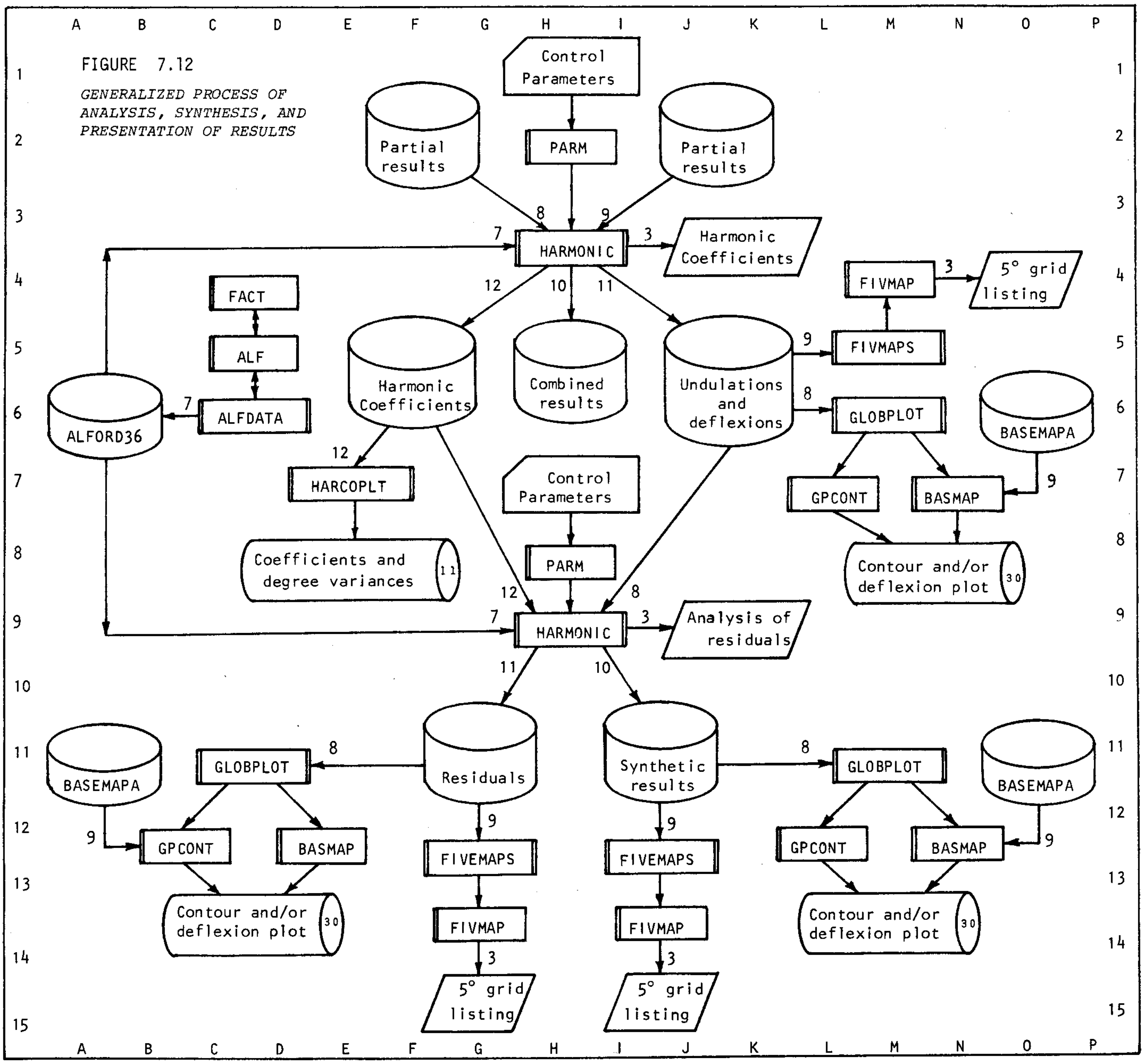

results were stored in datasets INNFIVEG (7.4,C13), INNFIVIC (7.4,A13), INNFCONT (7.4,E13), MIDFIVEG and MIDFIVIC (7.4,I13), and OUTFIVEG and OUTFIVIC (7.4,N13).

A single programme, HARMONIC, was used to:

(a) Sum the contributions from the separate causes within each zone and then sum the total contribution from each zone.

(b) Convert the potentials and attraction components to equipotential undulations and components of the deflexions of the vertical according to Bruns' theorem (equations 1.5 and 1.6).

(c) Compute fully normalized spherical harmonic coefficients and degree variances to degree 36, of the undulations and deflexions of the verical due to separte zones and the combined effects.

(d) Synthesize (that is, regenerate) the undulations and deflexions from the coefficients and compute residuals with respect to the original results data.

Development of the theoretical aspects of the analysis and synthesis can be found in §8.4.

The process of summation and the partial and total results datasets are depicted in the lower part of figure 7.4. A schema of the whole analysis and sythesis processes, including the routines and datasets used in presentation of the results, is displayed in a generalized form in figure 7.12. All of the routines are described briefly in the compendium of appendix A.

Spherical harmonic analysis was effected by global numerical integration, taking advantage of the orthogonality relations for the surface harmonics. Precomputed values of the associated Legendre function up to degree and order (36,36) for 5° intervals of latitude were stored in dataset ALFORD36 (7.12,A6) and read-in by programme HARMONIC as necessary. Figure 7.13 is a flow chart of programme HARMONIC, annotated with cross-references to the appropriate equations.

7.4 DATA MANAGEMENT ROUTINES

Data management routines come within one of two categories: (a) model data routines—employed in preparation, storage, accessing, and display of the model data—and (b) results data routines, used to store and display the results data. Some general purpose routines occur within both categories. All of the data management routines are described in the compendium presented in appendix A. Also, in a separate compendium in appendix B, all of the model and results datasets, arranged alphabetically by name, are briefly described and a list of their technical attributes is given.

MODEL DATA SUB-SYSTEM. A schematic representation of the interrelation of routines and datasets forming the model data sub-system is available in figure 7.14. The key to symbols in the previous section (figure 7.3) remains applicable. Central to the whole model data sub-system is the global 5'x5' mean elevation data, contained in datasets FIVMINEL (7.14,G12) and SIMINDEX (7.14,G16). Dataset FIVMINEL contains only real data derived from the Australian, North American, and European datasets (see table 6.1) and the remainder of the global data is simulated using the parameters stored in dataset SIMINDEX according to the procedure described in §6.4. All data is entered into dataset FIVMINEL by the subroutine PUTELS (7.14,E10) which simultaneously writes location, date, and time parameters into each record. This precaution enables the integrity of any record to be checked whenever it is extracted and allows the fidelity of the whole dataset to be checked periodically by programme STATUS (7.14,C14), which may also be used to delete a specified group of records from FIVMINEL and close up the resulting space. As it is not practical to maintain the records in FIVMINEL in "geographical" order, they must always be accessed through an index which is stored in dataset SIMINDEX via subroutines ELSIMW (7.14,B12) and WINDEX (7.14,B16). Each record of SIMINDEX comprises a 10°x10° block of index parameters refering to each 1°x1° block of 5' data. If real data is available the index parameter is merely a record number in dataset FIVMINEL, but, if data must be simulated, the parameters to be used in the transfer

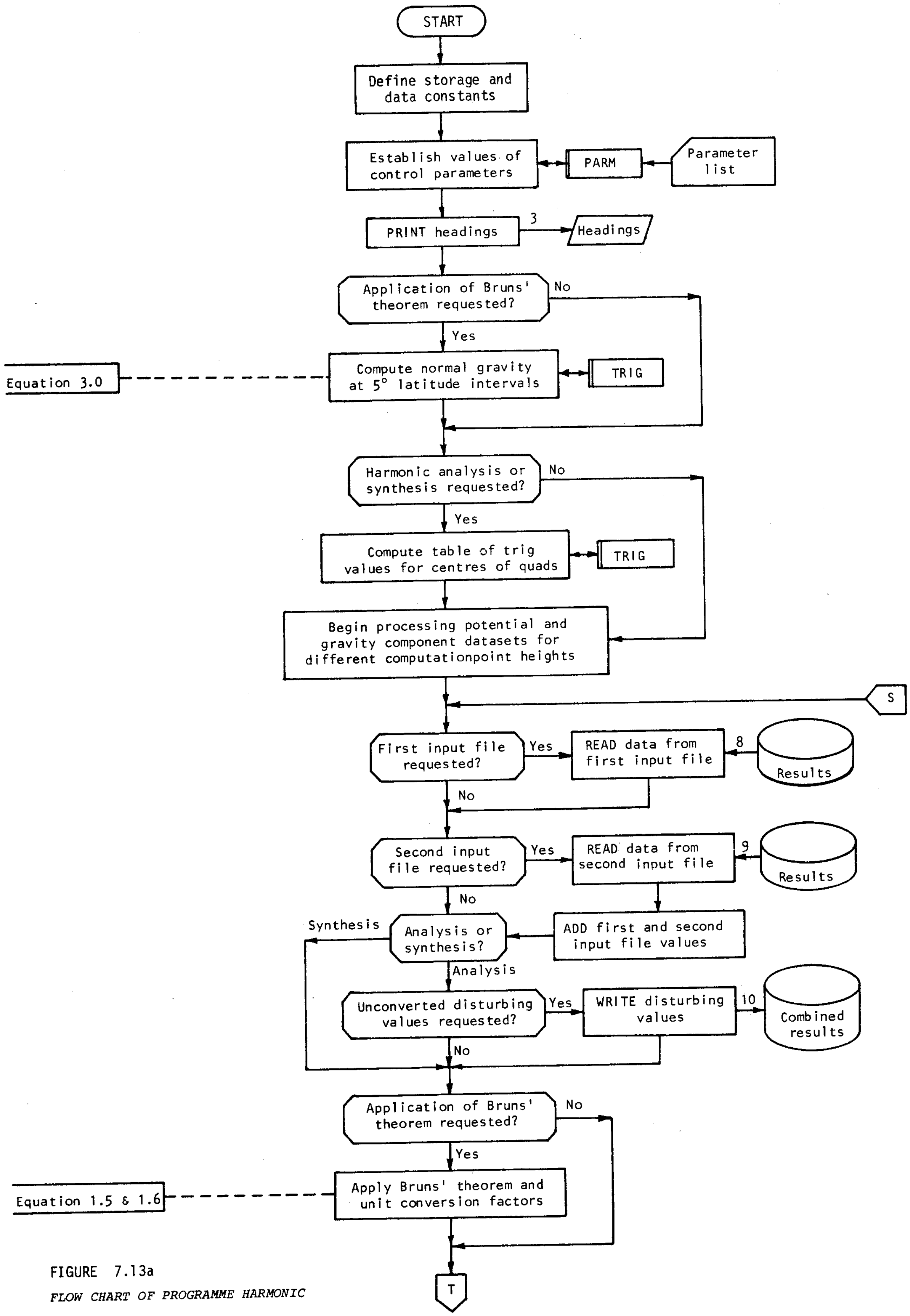

FIGURE 7.13a

FLOW CHART OF PROGRAMME HARMONIC

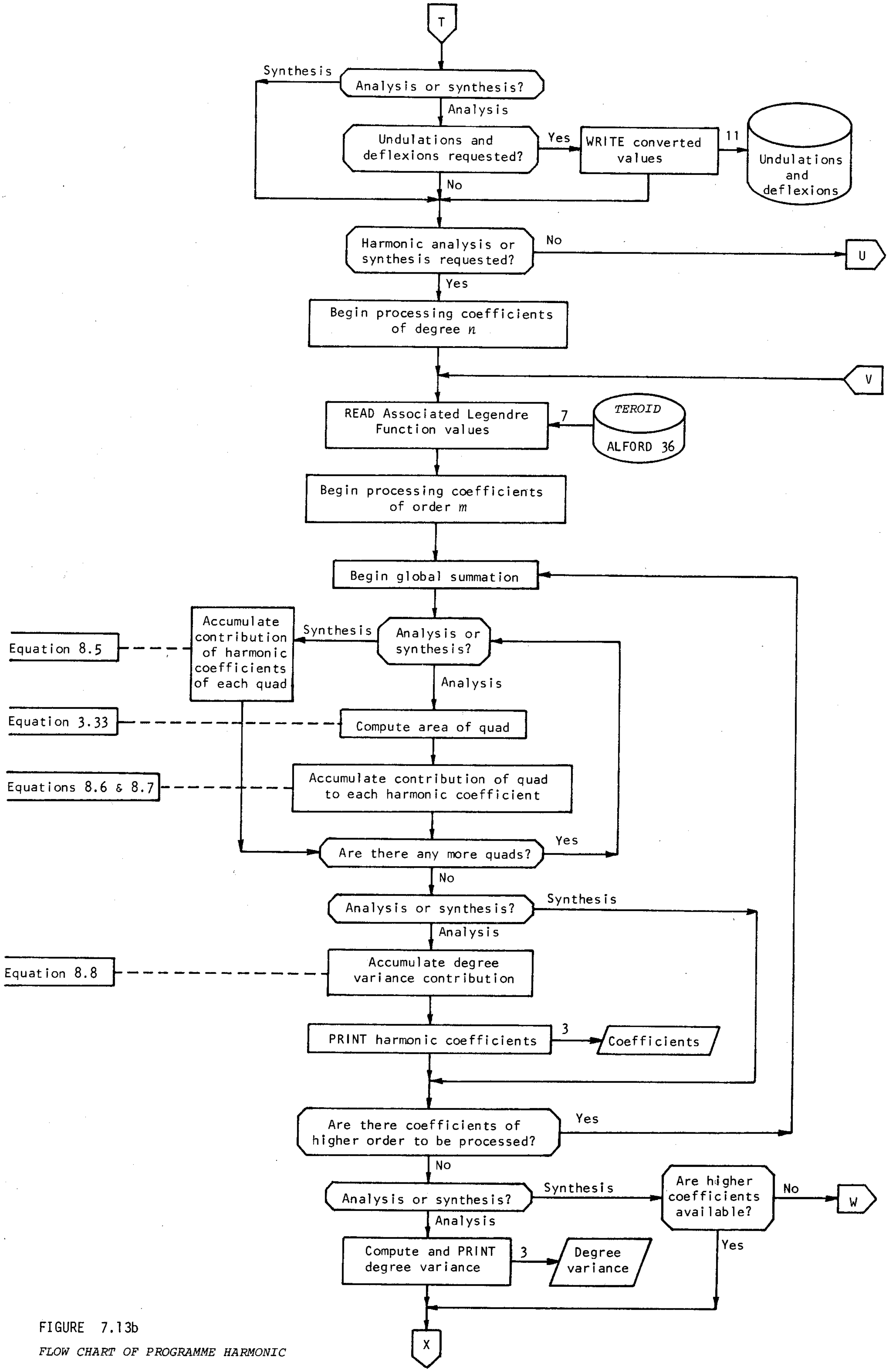

FIGURE 7.13b

FLOW CHART OF PROGRAMME HARMONIC

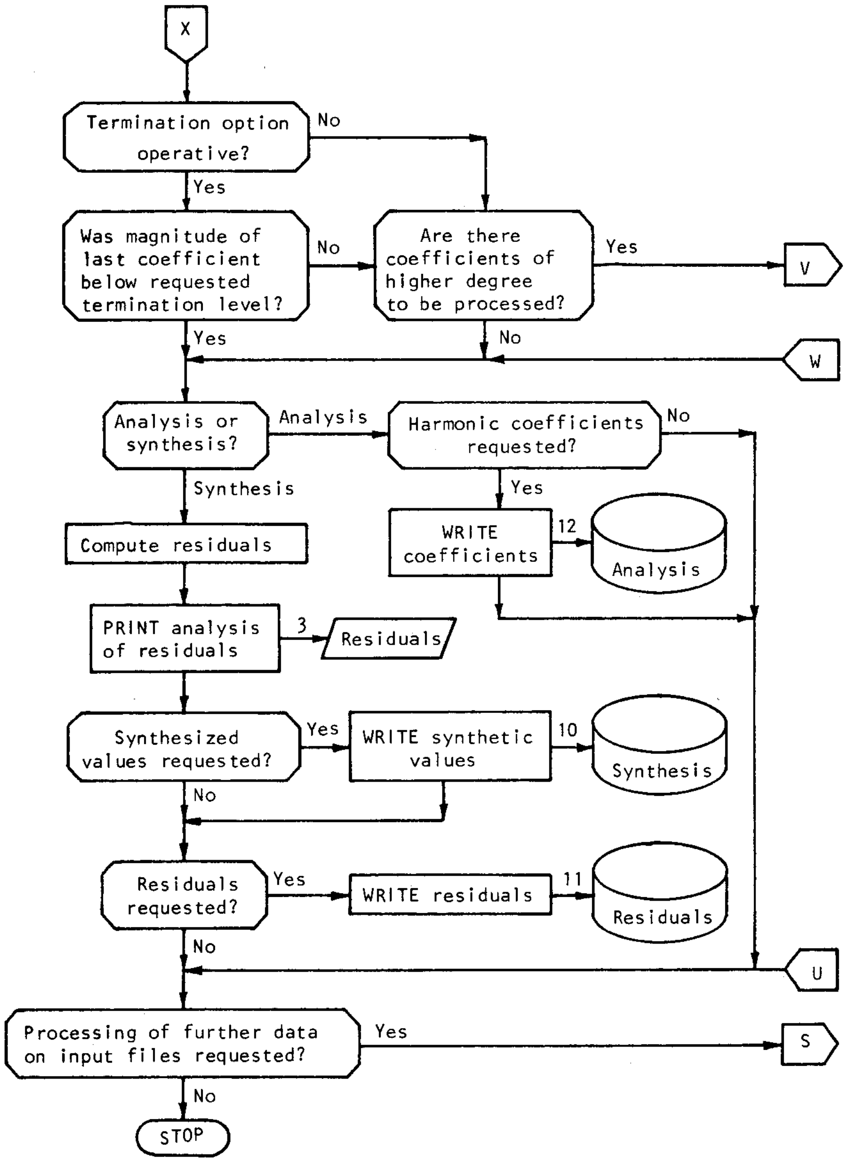

FIGURE 7.13c

FLOW CHART OF PROGRAMME HARMONIC

equation (equation 6.9) are also present in the index record. Originally, index records are stored in SIMINDEX either by subroutine PINDEX (7.14,G13), if real data is available, or by programme TOPOSIM (7.14,J15) which generates the simulation parameters.

All of the model data for larger quad sizes was derived from the 5' data, which in the case of simulated values, is compatible with the UCLA 1° data stored in dataset UCLA1SHT (7.14,014). Plots used for visual error screening of the 5' data were produced by programme WORLDPLT (7.14,B23).

Digital coordinates for an outline map of the world were generated by programme BASEMAPA (7.14,H19) and stored in a dataset of the same name (7.14,H22) for subsequent use by programme GLOBPLOT (7.14,H24), which was used to plot global contour or deflexion vector maps of the results data (see also figure 7.12).

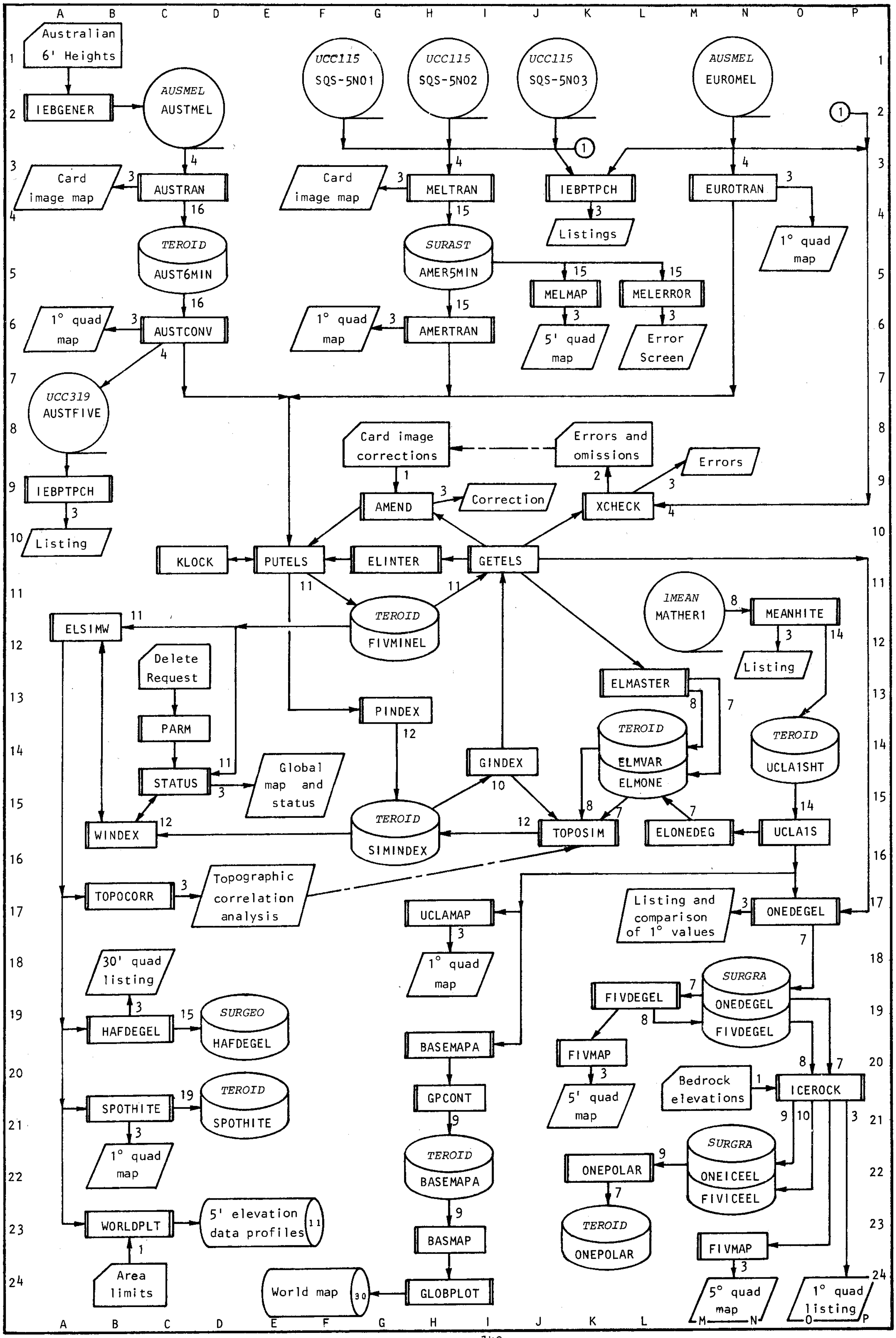
A B C D E F G H I J K L M N O P
Australian 6' Heights
IEBGENER
AUSMEL AUSTMEL
UCC115 SQS-5N01
UCC115 SQS-5N02
UCC115 SQS-5N03
AUSMEL EUROMEL
Card image map
AUSTRAN
MELTRAN
IEBPTPCH
EUROTRAN
Listings
1° quad map
TEROID AUST6MIN
SURAST AMER5MIN
MELMAP
MELERROR
AUSTCONV
AMERTRAN
5' quad map
Error Screen
UCC319 AUSTFIVE
Card image corrections
Errors and omissions
Errors
IEBPTPCH
AMEND
Correction
XCHECK
Listing
KLOCK
PUTELS
ELINTER
GETELS
TEROID FIVMINEL
1MEAN MATHER1
MEANHITE
ELSIMW
Delete Request
Listing
ELMASTER
PARM
PINDEX
TEROID ELMVAR ELMONE
TEROID UCLA1SHT
STATUS
Global map and status
GINDEX
TEROID SIMINDEX
WINDEX
TOPOSIM
ELONEDEG
UCLA1S
TOPOCORR
Topographic correlation analysis
UCLAMAP
Listing and comparison of 1° values
ONEDEGEL
30' quad listing
1° quad map
SURGRA ONEDEGEL FIVDEGEL
FIVDEGEL
HAFDEGEL
SURGEO HAFDEGEL
BASEMAPA
FIVMAP
Bedrock elevations
ICEROCK
SPOTHITE
TEROID SPOTHITE
GPCONT
5' quad map
TEROID BASEMAPA
SURGRA ONEICEEL FIVICEEL
ONEPOLAR
TEROID ONEPOLAR
WORLDPLT
5' elevation data profiles
BASMAP
FIVMAP
Area limits
World map
GLOBPLOT
5° quad map
1° quad listing

RESULTS DATA ROUTINES AND DATASETS. Manipulation of the results data was largely performed by the computation and analysis routines already described in §7.3 and illustrated particularly in figure 7.12.

One important difficulty experienced with the storage of the results data, particularly the 1° evaluation grid datasets used by the main computation routines, was that of the large quantity of disk space required. This was largely overcome by storing the horizontal components of the attraction vector, computed at geoid, surface, and orbital elevations, as half-word integers after magnifying them by a factor of 1000 and truncating the result. However, in some instances this scaled quantity could exceed the numeric range of a half-word number and in these circumstances a scale factor of 100 was applied. To indicate the presence of the smaller scale factor a single bit was set to unity in a bit string referring to the 100 computation points in a 10°x10° block of the evaluation grid. As it was possible to store this bit string in what would otherwise be wasted space at the end of each track on the 2311 disk accommodating the dataset, this arrangement was especially economical. Subroutines PUTBIT and GETBIT were developed for this purpose.

Display of the results data was achieved graphically by programme GLOBPLOT—which is capable of plotting global contour or deflexion vector maps of 5° grid data over an outline map of the world—or numerically by programme FIVEMAPS which lists the 5° grid data on the line printer in the form of a global map, after automatically scaling the values by an appropriate tertiary power of ten to fit the output format. Programme HARCOPLT (7.12,E7) was used to plot bar charts of the spherical harmonic coefficients and graph the degree variances and could also be used to print or punch the coefficients.

8

Results and Analysis

8.1 INTRODUCTION

METHODS OF PRESENTATION

Due to the large quantity of data, it is not feasible to reproduce numerically all of the computation results. Moreover, in some instances, a contour map of the data does not adequately convey the details of the results, because of large and rapid variations between neighbouring points. In these circumstances the contours may degenerate into a confusing miscellany of isolated "highs" and "lows". A compromise solution to this dilemma has been adopted, in which both graphical and numeric presentations are utilized, depending on the properties of the data and its significance. Even so, not all of the results could be accommodated in the following sections and in some circumstances recourse is had to condensed examples which portray only the distinctive features.

ACCURACY OF THE RESULTS

Throughout the development of the formulae used to calculate the gravitational effects an attempt was made to eliminate errors which might exceed the order of the flattening (that is, approximately 0.3%). The success of these precautions may be judged by the preliminary numerical investigations reported in chapters 2 and 3. However, these measures guarantee only the "internal" precision of the formulations. Before it would be possible to estimate the "external" accuracy of the results, some measure of the verity of the physical models employed in the computations would be needed. For instance, the degree of reality of the isostatic compensation and topographic density models is uncertain. And the deliberate introduction of simulated topographic data, though it affects only part of the solution, must be emphasized as a source of misrepresentation in the results. In the absence of more detailed knowledge of the earth's topography and crust, it is not possible to assess the magnitude of these inaccuracies. Nevertheless, it may be stated with some confidence that the results are as accurate as can be obtained from the available data.

8.2 CONTACT SUB-ZONE EFFECTS

Inspection of the results obtained from the inner zone revealed a number of values of extraordinarily large magnitude and seemingly incorrect sign. In particular the vertical component of the attraction vector for some computation points at the earth's surface was found to have a large positive (that is, upwards) value. Since the topography and compensation are treated in isolation from the remainder of the earth in the model adopted, this effect could occur if the topographic gradient in the region of the computation point was sufficiently large. However, its magnitude was unexpected. Closer examination disclosed that the four topographic quads in the contact sub-zone were predominantly responsible for the effect, particularly when two of the quads on one side of the computation point were much higher than the other two. Such a situation could occur in mountainous regions or at a coastline. The excessive magnitude of the effect arises from the extreme distortion of the real topographic gradient, caused by the use of *mean* elevations in the contact sub-zone quads. In effect the computation point—whose height is taken as the mean of the four contact quads—is situated on the side of the higher model parallelepipeds representing the contact quads, and the nearby topographic gradient becomes vertical (see figure 8.1).

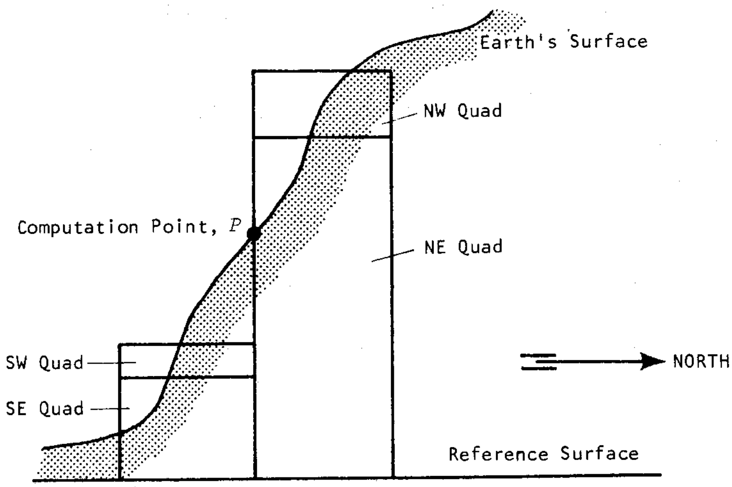

FIGURE 8.1

DISTORTION OF TOPOGRAPHIC GRADIENT IN CONTACT SUB-ZONE

A more realistic formulation of the contact sub-zone effects could be achieved if the contact parallelepipeds were replaced by right prisms with a sloping upper surface. Then formulation of the potential due to a homogeneous prism, for instance, would necessitate solution of the integrals (*c.f.* equation 4.20):

$$V_0 = \sigma k \int_0^{x_1} \int_0^{y_1} \int_0^{ux_0 + vy_0 + w} \frac{dz_0 \, dy_0 \, dx_0}{[x_0^2 + y_0^2 + (z_0 - z_2)^2]^{\frac{1}{2}}} \tag{8.1}$$

where u, v, and w are constants defining the upper surface of the prism and the remaining symbols have the same meaning as in equation 4.20. A cursory investigation suggests that the solution of such an equation is feasible but leads to a formula of unwarranted complexity.

A simpler alternative treatment was sought, which could be effected with the very limited computer time and access available at this stage. If the heights of the four contact quads are artificially made equal to the height of the computation point, gross distortion of the nearby topographic surface is avoided. While this amounts to complete suppression of the topographic gradient within the contact sub-zone, the resulting model provides a more realistic representation of the regional topographic morphology. With minor modifications, the programme already used to compute the inner zone effects (INNZONE) could be utilized to compute the necessary corrections to the potential and attraction components due to equalization of the heights of the contact quads and the appropriate adjustments to the isostatic compensation. This was achieved by programme INNCONT (see §7.3). Provision for the situation where the contact parallelepipeds may be partly composed of ice was included. Examples of the magnitude of these corrections are given in §8.3.

8.3 RESULTS

TERRESTRIAL TOPOGRAPHY AND COMPENSATION

EFFECT ON POTENTIAL. The disturbance of the gravitational potential at the earth's surface due to the adopted model of the terrestrial topography and isostatic compensation is shown in the contour map of figure 8.2 and the numerical results to the nearest metre on a global 5° grid are presented in figure 8.3. It must be stressed that these results are point values calculated at the grid intersections; they are *not* area mean values. For comparison, figure 8.4 is a contour map of the terrestrial topography, based on 5° mean elevations. A high degree of correlation between the effect on potential and the topography is evident. In the Himalayas, the maximum value of 23 metres is attained, while the next highest value of 16 metres occurs in the Andes. A value of approximately -0.7 metres predominates in ocean areas.

The results computed at geoid elevation (figure 8.5) behave almost identically to the surface effect except that the magnitude is slightly reduced. A maximum of 20 metres is reached in the Himalayas and the high in the Andes is 15 metres.

At an elevation representative of satellite orbits (1000 km) the effect of the topography is both reduced and smoothened (see figure 8.6). Nevertheless, the maximum attained over the Himalayas of 5.7 metres is appreciable and would appear to partly account for the small but definite "ridge" dividing an otherwise dominant trough which occurs in this region on extant satellite geoid maps [*e.g.* U.S. ARMY TOPOGRAPHIC COMMAND 1968 (see also FISCHER 1968); RAPP 1973; VINCENT and MARSH 1973]. Small negative values predominate in ocean areas, reaching a minimum of -0.48 metres in the mid Indian Ocean.

EFFECT ON THE VERTICAL COMPONENT OF GRAVITY. Figure 8.7 is a contour map of the results obtained for the vertical component of the attraction vector, computed at geoid level. Equivalent numerical data is presented in figure 8.8 to enable direct comparison with the results at surface level (figure 8.9). Rapid variations in the surface results make a contour map of that data too confusing to be useful.

Correlation of the vertical gravity at the geoid with the topography is even greater than was observed for the potential. Again the maximum occurs in the Himalayas where a value of 11290 μN/kg (1129 mgal) is reached, while values of 8281 μN/kg (828.1 mgal) and 5325 μN/kg (532.5 mgal) are observed in the Andes and Rocky Mountains respectively. Very small positive values occur in ocean areas. It must be emphasized that all of the data at geoid level is positive, indicating an *upwards* direction of the disturbing force vector. In this situation the attractive influences of both the topography and isostatic compensation near to the computation point are cumulative.

While the values derived for the vertical gravity effect at the earth's surface (figure 8.9) evince some dependence on the continental distribution of topography, their variation from point to point is often quite large and rapid and appears to be more dependent on local influences. Intuitively, it might be anticipated that the attraction at the surface, due to the topography and compensation in isolation, should be mostly a negative (downwards) directed quantity, but this is often contradicted by

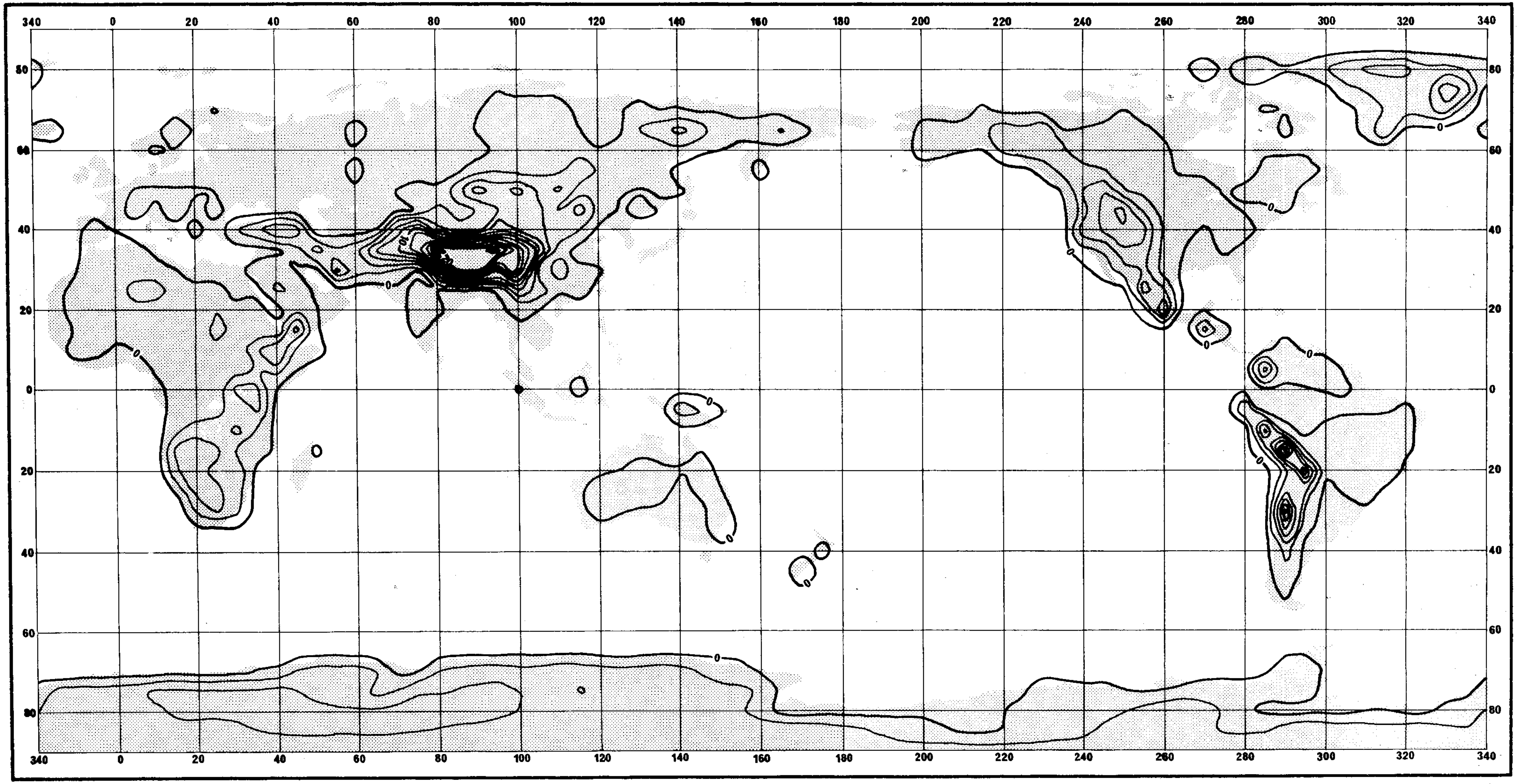

FIGURE 8.2

EQUIPOTENTIAL UNDULATIONS AT THE EARTH'S SURFACE DUE TO TOPOGRAPHIC-ISOSTATIC MODEL

Contour interval = 2 m

LAT | LON	0	5	10	15	20	25	30	35	40	45	50	55	60	65	70	75	80	85
90	-1	-1	-1	-1	-1	-1	-1	-1	-1	-1	-1	-1	-1	-1	-1	-1	-1	-1
85	-1	-1	-1	-1	-1	-1	-1	-1	-1	-1	-1	-1	-1	-1	-1	-1	-1	-1
80	-1	-1	-1	0	-1	0	-1	-1	-1	-1	-1	-1	-1	-1	-1	-1	-1	-1
75	-1	-1	-1	-1	-1	-1	-1	-1	-1	-1	-1	-1	0	-1	-1	-1	-1	-1
70	-1	-1	-1	-1	-1	0	-1	-1	-1	-1	-1	-1	-1	-1	-1	-1	-1	-1
65	-1	-1	-1	2	0	-1	0	-1	-1	-1	0	-1	-1	-1	-1	-1	-1	-1
60	-1	-1	0	0	-1	-1	-1	0	-1	-1	-1	-1	0	-1	-1	-1	-1	-1
55	-1	-1	-1	-1	-1	0	0	0	-1	-1	-1	0	0	-1	-1	-1	-1	0
50	-1	0	0	0	0	0	0	-1	-1	-1	-1	-1	0	-1	0	1	0	3
45	-1	1	0	1	0	1	-1	-1	0	-1	-1	-1	-1	-1	0	0	3	1
40	0	-1	-1	-1	1	-1	2	3	6	5	-1	-1	-1	0	7	12	4	3
35	2	1	0	-1	-1	0	-1	-1	0	1	5	2	4	8	10	13	23	21
30	1	0	1	0	-1	-1	0	1	2	0	-1	6	3	3	1	0	7	22
25	0	3	3	1	1	1	0	-1	2	2	-1	-1	-1	-1	-1	1	0	-1
20	1	1	1	1	1	2	0	2	-1	2	0	-1	-1	-1	-1	1	0	0
15	0	0	1	0	0	3	1	1	1	6	0	-1	-1	-1	-1	1	-1	-1
10	0	0	2	0	0	1	0	4	6	1	1	-1	-1	-1	-1	-1	-1	-1
5	-1	-1	0	2	1	1	1	2	3	0	-1	-1	-1	-1	-1	-1	-1	-1
0	-1	-1	0	1	0	1	5	4	0	-1	-1	-1	-1	-1	-1	-1	-1	-1
-5	-1	-1	-1	1	1	2	3	4	-1	-1	-1	-1	-1	-1	-1	-1	-1	-1
-10	-1	-1	-1	2	4	3	4	2	-1	-1	-1	-1	-1	-1	-1	-1	-1	-1
-15	-1	-1	-1	5	5	5	2	2	-1	-1	0	-1	-1	-1	-1	-1	-1	-1
-20	-1	-1	-1	4	5	3	4	-1	-1	0	-1	-1	-1	-1	-1	-1	-1	-1
-25	-1	-1	-1	0	5	5	2	-1	-1	0	-1	-1	-1	-1	-1	-1	-1	-1
-30	-1	-1	-1	-1	2	4	2	-1	-1	-1	-1	-1	-1	-1	-1	-1	-1	-1
-35	-1	-1	-1	-1	-1	-1	-1	-1	-1	-1	-1	-1	-1	-1	-1	-1	-1	-1
-40	-1	-1	-1	-1	-1	-1	-1	-1	-1	-1	-1	-1	-1	-1	-1	-1	-1	-1
-45	-1	-1	-1	-1	-1	-1	-1	-1	-1	-1	-1	-1	-1	-1	-1	-1	-1	-1
-50	-1	-1	-1	-1	-1	-1	-1	-1	-1	-1	-1	-1	-1	-1	-1	-1	-1	-1
-55	-1	-1	-1	-1	-1	-1	-1	-1	-1	-1	-1	-1	-1	-1	-1	-1	-1	-1
-60	-1	-1	-1	-1	-1	-1	-1	-1	-1	-1	-1	-1	-1	-1	-1	-1	-1	-1
-65	-1	-1	-1	-1	-1	-1	-1	-1	-1	-1	-1	-1	-1	-1	-1	-1	-1	-1
-70	-1	-1	0	0	-1	-1	0	0	0	2	3	3	3	2	-1	0	2	3
-75	3	4	5	5	4	5	4	5	5	4	3	4	3	1	2	4	4	4
-80	3	4	4	4	4	4	5	5	5	5	5	4	4	4	5	5	6	5
-85	3	3	3	3	3	3	3	4	4	4	4	4	4	4	4	4	4	3
-90	3	3	3	3	3	3	3	3	3	3	3	3	3	3	3	3	3	3

LAT | LON	90	95	100	105	110	115	120	125	130	135	140	145	150	155	160	165	170	175
90	-1	-1	-1	-1	-1	-1	-1	-1	-1	-1	-1	-1	-1	-1	-1	-1	-1	-1
85	-1	-1	-1	-1	-1	-1	-1	-1	-1	-1	-1	-1	-1	-1	-1	-1	-1	-1
80	-1	-1	-1	-1	-1	-1	-1	-1	-1	-1	-1	-1	-1	-1	-1	-1	-1	-1
75	0	0	0	0	0	-1	-1	-1	-1	-1	-1	-1	-1	-1	-1	-1	-1	-1
70	0	2	1	0	1	0	0	0	1	0	0	0	0	-1	-1	-1	-1	-1
65	0	0	1	1	1	0	0	-1	2	3	4	3	0	1	1	2	0	0
60	-1	0	0	0	1	1	0	1	0	0	2	0	0	0	-1	0	0	-1
55	1	2	1	1	2	3	2	1	1	1	-1	-1	-1	-1	1	-1	-1	-1
50	7	5	7	4	4	1	1	0	0	0	0	-1	-1	-1	-1	-1	-1	-1
45	2	4	5	5	2	5	2	0	1	0	-1	-1	-1	-1	-1	-1	-1	-1
40	2	8	6	4	3	2	-1	-1	-1	-1	-1	-1	-1	-1	-1	-1	-1	-1
35	22	23	18	9	1	-1	-1	-1	-1	0	-1	-1	-1	-1	-1	-1	-1	-1
30	21	12	19	0	4	1	0	-1	-1	-1	-1	-1	-1	-1	-1	-1	-1	-1
25	-1	0	6	3	0	1	-1	-1	-1	-1	-1	-1	-1	-1	-1	-1	-1	-1
20	-1	0	1	0	-1	-1	-1	-1	-1	-1	-1	-1	-1	-1	-1	-1	-1	-1
15	-1	-1	-1	-1	-1	-1	-1	-1	-1	-1	-1	-1	-1	-1	-1	-1	-1	-1
10	-1	-1	-1	-1	-1	-1	-1	-1	-1	-1	-1	-1	-1	-1	-1	-1	-1	-1
5	-1	-1	-1	-1	-1	0	-1	-1	-1	-1	-1	-1	-1	-1	-1	-1	-1	-1
0	-1	-1	0	-1	0	0	-1	-1	-1	-1	-1	-1	-1	-1	-1	-1	-1	-1
-5	-1	-1	-1	0	-1	-1	-1	-1	-1	-1	4	2	0	-1	-1	-1	-1	-1
-10	-1	-1	-1	-1	-1	-1	-1	-1	-1	-1	-1	-1	0	-1	-1	-1	-1	-1
-15	-1	-1	-1	-1	-1	-1	-1	-1	0	0	-1	0	-1	-1	-1	-1	-1	-1
-20	-1	-1	-1	-1	-1	-1	-1	0	1	0	0	2	-1	-1	-1	-1	-1	-1
-25	-1	-1	-1	-1	-1	0	2	1	1	0	0	0	0	-1	-1	-1	-1	-1
-30	-1	-1	-1	-1	-1	0	1	0	0	0	0	0	1	-1	-1	-1	-1	-1
-35	-1	-1	-1	-1	-1	-1	-1	-1	-1	-1	0	0	1	-1	-1	-1	-1	-1
-40	-1	-1	-1	-1	-1	-1	-1	-1	-1	-1	-1	-1	-1	-1	-1	-1	-1	0
-45	-1	-1	-1	-1	-1	-1	-1	-1	-1	-1	-1	-1	-1	-1	-1	-1	2	-1
-50	-1	-1	-1	-1	-1	-1	-1	-1	-1	-1	-1	-1	-1	-1	-1	-1	-1	-1
-55	-1	-1	-1	-1	-1	-1	-1	-1	-1	-1	-1	-1	-1	-1	-1	-1	-1	-1
-60	-1	-1	-1	-1	-1	-1	-1	-1	-1	-1	-1	-1	-1	-1	-1	-1	-1	-1
-65	-1	-1	-1	-1	-1	-1	-1	-1	-1	-1	-1	-1	-1	-1	-1	-1	-1	-1
-70	3	3	3	3	4	4	3	3	3	3	3	2	1	1	0	-1	-1	-1
-75	5	5	4	3	3	4	4	4	3	3	3	3	2	2	2	-1	-1	-1
-80	5	4	4	4	3	3	4	3	3	3	3	2	2	2	1	0	-1	-1
-85	3	3	3	4	4	3	3	3	3	4	3	3	3	3	3	3	3	3
-90	3	3	3	3	3	3	3	3	3	3	3	3	3	3	3	3	3	3

FIGURE 8.3a

Units: metres

FIVE DEGREE MAP OF EQUIPOTENTIAL UNDULATIONS AT THE EARTH'S SURFACE DUE TO THE TOPOGRAPHIC-ISOSTATIC MODEL

LAT	LON 180	185	190	195	200	205	210	215	220	225	230	235	240	245	250	255	260	265
90	-1	-1	-1	-1	-1	-1	-1	-1	-1	-1	-1	-1	-1	-1	-1	-1	-1	-1
85	-1	-1	-1	-1	-1	-1	-1	-1	-1	-1	-1	-1	-1	-1	-1	-1	-1	-1
80	-1	-1	-1	-1	-1	-1	-1	-1	-1	-1	-1	-1	-1	-1	-1	-1	-1	0
75	-1	-1	-1	-1	-1	-1	-1	-1	-1	-1	-1	-1	-1	-1	-1	-1	-1	-1
70	-1	-1	-1	-1	0	0	-1	0	0	-1	-1	-1	-1	-1	0	0	-1	0
65	-1	0	-1	0	0	0	0	1	3	3	4	0	0	0	1	0	0	0
60	-1	-1	-1	-1	1	0	0	0	2	4	3	2	1	0	0	1	0	-1
55	-1	-1	-1	-1	-1	-1	-1	-1	-1	-1	1	3	3	2	1	1	0	0
50	-1	-1	-1	-1	-1	-1	-1	-1	-1	-1	-1	0	4	6	2	1	1	0
45	-1	-1	-1	-1	-1	-1	-1	-1	-1	-1	-1	-1	3	7	9	3	1	0
40	-1	-1	-1	-1	-1	-1	-1	-1	-1	-1	-1	-1	5	6	8	7	2	0
35	-1	-1	-1	-1	-1	-1	-1	-1	-1	-1	-1	-1	2	2	6	6	1	0
30	-1	-1	-1	-1	-1	-1	-1	-1	-1	-1	-1	-1	-1	1	3	4	1	-1
25	-1	-1	-1	-1	-1	-1	-1	-1	-1	-1	-1	-1	-1	-1	-1	7	4	-1
20	-1	-1	-1	-1	-1	-1	-1	-1	-1	-1	-1	-1	-1	-1	-1	1	8	-1
15	-1	-1	-1	-1	-1	-1	-1	-1	-1	-1	-1	-1	-1	-1	-1	-1	-1	-1
10	-1	-1	-1	-1	-1	-1	-1	-1	-1	-1	-1	-1	-1	-1	-1	-1	-1	-1
5	-1	-1	-1	-1	-1	-1	-1	-1	-1	-1	-1	-1	-1	-1	-1	-1	-1	-1
0	-1	-1	-1	-1	-1	-1	-1	-1	-1	-1	-1	-1	-1	-1	-1	-1	-1	-1
-5	-1	-1	-1	-1	-1	-1	-1	-1	-1	-1	-1	-1	-1	-1	-1	-1	-1	-1
-10	-1	-1	-1	-1	-1	-1	-1	-1	-1	-1	-1	-1	-1	-1	-1	-1	-1	-1
-15	-1	-1	-1	-1	-1	-1	-1	-1	-1	-1	-1	-1	-1	-1	-1	-1	-1	-1
-20	-1	-1	-1	-1	-1	-1	-1	-1	-1	-1	-1	-1	-1	-1	-1	-1	-1	-1
-25	-1	-1	-1	-1	-1	-1	-1	-1	-1	-1	-1	-1	-1	-1	-1	-1	-1	-1
-30	-1	-1	-1	-1	-1	-1	-1	-1	-1	-1	-1	-1	-1	-1	-1	-1	-1	-1
-35	-1	-1	-1	-1	-1	-1	-1	-1	-1	-1	-1	-1	-1	-1	-1	-1	-1	-1
-40	-1	-1	-1	-1	-1	-1	-1	-1	-1	-1	-1	-1	-1	-1	-1	-1	-1	-1
-45	-1	-1	-1	-1	-1	-1	-1	-1	-1	-1	-1	-1	-1	-1	-1	-1	-1	-1
-50	-1	-1	-1	-1	-1	-1	-1	-1	-1	-1	-1	-1	-1	-1	-1	-1	-1	-1
-55	-1	-1	-1	-1	-1	-1	-1	-1	-1	-1	-1	-1	-1	-1	-1	-1	-1	-1
-60	-1	-1	-1	-1	-1	-1	-1	-1	-1	-1	-1	-1	-1	-1	-1	-1	-1	-1
-65	-1	-1	-1	-1	-1	-1	-1	-1	-1	-1	-1	-1	-1	-1	-1	-1	-1	-1
-70	-1	-1	-1	-1	-1	-1	-1	-1	-1	-1	-1	-1	-1	-1	-1	-1	-1	-1
-75	-1	-1	-1	-1	-1	-1	-1	-1	0	0	1	1	0	0	0	0	0	0
-80	-1	-1	-1	0	0	0	0	0	0	0	1	1	1	1	2	2	3	3
-85	2	2	2	1	0	0	0	0	0	0	1	1	2	2	3	3	2	3
-90	3	3	3	3	3	3	3	3	3	3	3	3	3	3	3	3	3	3

LAT	LON 270	275	280	285	290	295	300	305	310	315	320	325	330	335	340	345	350	355
90	-1	-1	-1	-1	-1	-1	-1	-1	-1	-1	-1	-1	-1	-1	-1	-1	-1	-1
85	-1	-1	-1	-1	-1	-1	-1	-1	-1	-1	-1	-1	-1	-1	-1	-1	-1	-1
80	1	0	1	1	0	0	2	3	4	5	5	2	3	2	1	-1	-1	-1
75	-1	0	-1	-1	-1	-1	-1	1	2	2	2	3	8	6	0	-1	-1	-1
70	-1	-1	-1	0	0	-1	-1	-1	1	2	2	3	5	1	-1	-1	-1	-1
65	0	-1	-1	-1	0	0	-1	-1	1	4	0	-1	-1	-1	1	1	-1	-1
60	-1	-1	-1	0	0	0	-1	-1	-1	0	-1	-1	-1	-1	-1	-1	-1	-1
55	0	-1	-1	0	1	1	0	-1	-1	-1	-1	-1	-1	-1	-1	-1	-1	-1
50	1	0	0	1	1	-1	-1	-1	-1	-1	-1	-1	-1	-1	-1	-1	-1	-1
45	1	0	0	0	0	0	-1	-1	-1	-1	-1	-1	-1	-1	-1	-1	-1	-1
40	0	0	1	0	-1	-1	-1	-1	-1	-1	-1	-1	-1	-1	-1	-1	-1	1
35	0	0	0	-1	-1	-1	-1	-1	-1	-1	-1	-1	-1	-1	-1	-1	-1	2
30	-1	-1	-1	-1	-1	-1	-1	-1	-1	-1	-1	-1	-1	-1	-1	-1	0	2
25	-1	-1	-1	-1	-1	-1	-1	-1	-1	-1	-1	-1	-1	-1	-1	-1	1	0
20	-1	-1	-1	0	-1	-1	-1	-1	-1	-1	-1	-1	-1	-1	-1	0	0	0
15	4	0	-1	-1	-1	-1	-1	-1	-1	-1	-1	-1	-1	-1	-1	0	0	0
10	-1	0	-1	-1	1	0	-1	-1	-1	-1	-1	-1	-1	-1	-1	-1	1	0
5	-1	-1	-1	7	0	2	1	0	-1	-1	-1	-1	-1	-1	-1	-1	-1	-1
0	-1	-1	0	0	0	0	0	0	-1	-1	-1	-1	-1	-1	-1	-1	-1	-1
-5	-1	-1	4	0	0	0	0	0	0	0	0	-1	-1	-1	-1	-1	-1	-1
-10	-1	-1	-1	8	0	0	0	0	0	1	1	-1	-1	-1	-1	-1	-1	-1
-15	-1	-1	-1	2	16	0	1	1	1	2	0	-1	-1	-1	-1	-1	-1	-1
-20	-1	-1	-1	-1	3	11	0	1	1	2	0	-1	-1	-1	-1	-1	-1	-1
-25	-1	-1	-1	-1	5	4	0	0	2	-1	-1	-1	-1	-1	-1	-1	-1	-1
-30	-1	-1	-1	-1	12	1	0	0	0	-1	-1	-1	-1	-1	-1	-1	-1	-1
-35	-1	-1	-1	-1	8	0	0	-1	-1	-1	-1	-1	-1	-1	-1	-1	-1	-1
-40	-1	-1	-1	-1	2	0	-1	-1	-1	-1	-1	-1	-1	-1	-1	-1	-1	-1
-45	-1	-1	-1	-1	2	-1	-1	-1	-1	-1	-1	-1	-1	-1	-1	-1	-1	-1
-50	-1	-1	-1	0	0	-1	-1	-1	-1	-1	-1	-1	-1	-1	-1	-1	-1	-1
-55	-1	-1	-1	-1	0	-1	-1	-1	-1	-1	-1	-1	-1	-1	-1	-1	-1	-1
-60	-1	-1	-1	-1	-1	-1	-1	-1	-1	-1	-1	-1	-1	-1	-1	-1	-1	-1
-65	-1	-1	-1	-1	-1	-1	0	-1	-1	-1	-1	-1	-1	-1	-1	-1	-1	-1
-70	-1	-1	-1	-1	1	2	-1	-1	-1	-1	-1	-1	-1	-1	-1	-1	-1	-1
-75	1	1	1	1	1	1	-1	-1	-1	-1	-1	-1	-1	-1	1	3	3	3
-80	3	2	0	0	-1	-1	-1	-1	0	0	-1	0	0	1	2	3	3	3
-85	2	2	2	2	3	3	3	3	3	2	3	3	2	2	2	2	2	2
-90	3	3	3	3	3	3	3	3	3	3	3	3	3	3	3	3	3	3

FIGURE 8.3b

Units: metres

FIVE DEGREE MAP OF EQUIPOTENTIAL UNDULATIONS AT THE EARTH'S SURFACE DUE TO THE TOPOGRAPHIC-ISOSTATIC MODEL

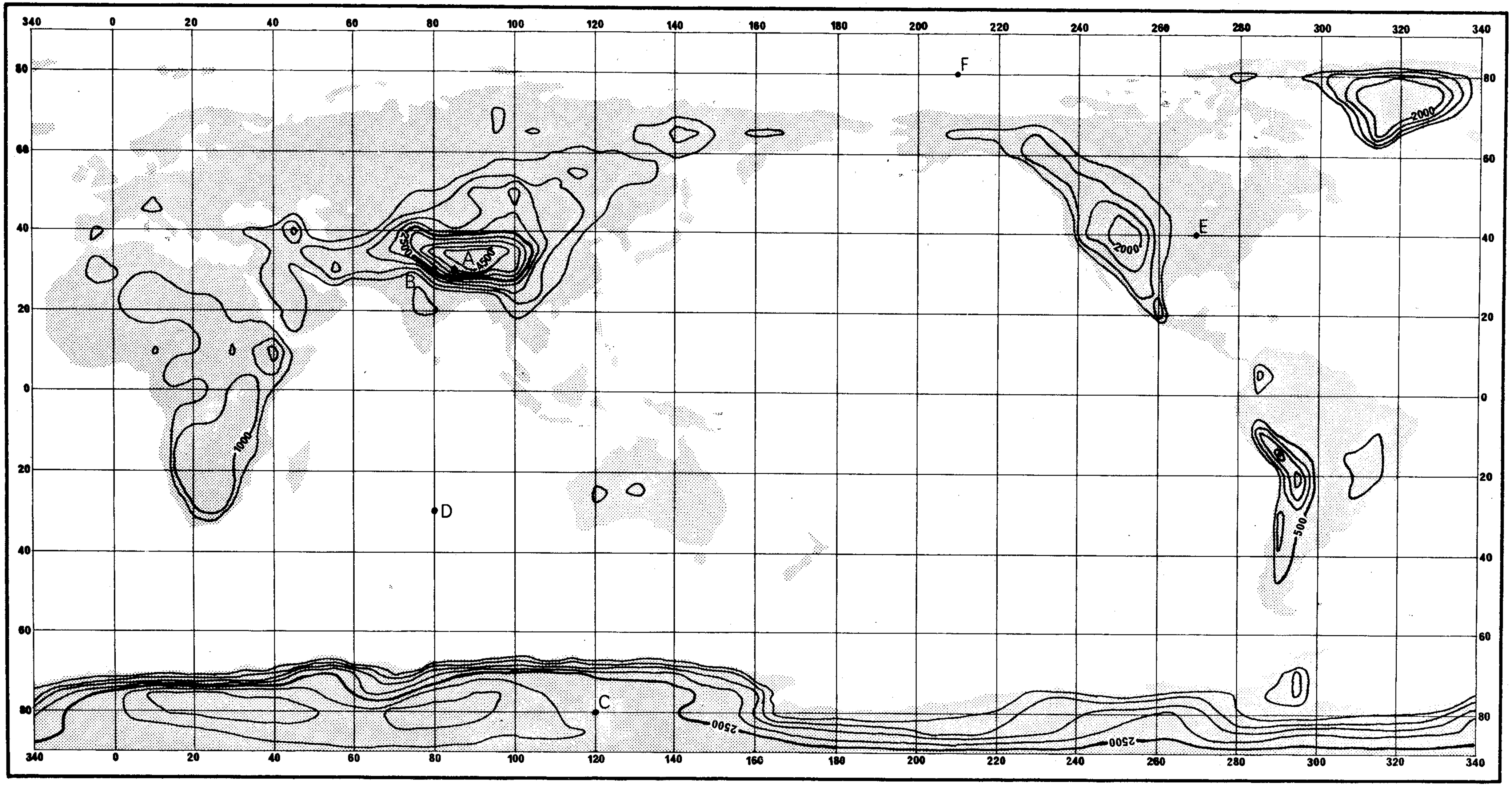

FIGURE 8.4

TERRESTRIAL TOPOGRAPHY BASED ON 5°x5° MEAN ELEVATIONS

Contour interval = 500 m

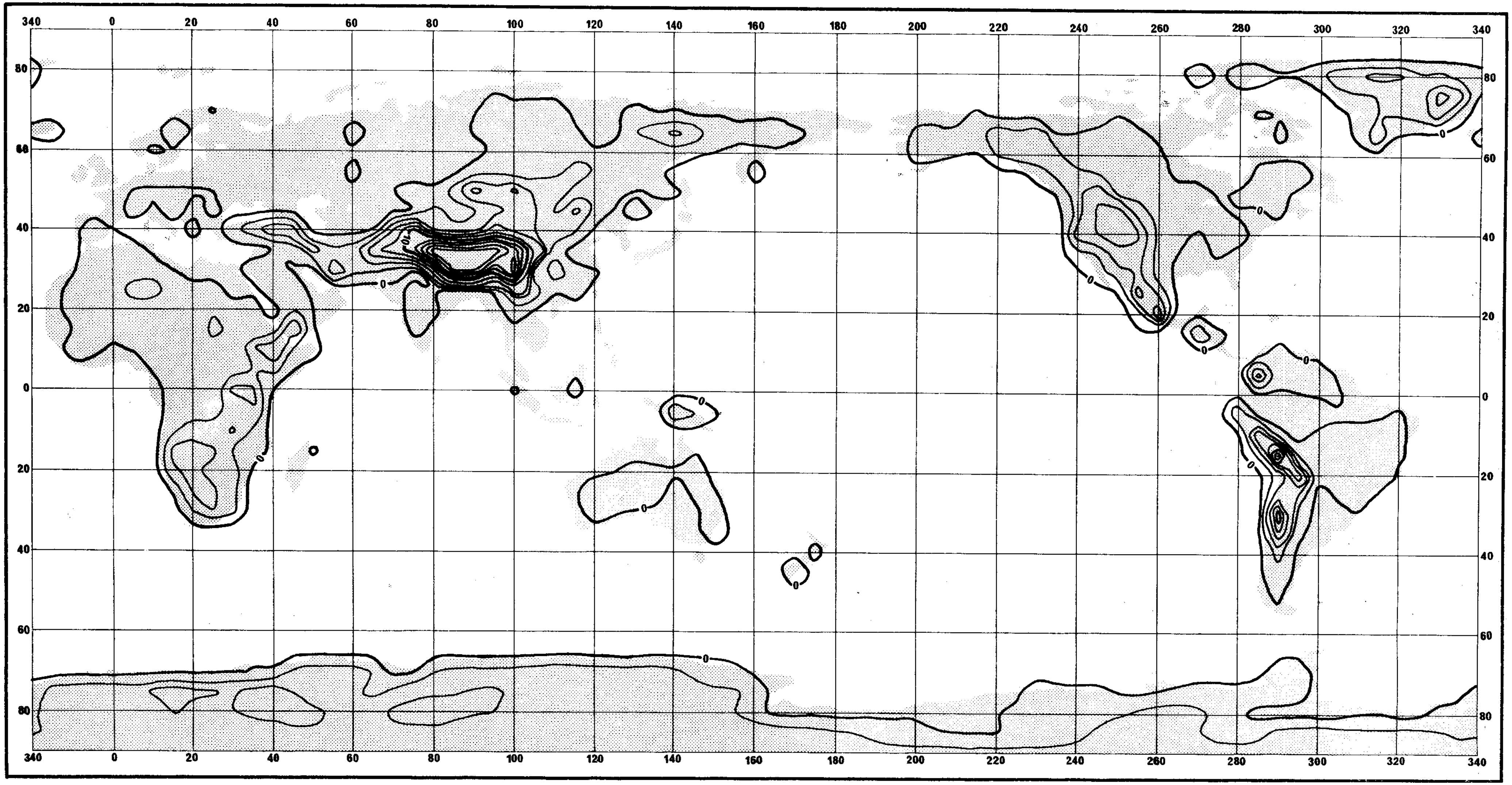

FIGURE 8.5

EQUIPOTENTIAL UNDULATIONS AT THE GEOID DUE TO TOPOGRAPHIC-ISOSTATIC MODEL

Contour interval = 2 m

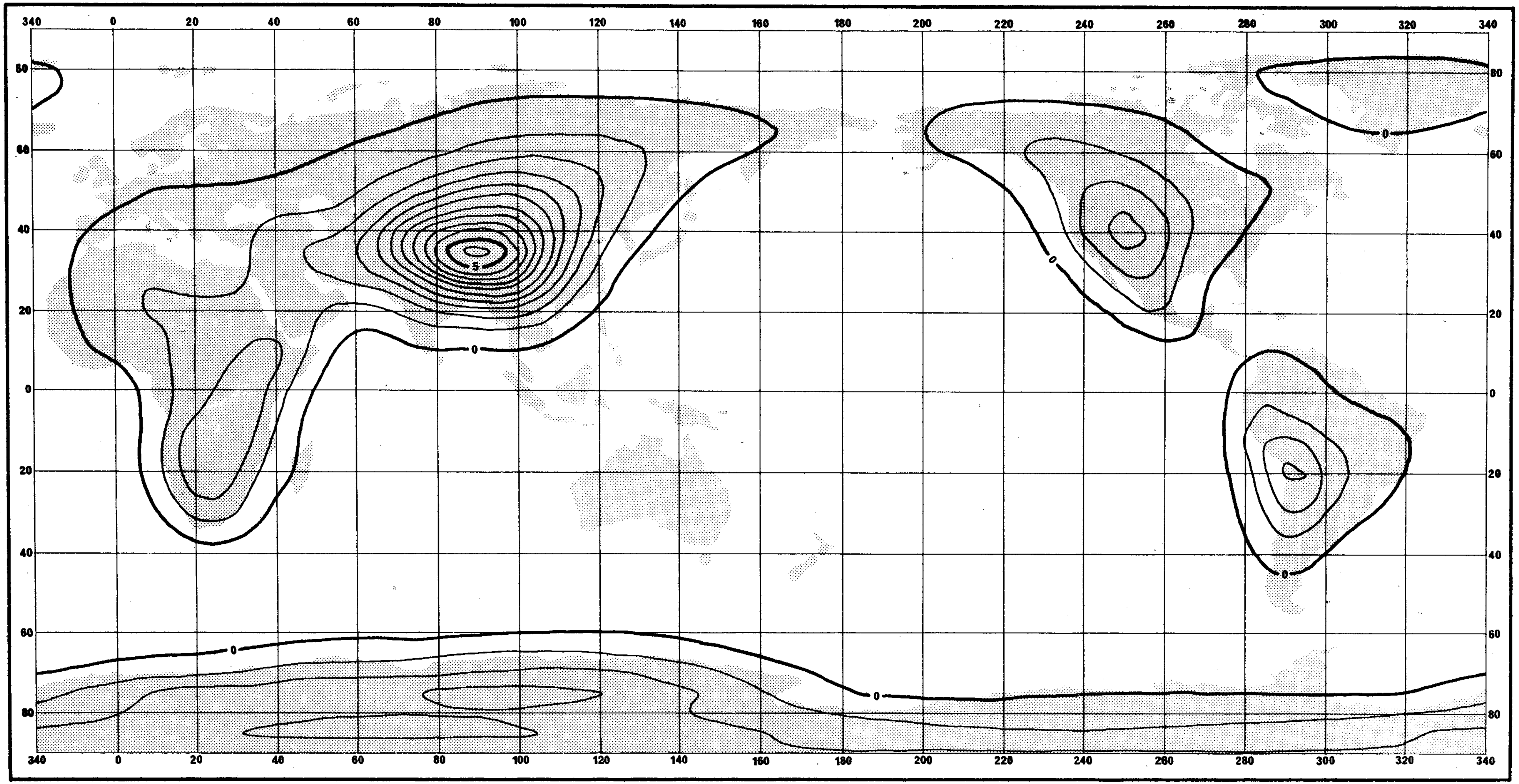

FIGURE 8.6

Contour interval = 0.5 m

EQUIPOTENTIAL UNDULATIONS AT SATELLITE ORBIT ALTITUDE (1000 km) DUE TO TOPOGRAPHIC-ISOSTATIC MODEL

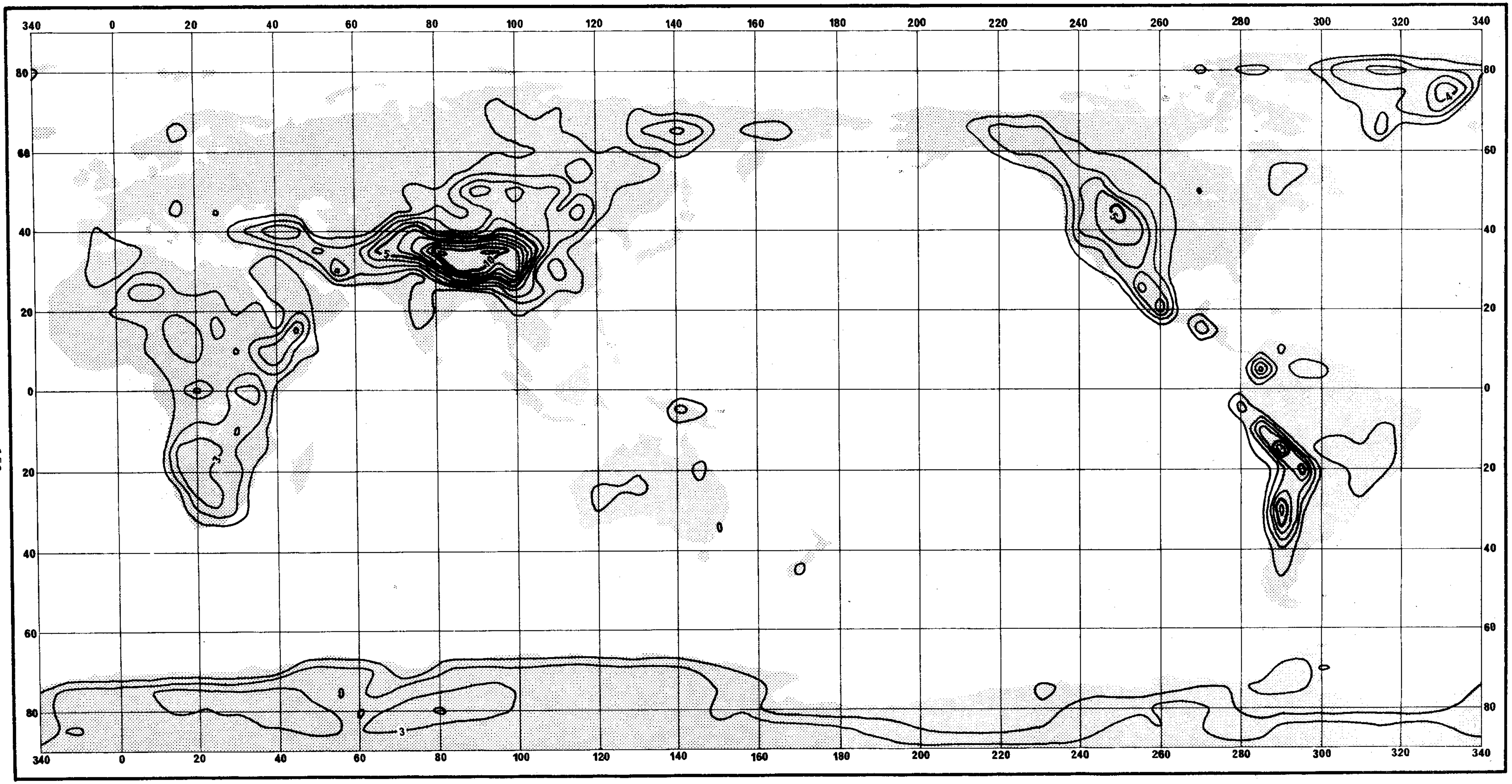

FIGURE 8.7

TOPOGRAPHIC-ISOSTATIC VERTICAL COMPONENT OF GRAVITY AT THE GEOID

Contour interval = 1 mN/kg
= 100 mgal

LAT	LON 0	5	10	15	20	25	30	35	40	45	50	55	60	65	70	75	80	85
90	9	9	9	9	9	9	9	9	9	9	9	9	9	9	9	9	9	9
85	15	14	13	12	11	10	10	9	9	9	8	8	8	8	8	8	8	8
80	23	22	53	185	120	379	27	12	10	13	15	9	8	8	9	9	9	11
75	15	13	12	11	11	10	10	9	9	10	13	52	352	25	14	13	16	25
70	11	12	16	33	179	505	126	30	16	14	16	18	22	29	240	213	273	266
65	13	22	71	1601	556	69	466	55	80	135	476	282	1217	303	262	280	287	302
60	17	146	685	562	31	40	67	436	251	270	274	345	547	287	277	275	289	288
55	27	16	39	31	33	306	389	433	281	312	163	496	1027	261	250	290	247	634
50	38	726	735	765	688	616	457	349	336	208	161	352	626	370	876	1351	1036	2847
45	207	906	423	1280	363	1031	47	242	524	317	44	131	59	268	789	1015	2554	1627
40	481	37	117	154	1186	93	1782	2501	4019	3755	158	362	342	893	4753	6848	3540	2772
35	1670	1299	436	26	24	497	59	136	723	1251	3505	2252	2909	5112	6156	7525	11212	10780
30	1123	695	998	742	81	348	448	1394	1766	678	303	4174	2478	2454	1833	817	4478	10855
25	729	2687	2565	997	1002	1033	561	349	1899	1837	450	114	110	163	497	1186	924	628
20	1068	1131	1011	1045	1408	1783	838	1599	268	1817	775	244	25	26	37	1555	946	510
15	838	893	1089	744	851	2459	1415	1248	989	4161	591	16	14	17	18	959	256	21
10	440	691	1591	843	890	1391	955	2910	3963	1277	1145	13	11	10	11	12	17	12
5	35	49	807	1767	1117	1621	1537	1738	2435	692	18	11	8	8	8	9	10	9
0	12	21	306	1060	870	1114	3215	3218	364	19	13	9	7	6	6	6	6	6
-5	7	17	37	1183	1185	1636	2158	2879	28	15	11	7	6	5	5	5	4	4
-10	7	22	32	1630	2761	2252	3150	1582	72	14	10	7	5	4	4	4	4	4
-15	7	13	45	3406	3405	3272	1651	1614	184	21	582	6	5	4	4	3	3	3
-20	6	14	41	2893	3397	2530	2698	59	16	501	11	5	5	4	3	3	3	3
-25	6	14	31	694	3369	3242	1939	34	13	260	7	5	4	3	3	3	3	3
-30	5	8	22	49	1957	2941	1906	13	10	7	6	4	4	3	3	3	3	3
-35	4	6	12	19	98	26	15	10	8	6	5	4	3	3	3	3	3	3
-40	4	5	6	8	10	10	8	7	5	5	4	3	3	3	3	3	3	3
-45	3	4	4	5	5	5	5	5	4	4	4	4	3	3	3	3	3	3
-50	3	4	4	4	4	4	4	4	4	4	4	4	4	4	38	4	4	4
-55	4	4	4	4	5	5	5	5	5	5	5	5	5	5	5	5	6	6
-60	5	5	6	6	6	7	7	8	9	9	10	10	10	10	10	10	11	12
-65	11	12	12	13	14	15	17	20	26	35	54	71	46	36	29	30	37	51
-70	105	144	200	254	127	130	310	732	781	2201	2786	2457	2436	1862	253	651	1701	2312
-75	2617	2643	3198	3380	3352	3205	3045	3183	3647	3053	2368	3040	2188	1460	2220	2789	2805	3078
-80	2629	2775	2636	3175	2960	3069	3072	3382	3395	3565	3269	2840	3009	2945	3206	3482	4190	3501
-85	2056	2250	2211	2282	2587	2591	2541	2890	2915	3086	3190	3004	2981	3174	3064	2925	2630	2568
-90	2216	2216	2216	2216	2216	2216	2216	2216	2216	2216	2216	2216	2216	2216	2216	2216	2216	2216

LAT	LON 90	95	100	105	110	115	120	125	130	135	140	145	150	155	160	165	170	175
90	9	9	9	9	9	9	9	9	9	9	9	9	9	9	9	9	9	9
85	8	7	7	7	7	7	7	7	7	7	7	7	7	7	7	7	7	7
80	18	191	81	16	11	10	9	9	9	9	8	8	8	8	8	7	7	7
75	266	602	394	573	384	33	20	18	17	16	40	21	13	12	11	10	10	10
70	560	1667	1016	775	1120	525	586	496	1164	567	738	356	278	101	133	69	69	172
65	838	1013	1306	1204	1067	775	552	343	1954	2447	3314	2527	773	944	1460	1850	760	425
60	387	917	800	993	1301	1483	777	1209	727	785	1596	792	507	299	89	217	233	22
55	1477	1900	1342	1623	1723	2579	1877	1609	1582	1093	53	24	18	51	1037	18	9	7
50	4697	3744	4441	3046	3179	1658	1587	874	649	733	821	36	11	11	10	6	5	4
45	2239	3254	3524	3545	1984	3512	1641	535	1106	507	32	28	8	6	5	4	4	3
40	2483	5642	4153	3367	2829	2357	219	286	66	19	169	11	6	4	4	3	3	3
35	10936	11290	9391	5381	1366	322	69	24	30	289	42	7	4	4	3	3	3	3
30	10789	6985	9914	1153	2882	1077	804	18	12	9	6	5	4	3	3	2	2	2
25	421	1108	3997	2678	888	1306	145	14	8	6	4	4	3	3	2	2	2	2
20	59	533	1391	663	178	18	12	8	6	4	4	3	3	2	2	2	2	2
15	25	33	343	294	15	11	32	7	5	4	3	3	3	2	2	2	2	2
10	13	14	26	124	10	9	7	13	5	4	3	3	3	2	2	2	2	2
5	9	20	22	10	10	375	9	5	5	5	4	4	3	2	2	2	2	1
0	7	7	552	10	290	744	73	7	7	16	21	9	4	3	2	2	2	1
-5	5	5	8	411	8	6	17	6	7	83	2450	1385	384	6	2	2	2	1
-10	4	4	4	5	7	5	6	8	7	12	14	21	110	4	2	2	2	1
-15	3	3	3	4	4	6	8	81	171	137	9	379	5	3	2	2	2	2
-20	3	3	3	4	6	15	92	472	915	720	442	1451	10	3	3	2	2	2
-25	3	3	3	4	7	335	1442	1036	1282	586	199	696	436	5	3	2	2	2
-30	3	3	3	4	6	138	1028	526	391	368	170	246	794	4	3	3	2	2
-35	3	3	3	3	5	10	12	10	9	19	138	188	1069	4	3	3	3	5
-40	3	3	3	3	3	4	4	4	5	6	7	8	5	4	3	4	8	547
-45	3	3	3	3	3	3	4	4	4	4	4	4	4	3	4	13	1351	6
-50	4	4	4	4	4	4	4	4	4	4	4	4	4	3	3	4	4	3
-55	6	6	6	6	6	6	6	6	6	5	5	5	4	4	4	4	3	3
-60	12	13	14	14	14	14	13	13	12	11	10	9	8	7	6	5	4	4
-65	65	79	93	98	95	92	69	67	71	79	56	37	24	16	12	9	8	6
-70	2241	2312	2186	2396	2566	2629	2367	2055	2051	2410	2298	1571	1174	828	197	52	29	14
-75	3257	3398	2756	2598	2328	2758	2652	2716	2512	2108	2462	1963	1935	1515	158	43	43	24
-80	3257	3143	2868	2829	2571	2423	2708	2383	2297	2078	2135	2137	1746	1856	939	245	169	156
-85	2760	2362	2366	2665	2619	2689	2513	2324	2492	2518	2322	2309	2143	2468	2640	2572	2467	2435
-90	2216	2216	2216	2216	2216	2216	2216	2216	2216	2216	2216	2216	2216	2216	2216	2216	2216	2216

FIGURE 8.8a

Units: μN/kg

FIVE DEGREE MAP OF THE VERTICAL COMPONENT OF GRAVITY AT THE GEOID DUE TO THE TOPOGRAPHIC-ISOSTATIC MODEL

LAT	LON 180	185	190	195	200	205	210	215	220	225	230	235	240	245	250	255	260	265
90	9	9	9	9	9	9	9	9	9	9	9	9	9	9	9	9	9	9
85	7	7	7	7	7	8	8	8	8	9	9	10	11	11	13	14	16	18
80	7	7	7	7	7	8	8	8	8	9	9	10	11	13	17	23	40	228
75	9	9	9	10	11	11	12	12	12	13	14	18	14	45	34	27	37	29
70	43	20	19	42	353	373	188	622	231	56	98	82	53	128	573	315	26	458
65	99	208	28	239	696	729	729	1463	2556	2162	2568	553	711	795	998	687	440	260
60	12	9	10	36	973	823	539	449	1603	2641	2511	2087	1168	785	806	978	714	143
55	6	5	6	24	18	13	14	17	26	55	960	2206	2125	2016	1490	944	709	482
50	4	4	4	4	5	6	7	9	12	19	47	516	3007	3952	1846	1468	1086	795
45	3	3	3	3	3	4	4	5	6	8	12	23	89	2506	4587	5325	2689	1392	818
40	3	3	3	3	3	3	4	5	6	9	17	100	3403	4055	4768	4331	1659	788
35	2	2	2	2	2	3	3	4	5	7	11	26	1552	1941	3778	3746	1413	553
30	2	2	2	2	2	2	3	3	4	5	7	12	24	1063	2525	2892	1439	79
25	2	2	2	2	2	2	2	2	3	4	5	7	11	23	87	4476	3018	32
20	2	2	2	2	2	2	2	2	2	3	4	5	7	27	24	1116	4916	47
15	2	1	1	1	2	2	2	2	2	2	3	3	4	6	17	22	47	72
10	1	1	1	1	1	1	2	2	2	2	2	3	3	4	5	8	11	14
5	1	1	1	1	1	1	1	2	2	2	2	2	3	3	4	4	5	6
0	1	1	1	1	1	1	1	1	1	2	2	2	2	2	3	3	4	4
-5	1	1	1	1	1	1	1	1	1	1	2	2	2	2	2	3	3	4
-10	1	1	1	1	1	1	1	1	1	1	1	2	2	2	2	3	3	4
-15	1	1	1	1	1	1	1	1	1	1	1	2	2	2	2	2	3	4
-20	1	1	1	1	1	1	1	1	1	1	1	1	2	2	2	2	3	4
-25	2	1	1	1	1	1	1	1	1	1	1	1	2	2	2	2	3	4
-30	2	2	1	1	1	1	1	1	1	1	1	2	2	2	2	2	3	4
-35	3	2	2	1	1	1	1	1	1	1	1	1	2	2	2	2	2	3
-40	4	2	2	2	2	1	1	1	1	1	2	2	2	2	2	2	3	3
-45	3	2	2	2	2	2	2	2	2	2	2	2	2	2	2	2	3	3
-50	2	2	2	2	2	2	2	2	2	2	2	2	2	2	2	2	2	2
-55	3	3	2	2	2	2	2	2	2	2	2	2	2	2	2	3	3	3
-60	4	3	3	3	3	3	3	3	3	3	3	3	3	3	3	3	3	3
-65	6	5	4	4	4	4	4	4	4	4	4	4	4	4	4	4	4	5
-70	10	8	7	7	6	6	7	7	7	8	8	9	9	9	9	10	11	12
-75	17	15	14	15	16	17	22	48	148	299	1313	887	731	724	429	193	473	619
-80	106	109	110	181	266	234	281	355	479	690	817	974	1159	1390	1444	1801	2360	2747
-85	2112	1922	1805	1272	920	641	439	529	540	758	960	1209	1495	1914	2477	2435	1994	2229
-90	2216	2216	2216	2216	2216	2216	2216	2216	2216	2216	2216	2216	2216	2216	2216	2216	2216	2216

LAT	LON 270	275	280	285	290	295	300	305	310	315	320	325	330	335	340	345	350	355
90	9	9	9	9	9	9	9	9	9	9	9	9	9	9	9	9	9	9
85	20	23	26	28	29	30	30	31	32	32	32	32	30	28	25	22	19	17
80	1288	324	1188	1296	597	705	1607	2636	2964	3273	3217	2043	2157	1568	1154	143	53	31
75	111	507	160	33	34	48	102	1524	1837	1935	2506	4813	3787	419	68	33	21	21
70	29	144	59	691	528	33	32	86	910	1895	2032	2381	3479	937	61	28	17	13
65	422	161	18	44	751	219	31	54	958	2637	390	95	40	45	781	1239	18	11
60	19	15	20	421	237	203	22	20	43	251	35	15	10	9	9	9	9	12
55	297	138	36	727	1350	1272	326	17	9	8	7	6	5	5	6	7	17	248
50	1012	480	662	879	1132	125	52	35	7	5	4	4	4	5	5	6	10	33
45	923	702	465	310	611	188	14	7	5	4	4	4	4	4	5	8	17	40
40	467	762	922	244	13	7	5	4	4	3	3	3	4	4	6	9	40	1204
35	232	701	273	12	6	5	4	3	3	3	3	3	3	4	6	10	29	1623
30	23	27	11	6	5	4	3	3	3	3	3	3	3	4	6	14	257	1724
25	14	9	8	6	5	4	4	3	3	3	3	3	3	4	7	76	966	789
20	133	11	8	208	40	5	4	4	3	3	3	3	3	4	9	355	779	856
15	2894	633	11	11	11	8	5	4	4	3	3	3	3	4	8	228	573	861
10	14	206	20	156	1187	182	15	6	5	4	3	3	3	4	7	23	1009	826
5	9	13	28	4383	672	1624	1370	247	8	5	4	4	3	4	6	8	25	59
0	7	11	379	514	426	380	517	623	76	12	8	5	4	4	4	5	6	7
-5	7	11	2548	314	252	263	266	396	448	294	706	17	4	4	3	4	4	5
-10	7	12	102	4998	697	357	682	795	582	1294	799	8	5	4	3	3	4	5
-15	6	49	31	1788	8281	748	1201	1345	1041	1652	665	7	5	4	3	3	4	5
-20	6	10	51	34	1811	6039	678	958	1129	1739	209	6	5	4	3	3	4	4
-25	5	8	17	35	3379	2931	265	578	1660	15	8	6	4	3	3	3	3	4
-30	5	8	14	33	6791	1151	250	362	272	9	7	5	4	3	3	3	3	4
-35	5	7	12	41	5088	663	166	45	9	7	5	4	3	3	3	3	3	4
-40	4	7	10	33	1931	237	10	8	6	5	4	3	3	3	3	3	3	3
-45	4	6	8	32	1358	22	7	6	5	4	3	3	3	3	3	3	3	3
-50	4	5	6	178	556	7	6	5	4	4	3	3	3	3	3	3	3	3
-55	3	4	5	6	287	9	5	4	4	4	4	11	3	3	3	3	3	4
-60	4	4	5	5	6	5	5	5	4	4	4	4	4	4	4	4	5	5
-65	5	5	6	7	12	46	163	8	5	5	5	6	6	6	7	8	9	10
-70	11	12	12	31	1188	1722	-3	5	7	8	9	10	12	16	20	26	37	48
-75	1007	1060	875	1360	1411	1100	22	16	18	20	24	29	42	96	1201	2165	2456	2456
-80	2139	1757	686	208	131	178	148	164	435	530	169	228	773	1222	1794	2105	2167	2036
-85	1991	1655	1629	1547	2423	2565	2681	2462	2337	1991	2392	2354	2068	1855	1649	2021	1944	2395
-90	2216	2216	2216	2216	2216	2216	2216	2216	2216	2216	2216	2216	2216	2216	2216	2216	2216	2216

FIGURE 8.8b

Units: μN/kg

FIVE DEGREE MAP OF THE VERTICAL COMPONENT OF GRAVITY AT THE GEOID DUE TO THE TOPOGRAPHIC-ISOSTATIC MODEL

LAT	LON 0	5	10	15	20	25	30	35	40	45	50	55	60	65	70	75	80	85
90	9	9	9	9	9	9	9	9	9	9	9	9	9	9	9	9	9	9
85	15	14	13	12	11	10	10	9	9	9	8	8	8	8	8	8	8	8
80	23	22	53	130	89	36	27	12	10	13	15	9	8	8	9	9	9	11
75	15	13	12	11	11	10	10	9	9	10	13	52	8	25	14	13	16	25
70	11	12	16	33	179	162	116	30	16	14	16	18	22	29	-22	-12	-29	5
65	13	22	71	-284	-7	69	-28	55	82	96	-73	-7	-223	-15	-16	-17	-20	-4
60	17	146	183	-85	31	40	67	-84	13	-11	-6	-13	-28	-4	-22	-2	-8	5
55	27	16	39	37	33	5	16	61	-17	11	64	3	-96	32	42	5	66	17
50	38	-122	38	52	120	9	-15	-20	37	68	79	38	37	78	-1	21	80	-259
45	76	458	310	-321	101	30	47	25	55	72	44	88	59	76	141	123	183	299
40	292	37	117	154	-238	93	-122	-181	-453	-132	142	56	52	123	-347	267	258	151
35	-35	-106	47	26	24	-132	59	136	126	115	25	-22	-50	-66	-803	-103	-947	-538
30	-3	13	114	-5	68	-19	-11	61	-84	34	298	-46	-191	13	-30	137	700	-445
25	61	-282	-281	30	-10	-43	89	173	56	-26	30	106	110	121	16	137	97	193
20	-112	54	106	81	-20	-91	-71	-97	212	-91	-73	3	25	26	37	-184	-105	110
15	-27	-31	-18	80	75	-157	-22	-55	273	-659	188	16	14	17	18	23	68	21
10	42	7	-60	39	61	44	29	-241	18	-49	-196	13	11	10	11	12	24	12
5	35	42	44	-28	8	45	-18	53	-176	-12	18	11	8	8	8	9	10	9
0	12	21	88	-5	2	65	-218	-385	-8	19	13	9	7	6	6	6	6	6
-5	7	17	37	19	100	28	-86	-396	33	15	11	7	6	5	5	5	4	4
-10	7	22	32	28	176	96	-243	-161	44	14	10	7	5	4	4	4	4	4
-15	7	13	45	-165	-146	-163	-30	-291	52	21	101	6	5	4	4	3	3	3
-20	6	14	41	-298	-138	-341	-441	36	16	-37	11	5	5	4	3	3	3	3
-25	6	14	31	210	-169	-423	-154	28	13	28	7	5	4	3	3	3	3	3
-30	5	8	22	49	-89	-384	-144	13	10	7	6	4	4	3	3	3	3	3
-35	4	6	12	19	26	61	15	10	8	6	5	4	3	3	3	3	3	3
-40	4	5	6	8	10	10	8	7	5	5	4	3	3	3	3	3	3	3
-45	3	4	4	5	5	5	5	5	4	4	4	4	3	3	3	3	3	3
-50	3	4	4	4	4	4	4	4	4	4	4	4	4	4	19	4	4	4
-55	4	4	4	4	5	5	5	5	5	5	5	5	5	5	5	5	6	6
-60	5	5	6	6	6	7	7	8	9	9	10	10	10	10	10	11	11	12
-65	11	12	12	13	14	15	17	20	26	35	54	71	46	36	29	30	37	51
-70	59	89	102	104	101	103	98	3	124	-194	-220	73	40	-118	172	110	92	-7
-75	-113	106	-107	-238	-351	-183	22	15	-193	-104	182	-430	-33	144	-223	-296	-177	-195
-80	-220	-118	62	-240	113	2	130	-183	-203	-300	8	238	27	34	61	14	-665	-162
-85	173	-70	54	15	-210	-153	67	-133	-94	-156	-272	-105	-51	-142	-91	-74	55	35
-90	-68	-68	-68	-68	-68	-68	-68	-68	-68	-68	-68	-68	-68	-68	-68	-68	-68	-68

LAT	LON 90	95	100	105	110	115	120	125	130	135	140	145	150	155	160	165	170	175
90	9	9	9	9	9	9	9	9	9	9	9	9	9	9	9	9	9	9
85	8	7	7	7	7	7	7	7	7	7	7	7	7	7	7	7	7	7
80	81	-26	50	16	11	10	9	9	9	9	8	8	8	8	8	7	7	7
75	48	-43	-3	-61	28	33	20	18	17	16	40	21	13	12	11	10	10	10
70	36	-146	36	56	-44	72	16	95	-121	36	-40	12	-96	-29	54	52	69	81
65	-23	-42	-105	-39	-38	6	4	55	-285	-135	-499	-116	178	39	-28	-181	-56	24
60	25	5	46	-5	-18	-70	77	-20	58	92	17	41	209	100	69	101	71	22
55	-107	-61	105	-35	121	-83	45	-5	50	34	53	24	18	51	-149	18	9	7
50	-92	13	97	-410	-80	139	131	79	-10	69	-100	36	11	11	10	6	5	4
45	339	247	329	-78	294	-398	108	24	-26	-6	32	28	8	6	5	4	4	4
40	374	-472	173	67	80	-249	135	126	66	19	73	11	6	4	4	3	3	3
35	-408	-1079	-753	367	281	98	60	24	20	17	42	7	4	4	3	3	2	2
30	-838	690	-925	288	-227	-146	16	18	12	9	6	5	4	3	3	2	2	2
25	230	181	-33	218	12	-106	88	14	8	6	4	4	3	3	2	2	2	2
20	59	41	-75	-13	42	18	12	8	6	5	4	3	3	2	2	2	2	2
15	25	33	8	-17	15	11	33	7	5	4	3	3	3	2	2	2	2	2
10	13	14	20	13	10	9	7	13	5	4	3	3	3	2	2	2	2	2
5	9	31	29	10	10	60	9	5	5	5	5	4	3	2	2	2	2	1
0	7	7	19	10	-5	-98	56	7	7	16	21	9	4	3	2	2	2	1
-5	5	5	8	-19	8	6	17	6	7	78	-240	164	51	6	2	2	2	1
-10	4	4	4	5	7	4	6	8	7	12	14	21	64	4	2	2	2	1
-15	3	3	3	4	4	6	8	47	22	22	9	-176	5	3	2	2	2	2
-20	3	3	3	4	6	15	53	29	-27	-22	6	-248	10	3	3	2	2	2
-25	3	3	3	4	7	49	-89	-27	-40	25	5	-69	39	5	3	2	2	2
-30	3	3	3	4	6	86	-102	36	8	6	46	1	-143	4	3	3	2	2
-35	3	3	3	3	4	10	12	10	9	19	27	-8	-108	4	3	3	3	5
-40	3	3	3	3	3	4	4	4	5	6	7	8	5	4	3	4	8	-8
-45	3	3	3	3	3	3	4	4	4	4	4	4	4	3	4	13	-135	6
-50	4	4	4	4	4	4	4	4	4	4	4	4	4	3	3	4	4	3
-55	6	6	6	6	6	6	6	6	6	5	5	5	4	4	4	4	3	3
-60	12	13	14	14	14	14	13	13	12	11	10	9	8	7	6	5	4	4
-65	65	79	93	98	95	92	69	67	71	79	56	37	24	16	12	9	8	6
-70	214	192	206	152	346	71	57	220	201	-49	-76	12	69	56	142	52	29	14
-75	-105	-205	59	10	138	85	30	-88	-113	178	23	-183	-5	-93	-47	135	43	24
-80	-65	-43	11	-131	4	10	-242	-10	-18	116	9	-90	249	-44	-205	187	85	71
-85	-98	136	148	-76	20	-195	-70	101	17	-63	34	-73	49	-223	-331	-297	-273	-311
-90	-68	-68	-68	-68	-68	-68	-68	-68	-68	-68	-68	-68	-68	-68	-68	-68	-68	-68

FIGURE 8.9a

Units: μN/kg

FIVE DEGREE MAP OF THE VERTICAL COMPONENT OF GRAVITY AT THE EARTH'S SURFACE DUE TO THE TOPOGRAPHIC-ISOSTATIC MODEL

LAT	LON 180	185	190	195	200	205	210	215	220	225	230	235	240	245	250	255	260	265
90	9	9	9	9	9	9	9	9	9	9	9	9	9	9	9	9	9	9
85	7	7	7	7	7	8	8	8	8	9	9	10	11	11	13	14	16	18
80	7	7	7	7	7	8	8	8	8	9	9	10	11	13	17	23	40	194
75	9	9	9	10	11	11	12	12	12	13	14	18	24	32	34	27	31	29
70	43	20	19	42	76	50	118	154	110	56	60	58	53	35	-95	-43	26	-126
65	68	37	28	12	-95	8	110	-30	-202	28	-168	174	-80	29	-102	-22	-81	25
60	12	9	10	43	-181	-30	55	236	589	-187	-15	-192	53	64	-23	-36	20	37
55	6	5	6	24	18	13	14	17	26	55	303	52	52	-246	-74	54	-23	-3
50	4	4	4	4	5	6	7	9	12	19	47	516	-364	-449	106	27	-27	-10
45	3	3	3	3	4	4	5	6	8	12	23	89	-329	-328	-653	-94	-54	20
40	3	3	3	3	3	3	4	5	6	9	17	100	-33	58	14	149	89	32
35	2	2	2	2	2	3	3	4	5	7	11	26	-380	-45	50	-26	45	17
30	2	2	2	2	2	2	3	3	4	5	7	12	24	-139	-224	14	-92	43
25	2	2	2	2	2	2	2	2	3	4	5	7	11	23	87	-313	-354	32
20	2	2	2	2	2	2	2	2	2	3	4	5	7	27	24	129	-942	47
15	2	1	1	1	2	2	2	2	2	2	3	3	4	6	17	22	47	72
10	1	1	1	1	1	1	2	2	2	2	2	3	3	4	5	8	11	14
5	1	1	1	1	1	1	1	2	2	2	2	2	3	3	4	4	5	6
0	1	1	1	1	1	1	1	1	1	2	2	2	2	2	3	3	4	5
-5	1	1	1	1	1	1	1	1	1	1	2	2	2	2	2	3	3	4
-10	1	1	1	1	1	1	1	1	1	1	1	2	2	2	2	3	3	4
-15	1	1	1	1	1	1	1	1	1	1	1	2	2	2	2	2	3	4
-20	1	1	1	1	1	1	1	1	1	1	1	1	2	2	2	2	3	4
-25	2	1	1	1	1	1	1	1	1	1	1	1	2	2	2	2	3	4
-30	2	2	1	1	1	1	1	1	1	1	1	2	2	2	2	2	3	4
-35	3	2	2	1	1	1	1	1	1	1	1	2	2	2	2	2	3	3
-40	4	2	2	2	2	1	1	1	1	1	2	2	2	2	2	2	3	3
-45	3	2	2	2	2	2	2	2	2	2	2	2	2	2	2	2	3	3
-50	2	2	2	2	2	2	2	2	2	2	2	2	2	2	2	2	3	3
-55	3	3	2	2	2	2	2	2	2	2	2	2	2	2	2	3	3	3
-60	4	3	3	3	3	3	3	3	3	3	3	3	3	3	3	3	3	3
-65	6	5	4	4	4	4	4	4	4	4	4	4	4	4	4	4	4	5
-70	10	8	7	7	6	6	7	7	7	8	8	9	9	9	9	10	11	12
-75	17	15	14	15	16	17	22	48	81	142	-550	-203	-26	-225	68	108	-6	54
-80	42	43	44	22	-110	27	34	37	48	20	100	47	59	-40	111	106	-195	-536
-85	-245	-345	-501	-216	-175	-113	119	66	113	54	63	47	27	-28	-272	-295	35	-248
-90	-68	-68	-68	-68	-68	-68	-68	-68	-68	-68	-68	-68	-68	-68	-68	-68	-68	-68

LAT	LON 270	275	280	285	290	295	300	305	310	315	320	325	330	335	340	345	350	355
90	9	9	9	9	9	9	9	9	9	9	9	9	9	9	9	9	9	9
85	20	23	26	28	29	30	30	31	32	32	32	32	30	28	25	22	19	17
80	-159	222	2	82	77	132	-214	-369	-277	-357	-279	129	-118	7	-52	143	53	31
75	55	-42	126	33	34	48	102	-330	-61	-47	-1	-8	-771	-610	299	68	33	21
70	29	11	39	-118	-73	33	32	86	-28	-16	52	102	-420	209	61	28	17	13
65	-66	5	18	44	-57	98	31	54	65	-59	296	95	40	45	142	-186	18	11
60	19	15	20	-20	36	63	22	20	43	141	35	15	10	9	9	9	9	12
55	27	9	36	-6	-108	-124	13	17	9	8	7	6	5	5	6	7	17	-67
50	-92	20	-79	-25	-49	125	52	35	7	5	4	4	4	5	5	6	10	33
45	-31	-75	60	106	43	2	14	7	5	4	4	4	4	4	5	8	17	40
40	20	-26	5	22	13	7	5	4	4	3	3	3	4	4	6	9	40	238
35	13	47	36	12	6	4	4	3	3	3	3	3	3	4	6	10	29	-441
30	23	41	11	6	5	4	3	3	3	3	3	3	3	4	6	14	222	-57
25	14	9	8	6	5	4	4	3	3	3	3	3	3	4	7	50	-63	28
20	4	11	8	26	40	5	4	4	3	3	3	3	3	4	9	24	-44	-30
15	-622	99	11	11	11	8	5	4	4	3	3	3	3	4	8	10	-12	-55
10	14	67	20	82	-78	69	15	6	5	4	3	3	3	4	7	23	-31	23
5	9	13	28	-491	-16	-132	-156	24	8	5	4	4	3	4	6	8	25	48
0	7	11	149	95	0	20	-25	-4	29	12	8	5	4	4	4	5	6	7
-5	7	11	-174	58	15	7	2	7	29	29	-46	16	4	4	3	4	4	5
-10	7	12	102	-460	48	42	56	63	36	-100	-52	8	5	4	3	3	4	5
-15	6	49	31	540	-496	202	-59	-44	-83	-455	-38	7	5	4	3	3	4	4
-20	6	10	51	34	909	-233	26	-53	-105	-254	61	6	5	4	3	3	4	4
-25	5	8	17	35	197	159	12	-23	-229	15	8	6	4	3	3	3	3	4
-30	5	8	14	33	-996	29	-10	-46	59	9	7	5	4	3	3	3	3	4
-35	5	7	12	41	-1007	18	33	48	9	7	5	4	3	3	3	3	3	4
-40	4	7	10	33	-165	12	10	8	6	5	4	3	3	3	3	3	3	3
-45	4	6	8	30	-153	28	7	6	5	4	3	3	3	3	3	3	3	3
-50	4	5	6	52	-71	7	6	5	4	4	3	3	3	3	3	3	3	3
-55	3	4	5	6	-21	9	5	4	4	4	4	11	3	3	3	3	3	4
-60	4	4	5	5	6	5	5	5	4	4	4	4	4	4	4	4	5	5
-65	5	5	6	7	12	52	40	8	5	5	5	6	6	6	7	8	9	10
-70	11	12	12	31	-304	-478	-3	5	7	8	9	10	12	16	20	26	37	48
-75	-66	-125	-71	-363	-490	-249	22	16	18	20	24	29	42	96	-65	-151	-211	4
-80	-293	-379	-20	105	90	79	82	62	-81	-144	86	114	44	31	-92	-174	-91	57
-85	-165	3	20	151	-360	-387	-416	-300	-271	11	-339	-349	-292	-81	201	-48	93	-221
-90	-68	-68	-68	-68	-68	-68	-68	-68	-68	-68	-68	-68	-68	-68	-68	-68	-68	-68

FIGURE 8.9b

Units: μN/kg

FIVE DEGREE MAP OF THE VERTICAL COMPONENT OF GRAVITY AT THE EARTH'S SURFACE DUE TO THE TOPOGRAPHIC-ISOSTATIC MODEL

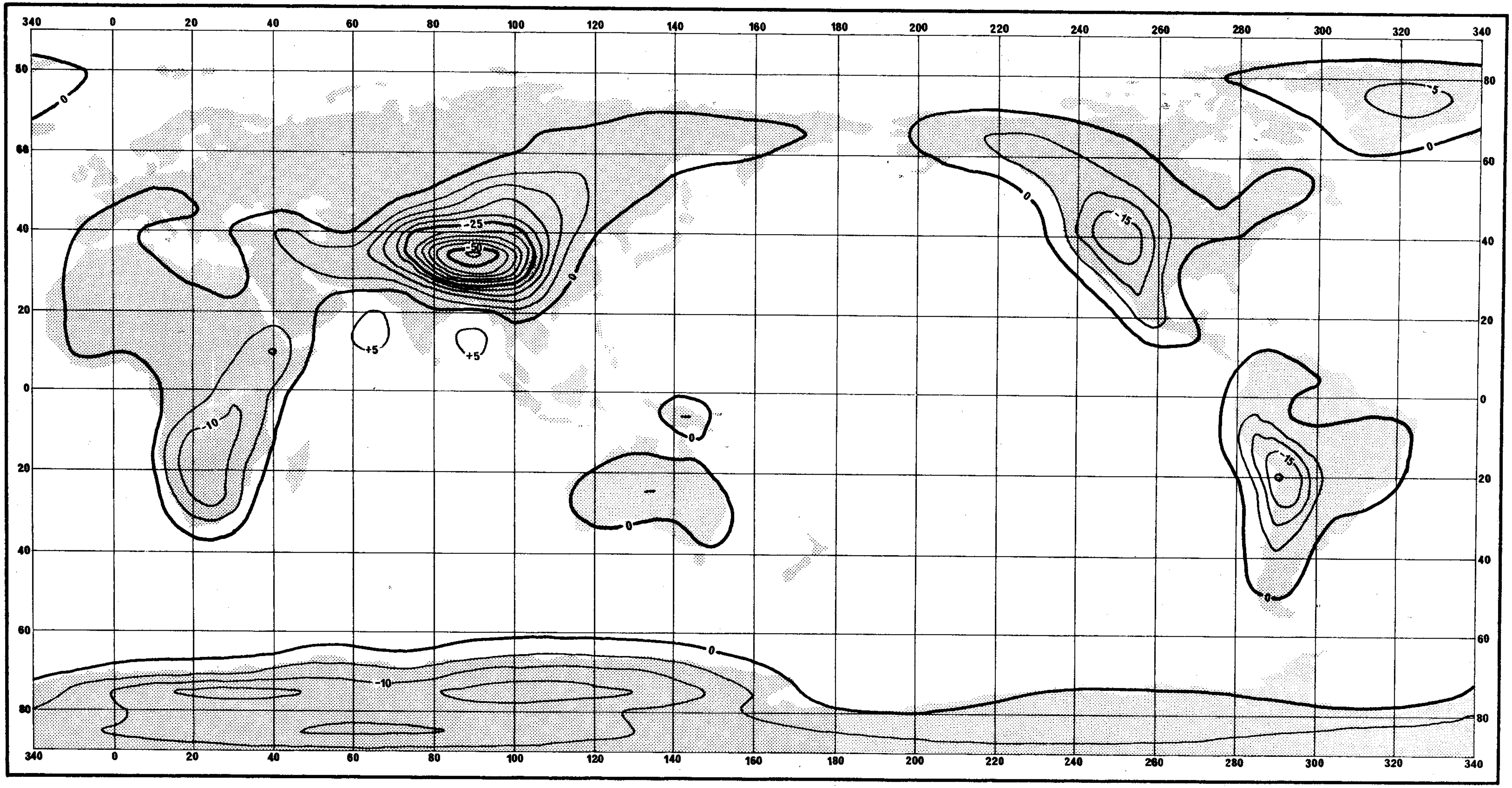

FIGURE 8.10

VERTICAL COMPONENT OF GRAVITY AT SATELLITE ORBIT ALTITUDE (1000 km)
DUE TO TOPOGRAPHIC-ISOSTATIC MODEL

Contour interval = 5 μN/kg
= 0.5 mgal

the computed results. There appears to be two prime factors which may contribute to the occurrence of the large positive values observed in the surface data:

(a) If the topographic gradients near the computation point are sufficiently large, the influence of nearby topography at a higher elevation than that of the point may predominate over the lower, but more distant, topography.

(b) The level at which the opposite global influences of the topography and the isostatic compensation cancel one another may be close to the elevation of the earth's surface, so that the attraction is strongly dependent on small variations in the height of the computation point.

Both factors will produce very localized effects. A more detailed investigation is deferred to the discussion of zone and source contributions below.

At orbital altitude, the vertical gravity again displays marked correlation with the continental masses (see figure 8.10). The maximum effect, in the Himalayas, is a value of -57 μN/kg (-5.7 mgal), whereas small positive values prevail over the oceans, due to the dominance of the isostatic compensation. This influence is greatest in the Arabian Sea and the Bay of Bengal, where two small "highs" of 6 μN/kg (0.6 mgal) occur.

EFFECTS ON THE HORIZONTAL COMPONENTS OF GRAVITY. Deflexions of the vertical at the earth's surface due to the topography and compensation model are illustrated in figure 8.11. Figures 8.12 and 8.13 are maps of the numerical results for the north and east components of the deflexion at the surface. Results at geoid level follow an almost identical pattern to that of the surface values with slight differences in magnitude. The deflexions appear to be strongly influenced by the local topography; indeed, when the zone contributions are considered (see below), the effect of the inner zone alone is seen usually to determine the size of the deflexions. Some quite large values are apparent in the results, but these are always associated with mountainous terrain. Furthermore—since they are highly dependent on the 5' mean elevations close to the computation point, and a large part of this data is simulated—care must be exercised in attempting to interpret specific results. However, deflexions up to 20" occur in areas of reliable topographic data (*e.g.* North America), suggesting that the calculated values which approach 40" in areas of more rugged terrain are not unreasonable, especially when the ameliorating effect of levelling any topographic gradient in the contact sub-zone is taken into account.

Resulting deflexions at satellite orbit altitude are mapped in figures 8.14 and 8.15. Correlation with the major topographic masses is, once again, evident. Both meridian and prime vertical components attain their largest values of -0.66" and +0.50" respectively in the Himalayas.

CONTRIBUTIONS TO THE TOPOGRAPHIC-ISOSTATIC EFFECT

The danger of attaching particular physical significance to the contributions of the separate zones to the total topographic-isostatic effect has already been mentioned (see §3.5). Nevertheless, the composition of the effect, in terms of zones and source materials, is of interest and may be of assistance in elucidating some general principles of behaviour from the results, provided that the arbitary nature of the zone boundaries and the limitations of the topographic-isostatic model are properly respected.

As it is not feasible to reproduce here all of the numeric data, the results for four representative points—referred to as A, B, C, and D and illustrated in figure 8.4—have been abstracted and are incorporated in tables 8.1 to 8.4. For each point the contributions from the inner, mid, and outer zones to the effects on the equipotential undulation, vertical gravity component, and meridian and prime vertical deflexions of the vertical are listed. The terminology used in subdividing the contributions according to source material require further explanation. The term "rock" refers to the contributions due to the terrestrial topography and compensation using the de Graaff-Hunter density model (equation 3.29). "Ice" is actually the ice correction necessary to allow for the over-estimation

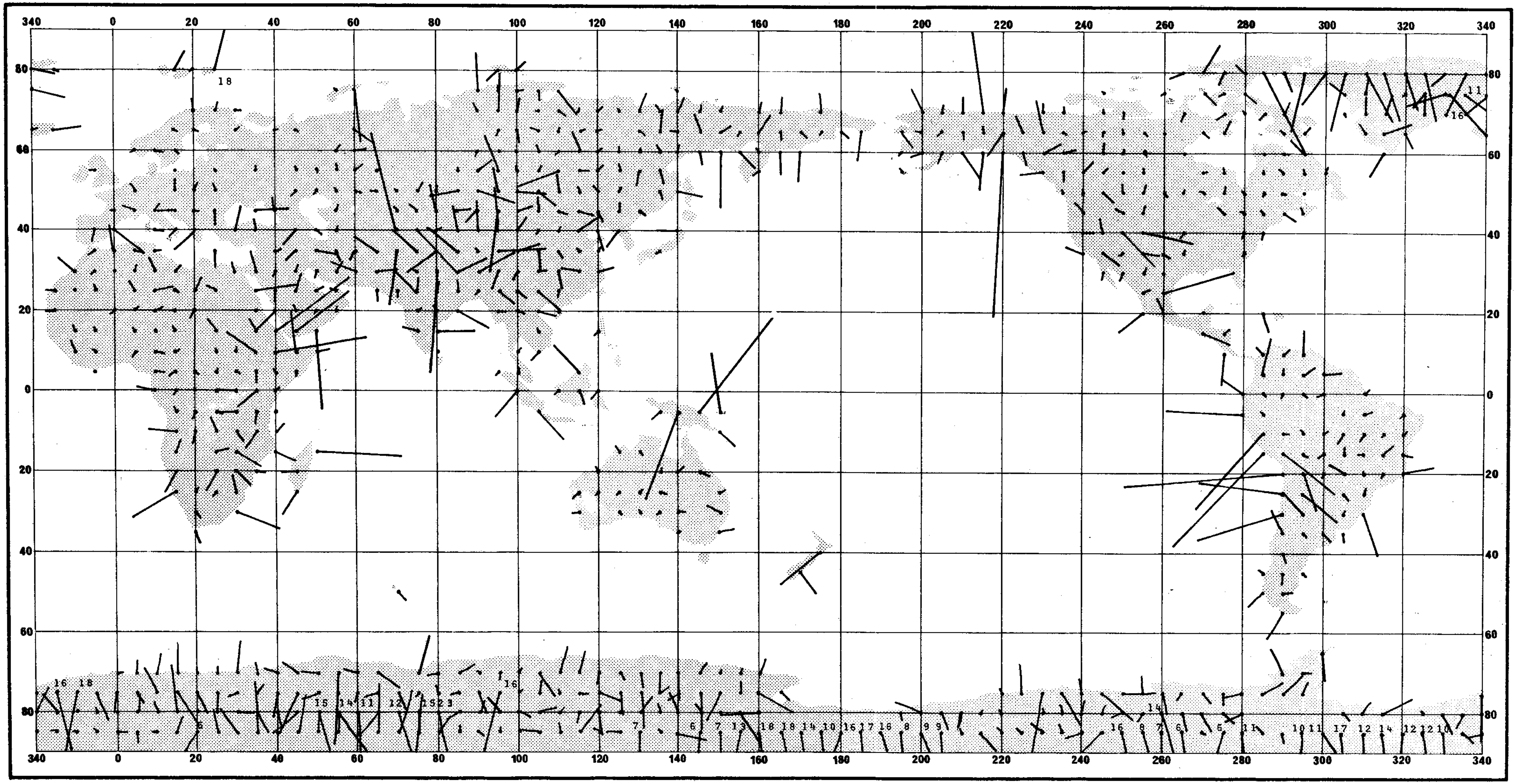

Vector scale: 1 cm = 10 arc seconds

FIGURE 8.11

DEFLEXIONS OF THE VERTICAL AT THE EARTH'S SURFACE DUE TO TOPOGRAPHIC-ISOSTATIC MODEL

LAT	LON 0	5	10	15	20	25	30	35	40	45	50	55	60	65	70	75	80	85
90	0	0	0	0	0	0	0	0	0	0	0	0	0	0	0	0	0	0
85	0	0	0	0	0	0	0	0	0	0	0	0	0	0	0	0	0	0
80	0	0	0	5	-1	16	0	0	0	0	0	0	0	0	0	0	0	0
75	0	0	0	0	0	0	0	0	0	0	0	0	-14	0	0	0	0	0
70	0	0	0	0	3	2	0	0	0	0	0	0	0	0	0	0	0	0
65	0	0	0	-1	0	0	0	0	1	0	0	0	-3	0	0	0	0	0
60	0	0	-1	0	0	0	0	0	0	0	0	1	0	0	0	0	0	0
55	0	0	0	-1	0	1	0	-1	0	1	-1	2	2	0	0	0	0	0
50	0	1	0	3	2	1	0	0	0	-1	-1	0	-1	0	0	2	1	-2
45	0	1	2	0	0	-4	0	0	4	0	0	1	0	0	1	1	7	1
40	-6	0	0	-2	-5	0	6	3	0	-4	-1	1	0	0	25	-11	0	6
35	6	-1	0	0	0	-4	0	0	0	-3	-1	-2	-3	4	-14	5	-6	6
30	-1	1	3	1	0	0	2	5	-1	1	-2	2	2	1	-6	0	-26	4
25	0	2	1	0	3	1	0	1	-3	4	1	0	0	-3	-1	3	3	3
20	0	0	0	0	-2	0	0	-1	-5	1	-1	1	0	0	0	0	1	-4
15	0	1	1	1	0	3	0	3	14	10	-20	0	0	0	0	1	0	0
10	0	-1	-1	0	0	1	1	5	4	10	1	0	0	0	0	0	0	0
5	0	0	0	-1	0	1	0	-3	-1	-1	0	0	0	0	0	0	0	0
0	0	0	1	0	0	1	0	-4	1	0	0	0	0	0	0	0	0	0
-5	0	0	0	1	-1	0	0	-3	0	0	0	0	0	0	0	0	0	0
-10	0	0	0	1	-4	3	-3	-4	2	0	0	0	0	0	0	0	0	0
-15	0	0	0	3	0	1	-4	0	-2	0	-1	0	0	0	0	0	0	0
-20	0	0	0	-6	0	-5	-4	0	0	0	0	0	0	0	0	0	0	0
-25	0	0	0	-7	0	-1	4	0	0	-6	0	0	0	0	0	0	0	0
-30	0	0	0	0	-1	0	-4	0	0	0	0	0	0	0	0	0	0	0
-35	0	0	0	0	-3	0	0	0	0	0	0	0	0	0	0	0	0	0
-40	0	0	0	0	0	0	0	0	0	0	0	0	0	0	0	0	0	0
-45	0	0	0	0	0	0	0	0	0	0	0	0	0	0	0	0	0	0
-50	0	0	0	0	0	0	0	0	0	0	0	0	0	0	-2	0	0	0
-55	0	0	0	0	0	0	0	0	0	0	0	0	0	0	0	0	0	0
-60	0	0	0	0	0	0	0	0	0	0	0	0	0	0	0	0	0	0
-65	0	0	0	0	0	0	0	0	0	0	0	0	0	0	0	0	0	0
-70	0	3	5	7	2	2	8	2	1	2	0	-6	1	-4	0	9	-1	2
-75	-5	-2	6	-7	-6	-4	-1	2	-6	-11	-1	-13	-3	-1	-6	-1	2	0
-80	10	5	3	12	5	1	0	-5	-3	-5	-15	-11	-11	-7	-11	-15	-23	-2
-85	0	-2	1	4	-5	5	6	13	11	10	6	6	7	13	11	10	4	2
-90	-3	-3	-3	-3	-3	-3	-3	-3	-3	-3	-3	-3	-3	-3	-3	-3	-3	-3

LAT	LON 90	95	100	105	110	115	120	125	130	135	140	145	150	155	160	165	170	175
90	0	0	0	0	0	0	0	0	0	0	0	0	0	0	0	0	0	0
85	0	0	0	0	0	0	0	0	0	0	0	0	0	0	0	0	0	0
80	0	-3	2	0	0	0	0	0	0	0	0	0	0	0	0	0	0	0
75	10	1	0	-3	-6	0	0	0	0	0	-1	0	0	0	0	0	0	0
70	2	11	3	0	-1	0	1	0	4	2	3	1	1	0	2	4	0	5
65	0	-1	-3	1	0	1	-1	0	-1	5	0	5	1	-1	4	-2	-2	0
60	-1	0	0	1	-1	5	0	1	0	2	2	-4	-15	-4	1	-6	-8	0
55	3	9	1	1	-4	0	1	2	-4	-4	0	0	0	0	-1	0	0	0
50	-3	6	-1	-3	5	2	1	1	0	-2	-2	0	0	0	0	0	0	0
45	-3	-16	1	3	-1	-1	-3	2	0	0	0	0	0	0	0	0	0	0
40	8	11	4	-1	1	3	-5	-4	0	0	0	0	0	0	0	0	0	0
35	0	1	2	-6	-2	0	1	0	0	0	0	0	0	0	0	0	0	0
30	5	-5	-3	0	-4	1	1	0	0	0	0	0	0	0	0	0	0	0
25	0	-3	-2	-5	-1	0	0	0	0	0	0	0	0	0	0	0	0	0
20	0	0	0	-1	7	0	0	0	0	0	0	0	0	0	0	0	0	0
15	0	0	0	1	0	0	-1	0	0	0	0	0	0	0	0	0	0	0
10	0	0	0	-2	0	0	0	0	0	0	0	0	0	0	0	0	0	0
5	0	-1	-1	0	0	7	0	0	0	0	0	0	0	0	0	0	0	0
0	0	0	-7	0	0	-3	-2	0	0	0	0	0	0	0	0	0	0	0
-5	0	0	0	-7	0	0	0	0	0	-2	-22	25	15	0	0	0	0	0
-10	0	0	0	0	0	0	0	0	0	0	0	0	-4	0	0	0	0	0
-15	0	0	0	0	0	0	0	1	0	0	0	0	0	0	0	0	0	0
-20	0	0	0	0	0	0	1	0	0	1	1	-1	0	0	0	0	0	0
-25	0	0	0	0	0	-1	0	0	1	-1	0	0	0	0	0	0	0	0
-30	0	0	0	0	0	0	0	0	-1	0	0	0	2	0	0	0	0	0
-35	0	0	0	0	0	0	0	0	0	0	0	0	1	0	0	0	0	0
-40	0	0	0	0	0	0	0	0	0	0	0	0	0	0	0	0	0	-9
-45	0	0	0	0	0	0	0	0	0	0	0	0	0	0	0	0	-5	0
-50	0	0	0	0	0	0	0	0	0	0	0	0	0	0	0	0	0	0
-55	0	0	0	0	0	0	0	0	0	0	0	0	0	0	0	0	0	0
-60	0	0	0	0	0	0	0	0	0	0	0	0	0	0	0	0	0	0
-65	0	0	0	0	0	0	0	0	0	0	0	0	0	0	0	0	0	0
-70	-1	-2	1	-7	7	5	-7	-2	-4	-6	-7	2	1	1	3	0	0	0
-75	-5	-15	-3	3	3	0	-2	-6	-8	1	-2	-9	-7	3	-5	-2	0	0
-80	2	4	-1	1	1	-3	-6	4	4	2	5	2	-2	-9	0	0	0	0
-85	-1	1	0	0	2	7	1	0	-7	-1	-2	-6	-7	-12	-18	-18	-14	-10
-90	-3	-3	-3	-3	-3	-3	-3	-3	-3	-3	-3	-3	-3	-3	-3	-3	-3	-3

FIGURE 8.12a

Units: arc seconds

FIVE DEGREE MAP OF THE MERIDIAN COMPONENT OF THE DEFLEXION OF THE VERTICAL AT THE EARTH'S SURFACE DUE TO THE TOPOGRAPHIC-ISOSTATIC MODEL

LAT	LON 180	185	190	195	200	205	210	215	220	225	230	235	240	245	250	255	260	265
90	0	0	0	0	0	0	0	0	0	0	0	0	0	0	0	0	0	0
85	0	0	0	0	0	0	0	0	0	0	0	0	0	0	0	0	0	0
80	0	0	0	0	0	0	0	0	0	0	0	0	0	0	0	0	0	-2
75	0	0	0	0	0	0	0	0	0	0	0	0	0	-1	0	0	-1	0
70	0	0	0	0	6	2	4	20	6	0	2	1	0	1	-2	0	0	-2
65	-2	-7	0	-4	0	-1	-2	2	-6	4	9	0	4	1	1	0	1	0
60	0	0	0	0	-1	-3	-7	-10	-42	-4	2	1	0	2	0	0	0	0
55	0	0	0	0	0	0	0	0	0	0	-1	-2	3	1	0	1	0	0
50	0	0	0	0	0	0	0	0	0	0	0	-1	2	-2	2	2	-1	1
45	0	0	0	0	0	0	0	0	0	0	0	0	3	0	1	2	0	0
40	0	0	0	0	0	0	0	0	0	0	0	0	0	4	-9	-3	1	-1
35	0	0	0	0	0	0	0	0	0	0	0	0	1	-3	0	-1	-1	1
30	0	0	0	0	0	0	0	0	0	0	0	0	0	-2	-2	1	-1	0
25	0	0	0	0	0	0	0	0	0	0	0	0	0	0	0	0	6	0
20	0	0	0	0	0	0	0	0	0	0	0	0	0	0	0	-5	3	0
15	0	0	0	0	0	0	0	0	0	0	0	0	0	0	0	0	0	0
10	0	0	0	0	0	0	0	0	0	0	0	0	0	0	0	0	0	0
5	0	0	0	0	0	0	0	0	0	0	0	0	0	0	0	0	0	0
0	0	0	0	0	0	0	0	0	0	0	0	0	0	0	0	0	0	0
-5	0	0	0	0	0	0	0	0	0	0	0	0	0	0	0	0	0	0
-10	0	0	0	0	0	0	0	0	0	0	0	0	0	0	0	0	0	0
-15	0	0	0	0	0	0	0	0	0	0	0	0	0	0	0	0	0	0
-20	0	0	0	0	0	0	0	0	0	0	0	0	0	0	0	0	0	0
-25	0	0	0	0	0	0	0	0	0	0	0	0	0	0	0	0	0	0
-30	0	0	0	0	0	0	0	0	0	0	0	0	0	0	0	0	0	0
-35	0	0	0	0	0	0	0	0	0	0	0	0	0	0	0	0	0	0
-40	0	0	0	0	0	0	0	0	0	0	0	0	0	0	0	0	0	0
-45	0	0	0	0	0	0	0	0	0	0	0	0	0	0	0	0	0	0
-50	0	0	0	0	0	0	0	0	0	0	0	0	0	0	0	0	0	0
-55	0	0	0	0	0	0	0	0	0	0	0	0	0	0	0	0	0	0
-60	0	0	0	0	0	0	0	0	0	0	0	0	0	0	0	0	0	0
-65	0	0	0	0	0	0	0	0	0	0	0	0	0	0	0	0	0	0
-70	0	0	0	0	0	0	0	0	0	0	0	0	0	0	0	0	0	0
-75	0	0	0	0	0	0	0	0	4	7	-14	-8	4	-7	0	4	-5	-1
-80	0	0	0	-2	2	-4	-2	-1	0	0	1	2	3	2	-1	-2	-14	-3
-85	-16	-17	-15	-8	-8	-9	1	-5	1	1	2	2	-1	-5	-15	-7	-7	-5
-90	-3	-3	-3	-3	-3	-3	-3	-3	-3	-3	-3	-3	-3	-3	-3	-3	-3	-3

LAT	LON 270	275	280	285	290	295	300	305	310	315	320	325	330	335	340	345	350	355
90	0	0	0	0	0	0	0	0	0	0	0	0	0	0	0	0	0	0
85	0	0	0	0	0	0	0	0	0	0	0	0	0	0	0	0	0	0
80	7	-3	2	-21	-5	-15	-8	-15	-12	-12	-9	-12	-3	0	-1	0	0	0
75	-3	-1	-2	0	0	0	0	3	5	0	0	-4	-3	-6	-2	0	0	0
70	0	-2	-1	-1	3	0	0	0	9	4	0	6	11	11	0	0	0	0
65	-1	3	0	0	1	1	0	0	3	3	-4	0	0	0	11	1	0	0
60	0	0	0	0	0	3	0	0	0	-6	0	0	0	0	0	0	0	0
55	1	1	0	0	1	1	1	0	0	0	0	0	0	0	0	0	0	0
50	1	2	1	1	-1	-1	0	0	0	0	0	0	0	0	0	0	0	0
45	0	1	0	1	-2	2	0	0	0	0	0	0	0	0	0	0	0	0
40	0	0	-1	-2	0	0	0	0	0	0	0	0	0	0	0	0	0	-3
35	0	0	-1	0	0	0	0	0	0	0	0	0	0	0	0	0	0	-1
30	0	0	0	0	0	0	0	0	0	0	0	0	0	0	0	0	4	-1
25	0	0	0	0	0	0	0	0	0	0	0	0	0	0	0	0	-1	1
20	0	0	0	-5	0	0	0	0	0	0	0	0	0	0	0	-1	0	0
15	-3	1	0	0	0	0	0	0	0	0	0	0	0	0	0	0	1	1
10	0	-8	0	2	1	6	0	0	0	0	0	0	0	0	0	0	2	1
5	0	0	0	9	1	2	0	0	0	0	0	0	0	0	0	0	0	-2
0	0	0	4	-1	-1	-1	0	0	1	0	0	0	0	0	0	0	0	0
-5	0	0	1	0	0	0	0	1	0	0	-1	0	0	0	0	0	0	0
-10	0	0	0	-20	0	1	1	-2	-1	0	1	0	0	0	0	0	0	0
-15	0	0	0	-24	-10	-1	0	2	0	2	-1	0	0	0	0	0	0	0
-20	0	0	0	0	-4	-9	0	2	-1	-1	1	0	0	0	0	0	0	0
-25	0	0	0	0	3	-7	0	-1	1	0	0	0	0	0	0	0	0	0
-30	0	0	0	0	-7	5	0	-1	-11	0	0	0	0	0	0	0	0	0
-35	0	0	0	0	6	0	-2	-2	0	0	0	0	0	0	0	0	0	0
-40	0	0	0	0	-2	0	0	0	0	0	0	0	0	0	0	0	0	0
-45	0	0	0	1	-3	-1	0	0	0	0	0	0	0	0	0	0	0	0
-50	0	0	0	-3	0	0	0	0	0	0	0	0	0	0	0	0	0	0
-55	0	0	0	0	-7	0	0	0	0	0	0	0	0	0	0	0	0	0
-60	0	0	0	0	0	0	0	0	0	0	0	0	0	0	0	0	0	0
-65	0	0	0	0	0	0	-7	0	0	0	0	0	0	0	0	0	0	0
-70	0	0	0	0	6	0	0	0	0	0	0	0	0	0	0	0	0	0
-75	-2	-3	-1	3	5	3	0	0	0	0	0	0	0	0	-12	-16	-18	-8
-80	-5	-2	-2	0	0	0	0	-2	3	4	0	0	-5	-4	6	4	1	1
-85	1	-6	-11	1	-3	-10	-9	-17	-12	-14	-12	-11	-10	-2	-1	0	0	1
-90	-3	-3	-3	-3	-3	-3	-3	-3	-3	-3	-3	-3	-3	-3	-3	-3	-3	-3

FIGURE 8.12b

Units: arc seconds

FIVE DEGREE MAP OF THE MERIDIAN COMPONENT OF THE DEFLEXION OF THE VERTICAL AT THE EARTH'S SURFACE DUE TO THE TOPOGRAPHIC-ISOSTATIC MODEL

LAT	LON 0	5	10	15	20	25	30	35	40	45	50	55	60	65	70	75	80	85
90	0	0	0	0	0	0	0	0	0	0	0	0	0	0	0	0	0	0
85	0	0	0	0	0	0	0	0	0	0	0	0	0	0	0	0	0	0
80	0	0	0	3	-1	4	0	0	0	0	0	0	0	0	0	0	0	0
75	0	0	0	0	0	0	0	0	0	0	0	-1	1	0	0	0	0	0
70	0	0	0	0	0	1	1	0	0	0	0	0	0	0	0	0	0	0
65	0	0	0	1	1	0	1	0	-1	0	0	0	4	0	0	0	0	0
60	0	-1	2	1	0	0	0	0	0	0	0	1	3	0	0	0	0	0
55	0	0	0	0	0	0	0	0	0	0	1	0	2	1	0	0	0	-1
50	0	-1	0	0	1	-1	0	0	0	-1	-1	-1	1	-1	-1	2	0	-7
45	-1	-3	1	-5	1	0	0	10	0	0	0	0	0	0	-1	-2	-2	4
40	7	0	1	-1	-6	0	1	-1	0	-4	1	0	0	0	-6	11	1	-1
35	-1	3	2	0	0	0	0	0	1	-3	6	1	-1	-6	-2	-7	-8	-8
30	0	0	-2	1	0	0	-1	-1	0	0	0	1	-7	5	5	-1	-2	8
25	0	-1	5	-1	1	-2	0	10	0	1	2	-1	0	0	0	0	0	-1
20	-1	1	2	-1	-1	0	0	0	-5	-1	-1	0	0	0	0	1	-1	8
15	0	-1	0	-1	0	-2	0	-2	19	13	1	0	0	0	0	-4	9	0
10	0	-1	2	1	0	0	0	-8	23	-2	3	0	0	0	0	0	0	0
5	0	0	2	-2	-1	1	1	0	0	0	0	0	0	0	0	0	0	0
0	0	0	-5	2	0	-1	-6	-5	1	0	0	0	0	0	0	0	0	0
-5	0	0	0	0	0	1	-5	0	0	0	0	0	0	0	0	0	0	0
-10	0	0	0	-7	-1	-1	2	-3	2	0	0	0	0	0	0	0	0	0
-15	0	0	0	1	0	3	6	0	4	0	21	0	0	0	0	0	0	0
-20	0	0	0	-3	0	-3	4	2	0	-4	0	0	0	0	0	0	0	0
-25	0	0	0	-11	0	0	-1	0	0	-4	0	0	0	0	0	0	0	0
-30	0	0	0	0	1	0	11	0	0	0	0	0	0	0	0	0	0	0
-35	0	0	0	0	1	0	0	0	0	0	0	0	0	0	0	0	0	0
-40	0	0	0	0	0	0	0	0	0	0	0	0	0	0	0	0	0	0
-45	0	0	0	0	0	0	0	0	0	0	0	0	0	0	0	0	0	0
-50	0	0	0	0	0	0	0	0	0	0	0	0	0	0	2	0	0	0
-55	0	0	0	0	0	0	0	0	0	0	0	0	0	0	0	0	0	0
-60	0	0	0	0	0	0	0	0	0	0	0	0	0	0	0	0	0	0
-65	0	0	0	0	0	0	0	0	0	0	0	0	0	0	0	0	0	0
-70	1	0	1	0	0	0	1	0	-4	-4	-4	0	-4	5	0	3	-3	4
-75	0	2	-3	5	2	0	-2	1	-1	-5	-3	-1	-1	-5	2	-1	-1	-2
-80	-1	1	-1	-1	1	0	4	3	1	-6	5	8	1	-6	4	-1	4	-3
-85	3	0	-1	1	-3	-1	-5	-1	0	2	1	0	-1	0	3	0	3	0
-90	0	0	0	0	0	0	0	0	0	0	0	0	0	0	0	0	0	0

LAT	LON 90	95	100	105	110	115	120	125	130	135	140	145	150	155	160	165	170	175
90	0	0	0	0	0	0	0	0	0	0	0	0	0	0	0	0	0	0
85	0	0	0	0	0	0	0	0	0	0	0	0	0	0	0	0	0	0
80	0	-3	2	0	0	0	0	0	0	0	0	0	0	0	0	0	0	0
75	0	0	1	0	5	0	0	0	0	0	1	0	0	0	0	0	0	0
70	-2	1	0	-1	2	-1	1	0	2	-1	1	0	1	0	0	0	0	0
65	0	-1	0	-2	0	1	1	0	1	1	-3	-2	3	-1	3	0	2	-1
60	-1	1	1	-1	-1	-3	1	0	1	-1	0	1	0	4	-1	0	0	0
55	4	-4	0	1	-10	2	1	0	-1	1	0	0	0	0	-2	0	0	0
50	9	-1	8	5	-1	-1	0	0	1	6	0	0	0	0	0	0	0	0
45	-3	-2	4	0	2	4	1	0	1	0	0	0	0	0	0	0	0	0
40	0	-1	2	-1	0	5	1	-3	0	0	-6	0	0	0	0	0	0	0
35	1	12	6	1	1	0	1	0	0	-1	0	0	0	0	0	0	0	0
30	9	-2	-1	2	1	-4	4	0	0	0	0	0	0	0	0	0	0	0
25	-1	4	2	5	0	0	0	0	0	0	0	0	0	0	0	0	0	0
20	0	1	1	4	1	0	0	0	0	0	0	0	0	0	0	0	0	0
15	0	0	0	0	0	0	-1	0	0	0	0	0	0	0	0	0	0	0
10	0	0	0	-2	0	0	0	0	0	0	0	0	0	0	0	0	0	0
5	0	-1	-1	0	0	-7	0	0	0	0	0	0	0	0	0	0	0	0
0	0	0	-6	0	-1	1	-2	0	0	0	0	0	0	0	0	0	0	0
-5	0	0	0	0	0	0	0	0	0	-2	-9	19	-2	0	0	0	0	0
-10	0	0	0	0	0	0	0	0	0	0	0	0	4	0	0	0	0	0
-15	0	0	0	0	0	0	0	-1	0	0	0	0	0	0	0	0	0	0
-20	0	0	0	0	0	0	0	0	0	0	1	3	0	0	0	0	0	0
-25	0	0	0	0	0	-1	0	-1	1	2	0	0	1	0	0	0	0	0
-30	0	0	0	0	0	-2	0	1	0	-1	2	0	-3	0	0	0	0	0
-35	0	0	0	0	0	0	0	0	0	0	0	0	3	0	0	0	0	0
-40	0	0	0	0	0	0	0	0	0	0	0	0	0	0	0	0	0	-10
-45	0	0	0	0	0	0	0	0	0	0	0	0	0	0	0	0	4	0
-50	0	0	0	0	0	0	0	0	0	0	0	0	0	0	0	0	0	0
-55	0	0	0	0	0	0	0	0	0	0	0	0	0	0	0	0	0	0
-60	0	0	0	0	0	0	0	0	0	0	0	0	0	0	0	0	0	0
-65	0	0	0	0	0	0	0	0	0	0	0	0	0	0	0	0	0	0
-70	0	0	0	4	2	1	0	1	1	0	0	1	0	1	1	0	0	0
-75	2	-4	0	1	-1	2	5	1	1	2	-3	0	-3	0	8	2	0	0
-80	2	-3	3	4	1	-1	1	-1	3	-1	-3	-2	2	6	-11	0	0	0
-85	1	0	0	-5	0	5	-2	-4	-1	0	7	-1	0	-3	1	5	2	2
-90	0	0	0	0	0	0	0	0	0	0	0	0	0	0	0	0	0	0

FIGURE 8.13a

Units: arc seconds

FIVE DEGREE MAP OF THE PRIME VERTICAL COMPONENT OF THE DEFLEXION OF THE VERTICAL AT THE EARTH'S SURFACE DUE TO THE TOPOGRAPHIC-ISOSTATIC MODEL

LAT	LON 180	185	190	195	200	205	210	215	220	225	230	235	240	245	250	255	260	265
90	0	0	0	0	0	0	0	0	0	0	0	0	0	0	0	0	0	0
85	0	0	0	0	0	0	0	0	0	0	0	0	0	0	0	0	0	0
80	0	0	0	0	0	0	0	0	0	0	0	0	0	0	0	0	0	-4
75	0	0	0	0	0	0	0	0	0	0	0	0	0	0	0	0	-1	0
70	0	0	0	0	-3	0	0	-3	1	0	0	0	0	0	0	0	0	-1
65	2	-1	0	3	-1	-1	0	0	-4	-2	-2	1	0	0	0	1	0	0
60	0	0	0	-1	-3	-1	5	-1	-2	1	5	3	0	0	-1	1	0	1
55	0	0	0	0	0	0	0	0	0	0	-6	0	3	1	1	0	0	0
50	0	0	0	0	0	0	0	0	0	0	0	0	1	2	0	1	1	0
45	0	0	0	0	0	0	0	0	0	0	0	0	0	-2	0	-2	1	0
40	0	0	0	0	0	0	0	0	0	0	0	0	3	-1	9	13	0	-1
35	0	0	0	0	0	0	0	0	0	0	0	0	-4	4	-1	4	1	0
30	0	0	0	0	0	0	0	0	0	0	0	0	0	-1	-1	1	0	0
25	0	0	0	0	0	0	0	0	0	0	0	0	0	0	0	1	18	0
20	0	0	0	0	0	0	0	0	0	0	0	0	0	0	0	-6	-2	0
15	0	0	0	0	0	0	0	0	0	0	0	0	0	0	0	0	0	0
10	0	0	0	0	0	0	0	0	0	0	0	0	0	0	0	0	0	0
5	0	0	0	0	0	0	0	0	0	0	0	0	0	0	0	0	0	0
0	0	0	0	0	0	0	0	0	0	0	0	0	0	0	0	0	0	0
-5	0	0	0	0	0	0	0	0	0	0	0	0	0	0	0	0	0	0
-10	0	0	0	0	0	0	0	0	0	0	0	0	0	0	0	0	0	0
-15	0	0	0	0	0	0	0	0	0	0	0	0	0	0	0	0	0	0
-20	0	0	0	0	0	0	0	0	0	0	0	0	0	0	0	0	0	0
-25	0	0	0	0	0	0	0	0	0	0	0	0	0	0	0	0	0	0
-30	0	0	0	0	0	0	0	0	0	0	0	0	0	0	0	0	0	0
-35	0	0	0	0	0	0	0	0	0	0	0	0	0	0	0	0	0	0
-40	0	0	0	0	0	0	0	0	0	0	0	0	0	0	0	0	0	0
-45	0	0	0	0	0	0	0	0	0	0	0	0	0	0	0	0	0	0
-50	0	0	0	0	0	0	0	0	0	0	0	0	0	0	0	0	0	0
-55	0	0	0	0	0	0	0	0	0	0	0	0	0	0	0	0	0	0
-60	0	0	0	0	0	0	0	0	0	0	0	0	0	0	0	0	0	0
-65	0	0	0	0	0	0	0	0	0	0	0	0	0	0	0	0	0	0
-70	0	0	0	0	0	0	0	0	0	0	0	0	0	0	0	0	0	0
-75	0	0	0	0	0	0	0	0	0	-1	-2	5	-1	8	8	0	1	-1
-80	0	0	0	1	-7	2	1	0	0	0	0	-1	1	1	-2	-1	4	1
-85	-5	2	5	1	3	0	-1	4	-1	-1	-3	-1	-4	-5	3	3	-1	1
-90	0	0	0	0	0	0	0	0	0	0	0	0	0	0	0	0	0	0

LAT	LON 270	275	280	285	290	295	300	305	310	315	320	325	330	335	340	345	350	355
90	0	0	0	0	0	0	0	0	0	0	0	0	0	0	0	0	0	0
85	0	0	0	0	0	0	0	0	0	0	0	0	0	0	0	0	0	0
80	4	-1	-2	11	2	-4	-6	-4	7	4	4	3	-4	0	6	1	0	0
75	3	-2	3	0	0	0	0	-4	1	0	-1	-3	-10	9	8	0	0	0
70	0	-2	0	-1	1	0	0	-1	0	2	0	0	6	14	0	0	0	0
65	2	2	0	0	-1	1	0	0	-2	7	2	0	0	0	-10	7	0	0
60	0	0	0	-1	1	-4	0	0	0	-4	0	0	0	0	0	0	0	0
55	0	0	0	-1	-1	0	1	0	0	0	0	0	0	0	0	0	0	-1
50	0	1	0	0	1	0	0	0	0	0	0	0	0	0	0	0	0	0
45	0	-2	-1	0	3	-1	0	0	0	0	0	0	0	0	0	0	0	0
40	0	0	0	0	0	0	0	0	0	0	0	0	0	0	0	0	0	-1
35	0	0	0	0	0	0	0	0	0	0	0	0	0	0	0	0	0	-2
30	0	0	0	0	0	0	0	0	0	0	0	0	0	0	0	0	-4	-1
25	0	0	0	0	0	0	0	0	0	0	0	0	0	0	0	-2	0	0
20	-1	0	0	1	0	0	0	0	0	0	0	0	0	0	0	-2	0	0
15	7	1	0	0	0	0	0	0	0	0	0	0	0	0	0	0	0	0
10	0	0	0	-2	1	0	0	0	0	0	0	0	0	0	0	0	-1	1
5	0	0	0	2	0	3	4	0	0	0	0	0	0	0	0	0	0	0
0	0	0	-6	0	0	1	-2	0	1	0	0	0	0	0	0	0	0	0
-5	0	0	-20	-1	0	0	0	0	1	0	-1	0	0	0	0	0	0	0
-10	0	0	0	-17	1	-1	1	-1	0	1	0	0	0	0	0	0	0	0
-15	0	0	0	-23	13	1	-1	1	-1	2	2	0	0	0	0	0	0	0
-20	0	0	0	0	-41	4	0	-3	0	-1	8	0	0	0	0	0	0	0
-25	0	0	0	0	-22	9	0	1	1	0	0	0	0	0	0	0	0	0
-30	0	0	0	0	-22	-5	0	0	4	0	0	0	0	0	0	0	0	0
-35	0	0	0	0	-3	0	2	0	0	0	0	0	0	0	0	0	0	0
-40	0	0	0	0	1	0	0	0	0	0	0	0	0	0	0	0	0	0
-45	0	0	0	-1	0	1	0	0	0	0	0	0	0	0	0	0	0	0
-50	0	0	0	-4	2	0	0	0	0	0	0	0	0	0	0	0	0	0
-55	0	0	0	0	-4	0	0	0	0	0	0	0	0	0	0	0	0	0
-60	0	0	0	0	0	0	0	0	0	0	0	0	0	0	0	0	0	0
-65	0	0	0	0	0	0	0	0	0	0	0	0	0	0	0	0	0	0
-70	0	0	0	0	-3	1	0	0	0	0	0	0	0	0	0	0	0	0
-75	2	0	-5	5	5	1	0	0	0	0	0	0	0	0	0	4	-3	3
-80	3	3	-5	0	0	0	0	1	2	7	0	-1	3	-2	3	-3	0	0
-85	0	-1	2	-1	1	-1	6	1	1	1	-1	2	1	2	-4	-1	-1	-1
-90	0	0	0	0	0	0	0	0	0	0	0	0	0	0	0	0	0	0

FIGURE 8.13b

Units: arc seconds

FIVE DEGREE MAP OF THE PRIME VERTICAL COMPONENT OF THE DEFLEXION OF THE VERTICAL AT THE EARTH'S SURFACE DUE TO THE TOPOGRAPHIC-ISOSTATIC MODEL

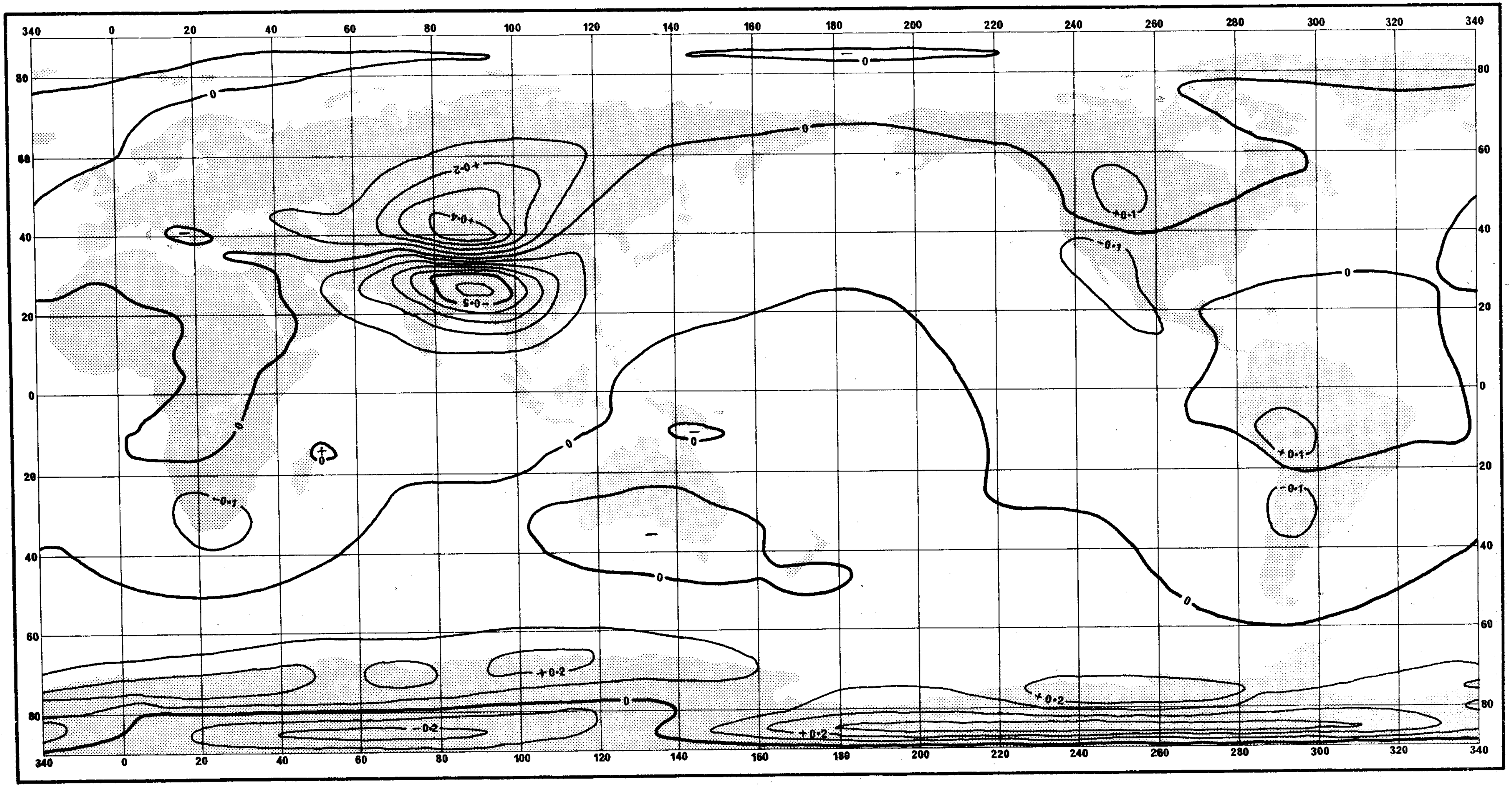

FIGURE 8.14

MERIDIAN COMPONENT OF THE DEFLEXION OF THE VERTICAL AT SATELLITE ORBIT ALTITUDE (1000 km) DUE TO TOPOGRAPHIC-ISOSTATIC MODEL

Contour interval = 0.1 arc secs.

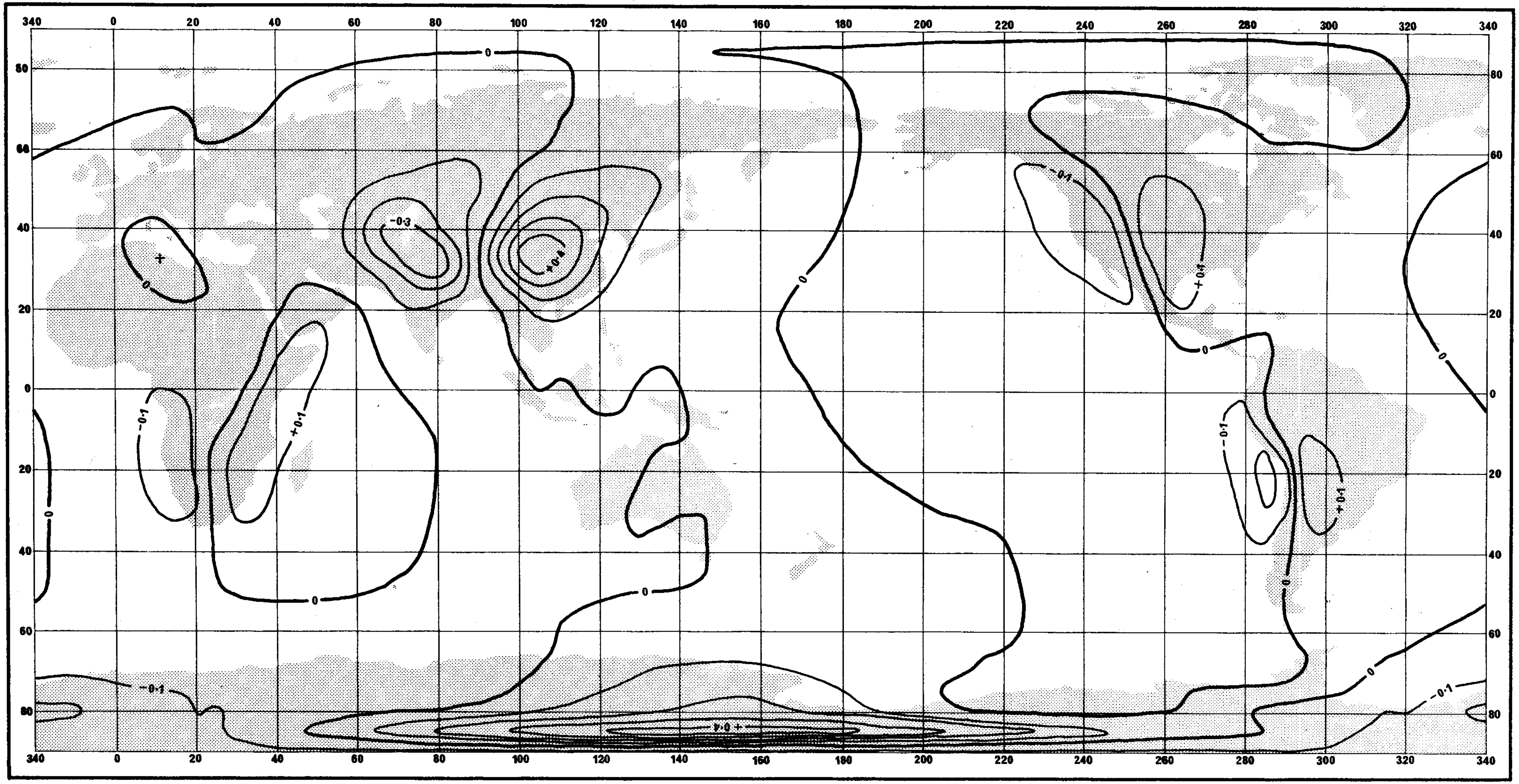

FIGURE 8.15

PRIME VERTICAL COMPONENT OF THE DEFLEXION OF THE VERTICAL AT SATELLITE ORBIT ALTITUDE (1000 km) DUE TO THE TOPOGRAPHIC-ISOSTATIC MODEL

Contour interval = 0.1 arc seconds

TABLE 8.1

CONTRIBUTIONS TO THE TOPOGRAPHIC-ISOSTATIC EFFECTS AT POINT (A)

Himalayas: Lat. = 30°N, Long. = 85°E, Height = 4982 m

EFFECT	LEVEL	SOURCE	INNER	MID	OUTER	TOTAL
EQUIPOTENTIAL UNDULATIONS (metres)	Geoid (0 m)	Rock	18.491	1.904	-1.095	19.301
		Ice	0	0	0.089	0.089
		Contact	0.005	--	--	0.005
		Total	18.497	1.904	-1.006	19.395
	Surface (4982 m)	Rock	20.398	2.639	-1.079	21.957
		Ice	0	0	0.088	0.088
		Contact	-0.004	--	--	-0.004
		Total	20.393	2.639	-0.991	22.041
	Orbit (1000 km)	Rock	--	--	--	4.569
		Ice	--	--	--	0.072
		Total	--	--	--	4.642
VERTICAL GRAVITY (μN/kg)	Geoid (0 m)	Rock	9348.87	1466.06	30.02	10 844.95
		Ice	0	0	-0.18	-0.18
		Contact	9.87	--	--	9.87
		Total	9358.75	1466.06	29.84	10 854.65
	Surface (4982 m)	Rock	-1483.40	1420.74	29.97	-32.69
		Ice	0	0	-0.18	-0.18
		Contact	-412.11	--	--	-412.11
		Total	-1895.51	1420.74	29.79	-444.98
	Orbit (1000 km)	Rock	--	--	--	-43.26
		Ice	--	--	--	-0.14
		Total	--	--	--	-43.40
MERIDIAN DEFLEXION (arc seconds)	Geoid (0 m)	Rock	3.366	-1.016	0.024	2.374
		Ice	0	0	0.001	0.001
		Contact	1.101	--	--	1.101
		Total	4.467	-1.016	0.024	3.476
	Surface (4982 m)	Rock	-0.446	-1.281	0.021	-1.706
		Ice	0	0	0.001	0.001
		Contact	5.398	--	--	5.398
		Total	4.952	-1.281	0.022	3.692
	Orbit (1000 km)	Rock	--	--	--	-0.567
		Ice	--	--	--	0.000
		Total	--	--	--	-0.566
PRIME VERTICAL DEFLEXION (arc seconds)	Geoid (0 m)	Rock	9.897	-0.260	0.006	9.643
		Ice	0	0	0.000	0.000
		Contact	-2.946	--	--	-2.946
		Total	6.952	-0.260	0.006	6.697
	Surface (4982 m)	Rock	28.485	-0.341	0.005	28.149
		Ice	0	0	0.000	0.000
		Contact	-20.127	--	--	-20.127
		Total	8.358	-0.341	0.005	8.022
	Orbit (1000 km)	Rock	--	--	--	-0.225
		Ice	--	--	--	0.000
		Total	--	--	--	-0.225

TABLE 8.2

CONTRIBUTIONS TO THE TOPOGRAPHIC-ISOSTATIC EFFECTS AT POINT (B)

Himalayan slopes: Lat. = 30°N, Long. = 80°E, Height = 1638 m

EFFECT	LEVEL	SOURCE	INNER	MID	OUTER	TOTAL
EQUIPOTENTIAL UNDULATIONS (metres)	Geoid (0 m)	Rock	6.545	0.820	-1.135	6.230
		Ice	0	0	0.089	0.089
		Contact	0.023	--	--	0.023
		Total	6.568	0.820	-1.046	6.341
	Surface (1638 m)	Rock	6.853	0.958	-1.130	6.682
		Ice	0	0	0.089	0.089
		Contact	0.003	--	--	0.003
		Total	6.857	0.958	-1.041	6.774
	Orbit (1000 km)	Rock	--	--	--	3.735
		Ice	--	--	--	0.072
		Total	--	--	--	3.807
VERTICAL GRAVITY (μN/kg)	Geoid (0 m)	Rock	3582.94	832.85	31.31	4447.10
		Ice	0	0	-0.18	-0.18
		Contact	31.00	--	--	31.00
		Total	3613.94	832.85	31.13	4477.92
	Surface (1638 m)	Rock	536.85	826.12	31.29	1394.26
		Ice	0	0	-0.18	-0.18
		Contact	-693.84	--	--	-693.84
		Total	-156.99	826.12	31.11	700.24
	Orbit (1000 km)	Rock	--	--	--	-29.55
		Ice	--	--	--	-0.14
		Total	--	--	--	-29.69
MERIDIAN DEFLEXION (arc seconds)	Geoid (0 m)	Rock	-37.268	-2.488	0.023	-39.734
		Ice	0	0	0.001	0.001
		Contact	14.741	--	--	14.741
		Total	-22.527	-2.488	0.024	-24.992
	Surface (1638 m)	Rock	-55.912	-2.699	0.022	-58.589
		Ice	0	0	0.001	0.001
		Contact	32.646	--	--	32.646
		Total	-23.267	-2.699	0.023	-25.943
	Orbit (1000 km)	Rock	--	--	--	-0.522
		Ice	--	--	--	0.000
		Total	--	--	--	-0.521
PRIME VERTICAL DEFLEXION (arc seconds)	Geoid (0 m)	Rock	-0.433	-1.114	0.013	-1.534
		Ice	0	0	0.000	0.000
		Contact	-0.709	--	--	-0.709
		Total	-1.142	-1.114	0.013	-2.243
	Surface (1638 m)	Rock	-1.670	-1.209	0.012	-2.866
		Ice	0	0	0.000	0.000
		Contact	0.435	--	--	0.435
		Total	-1.234	-1.209	0.012	-2.243
	Orbit (1000 km)	Rock	--	--	--	-0.367
		Ice	--	--	--	0.000
		Total	--	--	--	-0.367

TABLE 8.3

CONTRIBUTIONS TO THE TOPOGRAPHIC-ISOSTATIC EFFECTS AT POINT (C)

Antarctic: Lat. = 80°S, Long. = 120°E, Height = 3301 m, Ice = 3058 m

EFFECT	LEVEL	SOURCE	INNER	MID	OUTER	TOTAL
EQUIPOTENTIAL UNDULATIONS (metres)	Geoid (0 m)	Rock	10.347	0.780	-0.964	10.163
		Ice	-6.674	-0.573	0.291	-6.956
		Contact	0.002	--	--	0.002
		Total	3.675	0.207	-0.673	3.209
	Surface (3301 m)	Rock	11.102	1.084	-0.953	11.233
		Ice	-7.185	-0.774	0.285	-7.673
		Contact	0.001	--	--	0.001
		Total	3.917	0.311	-0.668	3.560
	Orbit (1000 km)	Rock	--	--	--	4.302
		Ice	--	--	--	-3.026
		Total	--	--	--	1.276
VERTICAL GRAVITY (μN/kg)	Geoid (0 m)	Rock	5895.02	921.15	31.33	6847.51
		Ice	-3523.67	-602.07	-16.80	-4142.53
		Contact	3.04	--	--	3.04
		Total	2374.39	319.08	14.54	2708.01
	Surface (3301 m)	Rock	-1078.88	905.74	31.30	-141.84
		Ice	626.85	-591.52	-16.78	18.55
		Contact	-118.43	--	--	-118.43
		Total	-570.46	314.22	14.52	-241.72
	Orbit (1000 km)	Rock	--	--	--	-35.80
		Ice	--	--	--	25.16
		Total	--	--	--	-10.64
MERIDIAN DEFLEXION (arc seconds)	Geoid (0 m)	Rock	-7.397	0.037	-0.015	-7.374
		Ice	-7.699	0.021	0.014	-7.665
		Contact	1.590	--	--	1.590
		Total	-13.506	0.058	-0.002	-13.449
	Surface (3301 m)	Rock	-22.719	0.041	-0.015	-22.693
		Ice	9.844	0.023	0.013	9.879
		Contact	6.832	--	--	6.832
		Total	-6.043	0.063	-0.002	-5.982
	Orbit (1000 km)	Rock	--	--	--	0.063
		Ice	--	--	--	-0.076
		Total	--	--	--	-0.013
PRIME VERTICAL DEFLEXION (arc seconds)	Geoid (0 m)	Rock	0.720	0.059	-0.022	0.758
		Ice	-0.650	-0.054	0.012	-0.692
		Contact	-0.204	--	--	-0.024
		Total	-0.134	0.006	-0.010	-0.139
	Surface (3301 m)	Rock	-0.508	0.076	-0.021	-0.453
		Ice	0.853	-0.071	0.011	0.793
		Contact	0.248	--	--	0.248
		Total	0.593	0.005	-0.010	0.588
	Orbit (1000 km)	Rock	--	--	--	0.283
		Ice	--	--	--	-0.191
		Total	--	--	--	0.092

TABLE 8.4

CONTRIBUTIONS TO THE TOPOGRAPHIC-ISOSTATIC EFFECTS AT POINT (D)

Indian Ocean: Lat. = 30°S, Long. = 80°E, Height = 0 m

EFFECT	LEVEL	SOURCE	INNER	MID	OUTER	TOTAL
EQUIPOTENTIAL UNDULATIONS (metres)	Geoid (0 m)	Rock	--	--	-0.857	-0.857
		Ice	--	--	0.159	0.159
		Contact	--	--	--	--
		Total	--	--	-0.698	-0.698
	Surface		As for Geoid			
	Orbit (1000 km)	Rock	--	--	--	-0.563
		Ice	--	--	--	0.093
		Total	--	--	--	-0.470
VERTICAL GRAVITY (μN/kg)	Geoid (0 m)	Rock	--	--	3.33	3.33
		Ice	--	--	-0.75	-0.75
		Contact	--	--	--	--
		Total	--	--	2.58	2.58
	Surface		As for Geoid			
	Orbit (1000 km)	Rock	--	--	--	2.44
		Ice	--	--	--	-0.54
		Total	--	--	--	1.90
MERIDIAN DEFLEXION (arc seconds)	Geoid (0 m)	Rock	--	--	-0.001	-0.001
		Ice	--	--	0.005	0.005
		Contact	--	--	--	--
		Total	--	--	0.003	0.003
	Surface		As for Geoid			
	Orbit (1000 km)	Rock	--	--	--	0.003
		Ice	--	--	--	-0.001
		Total	--	--	--	0.002
PRIME VERTICAL DEFLEXION (arc seconds)	Geoid (0 m)	Rock	--	--	-0.003	-0.003
		Ice	--	--	0.000	0.000
		Contact	--	--	--	--
		Total	--	--	-0.003	-0.003
	Surface		As for Geoid			
	Orbit (1000 km)	Rock	--	--	--	-0.0002
		Ice	--	--	--	0.000
		Total	--	--	--	-0.0002

which arises from treating the polar ice sheets as rock (see §3.3). Hence it is a correction due to material with a density equal to the difference between rock and ice (*i.e.* approximately -1753 kg/m^3) and therefore represents an effect with about double the magnitude of that which would be caused by the ice *per se*. "Contact" refers to the correction applied to bring the four 5'x5' quads in the contact sub-zone to the same height as the computation point. Results are given for the computation point at geoid, surface, and orbit elevations. In the latter case, all topography comes within the outer zone. (Note: in tables 8.1 to 8.4, the number of significant digits does not necessarily reflect the precision of the data and, due to round-off, given totals may not exactly equal the sums of the contributing values).

Point A (table 8.1) was chosen at a high part of the Himalayas, but the surrounding topography is somewhat plateau-like and excludes sustained, steep gradients. Notable features of the effect on the potential include: (a) a fairly large difference between the results at geoid and surface levels, (b) the tendency for cancellation of the mid and outer zone effects, (c) the ice correction of about 8 cm, despite the remoteness of the ice sheets, and (d) the small contact sub-zone correction. Results for the vertical component of attraction show: (a) an accumulation from all zones to the effect at geoid level, resulting in a large positive (upwards) effect, (b) almost complete cancellation of inner and mid zone effects and the consequent strong dependence of the total result on the contact sub-zone correction, and (c) the quite small outer zone effect. Moderate influence of the deflexion components is apparent. However, the large effect on the prime vertical component at the surface and the similarly large correction originating in the contact sub-zone illustrate the importance of the nearby topographic gradients.

A location with extreme asymmetry of topography is represented by point B (table 8.2), which was chosen at the edge of the Himalayas where a steep and sustained topographic gradient occurs. The only noticeable influence of this gradient on the potential is in the increased contact sub-zone correction, though this is still small. Comparison of the effects on the vertical gravity component for points A and B indicate that: (a) the effect at geoid level, though smaller at B, follows the same pattern, and (b) because of the large topographic gradient, a positive (upwards) effect occurs at the surface for point B, despite the large negative contact sub-zone correction. Very large consequences of the topographic gradient are evident in the meridian deflexions and the significance of the contact sub-zone is again confirmed.

Point C (table 8.3), in the Antarctic, illustrates the effect of a considerable thickness of ice, in this case almost the full height of the topography. The effect of the ice correction on the potential undulations exceeds 6 metres, indicating that the effect which could be expected from the actual ice sheet of this thickness would be approximately 3 metres. Rigorous treatment of the ice, as opposed to a process of condensation to equivalent rock thickness, therefore seems to be justified. Ice corrections to the attraction components follow a consistent and expected pattern of reducing the otherwise over-estimated effects, except for the meridian deflexion at geoid level which is reinforced by the correction. Unfortunately, comparison of these results with estimates of the gravitational influence of the Antarctic ice made by KIVIOJA [1967, table 1] is not possible as the effect of isostatic compensation was not included in the latter calculations.

To exemplify the case of a point in an ocean area, point D (table 8.4) was chosen in the Indian Ocean with the same distance from the equator as point A. Only outer zone effects are present and the influence of the ice correction is seen to be appreciable. The rock contribution is somewhat reduced by the remoteness of the point from the major topographic masses.

COMPOSITION OF THE OUTER ZONE EFFECT. A more detailed picture of the global composition of the outer zone contribution to the topographic-isostatic effects was generated by a modified version of programme OUTZONE (called OCONTRIB), which computed the individual contributions of each $5°\times5°$ quad in the outer zone to the total effect at a chosen point. Examples of the results for a point in the Himalayas are mapped in figures 8.16 to 8.18. Combined contributions from each $10°\times10°$ quad, to the potential and vertical attraction component at the surface and the potential at orbital altitude are expressed as a percentage of the total outer zone effect. The sign of the percentage reflects the sign of the actual contribution due to the topography and compensation in that quad. Diminished values appear in the four 10° quads adjacent to the computation point since the inner and mid zone ($\psi < 10°$) effects are excluded. The excluded topography is indicated by the circular region surrounding the compuation point.

All contributions to the potential at surface level (figure 8.16) are negative, indicating the dominance of the isostatic compensation. Slow attenuation of the contributions with increasing remoteness of the topography is apparent, in that the importance of quads on the opposite side of the earth to the computation point is often equal to that of nearby quads. The necessity for global coverage of the outer zone is thus verified.

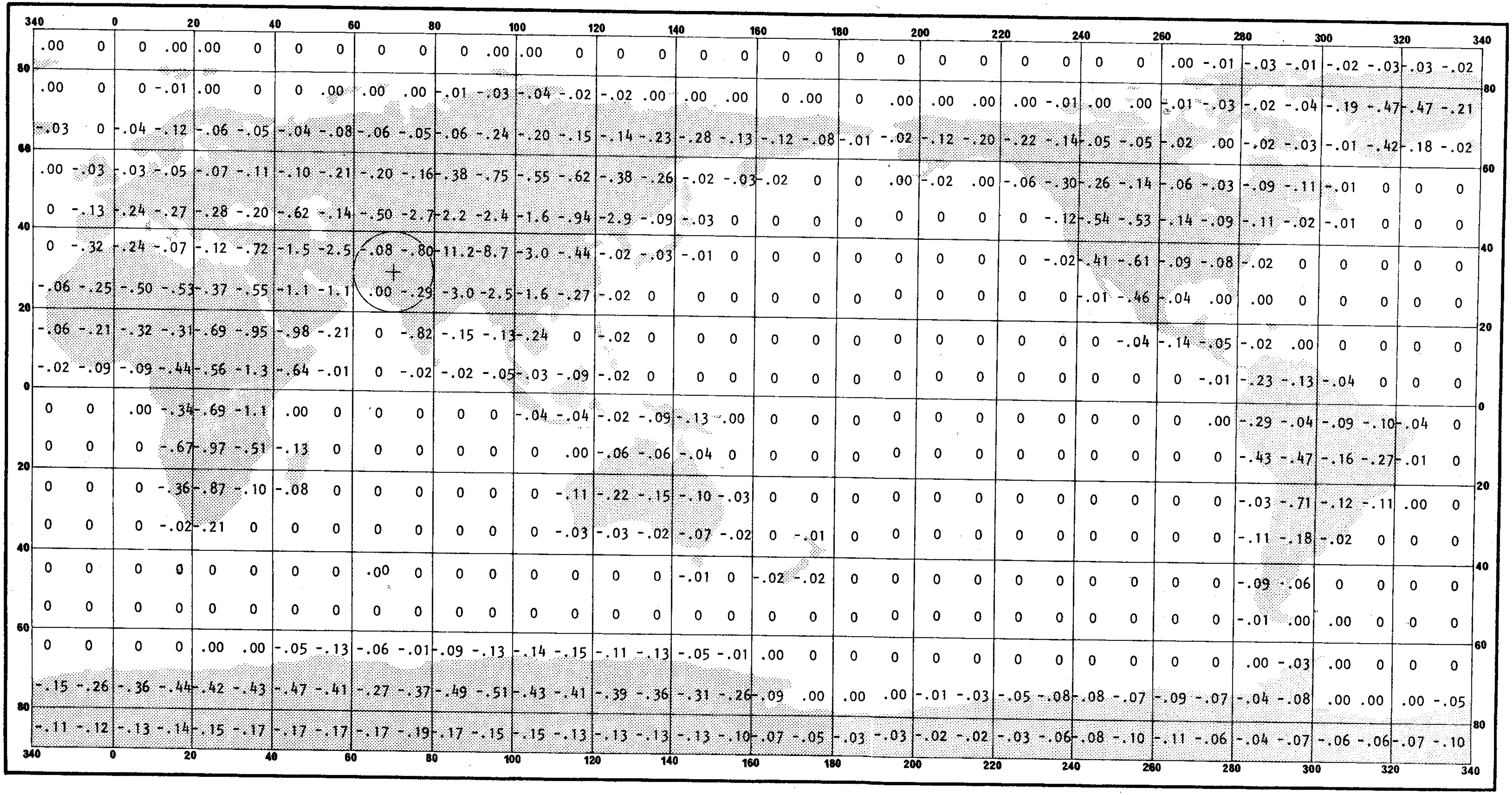

FIGURE 8.16

PERCENTAGE CONTRIBUTIONS OF 10°x10° QUADS TO THE POTENTIAL AT SURFACE LEVEL FOR A POINT AT LATITUDE 30°N, LONGITUDE 70°E, HEIGHT 811 m

Total potential of outer zone = -11.695 J/kg

Summation over 6400 1°x1° quads and 830 5°x5° quads.

(Sign of percentage corresponds to sign of contribution)

0	0	0	0	0	0	0	0	0	0	0	0	0	0	0	0	0	0	0	0	0	0	0	0	0	0	0	0	0	0	0	0	0	0	.01	0
0	0	0	0	0	0	0	0	0	0	0	.01	.01	.01	0	0	0	0	0	0	0	0	0	0	0	0	0	0	0	0	0	0	.02	.06	.06	.03
0	0	.01	.03	.01	.01	.01	.03	.02	.02	.02	.09	.06	.04	.03	.04	.04	.02	.01	.01	0	0	.01	.02	.02	.01	.01	.01	0	0	0	0	0	.05	.02	0
0	0	.01	.01	.02	.04	.05	.15	.17	.15	.29	.42	.23	.20	.09	.05	0	.01	0	0	0	0	0	0	0	.03	.03	.01	0	0	.01	.01	0	0	0	0
0	.02	.05	.07	.09	.10	.52	.16	1.3	7.8	3.3	1.8	.80	.33	.07	.02	0	0	0	0	0	0	0	0	0	.01	.04	.03	.01	.01	.01	0	0	0	0	0
0	.05	.05	.01	.04	.41	1.6	6.9	.36	3.7	31.4	9.2	1.7	.17	0	.01	0	0	0	0	0	0	0	0	0	0	.03	.05	.01	0	0	0	0	0	0	0
.01	.03	.09	.12	.11	.29	.96	3.3	0	1.2	7.7	2.5	.86	.08	.01	0	0	0	0	0	0	0	0	0	0	0	0	.03	0	0	0	0	0	0	0	0
.01	.03	.05	.06	.18	.38	.66	.24	0	1.8	.28	.07	.10	0	0	0	0	0	0	0	0	0	0	0	0	0	0	0	.01	0	0	0	0	0	0	0
0	.01	.01	.08	.13	.41	.28	0	0	.01	.01	.02	.01	.02	0	0	0	0	0	0	0	0	0	0	0	0	0	0	0	0	.02	.01	0	0	0	0
0	0	0	.06	.12	.25	0	0	0	0	0	0	.01	.01	0	.01	.01	0	0	0	0	0	0	0	0	0	0	0	0	0	.02	0	.01	.01	0	0
0	0	0	.09	.15	.10	.02	0	0	0	0	0	0	0	.01	.01	0	0	0	0	0	0	0	0	0	0	0	0	0	0	.02	.03	.01	.02	0	0
0	0	0	.04	.12	.01	.01	0	0	0	0	0	0	.01	.03	.01	.01	0	0	0	0	0	0	0	0	0	0	0	0	0	0	.05	.01	.01	0	0
0	0	0	0	.02	0	0	0	0	0	0	0	0	0	0	0	.01	0	0	0	0	0	0	0	0	0	0	0	0	0	.01	.01	0	0	0	0
0	0	0	0	0	0	0	0	0	0	0	0	0	0	0	0	0	0	0	0	0	0	0	0	0	0	0	0	0	0	.01	0	0	0	0	0
0	0	0	0	0	0	0	0	0	0	0	0	0	0	0	0	0	0	0	0	0	0	0	0	0	0	0	0	0	0	0	0	0	0	0	0
0	0	0	0	0	0	0	.01	0	0	.01	.01	.01	.01	.01	.01	0	0	0	0	0	0	0	0	0	0	0	0	0	0	0	0	0	0	0	0
.01	.02	.03	.04	.04	.04	.04	.04	.02	.03	.04	.04	.03	.03	.03	.03	.02	.02	.01	0	0	0	0	0	.01	.01	.01	.01	.01	0	0	.01	0	0	0	0
.01	.01	.01	.01	.01	.01	.01	.01	.01	.01	.01	.01	.01	.01	.01	.01	.01	.01	0	0	0	0	0	0	0	0	0	.01	.01	0	0	0	0	0	0	.01

FIGURE 8.17

PERCENTAGE CONTRIBUTIONS OF 10°x10° QUADS TO THE VERTICAL COMPONENT OF GRAVITY AT THE SURFACE FOR A POINT AT LATITUDE 30°N, LONGITUDE 70°E, HEIGHT 811 m

Total vertical component of gravity due to outer zone = 28.150 μN/kg (2.815 mgal)

340		0		20		40		60		80		100		120		140	
.00	0	0	.00	.00	0	0	0	0	0	0	.00	.00	0	0	0	0	0
.00	0	0	.00	.00	.00	0	.00	.00	.00	.00	-.01	-.01	-.01	-.01	.00	.00	.00
-.01	0	-.02	-.04	-.02	-.01	.00	-.01	-.01	0	-.01	-.05	-.05	-.04	-.05	-.08	-.11	-.05
.00	-.01	-.01	-.02	-.02	-.02	.01	.04	.06	.06	.08	.03	-.06	-.13	-.11	-.09	-.01	-.01
0	-.05	-.08	-.08	-.06	.00	.18	.11	.70	4.2	1.7	.56	-.02	-.17	-.08	-.03	-.01	0
.00	-.13	-.08	-.02	-.02	.04	.73	4.4	23.6	36.0	20.4	4.2	.20	-.07	-.01	-.02	-.01	0
-.03	-.10	-.18	-.17	-.08	.01	.35	2.0	6.8	5.0	4.5	1.1	.06	-.05	-.01	0	0	0
-.03	-.10	-.13	-.10	-.19	-.11	.15	.12	0	1.0	.16	.01	-.03	.00	-.01	0	0	0
-.01	-.04	-.04	-.17	-.18	-.29	-.05	0	0	.01	.01	-.01	-.01	-.04	.00	0	0	0
0	0	0	-.14	-.25	-.34	0	0	0	0	0	.00	-.02	-.02	-.01	-.04	-.06	.00
0	0	0	-.29	-.38	-.18	-.05	0	0	0	0	0	0	.00	-.03	-.03	-.02	0
0	0	0	-.16	-.37	-.05	-.03		0	0	0	0	0	-.05	-.10	-.07	-.05	-.01
0	0	0	-.01	-.09	0	0	0	0	0	0	0	0	-.02	-.02	-.01	-.04	-.01
0	0	0	0	0	0	0	0	0	0	0	0	0	0	0	0	-.01	0
0	0	0	0	0	0	0	0	0	0	0	0	0	0	0	0	0	0
0	0	0	0	0	0	-.03	-.06	-.03	-.01	-.04	-.06	-.07	-.07	-.05	-.06	-.03	-.01
-.08	-.12	-.18	-.22	-.20	-.21	-.23	-.20	-.14	-.18	-.23	-.24	-.21	-.20	-.19	-.18	-.15	-.12
-.05	-.05	-.06	-.06	-.08	-.09	-.09	-.09	-.09	-.09	-.09	-.08	-.07	-.07	-.07	-.06	-.06	-.06

160		180		200		220		240		260		280		300		320	
0	0	0	0	0	0	0	0	0	0	.00	-.01	-.01	-.01	-.01	-.01	-.01	-.01
.00	.00	0	.00	.00	.00	0	.00	.00	.00	.00	-.01	-.01	-.02	-.08	-.19	-.18	-.08
-.04	-.04	-.01	-.01	-.06	-.09	-.10	-.07	-.03	-.03	-.01	.00	-.01	-.02	-.01	-.18	-.07	-.01
-.01	0	0	.00	.00	0	-.03	-.15	-.12	-.06	-.03	-.01	-.03	-.05	-.01	0	0	0
0	0	0	0	0	0	0	-.06	-.27	-.21	-.07	-.04	-.06	-.01	-.01	0	0	0
0	0	0	0	0	0	0	-.01	-.19	-.31	-.05	-.04	-.01	0	0	0	0	0
0	0	0	0	0	0	0	0	-.01	-.23	-.02	.00	.00	0	0	0	0	0
0	0	0	0	0	0	0	0	0	-.02	-.07	-.03	-.01	.00	0	0	0	0
0	0	0	0	0	0	0	0	0	0	0	-.01	-.11	-.07	-.03	.00	0	0
0	0	0	0	0	0	0	0	0	0	0	.00	-.14	-.02	-.04	-.05	-.02	0
0	0	0	0	0	0	0	0	0	0	0	0	-.21	-.23	-.08	-.13	-.01	0
0	0	0	0	0	0	0	0	0	0	0	0	-.01	-.36	-.06	-.05	0	0
0	-.01	0	0	0	0	0	0	0	0	0	0	-.05	-.09	-.01	0	0	0
-.01	-.01	0	0	0	0	0	0	0	0	0	0	-.04	-.03	0	0	0	0
0	0	0	0	0	0	0	0	0	0	0	0	-.01	.00	.00	0	0	0
0	0	0	0	0	0	0	0	0	0	0	0	.00	-.01	.00	0	0	0
-.04	.00	.00	.00	-.01	-.02	-.04	-.04	-.03	-.03	-.05	-.03	-.04	-.05	.00	.00	.00	-.02
-.04	-.03	-.02	-.01	-.01	-.01	-.02	-.02	-.03	-.04	-.04	-.03	-.02	-.02	-.02	-.02	-.03	-.03

FIGURE 8.18

PERCENTAGE CONTRIBUTIONS OF $10^\circ x 10^\circ$ QUADS TO THE POTENTIAL AT SATELLITE ORBIT ALTITUDE (1000 km) FOR A POINT AT LATITUDE 30°N, LONGITUDE 70°E

Total potential due to outer zone = 19.625 J/kg

≡ 2.00 m

(Sign of percentage corresponds to sign of contribution)

In contrast, the contributions to the surface vertical component of gravity (figure 8.17) diminish more rapidly with distance from the computation point, so that the remote sub-zone contributes less than 3% of the outer zone effect. This is consistent with the higher power of the reciprocal distance term in the attraction as compared with the potential. All outer zone contributions to the vertical gravity are positive due to the compensation.

An example of the composition of the potential at orbital altitude is given in figure 8.18. The effect of all topography is included. A region of positive contributions surrounds the computation point and extends to an angular distance of about 30° (see equation 3.77) before the negative influence of the compensation becomes dominant. The negative effect makes up about 18% of the final value.

MARINE TOPOGRAPHY AND COMPENSATION

MARINE TOPOGRAPHIC-ISOSTATIC MODEL. An extension of the Airy-Heiskanen isostatic compensation system for oceans [HEISKANEN and MORITZ 1967, p.136] was adopted. Figure 8.19a illustrates the basic hypothesis.

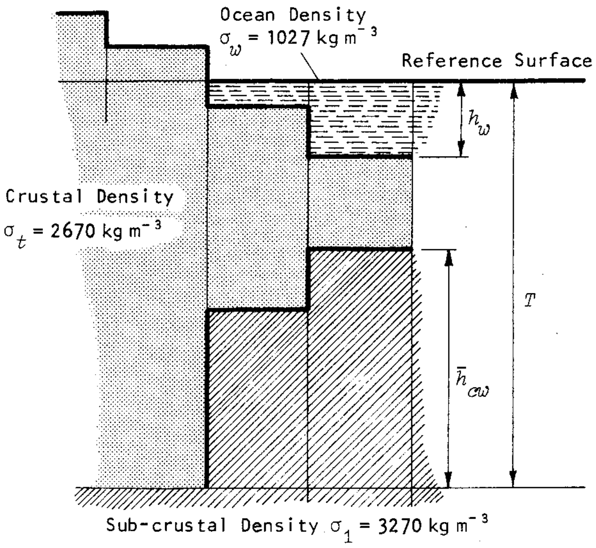

FIGURE 8.19a

AIRY-HEISKANEN ISOSTATIC COMPENSATION SYSTEM IN OCEAN AREAS

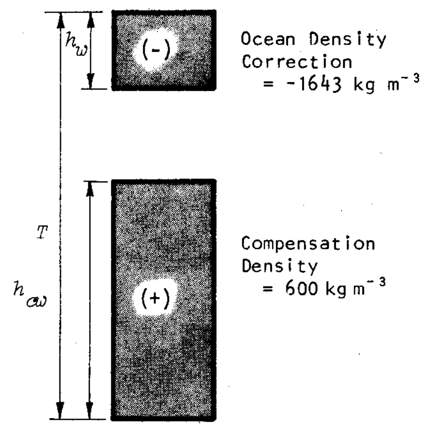

FIGURE 8.19b

MARINE TOPOGRAPHIC-ISOSTATIC DIPOLE MODEL

The height of the compensation $\bar{h}_{cw}$ is given by (*c.f.* equation 3.19):

$$\bar{h}_{cw} = \frac{\sigma_w - \sigma_t}{\sigma_c} h_w , \tag{8.2}$$

where h_w is the ocean depth,

σ_w is the density of the ocean,

and the remaining symbols remain as defined in §3.3. Constant values were adopted for the crust and ocean densities as follows [*ibid.,* equations 3.24 and 3.27]:

$$\sigma_t = 2670 \text{ kg/m}^3 , \tag{8.3}$$

$$\sigma_w = 1027 \text{ kg/m}^3 . \tag{8.4}$$

The resulting topographic-isostatic dipole model is shown in figure 8.19b. A sphericity correction was applied in accordance with the techniques and equations derived in §3.3. In all other respects, the topographic-isostatic model conformed with the specifications stated in chapter 3 (see table 3.4).

METHOD. Due to the limitations of the available bathymetric data and restrictions on computer time, only only outer zone effects were computed, and then only at selected points. A modified version of programme OUTZONE (called OUTSEAS) was used, relying on the same dipole point mass approximation and utilizing $1°\times1°$ and $5°\times5°$ mean solid earth elevation data (item 1, table 6.1).

TABLE 8.5

OUTER ZONE CONTRIBUTIONS TO MARINE TOPOGRAPHIC-ISOSTATIC EFFECTS

POINT	LOCATION	HEIGHT OF POINT	EQUIPOTENTIAL UNDULATION (m)	VERTICAL GRAVITY (μN/kg)	MERIDIAN DEFLEXION (arc sec)	PRIME VERT. DEFLEXION (arc sec.)
B	Lat. = 30°N	Geoid (0 m)	3.007	-13.550	-0.026	0.004
	Lon. = 80°E	Surface (1638 m)	3.004	-13.545	-0.026	0.005
		Orbit (1000 km)	1.892	-8.028	0.049	0.011
E	Lat. = 40°N	Geoid (0 m)	3.358	-23.843	-0.024	0.012
	Lon. = 270°E	Surface (187 m)	3.357	-23.840	-0.024	0.012
		Orbit (1000 km)	1.402	-9.600	0.095	-0.139
F	Lat. = 80°N	Geoid (0 m)	3.054	-16.931	-0.015	-0.003
	Lon. = 210°E	Surface (0 m)		As for	Geoid	
		Orbit (1000 km)	0.647	5.962	-0.061	0.032

RESULTS. Table 8.5 contains the results for three selected points (B, E, and F), the location of which is illustrated in figure 8.4. Point B is the same point as that dealt with in table 8.2 and—since no ocean areas occur within the inner and mid zones—the marine topographic-isostatic effect given in table 8.5 may be combined with the results in table 8.2 to complete the global effect at this point. A further 3 metres is added to the disturbance of the equipotentials at the geoid and surface levels and this order of magnitude for the marine topographic-isostatic effect appears to be sustained globally. This is a most significant effect in comparison with the terrestrial contributions.

Comparison of points B and E indicates the amount of variation to be expected between continents in opposite hemispheres, while point F was chosen in an ocean area, significantly surrounded by land masses. The ocean depth at point F exceeds 4500 metres and there is a substantial marine topographic gradient nearby. However, the results here are incomplete—except at orbital altitude—since the inner and mid zone effects are not available. A considerable reduction in the equipotential disturbance for point F at orbital level is apparently caused by the extra negative contribution from the ocean area surrounding the point. This effect is more noticeable in the vertical gravity component, where it is sufficient to reverse the sign of this quantity.

Generally, the influence of marine areas on the attraction vector, either horizontally or vertically, is much smaller than the terrestrial disturbance. A shorter dipole length (equation 3.78) and the lesser density of the marine topographic-isostatic model are partially responsible for this. Furthermore, the attenuating effect of distance from the computation point—observed in the composition of the outer zone effect of the terrestrial topography on the attraction vector—operates here also.

8.4 SPHERICAL HARMONIC ANALYSIS

INTRODUCTION

Spherical harmonic analysis of the results data was applied primarily as a mathematical device, to provide a compact numerical representation of the principal trends of the data, to facilitate comparisons within the results and with other data, and to elucidate any peculiar characteristics of the data which might not otherwise be evident. Essentially, the chief attributes of the process are those of a spectral analysis. Physical interpretation of the harmonic coefficients may be undertaken only with extreme caution and with full cognizance of the artificial nature and other limitations of the models upon which the original computations were based and the specific form and method of analysis. For these reasons, the association of physical characteristics with particular coefficients was not the main intent of the harmonic analysis.

Indeed, the strict validity of harmonic analysis of some of the results data may be questionable. Gravitational potential and attraction fields are not harmonic within the gravitating material (*e.g.* at the geoid) and even at the earth's surface the harmonic representation might be expected to diverge. RAPP [1973, p.61] has suggested that, at least in a practical sense, such concern is needless, since a finite number of harmonic coefficients are determined from a finite set of data values.

In accordance with usual practice, and for their convenience, *fully normalized, surface spherical* harmonic coefficients were determined, despite the lack of strict conformity of the models inherent in the results data with the precepts of this form of analysis. Any interpretation of the coefficients must be made in this context.

THERORETICAL DEVELOPMENT AND TESTS

Any of the results data may be treated as values of an arbitrary function $g(\phi,\lambda)$ at specific locations on the surface of a sphere which may be expanded in a series of fully normalized harmonics given by [HEISKANEN and MORITZ 1967, p.31]:

$$g(\phi,\lambda) = \sum_{n=0}^{\infty} \sum_{m=0}^{n} \bar{P}_{nm}(\sin \phi)[C_{nm} \cos m\lambda + S_{nm} \sin m\lambda] \tag{8.5}$$

where ϕ,λ specify the latitude and longitude of the data value,

n,m are the degree and order of the harmonic,

C_{nm}, S_{nm} are fully normalized harmonic coefficients, and

$\bar{P}_{nm}(\sin \phi)$ is the fully normalized associated Legendre function of the first kind.

The harmonic coefficients may be found by global integration, thus:

$$C_{nm} = \frac{1}{4\pi} \int_0^{2\pi} \int_{-\pi/2}^{\pi/2} g(\phi,\lambda)\, \bar{P}_{nm}(\sin \phi)\, \cos m\lambda\, \cos \phi\, d\phi\, d\lambda, \tag{8.6}$$

and

$$S_{nm} = \frac{1}{4\pi} \int_0^{2\pi} \int_{-\pi/2}^{\pi/2} g(\phi,\lambda)\, \bar{P}_{nm}(\sin \phi)\, \sin m\lambda\, \cos \phi\, d\phi\, d\lambda. \tag{8.7}$$

Evaluation of the associated Legendre function was based on the formulation of MATHER [1971, equations 4.32 and 3.39] which is essentially the same as that given by HEISKANEN and MORITZ [1967, equations 1-77a,b], but is somewhat more amenable to computer transcription.

8. RESULTS AND ANALYSIS

To determine the coefficients, the integration of equations 8.6 and 8.7 was replaced by summation. As values of $g(\phi,\lambda)$ were available on a 5°x5° global grid, each value was assumed to be representative of the 5°x5° quad within which it was centrally located. Values at the poles were assumed to prevail throughout the area of latitudes higher than 87½°. Associated Legendre function values were computed for the same latitude as that of the grid value—that is, at the mid-latitude of the quad. Equation 3.33 was used to rigorously compute the elemental area of each quad for a unit sphere. Unless the magnitude of the coefficients indicated that a lower degree would provide adequate representation, analysis was carried to degree 36, which gives resolution equivalent to the computation grid interval of 5°. As the number of coefficients for degree 36 is 1369—that is, $(n+1)^2$—and the number of data values on a global 5° grid, including the poles, is 2522, there is a reasonable amount of redundancy in the determination of the coefficients.

Harmonic *degree variances* Σ_n^2, given by [HEISKANEN and MORITZ 1967, p.259]:

$$\Sigma_n^2 = \sum_{m=0}^{n} (C_{nm}^2 + S_{nm}^2), \tag{8.8}$$

were also computed.

Synthesis of the data values from the harmonic coefficients, in accordance with equation 8.5, was used as an indication of the quality of the coefficients. Residuals, being the difference between the synthesized and original data values, were determined and statistically tested.

All of the computations necessary for analysis and synthesis were performed by programme HARMONIC (see ¶"*ANALYSIS PROGRAMMES*" in §7.3). Programme HARCOPLT (see appendix A) was employed to plot graphical representations of the harmonic coefficients and variances to facilitate visual comparisons.

SIGNIFICANCE OF THE LOW DEGREE HARMONICS OF THE TOPOGRAPHIC-ISOSTATIC DISTURBING POTENTIAL. If the reciprocal distance term in the basic expression for the topographic-isostatic disturbing potential is expanded as a set of zonal harmonics, so that [HEISKANEN and MORITZ 1967, p.58]:

$$V = \sum_{n=0}^{\infty} \frac{k}{d^{n+1}} \iiint t^n \, P_n(\cos \beta)\, dM, \tag{8.9}$$

where the notation is consistent with figure 5.1, it is possible to express the potential in the form of a convergent series, as given by equation 5.3. Term by term comparison of this series with a surface spherical harmonic series for the potential in the form of equation 8.5 provides a set of relations for the harmonic coefficients in terms of the dynamic properties of the topographic-isostatic model [*ibid.*, p.61]. Of these, the zero and first degree harmonics are of particular interest. The relevant relations are:

$$C_{00} = \frac{k}{R_p} \iiint dM = \frac{kM}{R_p}, \tag{8.10}$$

and

$$\begin{aligned} C_{10} &= \frac{k}{R_p^2} \iiint Z \, dM, \\ C_{11} &= \frac{k}{R_p^2} \iiint X \, dM, \\ S_{11} &= \frac{k}{R_p^2} \iiint Y \, dM, \end{aligned} \tag{8.11}$$

where X, Y, and Z are the geocentric coordinates of the elemental mass, and

R_p is the geocentric radius of the computation point denoted by d in equation 8.9. The integration is taken over the topographic-isostatic model, and the harmonic coefficients are non-normalized.

Equation 8.10 shows that the zero degree harmonic of the topographic-isostatic disturbing potential is a function of the mass. Since the combined mass of the topography and compensation is made zero in the model adopted, the zero degree harmonic should likewise be zero. By analogy with the dynamics of a system of particles [BULLEN 1951, p.166] the first degree harmonics (equations 8.11) are seen to be functions of the first moments of the topographic-isostatic mass with respect to the geocentric reference axes. Because its mass is zero, the "centre of mass" of the topographic-isostatic model in isolation is a meaningless concept. However, the first moments of the model exist and are finite because the spatial distribution of the topography and compensation differ. If the topography and compensation are treated as irregularities on what is otherwise a completely regular earth of total mass M_E, the geocentric coordinates of the centre of mass of the total irregular system will be given by:

$$X_E = \frac{\iiint X \, dM}{M_E} , \qquad Y_E = \frac{\iiint Y \, dM}{M_E} , \qquad Z_E = \frac{\iiint Z \, dM}{M_E} , \tag{8.12}$$

which become, on substituting 8.11:

$$X_E = \frac{C_{11} R_p^2}{kM_E} , \qquad Y_E = \frac{S_{11} R_p^2}{kM_E} , \qquad Z_E = \frac{C_{10} R_p^2}{kM_E} , \tag{8.13}$$

where R_p is the geocentric radius of the point of computation. Thus the non-normalized first degree harmonics of the disturbing potential due to the topographic-isostatic model may be used to determine the displacement of the centre of mass of a regular earth caused by the compensated topographic irregularities. The normalization factor for the first degree coefficients is: $(2n+1)^{\frac{1}{2}} = \sqrt{3}$.

TESTS. To test the computer routines, the solid surface (terrestrial and marine) topography and the terrestrial topography alone were analysed so that the coefficients could be compared with the published results of BALMINO *et al.* [1973], (see also LEE and KAULA [1967]). Such an analysis is also useful for comparison with the computed gravitational effects of the topography, to investigate the possibility of correlation between the respective spectral trends. Mean elevations for 5°x5° quads based on the UCLA 1° data were used in the test analysis. The resulting coefficients for the terrestrial topography are illustrated in figure 8.20 and the degree variances are included in figure 8.25. Satisfactory agreement was achieved between these results and the coefficients obtained for the "continental" topography through equation (8) of BALMINO *et al.* [1973, p.480].

ANALYSIS RESULTS

HARMONIC COEFFICIENTS. Complete sets of harmonic coefficients and degree variances for the potential undulations, vertical gravity, and deflexions of the vertical at geoid, surface, and orbital elevations are tabulated in appendix C. Figures 8.21 to 8.23 depict graphically the coefficients for the undulations at surface level, and the vertical gravity component at geoid and surface levels, respectively. They exemplify typical patterns. The pattern of coefficients observed in the analysis of the terrestrial topography (figure 8.20) appears in the undulation coefficients, at both geoid and surface levels (*e.g.* figure 8.21), but is most noticeable in the vertical gravity at geoid level (figure 8.22). This reflects the correlation with topography already observed in the results data (*c.f.* figures 8.7 and 8.4). A tendency for more of the power of the coefficients to be vested in the lower harmonics is evident in the vertical gravity as compared with the undulations and this is confirmed by the cumulative percentages graphed in figure 8.24. Analysis of the vertical gravity at surface level (figure 8.23) shows a contrasting trend, with the higher degrees just as important as the lower harmonics. This is a reflection of the

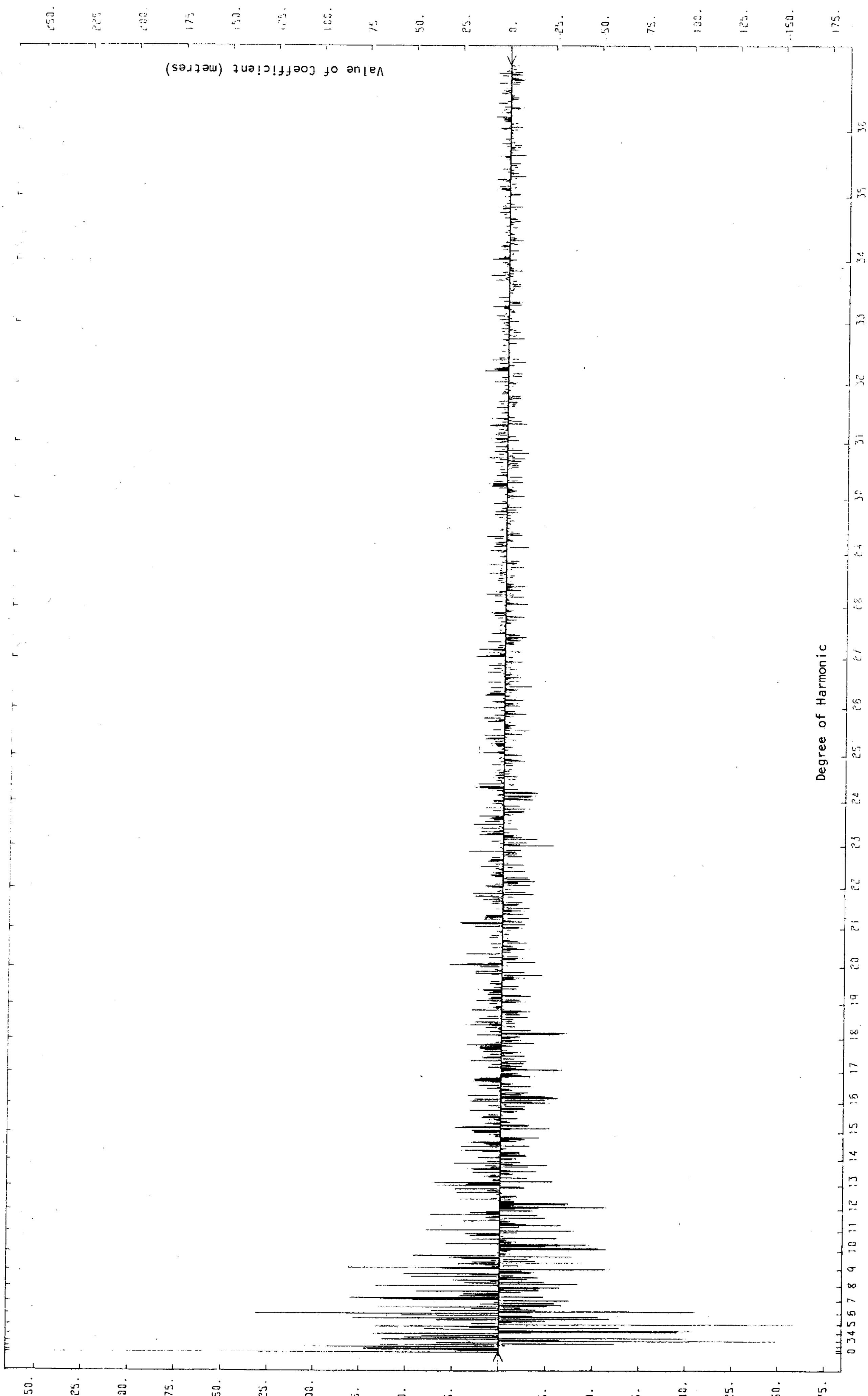

FIGURE 8.20

FULLY NORMALIZED SPHERICAL HARMONIC SPECTRUM OF TERRESTRIAL TOPOGRAPHY BASED ON 5°×5° MEAN ELEVATIONS

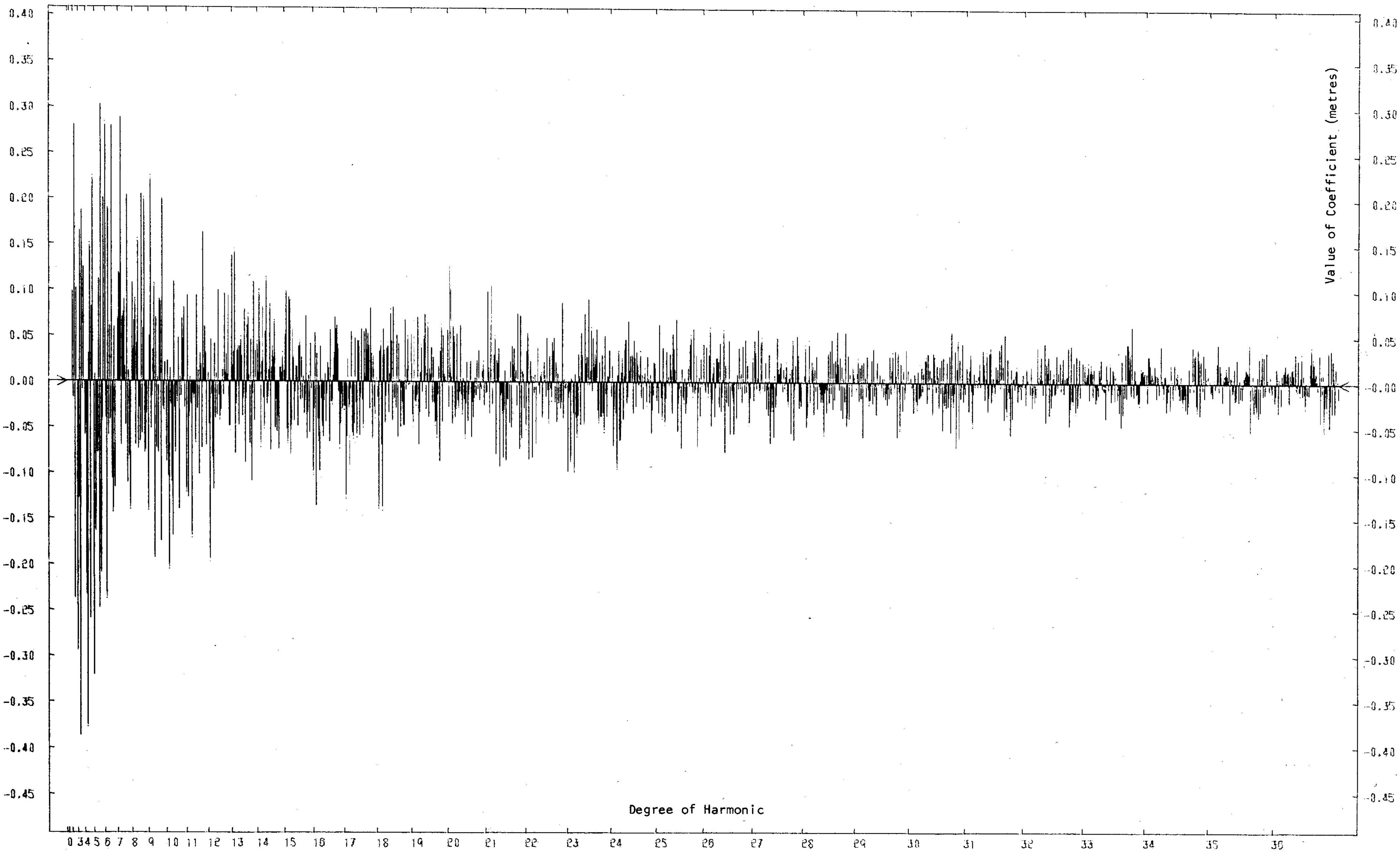

FIGURE 8.21

FULLY NORMALIZED SPHERICAL HARMONIC SPECTRUM OF TOPOGRAPHIC-ISOSTATIC EQUIPOTENTIAL UNDULATIONS AT THE EARTH'S SURFACE

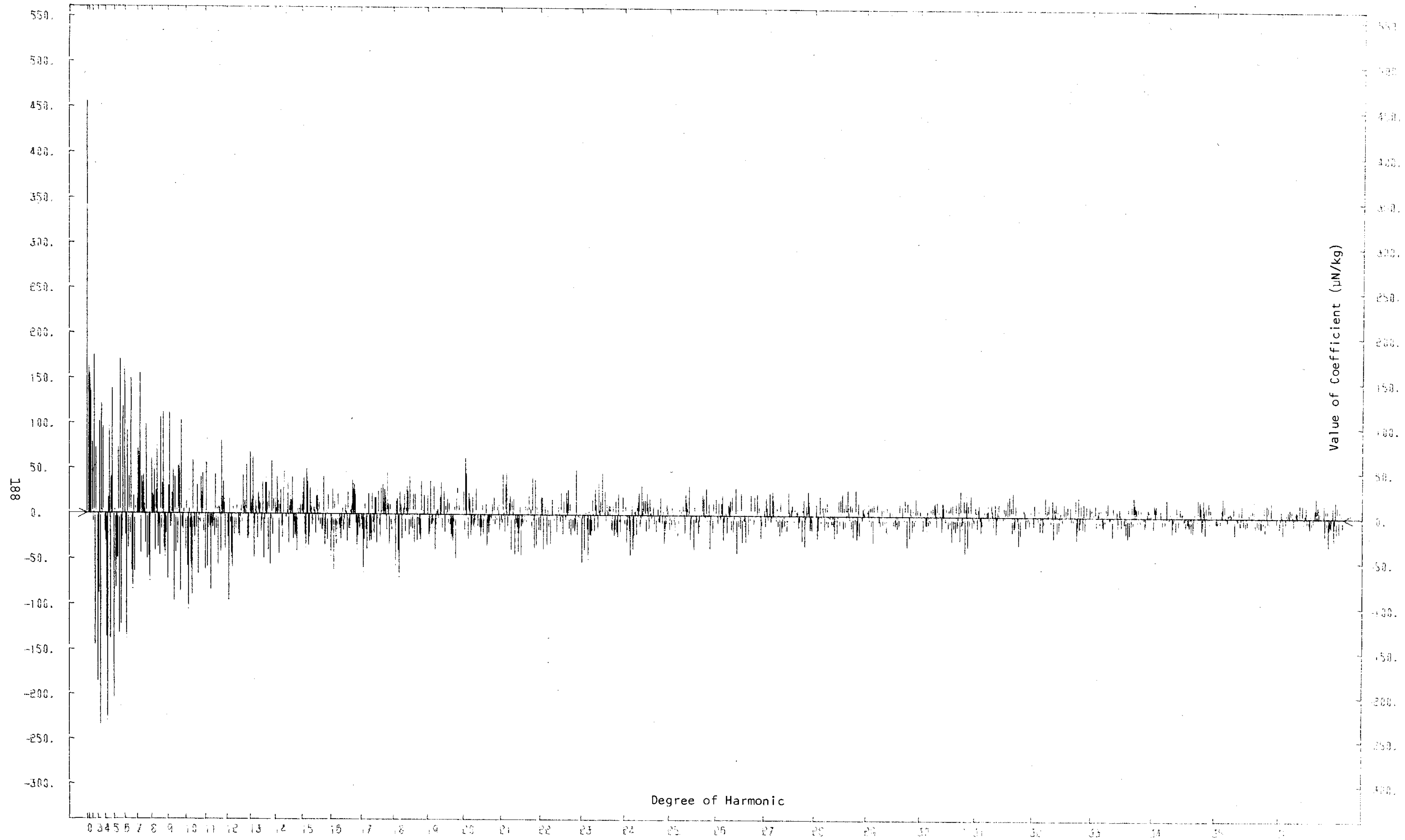

FIGURE 8.22

FULLY NORMALIZED SPHERICAL HARMONIC SPECTRUM OF THE TOPOGRAPHIC-ISOSTATIC VERTICAL COMPONENT OF GRAVITY AT THE GEOID

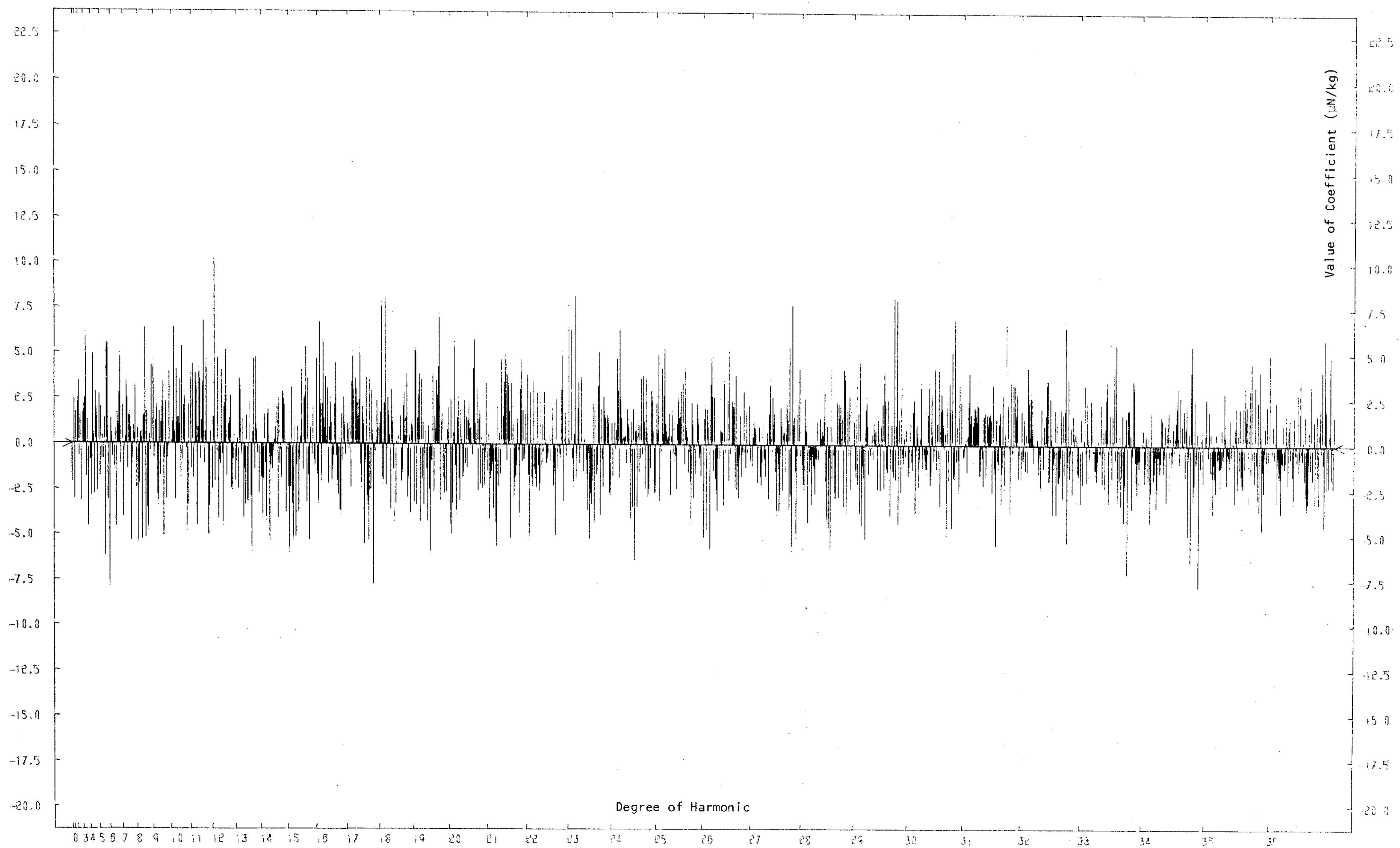

FIGURE 8.23

FULLY NORMALIZED SPHERICAL HARMONIC SPECTRUM OF THE TOPOGRAPHIC-ISOSTATIC VERTICAL COMPONENT OF GRAVITY AT THE EARTH'S SURFACE rapid and irregular variations in this quantity, observed in the results data (see figure 8.9).

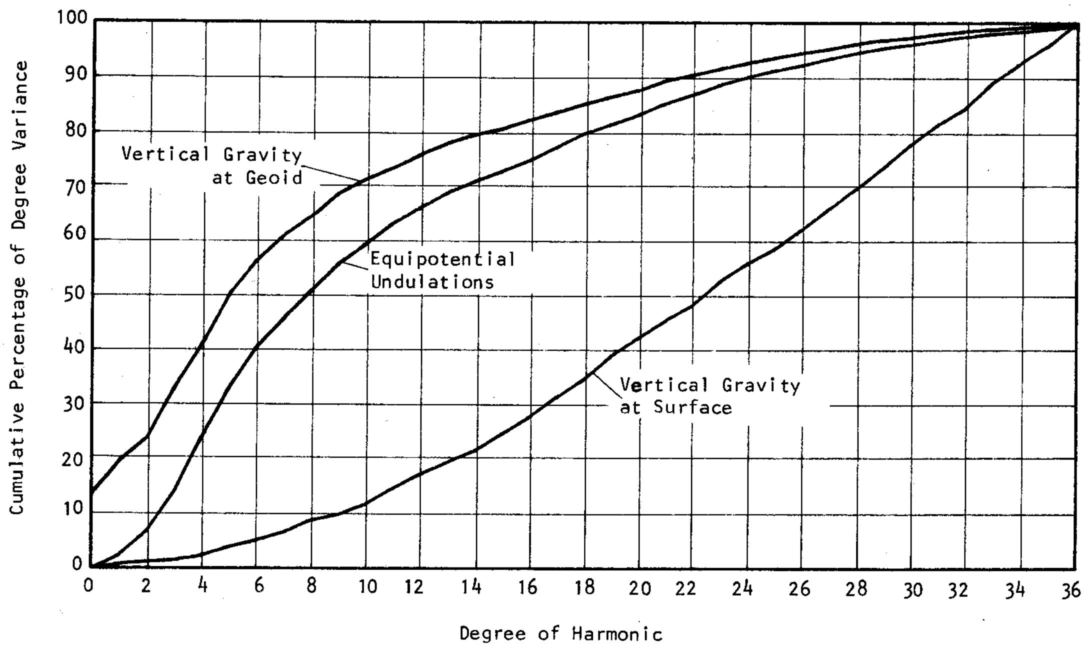

FIGURE 8.24

CUMULATIVE PERCENTAGE OF DEGREE VARIANCES

ZERO AND FIRST DEGREE HARMONICS. In table 8.6, the zero degree harmonics of the potential undulations at geoid, surface, and orbital levels are converted to equivalent topographic-isostatic masses in accordance with equation 8.10. Theoretically the combined masses of the topography and compensation

TABLE 8.6

TOPOGRAPHIC MASS DISCREPANCIES DERIVED FROM THE ZERO DEGREE HARMONICS OF THE DISTURBING POTENTIAL

LEVEL	UNDULATION COEFFICIENT C_{00} (m)	POTENTIAL COEFFICIENT C_{00} (J/kg)	R_p (m)	ΔM_T (kg)	$\lvert\Delta M_T\rvert/M_T$
Geoid	-0.0485	-0.4756	6 371 024	-4.5428×10^{16}	1 / 7 304
Surface	-0.0095	-0.0932	6 371 263	-0.8903×10^{16}	1 / 37 272
Orbit	-0.0013	-0.0127	7 371 024	-0.1406×10^{16}	1 / 236 040

should be zero and the masses computed from the zero degree harmonics must be presumed to be due to model and computation inaccuracies. A small discrepancy in the mass balance of the topographic-isostatic model was demonstrated in §3.4 (see equation 3.76). To compute the mass imbalance ΔM_T, the undulation harmonics were first reconverted to disturbing potentials using a global mean value of normal gravity at the geoid of:

$$M\{\gamma_0\} = \frac{\int_{-\pi/2}^{\pi/2} \gamma_0 \, d\phi}{\int_{-\pi/2}^{\pi/2} d\phi} = 9.806\,19\,\text{N/kg}, \tag{8.14}$$

where γ_0 is normal gravity at the reference surface (see table 3.4). Values of R_p used in equation 8.10 are based on an equivalent volume sphere of radius $R = 6\,371\,024$ metres. A global mean value of the heights of computation points at the terrain surface of

$$\mathrm{M}\{h\} = 239.47 \text{ metres,} \tag{8.15}$$

is given by the zero degree harmonic of the terrestrial topography (see ¶"*TESTS*" above). The derived mass discrepancies are expressed as a fraction of the total mass of the terrestrial topography M_T in the last column of the table.

A value of the total mass,

$$M_T = (3.318\,21 \pm 0.000\,08) \times 10^{20} \text{ kg,} \tag{8.16}$$

was computed by programme ICONTRIB (see appendix A) based on a global summation of 1°x1° quads using the UCLA 1° mean elevations and the de Graaff-Hunter density formula. This value, based on surface mean heights, ignores the ice/rock density contrast in the polar ice caps. Assuming that the mass of all polar ice is 0.237×10^{20} kg, [*e.g.*KIVIOJA 1967] the correct topographic mass would be

$$M_T = 2.865 \times 10^{20} \text{ kg.}$$

An alternative method of estimating this quantity is to derive the volume of the terrestrial topography from the global mean height given by the zero degree harmonic (equation 8.15) and compute the mass using a standard value of topographic density. This gives:

$$M_T = \frac{4}{3}\pi\,[(R + \mathrm{M}\{h\})^3 - R^3]\,\sigma_t$$

$$= 3.261\,4 \times 10^{20} \text{ kg.} \tag{8.17}$$

An under-estimate of the mass is expected, since a standard value of 2670 kg/m³ was used for the density σ_t compared with the greater values for topography below 2100 metres given by the de Graaff-Hunter formula. Nevertheless, the result provides a check.

Considerable differences occur in the values of ΔM_T derived from the coefficients at different levels. These are possibly due to the accumulated effects of computational inaccuracies in the coefficients. Certainly, the magnitude of the mass discrepancies, with respect to the total topographic mass, represents an accuracy somewhat beyond that expected of some aspects of the computations.

TABLE 8.7

DISPLACEMENT OF THE CENTRE OF MASS OF THE EARTH DUE TO THE TOPOGRAPHIC-ISOSTATIC MODEL

LEVEL	COEFF.	UNDULATION (non-normalized) (m)	POTENTIAL (J/kg)	R_p (m)	COORD.	VALUE (m)
Geoid	C_{11}	0.2891	2.835	6 371 024	X_E	0.289
	S_{11}	0.2629	2.578		Y_E	0.263
	C_{10}	0.3237	3.174		Z_E	0.323
Surface	C_{11}	0.3047	2.988	6 371 263	X_E	0.304
	S_{11}	0.2981	2.923		Y_E	0.298
	C_{10}	0.3488	3.421		Z_E	0.348
Orbit	C_{11}	0.2390	2.344	7 371 024	X_E	0.319
	S_{11}	0.2621	2.570		Y_E	0.350
	C_{10}	0.2501	2.453		Z_E	0.334

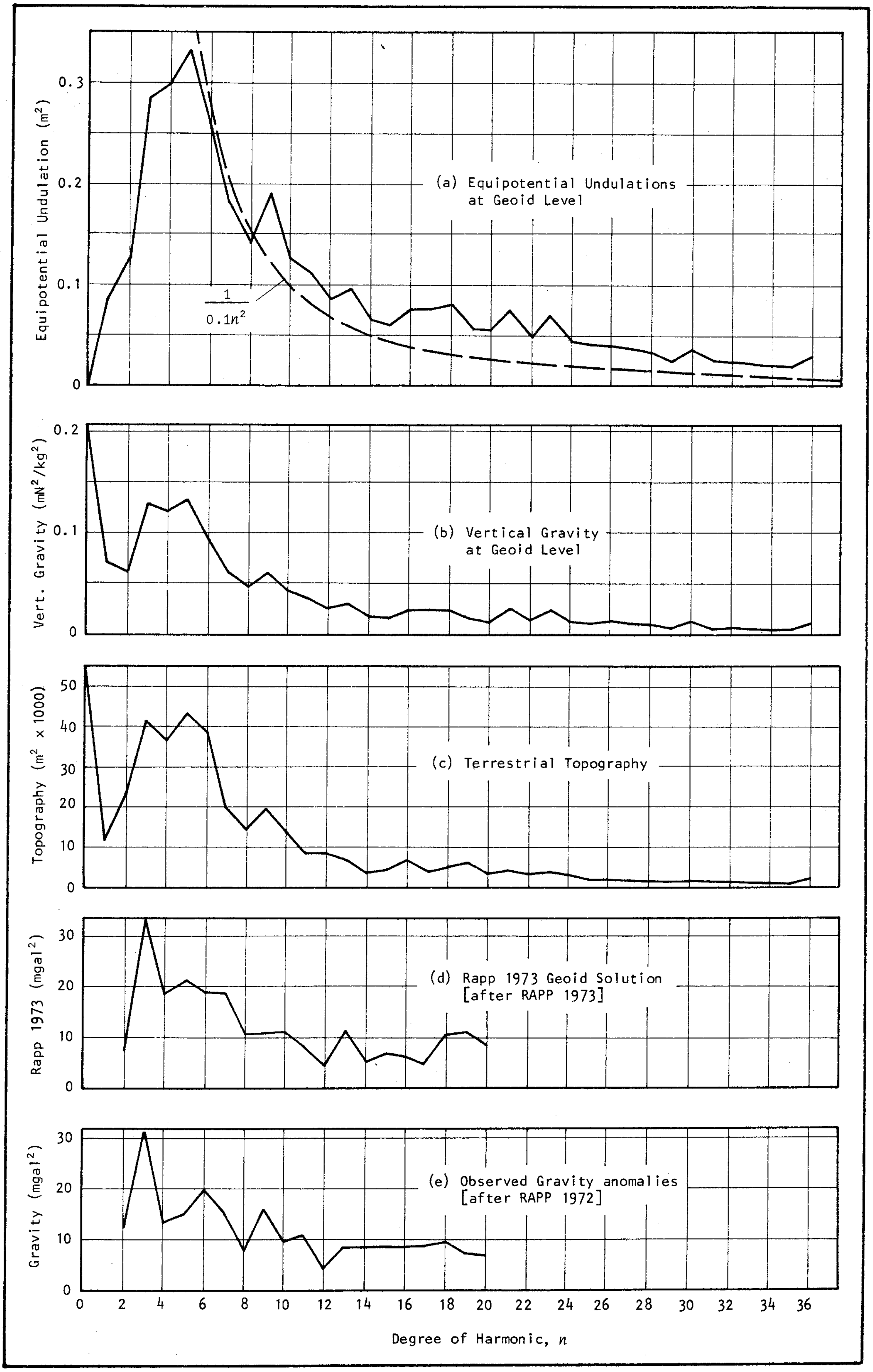

FIGURE 8.25

COMPARISON OF HARMONIC DEGREE VARIANCES

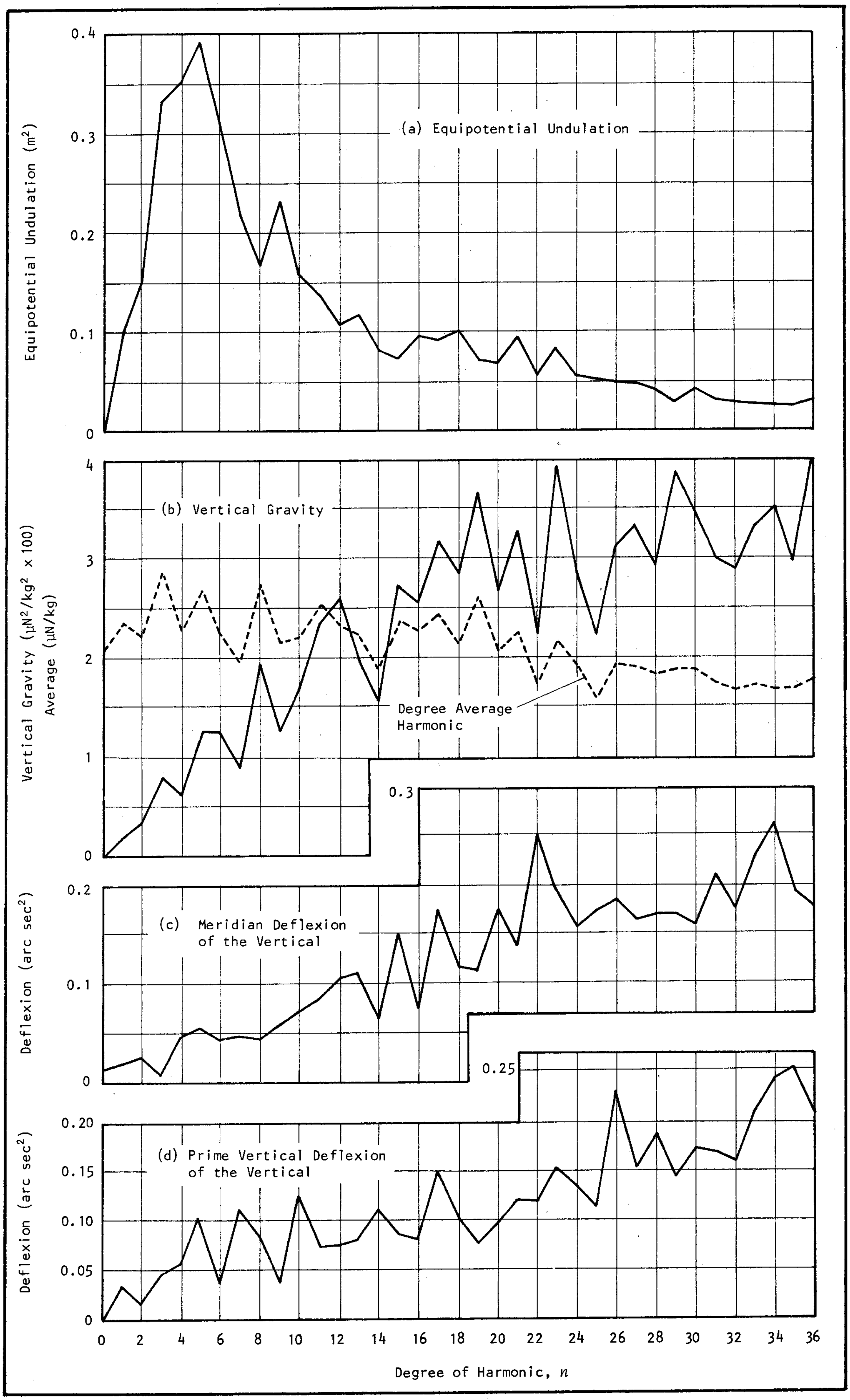

FIGURE 8.26

HARMONIC DEGREE VARIANCES OF GRAVITATIONAL EFFECTS AT SURFACE LEVEL

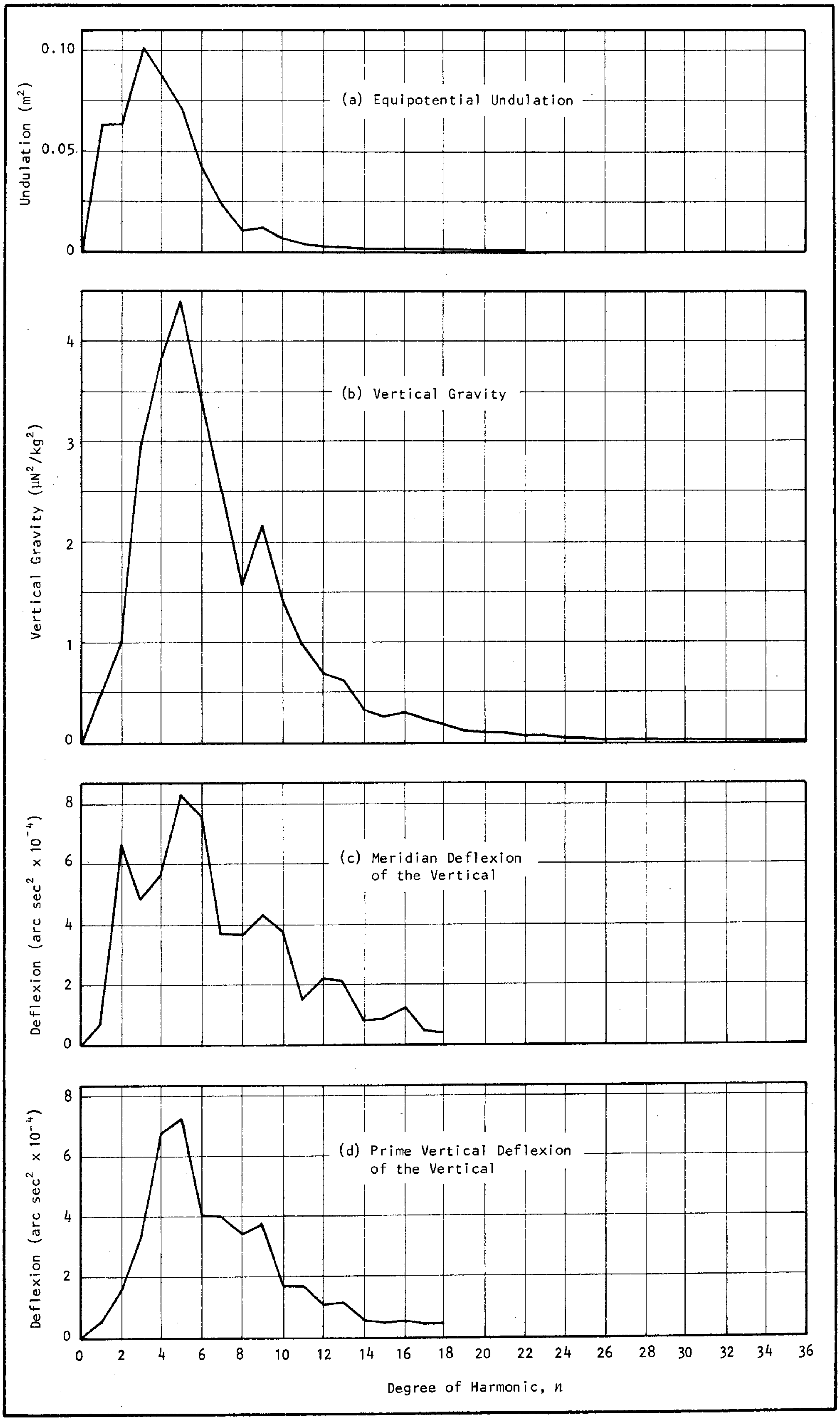

FIGURE 8.27

HARMONIC DEGREE VARIANCES OF GRAVITATIONAL EFFECTS AT ORBITAL ALTITUDE

Equations 8.13 provide the means of converting the non-normalized first degree harmonics of the topographic-isostatic potential to displacements of the earth's centre of mass. This conversion is performed in table 8.7 for coefficients available at geoid, surface, and orbital levels, using the value $kM_E = 3.986 \times 10^{14}$ m^3/s^2. All three components of the displacement are positive, which indicates movement of the centre of mass of about 0.5 metres towards the dominant continental masses of Europe and Asia. This is to be expected, since the greater geocentric radius of the positive topographic masses in comparison with the negative compensation, produces a larger moment about the geocentre.

HARMONIC DEGREE VARIANCES. Degree variances, as defined by equation 8.8, for the spheropotential undulations and vertical gravity at geoid level are compared with those of the terrestrial topography in figure 8.25. Also plotted, for comparison, are the anomaly degree variances of the earth's disturbing potential spectrum from Rapp's combination solution and those computed from the gravity data alone [RAPP 1973, table 3; RAPP 1972]. In figures 8.26 and 8.27 the degree variances for the undulations, vertical gravity, and deflexions of the vertical are plotted for surface and orbital elevations respectively.

Spectra for the undulations attenuate approximately in accordance with Kaula's "rule of thumb" [*e.g.* KAULA 1973, p.243]: in this case $\Sigma_n^2 \simeq 1/0.1n^2$, as plotted in figure 8.25a. This trend is observable —with some notable exceptions—in most of the analysis results. Correlation of the gravitational effects with the terrestrial topography is again clearly demonstrated in the variances, most noticeably in the vertical gravity at the geoid. RAPP [1973, p.64] has commented on the low value of the degree variance at $n=8$ in most geoid solutions and in the observed gravity anomalies and this phenomenon is a notable feature of the results presented here, even at satellite altitudes (figure 8.27). A similar effect is noticeable at $n=4$. As these characteristics are strongly portrayed in the analysis of the terrestrial topography, the inference that the topography may be a causative agent must be noted, but the possibility of a more fundamental geophysical origin—which could also dominate the distribution of topographic masses—cannot be overlooked [*e.g.* see KAULA 1973].

A remarkable exception to the general trend appears in the spectra of the effects on the gravity vector at the earth's surface (figure 8.26). The already noted preponderance of the higher degrees is distinctly confirmed. However, the deficiency of long wave effects at surface level is not unexpected when the tendency for cancellation of all but local influences of the topography is taken into account. Harmonics of the effect at the surface are approximately one order smaller than they are for the effect at geoid level. Moreover, the *average* value of the coefficients at surface level, calculated by degree (see figure 8.26) attenuate slowly for higher degrees.

9

Gravitational Effects of the Atmosphere

9.1 INTRODUCTION

In §1.1 it was pointed out that the earth's atmosphere cannot be ignored in gravimetric reduction procedures and determinations of the figure of the earth, if the anticipated precision of modern solutions is to be attained. It is not illogical to think of the atmosphere as an extension of the earth's topography. Like the crust, it forms a relatively thin, irregular layer and its lower boundary coincides with the terrain and ocean surfaces and may, therefore, be defined by the same numerical data. Only the reasonably large density contrast between atmosphere and crust (approximately three orders of magnitude) provides the conditions whereby the gravitational effects of the atmosphere can, as a practical expedient, be ignored or treated with less mathematical rigour. Admittedly, the gaseous nature of the atmosphere, and its attendant compressibility and mobility, introduce considerably greater complexity to the problem of evaluating its geodetic influence. Strictly, dynamic models would be required to represent the atmosphere with full theoretical rigour and this may not be compatible with conventional geodetic techniques. Presumably standardized static models, founded on statistical anlyses, will need to be defined and widely recognized for geodetic studies of high precision.

Tentative definitions and procedures for geodetic treatment of the atmosphere have been announced, such as the approach developed by ECKER and MITTERMAYER [1969] and included in the definition of the *Geodetic Reference System 1967* (GRS67) [IAG 1971] and the definitions incorporated in the recommendations of a special study group of the IAG [MORITZ 1975].

The influence of the atmosphere on solutions of the geodetic boundary value problem have been investigated theoretically by MATHER [1973] and compared with the GRS67 approach [ANDERSON *et al.* 1975]. Using the results of the present study, it has been demonstrated [*ibid.*] that the atmosphere effects cannot be neglected in studies of quasi-stationary sea surface topography [MATHER 1974; MATHER 1975].

EXTENSION OF THE EVALUATION METHOD TO THE ATMOSPHERE

Most of the resources necessary for an evaluation of the gravitational effects of a model of the atmosphere—including the theoretical development, computer routines, and digital data—had already been established for the evaluation of topographic effects which forms the major part of this thesis.

Consequently, it was recognized that fairly minor modifications, along with the development of an atmospheric model, would make it feasible to implement a direct evaluation of the gravitational effects of the atmosphere. Unfortunately, limitations on the time available to the writer to undertake such a research programme, and an accute shortage of computer allocations due to rearrangement of the University of New South Wales' central computing facilities at that time, meant that only an abbreviated study could be implemented.

Generally, computations for the atmospheric effects conformed with the specifications adopted for the topographic evaluation (see §2.4). Exceptions included:

(a) evaluation at geoid level was not undertaken;

(b) an evaluation grid interval of 30°, based on the Greenwich meridian and the equator, was adopted;

(c) an atmospheric model incorporating linear density variations with respect to height was used (see §9.2); and

(d) the atmosphere was divided vertically into two layers—upper and lower —and the effects of these were computed separately.

As a matter of expediency, these specifications were adopted without re-evaluating the accuracy of the techniques in the manner set out in §2.3. It is tacitly assumed that the relative accuracy of the results will be little affected by the introduction of the different geometric configuration and density model of the atmosphere.

9.2 ATMOSPHERIC MODEL

Elements of the atmospheric model and the geometric configuration are illustrated by figure 9.1. An ellipsoidal reference surface and appropriate normal gravity formula as stated in table 3.4 were retained.

DENSITY MODEL

Because of its ready availablility, the vertical density variation tablulated for the NACA Standard Atmosphere [SMITHSONIAN TABLES 1958, pp.267 & 284] was assumed to prevail globally. Thus lateral variations of density—due to climate and gravity variations with latitude—are suppressed and the model is static. However, the curvilinear relationship of the NACA model is not conveniently accommodated in the potential and gravity formulae, so a model based on stepwise linear regression of the NACA values was adopted. The density was defined within four "layers" by the basic linear equation:

$$\sigma_a = \sigma_{a0} + D_a z \tag{9.1}$$

where z is altitude in a local coordinate system,

σ_{a0} is a homogeneous component of the density, being the density at zero altitude, and

D_a is the vertical density gradient.

Each layer is 10 km thick so that the first 40 km of the atmosphere is contained in the model. Though the upper boundary, at 40 km above the reference surface, is arbitrary, calculations indicate that approximately 99.7% of the mass of the atmosphere occurs below this level (see §9.4). Table 9.1 contains the adopted values of the linear regression coefficients for each layer and figure 9.2 illustrates the fit to the NACA model.

UPPER AND LOWER ATMOSPHERE. An arbitrary subdivision of the atmosphere into upper and lower parts was made at an altitude of 10 km. By this means, the gravitational effects of the lowest layer—which alone

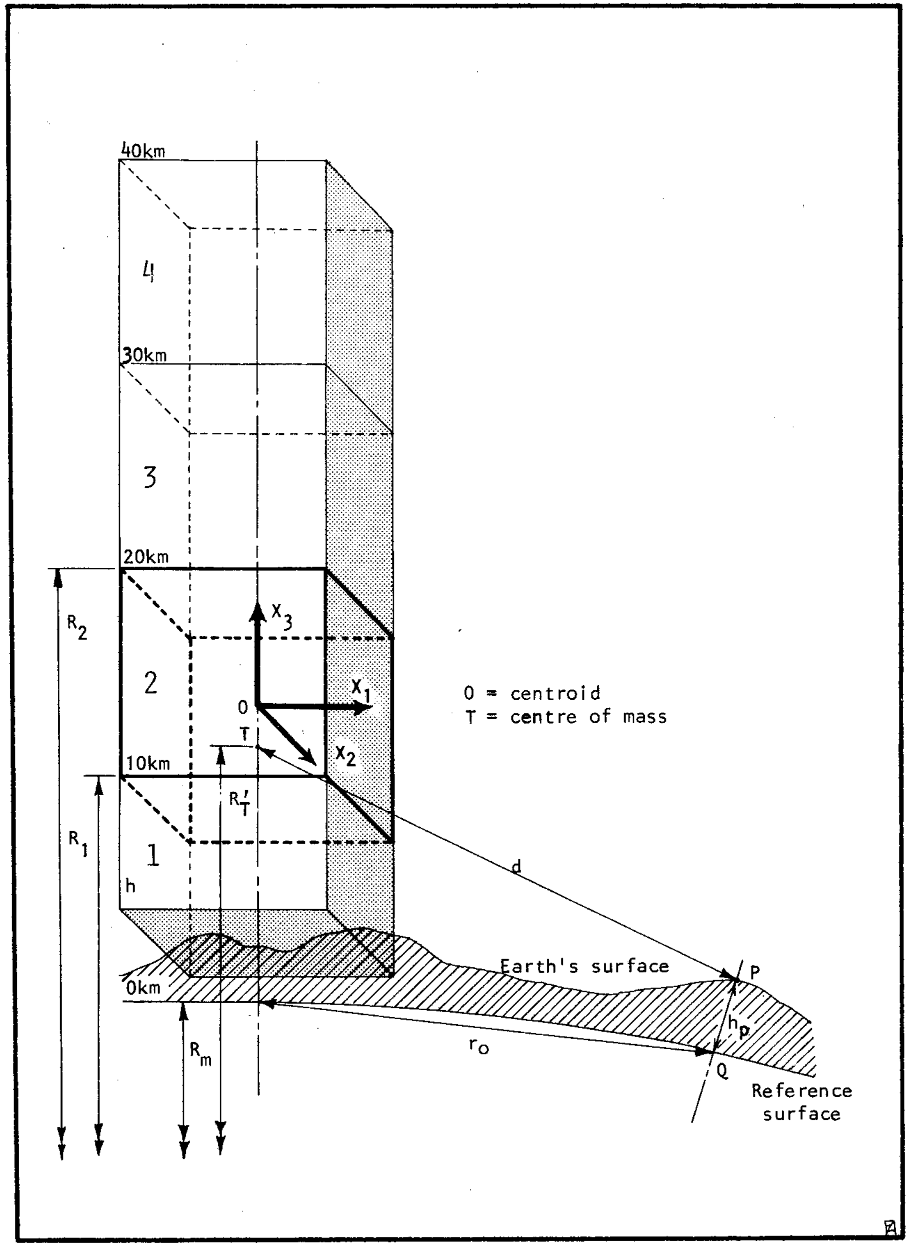

FIGURE 9.1

GEOMETRY OF ATMOSPHERIC MODEL

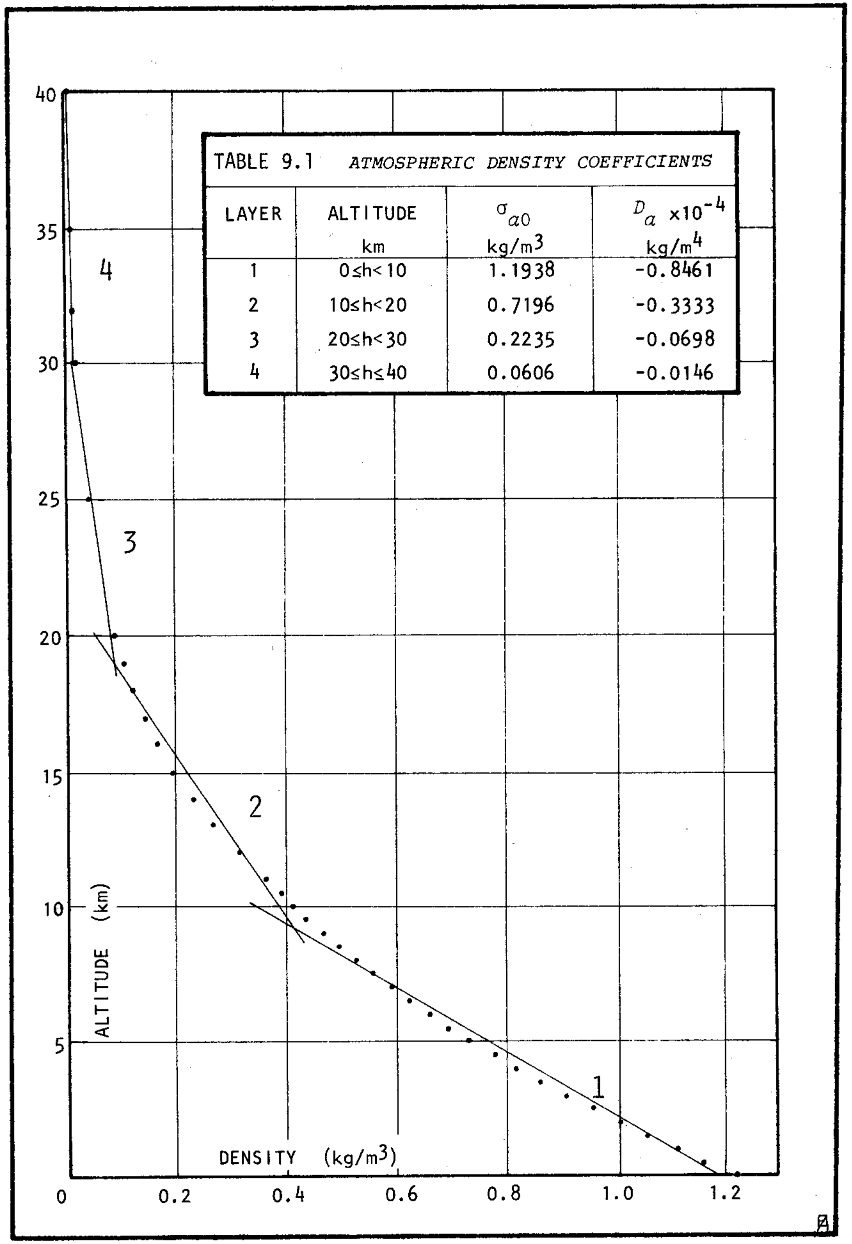

TABLE 9.1 *ATMOSPHERIC DENSITY COEFFICIENTS*

LAYER	ALTITUDE km	σ_{a0} kg/m^3	$D_a \times 10^{-4}$ kg/m^4
1	$0 \le h < 10$	1.1938	-0.8461
2	$10 \le h < 20$	0.7196	-0.3333
3	$20 \le h < 30$	0.2235	-0.0698
4	$30 \le h \le 40$	0.0606	-0.0146

FIGURE 9.2

NACA ATMOSPHERIC DENSITY AS A FUNCTION OF ALTITUDE contains the influence of the irregularities in the topographic surface forming the lower bound of the atmosphere—could be computed and analysed separately from the remaining three uppermost layers. Use of the terms "upper" and "lower" in this context has no connexion with their meteorological significance and does not conform with the division usually made at the tropopause [*e.g.* SMITHSONIAN TABLES 1958].

QUADRATURE MODELS

Zone boundaries and quadrature subdivision sizes as defined in table 2.3 were retained for the atmospheric computations.

INNER ZONE. Each subdivision, contained by equiangular geographical boundaries and layer boundaries above and below, was approximated by a coincident, right rectangular parallelepiped of equivalent volume with dimensions as defined in table 3.4. Vertical dimensions of quads in the three uppermost layers are constant at 10 km, but the first layer has a lower boundary defined by the topographic mean height h in each quad (see figure 9.1).

MID AND OUTER ZONES. Quads in the mid and outer zones for each layer were treated as an equivalent point mass located at their centre of mass T. Due to the linear density model within each quad, this point does not coincide with the centroid. Assuming a spherical approximation and small lateral dimensions of the quad, the approximate spherical coordinates of the centre of mass are $(\phi_\mu, \lambda_\mu, R_T')$, where ϕ_μ and λ_μ are the mid values of latitude and longitude referred to in §3.4 and R_T' is the geocentric radius given by equation 3.56. The mass of the quad, taken to be that of a spherical tesseroid, is given by equation 3.44. In both formulae the density coefficients must be replaced by their atmospheric equivalents, which necessitates extraploation of the constant part to a geocentric value.

9.3 FORMULAE AND COMPUTATIONAL METHOD

INNER ZONE

Potentials due to homogeneous and linear parts of each inner zone quad within each layer of the atmosphere were computed according to the rectangular parallelepiped equations, 4.34a and 4.35a. Equations 4.47, 4.48, 4.51, and 4.52 provided the basis for the evaluation of the gravitational attraction components. It should be noted that local coordinates used in these formulae refer to a reference frame located at the centroid of the parallelepiped (*not* the centre of mass) and this was constrained to coincide with the "mid point" of the spherical tesseroid (see figure 9.1)

Inner zone contributions were evaluated for points at the earth's surface only. Unreasonable contact sub-zone effects were controlled by equalizing the contact quad heights in the same manner as was used in the topographic calculations (see §8.2). Subsequent contact corrections were thereby avoided. Programme INNATMO (appendix A), a modified version of INNZONE, was developed for the inner zone calculations and the same topographic datasets were utilized.

MID AND OUTER ZONES

Point mass approximation formulae, given by the first term of each of the series 5.21, 5.32, 5.33, and 5.46 were used to compute the potential and attraction components due to quads in the mid and outer zones. In addition to the evaluation at surface level, global calculation of the atmospheric effects at satellite orbit altitude (1000 km) was included in the outer zone programme. The programmes used—MIDATMO and OUTATMO (see appendix A)—were based on the equivalent topographic routines and the same datasets were used to determine the topographic surface.

9. GRAVITATIONAL EFFECTS OF THE ATMOSPHERE

TREATMENT OF RESULTS DATA

Programme HARMONIC was again employed to combine the effects of all zones and, subsequently, to total the effects of the upper and lower atmosphere. This programme was also used to analyse the data for spherical harmonic coefficients.

CORRELATION WITH TOPOGRAPHIC HEIGHT. Prior to analysis, the results data was inspected to determine whether or not there was any correlation of the potential and attraction values with the topography. Should it exist, such correlation could provide a means of interpolating values on a finer evaluation grid, thereby improving the resolution of the results. ECKER and MITTERMAYER [1969] present their results as corrections to observed gravity which are a function of the height of the observation point. Accordingly, the present results were analysed for correlation with the height of the evaluation point at the surface of the earth, with the expectation that the vertical component of gravity, at least, should display this characteristic. Values of the potential and three components of the attraction due to the lower atmosphere at all 62 points of the global 30°x30° grid were submitted to a linear correlation analysis and were also plotted. Only the vertical gravity was found to be significantly correlated with the height of the computation point, though the potential appears to exhibit a degree of curvilinear correlation. Table 9.2 contains the least squares, linear regression coefficients g_0 and g_1 of the vertical component of gravity and the correlation coefficient r_g. The data is plotted in figure 9.3.

TABLE 9.2

LINEAR CORRELATION OF THE VERTICAL ATTRACTION OF THE ATMOSPHERE WITH HEIGHT.

n	g_0 µN/kg	g_1 µN/kg m	r_g
62	0.11956	3.98×10^{-4}	-0.997

Interpolated values of the vertical gravity due to the lower atmosphere G_{za} were, therefore, computed on the remainder of a 5°x5° global grid using the linear relationship:

$$G_{za} = g_0 + g_1 h_p, \tag{9.2}$$

where h_p is the height of the observation point at the surface of the earth. While the correlation is quite high, it is apparent from the plot that the data follows a slightly curvilinear trend, which is in agreement with the findings of Ecker and Mittermayer.

The remainder of the results data was analysed on a 30°x30° global grid. Values of the potential and the horizontal components of the attraction were converted to undulations and deflexions of the vertical in accordance with Bruns' theorem (equations 1.5 and 1.6).

9.4 RESULTS AND HARMONIC ANALYSIS

RESULTS

EFFECT ON POTENTIAL. Figure 9.4 depicts the disturbance of the gravitational potential at the earth's surface due to the adopted model of the atmosphere up to an altitude of 40 km. The contours are based on fully-normalized spherical harmonic coefficients up to (6,6) of the computed values on a 30°x30° grid. Broad negative correlation with the topography is evident, the minima and maxima occurring over the Himalayas and Pacific Ocean respectively.

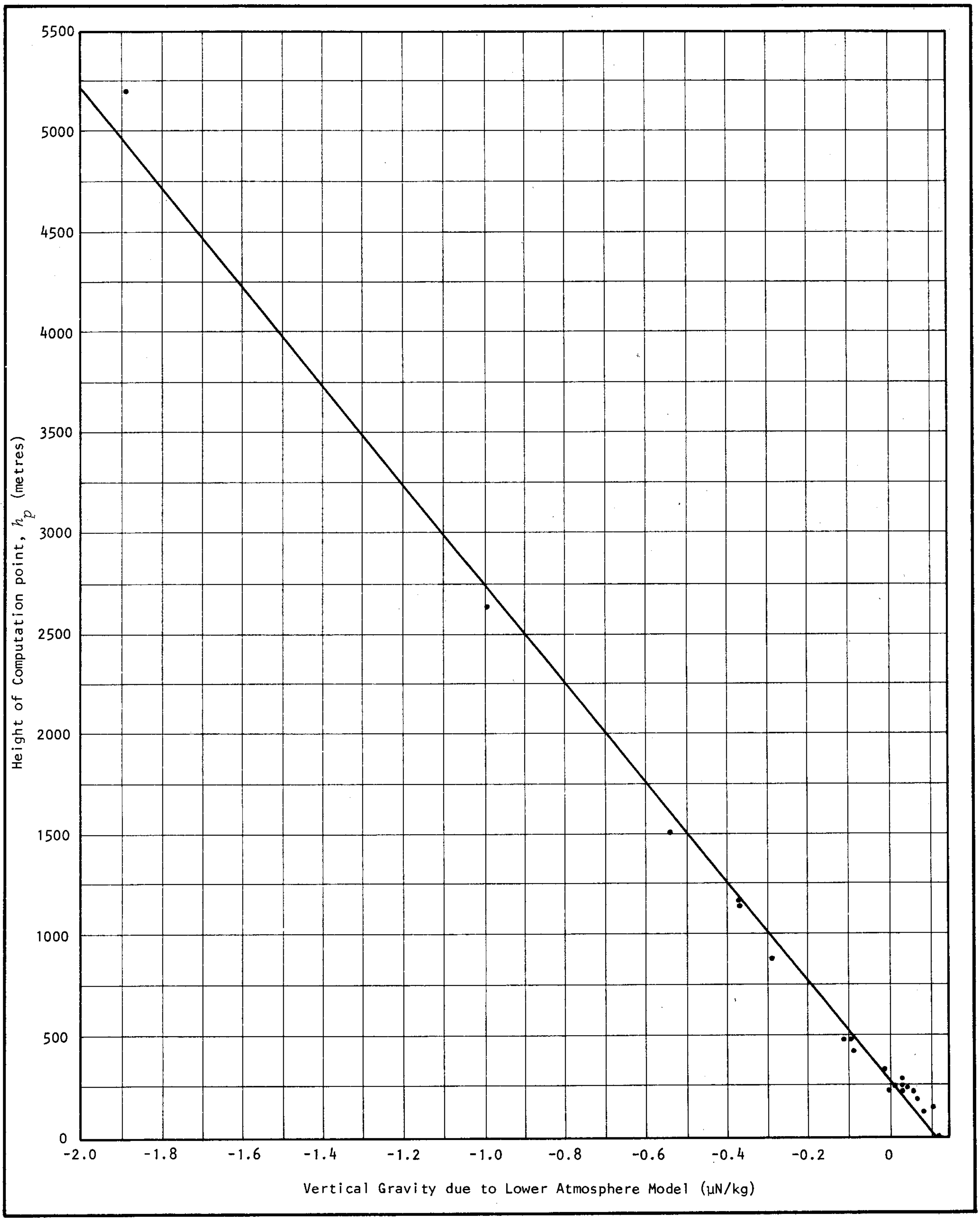

FIGURE 9.3

CORRELATION OF VERTICAL COMPONENT OF GRAVITY DUE TO LOWER ATMOSPHERE MODEL WITH HEIGHT OF COMPUTATION POINT

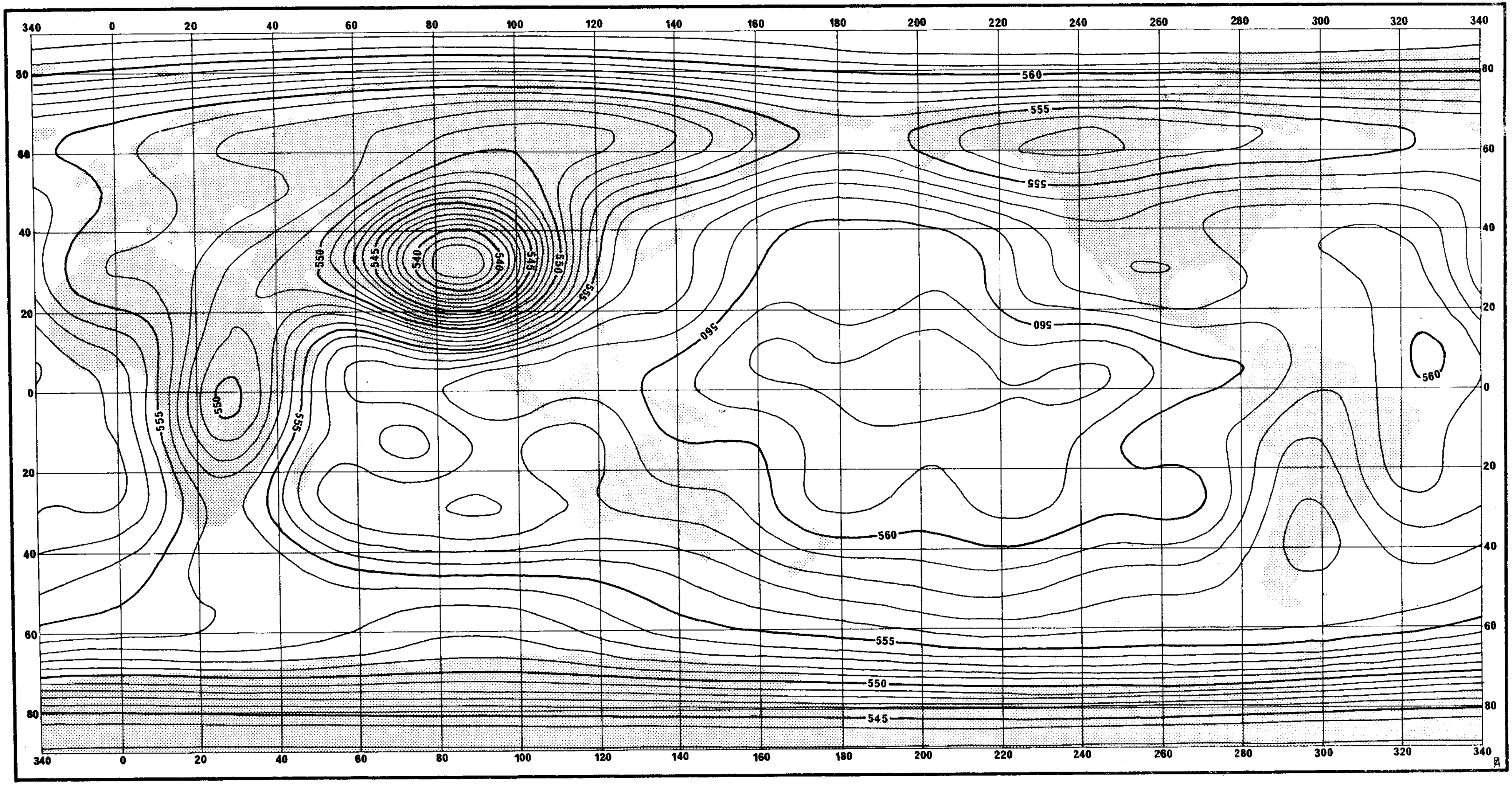

FIGURE 9.4

EQUIPOTENTIAL UNDULATIONS AT THE EARTH'S SURFACE DUE TO THE ATMOSPHERIC MODEL BASED ON A SPHERICAL HARMONIC ANALYSIS TO (6,6) OF DATA ON A 30° GRID

Contour interval = 1 cm

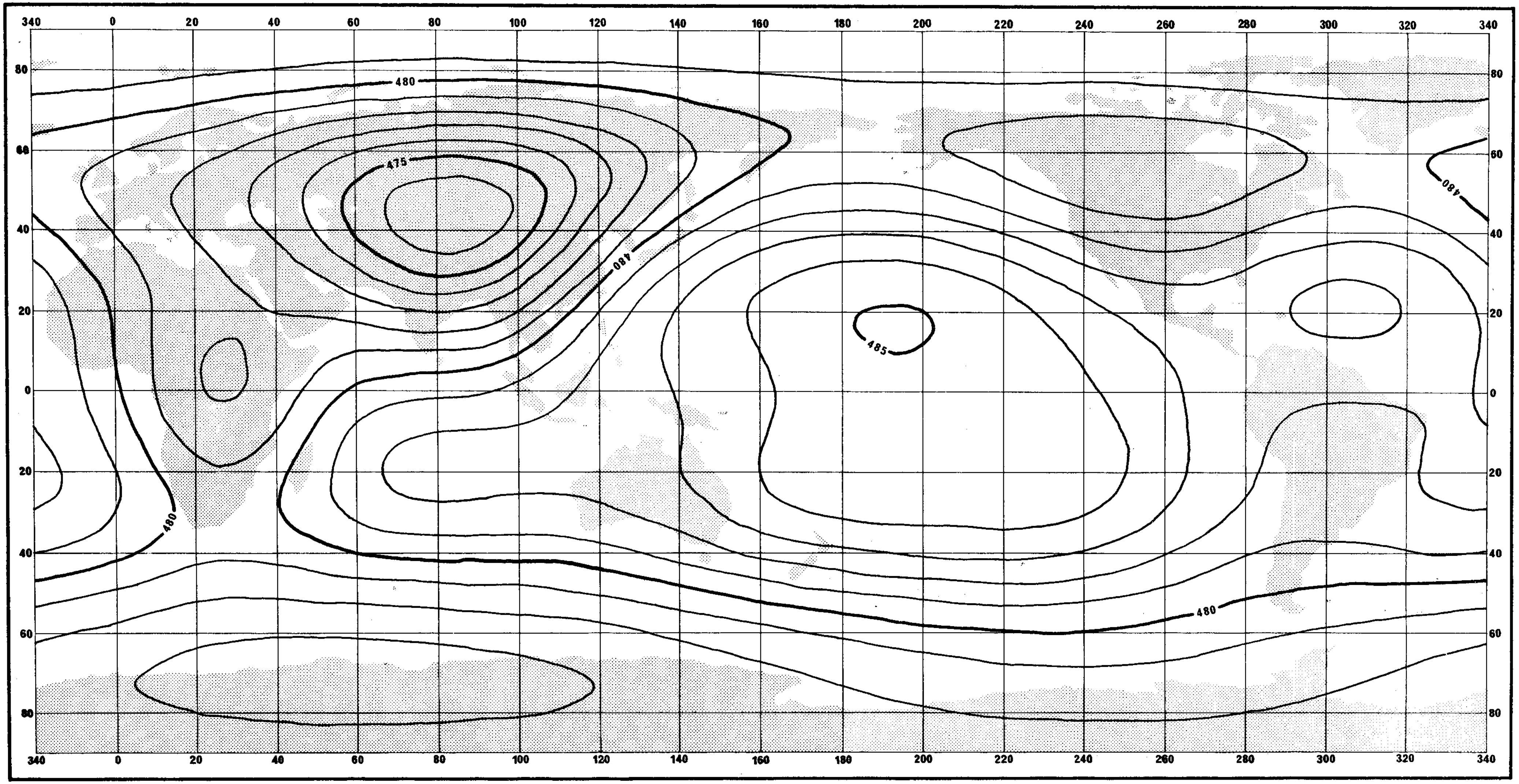

FIGURE 9.5

EQUIPOTENTIAL UNDULATIONS AT SATELLITE ORBIT ALTITUDE (1000 km) DUE TO THE ATMOSPHERIC MODEL

Contour interval = 1 cm

9. GRAVITATIONAL EFFECTS OF THE ATMOSPHERE

In the model of the atmosphere adopted, the three layers of the upper atmosphere are each defined to have a constant thickness of 10 km. Such a configuration conforms most nearly to the definition of *homothetic* ellipsoids [SOMMERVILLE 1946, p.203]. While the correspondence is not exact, the approximation is very good for the small eccentricity and large radius of the reference ellipsoid. It should be noted that the definition does not conform with that of *confocal* ellipsoids. MACMILLAN [1930, p.10] demonstrates that the attraction of an ellipsoidal homoeoid—which is homogeneous in concentric layers—upon an interior point is everywhere zero. It follows that the gravitational potential at any such point must be constant. Therefore, it may be anticipated that this condition would be approximately true for the model of the upper atmosphere. In practice the computed surface potential undulations due to the upper atmosphere were found to be truely constant with respect to longitude, but a small variation with latitude—ranging from 1.499 metres at the poles to an equatorial value of 1.517 metres—was observed. How much of this variation, which considerably exceeds the order of the flattening, can be attributed to the departures of the model from an exact ellipsoidal homoeoid and how much to the inaccuracies of the numerical integration process is uncertain.

Results of the computations at orbital altitude are illustrated by figure 9.5. Again, the contours are based on a harmonic spectrum to order (6,6). Similar trends with a higher degree of smoothing are noticeable, the range of undulations being approximately halved. The reduction in magnitude of the effect from surface to orbit levels agrees reasonably with that which would be expected over the distance of 1000 km, assuming a spherical shell model of the atmosphere.

The limitations of the coarse evaluation grid interval of 30° and truncation of the harmonic coefficients at degree 6 should be emphasized. A certain amount of smoothing is inevitable and the shape of the contours is partially dependent on the particular geographical location of the grid. For instance, the effect of the Himalayas is represented with reasonable accuracy since the chosen grid fortuitously falls on the most topographically significant point in that region. However, in North and South America, the grid happens to straddle the major topographic features—the Rocky Mountains and the Andes—so that their influence is largely suppressed. Despite these limitations, the range of values and general pattern of the results presented here should be substantially correct.

EFFECT ON VERTICAL GRAVITY. Contours of the atmospheric effect on vertical gravity at the surface are shown in figure 9.6. They are based on a harmonic expansion to (9,9) of values interpolated on a 5°x5° grid in accordance with equation 9.2. Truncation of the harmonic series has caused considerable smoothing of the results. For example, actual computed values at the minima which occur over the main continents are listed in table 9.3. Except for these localized distortions, the general pattern of the effect is

TABLE 9.3

SELECTED MINIMUM VALUES OF THE ATMOSPHERIC EFFECT ON GRAVITY AT THE EARTH'S SURFACE

LOCATION	POSITION		VALUE
	LAT.	LON.	(nN/kg)*
Himalayas	35	95	-2120
Antarctica	-80	80	-1607
Andes	-30	290	-1269
Rocky Mts.	45	250	-945
Southern Africa	-25	25	-529

* *1 nN/kg = 0.1 μgal.*

correctly portrayed. Over ocean areas the computed value is consistently positive at an average value of about 100 nN/kg (10 μgal).

Computed values of the effect of the upper atmosphere were found to vary with location, reaching a

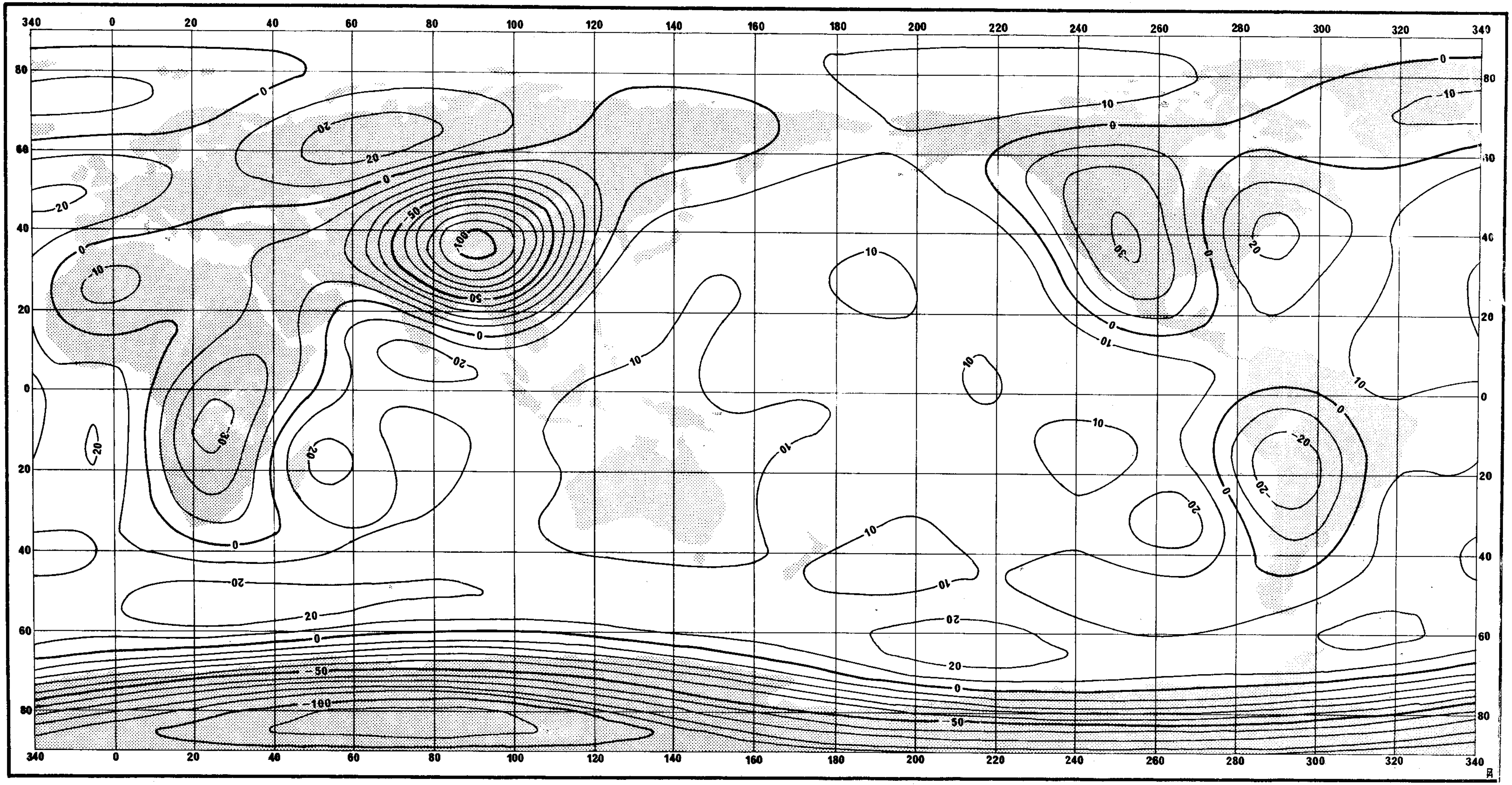

FIGURE 9.6

VERTICAL COMPONENT OF GRAVITY AT THE EARTH'S SURFACE DUE TO THE ATMOSPHERIC MODEL BASED ON A SPHERICAL HARMONIC ANALYSIS TO (9,9) OF DATA INTERPOLATED ON A 5° GRID

Contour interval = 10 μgal
= 100 nN/kg

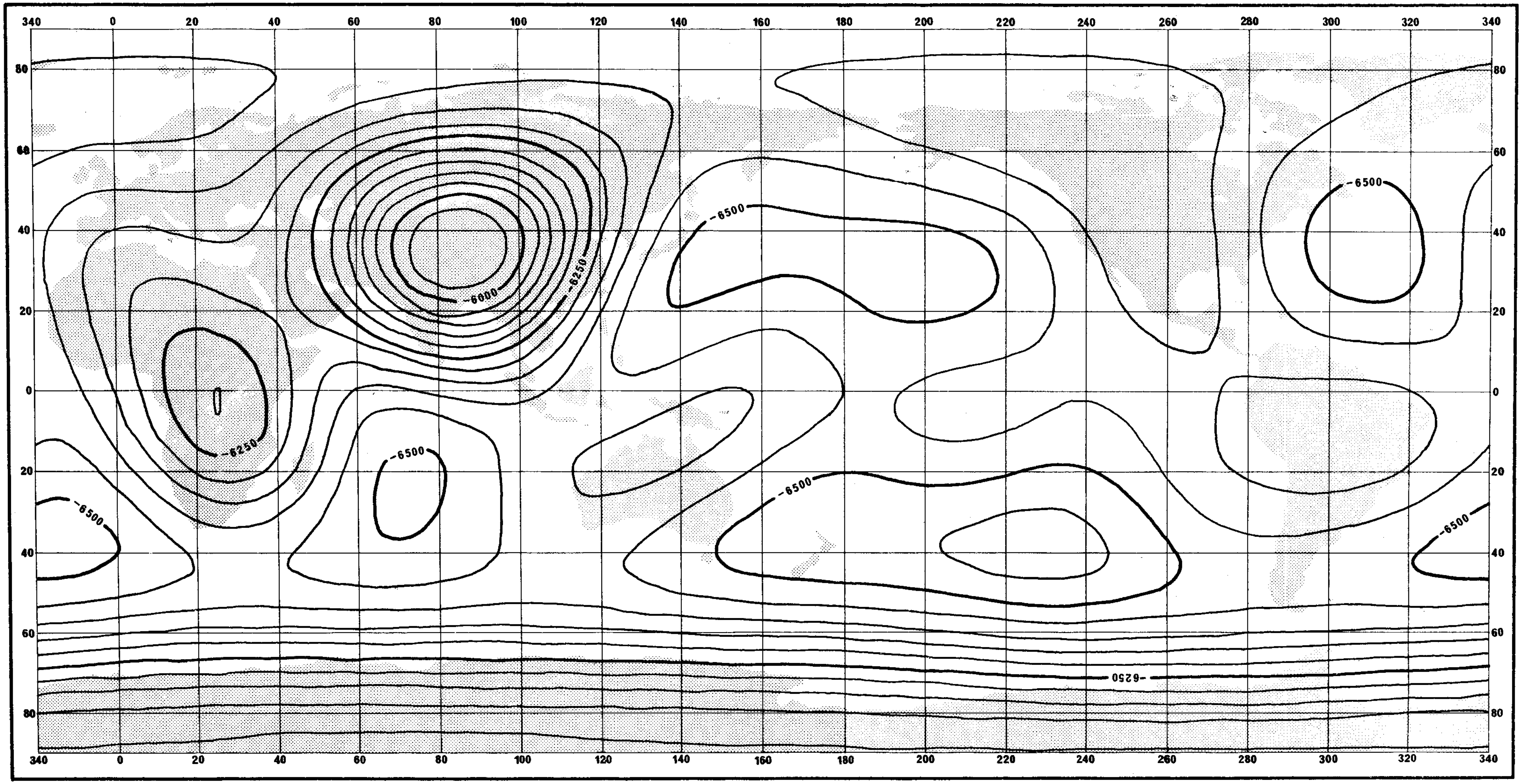

FIGURE 9.7

VERTICAL COMPONENT OF GRAVITY AT SATELLITE ORBIT ALTITUDE (1000 km) DUE TO THE ATMOSPHERIC MODEL

Contour interval = 50 nN/kg
= 5 µgal

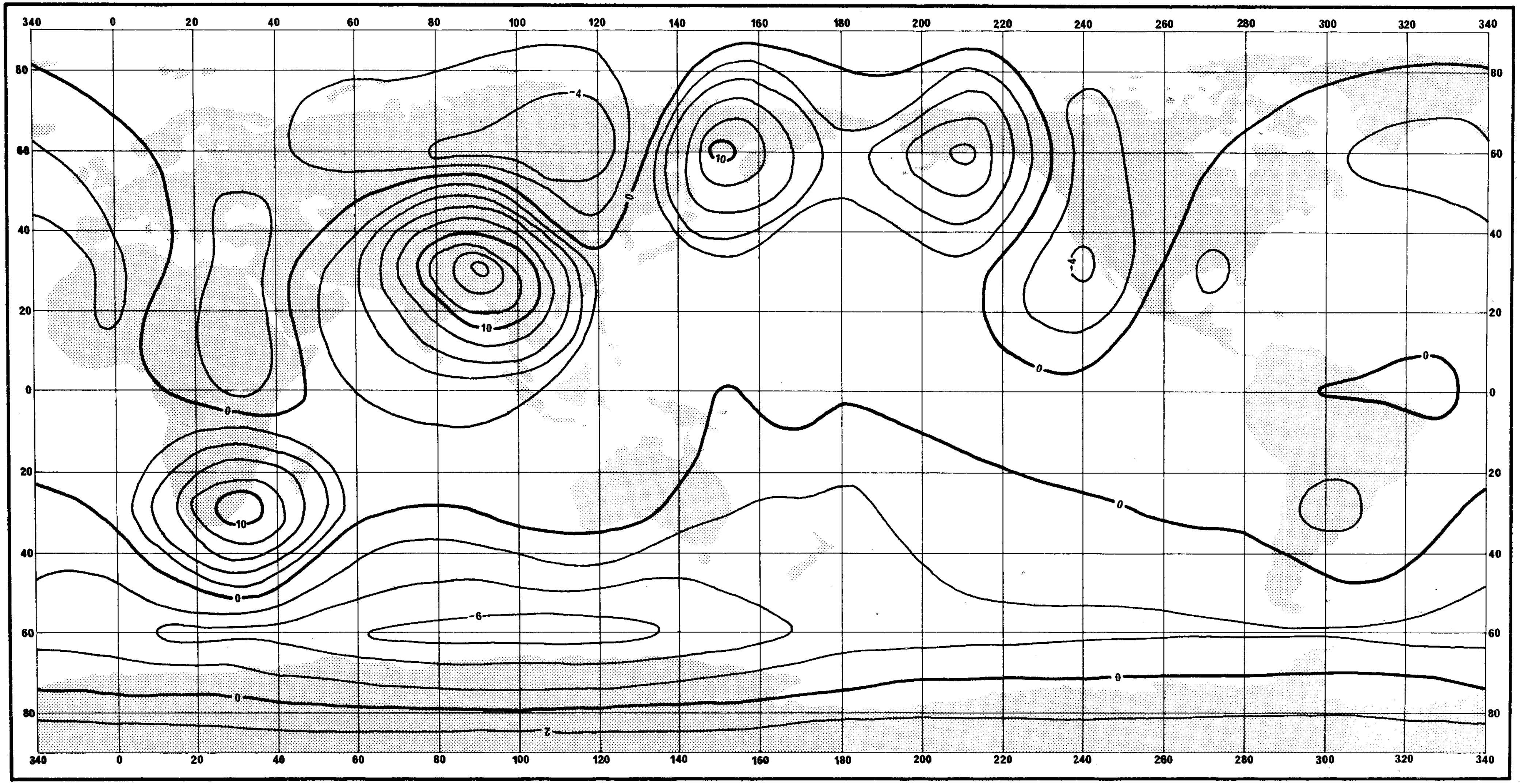

FIGURE 9.8

MERIDIAN COMPONENT OF THE DEFLEXION OF THE VERTICAL AT THE EARTH'S SURFACE DUE TO THE ATMOSPHERIC MODEL BASED ON A 30°×30° GRID EVALUATION

Contour interval = 2 arc milliseconds

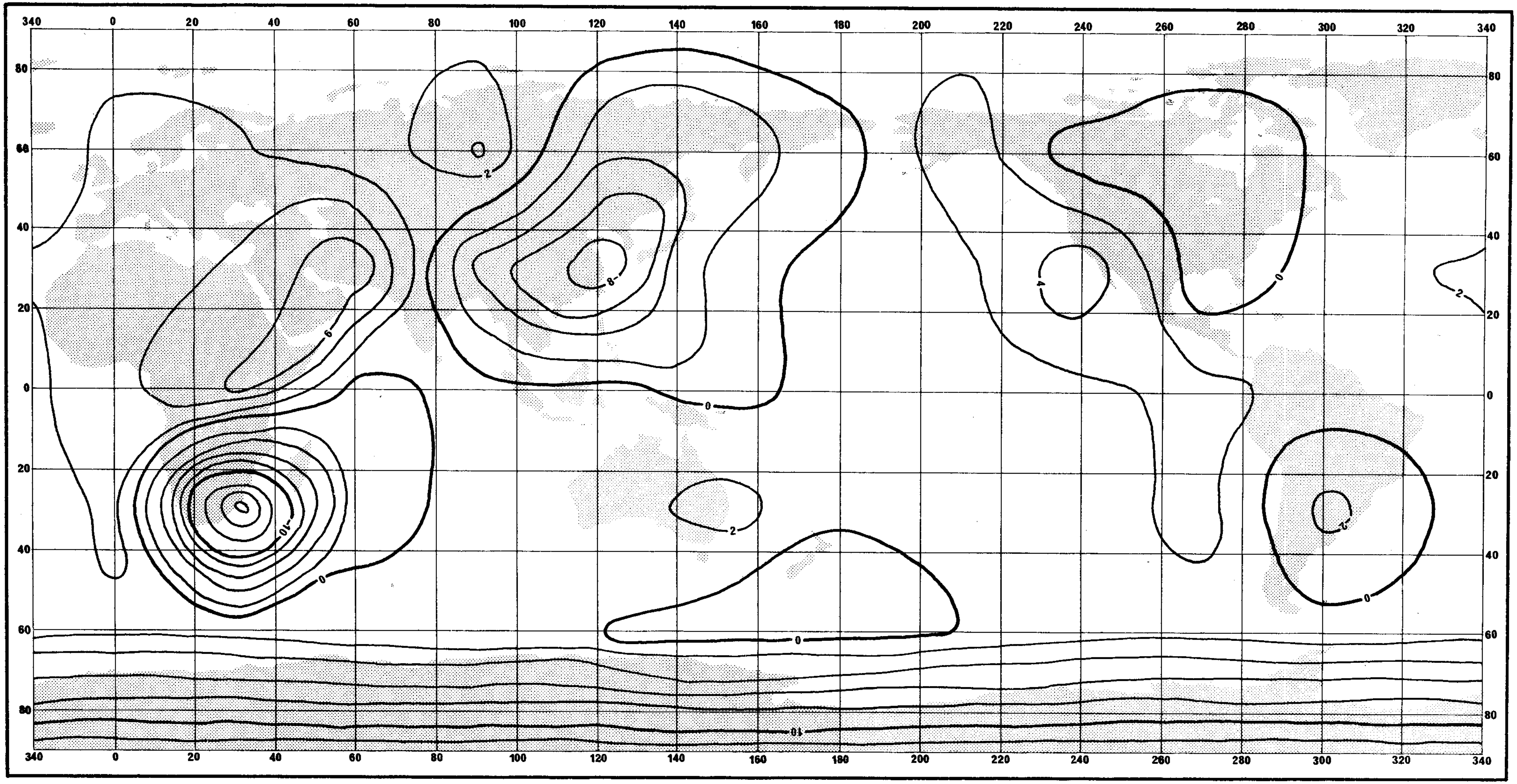

FIGURE 9.9

PRIME VERTICAL COMPONENT OF THE DEFLEXION OF THE VERTICAL AT THE EARTH'S SURFACE DUE TO THE ATMOSPHERIC MODEL BASED ON A 30°×30° GRID EVALUATION

Contour interval = 2 arc milliseconds

maximum of about 7 nN/kg (0.7 μgal). To the order of the flattening these results can be considered to conform with the theoretically expected value of zero.

Figure 9.7 depicts the influence of the atmospheric model on vertical gravity at orbital altitude (1000 km). Because the point of evaluation is outside the atmosphere the resulting effect is considerably greater than the surface values. A tendency towards correlation with the topography is noticeable, the atmospheric influence being diminished over the high mountain areas where the thickness of the atmosphere is reduced. Values range from -5.95 μN/kg (-595 μgal) to -6.55 μN/kg (655 μgal).

EFFECTS ON THE HORIZONTAL COMPONENTS OF GRAVITY. Meridian and prime vertical deflexions of the vertical at the surface due to the atmospheric model are presented in figures 9.8 and 9.9 respectively. The data contoured in these figures comprises the actual computed values on a 30° grid, since a harmonic analysis of the deflexions was not performed. Consequently, localized influences at particular points may tend to dominate the overall pattern. None of the deflexions exceed 17 arc milliseconds.

CONTRIBUTIONS TO THE ATMOSPHERIC EFFECT

Two representative points have been chosen to exemplify the compositon of the atmospheric effect — one in the Himalayas (30°N, 90°E) and one in the Indian Ocean (30°S, 90°E). These points have similar topographic characteristics to points A and D, respectively, which were used in §8.3 (see figure 8.4). Contributions to the potential undulations, vertical gravity, and deflexions of the verical, due to the upper and lower atmospheric models in each of the three zones are set out in tables 9.4 and 9.5.

TABLE 9.4

CONTRIBUTIONS TO THE ATMOSPHERIC EFFECTS AT A POINT IN THE HIMALAYAS

Lat. = 30°N, Long. = 90°E, Height = 5216 m

EQUIPOTENTIAL UNDULATIONS (m)					
LEVEL	SOURCE	INNER	MID	OUTER	TOTAL
Surface	Lower	0.0142	0.1948	3.6682	3.8773
	Upper	0.0122	0.1191	1.3845	1.5157
	Total	0.0263	0.3139	5.0528	5.3930
Orbit	Total	--	--	--	4.7441
VERTICAL GRAVITY (μN/kg)					
Surface	Lower	1.065	-0.136	-2.820	-1.891
	Upper	1.046	0.010	-1.054	0.003
	Total	2.111	-0.126	-3.874	-1.888
Orbit	Total	--	--	--	-5.915
MERIDIAN DEFLEXION (arc mseconds)					
Surface	Lower	-1.832	14.512	4.318	16.997
	Upper	-0.021	0.030	0.000	0.010
	Total	-1.853	14.542	4.318	17.007
Orbit	Total	--	--	--	4.465

TABLE 9.4 Continued

PRIME VERTICAL DEFLEXION (arc milliseconds)					
LEVEL	SOURCE	INNER	MID	OUTER	TOTAL
Surface	Lower	-3.581	-0.674	-0.421	-4.676
	Upper	0.021	0.295	0.000	0.316
	Total	-3.559	-0.379	-0.421	-4.360
Orbit	Total	--	--	--	-0.379

TABLE 9.5

CONTRIBUTIONS TO THE ATMOSPHERIC EFFECTS AT A POINT IN THE INDIAN OCEAN

Lat. = 30°S, Long. = 90°E, Height = 0 m

EQUIPOTENTIAL UNDULATIONS (m)					
LEVEL	SOURCE	INNER	MID	OUTER	TOTAL
Surface	Lower	0.0356	0.3307	3.7083	4.0746
	Upper	0.0116	0.1193	1.3821	1.5130
	Total	0.0473	0.4500	5.0903	5.5876
Orbit	Total	--	--	--	4.8268
VERTICAL GRAVITY (μN/kg)					
Surface	Lower	3.111	-0.148	-2.840	0.123
	Upper	0.995	0.058	-1.048	0.005
	Total	4.106	-0.090	-3.888	0.128
Orbit	Total	--	--	--	-6.447
MERIDIAN DEFLEXION (arc msec.)					
Surface	Lower	0.0632	-0.0842	-0.0211	-0.0421
	Upper	0.0211	-0.0211	0.1053	0.1053
	Total	0.0842	-0.1053	0.0842	0.0632
Orbit	Total	--	--	--	-0.2949
PRIME VERTICAL DEFLEXION (arc msec.)					
Surface	Lower	0.0211	0.4212	-0.3581	0.0842
	Upper	0.0000	0.2106	0.0000	0.2106
	Total	0.0211	0.6319	-0.3581	0.2949
Orbit	Total	--	--	--	-0.2949

EQUIPOTENTIAL UNDULATIONS. Its remoteness notwithstanding, the outer zone contributes the major portion of the atmospheric disturbance of the equipotential surfaces at both points—on land and ocean. Contributions from the mid and inner zones are seen to be diminished, successively, by approximately an order of magnitude each. This phenomenon appears to reflect the uneven distribution of atmospheric mass among the zones. Comparison of the two points demonstrates the small variation in the potential due to the upper atmosphere at different locations, for points within the atmospheric shell. Though small, this variation seems to be too large, relative to the total upper atmospheric effect, to be attributable to computational imprecision alone.

Comparison of the lower atmosphere effect reveals that most of the reduction observed at the point in the Himalayas comes from the mid zone. This is consistent with the reduction in atmospheric mass in the more dense lower layer, caused by the presence of the surrounding mountains.

An equally instructive comparison may be made between the total atmospheric effect on the potential and that of the topographic-isostatic model (*c.f.* tables 9.4 and 8.1). At the surface, the atmospheric disturbance is approximately one quarter as large as the topographic-isostatic effect, while at orbital altitude the effects are almost equal. The role of the isostatic compensation in diminishing the influence of the topography is thereby forcibly demonstrated. Though the mass of the atmosphere is relatively small, it exerts a disproportionately large gravitational influence, *if* it is assumed that there is no corresponding isostatic compensation. Intuitively, it would seem reasonable to suppose that the rigidity of the earth's crust is capable of sustaining the atmospheric load without isostatic compensation.

VERTICAL GRAVITY. The total vertical attraction of the upper atmosphere at the surface is effectively zero at both points. A substantial reduction in the upwards attraction of the atmosphere in the inner zone at the point in the Himalayas leads to a nett downwards attraction which contrasts with the one order smaller upwards attraction at the ocean point. Since the ocean point can be considered to be located entirely inside the atmospheric shell, the departure of the attraction there from the theoretically expected value of zero is presumably caused by the topographically induced irregularities in the lower boundary of the atmosphere.

DEFLEXIONS OF THE VERTICAL. Atmospheric influence of the vertical is seen to be generally quite small. Most of the effect on the meridian component at the surface, observed at the Himalayan point, arises from the mid zone, where the preponderance of topographic irregularity is concentrated.

SPHERICAL HARMONIC ANALYSIS

Fully normalized spherical harmonic coefficients and degree variances of the atmospheric effects were derived in the manner described in §8.4. Unfortunately, there was insufficient computer time available to complete the analysis so that harmonics for the deflexions of the vertical are not available.

ANALYSIS RESULTS. Coefficients and variances of the potential undulations and disturbance of vertical gravity at the earth's surface and at orbital altitude due to the total atmospheric model (*i.e.* up to 40 km) are listed in table 9.6. With the exception of the vertical gravity at surface level—which is analysed to (9,9) using data interpolated on a 5° grid—the coefficients were derived from 30° grid data and truncated at (6,6). The only significant effect of the upper atmosphere (10 km to 40 km) at the surface appears in the zonal harmonics of the potential undulations and these values are tabulated in the second column of coefficients. Clearly, given the laterally invariant properties of the atmospheric model, the ellipsoidal shells of the upper atmosphere should induce no tesseral harmonics.

A characteristically low value of the fourth degree harmonics, already observed in the topographic effects, is again evident in the potential and gravity effects of the atmospheric model at the surface. The same effect at n=8 is noticeable in the vertical gravity coefficients. Of course it must be remembered that a good deal of the vertical gravity data was derived by linear correlation with topographic elevations.

ZERO DEGREE HARMONIC OF THE ATMOSPHERIC DISTURBING POTENTIAL. The theoretical development relating to the low degree harmonics of the potential given in §8.4 may be applied to the atmospheric results. Table 9.7 contains the conversion of the zero degree harmonics to an equivalent atmospheric mass according to equations 8.10, 8.14, and 8.15.

TABLE 9.6

FULLY NORMALIZED SPHERICAL HARMONIC COEFFICIENTS AND DEGREE VARIANCES OF ATMOSPHERIC EFFECTS

Degree variances are shown in italics at the beginning of each degree in the 'S' column in mm^2 and nN^2/kg^2 for equipotential undulations and vertical gravity respectively.

		EQUIPOTENTIAL UNDULATIONS (millimetres)					VERTICAL GRAVITY (nN/kg)*			
		SURFACE LEVEL			ORBIT LEVEL		SURFACE LEVEL		ORBIT LEVEL	
		TOTAL ATMOSPHERE		UPPER	TOTAL ATMOSPHERE		TOTAL ATMOS.		TOTAL ATMOSPHERE	
n	*m*	C	S	C	C	S	C	S	C	S
0	0	5565.8	*30 978 000*	1512.7	4814.5	*23 179 000*	24.9	*620*	-6384.6	*40 763 000*
1	0	-1.5	*501.7*	2.3	-1.7	*246.5*	-8.6	*1584*	-1.6	*1918.4*
1	1	-15.5	-16.1		-11.6	-10.5	-28.3	-26.6	30.0	31.9
2	0	-18.6	*482.4*	-2.4	-13.0	*213.2*	-40.8	*3136*	31.6	*1814.8*
2	1	-1.0	-8.6		-0.5	-4.6	2.3	-24.6	2.2	20.7
2	2	6.2	-4.8		3.8	-2.8	26.3	-12.7	-15.5	11.9
3	0	13.3	*295.8*	0.4	6.6	*79.2*	58.4	*6577*	-39.1	*2460.2*
3	1	2.6	-4.6		1.3	-2.9	12.3	-24.1	-7.3	13.2
3	2	8.0	-4.6		4.0	-2.6	40.9	-21.3	-21.4	13.8
3	3	-0.3	-2.4		-0.3	-1.7	0.1	-17.7	0.8	7.3
4	0	1.0	*105.2*	1.2	2.5	*28.1*	-27.2	*5565*	11.0	*1102.2*
4	1	1.8	4.4		0.7	2.2	6.5	36.8	-5.7	-14.4
4	2	5.9	-0.5		2.9	-0.4	42.0	-1.8	-17.9	1.7
4	3	-0.6	5.5		-0.8	1.9	-17.1	25.6	3.3	-15.5
4	4	-1.2	-3.8		-0.5	-1.8	-6.5	-25.9	6.6	11.1
5	0	6.8	*117.6*	-0.0	2.1	*12.3*	60.8	*6561*	-21.7	*1129.0*
5	1	0.9	3.5		0.2	0.9	-6.4	3.2	-3.3	-9.4
5	2	-0.1	0.8		0.2	0.4	5.8	9.8	0.1	-3.2
5	3	-0.6	3.9		-0.4	1.3	-12.5	23.9	2.2	-11.5
5	4	-4.5	2.9		-1.5	1.1	-31.1	22.7	13.7	-9.6
5	5	0.7	-3.6		0.2	-1.3	5.9	-21.1	-1.9	11.4
6	0	-2.3	*34.5*	1.3	3.0	*11.6*	-54.4	*6304*	15.0	*488.4*
6	1	0.5	1.5		0.2	0.5	5.8	42.0	-1.8	-4.6
6	2	-2.5	0.6		-0.7	0.3	-13.7	8.8	7.0	-2.5
6	3	-0.6	0.5		-0.2	0.3	-6.2	4.9	1.6	-1.8
6	4	-2.9	1.6		-0.9	0.5	-26.6	11.2	9.7	-5.0
6	5	-0.9	-1.7		-0.0	-0.4	15.1	-2.9	1.9	4.3
6	6	2.1	-0.6		0.6	-0.2	12.1	-1.0	-6.0	1.6
7	0						15.2	*3249*		
7	1						-20.4	-25.5		
7	2						-32.0	10.0		
7	3						-6.9	-5.6		
7	4						-6.9	-1.1		
7	5						5.6	-18.4		
7	6						8.5	-0.1		
7	7						8.1	13.9		
8	0						-25.4	*2275*		
8	1						-0.7	13.0		
8	2						-5.3	10.2		
8	3						-2.1	-11.8		
8	4						7.5	2.6		
8	5						8.7	-20.0		
8	6						3.0	-6.3		
8	7						-21.7	6.4		
8	8						8.2	4.1		
9	0						24.9	*3329*		
9	1						-12.5	-33.8		
9	2						-3.0	4.9		
9	3						-4.5	-9.6		
9	4						17.8	-6.8		
9	5						7.8	-0.8		
9	6						6.5	-10.0		
9	7						-9.5	15.4		
9	8						-18.9	2.6		
9	9						3.6	-0.3		

1 nN/kg = 0.1 μgal

TABLE 9.7

MASS OF THE ATMOSPHERIC MODEL DERIVED FROM THE ZERO DEGREE HARMONIC OF THE DISTURBING POTENTIAL

LEVEL	UNDULATION COEFFICIENT C_{00} (m)	POTENTIAL COEFFICIENT C_{00} (J/kg)	R_p (m)	M_a ($\leq$ 40 km) (kg)
Surface	5.5658	54.5793	6 371 263	5.2135×10^{18}
Orbit	4.8145	47.2119	7 371 024	5.2174×10^{18}

These values of the mass—which are comparable to much better than 0.1%—apply to the atmospheric model below the upper boundary of 40 km.

A direct evaluation of the mass of the same atmospheric model by numerical integration, based on equation 3.44, was implemented using modified versions of programmes MIDATMO and OUTATMO and a separate estimation of the contribution from the inner zone, deliberately located in an ocean area and treated as a rectangular parallelepiped. This gave:

$$M_a\ (\leq 40\ \text{km}) = 5.2263 \pm 0.0005 \times 10^{18}\ \text{kg}, \tag{9.3}$$

where the stated precision is based on the internal consistency only, of the results of several separate evaluations. The number of quads within each 10 km layer of the atmosphere involved in the summation are listed in table 9.8. By choosing the "computation point" at different levels the quadrature

TABLE 9.8

NUMBER OF QUADS PER LAYER OF ATMOSPHERE USED IN NUMERICAL INTEGRATION FOR THE MASS

LEVEL	OUTER ZONE		MID ZONE	
	5°x5°	1°x1°	30'x30'	5'x5'
Surface	2242	8428	976	11054
Orbit	2242	8750	--	--

representation of the zones could be varied, thus providing independent summations for comparison and checking. To complete this determination of the mass the contribution of the remaining layers of the atmosphere up to an altitude of 122.5 km, treated as ellipsoidal shells, was calculated using the densities and altitude increments tabulated for the NACA Standard Atmosphere [SMITHSONIAN TABLES 1958, p.284]. Addition of this result brought the mass of the total atmospheric model to

$$M_a\ (\leq 122.5\ \text{km}) = 5.2415 \times 10^{18}\ \text{kg}, \tag{9.4}$$

indicating that 99.7% of the mass of the atmosphere is contained below an altitude of 40 km.

An estimate of the mass of atmosphere displaced by the terrestrial topography was prepared by comparing the different values of the mass of the first 10 km of atmosphere arrived at by numerical integration, taking into account the topographic boundary, and by treating this layer as an ellipsoidal shell. Results were as follows:

$$\begin{aligned} M_a\ (\leq 10\ \text{km}),\ \text{ellipsoidal shell} &= 3.8975 \times 10^{18}\ \text{kg} \\ M_a\ (\leq 10\ \text{km}),\ \text{topographic boundary} &= \underline{3.8000 \times 10^{18}\ \text{kg}} \\ M_a\ \text{displaced by topography} &= 0.0975 \times 10^{18}\ \text{kg} \end{aligned} \tag{9.5}$$

VERNIANI [1966] has reviewed the various estimates of the mass of the atmosphere up to 1965 and, using a quite different technique, has computed a value for the total atmospheric mass up to 100 km of

$$M_a\ (\leq 100\ \text{km}) = 5.136 \pm 0.007 \times 10^{18}\ \text{kg}. \tag{9.6}$$

The value given in 9.4 has been incorporated in the recommendations of the Special Study Group Number 5.39 of IAG on Fundamental Geodetic Constants [MORITZ 1975, p.5].

FIRST DEGREE HARMONICS OF THE ATMOSPHERIC DISTURBING POTENTIAL. Equations 8.13 may be applied to the non-normalized first degree harmonics of the atmosphere, in which case the displacement of the centre of mass of an otherwise regular earth due to the atmospheric model will be determined. Alternatively, if the mass of the atmosphere M_a is substituted in place of the mass of the earth M_E in these equations, they will provide the coordinates (X_a, Y_a, Z_a) of the centre of mass of the atmospheric model. These results are computed in table 9.9 for surface and orbital levels using the non-normalized coefficients of the total atmospheric model up to 40 km, so that $kM_a = 3.486 \times 10^8\ m^3/s^2$.

TABLE 9.9

CENTRE OF MASS OF THE ATMOSPHERIC MODEL

LEVEL	COEFFICIENT	UNDULATION (m)	POTENTIAL (J/kg)	R_p (m)	EARTH		ATMOSPHERE	
					COORD.	VALUE (m)	COORD.	VALUE (km)
Surface	C_{11}	-0.0268	-0.2633	6 371 263	X_E	-0.027	X_a	-30.7
	S_{11}	-0.0279	-0.2735		Y_E	-0.028	Y_a	-31.8
	C_{10}	-0.0026	-0.0255		Z_E	-0.003	Z_a	-3.0
Orbit	C_{11}	-0.0201	-0.1970	7 371 024	X_E	-0.027	X_a	-30.7
	S_{11}	-0.0182	-0.1783		Y_E	-0.024	Y_a	-27.8
	C_{10}	-0.0029	-0.0289		Z_E	-0.004	Z_a	-4.5

The displacements are in a direction opposite to that caused by the topographic-isostatic model since the topographic masses coincide with a reduction in the atmospheric mass. Approximately 4 cm displacement of the centre of mass of the earth is seen to be caused by the atmospheric model while the centre of mass of the atmospheric model itself is displaced rather more than 40 km.

9.5 COMPARISON AND CONCLUSIONS

A detailed comparison of the results described here with the consequential effects of the treatment of the atmosphere adopted in the GRS67 has been made elsewhere [ANDERSON *et al.* 1975]. Agreement between the two different approaches is generally acceptable. Specifically, the zero degree effects have been shown to differ by 6 cm — that is, by about 1%. The global patterns of atmospheric disturbing potential display remarkable agreement in form and in magnitude over ocean areas, but a maximum discrepancy of about 10 cm was observed over the Himalayas. To some extent, these differences can be attributed to the coarsness of global evaluation and truncation of the harmonic spectra.

CONCLUSIONS

In so far as the static atmospheric model adopted in the preceeding computations may be taken to correspond with the observed characteristics of the earth's atmosphere, the following conclusions — based on the results and analyses of §9.4 — are assumed to pertain to that reality.

(a) Correlation of the gravitational influence of the earth's atmosphere with topographic elevation pertains generally at the surface and to a lesser extent at orbital altitudes. Specifically, the vertical gravity at the surface due to topographically induced departures of the atmosphere from a regular homothetic ellipsoidal shell, displays a high degree of linear correlation with topographic elevations ($r_g = -0.997$).

(b) The disturbance of the equipotential surfaces at the earth's surface varies between approximately 5.38 m in the Himalayas and 5.62 m in the Pacific Ocean, the zero degree term in a spherical harmonic representation being 5.57 m.

(c) If solutions for the geoid or the height anomaly were derived entirely from gravity data observed at the earth's surface, the zero degree contribution of the atmosphere of about $5\frac{1}{2}$ m could not be ignored. However, the geometrical significance of this term can be interpreted correctly only in the context of a *complete* solution of the geodetic boundary value problem. To date, all low degree characteristics of the earth's equipotentials are derived from satellite orbital analysis, where the assumption of the harmonic nature of the geopotential field is valid, even when the effect of the atmosphere is correctly included.

(d) In view of the atmospherically induced undulations up to 25 cm in the surface equipotentials, future precise solutions involving combinations of orbital analysis and surface gravity data may need to take account of the atmospheric effects if biases in the harmonic representation are to be avoided.

(e) The mass of the atmosphere, determined by numerical integration up to an altitude of 40 km and ellipsoidal shells representing the remainder up to 122.5 km, was found to be 5.242×10^{18} kg. This value takes into account the irregular lower boundary; the mass of atmosphere displaced by topography being determined as 1.86% of the total mass.

(f) Departures of the atmosphere from a homothetic ellipsoidal shell cause a displacement of the centre of mass of an otherwise regular earth of about 4 cm. The centre of mass of the atmosphere alone is slightly more than 40 km from the reference system origin. Both departures are directed away from the major topographic masses of Europe and Asia.

(g) The use of atmospheric corrections in accordance with the procedure adopted in the definitions of the GRS67 produces results similar to those obtained from a conventional geodetic boundary value problem approach, except in mountainous regions such as the Himalayas, where discrepancies up to 10 cm in the Stokesian atmospheric contribution to the height anomaly may occur. It is anticipated that these discrepancies would be reduced by the use of higher degree harmonic representations of the disturbing potential.

10

Comparisons and Conclusions

10.1 INTRODUCTION — LIMITATIONS ON THE CONCLUSIONS

Before interpreting, comparing, or applying any of the results obtained in this study, the limitations imposed by the adopted physical and mathematical models, and the methods of computation and analysis must be recognized. In any context requiring an interpretation in terms of the physically observable characteristics of the earth's gravitational field, the results presented here may be held to conform with those characteristics only in so far as the underlying models and assumptions are valid. The degree of verity of the results — and hence their applicability in any particular circumstances — may be adjudged in terms of the precisions of the various contributing models and formulae.

In particular, the consequences of utilizing simulated 5'x5' mean topographic elevations in part of the computations must be included in any appraisal of the results. Of the remaining limitations, due to the physical models, perhaps that imposed by the simplicity of the topographic density model should cause the greatest concern. There can be little doubt that the adopted model may depart considerably from reality, and its influence is felt directly in the computed gravitational effects.

Despite these limitations, the generalized approach adopted throughout this investigation should broaden the applicability of the results and the degree of rigour incorporated in the models should be adequate in most of the anticipated applications. Generally, the intention of achieving the best results that could reasonably be obtained from extant data has been fulfilled.

10.2 COMPARISONS

The paucity of directly comparable investigations of the global gravitational effects of the topography and isostatic compensation has been mentioned in §1.1 (¶"*PREVIOUS EVALUATIONS OF TOPOGRAPHIC EFFECTS*"). While the present study was not specifically directed towards a determination of the indirect effect associated with Stokes' problem, it was in part motivated by the results obtained by FRYER [1970, chapter 6], wherein global estimates of the indirect effect for the free air geoid were obtained. Moreover, the particular quantities which were evaluated globally at geoid and surface levels in this study play a vital role in the formulation of the indirect effect. Therefore, the results and analyses described in chapter 8 may be usefully applied in an attempt to elucidate the general behaviour of some components of the indirect effect, as determined globally by Fryer and, in so far as they are relevant, the regional astro-geodetic studies in India of BHATTACHARJI [1973]. Unfortunately, the zero degree component of the Stokesian contributions to the indirect effect, as evaluated by Fryer, is relevant to a Stokesian term evaluated solely from surface gravity data and therefore cannot be considered as a correction to Stokesian contributions based on satellite determined low degree harmonics.

The magnitude of the non-Stokesian or potential term in the indirect effect as evaluated by FRYER [1970, figure 6.22] may be compared with the surface equipotential undulations portrayed in figure 8.2. Indeed, FRYER [*ibid.* p.152] has employed a simplisitic model of the Himalayan topography and compensation in checking the magnitude of the potential term. However, the indirect effect potential term is not influenced by the Airy-Heiskanen isostatic compensation, which is below the geoid — though it does partially depend on a surface condensation of the topographic mass — and cannot, therefore, be expected to vary in the same manner as the topographic-isostatic equipotential undulations. For instance, FRYER [*ibid.* p.127] finds that the outer zone contribution to the potential term is approximately constant at 6.3 m, whereas the outer zone component of the topographic-isostatic undulation tends to zero because of the lack of discrimination between the almost equal and opposite effects of the topography and compensation at such distances (*e.g.* see table 8.1). This fundamental difference in the geometry of the two evaluations influences the form of the results. The attenuation of the effect with increasing distance from major topographic masses appears slow in Fryer's solution [*e.g. ibid.*, figure 6.11] because of the accumulated influence of the outer zone, but is relatively rapid in the topographic-isostatic evaluation where the influence of the compensation tends to cancel that of the topography at distant points. This accumulative characteristic of the indirect effect potential term is aggravated in Fryer's results by the coarse evaluation interval of 15° [*ibid.*, p.94] and the smoothing inherent in the evaluation technique [*ibid.*, p.114].

A regional evaluation of "isostatic geoid" undulations, representing the difference between the geoid and the isostatic co-geoid in India and the southern margin of the Himalayas, has been described by BHATTACHARJI [1973, chart 6]. Inasmuch as these results are influenced by the global effects of the topographic-isostatic mass distribution, they provide additional confirmation of the quite strong correlation of such effects with the form of the topography and support the inference of rapid attenuation of topographic effects with increasing distance from the main masses. Unfortunately, the use of different isostatic models and the introduction of a number of assumptions for local technical reasons renders the Indian data unsuitable for direct quantitative comparison but, in a general qualitative sense, the results appear to provide a degree of practical confirmation of the trends found in the present study.

10.3 SUMMARY OF CONCLUSIONS

In summary, the findings of this study may be enumerated as follows:

(a) The feasibility of globally mapping the gravitational influence of a detailed model of the earth's topography and isostatic compensation, in accordance with specifications aimed at sustaining a relative precision of the results at the order of the flattening, has been demonstrated. Simultaneously, novel techniques for the maintenance and utilization of the large quantities of digital data required to realize a global topographic-isostatic model have been established and successfully tested (see chapters 6 and 7).

(b) The geometry of quadrature subdivisions for a spherical approximation of the earth have been developed in terms of a spherical tesseroid and its approximation by a rectangular parallel-epiped, and the necessary inertial properties formulated. Suitable modelling of an isostatic compensation system has been established, including provision for sphericity and ice corrections (see chapter 3).

(c) Formulations, in open and closed forms, of the gravitational potential and attraction vector components of a general rectangular parallelepiped with linear vertical density variation have been developed and tested. Thus the ability to determine the gravitational effects of crustal models with almost any degree of density elaboration has been assured (see chapters 4 and 5). A demonstration of the flexibility of the formulae was provided by their application to a model of the atmosphere, consisting of a stepwise, linear regression of its curvilinear density variation with altitude (see chapter 9).

(d) Detailed, general purpose global models of the topographic-isostatic disturbing potential and attraction vector have been evaluated at the geoid, the earth's surface, and at an altitude representative of satellite orbits and described in the form of fully normalized spherical harmonic representations (see chapter 8). These models have been designed to meet manifold requirements and may be applied wherever refinement of global gravitational information is sought.

(e) The working hypothesis set up in §1.1 has been substantially confirmed by the evidence of the experimental results and analyses. However, the contention of FRYER [1970, p.210] that the global indirect effect for the free air geoid displays variations with larger magnitude than has been conventionally anticipated is largely supported by the quantitative findings of this study. Although there is almost no evidence provided by the evaluation of the topographic-isostatic attraction which could confirm the suggestion that the Stokesian contributions of the earth's large mountainous regions accummulate to exaggerate their influence [*ibid.*, *p*.211], such a phenomenon is not precluded by the results. The geometry of the indirect effect formulation is not conducive to the high degree of cancellation of outer zone effects which has been shown to occur when the influence of the isostatic mass deficiencies is included (*e.g.* table 8.1). In the complete solution of Stokes' problem, the influence of the isostatic compensation enters directly through the gravity anomaly model employed in the Stokesian integration, and is felt, therefore, in the co-geoid solution. It has no influence on the magnitude of the indirect effect. When the total topographic-isostatic model is considered, the attenuation of gravitational effects with increasing distance from the major topographic masses has been shown to be virtually as rapid as the topographic morphology itself, with which, these effects are strongly correlated (see §8.3).

(f) While the topographic-isostatic disturbing potential varies smoothly, reflecting the major regional topographic trends, (figure 8.3), the associated attraction vector is found to vary rapidly as a function of localized topographic gradients — in some instances to such an extent that an upwards attraction component due to local topography may be experienced at the surface (figure 8.9). Similar tendencies are observed in the disturbance of the deflexions of the vertical (figure 8.11). By inference, the similar assertions of FRYER [*ibid.*], relating to the differential terrain correction within the indirect effect are substantiated. More detailed and accurate resolution of the disturbing attraction vector must be held in abeyance, pending the availability of a global coverage of 5'x5' mean topographic elevation data and realisitic crustal density models. A more realistic formulation of the gravitational effects of contact quadrature subdivisions may also be necessary (*e.g.* see §8.2).

(g) The effect of the compensated topography on equipotential surfaces at orbital altitudes is appreciable and disturbances with a wavelength greater than about 500 km may appear in satellite derived data (figure 8.6).

(h) Using numerical integration, the mass of the terrestrial topography (*i.e.* above the reference surface) was found to be 2.865×10^{20} kg, assuming that the mass of all polar ice is 0.237×10^{20} kg. This value is based on the de Graaff-Hunter global crustal density model.

(i) In accordance with the derived values of the first degree harmonics of the topographic-isostatic disturbing potential, the displacement of the centre of mass of an otherwise regular earth, due to the topographic-isostatic model, was estimated to be about 0.5 metres, directed towards the dominant continental masses of Europe and Asia (table 8.7).

(j) Global estimates of the gravitational effects of the atmosphere on solutions of Stokes' problem have been determined and shown to be of comparable magnitude to the topographic-isostatic effects, particularly at orbital altitudes. They are, therefore, of significance in definitions of sea surface topography based on surface gravity data alone. (See §9.5 for detailed conclusions).

References

ACIC 1965: *ACIC Standard Machine Punch Card Format for Mean Elevation Data.* Unpublished notes, 19 Jan. 1965, Defence Mapping Agency Aerospace Center, Missouri, U.S.A.

ANDERSON, E. G. 1973a: Evaluation of the Gravitational Potential and Attraction of a Model of the Earth's Topography and Compensation. *Proc. AAS/IAG Sympos. on Earth's Gravitational Field etc.*, Univ. of N.S.W., pp.106-116.

ANDERSON, E. G. 1973b: S. I. Units. Letter in *The Aust. Surv., 25* (3), pp.212-3.

ANDERSON, E. G., RIZOS, C., & MATHER, R. S. 1975: *Atmospheric Effects in Physical Geodesy.* Paper presented at XVI General Assembly of IUGG/IAG, Grenoble, August 18-23, 1975.

AUSTRALIAN STANDARD 1000 1970: *The International System (SI) Units and Their Application.* Standards Assoc. of Aust., Sydney.

BAESCHLIN, C. F. 1948: *Lehrbuch der Geodäsie.* Orell-Füssli, Zürich.

BALMINO, G., LAMBECK, K., & KAULA, W. M. 1973: A Spherical Harmonic Analysis of the Earth's Topography. Letter in *J. Geophys. Res., 78,* pp.478-481.

BHATTACHARJI, J. C. 1973: Geoid, Isostatic Geoid, Isostatic Co-geoid, and Indirect Effect on Gravity in India. *Proc. AAS/ IAG Sympos. on Earth's Gravitational Field etc.*, Univ. of N.S.W., pp.227-239.

BUDD, W. F., JENSSEN, D., & RADOK, U. 1971: Derived Physical Characteristics of the Antarctic Ice Sheet. *ANARE Interim Reports, Series A(IV), No. 120.* Antarctic Division, Dept. of Supply, Melbourne.

BULLEN, K. E. 1951: *An Introduction to the Theory of Mechanics,* (2nd ed.). Science Press, Sydney.

CASSINIS, G., DORE, P., & BALLARIN, S. 1937: Fundamental Tables for Reducing Gravity Observed Values. *R. Comm. Geod. Ital. Publ. No. 13.*

CZARNECKI, W. 1970: *The Geodetic Importance of Mean Elevation Data.* Paper presented at the 1970 ACSM/ASP Convention, Control Surveys Division, Washington, D.C.

DARLING, F. W. 1949: Fundamental Tables for the Deflection of the Vertical. *Spec. Publ. No. 243,* U.S. Coast and Geodetic Survey.

de GRAAFF-HUNTER, J. 1966: Earth Shape Studies and Relevant Assumptions. *Boll. de Uni. Fed. do Parana, Geodesia, 10,* 1966.

REFERENCES

ECKER, E., & MITTERMAYER, E. 1969: Gravity Corrections for the Influence of the Atmosphere. *Boll. Geofis. Teorica Appl. 11,* pp.70-80.

FISCHER, I. 1973: Deflections at Sea. *Proc. AAS/IAG Sympos. on Earth's Gravitational Field etc.,* Univ. of N.S.W., pp.36-50.

FISCHER, I., SLUTSKY, M., SHIRLEY, F. R., & WHATT III, P. Y. 1968: New Pieces in the Picture Puzzle of an Astrogeodetic Geoid Map of the World. *Bull. Géod., 88,* pp.199-221.

FREUND, J. E. 1962: *Mathematical Statistics.* Prentice-Hall Inc., Englewood Cliffs, N.J.

FRISCH, Von A. K. 1960: Die Methode der direkten Geländerkorrektion. *Schweizerische Zeitschrift für Vermessung, Kulturtechnik und Photogrammetrie, 58,* pp.240-253, 271-285, 314-332, 357-372.

FRYER, J. G. 1970: The Effect of the Geoid on the Australian Geodetic Network. *Unisurv Rep. 20.* School of Surv., Univ. of N.S.W.

GRÖBNER, W., & HOFREITER, N. 1961: *Integraltafel (Erster tiel) Unbestimmte Integrale.* Springer-Verlag, Wien.

HARDY, G. H. 1958: *A Course of Pure Mathematics (10th ed.).* Cambridge University Press.

HAYFORD, J. F., & BOWIE, W. 1912: The Effect of Topography and Isostatic Compensation upon the Intensity of Gravity. *Spec. Publ. No. 10,* U.S. Coast and Geodetic Survey.

HEISKANEN, W. A. 1953: Isostatic reductions of the gravity anomalies by the aid of high speed computing machines, *Publ. Isostat. Inst. Int. Assoc. Geod., No. 28,* Helsinki.

HEISKANEN, W. A. 1964: Activity of the Columbus Geodetic Group in Physical Geodesy since 1960. *Ann. Acad. Scient. Fenn.* A.III, 72, Helsinki.

HEISKANEN, W. A., & MORITZ, H. 1967: *Physical Geodesy.* W. H. Freeman & Co., San Francisco.

HEISKANEN, W. A., & NISKANEN, E. 1941: World Maps for the Indirect Effect of the Undulations of the Geoid on Gravity Anomalies. *Publ. Isostat. Inst. Int. Assoc. Geod., No. 7,* Helsinki.

HOLDEN, G. J. F. 1974: An Evaluation of Orthophotography in an Integrated Mapping System. *Unisurv Rep. S12,* School of Surv., Univ. of N.S.W.

HOPKINS, J. 1973: Mathematical Models of Geopotential Gradients. *Proc. AAS/IAG Sympos. on the Earth's Gravitational Field etc.,* Univ. of N.S.W., pp.93-105.

IAG 1967: Resolutions Adopted at the General Assembly, Int. Assoc. of Geod., Lucerne. *Bull. Géod. 86,* pp.367-383.

IAG 1971: *Geodetic Reference System 1967.* Spec. Publ. Int. Assoc. Geod., Paris.

IBM 1966a: IBM System/360 Operating System: *Assembler [F] Programmer's Guide,* 3rd ed., Form C26-3756-2.

IBM 1966b: IBM System/360: *Principles of Operation,* Form GA22-6821-8.

IBM 1968: IBM System/360 Operating System: *Fortran IV Language,* 8th ed., Form C28-6515-7.

IBM 1969: IBM System/360 Operating System: *Linkage Editor and Loader,* 9th ed., Form GC28-6538-8.

IBM 1970a: IBM System/360 Operating System: *Fortran IV (G & H) Programmer's Guide,* 3rd ed., Form GC28-6817-2.

IBM 1970b: IBM System/360 Operating System: *Utilities,* 12th ed., Form GC28-6586-11.

IBM 1971: IBM System/360 Operating System: *Supervisor and Data Management Macro Instructions,* 6th ed., Form GC28-6647-5.

JENNINGS, J. N. 1971: *An Introduction to Systematic Geomorphology (vol. 7): Karst.* Australian National University Press, Canberra.

JOHNSON, B. D., & LEE, T. J. 1973: A Rapid Method for the Computation of the Gravitational Anomaly Due to Complex Three Dimensional Structures. *Proc. AAS/IAG Sympos. on Earth's Gravitational Field etc.,* Univ. of N.S.W., pp.261-272.

JOHNSON, L. R., & LITEHISER, J. J. 1972: A Method for Computing the Gravitational Attraction of Three Dimensional Bodies in a Spherical or Ellipsoidal Earth. *J. Geophys. Res., 77* (35), pp.6999-7009.

R E F E R E N C E S

KÄRKI, P., KIVIOJA, L., & HEISKANEN, W. A. 1961: Topographic-isostatic Reduction Maps for the World for the Hayford Zones 18-1, Airy-Heiskanen System, T = 30 km. *Publ. Isostat. Inst. Int. Assoc. Geod., No. 35,* Helsinki.

KAULA, W. M. 1973: Mantle Convective Models Related to the Gravity Field and Tectonic Motion. *Proc. AAS/IAG Sympos. on Earth's Gravitational Field etc.,* Univ. of N.S.W., pp.240-247.

KELLOGG, O. D. 1929: *Foundations of the Potential Theory.* Berlin.

KIVIOJA, L. 1964: Effect of Topographic Masses and their Isostatic Compensation on the Mean Free Air Gravity Anomalies of 5°x5° Surface Elements. *Ann. Acad. Scient. Fenn.* A.III. 77, Helsinki.

KIVIOJA, L. A. 1967: Effects of Mass Transfers between Land-supported Ice Caps and Oceans on the Shape of the Earth and on the Observed Mean Sea Level. *Bull. Géod., 85,* pp.281-288.

KOEFOED, O. 1967: Units in Geophysical Prospecting (Official communication of the Committee on Geophysical Units and Nomenclature of the European Assoc. of Exploration Geophysicists). *Geophys. Prospect. XV* (1), pp.1-6.

KUKKAMÄKI, T. J. 1954: Gravimetric reductions with electronic computers. *Publ. Isostat. Inst. Int. Assoc. Geod., No. 30,* Helsinki.

LAMB, H. 1956: *An Elementary Course of Infinitesimal Calculus* (3rd ed., revised), Cambridge University Press.

LAMBERT, W. D. 1930: The Reduction of Observed Values of Gravity to Sea Level. *Bull. Géod., 26,* pp.107-181.

LAMBERT, W. D., & DARLING, F. W. 1936: Tables for Determining the Form of the Geoid and its Indirect Effect on Gravity. *Spec. Publ. No. 199,* U. S. Coast and Geodetic Survey.

LAMBERT, W. D., & DARLING, F. W. 1938: Formulas and Tables for the Deflection of the Vertical. *Bull. Géod., 57,* pp.29-71.

LEE, W. H. K., & KAULA, W. M. 1967: A spherical Harmonic Analysis of the Earth's Topography. *J. Geophys. Res., 72,* pp.753-758.

MACMILLAN, W. D. 1930: *The Theory of the Potential.* Dover Publ. Inc., New York.

MATHER, R. S. 1968a: The Free Air Geoid in South Australia and its Relation to the Equipotential Surfaces of the Earth's Gravitational Field. *Unisurv Rep. 6,* School of Surv., Univ. of N.S.W.

MATHER, R. S. 1968b: The Non-Regularised Geoid and its Relation to the Telluroid and Regularised Geoids. *Unisurv Rep. 11,* School of Surv., Univ. of N.S.W.

MATHER, R. S. 1971: *The Analysis of the Earth's Gravity Field,* Monograph 2, School of Surv., Univ. of N.S.W.

MATHER, R. S. 1973: A Solution of the Geodetic Boundary Value Problem to Order e^3. *Doc. X-592-73-11,* NASA Goddard Space Flight Centre, Greenbelt Md.

MATHER, R. S. 1974: On the Solution of the Geodetic Boundary Value Problem for the Definition of Sea Surface Topography. *Geophys. J. R. Astr. Soc., 39,* pp.87-109.

MATHER, R. S. 1975: On the Evaluation of Stationary Sea Surface Topography using Geodetic Techniques, *Bull. Géod., 115,* pp.65-82.

MATHER, R. S,, BARLOW, B. C., & FRYER, J. G. 1971: A Study of the Earth's Gravitational Field in The Australian Region. *Unisurv Rep. 22,* pp.1-37, School of Surv., Univ. of N.S.W.

METRIC CONVERSION BOARD 1973: *Metric Practice.* Australian Government Publishing Service, Canberra.

MILNE, W. E. 1949: *Numerical Calculus: Approximations, Interpolation, Finite Differences, Numerical Integration, and Curve Fitting.* Princeton University Press, Princeton.

MOLODENSKII, M. S., EREMEEV, V. F., & YURKINA, M. I. 1962: Methods for Study of the External Gravitational Field and Figure of the Earth; (Trans. from Russian 1960). *Israel Program for Scientific Translations,* Jerusalem.

MORITZ, H. 1965: The Boundary Value Problem of Physical Geodesy. *Ann. Acad. Scient. Fenn.* A.III. 83, Helsinki.

MORITZ, H. 1969: *Preliminary Computations for the Geodetic Reference System 1967.* Sympos. on European Triangulation, Paris.

REFERENCES

MORITZ, H. 1975: *Report of Special Study Group No. 5.39 of IAG: Fundamental Geodetic Constants.* Presented at XVI General Assembly of IUGG/IAG, Grenoble, 18 Aug. to 6 Sept., 1975.

NAGY, D. 1966: The Gravitational Attraction of a Right Rectangular Prism. *Geophysics 31,* pp.362-371.

PAUL, M. K. 1973: On Computation of Equal Area Blocks. *Bull. Géod. 107,* pp.73-84.

PELLINEN, L. P. 1962: Accounting for Topography in the Calculation of Quasigeoidal Heights and Plumb Line Deflections from Gravity Anomalies. *Bull. Géod. 63,* pp.57-66.

RAPP, R. H. 1972: The Formation and Analysis of a 5° Equal Area Block Terrestrial Gravity Field. *Rep. 178,* Dept. of Geodetic Science, Ohio State Univ.

RAPP, R. H. 1973: The Earth's Gravitational Field from the Combination of Satellite and Terrestrial Data. *Proc. AAS/IAG Sympos. on Earth's Gravitational Field etc.*, Univ. of N.S.W., pp.51-75.

SKILLING, H. H. 1957: *Electrical Engineering Circuits.* John Wiley & Sons, Inc., New York.

SMITHSONIAN TABLES 1958: *Smithsonian Meteorological Tables.* (6th ed., prepared by R. J. List). Smithsonian Inst., Washington, D.C.

SOMMERVILLE, D. M. Y. 1946: *Analytical Conics.* (3rd ed.). G. Bell & Sons, Ltd., London.

SPIEGEL, M. R. 1968: *Mathematical Handbook of Formulas and Tables.* McGraw-Hill Book Co., New York.

ST JOHN, V. P., & GREEN, R. 1967: Topographic and Isostatic Corrections to Gravity Surveys in Mountainous Areas. *Geophys. Prospect. XV* (1), pp.151-164.

STOLZ, A. 1972: Three Dimensional Cartesian Coordinates of Part of the Australian Geodetic Network by use of Local Astronomic Vector Systems. *Unisurv Rep. S8,* School of Surveying, Univ. of N.S.W.

SWINDELLS, B. 1971: Understanding Units of Force. *Engineering,* Jan./Feb. 1971, Aust. Inst. of Steel Construction.

THOMPSON, E. H. 1969: *An Introduction to the Algebra of Matrices with some Applications.* Adam Hilger Ltd., London.

UOTILA, U. A. 1964: Gravity Anomalies for a Mathematical Model of the Earth. *Ann. Acad. Scient. Fenn.* A.III. 74, Helsinki.

U.S. ARMY TOPOGRAPHIC COMMAND 1968: (Map) *Shape of the Geoid,* A modification of the Mercury Datum 1968. [Based on a harmonic representation to (13,13)]. Reference 8-70.

VERNIANI, F. 1966: The Total Mass of the Earth's Atmosphere. *J. Geophys. Res., 71* (2), pp.385-391.

VINCENT, S., & MARSH, J. G. 1973: Global Detailed Geoid Computation and Model Analysis. *Proc. AAS/IAG Sympos. on Earth's Gravitational Field etc.,* Univ. of N.S.W., pp.154-171.

WERNER, A. P. H., & ANDERSON, E. G. 1973: International Units (S.I. Units) in Gravimetry. *Proc. AAS/IAG Sympos. on Earth's Gravitational Field etc.,* Univ. of N.S.W., pp.699-701.

WILLERS, F. A. 1948: *Practical Analysis: Graphical and Numerical Methods.* Dover Publ. Inc., New York.

Appendix A

Compendium of Computer Routines

KEY TO ITEMS LISTED:

/ indicates end of item
- indicates item not applicable

NAME — *Computer: 360 = IBM 360/50, 9810 = Hewlett-Packard 9810 programmable calculator, 9830 = Hewlett-Packard 9830 programmable calculator / Description / Type of routine: P = programme, E = entry point (name of standard entry in parentheses), SS = subroutine subprogramme, FS = function subprogramme / Language: F = Fortran IV (G or H), A = Assembler (IBM), U = IBM OS/360 Utility programme, P = PL1 (IBM), B = Basic (H-P extended) / Names of subprogrammes referenced / Logical unit numbers and names of datasets accessed / Parameter (PARM) field used? Y = yes, N = no / Data cards used? Y = yes, N = no / Number of source statements or steps / Total memory requirements excluding buffer space: b = decimal bytes (360), w = words (9830), r = registers (9810) / Usual CPU time if relevant /.*

ALF — 360 / Returns in double precision a fully normalized value of the associated Legendre function for given values of latitude, degree ($n \leq 36$), and order, using an explicit formula [HEISKANEN and MORITZ 1967; equations 1-77 a, b; p.32]. / FS / F / FACT / - / N / N / 47 / 1372b / - /.

ALFDATA — 360 / Computes and stores values of the fully normalized associated Legendre function at 5° intervals of latitude up to degree and order (36,36). / P / F / ALF, FACT / 7 ALFORD36 / N / N / 26 / 26024b / 15 m /.

AMEND — 360 / Amends or inserts new 5' mean elevation values in dataset FIVMINEL and places new entries in dataset SIMINDEX. Input from single cards. / P / F / GETELS, PUTELS / 10 SIMINDEX, 11 FIVMINEL / N / Y / 118 / 103216b / 20 s for 300 cards. /.

AMERTRAN — 360 / Transfers North American 5' mean elevations from regional dataset AMER5MIN to global dataset FIVMINEL and updates dataset SIMINDEX. Maps available data by 1° quads. / P / F / NAMER, PUTELS / 10 SIMINDEX, 11 FIVMINEL, 15 AMER5MIN / N / N / 51 / 42752b / 4 m 59 s /.

A. COMPENDIUM OF COMPUTER ROUTINES

AUSTCONV 360 / Converts Australian 6'x6' mean elevations to equivalent 5'x5' values using two dimensional linear interpolation. Results are stored in dataset FIVMINEL and dataset SIMINDEX is updated. All data is copied to dataset AUSTFIVE on tape in card image DMA format / P / F / PUTELS / 4 AUSTFIVE, 10 SIMINDEX, 11 FIVMINEL, 16 AUST6MIN / N / Y / 125 / 348976b / 10 m 46 s /.

AUSTRAN 360 / Transfers Australian 6'x6' mean elevations from card image format in dataset AUSTMEL to direct access regional dataset AUST6MIN, and converts units from feet to metres. Maps card images / P / F / - / 4 AUSTMEL, 10 temporary, 16 AUST6MIN / N / Y / 112 / 59376b / 10 m 43 s /.

BASEMAPA 360 / Digitizes outline world map by plotting zero contour of UCLA 1° height data and stores resulting coordinates in dataset BASEMAPA / P / F / GPCONT, PLOT, UCLA1S / 9 BASEMAPA, 14 UCLA1SHT / N / N / 32 / 486784b / 14 m 49 s /.

BASMAP 360 / Plots outline map of the world and/or 20°x20° graticule of meridians and parallels to given scale / SS / F / - / 9 BASEMAPA, PLOTTER / N / N / 96 / 56728b / - /.

CONSOL 360 / Transmits and receives messages to and from operator's console typewriter using SVC 1 and 35 instructions / SS / A / - / - / N / N / 228 / 1192b / - /.

CONTINIT 360 / Initializes dataset INNCONTS and sets default values of parameters prior to running of programme INNCONT / P / F / PUTBIT / 20 INNCONTS / N / N / 25 / 31944b / 20 s /.

CYLINDER 9810 / Computes potential due to a cylinder of axial linear density variation at a point on its axis / P / - / - / - / - / - / 188 / 10r / - /.

DIPOLES 9810 / Computes potential and attraction components at geoid, surface and orbital elevations due to a point mass dipole representing the topography and compensation. Includes transformation of components to local coordinate system / P / - / - / - / - / - / 1374 / 90r / - /.

ELINTER 360 / Searches for and linearly interpolates isolated missing 5'x5' mean elevations in dataset FIVMINEL / P / F / PARM, ELSIMW, PUTELS, ITEST, GETELS, CONSOL, PARMNO / 10 SIMINDEX, 11 FIVMINEL / Y / N / 144 / 55352b / 39 m 13 s /.

ELMASTER 360 / Computes and lists mean elevations and topographic variance for 1°x1° quads using avaialable 5'x5' mean elevations and stores the results in datasets ELMONE and ELMVAR respectively for later use by programme TOPOSIM. One degree quads not entirely surrounded by available 5' data are signalled by a variance of -1 / P / F / GETELS / 7 ELMONE, 8 ELMVAR, 10 SIMINDEX, 11 FIVMINEL / N / N / 107 / 200352b / 17 m 47 s /.

ELONEDEG 360 / Completes global coverage of 1°x1° mean elevations in dataset ELMONE not computed from 5' data by programme ELMASTER, using UCLA 1° data. Corrects errors in UCLA data / P / F / UCLA1S / 7 ELMONE, 14 UCLA1SHT / N / N / 44 / 155576b / 3 m 56 s /.

ELSIMW 360 / Extracts a block of 5'x5' mean elevations with given dimensions and location from dataset FIVMINEL. If real data is not available, simulated values are generated using the parameters stored in dataset SIMINDEX. Values in ocean areas may be optionally zeroed or returned unaltered /SS / F / WINDEX / 11 FIVMINEL / N / N / 112 / 68438b / - /.

EUROTRAN 360 / Transfers European 5'x5' mean elevations from dataset EUROMEL on tape to dataset FIVMINEL and updates dataset SIMINDEX. Checks and lists values out of range in the card images and maps available data by 1° quads / P / F / PARM, GETELS, PUTELS / 4 EUROMEL, 10 SIMINDEX, 11 FIVMINEL / Y / N / 95 / 51560b / 9 m 58 s /.

FACT 360 / Extracts from a built-in table the factorial of numbers up to 118 and returns the result as a fractional component and the appropriate decimal exponent to avoid exceeding machine numeric range / FS / F / - / - / N / N / 23 / 1946b / - /.

FIVDEGEL 360 / Computes and lists global terrain 5°x5° mean elevations using dataset ONEDEGEL and stores the results in dataset FIVDEGEL / P / F / - / 7 ONEDEGEL, 8 FIVDEGEL / N / N / 36 / 156008b / 30 s /.

FIVEMAPS 360 / Prints a listing in global map form of results data on a 5° grid, with optional suppression of any of the twelve datasets on a results file. Data values are scaled by tertiary multiples of ten to fit the output format / P / F / FIVMAP, PARM / 9 Results dataset / Y / N / 77 / 42784b / 58 s for 12 datasets /.

FIVMAP 360 / Prints a listing in global map form of data on a 5° grid and a given title / SS / F / - / - / N / N / 25 / 818b / - /.

GETBIT (PUTBIT) 360 / Extracts the value of a given bit in a binary string of any length / ESS / A / - / - / N / N / 63 / 216b / - /.

GETELS (PUTELS) 360 / Returns a 1°x1° block of 5' mean elevations at a given location from dataset FIVMINEL / ESS / F / GINDEX / 11 FIVMINEL / N / N / 33 / 1616b / - /.

GINDEX (PINDEX) 360 / Returns the direct access record number (in dataset FIVMINEL) of a 1°x1° block of 5' mean elevations of given location or, if no data has been stored for that location, the number of the next unused record / ESS / F / - / 10 SIMINDEX / N / N / 51 / 1946b / - /.

GLOBPLOT 360 / Plots at a given scale selected contours of results data on a global 5° grid with chosen contours emphasized or, in the case of deflexions of the vertical, a vector representation of each value. Optionally plots outline map of the world and/or 20° graticule of meridians and parallels. Any of the twelve datasets on a results file may be selected. Contour interval and range may be optionally determined automatically, according to the range of values in the dataset / P / F / GPCONT, BASMAP / 8 Results dataset, PLOTTER / N / Y / 282 / 143456b / average 10 s per contour or 10 s per dataset for deflexions /.

GPCONT 360 / Plots contours of a rectangular array of equally spaced data values by linear interpolation and a linear fit of interpolated points. Based on a routine developed by the Commonwealth Scientific and Industrial Research Organization / SS / F - / - / N / N / 263 / 6464b / - /.

GRADERR 9830 / Computes by point mass assumption, the error due to suppression of topographic gradient when 1°x1° mean elevations are used to represent topography. Gradient, overall elevation, and distance of computation point may be varied / P / B / - / - / - / - / 55 / 458w / - /.

HAFDEGEL 360 / Computes global 30'x30' mean elevations using 5' data in dataset FIVMINEL and stores the results in dataset HAFDEGEL / P / F / ELSIMW / 11 FIVMINEL, 12 SIMINDEX, 15 HAFDEGEL / N / N / 58 / 114600b / 48 m 51 s /.

HARCOPLT 360 / Plots a bar chart of spherical harmonic coefficients up to (36,36) and a graph of degree variances. Scales may be determined automatically. Also optionally punches and lists harmonic coefficients / P / F / PARMNO, PARM / 12 Harmonic coefficients, PLOTTER / Y / Y / 341 / 48896b / 6 s per dataset /.

HARMONIC 360 / Operates in two modes on any of the twelve datasets on the input files: (1) Computes fully normalized spherical harmonic coefficients up to (36,36) and degree variances of results data on a 5° grid or coarser multiple of 5° by global numerical integration [HEISKANEN and MORITZ 1967, equations 1-76, p.31]. Options include: (a) Addition of two input datasets before analysis, (b) conversion of potentials and attraction components to equipotential undulations and deflexions of the vertical according to Bruns' theorem before analysis, (c) automatic cut-off of analysis at any degree if degree variance falls below a given tolerance level, (d) storage of combined datasets, converted or unconverted, and harmonic coefficients and degree variances. (2) Synthesizes values of a function given the fully normalized spherical harmonic coefficients [HEISKANEN and MORITZ 1967, equation 1-75, p.31]. Synthesized values and the residuals when compared with the original analysed data may be stored. Mean, root mean square, and maximum residuals are listed / P / F / PARM, TRIG, PARMNO / 7 ALFORD36, 8 First input file, 9 Second input file, 10 Unconverted values (analysis) or synthesized values (synthesis), 11 Undulations and deflexions (analysis) or residuals (synthesis), 12 Harmonic coefficients and degree variances / Y / N / 355 / 65648b / average 8 m 13 s per dataset for analysis to (36,36) and 11 m 18 s per dataset for systhesis /.

ICERINIT 360 / Initializes datasets INNICECS, MIDICECS, and OUTICECS and sets default values of all parameters prior to running computation routines / P / F / PUTBIT / 20 Results dataset / N / N / 25 / 31944b / 20 s /.

ICEROCK 360 / Computes and lists 1°x1° and 5°x5° mean ice thickness data for Greenland and Antarctica from given point values and stores the results in datasets ONEICEEL and FIVICEEL along with topographic mean elevations for use by programme OUTICEC / P / F / FIVMAP / 7 ONEDEGEL, 8 FIVDEGEL, 9 ONEICEEL, 10 FIVICEEL / N / Y / 134 / 178696b / 1 m 36 s /.

ICONTRIB 360 / Computes at selected points the contributions to the potential and attraction components at geoid, surface, and orbital levels due to topography in concentric zones of specified radius. Simultaneously computes the mass of the topography by numerical integration. All evaluations are based on 1°x1° quad sizes using UCLA 1° height data / P / F / UCLA1S / 9 COSINE, 14 UCLA1SHT / N / Y / 192 / 107624b / average 3 m per point /.

IEBGENER 360 / Copies card images to tape / P / U / - / Output dataset [IBM 1970b, p.257 *et seq.*] / N / Y / - / 17936b / variable /.

IEBPTPCH 360 / Copies card images to the line printer or card punch [IBM 1970b, p.301 *et seq.*] / P / U / - / Input dataset / N / N / - / 19984b / variable /.

INIT5MIN 360 / Initializes dataset SIMINDEX / P / F / - / 12 SIMINDEX / N / N / 26 / 25272b / 24 s /.

INNAINIT 360 / Initializes dataset INNATMOS and sets default values of parmaters prior to running programme INNATMO / P / F / PUTBIT / 20 INNATMOS / N / N / 25 / 31944b / 20 s /.

INNATMO 360 / Computes potential and attraction components at surface level on a 30° global grid due to the atmosphere in the inner zone using a rigorous rectangular parallelepiped formula, and a stepwise linear density model. (see also Computation Sub-system in §7.3) / P / F / PARM, CONSOL, ITEST, KLOCK, NOKHAR, TRIG, PARMNO, WINDEX, ELSIMW / 11 FIVMINEL, 12 SIMINDEX, 19 SPOTHITE, 20 INNATMOS / Y / N / 558 / 246040b / 5 h 03 m 36 s /.

INNCONT 360 / Computes corrections to potential and attraction components at geoid, and surface levels on a 5° global grid due to discrepancies in the heights of the four 5' topographic quads adjacent to the computation point / P / F / PARM, ELSIMW, NOKHAR, TRIG, CONSOL, PARMNO, ITEST, KLOCK, WINDEX / 7 ONEPOLAR, 11 FIVMINEL, 12 SIMINDEX, 19 SPOTHITE, 20 INNCONTS / Y / N / 576 / 264280b / 1 h 33 m /.

INNFCOPY 360 / Copies results data from 1° grid datasets INNZONES, INNICECS, and INNCONTS to 5° grid datasets INNFIVEG, INNFIVIC, and INNFCONT prior to analysis / P / F - / 9 Output dataset, 20 Input dataset / N / N / 139 / 138568b / 30 s /.

INNICEC 360 / Computes corrections to potential and attraction components at geoid and surface levels on a 5° grid due to the presence of the Greenland and Antarctic ice sheets in the inner zone using a rigorous rectangular parallelepiped formula (see §7.3 for details). / P / F / ITEST, KLOCK, PARM, WINDEX, ELSIMW, NOKHAR, TRIG, CONSOL, PARMNO / 7 ONEPOLAR, 11 FIVMINEL, 12 SIMINDEX, 19 SPOTHITE, 20 INNICECS / Y / N / 601 / 264664b / 6 h /.

ININIT 360 / Initializes datasets INNZONES and INNICECS and sets default values of parameters prior to running programmes INNZONE and INNICEC / P / F / PUTBIT / 20 Results dataset / N / N / 25 / 31944b / 20 s /.

A. COMPENDIUM OF COMPUTER ROUTINES

INNZONE 360 / Computes potential and attraction components at geoid and surface levels on a 5° grid due to the terrestrial topography and compensation in the inner zone using a rigorous rectangular parallelepiped formula (see §7.3 for details) / P / F / TRIG, PARM, ELSIMW, NOKHAR, CONSOL, PARMNO, ITEST, KLOCK, WINDEX / 11 FIVMINEL, 12 SIMINDEX, 19 SPOTHITE, 20 INNZONES / Y / N / 538 / 246184b / 30 h /.

ITEST 360 / Tests an event control block to determine whether it has been posted, indicating entry of a message at the operator's console typewritter / EFS / A / - / - / N / N / 228 / 1192b / - /.

JOBFILER 360 / Stores, replaces, or deletes sets of job control cards in dataset JOBFILE for use by programme JOBSTART and also lists the contents of the dataset. Jobs are stored in alphabetical order and card images are numbered sequentially in increments of 10 / P / F / - / 11 JOBFILE, 12 Temporary / N / Y / 101 / 2356b / approx. 20 s /.

JOBSTART 360 / Copies card images including job control cards from dataset JOBFILE or from the operator's console to the HASP internal reader for entry to the system input queue. Job requests and card editing commands or whole jobs may be entered from the operator's console / P / F / CONSOL, PARMNO / 11 JOBFILE, 12 Internal reader / N / N / 118 / 47104b / approx. 3 s /.

KLOCK 360 / Returns date and time of day to one hundredth of a second using SVC 11 instruction / FS / A / - / - / N / N / 24 / 168b / - /.

LEGENDRE 9810 / Checks summation of component terms of the associated Legendre function / P / - / - / - / N / N / 68 / 7r / - /.

MEANHITE 360 / Lists and transfers UCLA global 1°x1° mean elevations from dataset MATHER1 on tape to direct access dataset UCLA1SHT and replaces erroneous card images / P / F / - / 8 MATHER1, 14 UCLA1SHT / N / Y / 35 / 260722b / 6 m 00 s /.

MELERROR 360 / Screens North American 5'x5' mean elevations and their location parameters for errors and omissions. Elevations which differ from the mean of surrounding values by more than a given number of standard deviations are listed and identified in a 1° quad map / P / F / - / 15 AMER5MIN / N / Y / 145 / 54824b / 13 m 51 s /.

MELMAP 360 / Prints 50 metre interval hypsometric and 100 metre interval bathymetric maps (*e.g.* see figure 6.6) of North American 5'x5' mean elevations on line printer using alphanumeric and special symbols. Data type and precision, as coded by ACIC, may be mapped also / P / F/ - / 15 AMER5MIN / N / Y / 117 / 71768b / 1 h 18 m 33 s /.

MELTRAN 360 / Transfers North American 5'x5' mean elevations from datasets SQS-5N01, SQS-5N02, and SQS-5N03 on tape to direct access dataset AMER5MIN: checks and lists location parameters and maps card images. Lists index of dataset AMER5MIN and prints a 1° quad map of transferred data / P / F / - / 4 SQS-5N01, SQS-5N02, SQS-5N03; 15 AMER5MIN / N / Y / 280 / 43272b / 36 m 30 s /.

MIDAINIT 360 / Initializes dataset MIDATMOS and sets default values of parameters prior to running programme MIDATMO / P / F / PUTBIT / 20 MIDATMOS / N / N / 25 / 31944b / 20 s /.

MIDATMO 360 / Computes potential and attraction components at geoid and surface levels on a global 30° grid due to the atmosphere in the mid zone using a point mass approximation and a stepwise linear density model / P / F / TRIG, PARM, ITEST, KLOCK, NOKHAR, CONSOL, PARMNO, ELSIMW, WINDEX / 11 FIVMINEL, 12 SIMINDEX, 15 HAFDEGEL, 18 Temporary, 19 SPOTHITE, 20 MIDATMOS / Y / N / 536 / 260584b / 4 h 16 m 48 s /.

MIDFCOPY 360 / Copies results data from 1° grid datasets MIDZONES and MIDICECS to 5° grid datasets MIDFIEG and MIDFIVIC prior to analysis / P / F / - / 9 Output dataset, 20 Input dataset / N / N / 139 / 138568b / 31 s /.

A. COMPENDIUM OF COMPUTER ROUTINES

MIDICEC 360 / Computes corrections to potential and attraction components at geoid and surface elevations on a 5° grid due to the presence of the Greenland and Antarctic ice sheets in the mid zone using a point mass approximation (see §7.3 for details) / P / F / TRIG, PARM, ITEST, KLOCK, NOKHAR, CONSOL, PARMNO, ELSIMW, WINDEX / 7 ONEPOLAR, 11 FIVMINEL, 12 SIMINDEX, 15 HAFDEGEL, 18 Temporary, 19 SPOTHITE, 20 MIDICECS / Y / N / 595 / 279704 / 6 h 36 m /.

MIDINIT 360 / Initializes datasets MIDZONES and MIDICECS and sets default values of parameters prior to running programmes MIDZONE and MIDICEC / P / F / PUTBIT / 20 Results data / N / N / 25 / 31944b / 20 s /.

MIDZONE 360 / Computes potential and attraction components at geoid and surface levels on a 5° grid due to the terrestrial topography and compensation in the mid zone, using a dipole point mass approximation (see §7.3 for details) / P / F / TRIG, PARM, NOKHAR, CONSOL, PARMNO, ITEST, KLOCK, ELSIMW, WINDEX / 11 FIVMINEL, 12 SIMINDEX, 15 HAFDEGEL, 18 Temporary, 19 SPOTHITE, 20 MIDZONES / Y / N / 539 / 239272b / 28 h /.

NAMER 360 / Extracts a block of North American 5'x5' mean elevations with given dimensions and location from dataset AMER5MIN. Unavailable data is signalled by 9999 / SS / F / - / 15 AMER5MIN / N / N / 72 / 27504b / - /.

NOKHAR 360 / Converts a number stored as a 2-byte integer to character representation in a field of given length by adding 240 decimal (representing the zone digit) to each decimal digit. The character form is right justified and padded with blanks / SS / F / - / - / N / N / 30 / 488b / - /.

OCONTRIB 360 / Computes and stores the contribution to the total potential and attraction components at a given point at geoid, surface, and satellite orbit elevations due to the terrestrial topography and compensation in each 5° quad and prints a listing of the results in global map form / P / F / TRIG, CONSOL, PARMNO, PUTBIT, PARM, ITEST, KLOCK, FIVMAP, NOKHAR / 7 ONEDEGEL, 8 FIVDEGEL, 9 OCONTRIB, 19 SPOTHITE, 20 OUTZONES / Y / N / 623 / 378312b / 4 m per point /.

ONEDEGEL 360 / Computes 1°x1° mean terrestrial elevations from all available 5' data and combines the results with UCLA 1° data in remaining areas to form dataset ONEDEGEL. Values derived from the 5' data are compared with the UCLA 1° values and a listing of large discrepancies is printed along with the mean and rms discrepancies / P / F / GETELS, PARM, PARMNO, UCAL1S / 7 ONEDEGEL, 10 SIMINDEX, 11 FIVMINEL, 14 UCLA1SHT / Y / N / 87 / 163048b / 37 m 52 s /.

ONEPOLAR 360 / Converts 1°x1° mean ice thickness data stored in dataset ONEICEEL into a compressed form suitable for use by programmes INNICEC, INNCONT, and MIDICEC and stores the results in dataset ONEPOLAR / P / F / - / 7 ONEPOLAR, 9 ONIECEEL / N / N / 20 / 168032b / 14 s /.

ONEWORLD 360 / Transfers 1°x1° mean elevations from direct access dataset UCLA1SHT to sequential dataset ONEWORLD and computes global 5°x5° mean elevations including marine topography and stores the results in dataset FIVWORLD for use by programme OUTSEAS. Listings of both datasets are printed / P / F / UCLA1S / 7 ONEWORLD, 8 FIVWORLD, 14 UCLA1SHT / N / N / 78 / 156008b / 5 m 39 s /.

OUTAINIT 360 / Initializes dataset OUTATMOS and sets default values of parameters prior to running programme OUTATMO / P / F / PUTBIT / 20 OUTATMOS / N / N / 24 / 31944b / 19 s /.

OUTATMO 360 / Computes potential and attraction components at geoid, surface, and satellite orbit elevations on a global 30° grid due to the atmosphere in the outer zone using a point mass approximation and a stepwise linear density model (see also Computation Sub-system in §7.3) / P / F / PARM, TRIG, CONSOL, PUTBIT, NOKHAR, ITEST, KLOCK, PARMNO / 7 ONEDEGEL, 8 FIVDEGEL, 19 SPOTHITE, 20 OUTATMOS / Y / N / 497 / 182432b / 3 h 20 m /.

OUTFCOPY 360 / Copies results data from 1° grid datasets OUTZONES and OUTICECS to 5° grid datasets OUTFIVEG and OUTFIVIC prior to analysis / P / F / - / 9 Output dataset, 20 Input dataset /

N / N / 152 / 160416b / 17 s /.

OUTICEC 360 / Computes corrections to potential and attraction components at geoid, surface, and satellite orbit elevations on a 5° grid due to the presence of the Greenland and Antarctic ice sheets in the outer zone, using a point mass approximation (see §7.3 for details) / P / F / TRIG, PARM, ITEST, KLOCK, NOKHAR, CONSOL, PARMNO / 7 ONEICEEL, 8 FIVICEEL, 19 SPOTHITE, 20 OUTICECS / Y / N / 540 / 146504b / 6 h 12 m /.

OUTINIT 360 / Initializes datasets OUTZONES and OUTICECS and sets default values of parameters prior to running programmes OUTZONE and OUTICEC / P / F / PUTBIT / 20 Results dataset / N / N / 24 / 31944b / 17 s /.

OUTSEAS 360 / Computes potential and attraction components at geoid, surface, and satellite orbit elevations at selected points due to the marine topography and compensation in the outer zone, using a dipole point mass approximation (see also description of programme OUTZONE in §7.3) / P / F / ITEST, KLOCK, PARMNO, CONSOL, PUTBIT, PARM, TRIG, NOKHAR / 7 ONEWORLD, 8 FIVWORLD, 19 SPOTHITE, 20 OUTSEASS / Y / N / 486 / 182136b / approx. 1 m 30 s per point /.

OUTZONE 360 / Computes potential and attraction components at geoid, surface, and satellite orbit elevations on a 5° grid due to the terrestrial topography and compensation in the outer zone using a dipole point mass approximation (see §7.3 for details) / P / F / ITEST, KLOCK, PARMNO, CONSOL, PUTBIT, PARM, TRIG, NOKHAR / 7 ONEDEGEL, 8 FIVDEGEL, 19 SPOTHITE, 20 OUTZONES / Y / N / 483 / 182096b / 21 h /.

PARM 360 / Returns the character string and its length transferred to the problem programme through the PARM field (parameter list) of the EXEC statement [IBM 1966a, p.15] / SS / A / - / - / N / N / 24 / 168b / - /.

PARMNO 360 / Converts a character string of given length comprising numeric digits separated by commas to an ordered set of 4-byte integer numbers. Used to pick up numeric values of parameters in a parameter list or from the operator's console / SS / F / - / - / N / N / 28 / 624b / - /.

PINDEX 360 / Stores at a given location in dataset SIMINDEX the direct access record number of a 1°x1° block of 5'x5' mean elevations in dataset FIVMINEL. If the record is a new entry, the count of unused records is amended / SS / F / - / 10 SIMINDEX / N / N / 51 / 1946b / - /.

POTGRAV 9830 / Computes potential and attraction components at a given point due to a rectangular parallelepiped with an axial linear density variation, using a rigorous formula / P / B / - / - / - / - / 173 / 1803w / - /.

POTOPEN 9830 / Computes potential at a given point due to a pair of homogeneous rectangular parallelepipeds of given dimensions representing the topography and compensation, using an open series expansion in Legendre polynomials to four terms / P / B / - / - / - / - / 128 / 1482w / - /.

POTRIGOR 9830 / Computes potential at a given point due to a pair of homogeneous rectangular parallelepipeds of given dimensions representing the topography and compensation, using a rigorous formula / P / B / - / - / - / - / 72 / 1000w / - /.

PUTBIT 360 / Sets the given value of a given bit in a binary string of any length / SS / A / - / - / N / N / 63 / 216b / - /.

PUTELS 360 / Stores a 1°x1° block of 5' mean elevations at a given location in dataset FIVMINEL. If the block is a new entry SIMINDEX is updated by a call to routine PINDEX. The record written into FIVMINEL also contains location, date and time parameters / SS / F / GINDEX, PINDEX / 11 FIVMINEL / N / N / 33 / 1616b / - /.

A. COMPENDIUM OF COMPUTER ROUTINES

REGRESS 9810 / Computes least squares linear regression coefficients for any number of given values of a bivariate distribution and performs a complete regression analysis / P / - / - / - / - / - / 499 / 8r / - /.

SIMPSON 9810 / Performs a numerical integration between given limits in one, two, or three dimensions of a given function using Simpson's formula for a given even number of intervals / P / - / Given function / - / - / - / 1373 / 27r / - /.

SPOTHITE 360 / Computes and lists the elevation of points at the terrestrial surface on a global 1° grid by assuming that they are the mean of the four adjacent 5'x5' mean elevations stored in dataset FIVMINEL and stores the results in dataset SPOTHITE / P / F / ELSIMW, WINDEX / 11 FIVMINEL, 12 SIMINDEX, 19 SPOTHITE / N / N / 75 / 92032b / 1 h 08 m 17 s /.

STATUS 360 / Prints a global 1° quad map of the 5'x5' mean elevations contained in dataset FIVMINEL with records identified according to date and time of original entry. Optionally deletes groups of records and compresses the remaining records to remove resulting spaces. Entries in dataset SIMINDEX are amended appropriately / P / F / PARM, WINDEX, PARMNO / 10 SIMINDEX, 11 FIVMINEL / Y / N / 129 / 46128b / 1 m 57 s for map + approx. 1 m per group deleted./.

TOPOCORR 360 / Performs regression analysis of topographic standard deviation of 5'x5' mean elevations within 1°x1° quads with respect to the 1°x1° mean elevation and determines the correlation coefficient and linear regression coefficients. Analyses are performed for each of the continental sets of data, North America , Europe, and Australia, and for all data combined. Maps of the bivariate distributions are printed / P / F / ELSIMW, WINDEX / 10 SIMINDEX, 11 FIVMINEL / N / N / 119 / 90720b / 5 m 00 s /.

TOPOSIM 360 / Simulates 5'x5' mean elevations in areas where data is not available by transfering 1°x1° blocks of available data. Real data is selected from an area of morphological similarity, determined from the UCLA 1° data and modified by a linear function based on the global correlation of topographic variance with mean elevation. Resulting simulation parameters for each 1° block are stored in dataset SIMINDEX (see §6.4 for details) / P / F / PARMNO, ITEST, GINDEX, PARM, CONSOL, NOKHAR / 7 ELMONE, 8 ELMVAR, 9 ELSIMLOC, 12 SIMINDEX / Y / N / 233 / 184352b / 60 h /.

TRIG 360 / Returns single precision values of the sine and cosine functions of any given angle in degrees using a table at 1° intervals and series expansion of the remaining fraction. The routine is amost twice as fast as the built-in IBM functions with comparable precision / SS / A / - / - / N / N / 84 / 576b / average 460 µs per call /.

TRIGTIME 360 / Compares average computation time and accuracy of subroutine TRIG with that of IBM routines SIN and COS. Ten thousand randomly generated angles in the range -2π to $+2\pi$ are used as arguements / P / F / RANDU, TRIG / - / N / N / 42 / 51152b / 32 s /.

UCLAMAP 360 / Prints 200 metre interval hypsometric and/or bathymetric maps of the UCLA global 1°x1° mean elevations on the line printer using alphanumeric symbols / P / F / UCLA1S / 14 UCLA1SHT / N / Y / 236 / 210536b / 2 m per map /.

UCLA1S 360 / Extracts a block of UCLA 1°x1° mean elevations with given dimensions and location from dataset UCLA1SHT and checks stored location parameters of each record / SS / F / - / 14 UCLA1SHT / N / N / 39 / 1776b / - /.

UNSW5DEG 360 / Converts global 1°x1° mean elevations in dataset ONEWORLD to mean values of 5°x5° quads with bounding meridians and parallels offset from the universal origin by 2½° and stores the results in dataset UNSW5DEG for use in testing programme HARMONIC. Both solid earth and terrestrial elevations are stored separately / P / F / - / 7 ONEWORLD, 8 UNSW5DEG / N / N / 76 / 176536b / 57 s /.

A. COMPENDIUM OF COMPUTER ROUTINES

VTOCMAP 360 / Prints a concise map of the volume table of contents of a specified 2311 disk using alphanumeric symbols to represent the contents of each track / P / P and F / - / 9 Temporary / N / N / 131 / 84168b / 15 s /.

WINDEX 360 / Extracts a block of direct access record numbers referring to dataset FIVMINEL and simulation parameters of given dimensions and locations from dataset SIMINDEX. Called by subroutine ELSIMW to extract or simulate 5'x5' mean elevations / SS / F / - / 12 SIMINDEX / N / N / 21 / 904b / - /.

WORLDPLT 360 / Plots longitudinal profiles at a given vertical scale of the global 5'x5' mean elevations stored in dataset FIVMINEL within a given area, to enable visual error screening of the data / P / F / ELSIMW, PARM, WINDEX / 11 FIVMINEL, 12 SIMINDEX / Y / Y / 102 / 89168b / 9 s per 5°x5° block /.

XCHECK 360 / Compares 5'x5' mean elevation data stored in dataset FIVMINEL with original source datasets on tape and lists errors and omissions. Location parameters as well as elevations are checked for each card image and unsatisfactory card images are punched / P / F / GETELS / 4 SQS-5N01, SQS-5N02, SQS-5N03, EUROMEL; 10 SIMINDEX; 11 FIVMINEL / N / N / 75 / 30456b / 21 m 57 s /.

Appendix B

Compendium of IBM 360/50 Datasets

KEY TO ITEMS LISTED:

/ indicates end of item
- indicates item not applicable

NAME — *Contents and description / Storage unit: T = magnetic tape, D = 2311 disk / Volume names on which dataset resides / Label number on tape volumes / Dataset organization: S = sequential, DA = direct access, P = partitioned / Form of records: U = unformatted (Binary or internal), F = formatted (character or external) / Record format: F = fixed length, V = variable length, U = undefined length, B = blocked, S = spanned records / Block size (buffer length) in bytes / Logical record length in bytes / Number of records in dataset / Space occupied by dataset in 2311 disk tracks /.*

ALFORD36 — Values of the fully normalized associated Legendre function at 5° intervals of latitude from +90° to -90° for every degree and order from (0,0) to (36,36). Each record contains the 37 values for a particular order / D / TEROID, SURGRA / - / S / U / VBS / 3624 / 3620 / 1369 / 59 /.

AMER5MIN — North American 5' mean elevations and type and accuracy codes. Each record contains the 144 values within a 1°x1° quad. / D / SURAST / - / DA / U / F / 576 / - / 2332 / 480 /.

ATMGCOHA — Fully normalized spherical harmonic coefficients and degree variances of gravity corrections to account for the atmosphere according to the GRS67 computed on a 5° global grid. Each record contains an array dimensioned (1480). / D / TEROID / - / DA / U / F / 2960 / - / 24 / 24 /.

AUSTFIVE — Australian 5' mean elevations stored as card images according to DMA (ACIC) format. / T / UCC319 / 1 / S / F / FB / 1920 / 80 / 35928 records / - /.

AUSTMEL — Australian 6'x6' mean elevations in feet stored as card images with three different formats. / T / AUSMEL / 1, 2, 3 / S / F / FB / 80 / 80 / 10373 rec. / - /.

B. COMPENDIUM OF IBM 360/50 DATASETS

AUST6MIN Australian 6'x6' mean elevations. Each record contains the 100 values within a 1°x1° quad. / D / TEROID / - / DA / U / F / 200 / - / 1575 / 107 /.

BASEMAPA Coordinates of the digitized outline map of the world and plotter pen control parameter values. Each record contains a pair of coordinates (X,Y) and a value of the pen parameter. / D / TEROID, SURGRA, SURGEO / - / S / U / FB / 3624 / 12 / 4526 / 15 /.

ELMONE Global 1°x1° mean elevations compiled from all available 5' data and UCLA 1° data, stored as an array dimension (180,360). / D / TEROID / - / S / U / VBS / 3608 / 3604 / 36 / 36 /.

ELMVAR Topographic standard deviations within 1° quads, compiled from all available 5' mean elevations. Stored as an array dimension (50,80). / D / TEROID / - / S / U / VBS / 3608 / - / 5 / 5 /.

ELSIMLOC Parameters determining the current location of programme TOPOSIM, used as a continuity link between job runs. / D / TEROID / - / S / U / F / 12 / 12 / 1 / 1 /.

EUROMEL European 5' mean elevations stored as card images according to DMA (ACIC) format. / T / AUSMEL / 4, 5 / S / F / FB / 1320 / 132 / 37828 rec. / - /.

FIVDEGEL Global 5° mean terrestrial elevations compiled from dataset ONEDEGEL. Stored as an array dimensioned (36,72). / D / SURGRA / - / S / U / VBS / 3608 / 3604 / 2 / 2 /.

FIVICEEL Greenland and Antarctic 5° mean ice thicknesses and topographic surface elevations, stored as an array dimensioned (36,72) with vacant areas signalled by 9999. / D / SURGRA / - / S / U / VBS / 3608 / 3604 / 2 / 2 /.

FIVMINEL North American, European, and Australian 5' mean elevations. Each record contains the 144 values within a 1° quad and the location is recorded in dataset SIMINDEX. / D / SURGEO, TEROID / - / DA / U / F / 294 / - / 4751 / 650 /.

FIVWORLD Global 5° mean terrestrial and marine (solid earth) elevations, stored as an array dimensioned (36,72). / D / SURGRA / - / S / U / VBS / 3608 / 3604 / 2 / 2 /.

HAFDEGEL Global 30' mean terrain elevations compiled from global 5' data including simulated values. Each eight records contains an array dimensioned (720,20) comprising a block of data covering 360° longitude and 10° latitude. / D / SURGEO / - / DA / U / F / 3600 / - / 144 / 144 /.

INNATMOS Potential and attraction components computed on a global 30° grid at surface level due to atmosphere in inner zone. Each record contains a 10°x10° block of a global 1° grid. / D / SURGEO / - / DA / U / F / 3625 / - / 648 / 650 /.

INNCONTS Potential and attraction components computed on a global 5° grid at geoid and surface due to contact sub-zone 5'x5' mean elevation discrepancies. Each record contains a 10°x10° block of the grid. / D / TEROID / - / DA / U / F / 3625 / - / 648 / 650 /.

INNFATMO Compressed version of dataset INNATMOS. Each 3 records contain an array dimensioned (37,73). / D / SURGRA / - / DA / U / F / 3604 / - / 30 / 30 /.

INNFCONT Compressed version of dataset INNCONTS. Each 3 records contains an array dimensioned (37,73). / D / SURGRA / - / DA / U / F / 3604 / - / 30 / 30 /.

INNFIVCO Sum of datasets INNFIVEG and INNFCONT. Each 3 records contains an array dimensioned (37,73). / D / TEROID / - / DA / U / F / 3604 / - / 30 / 30 /.

INNFIVEG Compressed version of dataset INNZONES. Each 3 records contains an array dimensioned (37,73). / D / TEROID / - / DA / U / F / 3604 / - / 30 / 30 /.

INNFIVIC Compressed version of dataset INNICECS. Each 3 records contains an array dimensioned (37,73). / D / SURGEO / - / DA / U / F / 3604 / - / 30 / 30 /.

B. COMPENDIUM OF IBM 360/50 DATASETS

INNHARTO — Fully normalized spherical harmonic coefficients and degree variances of undulations and deflexions due to total inner zone effect. Each 2 records contains an array dimensioned (1480). / D / TEROID / - / DA / U / F / 2960 / - / 24 / 24 /.

INNICECS — Potential and attraction components computed on a global 5° grid at geoid and surface due to polar ice caps in the inner zone. Each record contains a 10°x10° block of the grid. / D / TEROID / - / DA / U / F / 3625 / - / 648 / 650 /.

INNMIDAT — Sum of datasets INNFATMO and MIDFATMO. Each 3 records contains an array dimensioned (37,73). / D / SURGRA / - / DA / U / F / 3604 / - / 24 / 24 /.

INNMIDGE — Sum of datasets INNTOTSI and MIDTOTSI converted to undulations and deflexions. Each 3 records contain an array dimensioned (37,73). / D / TEROID / - / DA / U / F / 3604 / - / 24 / 24 /.

INNMIDHA — Fully normalized spherical harmonic coefficients and degree variances of undulations and deflexions for combined inner and mid zone effects. Each 2 records contain an array dimensioned (1480). / D / TEROID / - / DA / U / F / 2960 / - / 24 / 24 /.

INNMIDSI — Sum of datasets INNTOTSI and MIDTOTSI. Each 3 records contain an array dimensioned (37,73). / D / TEROID / - / DA / U / F / 3604 / - / 24 / 24 /.

INNTOTGE — Undulations and deflexions due to the total inner zone effect. Each 3 records contain an array dimensioned (37,73). / D / TEROID / - / DA / U / F / 3604 / - / 24 / 24 /.

INNTOTSI — Sum of datasets INNFIVIC and INNFIVCO. Each 3 records contain an array dimensioned (37,73). / D / TEROID / - / DA / U / F / 3604 / - / 24 / 24 /.

INNZONES — Potential and attraction components computed on a global 5° grid at geoid and surface due to topography and compensation in inner zone. Each record contains a 10°x10° block of the grid. / D / TEROID / - / DA / U / F / 3625 / - / 648 / 650 /.

JOBFILE — Job control card images with jobs stored in alphabetical sequence. / D / TEROID, SURGRA, SURGEO / - / S / F / FB / 80 / 80 / variable / 10 /.

JOBSTART — Job control card images to initiate programme JOBSTART. / D / TEROID, SURGRA, SURGEO / - / S / F / FB / 80 / 80 / 7 / 1 /.

MATHER1 — UCLA global 1° mean solid earth elevations stored as card images. / T / 1MEAN / 1 / S / F / FB / 800 / 80 / 4320 rec. / - /.

MIDATMOS — As for dataset INNATMOS but for mid zone effect. / D / SURGRA / - / DA / U / F / 3625 / - / 648 / 650 /.

MIDFATMO — Compressed version of dataset MIDATMOS. Each 3 records contain an array dimensioned (37,73). / D / SURGRA / - / DA / U / F / 3604 / - / 30 / 30 /.

MIDFIVEG — Compressed version of dataset MIDZONES. Each 3 records contain an array dimensioned (37,73). / D / SURGEO / - / DA / U / F / 3604 / - / 30 / 30 /.

MIDFIVIC — Compressed version of dataset MIDICECS. Each 3 records contain an array dimensioned (37,73). / D / SURGEO / - / DA / U / F / 3604 / - / 30 / 30 /.

MIDHARTO — As for dataset INNHARTO but for total mid zone effect/ D / TEROID / - / DA / U / F / 2740 / - / 24 / 24 /.

MIDICECS — As for dataset INNICECS but for mid zone effect. / D / SURGEO / - / DA / U / F / 3625 / - / 648 / 650 /.

MIDTOTGE — As for dataset INNTOTGE but for mid zone effect. / D / TEROID / - / - / DA / U / F / 3604 / - / 24 / 24 /.

MIDTOTSI — Sum of datasets MIDFIVIC and MIDFIVEG. Each 3 records contain an array dimensioned (37,73). / D / TEROID / - / DA / U / F / 3604 / - / 24 / 24 /.

B. COMPENDIUM OF IBM 360/50 DATASETS

MIDZONES As for dataset INNZONES but for mid zone effect. / D / SURGEO / - / DA / U / F / 3625 / - / 648 / 650 /.

OCONTRIB Contributions to the potential and attraction components at a point with latitude 30°N and longitude 70°E (Himalayas) at geoid, surface, and satellite orbit elevations for each 5° quad. Each 3 records contain an array dimensioned (37,73). / D / SURGRA / - / DA / U / F / 3604 / - / 36 / 36 /.

OMIATMGE Undulations and deflexions due to the total global effect (inner, mid, and outer zones) of the atmosphere. Each 3 records contain an array dimensioned (37,73). / D / SURGRA / - / DA / U / F / 3604 / - / 36 / 36 /.

OMIATMHA As for dataset INNMIDHA but for total global effect (all zones). / D / SURGRA / - / DA / U / F / 2960 / - / 24 / 24 /.

OMIATMSI Sum of datasets INNMIDAT and OUTFATMO. Each 3 records contain an array dimensioned (37,73). / D / SURGRA / - / DA / U / F / 3604 / - / 36 / 36 /.

OMITOTGE Sum of datasets INNMIDSI and OUTTOTSI converted to undulations and deflexions. Each 3 records contain an array dimensioned (37,73). / D / TEROID / - / DA / U / F / 3604 / - / 36 / 36 /.

OMITOTHA As for dataset INNMIDHA but for total global effect (all zones). / D / TEROID / - / DA / U / F / 2960 / -/24 / 24 /.

OMITOTSI Sum of datasets INNMIDSI and OUTTOTSI. Each 3 records contain an array dimensioned (37,73). / D / TEROID / - / DA / U / F / 3604 / - / 36 / 36 /.

ONEDEGEL Global 1° mean terrestrial elevations compiled from datasets FIVMINEL and UCLA1SHT. Stored as an array dimensioned (180,360). / D / SURGRA / - / S / U / VBS / 3608 / 3604 / 36 / 36 /.

ONEICEEL Greenland and Antarctic 1° mean ice thicknesses and topographic surface elevations, stored as an array dimensioned (180,360) with vacant areas signalled by 9999. / D / SURGRA / - / S / U / VBS / 3608 / 3604 / 36 / 36 /.

ONEPOLAR Compressed version of dataset ONEICEEL containing only ice thicknesses stored as two arrays: Greenland, dimensioned (30,55), and Antarctica, dimensioned (20,360). / D / TEROID, SURGEO / - / S / U / VBS / 3608 / 3604 / 5 / 5 /.

ONEWORLD Global 1° mean terrestrial and marine (solid earth) elevations compiled from dataset UCLA1SHT and stored as an array dimensioned (180,360). / D / SURGRA / - / S . U / VBS / 3608 / 3604 / 36 / 36 /.

OUTATMOS As for dataset INNATMOS but for outer zone effects and including effects at satellite orbit elevations. / D / SURGRA / - / DA / U / F / 3625 / - / 648 / 650 /.

OUTFATMO Compressed version of dataset OUTATMOS. Each 3 records contain an array dimensioned (37,73). / D / SURGRA / - / DA / U / F / 3604 / - / 36 / 36 /.

OUTFIVEG Compressed version of dataset OUTZONES. Each 3 records contain an array dimensioned (37,73). / D / SURGRA / - / DA / U / F / 3604 / - / 36 / 36 /.

OUTFIVIC Compressed version of dataset OUTICECS. Each 3 records contain an array dimensioned (37,73). / D / SURGRA / - / DA / U / F / 3604 / - / 36 / 36 /.

OUTHARTO As for dataset INNHARTO but for total outer zone effect and including coefficients for effects at satellite orbit elevation. / D / TEROID / - / DA / U / F / 2740 / - / 24 / 24 /.

OUTICECS As for dataset INNICECS but for outer zone effects and including effects at satellite orbit elevations. / D / SURGEO / - / DA / U / F / 3625 / - / 648 / 650 /.

OUTSEAS As for dataset INNZONES but for outer zone effects at selected points due to marine topography and compensation and including effects at satellite orbit elevations. / D / SURGRA / - / DA / U / F / 3625 / - / variable / 650 /.

OUTTOTGE As for dataset INNTOTGE but for total outer zone effects. / D / TEROID / - / DA / U / F / 3604 / - / 36 / 36 /.

OUTTOTSI Sum of datasets OUTFIVEG and OUTFIVIC. Each 3 records contain an array dimensioned (37,73). / D / TEROID / - / DA / U / F / 3604 / - / 36 / 36 /.

OUTZONES As for dataset INNZONES but for outer zone effects and including effects at satellite orbit elevations. / D / SURGRA / - / DA / U / F / 3625 / - / 648 / 650 /.

SIMINDEX Index of direct access record numbers of all records in dataset FIVMINEL and three simulation parameters for each $1°\times1°$ quad in areas of unavailable 5' data. Each record contains a $10°\times10°$ block of record numbers and parameters referring to $1°\times1°$ quads stored in dataset FIVMINEL. Record 649 comprises three 4-byte integers indicating: (a) the record number of the next unused record in dataset FIVMINEL, (b) the total number of records in FIVMINEL (6500), and (c) the number of groups of data stored in FIVMINEL. Record 650 comprises an array dimensioned (10,10) containing, as 2-byte integers, the record numbers of the first record of each group of data in FIVMINEL. / D / TEROID, SURGEO / - / DA / U / F / 600 / - / 650 / 130 /.

SPOTHITE Terrestrial surface elevations of computation points on a global 1° grid computed from dataset FIVMINEL and stored with one $10°\times10°$ block per record. / D / TEROID, SURGEO, SURGRA / - / DA / U / F / 200 / - / 648 / 50 /.

SQS-5N01 North American 5' mean elevations between latitudes 65°N and 52°N stored as card images according to DMA (ACIC) format. Continued in datasets SQS-5N02 and SQS-5N03. / T / UCC115 / 2 / S / F / FB / 800 / 80 / 20136 rec. / - /.

SQS-5N02 As for dataset SQS-5N01 but between latitudes 51°N and 42°N. / T / UCC115 / 3 / S / F / FB / 800 / 80 / 16008 rec. / - /.

SQS-5N03 As for dataset SQS-5N01 but between latitudes 41°N and 13°N. / T / UCC115 / 4 / S / F / FB / 800 / 80 / 21264 rec. / - /.

TEDLIB Library of routines stored as object code in load module form. / D / TEROID, SURGEO, SURGRA / - / P / U / U / 3625 / 3625 / variable / variable /.

UCLA1SHT UCLA global 1° mean elevations (solid earth). Each record comprises a strip 1° wide and 180° long containing values between the north and south poles. / D / TEROID / - / DA / U / F / 724 / - / 360 / 90 /.

UNSW5DEG Global 5° mean elevations compiled from dataset ONEWORLD as two separate sets: one containing solid earth elevations and the other terrestrial mean elevations (ocean areas zeroed). Boundaries of the 5° quads are offset by $2\frac{1}{2}°$ in longitude and latitude from the universal origin. / D / TEROID / - / DA / U / F / 3604 / - / 6 / 6 /.

UNSW5HAR Fully normalized spherical harmonic coefficients and degree variances to degree and order (36,36) of global 5° mean, solid earth and terrestrial elevations. Each 2 records contain an array dimensioned (1480). / D / TEROID / - / DA / U / F / 2960 / - / 24 / 24 /.

Appendix C

Harmonic Coefficients and Degree Variances

TABLE A

FULLY NORMALIZED SPHERICAL HARMONIC COEFFICIENTS AND DEGREE VARIANCES OF THE TOPOGRAPHIC-ISOSTATIC DISTURBING POTENTIAL AND VERTICAL COMPONENT OF ATTRACTION

KEY TO COLUMNS:

(1) Disturbing potential at geoid level (cm)
(2) Disturbing potential at surface level (cm)
(3) Disturbing potential at orbital level (cm)
(4) Vertical component of attraction at geoid level (μN/kg)
(5) Vertical component of attraction at surface level (μN/kg)
(6) Vertical component of attraction at orbital level (μN/kg)

Degree variances are shown in italics at the beginning of each degree in the 'S' column in cm^2 and $\mu N^2/kg^2$ for potential and attraction respectively.

		(1)		(2)		(3)		(4)		(5)		(6)	
n	*m*	C	S	C	S	C	S	C	S	C	S	C	S
0	0	-4.85	*23.5*	-0.95	*0.9*	-0.13	*0.0*	454.8	*206880*	-2.064	*4.26*	-0.013	*0.0002*
1	0	18.69	*858.5*	20.14	*1011.2*	14.44	*628.0*	166.2	*71409*	2.402	*17.61*	-0.367	*0.4378*
1	1	16.69	15.18	17.59	17.21	13.80	15.13	154.4	141.2	-2.991	1.701	-0.370	-0.408
2	0	8.88	*1260.3*	9.73	*1540.6*	7.20	*632.0*	77.7	*62854*	2.451	*30.42*	-0.314	*1.0072*
2	1	-1.55	25.26	-1.73	27.96	-0.93	18.08	-7.7	175.2	3.423	-0.650	0.040	-0.712
2	2	-21.23	9.51	-23.66	10.04	-14.35	6.80	-144.3	72.4	1.612	-3.110	0.572	-0.271
3	0	-26.67	*2805.8*	-29.34	*3279.9*	-16.71	*1018.2*	-184.4	*129630*	1.663	*75.60*	0.916	*2.9440*
3	1	-12.31	14.78	-12.71	16.35	-7.64	10.26	-87.3	101.1	2.111	2.443	0.401	-0.564
3	2	-35.35	17.62	-38.63	18.55	-20.91	9.88	-232.6	120.8	6.100	-1.803	1.111	-0.525
3	3	-0.64	12.79	-0.81	12.37	-0.12	6.37	3.6	95.2	1.243	-4.517	0.006	-0.339

		(1)		(2)		(3)		(4)		(5)		(6)	
n	*m*	C	S	C	S	C	S	C	S	C	S	C	S
4	0	-5.10	*2984.4*	-5.79	*3494.0*	-2.88	*860.2*	-19.3	*123082*	-0.959	*60.83*	0.168	*3.8244*
4	1	-4.52	-21.11	-4.58	-23.22	-2.23	-12.48	-34.7	-134.6	-0.812	-3.060	0.154	0.849
4	2	-34.99	2.78	-37.73	2.95	-18.36	0.74	-229.0	17.1	4.888	0.585	1.222	-0.050
4	3	14.41	-23.16	15.09	-25.88	7.03	-12.88	96.4	-137.3	-2.748	2.814	-0.467	0.856
4	4	6.79	21.68	8.04	22.50	3.56	11.19	40.5	144.4	1.917	-2.551	-0.235	-0.743
5	0	-30.06	*3354.7*	-32.01	*3905.0*	-13.95	*686.4*	-202.5	*133439*	2.662	*123.88*	1.133	*4.3848*
5	1	0.49	-14.65	0.66	-16.32	-0.28	-6.04	3.8	-80.7	-1.738	1.950	0.016	0.460
5	2	-7.19	-7.40	-7.33	-7.73	-2.96	-2.89	-51.2	-48.3	-0.774	0.397	0.237	0.232
5	3	10.63	-22.30	11.03	-24.77	4.66	-10.46	71.9	-131.4	-0.788	1.352	-0.373	0.833
5	4	27.71	-19.61	30.17	-20.87	12.74	-8.30	170.6	-120.9	-6.121	5.528	-1.015	0.661
5	5	-4.28	18.67	-4.32	20.01	-2.25	8.42	-29.2	118.0	5.433	-3.040	0.179	-0.670
6	0	25.82	*2555.3*	28.34	*3083.6*	9.50	*388.1*	162.2	*94559*	-7.822	*123.96*	-0.894	*3.4158*
6	1	-3.75	-21.50	-3.96	-23.74	-1.74	-9.67	-23.4	-137.1	1.304	0.551	0.167	0.921
6	2	16.72	-5.47	18.83	-5.82	6.30	-1.96	90.9	-36.5	-0.703	0.159	-0.586	0.181
6	3	5.88	-3.54	6.01	-4.09	1.95	-1.41	40.2	-21.1	-1.251	0.766	-0.180	0.133
6	4	25.30	-9.93	27.85	-10.53	9.87	-3.38	148.7	-62.3	-4.553	1.680	-0.918	0.314
6	5	-13.50	4.46	-14.33	5.90	-4.49	2.35	-83.0	19.5	1.137	2.762	0.417	-0.217
6	6	-10.68	0.18	-11.54	0.06	-4.20	0.02	-62.7	7.5	4.944	-1.085	0.390	-0.002
7	0	5.85	*1802.0*	6.87	*2198.7*	2.50	*225.9*	20.8	*60871*	2.091	*88.31*	-0.270	*2.5770*
7	1	11.08	10.52	11.78	11.62	3.26	4.18	70.7	66.8	-3.978	-0.366	-0.351	-0.460
7	2	26.16	-6.53	28.74	-6.97	9.56	-1.68	155.3	-43.5	0.389	3.693	-1.018	0.180
7	3	6.53	6.47	6.99	7.49	2.61	2.21	40.2	33.0	2.463	-1.345	-0.280	-0.237
7	4	7.75	1.57	8.88	1.60	2.94	0.84	42.2	9.6	1.536	1.710	-0.313	-0.089
7	5	-4.58	17.92	-4.75	20.24	-1.10	6.31	-31.5	98.0	0.811	-5.282	0.116	-0.671
7	6	-9.50	0.69	-11.05	1.12	-3.31	0.10	-48.4	0.3	-1.048	0.969	0.352	-0.011
7	7	-7.57	-13.04	-8.01	-14.03	-2.63	-4.18	-45.8	-73.6	0.519	3.192	0.280	0.443
8	0	9.55	*1410.0*	10.69	*1672.0*	2.59	*110.9*	60.3	*49231*	-2.398	*195.60*	-0.298	*1.5773*
8	1	3.31	5.57	3.38	6.60	0.97	0.73	20.9	19.6	0.816	-5.403	-0.117	-0.079
8	2	8.49	-6.42	8.94	-6.92	2.39	-1.83	52.9	-40.3	-2.163	0.548	-0.288	0.219
8	3	3.93	13.81	4.04	15.62	1.22	4.03	24.8	74.6	0.633	-5.231	-0.143	-0.480
8	4	-6.54	-2.63	-7.33	-2.82	-1.62	-0.51	-35.7	-13.5	1.515	1.511	0.193	0.061
8	5	-6.36	18.57	-6.51	20.37	-1.74	5.34	-44.5	107.2	6.295	-5.127	0.208	-0.639
8	6	-4.30	5.35	-5.67	5.68	-1.53	1.38	-15.6	32.7	1.703	-3.490	0.183	-0.165
8	7	19.14	-6.72	20.09	-7.76	5.31	-2.16	118.1	-36.7	-4.794	0.468	-0.635	0.258
8	8	-7.25	-3.34	-7.44	-3.41	-1.81	-1.11	-46.8	-21.2	-0.348	4.287	0.216	0.132
9	0	-12.77	*1868.8*	-14.10	*2281.0*	-2.61	*121.2*	-76.7	*61441*	4.552	*125.50*	0.329	*2.1398*
9	1	4.51	20.06	4.92	22.45	1.15	5.78	30.3	115.8	-0.736	-0.170	-0.150	-0.773
9	2	-4.05	-1.49	-5.09	-1.56	-0.75	0.10	-13.5	-9.0	1.208	2.158	0.102	-0.019
9	3	3.22	9.55	3.33	10.65	0.64	2.54	22.4	52.9	-2.734	-3.366	-0.090	-0.341
9	4	-17.26	6.49	-19.21	6.83	-4.30	1.43	-95.4	40.3	1.711	-1.686	0.572	-0.189
9	5	-6.73	0.42	-7.20	0.36	-1.63	0.20	-42.2	5.1	1.138	2.282	0.217	-0.027
9	6	-6.57	8.48	-7.69	8.85	-1.87	1.58	-32.7	52.1	3.350	-5.019	0.249	-0.211
9	7	8.38	-15.48	8.71	-17.40	2.17	-4.11	54.4	-84.6	-0.807	2.273	-0.289	0.546
9	8	18.29	-2.48	19.89	-2.75	4.59	-0.34	102.9	-13.5	-2.982	-0.728	-0.610	0.046
9	9	-2.99	1.49	-3.10	2.00	-0.39	0.42	-21.1	4.8	-0.117	3.917	0.052	-0.056
10	0	-7.65	*1289.5*	-8.75	*1565.0*	-1.96	*63.2*	-38.7	*42252*	0.031	*168.64*	0.311	*1.3654*
10	1	2.26	-9.22	2.18	-10.23	0.29	-1.29	13.3	-57.0	0.095	1.325	-0.046	0.283
10	2	-18.46	1.25	-20.51	1.38	-4.03	0.50	-105.4	5.6	6.388	0.739	0.589	-0.072
10	3	-2.13	-10.07	-2.39	-10.94	-1.00	-1.77	-14.9	-58.9	-3.057	4.030	0.150	0.262
10	4	-15.32	10.03	-16.86	10.75	-3.66	2.30	-87.6	58.6	1.219	1.419	0.535	-0.338
10	5	-2.58	-6.59	-2.84	-7.77	-0.41	-1.10	-14.5	-31.2	1.025	3.471	0.060	0.161
10	6	-0.26	-2.22	-0.48	-2.18	-0.34	-0.37	-0.0	-16.5	-1.836	5.341	0.049	0.055
10	7	4.56	-12.30	4.65	-13.95	0.94	-2.86	30.9	-66.1	-0.839	2.073	-0.137	0.418
10	8	-0.23	-1.47	0.47	-1.54	0.28	-0.15	-6.9	-8.6	2.820	0.031	-0.043	0.022
10	9	6.58	4.11	6.80	4.55	1.25	1.02	40.3	23.3	-0.234	-4.763	-0.182	-0.149
10	10	7.71	-2.81	8.00	-2.86	1.51	-0.68	44.2	-18.9	-3.348	2.133	-0.221	0.099
11	0	-11.09	*1131.6*	-12.18	*1378.6*	-1.95	*38.7*	-65.6	*35854*	3.811	*232.08*	0.282	*0.9645*
11	1	8.81	-11.37	9.29	-12.64	1.71	-1.88	56.1	-58.4	-1.329	4.305	-0.270	0.305
11	2	-3.27	0.35	-3.78	0.39	-0.78	0.08	-14.7	-1.2	-1.815	-0.079	0.127	-0.005
11	3	-2.38	15.22	-2.46	-17.11	-01.5	-2.61	-15.6	-82.4	3.812	3.009	0.019	0.413
11	4	-1.24	-1.85	-1.27	-1.87	-0.63	-0.42	-9.9	-13.7	-4.485	0.874	0.101	0.069
11	5	-1.15	-5.48	-1.29	-6.74	0.03	-0.97	-6.8	-24.1	4.168	3.523	-0.005	0.155
11	6	8.21	-2.77	9.22	-2.97	1.59	0.26	43.6	-16.0	-0.786	1.215	-0.253	0.042
11	7	1.02	-9.39	1.07	-10.18	0.32	-1.71	5.9	-55.9	3.356	6.733	-0.051	0.272
11	8	2.20	1.69	2.97	1.73	0.86	0.27	7.4	10.6	-1.026	0.594	-0.137	-0.043
11	9	-6.81	14.57	-7.19	16.16	-1.38	2.87	-40.6	80.1	4.611	-0.003	0.220	-0.457
11	10	1.71	5.78	1.29	5.90	0.18	0.98	18.4	35.5	-0.134	-4.970	-0.030	-0.157
11	11	2.95	-6.43	3.19	-6.97	0.54	-1.25	16.2	-37.4	-3.375	0.607	-0.086	0.199

		(1)		(2)		(3)		(4)		(5)		(6)	
n	*m*	C	S	C	S	C	S	C	S	C	S	C	S
12	0	0.54	*853.8*	0.85	*1052.4*	-0.13	*21.9*	0.9	*27281*	-2.420	*259.21*	0.053	*0.6548*
12	1	-4.17	-17.54	-4.63	-19.69	-0.66	-2.58	-24.4	-99.6	1.418	10.360	0.111	0.439
12	2	3.82	-1.21	4.51	-1.29	0.30	-0.26	16.4	-9.1	-2.040	0.119	-0.055	0.045
12	3	-7.70	-10.40	-8.31	-11.76	-1.44	-1.70	-46.6	-57.8	-0.389	4.687	0.243	0.297
12	4	3.04	-3.72	4.06	-3.91	0.25	-0.51	7.2	-22.2	-4.100	-0.903	-0.043	0.085
12	5	0.83	-3.10	0.80	-3.62	0.14	-0.57	5.5	-15.9	-1.094	3.993	-0.024	0.098
12	6	8.59	-1.17	9.92	-1.44	1.63	-0.28	43.0	-3.6	-0.528	-4.495	-0.282	0.048
12	7	-4.08	-3.20	-4.18	-2.99	-0.54	-0.40	-26.4	-23.5	1.960	2.586	0.093	0.068
12	8	-0.52	1.18	-0.07	1.15	0.32	0.09	-9.0	9.0	5.117	-1.728	-0.055	-0.016
12	9	-1.39	8.32	-1.47	9.47	0.00	1.62	-8.1	42.2	-0.054	1.024	-0.000	-0.279
12	10	1.23	2.63	0.83	2.85	-0.07	0.48	11.5	14.2	1.345	2.632	0.011	-0.083
12	11	0.78	9.05	0.70	9.27	0.01	1.39	8.4	53.7	-2.385	-2.547	-0.001	-0.239
12	12	-4.61	-5.09	-4.84	-5.39	-0.79	-0.61	-27.2	-30.3	-0.805	0.487	0.135	0.106
13	0	12.32	*948.6*	13.63	*1146.5*	1.81	*18.1*	68.5	*30109*	-1.958	*202.21*	-0.373	*0.6467*
13	1	1.43	2.81	1.66	3.16	0.48	0.13	11.3	15.6	-0.954	0.245	-0.085	-0.015
13	2	12.70	-7.37	14.44	-7.83	1.83	-0.90	67.5	-46.6	-2.425	3.520	-0.338	0.166
13	3	-2.43	3.00	-2.40	3.31	0.00	0.20	-13.4	13.9	3.095	-0.565	-0.004	-0.041
13	4	2.78	-4.30	3.80	-4.77	0.54	-0.60	7.1	-25.9	-0.309	1.312	-0.101	0.113
13	5	3.69	4.09	3.82	4.88	0.35	0.44	23.4	18.3	-4.017	-1.308	-0.066	-0.089
13	6	2.19	-3.38	2.70	-3.69	0.41	-0.41	10.9	-19.0	-3.269	1.519	-0.075	0.076
13	7	-1.81	6.71	-1.75	7.76	-0.32	0.97	-11.8	33.9	-3.076	-3.149	0.060	-0.180
13	8	-8.20	-1.80	-8.83	-1.88	-1.02	-0.30	-48.0	-9.9	4.140	0.318	0.190	0.055
13	9	5.67	6.79	6.07	7.41	0.78	0.91	34.0	40.0	-2.824	-5.932	-0.145	-0.169
13	10	1.16	-6.39	0.61	-6.78	0.06	-0.79	12.4	-39.0	0.612	4.900	-0.011	0.146
13	11	4.13	-9.88	4.45	-10.82	0.48	-1.45	23.7	-54.8	-1.339	4.697	-0.088	0.268
13	12	-1.54	10.16	-1.37	10.80	-0.19	1.37	-10.9	57.8	1.022	-0.465	0.036	-0.253
13	13	-3.91	3.01	-4.20	3.23	-0.59	0.44	-21.4	16.0	0.183	-2.694	0.110	-0.081
14	0	3.77	*654.8*	4.36	*802.0*	0.49	*8.8*	17.3	*19463*	-1.773	*157.38*	-0.064	*0.3481*
14	1	0.96	8.86	0.85	10.00	0.04	0.96	5.7	45.9	-1.858	-4.108	-0.012	-0.200
14	2	3.41	-6.96	4.19	-7.28	0.49	-0.66	13.8	-42.4	-1.905	1.570	-0.101	0.133
14	3	2.01	7.31	2.02	8.55	0.07	0.62	9.8	32.2	-1.014	-4.226	-0.011	-0.121
14	4	-1.79	-5.02	-1.70	-5.28	-0.02	-0.48	-13.2	-30.1	1.601	2.123	0.004	0.093
14	5	4.96	10.01	5.40	11.41	0.64	1.12	28.1	52.5	-0.551	-5.528	-0.129	-0.223
14	6	-1.88	-1.61	-2.40	-1.68	-0.06	-0.30	-5.1	-9.3	-1.123	-0.672	0.013	0.059
14	7	0.90	7.37	1.12	8.35	0.06	1.10	4.2	38.7	-1.334	-0.359	-0.011	-0.220
14	8	-6.40	1.41	-7.41	1.52	-0.84	0.30	-32.0	7.9	0.227	1.111	0.167	-0.059
14	9	3.51	2.49	3.78	2.51	0.32	0.39	20.3	15.5	0.053	2.187	-0.064	-0.077
14	10	6.78	-4.66	6.68	-5.07	0.58	-0.38	45.8	-26.4	-4.103	2.472	-0.116	0.076
14	11	-1.90	-4.74	-1.96	-5.46	-0.25	-0.70	-11.6	-23.2	-1.064	-0.303	0.049	0.139
14	12	-3.77	-6.94	-3.73	-7.34	-0.39	-0.97	-23.6	-39.4	-1.840	2.811	0.078	0.193
14	13	1.27	1.15	1.47	1.45	0.20	0.19	5.3	5.9	2.670	2.139	-0.040	-0.037
14	14	0.82	2.87	0.90	3.12	0.11	0.34	5.1	15.1	0.176	-3.757	-0.022	-0.068
15	0	1.16	*595.4*	1.03	*738.8*	0.09	*5.7*	10.2	*18039*	-0.269	*271.50*	-0.054	*0.2605*
15	1	4.68	8.21	5.08	9.76	0.41	0.70	28.2	38.9	-2.350	-5.976	-0.084	-0.143
15	2	-4.52	-6.28	-5.09	-6.79	-0.48	-0.70	-21.8	-37.2	-2.357	3.085	0.106	0.146
15	3	8.37	7.60	9.08	8.74	0.72	0.89	48.9	39.6	-3.249	-5.310	-0.157	-0.192
15	4	-6.84	-4.28	-7.93	-4.73	-0.46	-0.44	-33.7	-24.4	2.649	0.154	0.099	0.097
15	5	5.08	2.65	5.54	3.27	0.30	0.36	28.4	12.4	-5.099	-1.151	-0.064	-0.078
15	6	-3.21	-1.14	-4.21	-1.11	-0.33	-0.21	-11.5	-5.8	0.964	-3.664	0.071	0.044
15	7	1.37	1.39	1.59	1.55	0.12	0.20	7.2	7.9	-0.842	0.372	-0.026	-0.042
15	8	-4.08	3.55	-4.81	3.81	-0.44	0.44	-21.0	20.6	4.278	0.042	0.093	-0.093
15	9	4.32	-1.45	4.51	-1.97	0.40	-0.17	25.6	-6.7	-1.393	2.475	-0.085	0.036
15	10	2.34	-1.70	2.55	-1.85	0.26	0.01	12.5	-11.4	2.943	5.325	-0.054	-0.003
15	11	0.53	-2.97	0.46	-3.44	-0.07	-0.29	4.5	-15.6	-3.164	3.545	0.015	0.062
15	12	-2.29	6.65	-1.99	7.03	-0.27	0.66	-16.4	40.7	-1.693	-5.483	0.058	-0.141
15	13	-5.76	-3.35	-6.24	-3.31	-0.56	-0.45	-32.4	-21.5	0.856	0.136	0.120	0.095
15	14	0.51	-5.20	0.53	-5.55	0.02	-0.55	3.2	-28.2	-0.519	2.017	-0.005	0.117
15	15	3.78	-0.70	4.05	-0.77	0.27	-0.13	21.2	-4.9	-0.847	-1.441	-0.058	0.029
16	0	-8.97	*739.8*	-10.18	*907.8*	-0.49	*5.8*	-45.9	*22509*	4.690	*253.15*	0.142	*0.3037*
16	1	-2.75	4.88	-2.93	5.26	-0.32	0.53	-17.8	28.5	-1.651	-3.299	0.070	-0.122
16	2	-11.94	2.84	-13.50	3.02	-0.83	0.37	-62.9	17.4	6.666	2.380	0.183	-0.081
16	3	-3.80	-6.22	-4.05	-6.55	-0.52	-0.50	-24.9	-37.7	-2.056	2.177	0.119	0.114
16	4	-8.37	3.50	-9.75	3.80	-0.68	0.58	-43.5	22.4	5.968	1.360	0.153	-0.134
16	5	-1.79	-4.34	-1.86	-4.84	-0.13	-0.15	-10.9	-21.3	0.843	3.692	0.029	0.035
16	6	-5.24	-2.08	-6.07	-2.06	-0.59	-0.02	-26.4	-13.2	0.361	3.012	0.135	0.005
16	7	0.78	-3.65	0.73	-4.35	0.05	-0.38	6.3	-16.5	-2.141	0.857	-0.012	0.087
16	8	-1.33	1.79	-1.36	2.00	-0.18	0.28	-9.4	10.5	2.515	1.129	0.040	-0.062
16	9	1.34	-5.71	1.33	-6.52	0.03	-0.64	9.0	-28.4	-1.957	-1.337	-0.007	0.146
16	10	4.88	-2.04	5.57	-2.10	0.48	-0.14	24.2	-14.5	-0.598	2.169	-0.108	0.032

		(1)		(2)		(3)		(4)		(5)		(6)	
n	*m*	C	S	C	S	C	S	C	S	C	S	C	S
16	11	-2.35	0.64	-2.50	0.62	-0.14	0.00	-14.7	4.4	4.608	-0.656	0.032	-0.000
16	12	2.71	6.45	3.10	6.98	0.25	0.52	13.6	37.0	-2.295	-2.736	-0.055	-0.117
16	13	5.44	5.55	5.64	6.03	0.49	0.53	32.8	31.7	0.251	-3.606	-0.109	-0.121
16	14	4.02	-1.02	3.99	-0.98	0.30	-0.09	26.0	-9.3	-3.876	1.632	-0.067	0.019
16	15	-6.93	-4.16	-7.33	-4.52	-0.66	-0.41	-38.6	-22.7	-0.903	2.530	0.149	0.092
16	16	-1.36	-2.70	-1.34	-2.94	-0.16	-0.35	-8.9	-14.8	1.108	-0.520	0.036	0.080
17	0	-2.62	*757.9*	-3.11	*913.9*	-0.40	*4.4*	-10.7	*23125*	1.048	*318.26*	0.062	*0.2431*
17	1	-2.64	-11.64	-2.63	-12.78	-0.16	-1.02	-16.2	-63.5	0.896	-0.240	0.038	0.239
17	2	-5.29	2.25	-6.06	2.35	-0.60	-0.03	-27.3	10.9	1.108	-2.311	0.147	0.004
17	3	-2.73	-8.52	-2.82	-9.73	0.00	-0.47	-15.6	-43.9	3.365	5.068	-0.001	0.112
17	4	-0.21	5.15	-0.70	5.42	-0.03	0.27	0.9	28.6	2.951	-0.069	0.007	-0.062
17	5	-4.96	-5.36	-5.52	-6.33	-0.21	-0.34	-28.7	-24.2	3.907	3.282	0.049	0.081
17	6	-4.39	4.25	-4.50	4.72	-0.37	0.39	-27.6	23.3	2.278	1.483	0.088	-0.095
17	7	-1.88	-5.25	-2.21	-6.17	-0.04	-0.34	-8.3	-26.3	2.373	5.256	0.010	0.081
17	8	3.74	4.03	4.39	4.35	0.30	0.31	17.9	23.7	-1.129	-2.363	-0.073	-0.075
17	9	-5.39	-1.33	-5.83	-1.74	-0.42	-0.04	-30.9	-3.7	2.047	1.202	0.101	0.009
17	10	4.94	-1.87	5.68	-1.96	0.23	-0.18	25.3	-10.7	-5.463	-0.992	-0.054	0.042
17	11	-4.76	4.92	-5.01	5.39	-0.32	-0.33	-28.6	27.8	3.609	-2.806	0.076	-0.080
17	12	0.39	5.33	0.51	5.70	-0.08	0.20	2.9	31.9	-3.316	-5.285	0.018	-0.047
17	13	3.25	4.77	3.39	5.21	0.32	0.31	17.2	27.6	3.508	-2.457	-0.078	-0.074
17	14	3.86	-2.70	3.88	-2.96	0.33	-0.21	23.2	-16.1	2.919	0.725	-0.078	0.049
17	15	7.54	2.93	7.95	3.00	0.56	0.31	45.2	16.5	-7.691	-0.328	-0.133	-0.073
17	16	-5.85	2.45	-6.28	2.63	-0.56	0.09	-32.9	13.9	-0.321	0.228	0.133	-0.022
17	17	-2.57	-3.87	-2.74	-4.05	-0.16	-0.33	-15.1	-22.0	2.591	0.892	0.038	0.080
18	0	0.39	*800.3*	0.38	*981.6*	0.16	*3.0*	2.6	*24305*	1.065	*284.16*	-0.012	*0.1912*
18	1	-1.46	-12.35	-1.67	-13.98	-0.10	-0.46	-8.9	-62.1	1.716	7.796	0.026	0.129
18	2	2.85	3.96	3.24	4.41	0.11	0.23	15.0	23.4	-1.788	-2.177	-0.028	-0.056
18	3	-6.34	-12.46	-6.87	-14.08	-0.49	-0.80	-39.0	-68.8	2.206	8.223	0.122	0.200
18	4	4.99	2.97	5.65	3.33	0.27	0.22	24.7	15.9	-2.227	-0.192	-0.067	-0.058
18	5	-4.15	-0.83	-4.48	-1.53	-0.21	-0.09	-25.9	1.2	2.507	1.770	0.053	0.024
18	6	2.84	3.91	3.57	4.30	0.23	0.15	8.9	22.5	0.451	-3.532	-0.058	-0.037
18	7	-3.09	0.90	-3.35	0.81	-0.22	0.01	-17.9	6.1	2.964	1.433	0.055	-0.002
18	8	6.90	4.12	7.88	4.36	0.51	0.14	35.8	24.9	-1.352	-4.238	-0.127	-0.035
18	9	-3.87	7.54	-4.19	8.09	-0.21	0.40	-22.0	42.6	1.195	-3.217	0.053	-0.102
18	10	-1.83	0.03	-1.78	-0.04	-0.12	0.01	-12.5	1.4	0.248	0.377	0.030	-0.003
18	11	-2.64	4.40	-2.81	4.98	-0.15	0.36	-15.3	22.5	0.426	-0.149	0.037	-0.091
18	12	-5.62	3.80	-6.03	4.06	-0.37	0.19	-30.2	22.0	1.516	-1.982	0.094	-0.048
18	13	0.26	-4.71	0.19	-4.93	-0.03	-0.31	2.4	-27.6	-1.566	2.062	0.008	0.078
18	14	-0.46	-1.91	-0.62	-2.11	-0.01	-0.24	-3.6	-10.4	3.139	0.404	0.004	0.062
18	15	-4.62	-4.41	-4.80	-4.73	-0.34	-0.32	-27.1	-27.3	1.678	3.819	0.086	0.081
18	16	6.22	-0.74	6.68	-0.88	0.49	-0.04	35.9	-2.9	-2.885	-1.840	-0.123	0.010
18	17	1.19	4.58	1.31	4.97	0.08	0.20	4.5	25.7	0.492	-3.715	-0.019	-0.050
18	18	-0.23	-0.27	-0.34	-0.20	0.08	-0.07	-0.5	-2.7	1.137	1.256	-0.021	0.016
19	0	4.29	*564.1*	5.06	*690.1*	0.02	*1.6*	20.5	*17055*	-3.125	*367.32*	-0.037	*0.1104*
19	1	-3.28	-4.39	-3.55	-4.97	-0.12	-0.33	-20.5	-24.3	5.131	5.291	0.029	0.073
19	2	7.06	-1.76	8.10	-2.03	0.37	-0.11	35.8	-9.7	-3.269	1.399	-0.099	0.028
19	3	-2.45	-1.22	-2.63	-1.41	-0.02	0.04	-14.5	-6.0	2.895	3.811	0.007	-0.010
19	4	6.01	-6.26	6.99	-6.83	0.33	-0.29	29.8	-37.7	-4.237	3.533	-0.087	0.078
19	5	-2.98	0.86	-3.36	1.02	-0.17	0.08	-16.4	3.2	-1.854	1.163	0.044	-0.022
19	6	3.20	-0.78	4.06	-0.98	0.09	0.02	10.8	-2.4	-3.293	-0.480	-0.025	-0.006
19	7	0.14	4.25	0.08	4.84	0.03	0.20	1.0	21.3	0.679	-1.292	-0.007	-0.052
19	8	6.51	-2.58	7.24	-2.90	0.25	-0.22	35.5	-13.7	-4.502	0.976	-0.067	0.058
19	9	0.83	5.64	0.89	6.39	0.02	0.16	5.3	29.8	-2.458	-6.105	-0.006	-0.043
19	10	-3.49	1.36	-3.80	1.33	-0.20	-0.00	-18.9	8.7	-0.866	-0.829	0.054	0.001
19	11	0.67	3.21	0.63	3.63	0.14	0.17	2.5	17.5	3.799	-2.591	-0.037	-0.045
19	12	-1.80	2.37	-2.19	2.55	-0.05	0.13	-8.0	12.1	1.480	0.798	0.013	-0.033
19	13	-1.98	-4.49	-2.12	-4.83	-0.03	-0.19	-10.3	-25.9	3.454	2.666	0.008	0.050
19	14	-3.95	-5.66	-4.25	-6.11	-0.16	-0.24	-23.9	-33.5	4.230	7.198	0.042	0.064
19	15	-1.30	1.57	-1.33	1.57	-0.12	0.03	-6.6	7.8	-3.075	1.243	0.032	-0.009
19	16	-8.24	3.10	-8.61	3.27	-0.50	0.13	-47.4	19.0	1.930	-1.410	01132	-0.034
19	17	5.89	-4.07	6.26	-4.32	0.40	-0.30	35.3	-22.5	-2.105	-2.616	-0.105	0.079
19	18	4.60	0.69	5.00	0.79	0.35	0.06	23.9	4.0	-0.478	-2.541	-0.092	-0.016
19	19	0.41	-0.08	0.42	0.04	0.11	-0.00	2.7	-2.5	0.789	2.285	-0.030	0.001
20	0	4.82	*548.0*	5.57	*669.3*	0.37	*1.4*	25.1	*16299*	-4.401	*262.74*	-0.077	*0.0948*
20	1	-2.55	11.44	-2.69	12.53	-0.06	0.55	-15.6	62.3	2.419	-4.942	0.019	-0.135
20	2	9.39	0.37	10.45	0.47	0.52	0.01	50.6	2.7	-3.201	0.629	-0.141	-0.005
20	3	-4.17	5.11	-4.55	5.93	-0.14	0.18	-26.3	23.2	5.617	-1.116	0.034	-0.052
20	4	4.14	-3.76	4.85	-3.86	0.18	-0.15	20.6	-22.1	-3.811	1.414	-0.050	0.039
20	5	-2.71	4.26	-2.92	5.12	-0.07	0.18	-15.5	19.5	2.546	-1.822	0.020	-0.049

		(1)		(2)		(3)		(4)		(5)		(6)	
n	*m*	C	S	C	S	C	S	C	S	C	S	C	S
20	6	-2.00	-2.47	-1.97	-2.80	-0.10	-0.11	-12.1	-13.0	-3.338	1.885	0.027	0.030
20	7	-0.92	5.35	-1.00	6.12	-0.02	0.34	-4.9	28.0	0.437	-1.780	0.007	-0.097
20	8	-1.13	-3.14	-1.35	-3.48	-0.03	-0.13	-3.2	-16.7	-1.718	2.346	0.009	0.036
20	9	0.16	-1.95	0.25	-1.86	0.03	-0.01	0.8	-12.8	-1.049	1.474	-0.009	0.003
20	10	-5.62	-2.20	-6.23	-2.35	-0.30	-0.16	-28.7	-13.1	-1.220	1.388	0.084	0.044
20	11	1.95	-3.95	2.04	-4.26	0.11	-0.11	10.1	-20.8	2.490	0.825	-0.031	0.031
20	12	-1.09	-0.04	-1.29	-0.02	-0.09	-0.04	-6.8	-1.4	1.144	0.065	0.025	0.010
20	13	2.04	-5.56	2.14	-6.03	0.11	-0.26	11.4	-32.6	-0.532	4.112	-0.031	0.074
20	14	-2.02	-3.53	-2.09	-3.98	0.03	-0.16	-13.7	-19.1	6.034	1.112	-0.009	0.046
20	15	-1.77	0.23	-1.77	0.33	-0.03	0.04	-11.0	-1.5	0.281	3.009	0.007	-0.011
20	16	-1.45	2.10	-1.48	2.22	-0.04	0.16	-6.5	11.2	-2.461	1.315	0.010	-0.044
20	17	-0.80	3.09	-0.75	3.33	-0.07	0.16	-5.6	19.4	1.843	-2.108	0.018	-0.044
20	18	-1.82	-0.52	-1.95	-0.53	-0.11	-0.06	-9.8	-3.4	0.391	-2.394	0.030	0.016
20	19	-0.68	1.21	-0.71	1.07	0.04	0.06	-4.4	9.4	-0.283	-2.256	-0.010	-0.017
20	20	2.08	-2.46	2.24	-2.52	0.09	-0.08	11.5	-15.8	-0.681	3.318	-0.024	0.022
21	0	-1.24	*790.2*	-1.17	*951.7*	-0.24	*1.2*	-9.5	*24237*	-1.420	*327.46*	0.041	*0.1035*
21	1	-1.03	8.56	-1.07	9.73	-0.08	0.25	-9.0	43.7	0.565	-4.061	0,024	-0.095
21	2	1.31	-3.14	1.42	-3.43	0.03	-0.13	7.8	-18.1	-1.816	-1.431	-0.014	0.043
21	3	5.75	9.79	6.15	11.06	0.24	0.44	33.5	51.9	-1.030	-3.490	-0.069	-0.129
21	4	-2.15	0.13	-2.42	-0.16	-0.12	-0.07	-11.9	1.5	0.231	-0.877	0.034	0.022
21	5	2.64	4.18	2.88	5.11	0.03	0.16	14.6	19.7	-4.601	-5.599	-0.009	-0.048
21	6	-7.16	2.15	-7.86	2.25	-0.24	0.04	-38.0	15.1	2.061	-2.305	0.069	-0.011
21	7	1.67	3.09	1.95	3.53	0.10	0.16	9.1	16.6	0.577	-1.575	-0.030	-0.045
21	8	-8.26	-1.38	-9.21	-1.39	-0.26	-0.07	-43.2	-8.7	4.597	-0.251	0.076	0.019
21	9	-1.17	-3.27	-1.17	-3.47	0.00	-0.04	-7.5	-19.3	1.517	3.383	-0.001	0.013
21	10	-7.47	-2.96	-8.27	-3.04	-0.21	-0.05	-40.3	-19.9	5.023	4.632	0.063	0.014
21	11	1.12	-7.87	1.15	-8.51	0.07	-0.26	8.0	-44.1	-0.824	3.770	-0.020	0.077
21	12	-1.61	-1.65	-1.72	-1.83	-0.03	0.00	-10.5	-8.9	3.297	1.772	0.009	0.000
21	13	0.18	-3.99	0.03	-4.44	-0.14	-0.17	0.5	-22.8	-5.155	3.340	0.042	0.049
21	14	1.95	-4.57	2.15	-4.97	0.13	-0.17	10.3	-24.6	0.108	1.070	-0.038	0.050
21	15	3.51	1.65	3.89	1.81	0.12	0.02	19.7	9.1	-2.876	-2.033	-0.035	-0.006
21	16	3.38	0.21	3.58	0.33	0.21	0.02	20.5	-0.0	-1.689	-1.085	-0.060	-0.005
21	17	1.08	-2.41	1.20	-2.57	0.10	-0.09	6.3	-13.2	1.376	-0.289	-0.028	0.027
21	18	6.92	-0.49	7.32	-0.37	0.26	0.03	40.8	-4.5	-3.983	2.993	-0.075	-0.008
21	19	-7.15	6.74	-7.64	7.17	-0.34	0.29	-41.7	38.1	4.885	-0.881	0.098	-0.084
21	20	-5.74	1.22	-6.14	1.10	-0.19	0.04	-32.6	8.2	1.824	-0.794	0.054	-0.011
21	21	0.73	-2.72	0.81	-2.88	0.03	-0.05	3.4	-15.9	-0.670	1.622	-0.008	0.014
22	0	-4.53	*449.9*	-5.24	*543.4*	0.03	*0.6*	-21.7	*13933*	4.085	*223.48*	0.015	*0.0545*
22	1	3.12	4.60	3.29	5.27	0.08	0.21	18.7	23.9	-1.626	-5.293	-0.024	-0.046
22	2	-7.34	-0.17	-8.41	-0.16	-0.20	-0.04	-36.8	0.1	2.798	0.206	0.069	0.009
22	3	1.94	0.34	2.15	0.62	0.02	-0.04	9.9	-0.8	-1.797	-2.569	-0.008	0.012
22	4	-7.26	0.41	-8.22	0.44	-0.26	0.02	-37.6	5.2	3.458	-1.284	0.079	-0.009
22	5	-1.43	0.67	-1.17	0.68	-0.12	-0.02	-11.9	4.7	-1.840	-2.344	0.037	0.008
22	6	-5.91	0.10	-6.77	0.13	-0.21	-0.01	-30.7	2.2	2.841	-1.105	0.063	0.002
22	7	3.77	-0.21	4.10	-0.35	0.10	0.01	21.1	3.2	-2.788	-2.107	-0.030	-0.002
22	8	-1.46	0.43	-1.79	0.58	-0.06	0.04	-5.9	2.5	2.494	-1.069	0.020	-0.011
22	9	0.84	-3.38	0.96	-0.38	0.07	-0.17	4.5	-17.8	1.067	-0.309	-0.021	0.051
22	10	-0.09	1.84	-0.11	2.07	0.01	0.08	-1.5	8.3	2.843	0.341	-0.005	-0.025
22	11	0.64	-1.28	0.65	-0.51	0.09	-0.09	5.7	-7.7	-0.979	-1.002	-0.027	0.027
22	12	4.35	-0.79	4.76	-0.84	0.20	0.00	24.1	-4.7	-0.446	-0.065	-0.062	-0.001
22	13	-4.39	2.67	-4.56	2.80	-0.17	0.09	-26.2	15.5	0.576	-0.870	0.051	-0.027
22	14	-0.69	-1.86	-0.63	-2.12	-0.02	0.01	-4.9	-9.7	0.338	2.261	0.005	-0.004
22	15	3.99	2.99	4.30	3.24	0.14	0.11	23.8	17.3	-2.218	-1.414	-0.041	-0.033
22	16	4.53	-2.17	4.75	-2.12	0.05	-0.02	27.6	-13.6	-4.971	2.450	-0.017	0.006
22	17	1.99	-4.01	2.10	-4.33	0.08	-0.17	12.0	-21.6	-1.225	-0.319	-0.024	0.052
22	18	0.76	-2.15	0.89	-2.19	-0.01	-0.11	3.9	-13.6	-0.078	-0.654	0.003	0.032
22	19	0.35	-2.77	0.22	-2.86	0.06	-0.11	3.5	-16.7	-0.755	2.966	-0.020	-0.095
22	20	-2.05	8.09	-2.14	8.53	-0.07	0.31	-13.6	48.7	5.128	-3.077	0.023	-0.095
22	21	-3.62	0.13	-3.89	0.19	-0.14	0.04	-20.6	-0.9	0.288	1.985	0.044	-0.012
22	22	-0.51	-0.51	-0.59	-0.59	0.00	0.05	-2.5	-2.3	-0.560	0.006	-0.000	-0.014
23	0	-8.96	*704.9*	-9.77	*852.6*			-51.9	*21610*	6.525	*390.93*	0.114	*0.0670*
23	1	-1.49	-0.80	-1.62	-0.96			-8.7	-1.1	0.256	-0.212	0.012	0.006
23	2	-7.68	0.26	-8.68	0.23			-40.2	1.9	6.296	-0.708	0.065	-0.013
23	3	0.04	-3.02	0.04	-3.34			2.2	-14.6	-2.295	0.581	-0.002	0.032
23	4	-8.78	0.70	-9.80	0.79			-48.6	4.0	8.401	-1.774	0.079	0.008
23	5	-3.54	-5.45	-2.88	-6.08			-20.9	-27.7	-0.465	1.983	0.035	0.037
23	6	-3.11	2.73	-3.58	3.00			-16.9	15.9	3.606	-0.999	0.034	-0.028
23	7	0.56	-3.84	0.53	-4.58			4.7	-17.3	-0.137	3.656	-0.023	0.030
23	8	4.98	2.68	5.24	2.86			27.8	15.8	-0.142	-1.609	-0.036	-0.016
23	9	-0.04	-3.95	-0.05	-4.59			-0.6	-18.4	0.325	0.203	0.004	0.033

		(1)		(2)		(3)		(4)		(5)		(6)	
n	*m*	C	S	C	S	C	S	C	S	C	S	C	S
23	10	6.55	1.81	7.33	1.99			34.3	10.6	-0.807	-1.896	-0.056	-0.015
23	11	2.52	-0.12	2.71	-0.24			15.1	0.5	-3.575	-0.449	-0.013	-0.003
23	12	8.21	-0.41	9.01	-0.37			45.9	-2.4	-5.185	-2.630	-0.070	0.017
23	13	1.03	5.49	1.19	5.93			4.9	31.0	-3.254	-1.937	0.001	-0.047
23	14	-0.94	4.46	-0.96	4.78			-6.7	25.9	2.240	-4.295	0.010	-0.018
23	15	1.53	2.67	1.60	2.92			9.1	13.8	1.934	0.164	-0.037	-0.032
23	16	2.39	5.23	2.49	5.69			15.2	28.6	-1.576	-1.383	-0.012	-0.053
23	17	-2.72	-4.02	-3.07	-4.38			-15.3	-22.3	3.221	5.371	0.025	0.016
23	18	1.92	-3.57	2.08	-3.75			11.6	-21.9	-3.838	1.927	0.008	0.046
23	19	-3.49	2.63	-3.77	2.85			-18.5	14.9	-0.716	-2.588	0.049	-0.026
23	20	-3.06	-5.10	-3.34	-5.52			-17.8	-28.5	2.599	1.816	0.013	-0.001
23	21	4.46	-1.16	4.94	-1.24			23.3	-5.5	1.408	-0.003	0.045	-0.010
23	22	-3.57	0.40	-3.72	0.57			-22.4	0.1	1.548	1.440	-0.004	-0.027
23	23	0.47	3.24	0.41	3.37			4.4	19.8	-2.594	-3.056	-0.051	-0.001
24	0	-1.41	*443.9*	-1.54	*536.4*			-8.4	*14115*	1.149	*290.63*	-0.006	*0.0352*
24	1	1.41	-6.01	1.66	-6.91			8.9	-29.3	-1.660	0.138	-0.000	0.066
24	2	-2.57	-0.13	-2.90	0.06			-15.1	-1.8	1.357	-0.164	0.030	0.008
24	3	-3.21	-8.42	-3.31	-9.51			-20.2	-44.3	0.751	4.965	0.026	0.064
24	4	0.66	2.93	0.68	3.35			3.3	15.2	2.897	-1.780	-0.014	-0.015
24	5	-5.93	-5.49	-6.29	-6.32			-37.1	-28.3	6.291	2.608	0.049	0.069
24	6	0.91	2.17	0.96	2.53			3.0	10.1	1.392	0.275	-0.017	-0.011
24	7	-3.70	0.83	-3.99	0.58			-20.8	7.8	0.391	0.651	0.026	-0.000
24	8	3.70	4.14	4.18	4.54			19.7	24.0	0.483	-0.981	-0.046	-0.040
24	9	-2.01	-1.39	-2.20	-1.58			-11.8	-8.2	1.919	1.376	0.010	0.011
24	10	5.96	1.13	6.55	1.14			31.6	7.6	0.892	-0.933	-0.054	-0.013
24	11	2.61	-0.11	2.73	0.00			16.2	-1.1	-4.413	1.234	-0.002	-0.010
24	12	2.62	-3.07	2.86	-3.34			15.9	-16.7	-3.360	1.929	-0.018	0.022
24	13	4.12	2.32	4.47	2.53			24.1	12.6	-6.322	0.696	-0.010	-0.023
24	14	-2.41	2.98	-2.63	3.18			-14.0	18.4	0.996	-3.392	0.025	-0.014
24	15	1.63	-0.29	1.80	-0.23			7.9	-2.6	1.327	-1.497	-0.015	0.015
24	16	0.67	3.03	0.70	3.41			3.7	15.0	0.993	-0.736	-0.015	-0.020
24	17	-1.42	0.69	-1.64	0.68			-8.2	4.8	3.609	-0.489	0.016	-0.013
24	18	-2.81	0.48	-2.92	0.51			-17.2	1.9	3.781	1.453	0.007	-0.005
24	19	1.44	-0.50	1.44	-0.34			10.2	-6.1	-2.387	3.606	0.003	-0.004
24	20	-2.43	2.64	-2.62	2.63			-13.3	18.7	0.864	-2.826	0.019	-0.025
24	21	0.18	-1.98	0.31	-2.18			-0.2	-11.2	-2.684	-0.012	0.014	0.029
24	22	0.61	-5.26	0.72	-5.56			3.9	-30.9	-1.325	2.900	-0.015	0.045
24	23	-2.99	-1.27	-3.04	-1.29			-19.2	-7.7	2.601	0.714	0.030	0.009
24	24	1.98	1.89	2.06	2.01			12.4	11.1	-2.588	-2.761	-0.008	-0.007
25	0	-2.00	*413.3*	-1.91	*502.7*			-15.3	*12229*	2.267	*226.25*	0.032	*0.0268*
25	1	-0.42	-2.75	-0.52	-3.38			-3.8	-10.5	0.776	4.926	-0.001	0.002
25	2	5.46	0.17	6.17	0.20			29.6	1.3	-3.043	-0.328	-0.045	-0.022
25	3	-1.46	-3.42	-1.59	-4.00			-8.1	-16.2	-0.290	4.156	0.023	0.031
25	4	3.12	-0.10	3.63	-0.30			12.1	-1.2	0.552	2.668	-0.027	0.002
25	5	-4.38	-1.50	-4.71	-1.70			-26.9	-7.7	5.470	1.107	0.009	-0.000
25	6	2.66	0.13	3.27	0.12			10.2	0.8	0.737	0.292	-0.038	-0.004
25	7	0.54	-0.38	0.51	-0.30			3.8	-4.9	0.727	1.668	-0.012	0.013
25	8	2.38	1.11	2.95	1.23			10.6	5.8	-2.747	0.442	-0.020	-0.007
25	9	-3.13	4.60	-3.31	5.15			-18.6	23.2	1.846	-0.446	0.029	-0.033
25	10	3.29	1.28	3.56	1.32			17.6	7.1	1.186	-0.870	-0.029	-0.005
25	11	0.23	6.10	0.20	6.74			2.2	32.5	-0.510	-2.396	0.002	-0.045
25	12	-4.84	-2.10	-5.29	-2.21			-26.3	-12.6	1.124	2.774	0.031	0.012
25	13	-0.51	0.23	-0.64	0.34			-1.3	0.4	1.408	1.791	-0.002	-0.009
25	14	-6.61	1.32	-7.14	1.37			-37.1	9.1	2.940	-0.143	0.048	-0.023
25	15	-1.29	-2.16	-1.52	-2.34			-6.8	-11.6	4.432	0.138	0.010	0.022
25	16	0.30	-3.17	0.37	-3.36			0.6	-19.1	-1.033	4.213	0.009	0.013
25	17	-2.04	-0.07	-2.25	-0.11			-11.3	0.2	0.930	0.394	0.026	0.004
25	18	1.33	-0.24	1.52	-0.47			7.0	-0.3	-1.478	-0.322	-0.006	0.013
25	19	3.82	4.64	4.08	5.15			22.3	24.7	-1.959	-4.341	-0.041	-0.014
25	20	-0.34	-1.46	-0.43	-1.62			-0.9	-7.2	2.284	1.293	-0.011	0.005
25	21	5.30	-1.04	5.79	-1.17			29.5	-4.5	-2.902	-0.235	-0.044	0.011
25	22	-0.80	2.62	-0.77	2.90			-6.2	12.6	-1.535	-0.078	0.022	-0.030
25	23	-6.45	-1.45	-6.99	-1.58			-36.9	-8.7	2.234	1.378	0.042	0.022
25	24	0.31	-3.33	0.44	-3.60			1.4	-17.5	-0.660	-0.484	0.005	0.022
25	25	2.35	-0.40	2.49	-0.43			13.5	-2.4	-1.668	0.119	-0.000	0.004
26	0	3.48	*400.0*	4.04	*476.5*			17.8	*12606*	-5.080	*312.66*	-0.050	*0.0214*
26	1	-0.23	-1.24	-0.28	-1.26			-0.7	-10.1	1.436	2.184	0.011	0.031
26	2	3.15	-0.35	3.78	-0.42			13.0	-3.9	-4.645	1.928	-0.013	0.021
26	3	-1.45	2.63	-1.62	2.87			-9.2	13.3	1.225	0.132	-0.033	-0.029
26	4	5.24	-4.49	5.93	-4.76			27.9	-26.4	-5.724	3.259	-0.005	0.022

		(1)		(2)		(3)		(4)		(5)		(6)	
n	*m*	C	S	C	S	C	S	C	S	C	S	C	S
26	5	-2.06	0.89	-2.28	0.97			-12.3	2.3	4.876	2.630	0.003	0.004
26	6	1.77	-3.43	2.07	-3.72			7.6	-19.1	-1.393	2.548	-0.015	0.012
26	7	-0.46	2.13	-0.56	2.54			-1.5	11.5	-1.854	-1.854	0.015	-0.016
26	8	2.18	2.26	2.54	2.22			13.3	15.7	-3.596	-0.705	-0.019	-0.017
26	9	-2.63	3.80	-2.63	4.18			-15.4	20.1	0.099	-0.719	0.018	-0.027
26	10	-2.91	-1.40	-3.09	-1.50			-16.8	-8.9	0.783	0.897	0.019	0.015
26	11	0.09	5.33	0.15	5.72			-0.2	29.9	0.652	-3.304	0.002	-0.028
26	12	-7.05	1.50	-7.64	1.77			-41.2	6.3	3.516	-0.371	0.044	-0.003
26	13	-1.90	-0.05	-2.09	0.01			-11.0	-0.5	2.878	0.192	0.010	0.003
26	14	-2.31	4.15	-2.55	4.48			-12.8	23.6	2.409	-1.937	0.004	-0.029
26	15	-5.15	0.16	-5.62	0.07			-29.0	1.7	5.138	-0.445	0.028	0.005
26	16	-0.80	-1.75	-0.86	-1.89			-4.7	-10.9	0.137	2.522	0.003	0.013
26	17	-5.19	-0.04	-5.65	-0.19			-28.9	0.9	2.070	2.257	0.027	-0.013
26	18	-0.10	-3.69	-0.07	-4.12			0.4	-20.2	-2.295	3.766	0.009	0.021
26	19	0.57	-0.68	0.82	-0.64			2.4	-4.3	-2.422	-1.075	-0.009	0.008
26	20	3.54	-0.57	3.69	-0.62			21.7	-2.7	-2.864	-0.764	-0.027	0.007
26	21	0.53	-1.83	0.82	-2.08			0.7	-8.3	1.549	-1.667	-0.012	0.022
26	22	3.62	-0.21	3.91	0.05			20.0	-3.8	-0.468	-0.336	-0.022	0.009
26	23	-0.92	4.27	-1.09	4.55			-4.7	23.5	2.862	-0.336	-0.006	-0.039
26	24	-0.79	1.68	-0.99	1.77			-3.4	9.1	-1.492	1.841	0.014	-0.014
26	25	-0.21	-4.48	-0.18	-4.76			-1.2	-25.5	-0.333	0.170	0.002	0.034
26	26	-1.55	0.55	-1.59	0.52			-10.1	4.1	2.321	-0.843	0.014	-0.001
27	0	2.23	*387.3*	2.65	*465.7*			11.4	*12151*	-1.451	*331.84*	0.010	*0.0199*
27	1	-1.79	3.95	-1.96	4.49			-10.4	19.4	0.402	1.554	-0.015	-0.070
27	2	2.61	-0.59	3.12	-0.65			12.8	-3.6	0.918	0.892	-0.018	-0.008
27	3	0.43	5.45	0.43	6.15			2.9	27.7	0.108	-2.009	0.015	-0.018
27	4	-0.87	-1.03	-0.82	-1.13			-6.9	-6.5	-0.075	0.978	0.010	0.002
27	5	4.26	4.21	4.38	4.89			25.6	21.9	-1.666	-2.471	-0.027	-0.040
27	6	-0.57	0.04	-0.61	-0.05			-1.2	1.0	-0.905	1.171	-0.008	-0.001
27	7	-0.93	1.74	-0.85	2.11			-5.0	7.9	-0.683	-1.024	0.010	-0.010
27	8	-2.43	-0.61	-2.85	-0.72			-10.7	-3.4	-1.674	0.113	0.025	0.013
27	9	-3.47	2.79	-3.51	2.99			-20.7	18.3	0.814	-2.939	0.021	-0.029
27	10	-6.06	-2.87	-6.63	-3.09			-31.9	-17.1	1.684	3.585	0.029	0.009
27	11	-0.47	-2.83	-0.52	-3.15			-2.9	-14.8	0.362	-0.631	0.005	0.023
27	12	-5.43	0.66	-5.90	0.68			-31.5	2.9	2.622	1.101	0.030	-0.005
27	13	-2.49	-1.14	-2.60	-1.35			-16.3	-5.2	1.667	-1.383	0.021	0.016
27	14	4.43	1.28	4.74	1.33			25.6	8.0	-3.850	-0.389	-0.023	-0.007
27	15	0.67	1.51	0.83	1.54			2.8	10.1	-1.210	-3.570	-0.001	-0.001
27	16	1.90	0.12	2.10	0.08			10.9	0.2	-2.683	2.017	-0.010	0.003
27	17	-0.91	1.24	-0.93	1.39			-6.0	6.6	1.247	-2.420	-0.003	-0.003
27	18	-0.37	0.61	-0.59	0.56			0.5	4.1	0.642	0.949	-0.009	-0.011
27	19	2.02	-1.85	2.30	-1.89			11.0	-11.7	-2.574	2.538	-0.011	0.007
27	20	-2.30	0.21	-2.65	0.33			-12.0	0.9	2.491	1.312	0.009	-0.012
27	21	0.87	-4.97	0.98	-5.51			5.4	-27.5	-3.526	5.323	0.011	0.021
27	22	1.18	4.17	1.42	4.62			5.6	22.9	-2.707	-5.848	0.003	-0.011
27	23	-5.78	-0.84	-6.18	-0.71			-32.9	-7.5	7.690	1.305	0.028	0.019
27	24	1.61	0.15	1.77	-0.04			9.8	3.4	1.505	-1.374	-0.029	0.002
27	25	4.62	2.62	4.98	2.86			26.0	15.4	-5.156	-0.553	-0.016	-0.030
27	26	-2.54	-1.93	-2.74	-1.96			-14.9	-12.3	2.286	-0.163	0.007	0.024
27	27	-2.41	0.38	-2.55	0.39			-14.5	2.7	4.116	-0.530	0.003	-0.002
28	0	-0.06	*343.4*	-0.14	*415.8*			0.8	*10528*	-1.291	*295.19*	-0.020	*0.0116*
28	1	0.54	3.54	0.67	4.06			3.5	17.3	-2.088	-2.734	0.014	0.018
28	2	-4.32	-3.51	-4.85	-3.77			-24.4	-20.4	2.510	1.056	0.022	0.021
28	3	0.09	4.08	0.21	4.57			-1.8	21.4	0.711	-4.239	-0.019	-0.033
28	4	-1.78	-0.38	-2.11	-0.42			-6.9	-0.9	-0.315	-1.268	0.015	-0.003
28	5	1.89	1.81	2.13	2.15			9.3	8.7	-0.710	-3.211	-0.001	-0.003
28	6	-2.93	1.30	-3.38	1.37			-13.9	8.7	-0.568	-1.016	0.023	-0.009
28	7	-1.00	2.46	-0.86	2.82			-7.1	14.4	-1.434	-2.638	0.009	-0.016
28	8	-2.58	-0.16	-2.86	-0.03			-11.8	-0.8	-0.661	-0.784	0.024	-0.001
28	9	-0.39	-1.00	-0.35	-1.13			-2.4	-5.6	1.277	-0.752	-0.004	0.011
28	10	-1.75	-1.18	-2.05	-1.23			-8.3	-7.7	0.073	1.559	0.012	-0.000
28	11	-1.81	-5.35	-2.00	-5.78			-9.5	-29.5	0.375	0.995	0.010	0.028
28	12	-0.94	-0.49	-1.04	-0.63			-4.9	-2.9	0.510	1.542	0.001	0.006
28	13	-3.00	-0.52	-3.26	-0.75			-17.6	-0.8	2.810	-1.940	0.014	0.005
28	14	2.79	-1.89	3.09	-2.16			16.2	-9.1	-4.116	1.010	-0.007	0.010
28	15	3.12	-1.02	3.38	-1.16			18.4	-4.2	-4.460	-0.620	-0.014	0.001
28	16	4.20	-2.46	4.63	-2.78			23.6	-13.2	-5.670	4.491	-0.007	0.008
28	17	1.80	-1.82	2.08	-1.81			8.6	-11.3	-1.762	0.474	-0.011	0.001
28	18	2.27	0.91	2.39	0.93			13.1	6.0	-0.507	-2.833	-0.009	-0.002
28	19	5.07	1.79	5.50	2.00			28.2	9.4	-2.903	-0.298	-0.025	-0.006
28	20	-0.62	2.28	-0.76	2.63			-3.9	12.1	2.232	1.467	0.002	-0.011

		(1)		(2)		(3)		(4)		(5)		(6)	
n	*m*	C	S	C	S	C	S	C	S	C	S	C	S
28	21	-2.59	1.71	-2.95	1.68			-12.9	10.2	2.232	1.467	0.007	-0.013
28	22	-3.70	0.40	-3.80	0.51			-23.1	1.6	2.124	0.363	0.023	-0.008
28	23	-1.71	4.92	-2.02	5.35			-8.2	27.8	1.421	-3.330	0.005	-0.026
28	24	-4.40	-3.45	-4.69	-3.84			-25.3	-19.5	4.126	3.804	0.018	0.021
28	25	2.48	-3.66	2.85	-3.92			14.4	-20.6	-3.788	-0.119	-0.011	0.026
28	26	0.73	-0.14	0.90	-0.00			1.5	-0.6	1.883	-0.475	-0.008	-0.006
28	27	-1.38	1.35	-1.48	1.55			-9.1	6.7	2.715	-2.386	0.002	0.-05
28	28	1.34	0.43	1.39	0.49			8.8	2.4	-0.067	0.045	-0.014	-0.000
29	0	-0.45	*232.3*	-0.81	*280.6*			1.3	*7444*	1.453	*384.51*	0.022	*0.0102*
29	1	0.84	2.42	0.92	2.70			4.9	13.1	-1.285	-2.043	-0.023	-0.052
29	2	-1.49	1.38	-1.89	1.57			-4.3	9.4	3.199	-2.077	0.006	-0.017
29	3	-1.55	1.80	-1.63	1.93			-9.8	11.1	1.738	-3.696	0.028	0.018
29	4	-5.26	2.01	-5.90	2.15			-28.8	13.2	4.515	-4.405	0.027	-0.007
29	5	-0.08	0.36	-0.05	0.46			-0.1	4.3	-1.117	-1.725	-0.005	-0.014
29	6	-1.19	2.54	-1.46	2.73			-4.2	16.2	-0.217	-5.109	0.008	-0.007
29	7	-0.67	-2.20	-0.64	-2.44			-4.8	-11.8	1.935	2.606	-0.005	0.010
29	8	-1.69	-0.44	-1.78	-0.33			-10.9	-3.5	1.032	-1.508	0.015	0.005
29	9	2.30	-1.94	2.39	-2.22			12.7	-9.0	-0.113	-0.502	-0.005	0.008
29	10	3.28	-1.40	3.58	-1.37			18.0	-9.8	-0.073	0.555	-0.019	0.010
29	11	-0.34	-3.13	-0.33	-3.43			-2.9	-16.7	-0.741	1.156	0.005	0.012
29	12	1.92	-0.23	2.20	-0.22			8.9	-2.2	0.599	0.757	-0.011	0.010
29	13	0.07	1.18	0.10	1.21			0.1	8.6	0.331	-2.386	-0.004	-0.009
29	14	-0.11	-0.86	-0.01	-0.97			-1.1	-5.3	1.353	0.343	-0.004	0.005
29	15	0.37	-0.14	0.36	-0.46			3.1	-8.4	-2.409	1.071	-0.003	0.000
29	16	0.43	-1.63	0.35	-0.77			3.3	-9.4	0.371	2.230	0.002	0.002
29	17	-1.10	-2.20	-0.10	-2.30			-6.9	-12.9	-2.307	3.959	0.009	0.003
29	18	-0.41	-1.61	-0.50	-1.63			-2.4	-9.8	2.417	-1.245	-0.000	0.009
29	19	2.52	-0.94	2.82	-1.18			13.1	-3.7	-1.744	2.477	-0.003	-0.003
29	20	1.09	2.88	1.32	3.23			3.7	15.8	0.089	-3.816	0.003	-0.009
29	21	0.18	-0.77	-0.04	-0.91			3.3	-4.7	-0.301	1.117	0.005	0.004
29	22	3.02	0.53	3.34	0.65			16.9	2.5	-1.370	-1.990	-0.018	0.002
29	23	-5.50	2.78	-5.94	3.22			-32.6	14.4	8.071	-1.839	0.015	-0.018
29	24	-0.68	-4.77	-0.81	-5.24			-2.7	-27.4	1.077	8.220	-0.008	0.010
29	25	1.68	0.26	1.98	0.18			8.8	2.3	-4.269	1.348	0.006	-0.012
29	26	-2.90	1.21	-3.06	1.41			-15.9	6.3	-0.180	-2.773	0.024	0.002
29	27	-1.55	-0.85	-1.71	-0.95			-9.4	-3.9	3.296	-0.562	-0.002	0.009
29	28	3.34	0.08	3.54	0.14			18.7	-0.5	-1.223	0.379	-0.017	-0.004
29	29	1.17	0.02	1.26	0.06			7.2	-0.4	-0.536	0.815	-0.009	0.003
30	0	0.67	*340.8*	0.45	*406.0*			5.2	*11005*	-1.654	*343.62*	-0.013	*0.0126*
30	1	-0.53	-0.69	-0.57	-0.93			-3.3	-0.7	-1.414	-0.263	0.032	0.062
30	2	-2.73	0.73	-3.18	0.83			-14.9	2.9	1.191	-0.811	0.014	0.008
30	3	0.48	-1.76	0.49	-1.97			2.9	-8.5	-1.600	1.824	-0.024	-0.013
30	4	-2.64	0.96	-2.96	1.16			-14.4	5.0	2.715	-3.682	0.012	0.008
30	5	-1.58	-1.11	-1.65	-1.48			-8.7	-4.1	-0.496	1.104	0.013	0.013
30	6	-1.11	1.25	-1.31	1.55			-6.4	7.0	0.651	-2.209	0.013	-0.005
30	7	-0.69	1.11	-0.87	1.01			-2.9	8.6	-0.847	0.356	0.008	-0.004
30	8	-0.19	2.16	-0.10	2.39			-1.9	12.9	3.413	-1.189	-0.011	-0.006
30	9	2.66	-1.87	2.76	-2.09			15.4	-9.9	-0.087	-0.452	-0.012	0.014
30	10	2.81	-0.53	3.11	-0.62			15.3	-3.0	-1.021	-1.246	-0.016	0.013
30	11	1.19	-0.01	1.33	-0.02			5.6	0.9	-1.525	-0.391	-0.002	-0.003
30	12	0.30	-3.26	0.53	-3.46			-1.5	-19.6	1.680	3.393	-0.004	0.016
30	13	2.86	2.55	3.22	2.79			14.4	14.5	-2.131	-1.779	-0.008	-0.012
30	14	0.20	-0.78	0.29	-0.89			0.1	-4.8	2.840	0.782	-0.007	0.000
30	15	1.63	0.32	1.81	0.53			8.2	0.1	-0.787	-0.189	-0.006	-0.001
30	16	-2.27	1.48	-2.59	1.66			-12.1	7.6	4.186	-1.211	0.004	-0.011
30	17	-1.05	2.19	-1.07	2.43			-6.8	11.3	1.154	-0.640	0.005	-0.005
30	18	-4.72	2.33	-5.14	2.69			-26.5	12.0	4.047	-3.271	0.010	-0.009
30	19	-2.14	-0.92	-2.33	-1.06			-12.3	-5.3	1.883	3.085	0.012	0.000
30	20	-2.50	2.12	-2.59	2.21			-15.0	13.0	1.994	1.097	0.007	-0.016
30	21	-2.28	-1.38	-2.58	-1.57			-11.2	-8.1	-0.075	0.639	0.019	0.005
30	22	2.64	-4.77	2.88	-5.30			16.4	-26.1	-5.054	2.785	-0.007	0.019
30	23	5.04	-1.38	5.44	-1.26			27.8	-8.4	-2.729	-2.153	-0.018	0.009
30	24	-2.32	-0.89	-2.51	-1.07			-13.4	-4.4	3.381	1.997	0.004	0.007
30	25	2.95	-6.68	3.33	-7.04			16.9	-39.7	-4.543	5.071	-0.013	0.023
30	26	1.36	4.16	1.46	4.59			8.1	22.9	-1.740	-1.779	-0.007	-0.023
30	27	-5.55	2.21	-6.01	2.43			-32.6	12.3	6.935	-0.829	0.021	-0.013
30	28	-1.41	-0.17	-1.67	-0.29			-8.3	-0.2	1.022	-0.723	0.007	0.003
30	29	3.98	-1.80	4.21	-1.94			23.4	-10.4	-2.570	3.257	-0.018	-0.005
30	30	-0.51	-1.07	-0.51	-1.10			-3.1	-6.6	-0.151	2.296	0.003	-0.000

		(1)		(2)		(3)		(4)		(5)		(6)	
n	*m*	C	S	C	S	C	S	C	S	C	S	C	S
31	0	1.56	*252.2*	1.60	*302.4*			10.6	*7928*	-0.576	*301.11*	-0.007	*0.0079*
31	1	0.58	-2.58	0.61	-3.06			3.9	-11.5	-0.495	0.135	-0.026	-0.046
31	2	1.18	2.87	1.30	3.06			6.8	17.0	0.324	-1.413	-0.005	-0.013
31	3	-0.67	-4.29	-0.74	-4.81			-3.2	-22.2	0.457	2.430	0.028	0.033
31	4	-1.11	0.81	-1.16	1.00			-9.2	3.8	3.927	1.213	-0.004	-0.011
31	5	-0.29	0.41	-0.36	0.27			-1.9	5.0	1.676	0.071	0.001	-0.004
31	6	0.01	-0.27	0.25	-0.28			-1.9	-2.0	1.083	1.527	-0.005	0.002
31	7	0.81	2.10	0.68	2.10			4.9	11.8	3.050	1.932	0.001	-0.004
31	8	-0.32	0.31	-0.32	0.28			-3.5	0.9	1.277	2.402	-0.003	0.002
31	9	0.09	3.16	0.01	3.48			0.5	18.3	2.104	-1.618	-0.003	-0.014
31	10	1.89	-1.64	2.12	-1.76			11.5	-10.0	-1.526	-0.127	-0.012	0.012
31	11	0.04	3.08	0.44	3.40			2.2	16.8	-0.822	-2.194	-0.001	-0.011
31	12	-2.93	-1.35	-3.01	-1.51			-18.2	-7.7	1.573	2.086	0.009	-0.000
31	13	2.98	3.49	3.16	3.80			16.8	19.5	-1.680	-0.018	-0.008	-0.012
31	14	-1.88	-0.79	-2.01	-0.88			-11.4	-4.1	1.680	1.219	0.004	0.000
31	15	0.34	-0.38	0.44	-0.36			0.8	-3.4	1.620	1.778	-0.001	0.003
31	16	-1.17	1.58	-1.29	1.73			-7.3	9.6	1.433	-2.532	0.002	-0.008
31	17	0.44	1.35	0.44	1.45			1.8	7.6	3.289	-1.154	-0.001	-0.001
31	18	0.11	3.17	0.26	3.55			-0.2	17.9	-1.727	-5.477	-0.001	-0.005
31	19	-0.34	3.98	-0.56	4.24			-0.2	22.0	1.448	-0.800	0.001	-0.013
31	20	-0.46	1.70	-0.39	1.75			-3.8	10.1	-1.251	1.147	0.004	-0.006
31	21	-3.45	4.72	-3.92	5.13			-17.2	25.6	2.086	-3.129	0.008	-0.011
31	22	-2.44	-2.97	-2.63	-3.52			-12.3	-14.7	-1.452	2.761	0.010	0.010
31	23	2.34	-0.78	2.61	-0.82			12.2	-2.9	-0.360	-2.387	-0.010	-0.000
31	24	-1.36	-5.25	-1.50	-5.72			-8.1	-30.6	0.686	6.929	0.012	0.011
31	25	1.10	-3.52	1.44	-3.83			4.5	-20.0	-3.800	2.217	0.004	0.015
31	26	0.25	0.48	0.34	0.86			1.0	0.8	-0.112	-3.859	0.005	0.001
31	27	-0.43	1.17	-0.63	1.23			-0.7	7.2	3.440	-0.332	-0.012	-0.001
31	28	1.73	-1.90	1.81	-1.98			9.7	-11.3	-0.693	3.262	-0.007	-0.006
31	29	-0.60	-0.30	-0.70	-0.23			-3.3	-4.2	-0.186	3.312	0.010	-0.003
31	30	-0.39	-1.50	-0.50	-1.61			-1.5	-8.8	1.604	2.742	-0.004	0.002
31	31	-0.26	0.83	-.030	0.88			-1.1	5.8	-1.727	-0.588	0.004	-0.007
32	0	-0.52	*229.2*	-0.37	*269.0*			-5.0	*7623*	-1.770	*291.34*	0.002	*0.0080*
32	1	-2.52	1.56	-2.69	1.44			-14.9	12.9	1.846	-0.726	0.029	0.058
32	2	0.04	-0.00	0.23	-0.07			-2.3	0.2	-0.767	1.431	-0.002	0.001
32	3	0.12	-0.89	0.06	-1.08			2.4	-4.1	-1.349	0.700	-0.027	-0.014
32	4	1.44	-2.41	1.69	-2.61			6.7	-14.9	-1.404	4.236	-0.007	0.013
32	5	-1.21	-0.20	-1.42	-0.33			-6.8	-0.9	2.565	0.491	0.000	0.003
32	6	-2.47	-1.27	-2.45	-1.43			-18.1	-6.6	2.849	2.563	0.009	0.003
32	7	-0.46	3.62	-0.53	3.87			-2.1	20.9	0.924	-0.901	-0.001	-0.016
32	8	0.57	0.82	0.07	0.69			3.1	7.0	0.250	0.287	-0.006	-0.006
32	9	0.96	2.57	0.98	2.79			6.8	13.2	0.167	0.557	-0.009	-0.009
32	10	0.34	-1.06	0.34	-1.11			2.0	-6.6	-1.505	-0.812	0.004	0.005
32	11	0.04	3.99	0.10	4.36			0.7	22.3	-0.398	-2.557	-0.001	-0.013
32	12	-3.93	1.84	-4.19	1.97			-23.5	9.2	2.039	-0.057	0.013	-0.008
32	13	1.04	2.57	1.07	2.74			6.9	14.0	-1.306	1.082	-0.001	-0.012
32	14	-3.09	1.31	-3.40	1.50			-16.8	5.8	0.212	1.627	0.007	-0.007
32	15	-2.32	-1.11	-2.53	-1.26			-13.5	-7.1	3.493	3.522	0.005	0.005
32	16	0.52	0.91	0.48	1.08			3.7	5.2	-1.917	-2.017	0.001	-0.004
32	17	-1.01	-0.75	-1.14	-0.97			-5.1	-2.4	2.566	0.614	0.005	0.001
32	18	2.60	-0.23	2.93	-0.32			14.4	-0.4	-3.757	-1.162	-0.006	0.006
32	19	1.15	0.11	1.11	0.00			7.6	1.2	-0.575	1.897	-0.001	-0.002
32	20	1.93	-0.60	2.17	-0.76			10.9	-2.2	-3.742	1.285	-0.003	0.006
32	21	0.36	2.86	0.43	3.15			1.5	15.4	-1.908	-2.307	0.001	-0.007
32	22	-0.89	0.43	-1.00	0.52			-3.4	1.7	-1.616	-0.830	0.002	0.008
32	23	-0.16	0.54	0.02	0.59			-3.7	5.2	1.956	-2.830	-0.003	0.001
32	24	0.73	3.41	0.63	3.74			4.7	18.1	1.687	-1.523	-0.003	-0.009
32	25	-4.30	-2.38	-4.60	-2.70			-24.8	-13.8	1.856	6.791	0.017	-0.001
32	26	3.66	-1.94	3.92	-1.81			21.6	-13.0	-5.327	-1.100	-0.001	0.006
32	27	-1.97	1.99	-2.24	2.13			-10.7	11.7	3.596	-1.749	0.009	-0.003
32	28	-0.31	-3.02	-0.23	-2.53			-1.8	-15.6	-0.626	0.960	-0.002	0.016
32	29	2.56	-2.44	-0.63	2.52			14.0	-13.9	-2.585	1.635	-0.009	0.003
32	30	-0.51	2.32	-1.41	0.10			-3.0	12.0	0.699	-0.043	0.006	-0.009
32	31	-1.22	0.06	-0.00	2.14			-5.2	-0.2	0.755	0.514	0.001	0.003
32	32	0.03	2.04	2.83	-2.53			0.8	13.4	-1.465	-1.953	-0.001	-0.010
33	0	1.57	*218.7*	1.86	*257.3*			8.2	*7179*	-3.110	*333.42*	-0.017	*0.0075*
33	1	0.12	0.62	0.14	0.71			0.4	2.2	1.454	-2.065	-0.026	-0.060
33	2	0.72	2.11	1.02	2.21			1.7	13.2	0.114	0.457	-0.002	-0.008
33	3	-1.68	1.01	-1.76	1.06			-10.2	5.1	3.266	-0.265	0.026	0.012
33	4	1.72	1.14	2.00	1.06			9.1	6.8	-2.290	2.449	-0.007	-0.014

		(1)		(2)		(3)		(4)		(5)		(6)	
n	m	C	S	C	S	C	S	C	S	C	S	C	S
33	5	-1.24	1.31	-1.31	1.50			-6.7	6.8	0.471	-0.682	0.001	-0.003
33	6	-0.28	-2.17	-0.21	-2.43			-2.0	-12.9	0.250	2.658	-0.002	0.007
33	7	-1.63	-0.67	-1.65	-0.63			-10.5	-4.2	1.981	-0.320	0.002	0.004
33	8	-1.05	1.52	-1.20	1.50			-5.2	10.3	-0.591	-1.268	0.006	-0.004
33	9	0.49	2.29	0.59	2.44			3.7	14.9	-1.578	-1.905	-0.005	-0.010
33	10	-0.41	-0.60	-0.51	-0.63			-0.6	-4.4	-1.088	0.282	0.002	0.002
33	11	-0.73	-0.73	-0.70	-0.79			-4.2	-4.9	-0.314	-0.720	-0.002	0.002
33	12	-3.52	1.76	-3.84	1.93			-20.9	10.2	2.238	-2.025	0.007	-0.009
33	13	0.36	-0.54	0.43	-0.64			1.9	-2.6	-0.508	0.765	-0.007	-0.002
33	14	0.26	1.95	0.17	2.16			2.2	10.1	-2.322	0.927	-0.001	-0.008
33	15	-1.77	-0.92	-1.91	-1.04			-10.8	-6.2	2.922	3.453	0.004	0.002
33	16	1.41	1.14	1.50	1.28			9.1	5.9	-3.156	-0.375	-0.003	-0.004
33	17	-1.72	0.70	-1.85	0.71			-9.7	3.8	1.676	-0.376	0.005	-0.003
33	18	0.08	-1.44	0.12	-1.68			1.1	-6.8	-2.057	1.719	0.001	0.006
33	19	-1.08	-2.90	-1.16	-3.09			-6.5	-17.6	0.156	4.266	0.004	0.003
33	20	-0.90	-4.23	-1.07	-4.75			-2.9	-22.5	-0.754	5.507	0.005	0.009
33	21	2.04	-3.22	2.33	-3.34			10.1	-18.6	-3.075	-0.270	-0.002	0.010
33	22	0.05	-1.34	-0.08	-1.39			1.8	-8.2	-1.882	0.518	0.006	0.003
33	23	2.69	-1.44	2.20	-1.53			12.3	-6.6	-3.285	-1.618	-0.003	0.007
33	24	3.99	3.61	4.16	4.14			22.2	18.7	1.690	-4.180	-0.011	-0.002
33	25	1.49	2.80	1.50	2.96			10.3	14.4	-2.330	0.101	-0.004	-0.002
33	26	-1.13	5.56	-1.24	6.04			-6.1	32.6	1.702	-7.099	0.000	-0.014
33	27	0.11	-1.53	-0.14	-1.63			2.5	-9.2	1.930	2.254	-0.005	0.004
33	28	1.34	0.61	1.44	0.38			7.5	6.6	0.134	0.698	-0.004	-0.006
33	29	-1.29	-1.07	-1.14	-1.08			-8.8	-6.5	-3.449	-0.768	0.015	0.003
33	30	-1.89	-2.38	-2.05	-2.43			-11.3	-14.5	3.572	3.361	0.003	0.009
33	31	0.26	1.49	0.28	1.53			1.0	9.5	-0.808	-2.270	0.007	-0.003
33	32	1.22	1.23	1.29	1.37			8.2	6.3	-2.645	-0.764	0.002	-0.003
33	33	0.72	1.05	0.74	1.11			4.4	7.0	-1.191	-0.987	-0.002	-0.005
34	0	0.83	*198.0*	0.98	*235.6*			2.9	*6621*	0.077	*350.01*	0.019	*0.0056*
34	1	-1.88	2.55	-1.99	2.89			-12.3	13.0	0.384	0.833	0.027	0.047
34	2	2.63	1.88	2.87	1.89			15.2	12.0	-1.988	-1.451	-0.005	-0.007
34	3	0.45	0.73	0.49	1.00			1.7	2.0	0.507	0.181	-0.021	-0.017
34	4	0.03	0.29	0.47	0.20			1.7	2.2	-1.884	0.459	0.003	0.006
34	5	1.93	0.69	2.18	0.87			11.5	3.4	-4.248	-2.765	-0.003	-0.004
34	6	-1.39	0.68	-1.58	0.78			-7.8	3.8	1.824	-0.214	0.007	-0.002
34	7	0.40	-1.17	0.53	-1.10			2.4	-7.0	-2.168	-1.477	-0.002	0.003
34	8	-0.01	3.72	-0.07	3.95			1.5	22.8	-0.784	-3.390	0.002	-0.008
34	9	0.04	-0.27	0.23	-0.32			1.4	-1.3	-2.465	-0.513	-0.001	0.005
34	10	-1.35	0.68	-1.50	0.72			-6.8	3.5	-0.820	-1.478	0.-09	-0.003
34	11	0.67	-2.83	0.74	-3.05			4.7	-17.3	-1.195	1.577	-0.002	0.008
34	12	-1.71	-0.71	-1.91	-0.76			-9.7	-3.2	1.626	-1.418	0.-01	0.002
34	13	0.16	-2.56	0.10	-2.83			1.2	-13.6	-0.943	1.126	0.003	0.005
34	14	1.82	0.17	1.96	0.17			11.1	2.2	-3.996	0.661	-0.003	-0.001
34	15	-1.53	-0.34	-1.61	-0.41			-8.7	-2.0	1.263	1.917	0.003	0.002
34	16	1.71	-0.46	1.97	-0.58			9.1	-1.3	-2.528	0.464	-0.004	0.002
34	17	0.65	0.96	0.71	1.10			3.7	-7.4	-1.063	-1.130	-0.003	-0.003
34	18	-0.57	-1.50	-0.48	-1.67			-4.4	3.7	0.903	-0.302	0.001	0.007
34	19	-1.55	0.47	-1.59	0.63			-10.4	0.8	0.479	1.543	0.002	-0.004
34	20	-1.24	-2.24	-1.48	-2.43			-6.1	-13.2	2.010	3.362	0.006	0.004
34	21	-1.55	-1.15	-1.55	-1.12			-9.5	-6.4	0.410	-0.955	0.001	0.006
34	22	-2.55	-0.13	-2.86	-0.02			-15.1	-2.0	2.679	0.009	0.009	-0.002
34	23	-2.88	-2.00	-3.10	-2.29			-16.4	-9.4	1.092	0.353	0.005	0.005
34	24	1.38	-0.72	1.59	-0.70			5.5	-3.9	1.897	-1.667	-0.004	0.003
34	25	0.06	-0.12	-0.08	-0.12			2.0	-2.6	0.873	2.456	-0.005	0.003
34	26	3.51	-0.65	3.89	-0.73			20.0	-2.6	-4.943	-0.729	-0.005	0.003
34	27	2.85	2.77	2.92	3.07			17.1	15.9	0.691	-6.373	-0.009	0.001
34	28	-2.25	-2.71	-2.38	-3.10			-14.1	-14.9	4.114	5.742	-0.003	0.004
34	29	3.35	2.30	3.70	2.52			18.7	13.8	-3.145	-2.418	-0.007	-0.010
34	30	-3.20	2.11	-3.42	2.39			-19.3	11.1	2.532	-0.926	0.015	-0.009
34	31	0.37	-0.57	0.20	-0.76			4.1	-3.2	-0.905	0.652	0.003	0.008
34	32	2.88	-1.30	3.02	-1.42			18.5	-6.0	-7.797	-0.245	-0.004	0.004
34	33	1.61	0.43	1.74	0.05			9.0	1.8	-1.203	0.302	-0.002	-0.003
34	34	-0.02	0.66	-0.03	0.70			-0.4	4.5	0.714	-1.995	0.002	0.001
35	0	0.38	*195.4*	0.32	*236.2*			2.9	*6138*	0.091	*299.39*	-0.035	*0.0052*
35	1	-0.95	-1.23	-0.88	-1.07			-6.2	-12.3	0.597	2.634	-0.017	-0.046
35	2	-1.20	0.29	-1.38	0.30			-6.4	1.6	-0.009	-0.724	0.002	0.002
35	3	0.34	-0.65	0.39	-0.49			0.6	-5.4	1.846	-1.372	0.015	0.011
35	4	0.14	2.02	0.05	2.21			2.1	12.2	0.686	-1.662	-0.003	-0.016
35	5	3.82	-0.79	4.20	-0.68			21.4	-5.3	-3.981	-0.915	-0.005	0.005
35	6	1.89	1.15	1.96	1.32			12.8	6.2	-2.021	-2.511	-0.004	-0.003

		(1)		(2)		(3)		(4)		(5)		(6)	
n	m	C	S	C	S	C	S	C	S	C	S	C	S
35	7	-0.06	-1.82	0.06	-1.94			-1.3	-10.3	0.662	-0.664	-0.001	0.007
35	8	0.52	0.59	0.48	0.74			3.4	2.9	-0.571	-1.191	-0.001	-0.002
35	9	0.74	1.47	0.87	1.64			5.0	8.7	-2.637	-1.065	-0.000	-0.003
35	10	0.67	0.25	0.79	0.35			3.9	1.3	0.853	-0.704	-0.003	-0.000
35	11	1.91	-3.04	1.99	-3.23			10.9	-19.1	-0.693	2.865	0.001	0.007
35	12	0.56	0.45	0.60	0.43			2.5	2.6	0.693	-2.093	-0.002	0.001
35	13	-0.78	-0.58	-0.95	-0.67			-3.6	-2.4	-0.657	-0.545	0.005	0.002
35	14	1.34	-1.69	1.52	-1.84			7.2	-8.8	-1.487	1.424	-0.001	0.005
35	15	-1.50	2.47	-1.61	2.60			-7.4	14.4	-0.551	-0.504	0.005	-0.003
35	16	-0.11	-2.09	-0.00	-2.25			-1.1	-10.6	0.160	0.430	0.001	0.007
35	17	0.23	-1.50	0.30	-1.53			1.8	-9.8	-3.085	0.076	-0.002	0.004
35	18	-0.31	-1.52	-0.31	-1.67			-2.5	-8.3	2.379	-2.278	0.001	0.006
35	19	-0.41	0.49	-0.32	0.54			-4.6	3.4	0.590	-1.252	-0.002	0.001
35	20	0.89	1.21	0.85	1.46			4.4	5.2	2.025	-1.569	-0.000	-0.003
35	21	1.10	1.21	1.33	1.20			6.0	8.2	-2.341	-2.263	-0.003	0.003
35	22	0.90	3.72	0.94	4.29			3.6	17.7	2.062	-1.193	-0.006	-0.008
35	23	-4.76	-0.00	-5.29	-0.16			-26.1	0.7	3.183	1.585	0.009	-0.002
35	24	-1.49	0.78	-1.56	0.87			-9.3	4.4	2.216	-3.079	-0.003	0.002
35	25	-2.61	-0.41	-3.10	-0.55			-12.0	-3.1	4.035	3.530	-0.003	-0.004
35	26	-2.26	-3.05	-2.28	-3.46			-12.9	-15.8	-1.545	4.510	0.003	-0.002
35	27	0.55	-3.39	0.66	-3.67			2.1	-18.1	-0.648	0.223	0.004	0.008
35	28	2.42	-2.70	2.71	-3.06			12.5	-15.3	-2.007	3.218	-0.003	0.010
35	29	0.31	3.14	0.58	3.45			0.1	17.7	-0.912	-3.192	-0.001	-0.006
35	30	-1.05	2.47	-1.20	2.86			-5.6	12.5	2.415	-3.579	0.001	-0.000
35	31	-1.00	-0.57	-1.15	-0.60			-6.1	-2.9	4.059	0.789	-0.003	-0.003
35	32	3.11	0.34	3.32	0.34			18.5	1.9	-4.619	-1.559	-0.003	0.003
35	33	0.10	-0.62	0.06	-0.77			2.4	-2.1	-2.539	-0.530	0.001	0.002
35	34	0.65	-0.33	0.69	-0.38			3.4	-0.7	0.966	-0.847	-0.003	-0.001
35	35	-1.36	-0.03	-1.44	-0.04			-8.9	0.5	1.187	-1.282	0.004	0.001
36	0	-1.85	*249.3*	-2.12	*290.4*			-10.9	*8348*	4.947	*406.52*	0.035	*0.0045*
36	1	-1.20	1.40	-1.27	1.54			-7.6	7.8	0.261	0.204	0.019	0.035
36	2	0.59	-3.08	0.47	-3.13			6.6	-18.4	-0.396	1.086	-0.001	0.005
36	3	0.46	-0.03	0.48	0.03			2.9	-0.8	-0.680	0.205	-0.012	-0.007
36	4	-1.94	0.82	-2.27	0.89			-10.6	4.3	2.600	-3.087	0.006	0.012
36	5	0.19	1.04	0.-8	1.13			1.5	6.7	-0.801	-1.730	-0.002	-0.007
36	6	1.44	1.67	1.48	2.00			9.2	9.7	-1.713	-3.691	-0.003	-0.004
36	7	0.45	1.08	0.45	1.16			3.9	6.6	-1.054	-0.899	-0.001	-0.004
36	8	1.24	-2.02	1.38	-2.06			6.9	-11.1	1.138	-1.199	-0.007	0.003
36	9	0.96	0.12	0.95	1.97			6.5	-0.1	-1.174	1.672	0.001	0.001
36	10	1.39	1.86	1.52	0.14			7.0	11.4	0.337	-2.099	-0.003	-0.005
36	11	0.90	0.03	0.89	0.04			5.3	-0.2	0.862	1.695	0.000	-0.002
36	12	2.89	-0.57	3.18	-0.60			15.4	-3.9	-0.704	0.295	-0.007	0.005
36	13	-0.75	2.33	-0.84	2.49			-3.9	14.3	-1.615	-3.201	0.006	-0.003
36	14	-0.83	-1.12	-0.75	-1.20			-5.9	-5.9	1.560	-0.451	0.003	0.001
36	15	0.65	3.01	0.70	3.25			3.3	16.8	-0.360	-0.824	-0.000	-0.007
36	16	-1.09	0.80	-1.19	0.89			-6.3	4.6	2.815	-1.335	0.003	-0.002
36	17	-1.04	-2.62	-1.06	-2.69			-6.4	-16.7	-0.883	3.561	-0.001	0.006
36	18	0.29	-1.06	0.11	-1.07			3.4	-7.3	-0.342	-1.028	0.003	0.003
36	19	-0.09	-1.02	-0.04	-1.13			-0.9	-4.7	0.204	-1.834	-0.000	0.004
36	20	-0.00	1.98	-0.12	2.22			0.4	10.7	1.630	-2.736	-0.001	-0.004
36	21	3.69	0.94	3.95	0.79			22.1	7.8	-3.761	-3.135	-0.005	0.001
36	22	2.40	1.86	2.72	2.05			11.8	9.1	-1.013	0.794	-0.007	-0.003
36	23	0.81	1.02	0.72	1.02			6.0	4.8	-1.250	3.133	-0.001	-0.004
36	24	0.16	-0.41	0.23	-0.59			0.9	-1.1	-1.841	0.098	-0.002	0.003
36	25	0.04	2.99	0.01	3.28			0.4	15.5	1.513	-3.129	-0.004	-0.002
36	26	-3.89	0.99	-4.25	0.86			-20.3	8.0	0.183	1.986	0.004	-0.009
36	27	-0.99	1.06	-0.90	1.13			-7.1	7.8	-1.628	-3.503	0.005	-0.004
36	28	-5.11	-2.79	-5.50	-3.01			-30.4	-16.5	8.107	2.428	0.007	0.006
36	29	-1.00	-2.75	-0.77	-2.95			-8.3	-16.1	-0.397	4.048	0.004	0.001
36	30	0.12	3.28	0.11	3.74			1.3	17.5	-0.914	-4.839	0.002	-0.006
36	31	-4.30	-1.96	-4.69	-2.19			-25.0	-11.1	5.828	2.181	0.006	0.010
36	32	3.27	-2.98	3.52	-3.14			18.6	-16.5	-2.327	0.042	-0.010	0.006
36	33	2.34	0.54	2.52	0.68			12.5	2.1	-2.222	0.601	-0.003	-0.004
36	34	-2.84	1.44	-3.08	1.56			-16.4	8.3	5.135	-1.758	0.004	-0.001
36	35	-0.02	0.21	-0.08	0.18			0.5	2.8	-0.276	-2.291	-0.001	0.002
36	36	-1.42	0.0	-1.51	0.0			-9.5	0.0	1.604	0.0	0.005	0.0

C. HARMONIC COEFFICIENTS AND DEGREE VARIANCES

TABLE B

FULLY NORMALIZED SPHERICAL HARMONIC COEFFICIENTS AND DEGREE VARIANCES OF THE TOPOGRAPHIC-ISOSTATIC MERIDIAN AND PRIME VERTICAL COMPONENTS OF THE DEFLEXION OF THE VERTICAL

KEY TO COLUMNS:

(1) Meridian component of deflexion at geoid level (arc ms)
(2) Meridian component of deflexion at surface level (arc ms)
(3) Meridian component of deflexion at orbital level (arc ms)
(4) Prime vertical component of deflexion at geoid level (arc ms)
(5) Prime vertical component of deflexion at surface level (arc ms)
(6) Prime vertical component of deflexion at orbital level (arc ms)

Degree variances are shown in italics at the beginning of each degree in the 'S' column in arc ms^2.

		(1)		(2)		(3)		(4)		(5)		(6)	
n	*m*	C	S	C	S	C	S	C	S	C	S	C	S
0	0	-134.8	*18171*	-113.5	*12882*	0.7	*0.5*	38.2	*1459*	43.1	*1858*	0.4	*0.2*
1	0	169.7	*30241*	132.1	*19404*	-6.9	*72.3*	90.3	*28392*	90.7	*32616*	-0.7	*49.0*
1	1	2.0	38.1	1.3	44.1	0.7	-4.8	-1.6	142.3	-3.1	156.2	-5.7	4.1
2	0	-111.5	*30695*	-72.5	*24680*	22.9	*665.6*	52.5	*17109*	48.1	*17082*	1.0	*153.8*
2	1	102.5	-8.2	105.8	-12.7	6.6	-2.9	19.-	-56.4	20.1	-54.6	-5.2	-0.7
2	2	84.1	24.4	85.9	26.3	8.5	-3.8	26.6	100.4	25.2	103.8	-4.2	-10.3
3	0	97.7	*17662*	35.8	*8464*	-1.6	*475.2*	-103.4	*41290*	-113.6	*44986*	-1.1	*327.6*
3	1	80.7	-8.4	73.4	5.9	1.9	19.2	-0.7	-74.7	-9.1	-62.7	-5.6	-2.1
3	2	-13.3	-13.7	-14.3	-10.0	7.0	1.8	-147.6	-22.1	-158.2	-22.1	-6.6	-14.9
3	3	33.9	-3.3	38.1	-3.8	-3.3	5.9	25.3	-45.8	25.2	-43.7	-4.8	0.4
4	0	-124.7	*53917*	-81.9	*46656*	12.2	*566.4*	12.9	*52808*	8.9	*53731*	1.3	*676.0*
4	1	-33.0	89.5	-39.0	85.4	-4.7	10.1	-19.4	71.3	-22.0	67.6	6.1	-1.5
4	2	-78.4	9.1	-79.4	9.1	-9.1	7.5	-66.0	-34.6	-69.6	-31.3	-0.6	-14.7
4	3	-72.1	83.4	-70.3	91.1	-3.7	9.2	-42.5	82.5	-40.1	81.1	13.1	7.4
4	4	-49.3	-91.9	-49.4	-95.1	-6.4	4.0	-121.6	-135.0	-128.4	-134.5	-12.9	5.1
5	0	214.1	*72630*	169.3	*55932*	-16.8	*835.2*	58.9	*94065*	58.2	*100679*	-1.3	*729.0*
5	1	47.7	-30.4	36.0	-5.3	0.3	5.4	29.5	-36.5	20.3	-21.8	-0.5	0.2
5	2	-57.7	-34.9	-59.3	-32.6	-19.5	3.4	95.7	4.3	95.6	2.3	1.5	-3.4
5	3	24.0	-32.0	30.7	-28.6	1.9	-6.3	101.2	4.2	107.2	6.9	10.4	5.7
5	4	-8.6	130.0	-7.5	138.0	-5.7	6.9	120.8	148.7	129.6	155.5	10.6	16.8
5	5	-20.5	4.7	-22.3	3.6	2.5	-1.5	-179.6	2.5	-186.3	5.1	-12.9	-3.4
6	0	-186.8	*54056*	-152.6	*45882*	-12.1	*767.3*	35.6	*35834*	42.3	*38377*	1.4	*408.0*
6	1	55.0	6.3	61.8	-3.6	-7.0	-10.8	87.9	-19.6	93.7	-25.5	7.0	-1.3
6	2	-39.4	-22.1	-49.6	-26.5	-16.6	1.1	31.4	-57.0	30.5	-47.0	2.0	1.8
6	3	20.4	-79.6	22.1	-89.1	0.3	-10.2	78.1	-56.9	84.3	-57.9	2.9	3.6
6	4	50.8	8.6	49.9	9.4	5.7	-6.1	55.9	30.0	62.7	28.8	3.6	13.5
6	5	7.0	41.4	7.9	41.4	0.1	-1.4	47.6	18.4	44.2	16.7	-4.5	-7.4
6	6	-33.6	42.3	-30.3	43.7	2.0	-0.1	-62.7	48.2	-64.3	49.5	-0.2	-7.5
7	0	61.4	*52578*	19.0	*49195*	4.1	*372.5*	-39.3	*103169*	-33.2	*112493*	-1.4	*404.0*
7	1	-42.2	-36.5	-49.8	-13.2	-3.7	-11.3	34.6	37.0	23.8	59.5	-3.7	2.1
7	2	-97.1	-47.1	-96.1	-34.3	1.0	0.8	-11.8	22.7	-9.0	28.3	1.8	7.0
7	3	-49.3	21.0	-42.5	20.5	1.4	-7.3	-38.8	5.2	-46.8	15.4	-1.2	4.5
7	4	55.8	-121.3	56.5	-124.0	11.0	-2.1	-43.8	-87.9	-39.3	-87.1	-0.2	5.2
7	5	-23.5	-38.4	-28.8	-35.4	-1.2	-3.8	-137.4	6.6	-140.2	5.7	-11.5	-2.4
7	6	10.2	-78.2	9.5	-83.2	-0.7	-1.1	7.7	-145.0	6.8	-154.0	-0.4	-6.4
7	7	70.8	-8.2	76.3	-7.0	-3.2	1.4	208.2	-62.4	215.9	-69.3	8.9	-5.1
8	0	-83.2	*44142*	-64.1	*45284*	6.5	*364.8*	-21.5	*87912*	-18.5	*87438*	1.5	*346.0*
8	1	-91.3	56.1	-98.4	46.6	-0.1	-4.1	-31.2	44.4	-19.7	25.2	3.5	-0.2
8	2	68.5	-7.5	68.4	-0.3	10.9	-1.7	19.1	26.6	15.1	36.7	2.2	1.0
8	3	-10.9	50.9	-19.3	50.5	2.6	-2.0	-85.6	64.2	-75.6	62.4	-3.3	1.9
8	4	31.4	-4.0	34.0	-1.7	10.4	-1.8	-9.6	2.7	-12.0	-0.6	0.6	-1.5
8	5	-25.5	35.1	-32.1	34.4	1.0	5.9	-130.8	11.1	-128.4	12.1	-9.6	-3.9

		(1)		(2)		(3)		(4)		(5)		(6)	
n	*m*	C	S	C	S	C	S	C	S	C	S	C	S
8	6	-25.5	35.1	-34.2	-6.7	-0.6	-1.6	-98.4	36.0	-102.1	38.1	-2.6	-3.4
8	7	-30.1	-9.6	-81.6	-87.4	-3.3	1.6	-53.6	-92.3	-51.8	-90.2	5.1	11.6
8	8	20.3	-44.5	23.6	-47.9	-2.9	0.2	160.3	-80.9	165.8	-89.0	2.6	-4.1
9	0	93.6	*56454*	87.2	*59780*	8.6	*428.5*	-14.8	*41372*	-13.0	*40240*	-1.5	*368.6*
9	1	-52.1	-80.1	-66.3	-63.9	0.5	1.9	-5.3	-130.7	-15.7	-115.3	-4.4	2.0
9	2	93.0	-41.0	103.6	-27.9	10.6	-3.7	6.9	-24.9	3.9	-27.7	0.7	1.2
9	3	75.0	-23.4	87.0	-14.5	4.7	8.2	-4.7	-12.8	-13.4	3.2	-2.4	2.1
9	4	28.7	41.3	39.8	47.9	5.4	-4.4	-39.7	0.8	-35.3	-2.6	-1.9	-5.8
9	5	41.2	43.3	42.8	40.5	-1.8	7.7	77.8	18.3	77.6	15.8	-1.7	-3.3
9	6	-4.6	90.7	-3.2	91.1	-1.5	1.9	23.8	33.0	27.5	31.4	-3.2	-4.0
9	7	-1.4	2.2	-0.5	2.4	3.2	1.6	73.9	30.8	81.5	33.4	10.1	4.7
9	8	-34.3	-29.1	-40.2	-29.5	-1.3	-0.5	-26.7	62.6	-25.6	68.4	0.8	11.3
9	9	27.2	-70.3	29.6	-73.4	-0.8	-0.7	-21.3	-45.5	-24.9	-50.8	-1.4	-1.1
10	0	-111.8	*72630*	-105.9	*72092*	-0.7	*392.0*	38.0	*120965*	41.6	*127021*	1.6	*190.4*
10	1	-92.1	74.8	-91.0	74.2	-1.6	14.6	3.9	9.9	22.0	-12.5	3.8	-0.4
10	2	45.3	-25.5	39.0	-22.7	1.9	0.7	-5.8	-112.2	-8.1	-100.9	0.7	-3.4
10	3	10.3	4.4	97.4	0.3	2.1	8.6	-29.3	-13.1	-11.0	-20.4	2.2	-1.3
10	4	12.9	-19.7	10.9	-27.8	-4.0	3.0	-34.2	-52.3	-40.8	-58.6	-3.4	-6.0
10	5	-15.7	-36.4	-13.0	-32.8	-2.5	2.7	11.4	-42.9	10.1	-44.3	0.7	-1.3
10	6	-13.8	2.0	-12.6	-4.7	-5.0	2.4	88.1	-26.0	87.5	-26.7	0.6	-0.6
10	7	60.7	65.6	66.4	66.4	1.7	-2.2	126.8	4.2	131.3	-1.0	7.2	3.0
10	8	70.2	-10.6	73.7	-10.9	3.0	-0.6	100.5	-36.8	108.9	-31.3	0.5	0.6
10	9	31.2	57.6	35.6	61.7	1.1	-2.6	64.3	196.3	71.3	202.2	-3.0	3.4
10	10	-12.7	113.1	-15.1	116.4	-0.1	-0.6	-31.1	142.5	-33.8	145.3	1.9	4.3
11	0	-58.3	*76066*	-53.5	*83002*	-1.7	*156.3*	7.2	*70172*	11.1	*71556*	-1.4	*176.9*
11	1	-48.1	96.1	-54.4	113.1	2.1	-0.4	67.5	46.2	54.7	56.2	-1.7	2.2
11	2	-21.2	24.9	-8.1	30.5	-6.8	0.5	51.3	22.0	57.0	23.1	0.8	2.2
11	3	-45.6	39.9	-27.4	55.9	2.3	1.4	68.7	-52.8	64.6	-31.6	2.6	0.6
11	4	-28.7	-52.0	-22.8	-53.9	-0.6	4.6	-6.9	-14.1	14.1	-11.3	0.6	-2.1
11	5	-164.8	-8.3	-161.6	-12.9	-1.5	0.1	-51.0	-24.3	-43.0	-35.3	1.2	-0.4
11	6	38.2	-66.8	35.7	-70.9	-3.5	0.2	-17.7	-11.5	-20.8	-8.9	0.3	3.0
11	7	-32.2	-45.8	-33.2	-46.6	2.4	-3.3	31.0	-50.3	30.2	-49.3	4.9	1.1
11	8	67.1	6.6	73.4	5.8	-0.1	-0.4	-40.5	14.5	-42.0	15.0	-0.6	2.7
11	9	5.3	-9.2	6.0	-11.7	1.1	-1.1	12.4	-72.8	9.4	-70.4	-8.4	-3.7
11	10	92.9	9.3	102.0	10.3	1.0	-0.9	99.5	91.2	106.3	93.8	-2.8	0.6
11	11	-55.7	16.2	-61.8	20.3	0.0	-1.0	-2.4	141.1	-0.2	148.1	4.1	1.8
12	0	-81.8	*96845*	-95.5	*104071*	-9.2	*216.1*	-83.9	*75240*	-83.7	*75625*	1.5	*108.2*
12	1	-47.6	26.6	-45.9	36.6	3.0	0.0	-38.0	71.9	-19.1	53.5	3.7	-0.8
12	2	73.7	77.9	63.3	90.0	-4.6	3.0	-1.1	13.1	-13.2	12.5	0.8	-0.9
12	3	11.6	-86.0	8.3	-90.8	-0.1	-4.7	-31.3	18.2	-10.3	11.4	2.8	-2.3
12	4	52.3	37.8	46.0	32.9	-3.0	1.1	75.7	-23.7	74.3	-34.0	0.1	-1.2
12	5	-23.1	-26.6	-28.4	-26.5	-1.2	-2.3	61.1	35.1	67.1	37.4	0.6	0.2
12	6	47.5	95.4	47.8	101.1	1.5	0.7	-41.9	-18.1	-33.1	-24.2	0.8	3.5
12	7	-106.1	-75.1	-109.1	-73.1	1.3	-4.8	-30.8	-24.6	-34.5	-22.8	1.4	-0.9
12	8	-64.8	93.2	-66.8	98.5	3.2	0.7	-130.1	21.7	-133.5	23.9	-0.3	0.6
12	9	-72.2	-42.6	-74.1	-43.6	-2.8	1.9	-112.5	48.1	-118.2	57.3	-5.0	0.3
12	10	-22.7	-36.6	-27.7	-37.5	0.1	1.9	-46.2	-70.3	-45.6	-70.6	-1.3	0.1
12	11	60.7	-22.1	62.8	-27.7	-0.1	0.7	22.2	-4.5	24.2	-5.8	-4.4	-0.0
12	12	92.9	-1.0	89.9	-0.4	0.2	-1.0	57.7	-43.6	62.9	-39.4	2.2	-2.7
13	0	-113.7	*111489*	-92.6	*110290*	-1.3	*210.3*	-17.3	*79130*	-10.1	*81054*	-1.4	*114.5*
13	1	-16.6	-39.4	-24.2	-53.3	-1.4	-11.0	-53.9	-34.4	-66.4	-22.5	-1.9	1.7
13	2	29.5	95.0	44.8	98.0	-1.7	0.2	-27.0	-29.5	-12.0	-25.8	1.5	1.9
13	3	-2.4	-144.0	23.4	-136.3	-2.6	-4.8	17.8	19.9	-4.4	45.0	0.1	0.7
13	4	-77.7	-14.4	-63.6	-4.3	-0.4	0.6	-42.2	-49.8	-16.2	-41.5	1.4	0.0
13	5	21.1	-29.9	28.5	-35.5	-1.4	-3.5	35.0	58.2	37.8	51.0	-0.8	0.7
13	6	49.3	77.8	50.2	76.7	3.1	0.1	-14.2	12.3	-10.7	12.4	1.0	1.2
13	7	24.0	-11.8	25.4	-8.9	-0.7	-3.3	-0.1	-33.4	-6.3	-35.2	-1.8	-0.7
13	8	-42.1	-13.2	-43.3	-6.7	2.1	-0.5	71.7	-43.8	60.5	-39.9	0.6	-2.7
13	9	20.2	24.9	19.9	24.2	-0.5	1.7	-62.6	51.9	-71.5	52.7	-3.4	2.2
13	10	-141.7	7.8	-150.7	7.4	-1.0	1.2	50.8	46.8	52.5	48.4	2.4	0.3
13	11	102.6	37.9	98.9	39.4	0.4	2.3	30.4	44.1	33.2	50.3	5.1	1.6
13	12	-88.9	-20.6	-94.6	-30.8	-0.1	0.6	-165.8	39.1	-170.6	41.3	-5.0	-0.7
13	13	-68.5	34.7	-66.6	30.9	-0.2	-0.2	-43.9	-105.6	-41.9	-105.8	-1.6	-2.2
14	0	-19.4	*66616*	-39.0	*69274*	2.5	*75.7*	40.4	*102848*	37.3	*111556*	1.4	*62.4*
14	1	24.6	-3.1	35.6	6.6	2.3	0.8	-8.6	-14.7	9.0	-34.4	2.3	-0.8
14	2	77.7	11.0	61.4	27.2	5.8	0.3	-4.4	-66.8	-14.3	-76.2	0.9	-0.3
14	3	4.9	-50.1	0.9	-61.9	-1.8	-2.5	-18.0	-28.8	3.9	-41.5	0.5	-1.0
14	4	-63.9	38.7	-68.4	26.2	1.7	-0.4	-24.7	34.7	-42.5	27.3	0.4	-0.9

		(1)		(2)		(3)		(4)		(5)		(6)	
n	*m*	C	S	C	S	C	S	C	S	C	S	C	S
14	5	-63.0	-56.1	-68.5	-49.6	0.0	-0.0	-28.2	-31.9	-23.5	-25.5	-2.1	1.2
14	6	47.8	-14.4	46.1	-14.2	2.1	-0.5	-13.9	106.7	-14.5	109.8	0.9	0.2
14	7	10.6	-17.7	13.6	-15.4	-0.7	0.9	-12.8	-26.6	-17.9	-25.1	-2.4	0.0
14	8	4.9	-83.0	9.6	-85.3	-0.7	-1.5	44.8	-12.4	39.5	-12.8	-1.0	-2.4
14	9	50.3	18.5	52.0	17.6	0.4	2.1	59.7	-14.6	53.2	-13.2	-1.5	1.0
14	10	4.1	15.5	2.3	11.5	-0.4	-1.0	44.4	2.0	38.4	-8.1	1.2	2.1
14	11	-33.5	7.4	-33.0	11.7	0.8	-1.4	64.9	-69.0	76.1	-77.5	2.2	-0.9
14	12	44.8	43.7	45.6	45.5	0.2	0.4	65.7	123.9	66.3	129.5	3.5	-1.5
14	13	-74.5	80.3	-78.0	79.1	0.2	0.8	-155.9	80.4	-160.8	85.1	-0.8	0.9
14	14	-63.8	-100.4	-59.2	-105.4	-0.0	0.4	-90.8	-60.7	-88.2	-63.9	-1.4	0.5
15	0	-51.1	*160721*	-23.3	*149924*	2.5	*88.4*	-11.2	*88090*	-11.9	*84797*	-1.2	*49.0*
15	1	84.5	174.9	74.6	154.7	0.1	-2.9	84.3	-7.3	69.1	0.9	-2.0	1.6
15	2	3.3	83.2	27.3	76.7	2.7	-3.5	-14.3	12.3	-2.6	8.6	1.4	0.2
15	3	-25.3	-15.6	-11.3	1.2	1.4	2.4	69.5	-93.1	50.3	-81.0	-0.9	1.3
15	4	-59.7	-117.3	-39.0	-111.9	1.2	-2.6	-28.0	-30.5	-4.7	-22.5	1.2	-0.9
15	5	-81.6	81.4	-72.5	73.6	1.9	2.7	-44.2	-2.2	-41.6	-23.3	-0.8	0.6
15	6	68.6	17.9	66.3	10.2	1.8	-0.8	-5.2	21.1	-5.6	16.9	0.5	-0.7
15	7	-42.1	-1.1	-46.9	-3.3	0.0	2.9	-47.3	60.9	-48.6	62.0	-0.6	0.2
15	8	-91.9	37.3	-94.9	33.3	-1.3	-0.1	-44.3	16.1	-47.7	10.2	-1.3	-1.5
15	9	13.1	-94.8	13.6	-97.9	0.6	2.2	68.2	19.4	72.1	23.6	0.1	1.3
15	10	71.0	-80.2	71.7	-87.8	0.0	-0.3	23.3	-72.1	19.4	-82.2	0.2	1.0
15	11	-1.1	-111.7	0.7	-115.7	-0.1	-1.0	51.0	-85.6	52.6	-95.0	1.3	-0.2
15	12	141.1	2.9	149.2	4.5	-0.9	-2.1	11.3	-95.7	15.1	-94.4	-2.8	-1.1
15	13	27.1	9.4	28.1	8.7	-0.5	-0.5	121.4	17.1	123.2	20.9	1.7	-2.2
15	14	-33.6	101.3	-33.1	106.4	-0.3	0.4	-14.6	53.2	-15.3	54.3	2.3	0.1
15	15	-5.0	10.5	-4.1	6.0	0.6	0.3	-10.1	80.4	-5.9	79.7	0.5	1.2
16	0	92.3	*79411*	75.5	*79750*	1.9	*118.8*	-34.9	*86318*	-39.8	*81282*	1.3	*56.3*
16	1	-30.0	27.5	-10.5	55.8	3.9	6.9	-84.2	8.6	-67.8	0.3	2.2	-1.0
16	2	97.2	15.1	83.3	36.5	1.6	-1.9	27.9	76.3	14.3	60.0	0.0	-1.0
16	3	60.2	-15.2	62.0	-16.2	1.8	3.3	-62.9	43.6	-41.7	31.8	1.4	-1.4
16	4	-17.7	25.2	-24.8	9.9	-1.2	-2.1	72.4	-30.4	53.9	-36.2	-1.0	-1.4
16	5	60.3	26.8	55.8	37.7	1.6	2.0	-59.8	-29.5	-59.1	-20.2	-0.2	-0.1
16	6	-1.8	-16.4	0.3	-14.5	0.5	-1.8	13.8	-50.2	15.1	-59.8	0.2	-1.3
16	7	8.9	-68.7	6.1	-69.1	0.2	1.4	-17.0	18.4	-19.7	10.8	0.5	0.0
16	8	-47.1	78.1	-50.4	81.2	-2.0	0.2	2.2	-4.8	1.3	-6.8	-1.1	-0.6
16	9	33.4	-29.3	31.6	-34.1	1.9	-0.2	-17.5	-42.0	-11.2	-49.8	1.7	0.1
16	10	2.7	14.7	0.2	15.0	0.1	0.3	51.5	58.7	54.2	58.1	0.6	1.8
16	11	56.7	35.5	60.4	32.2	0.5	-1.4	-11.3	5.6	-9.6	-0.5	0.0	-0.7
16	12	61.9	-15.9	71.5	-16.3	-0.3	0.7	-3.6	43.4	-1.0	48.4	-1.9	0.7
16	13	-3.6	35.9	-0.5	35.5	-1.3	-1.1	-98.8	32.5	-104.6	41.7	-2.1	2.0
16	14	-71.7	52.5	-71.4	51.0	-0.4	-0.4	39.4	-37.2	35.7	-37.4	0.4	1.3
16	15	35.0	-122.9	40.3	-122.6	-0.5	-0.5	26.0	-148.0	27.0	-154.6	1.9	-3.0
16	16	-2.2	-27.3	-0.8	-32.1	0.5	-0.1	70.1	-0.3	72.5	-2.4	1.6	-0.7
17	0	26.1	*176568*	48.4	*171479*	-1.6	*50.4*	58.7	*144856*	62.8	*149692*	-1.1	*42.3*
17	1	80.8	141.3	60.8	110.6	-1.7	0.0	-7.6	-45.0	-17.1	-41.2	-1.5	1.3
17	2	-67.5	56.5	-41.1	42.3	-3.0	-0.6	0.1	-17.5	25.5	-3.1	0.8	-0.2
17	3	35.2	11.6	44.7	25.0	0.2	1.0	10.4	40.3	-5.4	40.1	0.3	0.5
17	4	-117.0	-52.5	-101.0	-37.8	-3.0	0.9	-61.6	28.5	-29.3	40.8	0.1	-0.2
17	5	73.8	70.9	91.1	53.5	0.7	0.3	1.9	25.7	11.0	2.4	0.4	-0.4
17	6	-52.9	-19.5	-54.8	-29.8	-1.9	-0.6	38.7	-23.4	33.0	-24.4	-0.9	-1.1
17	7	3.8	-121.2	6.5	-131.9	0.8	-0.8	26.9	-20.9	32.0	-30.1	0.6	-0.0
17	8	22.5	23.7	20.1	26.2	-2.0	0.4	11.1	55.0	10.9	55.6	-1.0	0.8
17	9	47.0	6.0	44.3	5.9	0.7	-2.3	-69.5	-62.6	-64.5	-65.9	0.0	-1.2
17	10	72.4	59.7	72.5	67.0	1.5	-0.3	46.3	3.0	45.8	4.5	0.7	0.8
17	11	41.9	145.4	44.3	150.9	-0.0	-0.9	-15.8	22.9	-12.7	20.1	-1.2	-1.1
17	12	-25.4	42.4	-20.6	45.3	1.2	0.4	12.8	86.4	5.5	91.4	-1.1	-0.4
17	13	-25.2	112.1	-27.0	118.1	0.8	1.5	17.2	94.0	21.2	100.4	-1.1	1.2
17	14	-48.8	-54.2	-55.7	-52.9	0.4	0.3	-0.8	48.8	-1.5	55.9	1.1	1.4
17	15	-70.8	-48.9	-75.4	-51.6	-0.2	0.0	-105.9	-0.3	-111.7	-4.2	-1.4	2.5
17	16	40.5	-108.1	44.3	-109.0	-0.7	-0.2	15.7	-226.0	15.2	-230.0	-0.4	-2.7
17	17	129.3	46.0	134.0	46.9	-0.1	-0.2	173.6	-47.6	175.9	-47.2	1.6	-0.7
18	0	154.2	*127235*	142.0	*119993*	-0.7	*34.8*	39.9	*103813*	29.6	*105755*	1.1	*38.4*
18	1	-55.4	-37.7	-26.5	-3.8	2.5	0.5	29.4	-23.1	36.8	-25.5	2.4	-1.0
18	2	-65.2	-43.6	-90.4	-27.0	-2.8	-0.4	-2.8	22.0	-15.8	3.5	-0.1	-0.3
18	3	-20.5	32.3	-6.6	24.4	0.2	-1.5	14.6	-44.5	29.5	-56.1	1.7	-1.4
18	4	-50.3	135.3	-59.1	118.2	-1.3	1.2	6.8	35.7	-12.4	25.7	-0.7	-0.0
18	5	43.3	-55.5	30.2	-50.0	0.2	-1.0	-10.3	-32.2	-2.0	-19.3	-0.0	-0.6
18	6	-57.7	41.3	-56.6	48.7	-1.2	0.8	27.7	35.7	34.6	27.4	-0.2	0.2

		(1)		(2)		(3)		(4)		(5)		(6)	
n	*m*	C	S	C	S	C	S	C	S	C	S	C	S
18	7	-42.1	-140.8	-86.5	-145.5	-0.2	-1.4	51.7	28.3	46.7	18.2	-0.2	-0.6
18	8	-5.9	5.7	1.3	8.2	-0.1	1.6	37.1	22.6	41.3	26.1	-0.6	1.4
18	9	-2.4	70.0	-2.3	69.6	-0.9	-0.5	-40.6	59.1	-37.6	66.2	-1.1	-0.7
18	10	-15.7	-20.3	-14.3	-18.7	1.2	-0.4	-6.3	-94.1	-5.6	-91.8	0.1	-0.3
18	11	-12.9	57.0	-16.6	62.3	-1.1	0.3	-21.8	29.8	-24.2	34.4	-1.3	-0.6
18	12	-11.2	75.6	-4.8	79.9	-0.1	0.2	-36.7	-14.0	-41.9	-11.0	-0.9	-1.5
18	13	19.9	76.8	17.6	81.5	0.6	1.0	66.8	38.5	62.6	37.9	1.3	0.0
18	14	6.9	63.9	-0.5	67.5	0.8	0.1	71.9	0.0	75.5	-8.1	1.2	0.0
18	15	-5.9	42.2	-10.0	38.2	1.0	0.4	116.7	80.1	120.6	83.2	1.5	-1.7
18	16	15.8	34.1	11.0	31.7	0.1	-0.1	-91.0	150.6	-90.6	150.4	0.2	2.3
18	17	-88.6	-1.9	-87.9	-2.4	-0.6	0.1	-33.6	-79.3	-34.0	-77.1	-1.0	0.4
18	18	-32.1	38.5	-31.1	41.5	-0.3	-0.1	-12.2	40.8	-13.3	44.3	0.3	0.4

Publications from

THE SCHOOL OF SURVEYING, THE UNIVERSITY OF NEW SOUTH WALES

P.O. Box I, Kensington, N.S.W. 2033

AUSTRALIA

Reports

1.*	The discrimination of radio time signals in Australia *G.G. Bennett*		*Uniciv Rep.* D-1	(G 1)
2.*	A comparator for the accurate measurement of differential barometric pressure *J.S. Allman*	9pp	*Uniciv Rep.* D-3	(G 2)
3.	The establishment of geodetic gravity networks in South Australia *R.S. Mather*	26pp	*Uniciv Rep.* R-17	(G 3)
4.	The extension of the gravity field in South Australia *R.S. Mather*	26pp	*Uniciv Rep.* R-19	(G 4)
5.*	An analysis of the reliability of barometric elevations *J.S. Allman*	335pp	*Unisurv Rep.* 5	(S 1)
6.*	The free air geoid for South Australia and its relation to the equipotential surfaces of the earth's gravitational field *R.S. Mather*	491pp	*Unisurv Rep.* 6	(S 2)
7.*	Control for mapping (Proceedings of Conference, May 1967) *P.V. Angus-Leppan (Editor)*	329pp	*Unisurv Rep.* 7	(G 5)
8.*	The teaching of field astronomy *G.G. Bennett & J.G. Freislich*	30pp	*Unisurv Rep.* 8	(G 6)
9.*	Photogrammetric pointing accuracy as a function of properties of the visual image *J.C. Trinder*	64pp	*Unisurv Rep.* 9	(G 7)
10.*	An experimental determination of refraction over an icefield *P.V. Angus-Leppan*	23pp	*Unisurv Rep.* 10	(G 8)
11.*	The non-regularised geoid and its relation to the telluroid and regularised geoids *R.S. Mather*	49pp	*Unisurv Rep.* 11	(G 9)
12.*	The least squares adjustment of gyro-theodolite observations *G.G. Bennett*	53pp	*Unisurv Rep.* 12	(G 10)
13.*	The free air geoid for Australia from gravity data available in 1968 *R.S. Mather*	38pp	*Unisurv Rep.* 13	(G 11)
14.*	Verification of geoidal solutions by the adjustment of control networks using geocentric Cartesian co-ordinate systems *R.S. Mather*	42pp	*Unisurv Rep.* 14	(G 12)
15.*	New methods of observation with the Wild GAKI gyro-theodolite *G.G. Bennett*	68pp	*Unisurv Rep.* 15	(G 13)
16.*	Theoretical and practical study of a gyroscopic attachment for a theodolite *G.G. Bennett*	343pp	*Unisurv Rep.* 16	(S 3)
17.	Accuracy of monocular pointing to blurred photogrammetric singals *J.C. Trinder*	231pp	*Unisurv Rep.* 17	(S 4)
18.	The computation of three dimensional Cartesian co-ordinates of terrestrial networks by the use of local astronomic vector systems *A. Stolz*	47pp	*Unisurv Rep.* 18	(G 14)
19.	The Australian geodetic datum in earth space *R.S. Mather*	130pp	*Unisurv Rep.* 19	(G 15)
20.*	The effect of the geoid on the Australian geodetic network *J.G. Fryer*	221pp	*Unisurv Rep.* 20	(S 5)
21.*	The registration and cadastral survey of native-held rural land in the Territory of Papua and New Guinea *G.F. Toft*	441pp	*Unisurv Rep.* 21	(S 6)
22.	Communications from Australia to Section V, International Association of Geodesy, XV General Assembly, International Union of Geodesy & Geophysics, Moscow 1971 *R.S. Mather et al*	72pp	*Unisurv Rep.* 22	(G 16)
23.	The dynamics of temperature in surveying steel and invar measuring bands *A.H. Campbell*	195pp	*Unisurv Rep.* S 7	

* Out of print

Reports (contd)

24. Three-D Cartesian co-ordinates of part of the Australian geodetic network by the use of local astronomic vector systems
A. Stolz 182pp *Unisurv Rep.* S 8

25. Papers on Four-dimensional Geodesy, Network Adjustments and Sea Surface Topography
R.S. Mather, H.L. Mitchell, A. Stolz 73pp *Unisurv* G 17

26. Papers on photogrammetry, co-ordinate systems for survey integration, geopotential networks and linear measurement
L. Berlin, G.J.F. Holden, P.V. Angus-Leppan, H.L. Mitchell and A. Campbell 80pp *Unisurv* G 18

27. Aspects of Four-dimensional Geodesy
R.S. Mather, P.V. Angus-Leppan, A. Stolz and I. Lloyd 100pp *Unisurv* G 19

28. Relations between MSL & Geodetic Levelling in Australia
H.L. Mitchell 264pp *Unisurv Rep.* S 9

29. Study of Zero Error & Ground Swing of the Model MRA101 Tellurometer
A.J. Robinson 200pp *Unisurv Rep.* S 10

30. Papers on Network Adjustments, Photogrammetry and 4-Dimensional Geodesy
J.S. Allman, R.D. Lister, J.C. Trinder and R.S. Mather 133pp *Unisurv* G 20

31. An Evaluation of Orthophotography in an integrated Mapping System
G.J.F. Holden 232pp *Unisurv Rep.* S 12

32. The Analysis Precision and Optimization of Control Surveys
G.J. Hoar 200pp *Unisurv Rep.* S 13

33. Papers on Mathematical Geodesy, Coastal Geodesy and Refraction
E. Grafarend, R.S. Mather and P.V. Angus-Leppan 100pp *Unisurv* G 21

34. Papers on Gravity, Levelling, Refraction, ERTS Imagery, Tidal Effects on Satellite Orbits & Photogrammetry
R.S. Mather, J.R. Gilliland, F.K. Brunner, J.C. Trinder, K. Bretreger and G. Halsey 96pp *Unisurv* G 22

35. Papers on Earth Tides, Sea Surface Topography, Atmospheric effects in physical geodesy, Mean sea level, Systematic errors in levelling
R.S. Mather, E.G. Anderson, C. Rizos, K. Bretreger, K. Leppert, B.V. Hamon, P.V. Angus-Leppan 96pp *Unisurv* G 23

36. Papers on Adjustment theory, Sea surface topography determinations, applications of Landsat imagery, Ocean loading of Earth tides, physical geodesy, photogrammetry and oceanographic applications of satellites
R. Patterson, R.S. Mather, R.C. Coleman, O.L. Colombo, J.C. Trinder, S.U. Nasca, T.L. Duyet, K. Bretreger *Unisurv* G 24

37. The Effect of Topography on Solutions of Stokes' Problem
E.G. Anderson 252pp *Unisurv Rep.* S 14

Prices

G. General Series

Subscription for 1976 Postfree
To Libraries $11.00
To Individuals $8.00

S. Special Series (Limited Printing)

Postfree
To Libraries $11.00 each copy.
To Individuals $8.00 each copy.

Publications from the School of Surveying (contd.)

Proceedings

Proceedings of conferences on refraction effects in geodesy & electronic distance measurement
P.V. Angus-Leppan (Editor) 264pp Price: $10.00**

Australian Academy of Science/International Association of Geodesy Symposium on Earth's Gravitational Field & Secular Variations in Position
R.S. Mather & P.V. Angus-Leppan (eds) 764pp Price: (A)

(A) Price to Libraries, etc.
& individuals $20.00**

Monographs

1. The theory and geodetic use of some common projections (2nd edition)
R.S. Mather 125pp Price: $5.00**

2. The analysis of the earth's gravity field
R.S. Mather 172pp Price: $5.00**

3. Tables for Prediction of Daylight Stars
G.G. Bennett 24pp Price: $2.25**

4. Star Prediction Tables for the fixing of position
G.G. Bennett; J.G. Freislich & M. Maughan 200pp Price: $8.00**

5. Survey Computations
M. Maughan 98pp Price: $3.50**

6. Adjustment of Observations by Least Squares
M. Maughan 57pp Price: $3.50**

** including postage